NOVEL *N*-(1,3,4-OXADIAZOL-2-YL)BENZAMIDES AS ANTIMICROBIAL AGENTS

by

George Alfred Naclerio III

A Dissertation

Submitted to the Faculty of Purdue University

In Partial Fulfillment of the Requirements for the degree of

Doctor of Philosophy

Department of Chemistry

West Lafayette, Indiana

December 2021

THE PURDUE UNIVERSITY GRADUATE SCHOOL
STATEMENT OF COMMITTEE APPROVAL

Dr. Herman Sintim, Chair

Department of Chemistry

Dr. Jean Chmielewski

Department of Chemistry

Dr. P. V. Ramachandran

Department of Chemistry

Dr. Mingji Dai

Department of Chemistry

Dr. Rob Stahelin

Department of Medicinal Chemistry and Molecular Pharmacology

Approved by:

Dr. Christine Hrycyna

I dedicate this work to my wife, Marcella. Thank you so much for all your love, support, and encouragement over these past 10 years. I would have never had been able to get through this PhD without you. I love you more than anything.

ACKNOWLEDGMENTS

I would like to thank Dr. Sintim for his guidance and mentorship during my time at Purdue University. You pushed me to be the best scientist I could and because of that I discovered my passion for drug development. I also appreciated our talks about topics other than science, like family and life. Your guidance not only made me into a great scientist but also a better man and for that I am grateful.

I would also like to thank my committee members—Dr. Jean Chmielewski, Dr. P.V. Ramachandran, Dr. Mingji Dai, and Dr. Rob Stahelin. Your encouragement and support helped me greatly throughout my doctoral studies.

I am also grateful to the I3D Committee—Dr. Rob Stahelin, Dr. Yoon Yeo, and Dr. Tommy Sors. Thank you all for giving me the opportunity to be part of such a great training program. I learned many important aspect about infectious diseases which will help me throughout my career as a medicinal chemist.

I would also like to thank my current colleagues in the Sintim laboratory for all of their support over the years. In particular, I would like to thank Dr. Neetu Dayal. Neetu, thank you so much for your guidance and patience over these past 4.5 years. I would not be the scientist I am today without all of your help.

I am grateful to my collaborators, Dr. Mohamed Seleem and Dr. Nader Abutaleb. Thank you both so much for your help and guidance. You both played a significant role in the development of my research studies and allowed us to push the project into new heights.

I would like to express my appreciation to the department of chemistry for giving me an opportunity to pursue my doctoral studies at such a prominent institution.

To my brothers Nick and Mike. Words cannot describe how grateful I am for you both. Growing up, you two were the only role models in my life and you both have shown me that hard work does indeed pay off. I would not be where I am today without you both.

To Brian Clark and Ring One Boxing. Brian, you allowed a broken and homeless family to come into your gym free of charge. Your training allowed me to develop critical life skills such as hard work, dedication, and perseverance which have attributed to my success. I am forever grateful for everything you did for me and my family. This PhD could not be possible without you.

TABLE OF CONTENTS

LIST OF TABLES

LIST OF FIGURES

LIST OF ABBREVIATIONS

ATCC	American type culture collection
BHIS	brain heart infusion supplemented
BOP	benzotriazol-1-yloxytris(dimethylamino)phosphonium hexafluorophosphate
CDI	*Clostridium difficile* infection
CLSI	clinical and laboratory standards institute
DIPEA	diisopropylethylamine
DMEM	dulbecco's modified eagle medium
DMF	dimethylformamide
DMSO	dimethyl sulfoxide
FBS	fetal bovine serum
H_2O	water
LTA	lipoteichoic acid
MeOH	methanol

MIC	minimum inhibitory concentration
MRSA	methicillin-resistant *Staphylococcus aureus*
MTS	3-(4,5-dimethylthiazol-2-yl)-5-(3-carboxymethoxyphenyl)-2-(4-sulfophenyl)-2H-tetrazolium)
NaOAc	sodium acetate
PAINS	pan assay interference compounds
PCA	principle component analysis
PBS	phosphate buffered saline
RT	room temperature
TLC	thin layer chromatography
TSA	tryptic soy agar
TSB	tryptic soy broth
VRE	vancomycin-resistant enterococci
WTA	wall teichoic acid

ABSTRACT

Antibiotic resistance has become a major threat to human health. For instance, globally, it is estimated that more than 700,000 people die annually from infections caused by drug-resistant bacterial pathogens. In the United States, antibiotic resistance is also a major issue as the Centers for Disease Control and Prevention (CDC) reports that more than 2.8 million antibiotic-resistant infections occur each year, resulting in more than 35,000 deaths. At the same time, the antibiotic pipeline remains dry – exemplified by the paucity of novel antibiotics introduced into clinical use and the number of active pharmaceutical companies working on antibiotic development. Still, antibiotics that have either entered clinical trials or have been FDA approved recently are just derivatives of other drugs. This means that resistance mechanisms affecting the older drugs will likely affect the newer ones as well. Therefore, this is a dire need to develop antibiotics containing new chemotypes and novel mechanisms of action to slow down the generation of resistance.

Lipoteichoic acid (LTA) is an anionic polymer attached to the cell membrane of Gram-positive bacteria such as *Staphylococcus aureus, Enterococci, Listeria monocytogenes, Streptococcus pneumoniae,* and *Bacillus subtilis*. It's been found that LTA is highly important for several bacterial processes such as growth, virulence, biofilm formation, and inflammation. Because of this, LTA has been deemed a potential new antibiotic target. Inhibitors of LTA have been reported but they contain several unfavorable properties such as low to moderate antibacterial activity.

This dissertation reports a novel class of sulfonamide containing *N*-(1,3,4-oxadiazol-2-yl)benzamides which potently inhibit *Staphylococcus aureus* (*S. aureus*) LTA biosynthesis with minimum inhibitory concentrations (MICs) of 0.25 μg/mL. Additonally, this dissertation will discuss the discovery of trifluoromethoxy (OCF_3), trifluoromethylthio (SCF_3) and pentafluorosulfanyl (SF_5) containing *N*-(1,3,4-oxadiazol-2-yl)benzamides exhibiting strong antibacterial activities against a wide-range of clinically important bacterial pathogens such as methicillin-resistant *S. aureus* (MRSA), vancomycin resistant *enterococcus* (VRE), *Clostridioides difficile* (*C. difficile*), and *Neisseria gonorrhoeae* (*N. gonorrhoeae*) with MICs as low as 0.003 μg/mL. Halogenated *N*-(1,3,4-oxadiazol-2-yl)benzamides which eradicate MRSA preformed biofilm have also been characterized.

CHAPTER 1. INTRODUCTION

1.1 Bacterial Infections

Bacteria are a group of microscopic, unicellular organisms, which are classified as prokaryotic cells. Bacteria comprise a physical structure consisting of a cell wall, DNA, RNA, pili, flagellum, cytoplasm, and ribosomes. Bacteria can be Gram-positive or Gram-negative and can be distinguished based on physical composition or stain. Regarding physical composition, Gram-positive bacteria contain a thick peptidoglycan cell wall which is decorated with teichoic and protects the cell membrane[1]. In contrast, Gram-negative bacteria contain a thin peptidoglycan cell wall which is sandwiched between outer and inner membranes[2]. Additionally, Gram-positive stain a deep violet color, whereas Gram-negative bacteria stain a red or pink color[1-2].

Bacteria have the ability to cause infections. A bacterial infection is when a bacterium colonizes in a host and uses the host's resources as a means for self-replication, which then leads to the formation of disease. Germ theory is the scientific principle that attributes certain diseases to the infiltration of the body by microorganisms like bacteria. Germ theory became accepted among the scientific and general community after careful experimentation by both Louis Pasteur and Robert Koch[3]. Louis Pasteur discovered that *pébrine* (a protozoa) and *flacherie* (a bacterium) were responsible for the contamination of food spoilage[4-5]. Robert Koch revealed that a particular bacteria (anthrax) could cause a specific disease[6-7]. Thus, both Pasteur and Koch played a significant role in the conception that bacterial infections are a potential threat to human health, and they are both the reason why germ theory is globally accepted today.

Bacterial infections can be detrimental and sometimes fatal to the host. For centuries infectious diseases, including bacterial infections, have been a leading cause of death. For instance, throughout history bacterial infections have been the culprit for epidemics and pandemics which have claimed millions of lives (Table 1.1)[8-12]. One of the earliest epidemics, The Plague of Athens (431-404 BC), was caused by a pathogenic bacterium, *Salmonella enterica* serovar typhi, leading to typhoid fever[13]. The Plague of Athens caused around 75,000 to 100,000 deaths (25% of the city's population)[13]. Additionally, two of the deadliest pandemics in history, the Plague of Justinian and Black Death (both caused by *Yersinia pestis*), had a detrimental effect to the world's population. In fact, the Plague of Justinian is estimated to have killed around 100 million people

in the Roman Empire, while the Black Death killed 200 million people (30% of Europe's population)[14]. Moreover, cholera, caused by the bacterium *Vibrio cholerae*, has resulted in seven pandemics (see Table 1.1). Cholera was primarily found in Asia until 1817 where it spread from India to several other regions of the world. The emergence of these cholera pandemics is attributed to contaminated water found in public pumps used for water supply[15]. Therefore, bacterial infections can become quite deadly and wreak havoc on human health.

Table 1.1 Epidemics and Pandemics Throughout History Caused by Bacterial Infections

Years	Epidemic/Pandemic	Pathogen	Causes
431-404 BC	The Plague of Athens	*Salmonella enterica* serovar typhi	Overcrowding/poor hygiene
541-750	The Plague of Justinian	*Yersinia pestis*	Fleas from rodents
1346-1361	The Black Death	*Yersinia pestis*	Fleas from rodents
1817-1824	1st Cholera Pandemic	*Vibrio cholerae*	Contaminated water
1827-1835	2nd Cholera Pandemic	*Vibrio cholerae*	Contaminated water
1839-1856	3rd Cholera Pandemic	*Vibrio cholerae*	Contaminated water
1863-1875	4th Cholera Pandemic	*Vibrio cholerae*	Contaminated water
1881-1886	5th Cholera Pandemic	*Vibrio cholerae*	Contaminated water
1899-1923	6th Cholera Pandemic	*Vibrio cholerae*	Contaminated water
1961-ongoing	7th Cholera Pandemic	*Vibrio cholerae*	Contaminated water

Regardless of global advancements in medicine, bacterial infections are still associated with high mortality rates, causing almost one million deaths every year[16-17]. This is due to poverty as well as the emergence and re-emergence of bacterial infections. Regarding poverty, a recent report found that more than half of the deaths in low income countries were caused from conditions like communicable diseases, maternal, prenatal, and nutritional conditions[16]. However, these conditions were less likely to effect high income countries, resulting in less than 7% of total deaths. This difference can be credited to the population of low income countries' increased exposure to risk factors such as: unsafe sex, poor hygiene, poor sanitation, unsafe water, and limited supply of drugs[18-19].

Several bacterial pathogens have emerged as potential threats to human society. These pathogens consist of older bacteria that have re-emerged due to resistance or newer bacteria that have arisen (see Table 1.2). The bacterial pathogens that re-emerged include *Plasmodium falciparum* malaria, *Mycobacterium tuberculosis*, and *Neisseria gonorrhoeae*. Malaria was

neglected due to effective therapeutic treatment with dichlorodiphenyltrichloroethane (DDT) but the bacterium has re-emerged due to DTT's toxicity concerns along with drug-resistance to chloroquine and mefloquine[20]. Like malaria, tuberculosis was also neglected after the therapeutic use of isoniazid led to cures and the ability for developed nations to dismantle public health control systems. Yet, tuberculosis has re-emerged worldwide due to immune deficiencies of people with AIDS and other autoimmune conditions, increase in poverty, and drug-resistant strains[21]. *Neisseria gonorrhoeae* was also a forgotten pathogen due to therapeutic treatment with ceftriaxone and azithromycin but has re-emerged because of unsafe sex practices along with drug-resistance[22].

Emerging pathogens that have become a serious threat include *Clostridioides difficile*, *Borrelia burgdorferi*, *Helicobacter pylori*, and *Neoehrlichia mikurensis*. *Clostridioides difficile* and *Helicobacter pylori* are both gut pathogens, resulting in pseudo-membrane colitis and gastric ulcers respectively[23-24]. *Borrelia burgdorferi* and *Neoehrlichia mikurensis* come from ticks and have been shown to cause inflammatory responses as well as vascular and thromboembolic events[25-26]. Recently, because of the threat of emerging bacterial pathogens, large pharmaceutical companies like Pfizer, Merck, and Johnson & Johnson have recently created the AMR Action Fund, which will invest $1 billion in small antibiotic development companies with hopes of created 2-4 novel antibiotics by 2030[27].

Table 1.2 List of Re-emerging and Emerging Pathogens that Threaten Human Health

Pathogen	Re-emerging/Emerging	Transmission
Plasmodium falciparum malaria	Re-emerging	Zoonosis (mosquitoes)
Mycobacterium tuberculosis	Re-emerging	Person to person
Neisseria gonorrhoeae	Re-emerging	Sexually transmitted
Clostridioides difficile	Emerging	Part of normal microflora
Helicobacter pylori	Emerging	Person to person
Borrelia burgdorferi	Emerging	Zoonosis (ticks)
Neoehrlichia mikurensis	Emerging	Zoonosis (ticks)

1.2 History of Antibiotics and Their Development

An antibiotic or antibacterial is an agent that kills or inhibits the growth of bacteria. Antibiotics can be extracted from nature or synthesized in a laboratory. Contrary to widespread belief, humans have been exposed to antibiotics since prehistoric times. For instance, archeologists discovered traces of tetracycline in human skeletal remains from ancient Sudanese Nubia (350-

550) as well as in femoral midshafts of Roman period skeletons from Egypt[28-30]. Similarly, red soils used treat skin infection from ancient Jordan led to the discovery of actinomycete bacteria which produce actinomycin C2 and actinomycin C3, polypeptide antibiotics that bind to a pre-melted DNA conformation present within the transcriptional complex[31-32]. Still, the widespread use of antibiotics for controlling bacterial infections did not start until the 20th century[33-34]. Prior to the widespread use of antibiotics, the global average life expectancy was around 47 years[35-36], however, the introduction of antibiotics for treatment of bacterial infections resulted in increased life expectancy to around 77 years[34, 37].

The first antibiotic used to treat bacterial infections was pyocyanase. Both Rudolf Emmerich and Oscar Low discovered that green bacteria (*Pseudomonas aeruginosa*) isolated from injured patients' dressings inhibited the growth of other bacterial organisms[38]. Both Emmerich and Low grew the bacteria in batches and used the supernatant (pyocyanase) as a treatment resulting in mixed success due to toxicity, ultimately leading to the abandonment of the drug[38]. The dawn of the antibiotic era really began with Paul Ehrlich's idea of a "magic bullet" which would selectively target disease causing bacteria but not the host[33, 39-40]. This idea was based on his observation that aniline based dyes could stain specific bacteria but not others. Thus, Ehrlich began a systematic screening program for the treatment of syphilis. In collaboration with chemist Alfred Bertheim and bacteriologist Sahachiro Hata, they synthesized hundreds of organoarsenic derivatives (based off the highly toxic drug atoxyl), leading to the identification of compound 606 which cured syphilis-infected rabbits and showed significant promise for the treatment of patients with this disease in human trials. The drug was marketed as salvarsan and was used until it was replaced by penicillin in the mid-1940s[41].

Probably the most famous story of antibiotic development is Alexander Fleming's serendipitous discovery of penicillin. Fleming found that petri dishes contaminated with mold came from the *penicillium* genus. Fleming isolated the bacterium and found that the ingredient in the mold juice, penicillin, had antibiotic activity against a variety of bacteria[42]. However, Fleming had much difficulty trying to purify penicillin until a team of scientists at Oxford led by Howard Florey and Ernest Chain published a paper describing the purification of penicillin in quantities necessary for clinical testing[43]. This protocol led to penicillin's mass production and distribution in 1945.

The discovery of these first antibiotics salvarsan and penicillin, set up the ideas for future antibiotic drug discovery research. Research aimed at replicating the work put forth by Ehrlich and Flemming resulted in several new antibiotics, some of which made their way to the patients' bedside. The period between the 1950s-1970s was indeed the golden era of discovery of novel antibiotics classes (see Figure 1.1) but the years following showed an increase in antibiotic resistance and only few new classes of antibiotics discovered (Figure 1.1).

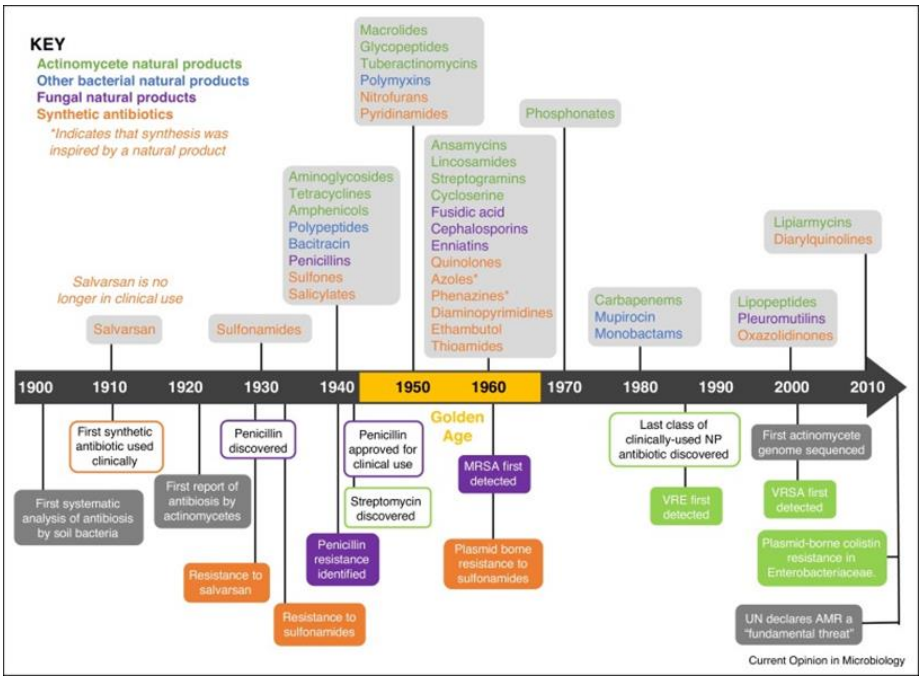

Figure 1.1 History of Antibiotic Drug Discovery. Image provided by Elsevier https://doi.org/10.1016/j.mib.2019.10.008

1.3 Rise of Antimicrobial Resistance

The discovery of antibiotics has benefited healthcare significantly since several bacterial infections that were considered deadly can now be adequately treated[44-45]. However, the rise of antibiotic resistant strains has led to the unsuccessful treatment of bacterial infections by antibiotics[46]. Consequently, antibiotic resistant infections impact millions of people annually, resulting in thousands of deaths. In 2017, the Centers for Disease Control and Prevention (CDC) reported that on average 2.8 million people are inflicted with an antibiotic-resistant infection every year, resulting in at least 35,000 deaths[47] as well as more than $20 billion in healthcare costs[48-49]. Globally, the World Health Organization (WHO) predicts that if antimicrobial resistance is not

tackled now then annual deaths from drug-resistant bacterial infections could reach 10 million by the year 2050[50].

The increase of antibiotic resistant bacteria has been partially credited to the lack of development of antibiotics with novel mechanisms of action as well as well the irresponsible prescription of current antibiotics[46]. The current antibiotic pipeline is dry as pharmaceutical companies believe that there is a low profitability of developing antibiotics due to the fact that it costs millions of dollars to conduct clinical trials, but it is guaranteed that resistant strains will emerge against any antibiotic agent[45-46]. Thus, pharmaceutical companies believe that the "safe" way to develop antibiotics is to concentrate on drug classes that have a high likelihood of being approved. Because of this, newer antibiotics that have been recently approved or in clinical trials are analogs of existing drugs (Figure 1.2). Since the compounds share both structural and mechanistic similarities, it is likely that the resistance mechanisms that inactivate the old drugs are likely to affect the newer analogs. For example, both tetracycline and ciprofloxacin are inactivated by bacterial enzymes tetracycline monooxygenase and DNA gyrase, respectively[51]. Therefore, it is likely that newer versions of these drugs, omadacycline and delafloxacin, will suffer from same mechanisms of resistance. As a result, antibiotic discovery must be focused on developing new antibacterial agents with novel chemical scaffolds and new mechanisms of action[45].

A large number of FDA approved antibiotics target either the cell membrane[52] or cell wall synthesis[53-54]. Still, these drugs target only a minor number of proteins involved in cell wall synthesis or sections of the cell wall. Several macromolecules attached to cell wall components or cell membranes have been found to be essential for bacterial growth and/or virulence, making these superb targets for new antibiotics.

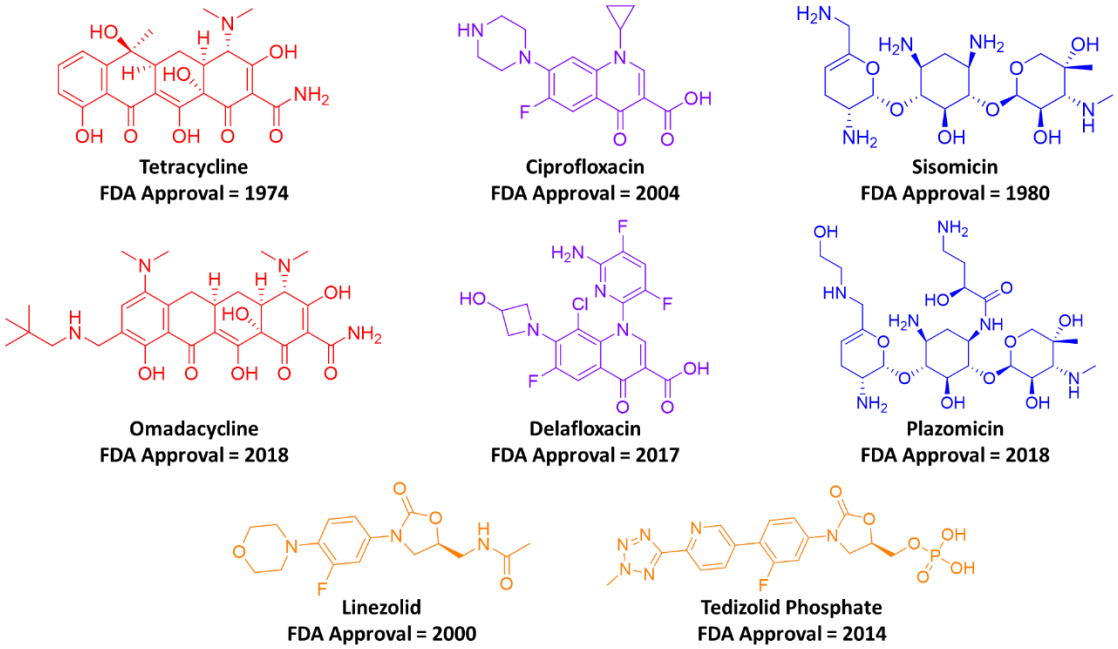

Figure 1.2 Old vs. Recently FDA-Approved Antibiotics.

1.4 Persistent Infections

Many bacterial infections can persist in the host for long periods of time, even during antibiotic treatment. Various factors in both the pathogen and host are thought to aid in the establishment and maintenance of persistent infections, infective clearance by host or antibiotics. Ineffective clearance by the host can arise due to failure of the host's immune system to detect the bacterial pathogen. For instance, *Borrelia* spp. can alter the expression of surface antigens during infection[55]. Similarly, *Mycobacterium tuberculosis* and *Listeria monocytogenes* vary the host immune response which triggers an improper anti-inflammatory response and decreases the chance of clearance[56-57]. Regarding ineffective clearance by antibiotics, this can be due to several factors including antibiotic tolerance[58]. Antibiotic tolerance is considered either inability of bacteria to be killed by a bactericidal antibiotic or an increased time for a bacteria population to be eradicated[58]. Antibiotic tolerance can happen among an entire bacteria population or in a subpopulation with phenotypic heterogeneity known as persister cells[59].

1.4.1 Persister Cells and Biofilm

Persister cells are thought to be ubiquitous among bacterial species and have been well described in *Escherichia coli*, *Pseudomonas aeruginosa*, *Mycobacterium tuberculosis*, *Salmonella* enterica subsp. enterica serovar *Typhimurium* and *Staphylococcus aureus*[60-62]. Persisters are in an inactive or dormant state which grow slowly or not at all[63]. Since persister cells are metabolically inactive, they show decreases in activity of many antibiotic drug targets (i.e., DNA, RNA, cell wall, and protein synthesis) which allows them to escape eradication[63]. Additionally, persister cells have been found to make up around 1% of biofilms[64]. Biofilm is the organization of bacteria into matrix-enclosed aggregates[65]. Biofilms grow on immobile surfaces, or on dead tissue, like medical devices or dead bone which can lead to infections like osteomyelitis or endocarditis[66]. Moreover, biofilm are 10-10,000 times more resistant to antibiotics than planktonic bacteria[67]. Much of this is because of the presence of persister cells, particularly in the middle of the biofilm. Biofilms form a shield for persisters, protecting them from both antibiotics and the host's immune system[68]. The ability for bacteria to form persister cells as well as biofilm fosters the challenge in treating chronic bacterial infections.

1.4.2 Bacterial Membrane as Antibacterial Target for Persisters and Biofilm

Bacterial membranes have become an attractive target to eradicate persisters and biofilm because they can be disrupted independently of growth[69]. There have been several reports that demonstrate the synthesis of membrane targeting small molecules that kill persister cells and eradicate biofilm (Figure 1.3). Synthetic retinoids have shown the ability to kill persisters. For instance, the synthetic retinoid PPARγ partial agonist nTZDpa was found to have potent antimicrobial activity against persistent *S. aureus* (Figure 1.3)[70]. nTZDpa was also shown to disrupt lipid bilayers, permitting it to kill *S. aureus*. Moreover, nTZDpa did not develop resistance and synergized with aminoglycosides against MRSA[70]. Likewise, the synthetic retinoid Analog 2 showed potent activity towards methicillin-resistant *S. aureus* (MRSA) persisters. Analog 2 was discovered to selectively target bacterial membranes and possess low toxicity to mammalian cells (Figure 1.3)[71]. Analog 2 synergized with gentamicin in a MRSA mouse deep-seated thigh infection model[71].

Moreover, the FDA approved anthelmintic bithionol showed potent antimicrobial activity against drug-resistant Gram-positive bacterial pathogens (Figure 1.3)[69]. Additionally, bithionol selectively targets bacterial membranes which contributes to its activity against MRSA persisters. The compound showed efficacy in combination with gentamicin in a mouse model of chronic deep-seated MRSA infection[69].

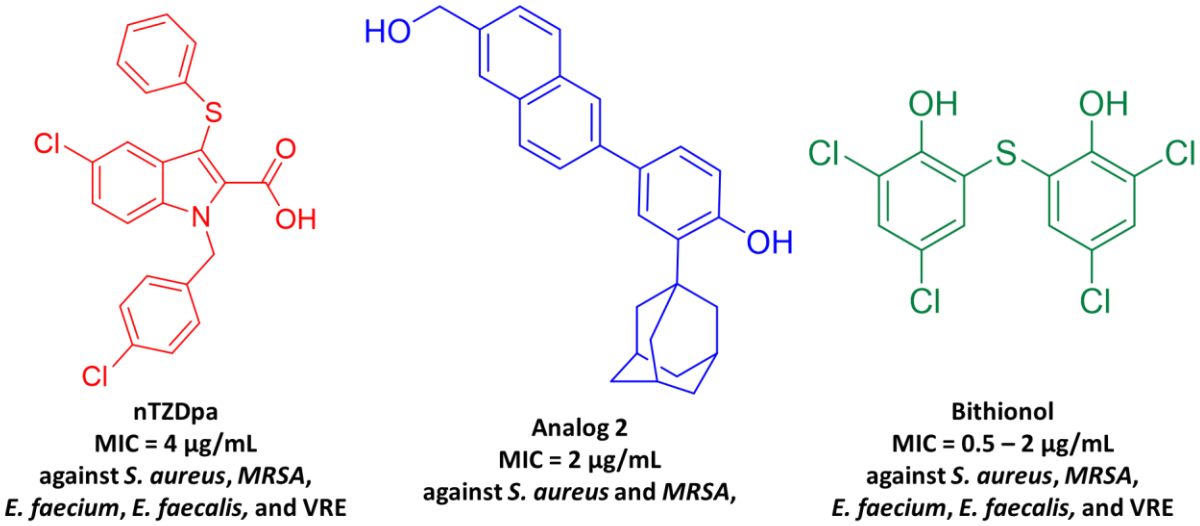

Figure 1.3 Small molecules that show highly potent activity against MRSA biofilm and persister cells.

1.5 Teichoic Acids in Bacteria

Teichoic acids (TAs) located all over the cell envelope in Gram-positive bacterial pathogens like *Staphylococcus aureus*, *Listeria monocytogenes*, enterococci, *Streptococcus pneumoniae*, and *Bacillus subtilis*[72]. TAs contain a repeating alditol phosphate backbone paired with D-alanyl and glycolyl components[73-78]. TAs are split into two types: lipoteichoic acids (LTAs) and wall teichoic acids (WTAs). LTA is a membrane-anchored anionic polymer containing 1,3-glycerolphosphate; whereas WTA is a glycopolymer that is located within the cell surface and covalently linked to peptidoglycan which expands beyond the cell wall[75, 79]. Both LTA and WTA undergo different biosyntheses (Figure 1.4). For instance, the biosynthesis of LTA begins when the α-phosphoglucomutase PgcA converts glucose-6-phosphate to glucose-1-phosphate. Then, uridyltransferase GtaB activates UTP to produce UDP-Glc. YpfP transfers two glucose molecules from UDP-Glc to DAG producing Glc_2-DAG. Glc_2-DAG is flipped to the outer membrane by the flippase LtaA followed by LtaS catalyzing the addition of glycerol phosphate to Glc_2-DAG,

generating LTA[80-81]. WTA biosynthesis begins in the cytoplasm where the diphospho-ManNAc-GlcNAc-GroP polymer is made using TarO as a key enzyme. Next, TarGH transfers the WTA polymer to the cell membrane and LCP forms the covalent bond between the peptidoglycan and WTA. DltABC then adds D-alanine to LTA or WTA[75, 79].

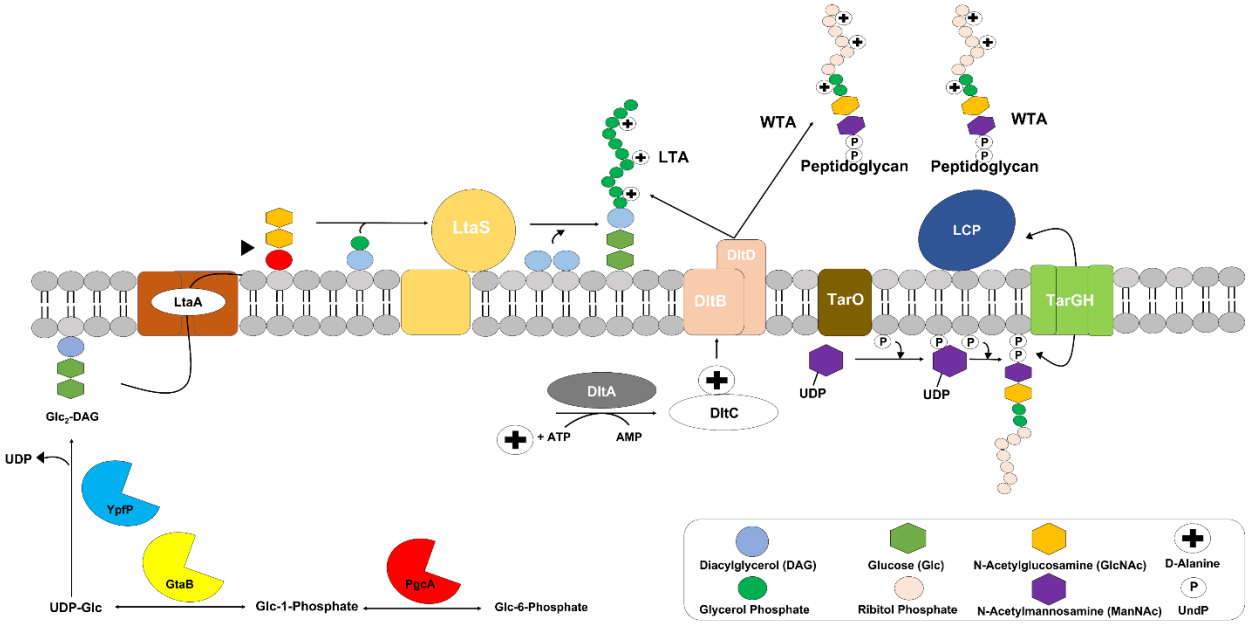

Figure 1.4 Teichoic Acid Biosynthesis in Gram-positive Bacteria.

Regarding LTA, there exitsit four distinct types (Figure 1.5A-D). Type I LTA is most frequently encountered polymer as it is found in several Gram-positive bacterial species like *Staphylococcus aureus*, *Bacillus subtilis*, *Enterococcus faecalis*, *Listeria monocytogenes*, *Streptococcus agalactiae*, and *Streptococcus pyogenes*[82]. Type I LTA is comprised of roughly 15 to 50 repeating 1,3-polyglycerolphosphate (poly(Gro-P)) units anchored to Glc_2DAG[83] (Figure 1.5A). Additionally, Type II and III LTAs have repeating units of glycosylalditol-phosphate[84]. Type II and III LTA is found in *Lactococcus garvieae* and *Clostridium innocuum* as these bacteria contain repeating units $(Gal\text{-}Gal\text{-}Gro\text{-}P)_n$ and $(Gal\text{-}Gro\text{-}P)_n$, respectively[84-85] (Figure1.5B and C). Furthermore, Type IV LTA is typically found in *Streptococcus pneumoniae* and is among the most diverse of all the LTA types[86]. For instance, Type IV LTA is substituted with choline and consists of repeating unit such as: pseudopentasaccharide 2-acetamido-4-amino-2,4,6-trideoxygalactose

(AATGal), glucose, and ribitol-phosphate along with two *N*-acetylgalactosamine moieties[87] (Figure 1.5D).

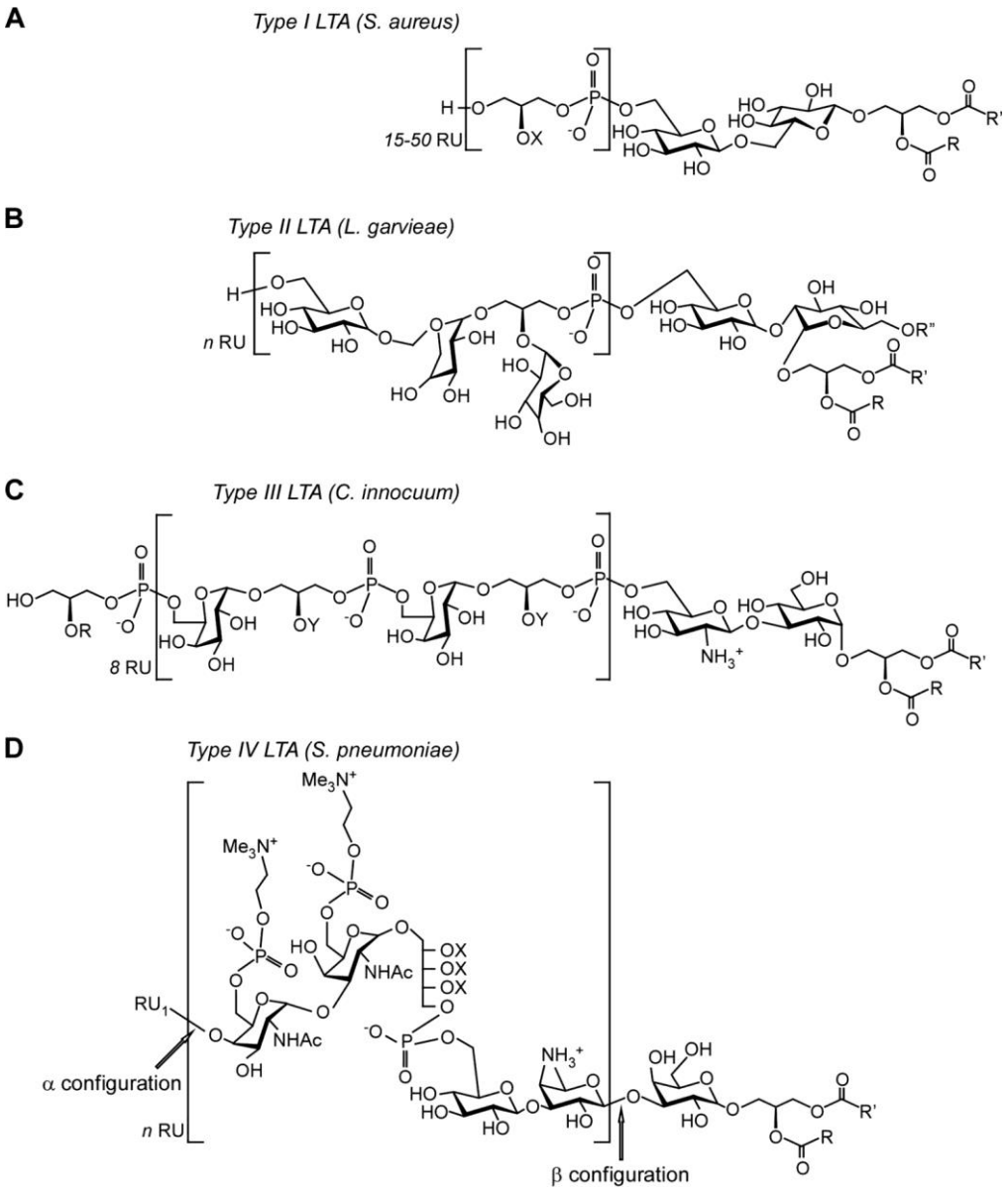

Figure 1.5 Structure of the four types of LTA found in Gram-positive bacteria. (A) Type I LTA. (B) Type II LTA. (C) Type III LTA. (D) Type IV LTA. Image provided by the American Society for Microbiology (ASM) https://doi.org/10.1128/JB.01155-13.

1.5.1 Teichoic Acids as an Antibacterial Target

TAs have been deemed a potential antimicrobial target due to their importance in the existence of Gram-positive bacterial pathogens. For example, LTA and WTA are vital for bacterial

cell wall physiology, growth, membrane homeostasis, virulence, and biofilm formation[88]. In particular, bacteria which lack WTAs have been found to grow slower and show clumping in solution when compared wildtype strains. WTA mutant strains also show many abnormalities like cell wall thickening, increased cell size, and defects in septal positioning and number[89-90]. Likewise, deletion of LtaS in *S. aureus* results in cell division and cell wall defects as well as in growth arrest[80].

Regarding virulence, TacL is an important ligase involved in LTA assembly. *S. pneumoniae* mutants lacking TacL demonstrate reduced virulence in mouse models of acute pneumonia infections[91]. Additionally, the Agr system increases the expression of virulence factors during the transition from late-exponential to stationary growth phase in Gram-positive bacteria[92-93]. Wanner et. al showed that *S. aureus* strains lacking agr had little WTA content in their cell wall compared to wild-type strains, demonstrating that the agr system regulates the WTA biosynthesis gene tarH[94]. Furthermore, D-alanyl-TA deficient *S. agalactiae* (DltA mutant) show impaired virulence in mouse and rat models because of cell wall charge disruption[95]. The DltA mutant is also more susceptible to antimicrobial peptides[95] as well as killing by mouse macrophages and human neutrophils than the wild-type strain.

TAs have also been found to be vital for biofilm formation. *S. aureus* YpfP mutants show considerably less surface charge. For instance, YpfP mutants show little to no detectable biofilm while the wild type clearly forms biofilms on polystyrene plates[96]. YpfP mutants had less biofilm formation than the PIA deficient ica mutant with a known biofilm defect[97]. Moreover, TA mutants lacking D-alanine showed decreased colonization of both MRSA and VRE, as well as reduced adherence of these bacterial pathogens to nasal epithelial cells[74, 98-99]. LTA's and WTA's essential responsibilities in biofilm formation come from altered hydrophobicity resulting in disruption of the bacterial cell wall's negative charge[100].

1.5.2 Inhibitors of Teichoic Acid Biosynthesis

Since TAs have been shown to be important to Gram-positive bacterial pathogens, inhibitors of these essential molecules have been developed. One of the first inhibitors of TAs developed. 5′-*O*-[*N*-(D-alanyl)-sulfamoyl]-adenosine (Compound 5) was discovered to prevent the D-alanyl carrier protein ligase (DltA) in *B. subtilis*. Compound 5 demonstrated potent activity

against *B. subtilis* with a MIC of 0.01 µg/mL and potentiated vancomycin against vancomycin-resistant *B. subtilis* (Figure 1.5)[101].

Furthermore, inhibitors of WTA have been developed as well (Figure 1.5)[102-103]. Targocil, a novel antibiotic, was found to inhibit TarG which is a protein that is a major part of the ABC transporter TarGH[89, 102]. Similarly, tunicamycin, a natural product, was found to inhibit TarO which is an enzyme involved in the first step of the WTA biosynthesis pathway[103]. Interestingly, targocil and tunicamycin have been found to potentiate antibiotics against drug-resistant bacteria as well as have biofilm formation inhibition[102-104].

Inhibitors of LTA biosynthesis have also been described (Figure 1.5**)**. Compound 177 was the first LTA biosynthesis inhibitor reported and was shown to have moderate antibiotic activity with a MIC of 5.34 µg/mL against *S. aureus*[105]. Furthermore, the Susan Walker group showed that the probe like molecule Congo red specifically targeted LtaS, therey contributing to its LTA biosynthesis inhibition[106]. Still, Congo Red possessed little to no antimicrobial activity with a MIC of 1024 µg/mL against *S. aureus*[106].

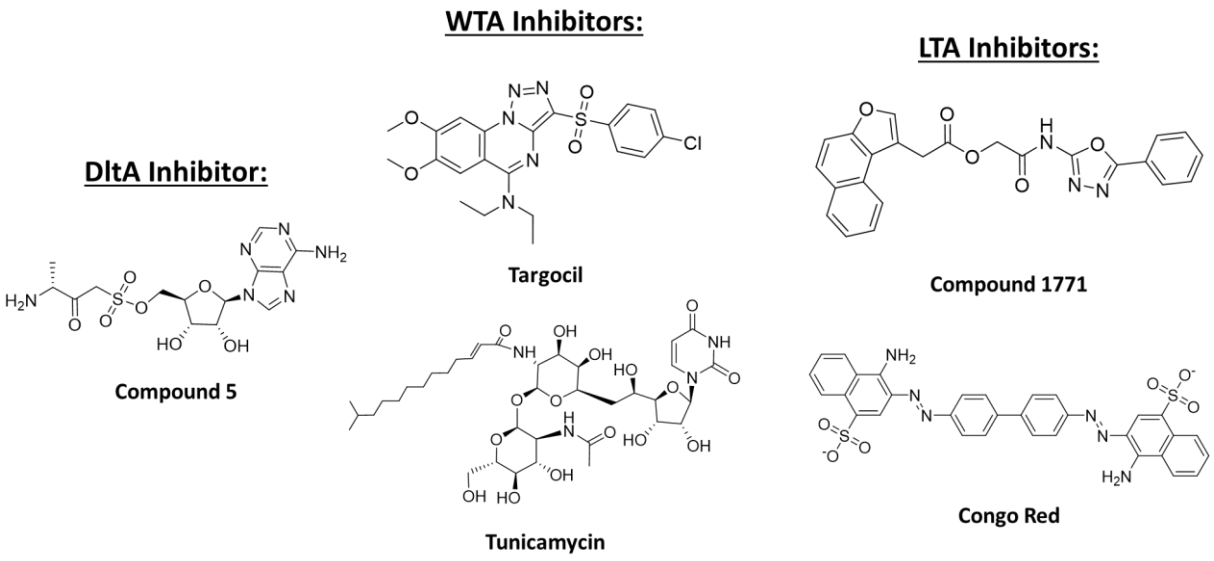

Figure 1.6 Previously Reported Teichoic Acid Biosynthesis Inhibitors. Compounds are separated by the process they inhibit (i.e., DltA, WTA, or LTA).

CHAPTER 2. ANTIBACTERIAL SMALL MOLECULES THAT POTENTLY INHIBIT *STAPHYLOCOCCUS AUREUS* LIPOTEICHOIC ACID BIOSYNTHESIS

This chapter was reprinted with permission from John Wiley and Sons. Original article can be found at Naclerio, G. A., Karanja, C. W., Opoku-Temeng, C., & Sintim, H. O. Antibacterial Small Molecules That Potently Inhibit *Staphylococcus aureus* Lipoteichoic Acid Biosynthesis. *ChemMedChem* **14**, 1000–1004 (2019).

2.1 Abstract

The rise of antibiotic resistance, especially in *Staphylococcus aureus* (*S. aureus*), and the increasing death rate due to multi-resistant bacteria have been well documented. The need for new chemical entities and/or the identification of novel targets for antibacterial drug development is high. Lipoteichoic acid (LTA), a membrane attached anionic polymer, is important for the growth and virulence of many Gram-positive bacteria and interest has been high in the discovery of LTA biosynthesis inhibitors. Thus far only a handful of LTA biosynthesis inhibitors have been described with moderate (MIC = 5.34 μg/mL) to low (MIC = 1024 μg/mL) activities against *S. aureus*. Here we describe the identification of novel compounds that potently inhibit LTA biosynthesis in *S. aureus*, displaying impressive antibacterial activities (MIC as low as 0.25 μg/mL) against methicillin-resistant *S. aureus* (MRSA). Under similar *in-vitro* assay conditions, these compounds are 4X more potent than vancomycin and 8X more potent than Linezolid against MRSA.

2.2 Introduction

The rise of antibiotic resistance and the increasing death rate due to infections with multidrug-resistant bacteria and *Staphylococcus aureus* (*S. aureus*) have been well documented. *S. aureus,* a Gram-positive bacterial pathogen, is one of the leading causes of community- and hospital- acquired bacteremia[107]. The rise of antimicrobial resistance strains partly contributes to the increasing death rate associated with *S. aureus* infection[108]. Methicillin-resistant *S. aureus* (MRSA) bacteremia is accompanied by higher mortality rates compared to methicillin-sensitive *S. aureus* (MSSA) bacteremia[109]. In 2013, the Center for Disease Control and Prevention (CDC) estimated that bacterial infections kill at least 23,000 annually in the US alone with MRSA being

responsible for nearly half of the mortalities[110-111]. Vancomycin, a glycopeptide antibiotic, is used for the treatment of severe MRSA infections. However, emergence of vancomycin intermediate and resistant *S. aureus* (VISA/VRSA) strains further limits therapy [112]. The discovery of antimicrobial agents with a novel mode of action is vital for the successful treatment of *S. aureus* infections.

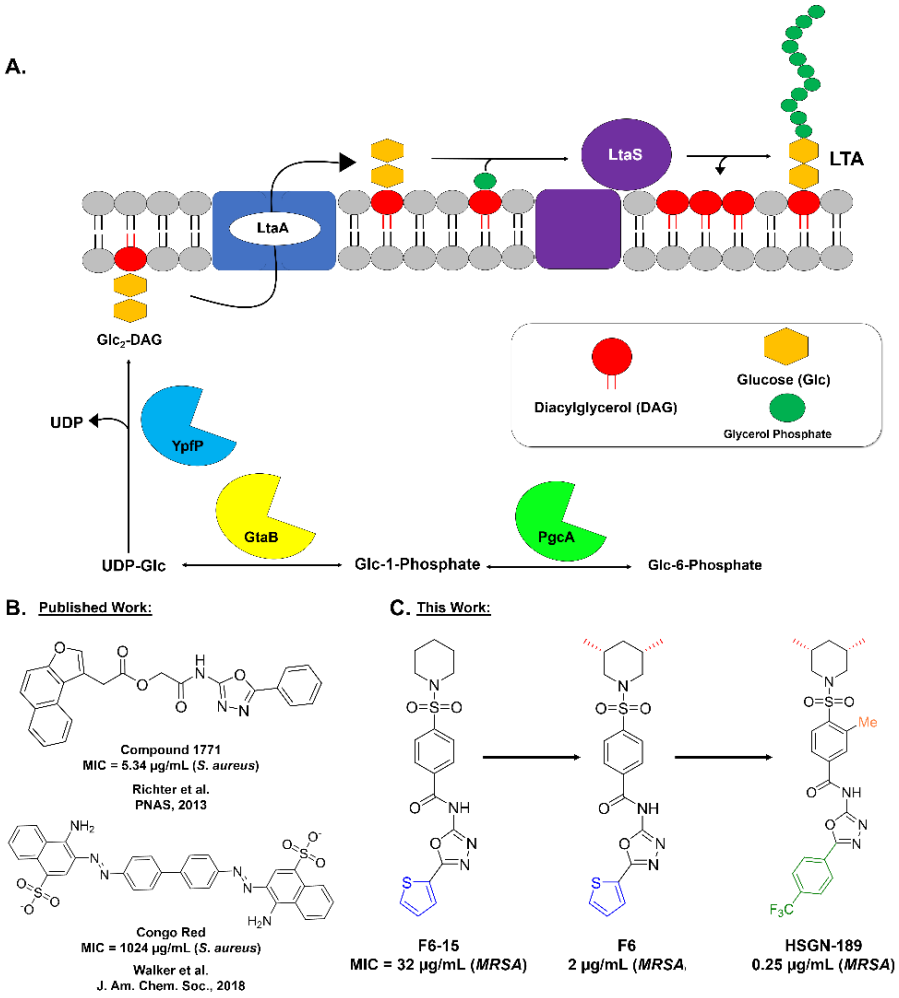

Figure 2.1 HSGN-189 has potent antibacterial activity and inhibits LTA biosynthesis in *S. aureus*. (A) The biosynthesis of LTA takes place at the cell membrane. UDP-Glc is produced by the conversion of glucose-6-phosphate to glucose-1-phosphate by the α-phosphoglucomutase PgcA, followed by activation of UTP:α-glucose-1-phosphate by uridyltransferase GtaB. The glycosyltransferase YpfP transfers two glucose molecules from UDP-Glc to diacylglycerol (DAG), generating the glycolipid Glc_2-DAG. Glc_2-DAG is then displaced to the outer membrane by LtaA. LtaS uses glycerol phosphate as a substrate to repeatedly transfer glycerol phosphate to the Glc2-DAG anchor, producing LTA. (B) Previous LTA biosynthesis inhibitors include Compound 1771 and the probe-like molecule Congo Red. These molecules exhibit moderate to low antimicrobial activity with MIC values of 5.34 µg/mL and 1024 µg/mL against *S. aureus* respectively. (C) We previously identified F6-15 as a weak antibacterial agent against MRSA.[11] With further optimization, HSGN-189 was indentified to be a potent anti-MRSA agent (MIC = 0.25 µg/mL) and LTA biosynthesis inhibitor.glycolipid[88, 113].

The Gram-positive bacteria cell envelope consists of a membrane and a peptidoglycan cell wall with anchored anionic polymers (teichoic acids). Teichoic acids include wall teichoic acids (WTA), which are covalently linked to the peptidoglycan, and lipoteichoic acids (LTA), which are anchored together via a glycolipid[88, 113]. Both polymers are vital components of the cell envelope

involved in bacterial growth, replication, colonization and virulence[74, 114]. LTA in *S. aureus*, is composed of a 1,3-glycerol phosphate polymer linked by a diglucosyl diacylglycerol glycolipid anchored to the membrane[88]. The LTA varies greatly amongst Gram-positive bacteria. Yet, several Gram-positive pathogens, including *Bacillus subtilis, Enterococcus faecalis, and Listeria monocytogenes*, produce the same polyglycerol phosphate polymer as *S. aureus* [88, 114]. LTA is synthesized by lipoteichoic acid synthase (LtaS) from phosphatidylglycerol. Depletion of *ltaS* (gene for LtaS) and LTA in *S. aureus* results in growth arrest, cell wall envelope and cell division defects[80]. The essential nature of LTA in *S. aureus*, along with the fact that it is not present in eukaryotic cells, makes LTA an ideal antimicrobial target.

Thus far, there have been efforts to develop potent LTA biosynthesis inhibitors with antibacterial activity by few groups. However, the compounds developed to date are significantly less potent than vancomycin. For example, the first LTA biosynthesis inhibitor, Compound 1771 possessed a minimum inhibitory concentration (MIC) of 5.34 μg/mL against *S. aureus*.[115] Compound 1771 contains an ester moiety, a potential liability due to esterase hydrolysis in blood. In a more recent publication Walker et al. demonstrated that Congo red inhibits LtaS activity[116], however exhibited very low antimicrobial activity (MIC of 1024 μg/mL) against *S. aureus*[116].

Due to the essential nature of LTA, we have been interested in developing antibacterial agents that inhibit LTA biosynthesis. Our group has demonstrated that *N*-(1,3,4-oxadiazol-2-yl)benzamides are potent antibacterial agents with MIC values of 2 μg/mL against MRSA[117]. Here, we report a new generation of *N*-(1,3,4-oxadiazol-2-yl)benzamides, exhibiting MIC values as low as 0.25 μg/mL against MRSA and are more potent than frontline antibiotics used for MRSA infections (4X more potent than vancomycin and 8X more potent than linezolid).

2.3 Results and Discussion

2.3.1 Oxadiazole as a Privileged Scaffold in Medicinal Chemistry

Our group has embarked on the generation of proprietary compounds for evaluation against drug resistant bacteria. As a strategy to increase the chances of advancing a hit molecule to the clinic, we have prepared a library that is enriched with moieties typically found in other clinical compounds. Several compounds containing the 1,3,4-oxadiazolyl unit have demonstrated interesting biological activities, as exemplified by the drugs such as furamizole[118-119]

(antibacterial), nesapidil[118-119] (antiarrhythmic), raltegravir (HIV antiviral)[120] and zibotentan (underwent clinical trials for prostate cancer)[121] (see Figure 2.2).

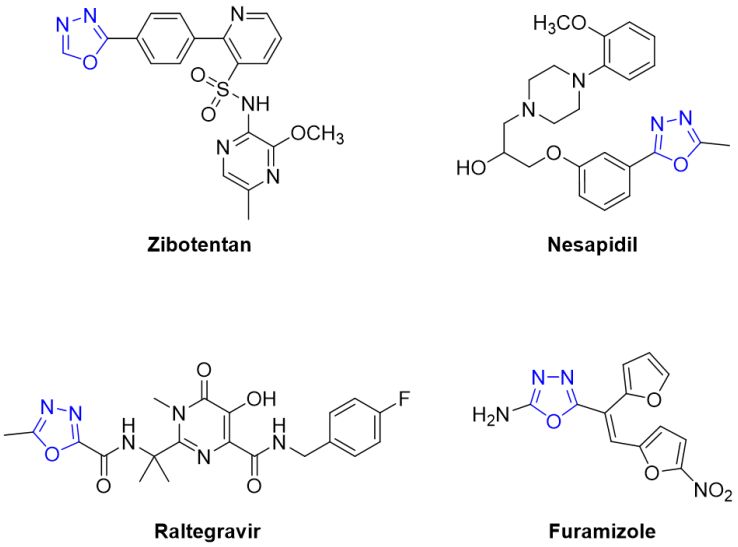

Figure 2.2 Clinical compounds containing 1,3,4-oxadiazole unit.

2.3.2 Synthesis and Antibacterial Evaluation of New N-(1,3,4-oxadiazol-2-yl)benzamides

We previously discovered that compound F6-15 displayed weak antibacterial properties with a MIC of 32 μg/mL against *S. aureus*. Remarkable enhancements in the activity of the lead compound were obtained upon strategic methyl group substitution (the methylation effect)[122]. The installment of the 3,5-dimethyl groups on the piperidine ring gave rise to F6, which displayed MIC of 2 μg/mL[117] Notably F6 was well tolerated in mice and capable of reducing bacterial burden in a wound infection model[11]. While a MIC of 2 μg/mL is respectable, we desired to further optimize this compound by the synthesis of new analogues, which were initially screened for their ability to inhibit the growth of *S. aureus* at 16 μg/mL (ESI, Figure S1).

For compounds that showed inhibitory activity, we determined the MIC (Table 2.1). For synthesis of compounds see ESI Figure S1. Four types of compounds were made (series 1-4, Figure 2.3). The compounds contained four rings (labeled rings A, B, C and D, see Figure 2.3). Series 1 was made up of compounds with various substitution (halogens, CF_3, CN, OMe, tetrazole, NH_2, OH, Me, hydroxyamidine) to phenyl ring D. Halogen substitutions (especially the Cl, F or CF_3 groups) resulted in the most active compounds. Hydrophilic substituents, such as the NH_2, CN,

OH and tetrazole were not active. For the halogen substituents, the position on the ring was also important. For example, the MIC for para-CF_3 (12, HSGN-94) was 0.25 µg/mL, whereas that for the meta-analog (5) was 1 µg/mL against MRSA (Table 2.1). In series 2, we investigated other heteroaromatics, such as pyridinyl (25 and 26), chlorothiophenyl (27), dimethylthiazolyl (28), pyrazolyl (29) as ring D. For these compounds, the chlorothiophenyl analog 27 was the most potent (MIC = 2 µg/mL against MRSA). Series 3 explored structure-activity-relationships (SAR) of the sulfonamide moiety (ring A). Here both the methyl substituted piperidine and *N*-substituted aniline substituents were highly active (MIC for compounds 30, 31, 32, and 35 are 0.5, 0.25, 1 and 0.5 µg/mL respectively). Considering that the 3,5-dimethyl piperidine sulfonamide (HSGN-94) was one of the best compounds, we proceeded to investigate how substitution of ring B and/or position of the 3,5-dimethyl piperidine sulfonamide (series 4) affected antibacterial activity. Replacement of the phenyl group with thiophenyl (37) or pyridinyl (39) led to a small reduction in antibacterial activity (MIC = 1 µg/mL and 2 µg/mL for compounds 37 and 39 respectively). Addition of a methyl group to the 3 position of ring B (36, HSGN-189) did not effect activity (MIC = 0.25 µg/mL). Changing the position of the 3,5-dimethylpiperidine sulfonamide moiety from *para* to *meta*, (compounds 38 and 40) on ring B resulted in reduced activity against MRSA (compare MIC of 0.25 µg/mL for HSGN-94 and HSGN-189 with 8 µg/mL and 1 µg/mL for compounds 38 and 40 respectively).

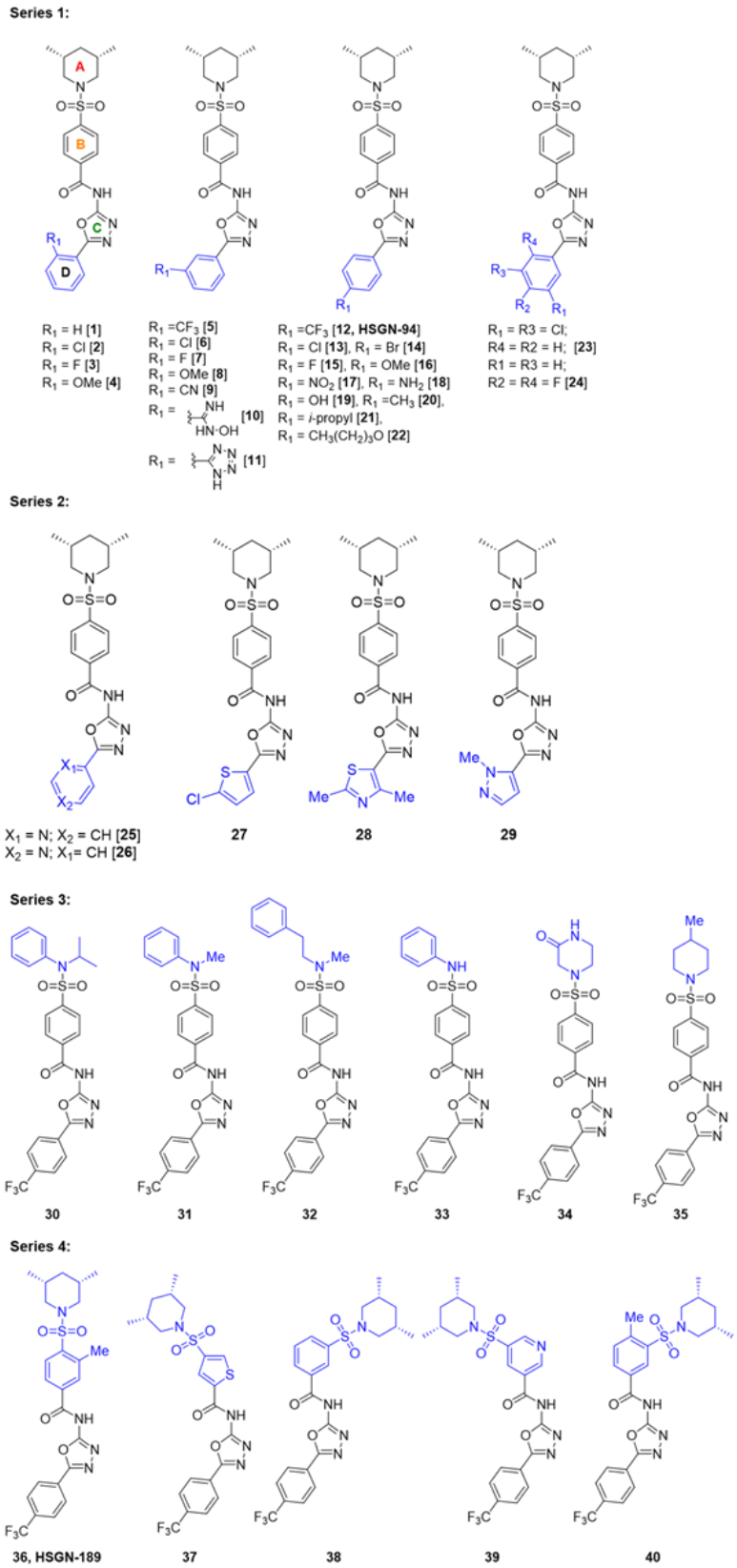

Figure 2.3 Series of 1,3,4-oxiadizolyl-based compounds synthesized for study.

Table 2.1 MIC (μg/mL) of HSGN-94, HSGN-189, analogs, vancomycin, and linezolid against a panel of Gram-positive bacterial pathogens. † Samples were done in triplicate and performed at least 3-4 times with reproducibility each time.

Compounds/ Control Antibiotic	*S. aureus* ATCC 25923	MRSA ATCC 33592	*E. faecalis* ATCC 29212	VRE. *faecalis* ATCC 51575	*L. monocytogenes* ATCC 19115
F6-15	32	32	16	64	32
F6	2	2	4	4	4
1	4	4	16	8	8
2	32	32	64	64	32
3	2	4	16	8	4
5	2	2	4	8	2
6	1	0.5	1	2	1
7	2	0.5	2	2	2
8	4	2	8	4	4
9	16	8	32	16	8
11	16	16	64	32	32
12, HSGN-94	0.25	0.25	2	1	0.5
13	2	1	4	2	2
14	2	4	4	4	4
15	4	4	4	4	4
16	4	4	4	4	4
17	32	16	64	32	32
20	16	8	32	16	16
21	2	1	4	2	2
22	16	16	16	8	16
23	0.5	0.25	2	1	1
24	8	8	32	32	32
26	16	32	64	64	32
27	2	2	64	32	32
28	16	8	32	64	16
29	8	4	16	128	8
30	1	0.5	4	4	2
31	0.25	0.25	2	2	1
32	1	2	8	8	4
33	4	4	8	8	8
35	1	0.5	4	4	2
36, HSGN-189	0.25	0.25	8	8	4
37	0.5	1	16	16	8
38	8	8	>16	>16	>16
39	2	2	4	4	2
40	2	1	8	4	4
Vancomycin	1	1	2	>128	1
Linezolid	2	2	2	2	2

2.3.3 HSGN-189 Potently Inhibits LTA Biosynthesis

HSGN-189 appears more selective than HSGN-94 (see Table 2.1 for comaprision of MICs against other Gram-postive bacteria), thus we proceeded to identify its mode of action. Traditional ways to do this are to generate bacteria that are resistant to the compound and use global sequencing to identify genes that are mutated in the presence of the compound or to use affinity probes to identify binding proteins[123-125]. Despite many attempts, we have been unable to generate resistant strains towards HSGN-189 (which looks promising for the eventual translation of this compound or analogs thereof). Given that HSGN-189 and the known LTA biosynthesis inhibitor, Compound 1771, both contain aryl substituted 1,3,4-oxadiazolyl unit, we investigated the effects of selected compounds on LTA levels in S. aureus Excitingly, when we investigated the effects of F6-15, F6 and HSGN-189 on LTA biosynthesis in *S. aureus*, following the protocol utilized by Walker and Richter, we observed potent inhibition of LTA by these compounds (Figure 2.4 and ESI, Figure S2). Interestingly, the degree of LTA biosynthesis inhibition correlated with the MIC values, strongly hinting that LTA biosynthesis inhibition is responsible (at least in part) for the antibacterial activities of the compounds. Vancomycin and Congo Red were used as negative and positive controls respectively (see Figure S2). Whereas Congo Red reduced LTA biosynthesis in *S. aureus*, vancomycin increased LTA content (see Figure S2).

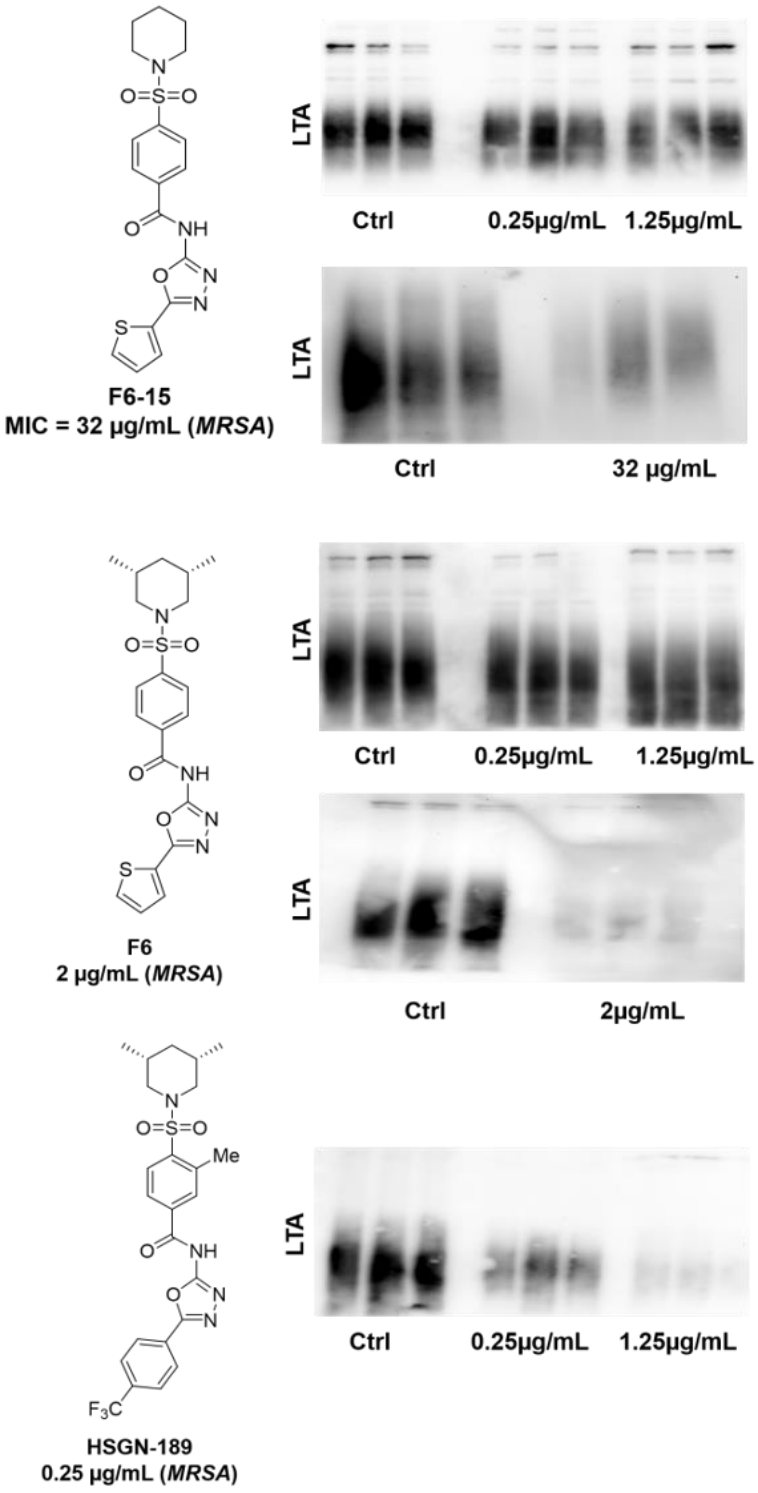

Figure 2.4 LTA biosynthesis inhibition by 1,3,4-oxadiazolyl –based compounds. The MIC of HSGN-189 (0.25 µg/mL) is lower than F6-15 (32 µg/mL) and F6 (2 µg/mL). At lower concentrations (0.25 µg/mL), only HSGN-189 significantly inhibited the biosynthesis of LTA. Yet, at the MIC concentration of F6-15 (32 µg/mL) and F6 (2 µg/mL), LTA biosynthesis was inhibited.

2.4 Conclusion

In conclusion, we have identified potent inhibitors of LTA biosynthesis. These compounds potently inhibit MRSA with MIC values that are 4X lower than vancomycin and 8X lower than linezolid, two antibiotics commonly used to treat MRSA infections. However, both traditional antibiotics have many disadvantages. For vancomycin, it is not orally bioavailable and displays nephrotoxicity. Likewise, linezolid can cause serious side effects like bone-marrow suppression, lactic acidosis, peripheral and optic neuropathy, etc[126]. Thus, alternatives to vancomycin and linezolid are needed. Future work will focus on the activities of the potent compounds (MIC less than 0.5 μg/mL) in mice infection models. We will also investigate which of the many enzymes involved in LTA biosynthesis is/are the targets of the described compounds. This work adds to the increasing number of reports that have attempted to address the anti-bacterial resistance issue with novel small molecules[16, 70, 127-130].

2.5 Supplementary Information

For experimental procedures, compound syntheses, characterization data, ^{1}H and ^{13}C NMR spectra, please see the electronic supplementary information located on the ChemMedChem website.

2.6 Author Contributions

G. Naclerio synthesized all compounds in study, performed MIC assays, and did western blot experiments. C. Karanja performed western blot experiments. C. Opoku-Temeng performed MIC assays. G. Naclerio and H. Sintim wrote the manuscript.

CHAPTER 3. LIPOTEICHOIC ACID BIOSYNTHESIS INHIBITORS AS POTENT INHIBITORS OF *S. AUREUS* AND *E. FAECALIS* GROWTH AND BIOFILM FORMATION

This chapter was reprinted with permission from MDPI. Original article can be found at Naclerio, G. A., Onyedibe, K. I., & Sintim, H. O. Lipoteichoic Acid Biosynthesis Inhibitors as Potent Inhibitors of *S. aureus* and *E. faecalis* Growth and Biofilm Formation. *Molecules* **2020**, *25*(10), 2277.

3.1 Abstract

Methicillin-resistant *Staphylococcus aureus* (MRSA) and vancomycin-resistant *Enterococcus faecalis* (VRE) have been deemed as serious threats by the CDC. Many chronic MRSA and VRE infections are due to biofilm formation. Biofilm are considered to be between 10–10,000 times more resistant to antibiotics, and therefore new chemical entities that inhibit and/or eradicate biofilm formation are needed. Teichoic acids, such as lipoteichoic acids (LTAs) and wall teichoic acids (WTAs), play pivotal roles in Gram-positive bacteria's ability to grow, replicate, and form biofilms, making the inhibition of these teichoic acids a promising approach to fight infections by biofilm forming bacteria. Here, we describe the potent biofilm inhibition activity against MRSA and VRE biofilms by two LTA biosynthesis inhibitors HSGN-94 and HSGN-189 with MBICs as low as 0.0625 μg/mL against MRSA biofilms and 0.5 μg/mL against VRE biofilms. Additionally, both HSGN-94 and HSGN-189 were shown to potently synergize with the WTA inhibitor Tunicamycin in inhibiting MRSA and VRE biofilm formation.

3.2 Introduction

Antimicrobial-resistant bacteria have become a serious global health issue. The World Health Organization (WHO) acknowledges that every year 700,000 people die from drug-resistant infections worldwide. It has been estimated that deaths from drug-resistant infections will reach 10 million people per year by 2050, surpassing deaths due to cancer [131]. The Centers for Disease Control Prevention (CDC, US) has reported that on average 2 million people are inflicted with an antibiotic-resistant infection every year, and at least 23,000 people die from these infections [132]. Of these drug-resistant bacteria, methicillin-resistant *Staphylococcus aureus* (MRSA) and vancomycin-resistant *Enterococcus faecalis* (VRE) are recognized as serious threats by the CDC.

MRSA accounts for 80,461 infections and 11,285 deaths annually; while VRE accounts for 20,000 infections and 1,300 deaths per year [132].

The majority of chronic MRSA and VRE infections are due to biofilm formation. Biofilm is a group of bacterial pathogens that anchors to a biological (lung, intestine, tooth) or non-biological (medical devices) surface and biofilm bacteria are 10-1,000 times more resistant to antibiotics than planktonic bacteria [67]. Currently, treatment for MRSA and VRE biofilm infections involves long-term antibiotic therapy, which leads to increased persistence and destruction of inflamed tissue [133]. Thus, new agents that eradicate or inhibit MRSA and VRE biofilm formation via novel mechanisms are needed.

Teichoic acids are abundant throughout the cell envelopes of Gram-positive bacterial pathogens such as *S. aureus*, enterococci, *Listeria monocytogenes*, *Streptococcus pneumoniae*, and *Bacillus subtilis*. [72]. Teichoic acids are divided into two classes: lipoteichoic acids (LTAs) and wall teichoic acids (WTAs) (Figure 3.1A). Both LTA and WTA play major roles in Gram-positive bacterial cell processes that are vital to their survival [72]. Specifically, LTA is an anionic 1,3-glycerolphosphate containing polymer anchored to the cell wall; while WTA is a cell surface glycopolymer that is covalently linked to peptidoglycan and expands beyond the cell wall [75, 79]. Both LTA and WTA are very important for bacterial growth, cell wall physiology, membrane homeostasis, and virulence [88]. Regarding biofilm formation, both LTA and WTA are vital. For instance, teichoic acids lacking D-alanine showed decreased colonization of both MRSA and VRE, as well as reduced adherence of these bacterial pathogens to nasal epithelial cells [74, 98-99]. Both LTA's and WTA's important roles in biofilm formation have been linked to disruption of the negative charge of the bacterial cell wall resulting in altered hydrophobicity [100]. Therefore, both LTA and WTA can be potential targets in the development for new antibacterial agents against biofilm forming Gram-positive infections.

WTA inhibitors have been developed [102-103]. Tunicamycin, a natural product, is an inhibitor of TarO, a biocatalyst in the first step of WTA biosynthesis (Figure 3.1). Likewise, the novel antibiotic targocil, inhibits TarG, a main component of the ABC transporter TarGH (Figure 3.1) [89, 102]. Both tunicamycin and targocil possess antibiofilm activities as well as potentiate the effects of other antibiotics [102-104].

Very few LTA biosynthesis inhibitors exist [105-106]. Recently, we reported novel *N*-(1,3,4-oxadiazol-2-yl)benzamide containing LTA biosynthesis inhibitors with MIC values as low as 0.25

μg/mL and 1 μg/mL against MRSA and VRE respectively (Figure 3.1) [117, 134]. In this follow-up study, we sought to determine the activity of our two most potent LTA biosynthesis inhibitors, HSGN-94 and HSGN-189, against MRSA and VRE biofilm formation. Here, we report HSGN-94 and HSGN-189 as having potent biofilm inhibition activity against MRSA and VRE with minimum biofilm inhibition concentrations (MBICs) as low as 0.125 μg/mL and 0.5 μg/mL respectively. Additionally, HSGN-94 and HSGN-189 showed potent synergism or additivity when tested in combination with tunicamycin and targocil against MRSA and VRE strains and biofilms.

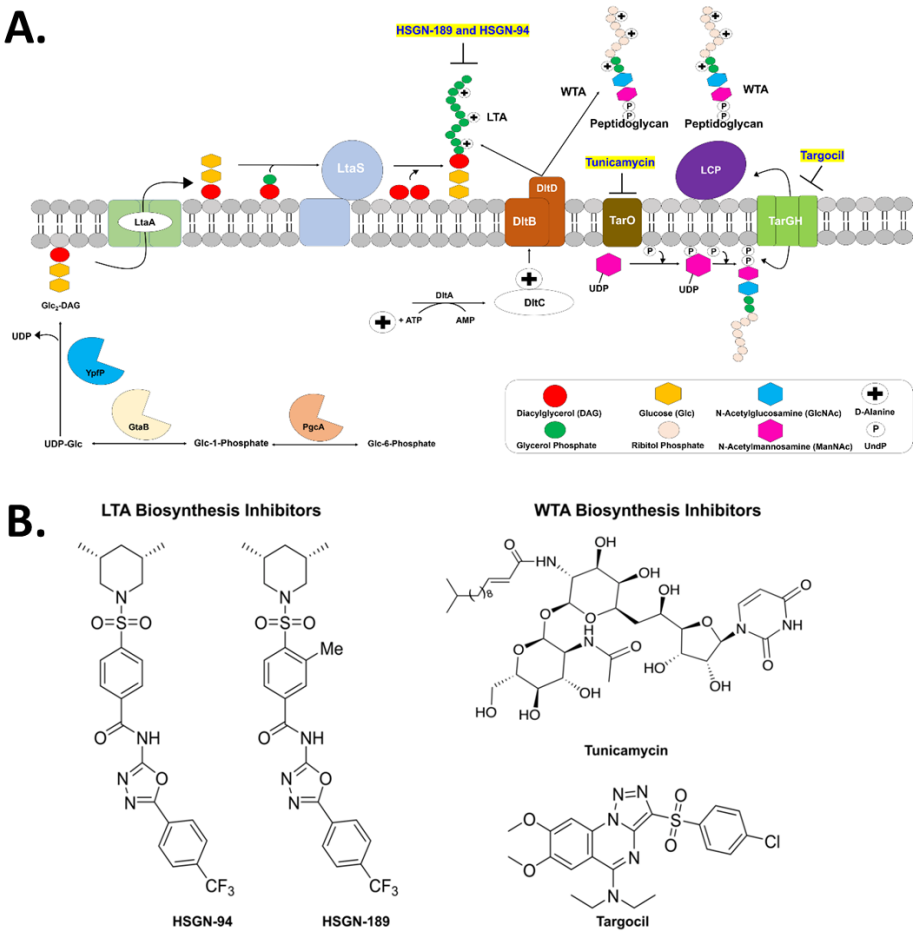

Figure 3.1 Teichoic Acid Biosynthesis and Reported Inhibitors. A) LTA biosynthesis occurs at the Gram-positive bacterial cell membrane. The α-phosphoglucomutase PgcA converts glucose-6-phosphate to glucose-1-phosphate, then uridyltransferase GtaB activates UTP to produce UDP-glc. Glc_2-DAG is then produced from YpfP transfering two glucose molecules from UDP-Glc to DAG. Glc_2-DAG is moved to the outer membrane by LtaA followed by LtaS adding glycerol phosphate to Glc_2-DAG generate LTA. WTA biosynthesis begins in the cytoplasm where TarO plays a key role in generate the diphospho-ManNAc-GlcNAc-GroP polymer. TarGH then exports the WTA polymer to the cell membrane where LCP catalyzes the covalent bond between the WTA and peptidoglycan. The D-alanine moieties are added by DltABC. B) HSGN-94 and HSGN-189 inhibit LTA biosynthesis. Tunicamycin and Targocil inhibit WTA biosynthesis via inhibition of TarO and TarGH respectively.

3.3 Results and Discussion

3.3.1 Biofilm Inhibition Activity of HSGN-94 and HSGN-189 Against MRSA and VRE Strains:

The synthesis and characterization of both HSGN-94 and HSGN-189 have been previously described[134]. Additionally, HSGN-94 and HSGN-189 were found to have potent antibacterial activity against both MRSA and VRE with MICs as low as 0.25 µg/mL and 1 µg/mL respectively.

Furthermore, both compounds proved to be the most potent LTA biosynthesis inhibitors published[134]. As mentioned above, since LTA plays a major role in biofilm formation of both MRSA and VRE, we aimed to test whether HSGN-94 or HSGN-189 could have antibiofilm activity. Both HSGN-94 and HSGN-189 showed potent biofilm formation inhibition against MRSA and VRE with minimum biofilm formation inhibition concentrations (MBICs) at or below their MIC values. For instance, the MBIC of HSGN-94 against MRSA ATCC 33592, MRSA USA300, and VRE ATCC 51575 was found to be 0.125 µg/mL, 0.5 µg/mL, and 0.5 µg/mL respectively (compare with MICs of HSGN-94 to these strains being 0.25 µg/mL, 2 µg/mL, and 1 µg/mL respectively; see Figure 3.2). Similarly, HSGN-189 also had potent MBIC values against MRSA ATCC 33592, MRSA USA300, and VRE ATCC 51575 and was found to be 0.0625 µg/mL, 0.5 µg/mL, and 1 µg/mL respectively, which are all below the reported MIC values (see Figure 3.2). Both HSGN-94 and HSGN-189 did not disperse established biofilms. Since the MBIC values of the compounds are lower than MIC (for example HSGN-189 inhibits biofilm formation of MRSA ATCC 33592 at a concentration that is 4X lower than MIC (MIC = 0.25 µg/mL and MBIC is 0.0625 µg/mL), we conclude that the mode of biofilm inhibition is not entirely due to bacterial death. We do not discount that some bacterial death also accounts for biofilm formation inhibition since at the MBIC concentrations, some bacterial death (not 100%) was also observed, see Figures 3.2A and 3.2C. Thus, it appears that although LTA is critical for initial biofilm formation, other factors are also important for biofilm maturation and persistence[135-136]. Established biofilms contain many adhesive and connective compounds, including DNA, proteins and polysaccharide[137-140]. Thus, agents that degrade these would also be needed to eliminate established biofilms. In any case, combining LTA and WTA inhibitors with biofilm degraders, such as proteases[141], DNAses[142-143], β-hexosaminidases[144-145] could lead to enhanced biofilm clearance and worthy of future investigations.

A.

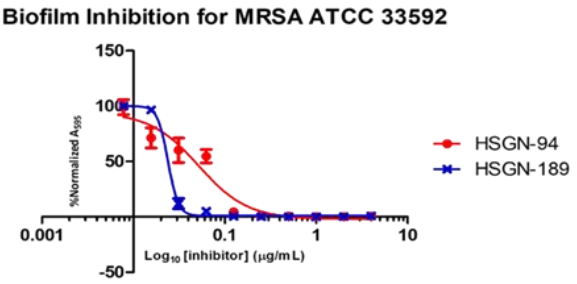

Compound	MIC (µg/mL)	MBIC (µg/mL)	MBEC (µg/mL)	IC_{50} (µg/mL)	IC_{99} (µg/mL)
HSGN-94	0.25	0.125	>256	0.044	0.94
HSGN-189	0.25	0.0625	>256	0.024	0.044

B.

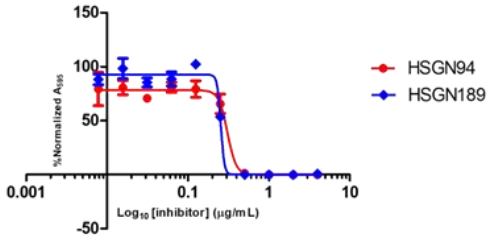

Compound	MIC (µg/mL)	MBIC (µg/mL)	MBEC (µg/mL)	IC_{50} (µg/mL)	IC_{99} (µg/mL)
HSGN-94	2	0.5	>256	0.25	1.78
HSGN-189	2	0.5	>256	0.25	0.32

C.

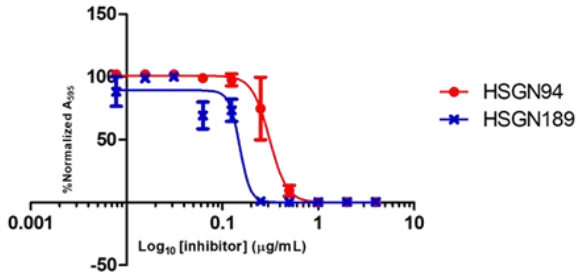

Compound	MIC (µg/mL)	MBIC (µg/mL)	MBEC (µg/mL)	IC_{50} (µg/mL)	IC_{99} (µg/mL)
HSGN-94	1	0.5	>256	0.31	0.81
HSGN-189	2	1	>256	0.61	1.25

Figure 3.2 Biofilm inhibition of HSGN-94 and -189 against Gram-positive bacteria. A) Biofilm Inhibition Curves for HSGN-94 and HSGN-189 against MRSA ATCC 33592. B) Biofilm Inhibition Curves for HSGN-94 and HSGN-189 against MRSA USA300. C) Biofilm Inhibition Curves for HSGN-94 and HSGN-189 against VRE ATCC 51575.

3.3.2 HSGN-94 and HSGN-189 Synergize with Tunicamycin and Targocil Against MRSA and VRE strains

Tunicamycin's and targocil's effect on WTA biosynthesis has been linked to their ability to synergize with cell-wall targeting antibiotics[89, 146]. For instance, Tunicamycin was shown to synergize with β-lactam containing antibiotics such as cefotaxime, ceftazidime, methicillin, oxacillin, and cephradine; tunicamycin enhanced the activities of these antibiotics by 4 to 64 times [89]. Similarly, targocil was also tested in combination with representative antibiotics of different classes but only synergized with methicillin (the cell-wall targeting antibiotic) with a ∑FICI of 0.4 [146]. Considering that HSGN-94 and HSGN-189 act on the cell-wall via inhibition of LTA biosynthesis, we wondered if our compounds would be synergistic with targocil or tunicamycin against MRSA and VRE. Using the checkerboard assay described above, we probed interactions between HSGN-94 and HSGN-189 in combination with WTA inhibitors against drug resistant MRSA ATCC 33592, MRSA USA300 and VRE ATCC 51575 strains (Table 3.1).

Table 3.1 HSGN-94 and -189 synergy with WTA inhibitors. (A) The cumulative fractional inhibitory concentration index (∑FICI) range of HSGN-94 and HSGN-189 in combination with Tunicamycin and Targocil against MRSA ATCC 33592. (B) The cumulative fractional inhibitory concentration index (∑FICI) range of HSGN-94 and HSGN-189 in combination with Tunicamycin and Targocil against MRSA USA300. (C) The cumulative fractional inhibitory concentration index (∑FICI) range of HSGN-94 and HSGN-189 in combination with Tunicamycin and Targocil against VRE ATCC 51575. Note: ∑FICI was interpreted as follows: ∑FICI of ≤0.5 is considered to demonstrate synergy (SYN). An ΣFICI of >0.5–1.25 was categorized as additive (ADD). ΣFICI of >1.25–4 was considered as indifference (IND), while ΣFICI values of >4 were categorized as antagonistic.

A	MRSA ATCC 33592											
	MIC Alone		Combination MIC		∑FICI	SYN/ADD/IND	MIC Alone		Combination MIC		∑FICI	SYN/ADD/IND
Antibiotic	Antibiotic	HSGN-94	Antibiotic	HSGN-94			Antibiotic	HSGN-189	Antibiotic	HSGN-189		
Targocil	16	0.5	2	0.25	0.6	ADD	32	0.5	16	0.5	1.5	IND
Tunicamycin	256	0.5	64	0.125	0.5	SYN	256	0.5	32	0.25	0.6	ADD
B	MRSA USA300											
	MIC Alone		Combination MIC		∑FICI	SYN/ADD/IND	MIC Alone		Combination MIC		∑FICI	SYN/ADD/IND
Antibiotic	Antibiotic	HSGN-94	Antibiotic	HSGN-94			Antibiotic	HSGN-189	Antibiotic	HSGN-189		
Targocil	>1024	2	16	2	1.0	ADD	>1024	2	16	2	1.0	ADD
Tunicamycin	32	2	2	1	0.6	ADD	64	2	4	0.5	0.3	SYN
C	VRE Faecalis ATCC 51575											
	MIC Alone		Combination MIC		∑FICI	SYN/ADD/IND	MIC Alone		Combination MIC		∑FICI	SYN/ADD/IND
Antibiotic	Antibiotic	HSGN-94	Antibiotic	HSGN-94			Antibiotic	HSGN-189	Antibiotic	HSGN-189		
Targocil	>1024	2	16	2	1.0	ADD	>1024	2	16	2	1.0	IND
Tunicamycin	16	2	4	0.5	0.5	SYN	16	2	0.5	1	0.5	SYN

HSGN-94 or HSGN-189 in combination with targocil resulted in additivity or indifference for all three strains. Combining HSGN-94 with targocil against MRSA ATCC 33592 resulted in an eight-fold decrease in MIC for targocil, from 16 µg/mL to 2 µg/mL while also decreasing the MIC for HSGN-94 from 0.5 µg/mL to 0.25 µg/mL (Table 3.1A). Although, either HSGN-94 or HSGN-189 did not show significant synergy in combination with targocil, there was remarkable reduction in targocil's MIC against MRSA USA300 or VRE, from >1024 µg/mL to 16 µg/mL (approximately a hundred-fold decrease in targocil's MIC) (See Table 3.1B and 3.1C). However, HSGN-94 in combination with tunicamycin resulted in synergy against MRSA ATCC 33592 and VRE ATCC 51575. Against MRSA ATCC 33592, tunicamycin's MIC decreased from 256 µg/mL to 64 µg/mL while HSGN-94's MIC went from 0.5 µg/mL to 0.125 µg/mL (Table 1A). Against VRE ATCC 51575, tunicamycin's MIC went from 16 µg/mL to 4 µg/mL, resulting in a 4-fold change (Table 1C). Combining HSGN-94 with tunicamycin against MRSA USA300 resulted in additivity with tunicamycin with a 16-fold change in MIC (Table 3.1B). Likewise, combinations with HSGN-189 and tunicamycin resulted in synergy when tested against MRSA USA300 and VRE ATCC 51575. Against MRSA USA300, synergy between HSGN-189 and tunicamycin resulted in a 16-fold decrease in MIC for tunicamycin (Table 3.1B). Similarly, for VRE ATCC 51575, combinations with HSGN-189 and tunicamycin resulted in tunicamycin's MIC decreasing from 16 µg/mL all the way down to 0.5 µg/mL (Table 3.1C). Against MRSA ATCC 33592, combinations between HSGN-189 and tunicamycin resulted in additivity with tunicamycin experiencing an 8-fold change in MIC (Table 3.1A).

3.3.3 HSGN-94 and HSGN-189 Shows Synergy with Tunicamycin in inhibiting MRSA and VRE biofilms

Tunicamycin has been previously reported to inhibit *S. aureus* and *L. monocytogenes* biofilm formation. Since HSGN-94 and HSGN-189 showed synergistic activity with tunicamycin, we sought to determine if these compounds could synergize with tunicamycin to inhibit MRSA and VRE biofilms. Thus, following a previously reported procedure[147], we determined the MBIC values of HSGN-94 and HSGN-189 in combination with tunicamycin against clinically relevant MRSA USA300 and VRE ATCC 51575 biofilms. Interestingly, both HSGN-94 and HSGN-189 showed synergy with tunicamycin in inhibiting MRSA USA300 and VRE biofilm formation. Alone, the MBIC of tunicamycin was found to be 64 µg/mL against MRSA USA300 biofilms but,

in combination with HSGN-94, the MBIC of tunicamycin decreased 32-fold to 2 µg/mL, resulting in a ∑FICI of 0.5 (Table 3.2A). HSGN-94 also showed potent synergy with tunicamycin against inhibiting VRE biofilms (Table 3.2B). Additionally, HSGN-189 showed synergy with tunicamycin against MRSA USA300 biofilm formation. Tunicamycin's MBIC went from 64 µg/mL to 4 µg/mL when combined with HSGN-189 (Table 3.2A). Furthermore, combinations with HSGN-189 and tunicamycin resulted in synergism in inhibiting VRE ATCC 51575 biofilm formation resulting in a ∑FICI of 0.3 (Table 3.2B).

Table 3.2 HSGN-94 and -189 MBIC synergy with WTA inhibitors. (A) MBIC of HSGN-94 and HSGN-189 in combination with Tunicamycin against MRSA USA300 biofilms. (B) MBIC of HSGN-94 and HSGN-189 in combination with Tunicamycin against VRE ATCC 51575 biofilms. ∑FICI was calculated and interpreted as follows: ∑FICI of ≤0.5 is considered to demonstrate synergy (SYN). An ΣFICI of >0.5–1.25 was categorized as additive (ADD). ΣFICI of >1.25–4 was considered as indifference (IND), while ΣFICI values of >4 were categorized as antagonistic.

A	MRSA USA300											
	MBIC Alone		Combination MBIC		∑FICI	SYN/ADD/IND	MBIC Alone		Combination MBIC		∑FICI	SYN/ADD/IND
Antibiotic	Antibiotic	HSGN-94	Antibiotic	HSGN-94			Antibiotic	HSGN-189	Antibiotic	HSGN-189		
Tunicamycin	64	2	2	1	0.5	SYN	64	2	4	0.5	0.3	SYN
B	VRE Faecalis ATCC 51575											
	MBIC Alone		Combination MBIC		∑FICI	SYN/ADD/IND	MBIC Alone		Combination MBIC		∑FICI	SYN/ADD/IND
Antibiotic	Antibiotic	HSGN-94	Antibiotic	HSGN-94			Antibiotic	HSGN-189	Antibiotic	HSGN-189		
Tunicamycin	32	2	8	0.06	0.3	SYN	32	2	8	0.06	0.3	SYN

3.4 Materials and Methods

3.4.1 Bacterial strains and chemical compounds

Bacterial strains used in this study were obtained from the American Type Culture Collection (ATCC). Tunicamycin and targocil were purchased from Cayman Chemical (Cayman Chemical Company, 1180 East Ellsworth Road, Ann Arbor, Michigan 48108, USA). HSGN-94 and HSGN-189 were previously synthesized from commercial sources in our laboratory.

3.4.2 Synergistic interactions of HSGN-94 and HSGN-189 with Tunicamycin and Targocil

The checkerboard assay[148-149] was used to determine synergistic interactions of antibiotic-compound combinations against MRSA ATCC 33592, MRSA USA300 and VRE ATCC 51575. Tunicamycin and targocil were tested in combination with compounds HSGN-94 or HSGN-189. The ΣFICI was calculated for each combination as follows:

$FICI_{compound}$ = MIC of HSGN-94 or HSGN-189 in combination/MIC of HSGN-94 or HSGN-189 alone

$FICI_{antibiotic}$ = MIC of antibiotic in combination/MIC of antibiotic alone

The cumulative FICI (∑FICI) was then calculated as:

$$\sum FICI = FICI_{compound} + FICI_{antibiotic}$$

Interactions where the ΣFICI was ≤ 0.5 were categorized as synergistic (SYN). An ΣFICI of >0.5-1.25 was categorized as additive (ADD). ΣFICI of >1.25-4 was considered as indifference (IND), while ΣFICI values of > 4 were categorized as antagonistic[150].

3.4.3 Biofilm Inhibition Assay and Minimum Biofilm Inhibition Concentration (MBIC):

MRSA and VRE biofilm inhibition were performed in tissue culture treated 96 well plates. Overnight cultures of MRSA ATCC 33592, MRSA USA300, and VRE ATCC 51575 were diluted 1 : 100 in tryptic soy broth (TSB) supplemented with 1% glucose. The diluted culture was inoculated into wells with 1 mg/mL stock solution of compound in DMSO (at 4 μg/mL to 0.0078

μg/mL). DMSO content in the 4 μg/mL and 0.0078 μg/mL wells was 0.8% and 0.002% respectively. The growth control contained diluted bacteria inoculum with 0% DMSO. The sterility control contained only media (TSB supplemented with 1% glucose) with 0% DMSO. The plates were incubated at 37 °C for 48 h after which the minimum biofilm inhibition concentration (MBIC) was read as the minimum concentration of the compounds that completely inhibited the visual growth of biofilm. Next, medium was carefully discarded, and the unattached cells washed away. The biofilms were stained with 0.5% crystal violet for 30 min. The crystal violet was discarded, and wells washed. The dye was solubilized with 100% ethanol for 1 h and the biofilm mass was quantified by measuring absorbance at 595 nm on a BioTek Cytation 5 Cell Imaging Multi-Mode Reader (BioTek, 100 Tigan St, Winooski, VT 05404, USA). The A595 value for any absorbance reading, A was normalized to the no compound (A_T) and broth (A_o) controls using the equation:

$$\%\ Normalized\ A595 = \left(\frac{A - A_0}{A_r - A_0}\right) X\ 100$$

3.4.4 Biofilm Eradication Assay and Minimum Biofilm Eradication Concentration (MBEC):

MRSA and VRE biofilm eradication were performed in tissue culture treated 96 well plates. Overnight cultures of MRSA ATCC 33592, MRSA USA300, and VRE ATCC 51575 were diluted 1 : 100 in tryptic soy broth (TSB) supplemented with 1% glucose and further incubated to OD_{600} 0.2. Next, the culture was diluted 1: 10 in TSB supplemented with 1% glucose and inoculated into wells. The plates were incubated at 37 °C for 24 h. Then, the medium was carefully discarded, and the unattached cells washed away. 10 mg/mL stock solutions of compound in DMSO, at 256 μg/mL to 0.5 μg/mL in TSB supplemented with 1% glucose, was added to the preformed biofilm. DMSO content in the 256 μg/mL and 0.5 μg/mL wells was 5% and 0.01% respectively. The growth control contained diluted bacteria inoculum with 0% DMSO. The sterility control contained only media (TSB supplemented with 1% glucose) with 0% DMSO. The plates were incubated at 37 °C for 24 h after which the minimum biofilm eradication concentration (MBEC) was read as the minimum concentration of the compounds that completely eradicated the preformed biofilm. Next, medium was carefully discarded, and the unattached cells washed away. The biofilms were stained with 0.5% crystal violet for 30 min. The crystal violet was discarded, and wells washed. The dye

was solubilized with 100% ethanol for 1 h and the biofilm mass was quantified by measuring absorbance at 595 nm on a BioTek Cytation 5 Cell Imaging Multi-Mode Reader (BioTek, 100 Tigan St, Winooski, VT 05404, USA). The A595 value for any absorbance reading, *A* was normalized to the no compound (A_T) and broth (A_o) controls using the equation:

$$\%\ Normalized\ A595 = \left(\frac{A - A_0}{A_r - A_0}\right) X\ 100$$

3.4.5 MBIC Synergy with Tunicamycin:

The checkerboard assay was utilized as described above. However, tryptic soy broth (TSB) supplemented with 1% glucose was used as the primary medium and the plates were incubated at 37 °C for 48 h. After, the medium was discarded, and the unattached cells washed away. The biofilms were stained with 0.5% crystal violet for 30 min. The crystal violet was discarded, and wells washed. The ΣFICI was calculated for each combination as follows:

FICI $_{compound}$ = MBIC of HSGN-94 or HSGN-189 in combination/MBIC of HSGN-94 or HSGN-189 alone

FICI $_{antibiotic}$ = MBIC of antibiotic in combination/MBIC of antibiotic alone

The cumulative FICI (∑FICI) was then calculated as:

∑FICI = FICI $_{compound}$ + FICI $_{antibiotic}$

Interactions where the ΣFICI was ≤ 0.5 were categorized as synergistic (SYN). An ΣFICI of >0.5-1.25 was categorized as additive (ADD). ΣFICI of >1.25-4 was considered as indifference (IND), while ΣFICI values of > 4 were categorized as antagonistic[150].

3.5 Conclusion

We previously identified HSGN-94 and HSGN-189 as novel LTA biosynthesis inhibitors. Here, we demonstrate that these compounds have potent inhibition of MRSA and VRE biofilms with MBICs well below compounds' MICs. Additionally, these compounds showed synergistic activity when combined with WTA inhibitors tunicamycin and targocil. Furthermore, HSGN-94 and HSGN-189 also showed potent synergy with tunicamycin in inhibiting MRSA and VRE

biofilms; significantly decreasing the MBIC of tunicamycin from 64 µg/mL to 2 µg/mL against MRSA. Therefore, we demonstrate that potent inhibitors of LTA biosynthesis (such as HSGN-94 and HSGN-189) can be used to inhibit biofilm infections from Gram-postive bacterial pathogens either alone or in combination with WTA inhibitors. Opoku-Temeng et al. reported that compounds containing the *N*-(1,3,4-oxadiazol-2-yl)benzamide moiety, as found in HSGN-189 and HSGN-94 were efficacious *in vivo* and reduced bacterial load in a mouse wound infection model. Future work will be focused on making HSGN-94/189 analogs thereof and evaluating these compounds *in vivo*[117].

3.6 Author Contributions

H. Sintim designed overall study, managed overall study and secured funding for study. H. Sintim and G. Naclerio wrote the manuscript. K. Onyedibe edited the manuscript. G. Naclerio performed biofilm inhibition and eradication assays. G. Naclerio and K. Onyedibe performed synergy checkerboard assays. G. Naclerio performed MBIC synergy checkerboard assay. H. Sintim, G. Naclerio, and K. Onyedibe analyzed and interpreted data.

CHAPTER 4. MECHANISTIC STUDIES AND *IN VIVO* EFFICACY OF THE OXADIAZOLE-CONTAINING ANTIBIOTIC, HSGN-94, WHICH INHIBITS LIPOTEICHOIC ACID BIOSYNTHESIS IN *STAPHYLOCOCCUS AUREUS*

4.1 Abstract

Methicillin-resistant *Staphylococcus aureus* (MRSA) is considered a serious threat that requires development of new therapeutics. MRSA affects around 330,000 patients every year, resulting in almost 11,000 deaths. Despite the availability of FDA-approved therapeutics to combat this pathogen, there is a need for new chemical entities. The oxadiazole-containing compound, HSGN-94, has been shown to reduce lipoteichoic acid (LTA) in *S. aureus*, but the mechanism that accounts for LTA biosynthesis inhibition remains uncharacterized. Here, we report the elucidation of the mechanism by which HSGN-94 inhibits LTA biosynthesis via utilization of global proteomics, activity-based protein profiling, and lipid analysis via multiple reaction monitoring (MRM). Our data suggest that HSGN-94 inhibits LTA biosynthesis via direct binding to PgcA and downregulation of PgsA. We further show that HSGN-94 reduces MRSA load in a murine model of skin infection and reduced the pro-inflammatory cytokines in MRSA infected wounds. Collectively, these results indicate that HSGN-94 merits further consideration as a new therapeutic option for treatment of staphylococcal infections.

4.2 Introduction

Staphylococcus aureus is one of the leading causes of community- and hospital-acquired bacteremia, surgical site infections, osteomyelitis, pneumonia, and skin infections[107]. The rise of antimicrobial-resistant *S. aureus* strains largely contributed to the increasing death rate associated with *S. aureus* infections[108]. For instance, methicillin-resistant *S. aureus* (MRSA) bacteremia leads to higher mortality rates as compared to methicillin-sensitive *S. aureus* (MSSA)[109]. Although there are several antibiotics used to treat MRSA such as trimethoprim–sulfamethoxazole, clindamycin, tetracycline, doxycycline, minocycline, daptomycin, rifampin, linezolid, or vancomycin[151], resistance to these agents has been documented, attributing to the fact that 14% of patients who get serious MRSA infections die[151-155]. Additionally, newer antibacterial agents developed to treat drug-resistant bacterial pathogens like MRSA are only derivatives of existing drugs. This means

that resistance mechanisms affecting the older drugs would likely alter the activity of the newer ones[156]. Consequently, there is a dire need for development of antibacterial agents with novel scaffolds and new mechanisms of action.

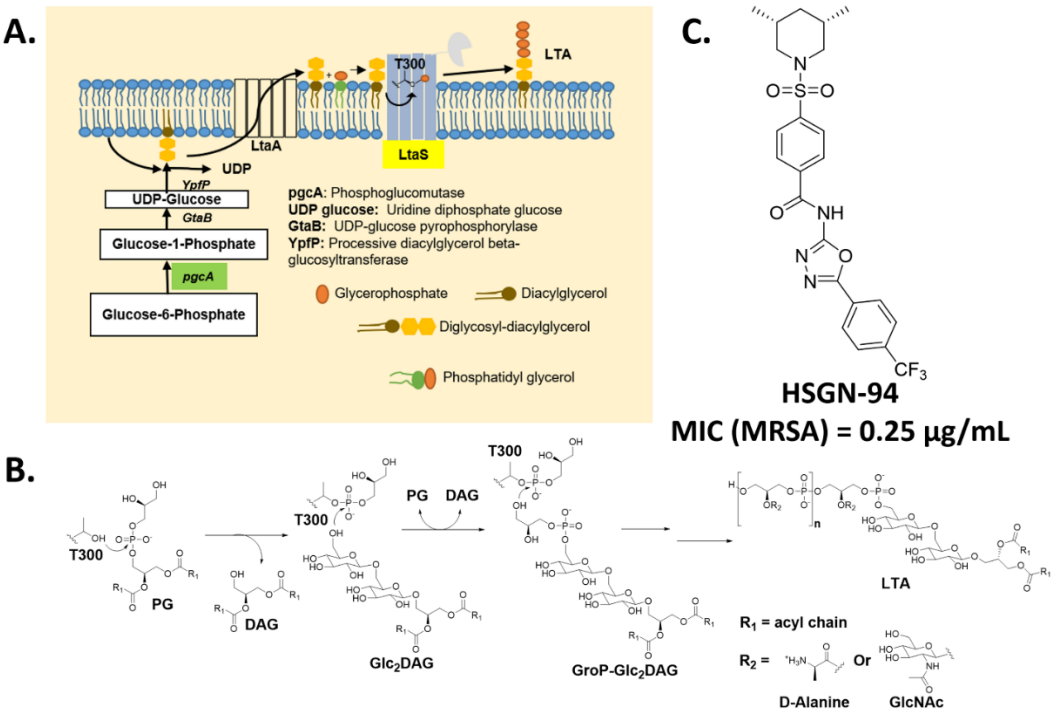

Figure 4.1 LTA biosynthesis in S. aureus involves both Glc_2DAG and PG. (A) PgcA converts glucose-6-phosphate to glucose-1-phosphate. Next, GtaB activates UTP to produce UDP-glc. Glc_2-DAG is then produced from YpfP via the transfer of two glucose molecules from UDP-Glc to DAG. Then, Glc_2-DAG is flipped the outer membrane by LtaA where LtaS catalyzes the addition of glycerol phosphate to Glc_2-DAG, generating LTA[80]. (B) LtaS synthesizes LTA via utilization of catalytic T300. PG transfers phosphoglycerol units to T300 formig a covalent intermediate. Then, phosphoglycerol units are transferred to Glc_2DAG through a reaction with the covalent intermediate, giving rise to GroP-Glc_2DAG. Repeat units are then added to the polymer, producing LTA. (C) HSGN-94 is a highly potent antimicrobial agent discovered to inhibit LTA biosynthesis.

The Gram-positive bacterial cell envelope is decorated with lipoteichoic acid (LTA), a membrane-anchored anionic 1,3-glycerolphosphate containing polymer. LTA is abundant in several Gram-positive pathogens like *S. aureus, enterococci, Listeria monocytogenes, Streptococcus pneumoniae, and Bacillus subtilis*[72]. In *S. aureus*, LTA has been shown to play an important role in the bacteria's growth[80], cell wall physiology[157], membrane homeostasis[73], virulence[158-159], and biofilm formation[88]. LTA synthesis begins in the cytoplasm where the α-phosphoglucomutase PgcA converts glucose-6-phosphate to glucose-1-phosphate. Next,

uridyltransferase GtaB activates UTP to produce UDP-glucose. Then, YpfP transfers two glucose molecules from UDP-Glucose to DAG to give Glc_2-DAG. Glc_2-DAG is flipped to membrane by the flippase LtaA where it then acts as a starting unit for LTA. Lastly, the synthase LtaS catalyzes the addition of glycerol phosphate to Glc_2-DAG, thereby generating LTA[80-81] (Figure 4.1A). The mechanism by which LtaS generates LTA involves the use of catalytic threonine (T300)[114, 160-161]. Phosphatidyl glycerol (PG) transfers phosphoglycerol units to T300, realeasing diacylglycerol (DAG) to form a covalent intermediate. Then, phosphoglycerol is transferred to Glc_2DAG via reaction with the covalent intermediate to give GroP-Glc_2DAG. Repeat units are then added to the glycerol tip, giving rise to LTA (Figure 4.1B). Since LTA is essential to *S. aureus* for many of the organism's biological processes, it has been deemed a potential antimicrobial target[162].

Our lab has focused on the development of *N*-(1,3,4-oxadiazol-2-yl)benzamides as antimicrobial agents[117, 134, 163-166]. We recently reported that the sulfonamide containing *N*-(1,3,4-oxadiazol-2-yl)benzamide HSGN-94 was a highly potent antimicrobial agent against drug-resistant Gram-positive bacteria with minimum inhibitory concentrations (MICs) ranging from 0.25 μg/mL to 2 μg/mL[134] (Figure 4.1C). Additionally, HSGN-94 was found to be a highly potent small molecule inhibitor of LTA biosynthesis in *S. aureus*[134]. We also demonstrated HSGN-94's ability to inhibit MRSA and vancomycin-resistant *Enterococci* biofilm formation[166].

Building upon our previous studies, this study investigated the antibacterial profile of HSGN-94 including structure-activity relationship studies, MICs against a panel of multidrug-resistant Gram-positive bacteria, cytotoxicity assessment, and the resistance development assay. We also elucidated the mechanism by which HSGN-94 inhibits LTA biosynthesis in *S. aureus*, utilizing several mechanistic studies, including global proteomics, activity-based protein, and transcriptional profiling, lipidomics, and macromolecular synthesis inhibition. Finally, we evaluated HSGN-94's *in vivo* efficacy in a MRSA murine wound infection model as well as its ability to inhibit the expression of pro-inflammatory cytokines and the effect of HSGN-94's treatment on the histopathological features of the mice skin.

4.3 Results and Discussion

4.3.1 Structure-activity relationship studies

We established structure-activity-relationship (SAR) studies of HSGN-94, which has indicated important structural features of the molecule that account for its potent antibacterial

activity. The synthetic schemes of these new analogs can be found in the supporting information (Appendix A; Schemes A.1-A.8). The results of the initial screening of the synthesized analogs against *S. aureus* ATCC 25923 and MRSA ATCC 33592 are included in Table A.1. We discovered that the size of the sulfonamide ring A (Figure 2, Series 1) and nature of substitution were all critical for antibacterial activity. For instance, while HSGN-94 (3,5-dimethylpiperidine) had an MIC of 0.25 µg/mL (0.5 µM), the analog 2-azabicyclo [2.2.1]heptane (5) had an MIC value of 2 µg/mL (4.1 µM). Furthermore, monomethyl substituted analogs 6, 7, and 8, also had less antibacterial activity with MICs of 1 µg/mL (2 µM), 2 µg/mL (4 µM), and 2 µg/mL (4 µM) respectively. Analogs containing smaller ring systems (1, 2, 3, and 4) showed less activity than HSGN-94 as well, with MIC values ranging from 2 µg/mL (4.2 µM) to 16 µg/mL (36.3 µM) (Table A.1).

Moreover, we determined that an unsubstituted phenyl moiety of the benzamide (ring B) was optimal for the antibacterial activity, as replacing ring B with other heterocycles (Figure 2, Series 2) or substituting ring B with electron-donating or electron-withdrawing groups (Figure 2, Series 3) showed a decrease in the antibacterial activity by 4 to >256 times (Table A.1). Likewise, both the amide bond and trifluoromethylphenyl group (ring C) were imperative for antibacterial activity. Conversion of the amide to a tertiary amide (17) or reversion of the amide (18) completely abrogated the anti-*S. aureus* activity (MICs of >64 µg/mL). Substitution of ring C with alkyl-containing groups (19 and 20) showed a reduction in antibacterial activity (MICs = 64 - >64 µg/mL) (Table A.1). Altogether, our SAR investigations demonstrated that HSGN-94 displayed the most potent activity against staphylococci. Therefore, it was selected for further characterization.

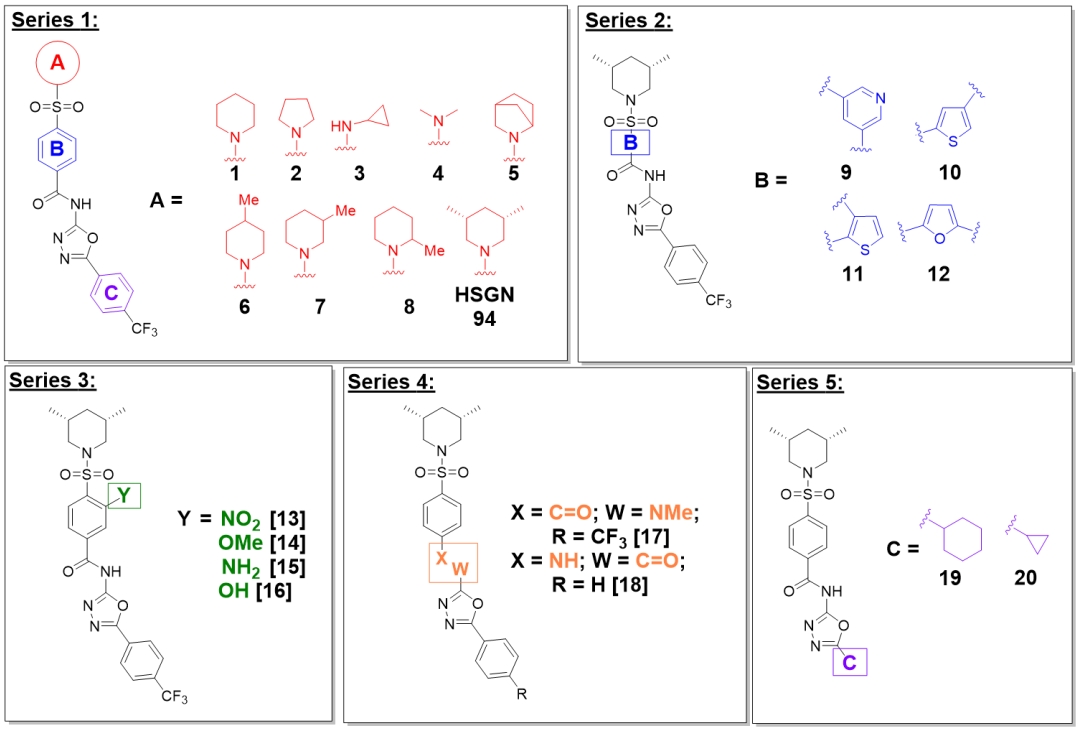

Figure 4.2 Summary of structure-activity-relationship study of sulfonamide-containing N-(1,3,4-oxadiazol-2-yl)benzamides.

4.3.2 Profiling the antibacterial activity of HSGN-94

We investigated the antibacterial activity of HSGN-94 against a panel of multidrug-resistant bacterial strains, including methicillin-sensitive, methicillin-resistant, and vancomycin-resistant *S. aureus*, *S. epidermidis*, *Streptococcus pneumonia*, *S. pyogenes*, vancomycin-resistant *Enterococcus faecium* and *E. faecalis, and Listeria monocytogenes.* As reported in our study before[134], HSGN-94 exhibited potent activity against the tested staphylococcal strains with MIC values ranging from 0.25 μg/mL (0.5 μM) to 1 μg/mL (2 μM) (Table A.2). The potent activity of HSGN-94 was extended to include drug-resistant *S. pneumoniae* and *S. pyogenes* as well (MICs ranging from 0.06 μg/mL (0.1 μM) to 0.25 μg/mL (0.5 μM), outperforming the activity of linezolid and vancomycin (Table A.3). *S. pneumoniae* causes infections ranging from ear and sinus infections to fatal pneumonia, bloodstream infections, and meningitis[167-168]. *S. pneumoniae* is a leading cause of bacterial pneumonia and meningitis in the United States. It has been reported that over 2 million pneumococcal infections occur annually in the United States, resulting in more than 6,000 deaths and $4 billion in total health-care costs. In addition, more than 30% of pneumococcal

infections are resistant to one or more clinically relevant antibiotics[169-170]. Consequently, this pathogen is classified by CDC as a serious threat bacterium for which new effective agents are sought[170]. Additionally, the compound maintained the same potency against vancomycin-resistance enterococci (MIC = 0.25 µg/mL (0.5 µM)), a serious threat pathogen that critically requires development of new drugs[171-173]. HSGN-94 was also superior to linezolid and vancomycin against *L. monocytogenes* with an MIC of 0.06 µg/mL (0.1 µM) (Table A.3). These results suggested that HSGN-94 demonstrated a broad spectrum of activity against the Gram-positive bacterial strains.

The cytotoxicity profile of HSGN-94 was assessed against human keratinocyte (HaCaT) cells (Figure A.1). The compound was tolerable to HaCaT cells at a concentration as high as 64 µg/mL, which represents 64 to 256 times its MIC values against staphylococcal strains.

Moreover, we assessed MRSA USA300's ability to form resistance to HSGN-94, using the multi-step resistance selection assay. Excitingly, the compound displayed low propensity to develop resistance to MRSA USA300, where its MIC remained unchanged over 65 passages (Figure A.2). In contrast, MRSA formed rapid resistance to ciprofloxacin where its MIC progressively increased after following passages reaching 128-fold increase in the MIC by the end of the experiment (Figure A.2).

4.3.3 Effects of HSGN-94 on global proteomics in *S. aureus*

Since we could not obtain HSGN-94 resistant-mutants via serial passaging (Figure A.2), we decided to use global proteomics in order to evaluate the pathways and proteins that are impacted by the treatment with this compound. We treated *S. aureus* with HSGN-94 for 2 hours and extracted the total protein for profiling using liquid chromatography-tandem mass spectrometry (LC-MS/MS). Samples treated with HSGN-94 were compared with samples treated only with DMSO (control). Proteomics data was filtered using label-free quantitation (LFQ) and analysis was pursued for proteins showing LFQ reponse in all 3 samples tested. From the analysis of the proteomics data, we indentified a total number of 1475 proteins. Yet, out of these proteins, 1431 proteins (97.0%) were observed to be shared by both DMSO and HSGN-94, while 30 proteins (3.0%) were only identified in DMSO, and 14 proteins (1.0%) were only identified in HSGN-94 (Figure 4.3A). Stringent filtration using statistical analysis of the 1475 total proteins (where $p < 0.05$) gave423 proteins which demonstrated that the control and treatment samples

clustered into two differentially expressed groups (Figure 4.3B). From those 423 significant proteins, 198 were downregulated, while 225 were upregulated. We then filtered this data set using p-value (p) and fold change (Log_2FC). Based on this analysis, 30 proteins were considered downregulated ($p \leq 0.05$ and $Log_2FC \leq -2$) whereas 7 proteins were upregulated ($p \leq 0.05$ and $Log_2FC \geq 2$) after HSGN-94 treatment (Figure 4.3B & 4.3C).

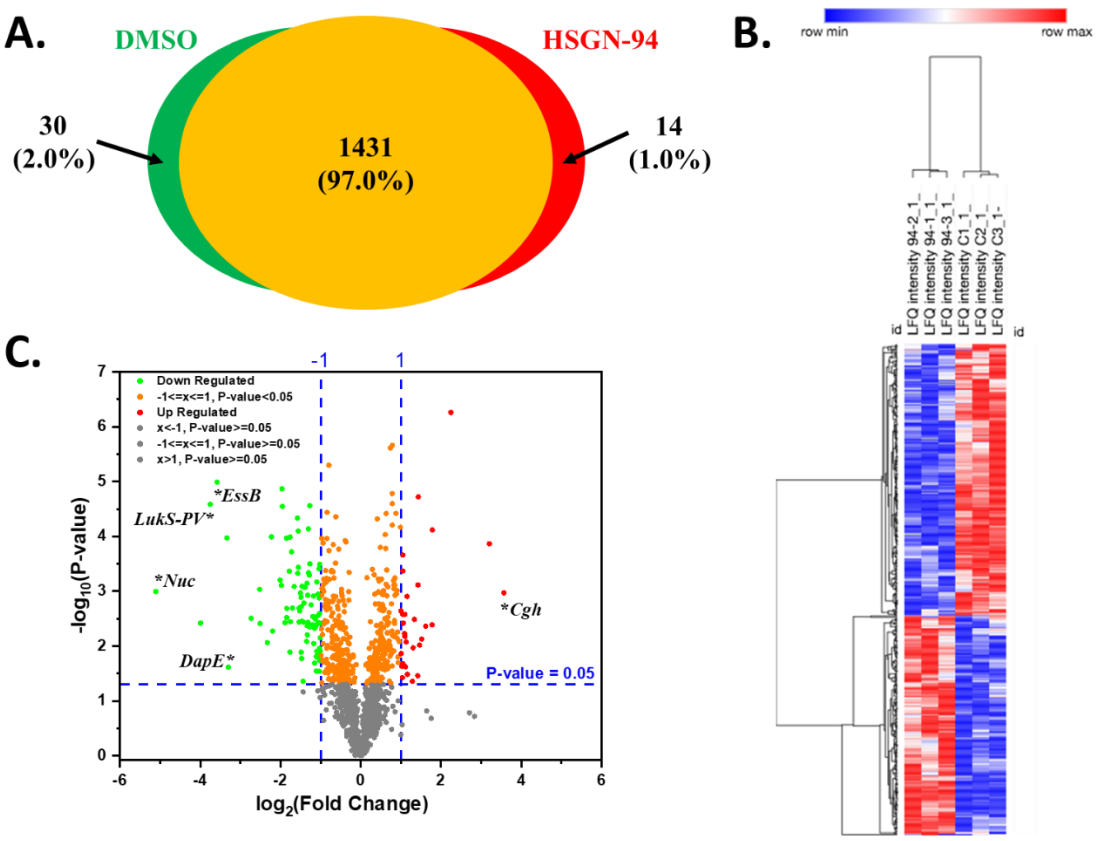

Figure 4.3 Global proteomics analysis of *S. aureus* cells treated with HSGN-94. (A) A Venn diagram was constrcuted to compare proteins found in DMSO-treated cells alone, HSGN-94-treated cells alone and in both groups. (B) Heatmap analysis of significant proteins ($p < 0.5$) demonstrating differentially expressed proteins between DMSO- and HSGN-94-treated *S. aureus*. (C) Volcano plot of significant proteins displaying the Log_2 fold change (Log_2FC, x-axis) vs. p-value (y-axis). Most down and upregulated proteins have been labled. The differential expression was defined as $p \leq 0.05$ and $Log_2FC \leq -2$ for downregulated proteins or $p \leq 0.05$ and $Log_2FC \geq 2$ for upregulated ones. The Perseus software was used to analyze data[174]. OriginPro 2017 Software (OriginLab, Massachusetts, USA) was utilized to construct the volcano plot.

Evaluation of the 30 downregulated proteins (those with $Log_2FC \leq -2$) demonstrated that *S. aureus* treatment with HSGN-94 impacted several bacterial processes such as transcription,

translation, nucleotide metabolism, amino acid biosynthesis, and carbohydrate biosynthesis (Table A.4). Impotrantly, HSGN-94 seemed to have the most significant impact on virulence (Figure A.3 and Table A.4). For instance, thermonuclease (Nuc) which is an important virulence factor in *S. aureus* as it is vital for DNA and RNA degradation, a crucial part of the organism's denfense mechanism[175-176], was the most downregulated protein (Log_2FC = -5.1) (Figure A.3 and Table A.4). Likewise, other virulence factors were also downregulated such as gamma-hemolysin subunit B, LukS-PV (Log_2FC = -3.7), leucotoxin LukD (Log_2FC = -2), Nitrate reductase subunit alpha NarG (Log_2FC = -2), Lipoyl synthase LipA (Log_2FC = -2), and hydrolase SdrD (Log_2FC = -2) (Figure A.3 and Table A.4). Additionally, HSGN-94 appears to substantially affect the type VII secretion system (T7SS) of *S. aureus* which is an essential pathway for bacterial virulence[177]. The T7SS consists of four membrane-associated proteins (EsaA, EssA, EssB, and EssC), three cytosolic proteins (EsaB, EsaE, and EsaG), and five virulence factors that are produced (EsxA, EsxC, EsxB, EsxD, and EsaD)[178]. *S. aureus* treatment with HSGN-94 showed downregulation of several proteins in the T7SS pathway like EsaA (Log_2FC = -2.0), EsxA (Log_2FC = -2.0), and EssB (Log_2FC = -3.3) (Figure A.3 and Table A.4). Similarly, both EssC and EsaB were also downregulated by HSGN-94 treatment as they were only identified in the DMSO-treated group (Table A.5). The fact that HSGN-94 downregulates important proteins in the T7SS pathway was very interesting to us because it has been shown that T7SS activation requires incorporation of *cis*-unsaturated fatty acids into *S. aureus* lipid molecules such as phospholipids, lipoproteins, cardiolipin, and LTA[179]. Thus, we speculate that downregulation of this pathway can be due to HSGN-94's inhibition of LTA.

Furthermore, we also analyzed the 30 proteins that were only detected in the DMSO-treated group (see figure Figure 4.3A and Table A.5). Detection of these proteins in the DMSO group only indicates that they were massively downregulated by HSGN-94. In this group of proteins, we utilized the comprehensive list of *S. aureus* essential genes developed by Charles et al[180] to identify essential proteins that were only found in the DMSO-treated group. We discovered that HSGN-94 downregulated CDP-diacylglycerol--glycerol-3-phosphate 3-phosphatidyltransferase (PgsA). PgsA is an essential protein in *S. aureus* because it is vital for the synthesis of phosphatidyl glycerol (PG), the most abundant membrane phospholipid in the bacteria[181]. PgsA synthesizes phosphatidylglycerol phosphate (PG-P) from cytosine diphosphate diacylglycerol (CDP-DAG) by exhanging glycerol-3-phosphate (Gro-3-P) for cytosine monophosphate (CMP). Then,

phosphatidylglycerol phosphate phosphatase (PgpP) rapdily dephosphorylates PG-P to give PG. Next, cardiolipin synthase (Cls) synthesizes cardiolipin (CL) via the condensation of two PG molecules[182]. Additionally, as mentioned above, LtaS also uses PG to synthesize LTA. PgsA is essential for the synthesis of PG and PG is important for LTA biosynthesis (Figure 4.4A). Next, we sought to validate that HSGN-94 does indeed downregulate PgsA. Therefore, we performed RT-qPCR which demonstrated that *S. aureus* treated with HSGN-94 showed a decrease in mRNA expression levels of PgsA (Figure 4.4B), which confirmed our global proteomics analysis.

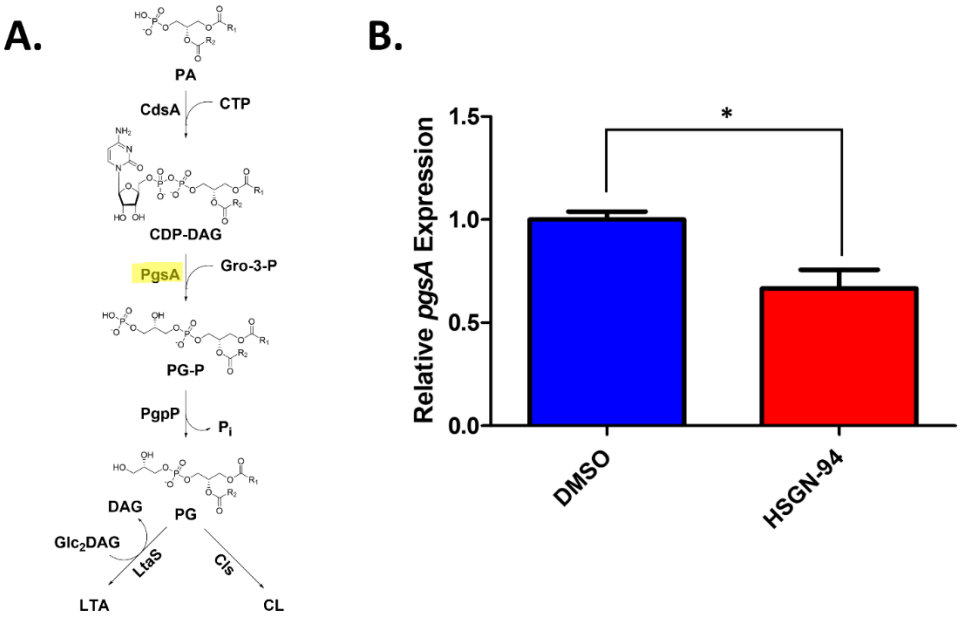

Figure 4.4 HSGN-94 downregulates PgsA. (A) PgsA synthesizes phosphatidylglycerol phosphate (PG-P) from cytosine diphosphate diacylglycerol (CDP-DAG) by exhanging glycerol-3-phosphate (Gro-3-P) for cytosine monophosphate (CMP). Phosphatidylglycerol phosphate phosphatase (PgpP) rapdily dephosphorylates PG-P to give PG. Cardiolipin synthase (Cls) synthesizes cardiolipin (CL) via the condensation of two PG molecules. LtaS also uses PG in order to synthesize LTA. (B) The effect of HSGN-94 (0.25 µg/mL) treatment on the transcription of *pgsA*. Experiments were performed in triplicate and normalized with 16S RNA. Error bars represent standard-deviation. Statistically significant differences between DMSO-treatment and HSGN-94-treatment were established by Student's *t*-test analysis (unpaired, two-tailed) and is represented as $*p \leq 0.05$.

4.3.4 HSGN-94 inhibits Glc_2-DAG in *S. aureus*

The global proteomics analysis demonstrated that HSGN-94 had an effect on numerous biological processes in *S. aureus* (Figure A.3 and Table A.4) and the levels of several proteins (~80) were impacted by HSGN-94. However global proteomics does not reveal the actual binding protein(s) to the compound, so we further performed activity-based protein profiling to identify

the putative targets of HSGN-94[183-186]. An affinity probe (HSGN-probe) was synthesized in 3 steps via click chemistry between the biotin azide and an alkynyl oxadiazole benzamide (I11) (Figure 4.5A). Then, a pull-down assay was performed. To ensure that proteins being captured with the HSGN-Probe also bind the unlabeled compound HSGN-94, we used a competition strategy, *vide infra*, to identify proteins that putatively bind to HSGN-94. Briefly, *S. aureus* ATCC 25923 cells (at the exponential phase) were incubated with HSGN-Probe only (sample A) or with HSGN-Probe plus 50 µM HSGN-94 (sample B) for 4 hours at 25ºC with gentle agitation (Figure 4.5B). Then, cells were lysed, and the biotinylated probes were captured with streptavidin beads, and enriched proteins were evaluated via SDS-PAGE. The bands that show on sample A lane but not on sample B lane (i.e., unique to the HSGN-probe without HSGN-94 competition) would be the proteins that bind to HSGN-94.

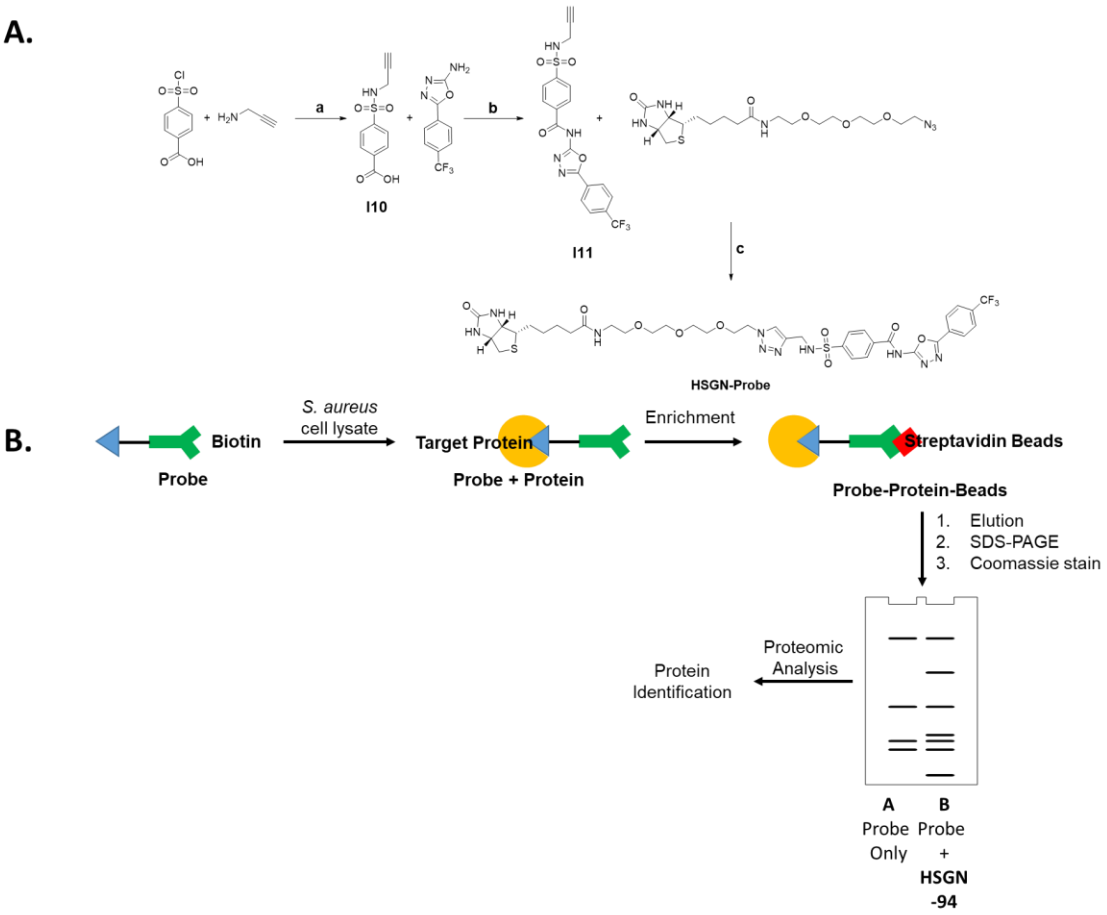

Figure 4.5 Probe Synthesis and Pull-Down Assay. (A) Synthesis of HSGN-Probe[a]. [a]Reagents and Conditions: (a) MeOH, rt, 12 h 53% (b) BOP Reagent, DIPEA, DMF, rt, 12 h, 24% (c) $CuSO_4 \cdot 5H_2O$, Na Ascorbate, DMF: H2O (10:1), 60°C, 12 h, 77%. (B) Schematic of pull-down assay experiment to identify target(s) of HSGN-94.

Phosphoglucomutase (PgcA), a protein inlvoled in LTA biosyntheis, was one of the proteins unique to HSGN-Probe group (Table A.6). PgcA converts glucose-6-phosphate to glucose-1-phosphate (the first step in the LTA biosynthesis pathway, Figure 4.1A) which later gives rise to Glc_2-DAG. Thus, since HSGN-94 inhibits PgcA, it would also inhibit Glc_2-DAG formation. To test this hypothesis, we treated *S. aureus* ATCC 25923 with HSGN-94 (0.25×, 1×, and 8×MIC) for 5 hours and then extracted total membrane lipids using a similar procedure outlined by Scheewind et al[187]. The lipids were then separated by thin layer chromatography (TLC) and visualized by α-naphthol/sulfuric acid staining. The TLC indicated that HSGN-94 treatment reduced the amount of the α-naphthol-reactive species, which we tentatively assigned as Glc_2-DAG and further characterized (Figure 4.6A). To verify the identity of this stained species, lipids were extracted from TLC plates and analyzed by MALDI-TOF mass spectrometry, and spectra were recorded in the positive ion mode. The mass-to-charge (*m/z*) ratio of the major ion signal of the stained species was in agreement with the predicted mass of Glc_2-DAG $[M + H]^+$ adduct harboring fatty acids with chain lengths ranging from C_{15} to C_{18} (Figure 4.6B). For instance, the predicted *m/z* for the $[M + H]^+$ of Glc_2-DAG harboring C_{18} and C_{15} acyl chains was 907.63 and the observed *m/z* for DMSO and HSGN-94 treated samples were the same as that of the predicted *m/z* (907.62 -907.63) (Figure 4.6B and SI for mass spectra). In summary, our results reveal that, compared to DMSO-treated *S. aureus*, HSGN-94 (0.25×, 1×, and 8×MIC) inhibits Glc_2-DAG which we hypothesize is a result of HSGN-94's direct binding to PgcA.

A.

B.

			Observed Molecular Mass For:			
Possible Fatty Acid Chain Length	Chemical Formula $[M + H]^+$	Predicted Molecular Mass	DMSO-treated	HSGN-94 0.25X MIC	HSGN-94 1X MIC	HSGN-94 8X MIC
C_{15}/C_{18}	$C_{48}H_{91}O_{15}$	907.63	907.62	907.63	907.63	907.63

Figure 4.6 HSGN-94 inhibits Glc_2-DAG. (A) TLC analysis of *S. aureus* glycolipids. Membrane lipids were extracted from *S. aureus* ATCC 25923, treated with either DMSO (control) or HSGN-94 (0.25×, 1×, and 8×MIC). Glycolipids were separated from TLC and assessed via MALDI mass spectroscopy.

4.3.5 Multiple reaction monitoring profiling (MRM-Profiling) of lipids demonstrates HSGN-94 selectively effects phosphaditlyglycerol (PG) in *S. aureus*

It has been shown that even in the absence of Glc_2-DAG, LTA can still be made as LtaS uses PG as an alternative starter unit[157]. Polymers formed on PG to make the alternative PG-LTA are much longer than polymers formed on Glc_2-DAG[157, 187]. Additionally, *S. aureus* cells that make these longer polymers have cell division defects[157, 188], are less virulence[159, 187], and are more sensitive to β-lactam antibiotics as well as other cell envelope stresses[157]. However, since inhibition of Glc_2-DAG would not completely deplete LTA, but HSGN-94 potently depletes LTA from *S. aureus*, we hypothesized there must be another mechanism by which HSGN-94 inhibits LTA biosynthesis. Since global proteomics and RT-qPCR shows HSGN-94 downregulates PgsA, an essential protein in *S. aureus* for PG synthesis, we wondered if HSGN-94 also had an effect on PG. To determine this, we proceeded to perform multiple reaction monitoring profiling[189] (MRM-Profiling) to differentiate lipid profile differences among *S. aureus* ATCC 25923 treated with DMSO (control) or HSGN-94 (1× and 8× MIC) for 5 hours. Lipids were extracted and analyzed

using electrospray ionization MS (ESI-MS). MRMs were filtered by ion counts and false discovery rate (FDR) adjusted *p*-value in ANOVA, and then analyzed by differentiated using principal component analysis **(**PCA). Our experiment focused on analyzing differences in glycerophospholipids and total membrane lipids in *S. aureus* treated cells. After obtaining this data, PCA scores plots were generated to evaluate HSGN-94's effects on PG (Figure 4.7A), total membrane lipids (Figure 4.7B), phosphatidylcholine (PC) (Figure 4.7C), and phosphatidylethanolamine (PE) (Figure 4.7D). Each point in the PCA plot represents an individual lipid extract sample from the staphylococci and the elliptical shaded area is the calculated 95% confidence region for each group. Interestingly, we discovered that HSGN-94 seemed to effect PG (Figure 4.7A). However, HSGN-94 did not affect total lipids, PC or PE (Figures 4.7B-D).

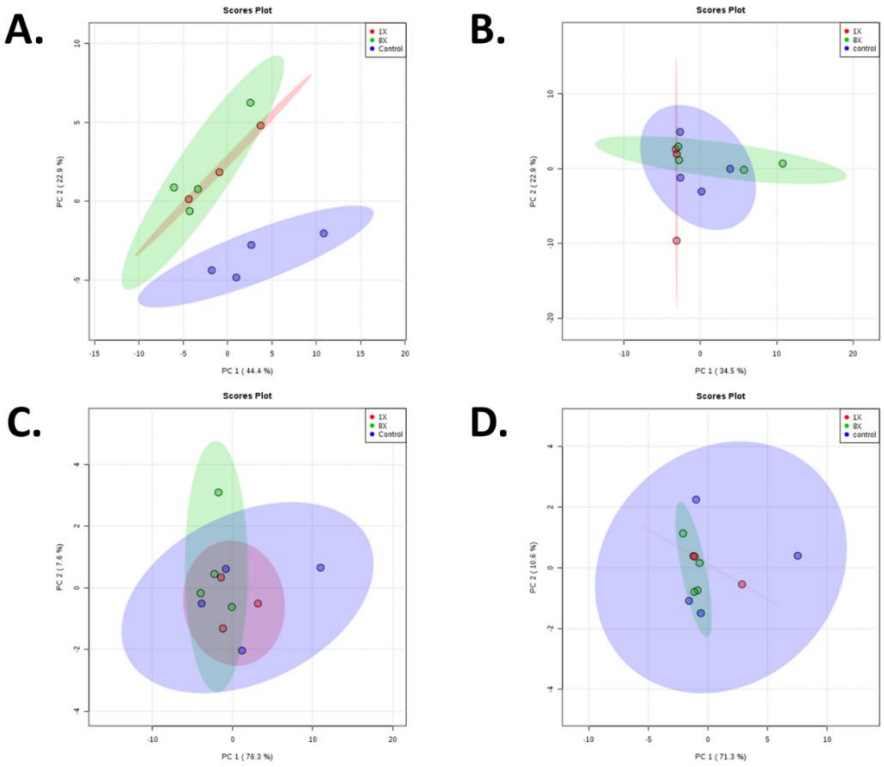

Figure 4.7 PCA scores plots of S. aureus treated with DMSO (control) or HSGN-94 (1× and 8× MIC). (A) Effects on PG synthesis. (B) Effects on total membrane lipids. (C) Effects on PC synthesis. (D) Effects on PE synthesis.

4.3.6 Proposed Mechanism for HSGN-94's Inhibition of LTA Biosynthesis

Since our data demonstrates that HSGN-94 directly binds to PgcA as well as downregulates *pgsA*, we hypothesized that HSGN-94 inhibits LTA biosynthesis in two distinct manners (Figure 4.8). First, HSGN-94 directly binds to PgcA thereby inhibiting the synthesis of Glc_2-DAG. Secondly, HSGN-94 downregulates PgsA expression, which causes an effect on PG synthesis

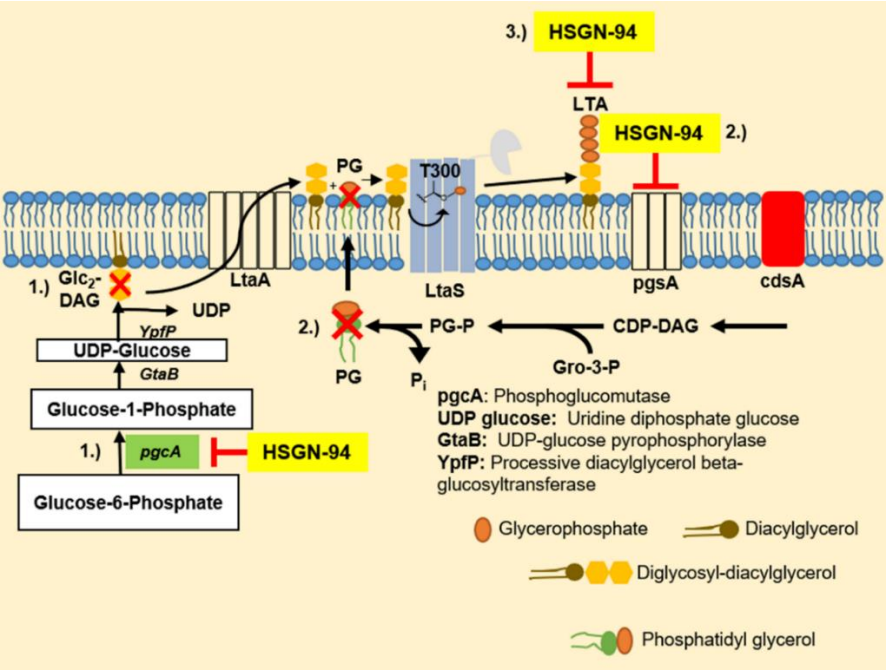

Figure 4.8 Proposed Mechanism for HSGN-94 Inhibition of LTA Biosynthesis. We hypothesize that HSGN-94 inhibits LTA biosynthesis in a dual-mechanistic way.

In addition to LTA inhibition, the global proteomics data (Tables A.4 and A.5) also showed that treatment of *S. aureus* with HSGN-94 downregulated proteins involved in translation (mtaB), transcription (SarR and GntR), and nucleotide metabolism (GloB, PyrF, and CarB). Furthermore, we performed GO function analysis using Metascape™ software of the 423 significant proteins ($p < 0.05$) and identified that nucleotide metabolic and small molecules catabolic processes, as well as precursor metabolites and energy were the most significantly regulated biological processes identified (-log10(p) >10, see Figure A.4). Likewise, the proteomics data using affinity HSGN-probe (Table A.6) indicated that HSGN-94 interacted with proteins involved in protein synthesis (miaB, rplD, PheT, rplJ, and trmFO), DNA/RNA synthesis (SigA, rpiA, Xpt, RecA, adk, and guaA), as well as cell-wall synthesis (IsaA). Therefore, to further evaluate this, we performed a

macromolecular biosynthesis inhibition assay to analyze the incorporation of radiolabeled precursors into the biosynthesis of macromolecules (DNA, RNA, cell wall, and proteins). As expected from data outlined in Tables A.4, A.5, and A.6, HSGN-94 inhibited the biosynthesis of each macromolecule assayed with similar or better potencies than the corresponding antibiotics (Figure A.5A-D). It thus appears that the potent antimicrobial activity of HSGN-94 is derived from LTA biosynthesis inhibition and the inhibition of other essential processes in bacteria. This multi-pronged inhibition of essential processes in bacteria explains why attempts to generate resistant clones towards HSGN-94 failed. It has emerged that successful antibiotics used in the clinic, while developed against single targets, are successful because they indeed target other pathways[190]. For example, daptomycin, which has long been categorized as mainly acting via depolarization of bacterial membrane has now been shown to also target cell wall biosynthesis via a mechanism that involves complex formation with undecaprenyl-coupled intermediates and membrane lipids[191]. Recently, it was also reported that tetracyclines, long thought of as mainly acting via ribosome inhibition, also act via bacterial membrane targeting[192].

4.3.7 *In vivo* Efficacy of HSGN-94 in a MRSA Murine Skin Infection

Based on its potent antibacterial activity, interesting mechanism of action, and the fact that HSGN-94 was not toxic to HaCat cells at concentrations as high as 64 µg/mL, the compound was evaluated for its *in vivo* efficacy in a MRSA murine skin infection model. MRSA-infected wounds were treated as either clindamycin I.P. (25 mg/kg once daily), 2% HSGN-94, 2% mupirocin, or the vehicle alone (petroleum jelly) for five days. twice daily with either 2% HSGN-94, 2% mupirocin, or the vehicle alone (petroleum jelly). It was observed that HSGN-94 (93.84% reduction) performed similarly to FDA-approved antibiotics clindamycin (93.39% reduction) and mupirocin (98.77% reduction) in reducing the burden of MRSA in the wounds of infected mice after (Figure 4.9).

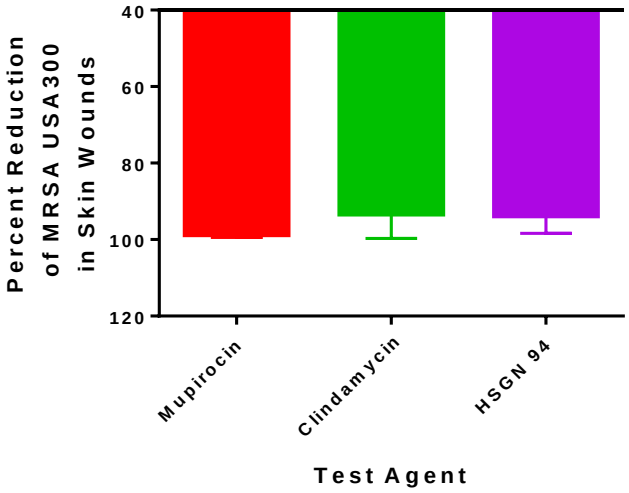

Figure 4.9 Reduction of MRSA USA300 in infected wounds of mice. The data are presented as average percent reduction of MRSA CFU/mL in murine skin wounds. A one-way ANOVA with post-hoc Dunnet's multiple comparisons found no statistical difference between mice treated with mupirocin or clindamycin and mice treated with HSGN-94 (2%).

4.3.8 HSGN-94 Reduces Pro-Inflammatory Cytokines

The clinical severity of *S. aureus* skin infections is driven by the excess host pro-inflammatory cytokines[193]. Several reports have shown that in *S. aureus* infected wounds, LTA contributes to the increased development of inflammation and skin barrier defects[194-197]. Since HSGN-94 is a potent LTA inhibitor and effectively reduced MRSA USA300 in infected wounds, we proceeded to examine its effect on pro-inflammatory cytokine expression in the treated wounds. As depicted from Figure 4.10A-C, HSGN-94 significantly reduced the levels of the pro-inflammatory cytokines, interleukin-1 beta (IL-1β), monocyte chemo attractant protein-1 (MCP-1), and tumor necrosis factor-α (TNF-α) in MRSA USA300 skin lesions. Additionally, HSGN-94 was superior to mupirocin and clindamycin in reducing the levels of IL-1β and MCP-1 (Figure 4.10A and 4.10B). it was reported that prolonged inflammation especially due to inflammatory cytokines such as TNF-α, and MCP-1, greatly delays healing in chronic wounds[198]. Therefore, HSGN-94 treatment resulted in the reduction of pro-inflammator cytokines, which could result in acceleration of wound healing.

To further evaluate HSGN-94's effect on pro-inflammatory cytokines, we performed histopathology (Figure 4.10D-G). It is evident that MRSA infected wounds treated with mupirocin (Figure 4.10E), clidamycin (Figure 4.10F), or HSGN-94 (Figure 4.10G) demonstrate evidence of

necrosis, hemorrhage, and a chronic inflammatory response. However, the response is less pronounced than the than vehicle treated group (Figure 4.10D). However, HSGN-94 showed resolution of inflammation and necrosis which was similar to clidamycin treatment but was much superior than mupriocin treatment (see Figure 4.10E-G). Therefore, MRSA infected wounds treated with HSGN-94 show reduced levels of pro-inflammatory cytokines which is superior to that of wounds treated with clindamycin or mupirocin and may be a result of HSGN-94's ability to inhibit LTA biosynthesis.

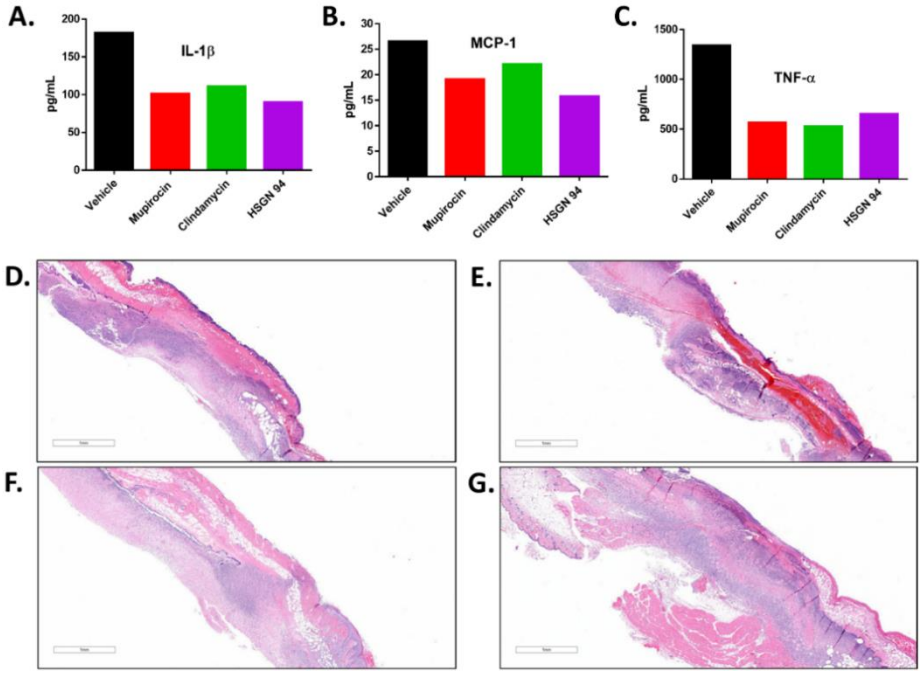

Figure 4.10 HSGN-94 Reduces Pro-Inflammatory Cytokines in MRSA Infected Wounds. (A) Level (pg/mL) of IL-1β in MRSA infected wound treated with vehicle, mupirocin, clidamycin, or HSGN-94. (B) Level (pg/mL) of MCP-1 in MRSA infected wound treated with vehicle, mupirocin, clidamycin, or HSGN-94. (C) Level (pg/mL) of TNF-α in MRSA infected wound treated with vehicle, mupirocin, clidamycin, or HSGN-94. (D) MRSA infected wound treated with vehicle with diffuse necrosis, chronic inflammation, edema and bacterial colonization present. (E) MRSA infected wound treated with mupirocin with moderate necrosis, chronic inflammation, and hemorrahge. (F) MRSA infected wound treated with clidamycin demonstrated epithelial hyperplasia on wound periphery, with moderate chronic inflammation and necrosis. (G) Histopathology of MRSA infected wound treated with HSGN-94 demonstrated resolution of inflammation within the deep dermis and subcutis.

4.4 Conclusion:

In conclusion, using a panoply of techniques, including global proteomics, activity-based protein profiling, lipid analysis, and MRM profiling experiments, we have been able to propose

how **HSGN-94** inhibits LTA biosynthesis. We propose that **HSGN-94** inhibits LTA in two ways: direct binding to PgcA which causes inhibition of Glc_2-DAG; and downregulation of PgsA, which leads to a reduction in PG synthesis. Excitingly, **HSGN-94** showed high efficacy in reducing the burden of MRSA in a murine skin infection model and also reduced the pro-inflammatory cytokines in MRSA infected wounds. Antimicrobial resistance is a growing threat and many groups have disclosed new chemical scaffolds that inhibit bacterial growth[199-209]. Detailed mechanistic work to uncover how each of these unique compounds killing bacteria would likely reveal many novel tactics to tackle this global health challenge.

4.5 Experimental Section

4.5.1 Chemistry:

All reagents and solvents were purchased from commercial sources and utilized without purification. The ^{1}H, ^{13}C, and ^{19}F NMR spectra were obtained in DMSO-*d*6, chloroform-*d*, or methanol-d_4 as solvent using a 500 MHz or 800 MHz spectrometer with tetramethylsilane as the internal standard. ^{1}H NMR spectra data are reported as chemical shift (δ ppm) (multiplicity, coupling constant (Hz), integration). High resolution mass spectra (HRMS) were taken using electron spray ionization (ESI) and a TOF mass analyzer. Characterization of compounds was done using ^{1}H NMR, ^{13}C NMR, ^{19}F NMR, and HRMS data. The purity of compounds was determined to be ≥95% by measuring the absorbance at 280 nm with high performance liquid chromatography (HPLC). HPLC spectra were recorded on an Agilent 1260 Infinity system using a ZORBAX SB-C18 column.

4.5.2 Synthetic Procedures:

4.5.3 General Procedure I: Synthesis of Sulfonamide-Containing Intermediates S1-S10, E1-E2, I5, I6, I8, and I10

To a solution of chlorosulfonyl-containing intermediate (1 eq) in methanol (25 mL) was added amine (3 eq). This mixture was stirred overnight at room temperature. Next, the mixture was concentrated under reduced pressure, diluted with ethyl acetate (20 mL), washed twice with water (10 mL), once with brine (10 mL), dried over Na_2SO_4, and concentrated under reduced pressure. The crude mixture was then purified via column chromatography using hexanes: ethyl acetate (80:20) as solvent system to give pure product.

4.5.4 General Procedure II: Synthesis of Aromatic 1,3,4-oxadiazol-2-amines A1:

The synthesis of A1 was performed using a literature-reported procedure[210]. Obtained ^{1}H, ^{13}C, and ^{19}F spectra were in agreement with literature-reported data.

4.5.5 General Procedure III: Sandmeyer Reaction for the Synthesis of I1, I3, and I4

Thionyl chloride (5.5 eq) was added dropwise to water (15 mL) at 0°C and then stirred for 18 hours at room temperature. $CuCl_2$ (0.05 eq) was added at 0°C and the mixture was stirred for 15 minutes. In a separate flask, a solution of $NaNO_2$ (1.5 eq) in water (5 mL) was added to a stirred solution of 4-amino-3-nitrobenzonitrile (1 eq), 4-amino3-methoxybenzonitrile (1 eq), or 5-aminonicotinic acid (1 eq) in concentrated HCl (5 mL) at 0°C, over 15 minutes. The diazonium salt solution was added dropwise to the thionyl chloride/$CuCl_2$ solution at 0°C and stirred for 1 hour. Over this time, a precipitate formed which was collected via vacuum filtration and washed with water (10 mL) which gave the sulfonyl chloride intermediates I1, I3, or I4. These intermediates were used in the next step without purification or characterization.

4.5.6 General Procedure IV: Hydrolysis of Benzonitriles I5-I7 to Benzoic Acids S13, S14, and S15

To a mixture of benzonitriles I5-I7 in ethanol (10 mL) was added sodium hydroxide (2M in H_2O) (16.6 mL) and the solution was refluxed at 100°C overnight. After, the reaction was cooled to room temperature and concentrated under reduced pressure. The crude material was dissolved in H_2O and acidified to pH = 1 with 6 M HCl to give an off-white precipitate which was collected via vacuum filtration to give desired product which was continued without further purification or characterization.

4.5.7 General Procedure V: Hydrolysis of Esters E1 and E2 to Carboxylic Acids S11 and S12

To a solution of methyl ester E1 or E2 (1 eq) in MeOH: H_2O (2:1) was added LiOH (22 eq) and the solution was stirred at room temperature for 12 hours. After, the mixture was concentrated under reduced pressure and the crude product was dissolved in H_2O and acidified to

pH = 1 with 6 M HCl to afford the carboxylic acid intermediate as an off-white solid which was collected via vacuum filtration.

4.5.8 General Procedure VI: Reduction of Nitro for the Synthesis of 15 and I9:

To a 50 mL round-bottom flask charged with nitro containing compound 13 (1 eq) or intermediate I8 (1 eq) was dissolved in DMF: H_2O (9:1). $Na_2S_2O_4$ (3.5 eq) was added, and the reaction was run at 90°C for 12 hours. After, the reaction mixture was concentrated under reduced pressure and diluted with ethyl acetate (20 mL). The organic layer was washed twice with H_2O (10 mL) and once with brine (10 mL). The organic layer was separated, dried over Na_2SO_4, and concentrated under reduced pressure to give a crude mixture which was purified via column chromatography (hexanes/ethyl acetate 70:30).

4.5.9 General Procedure VII: Synthesis of Alkyl containing 1,3,4-oxadiazol-2-amines A2 and A3:

The synthesis of A2 and A3 was performed using a literature-reported procedure[211]. Obtained ^{1}H, and ^{13}C spectra were in agreement with literature-reported data.

4.5.10 General Procedure VIII: Amide Coupling for the Synthesis of Compounds 1-14, 16, 18, and I11

To a round-bottomed flask was added benzoic acid (1 eq), amine (1 eq), BOP reagent (2.7 eq), and DIPEA (1.5 mL) in DMF solvent (5 mL) was stirred at room temperature for 24 h. After completion, the reaction mixture was concentrated under reduced pressure. The crude reaction mixture was purified by flash column chromatography (hexanes/ethyl acetate 90:10 to 70:30) to give the desired product.

4.5.11 General Procedure IX: Synthesis of Compounds 19 and 20:

To a round-bottom flask with acyl chloride (1.4 eq) and 1,3,4-oxadiazol-2-amine (1 eq) in 1,4, -dioxane (5 mL) was added *N*-methylimidazole (5.5 eq). The mixture was stirred at 90°C for 2 hours and then concentrated under reduced pressure. The crude mixture was diluted in ethyl acetate (20 mL), washed twice with water (10 mL), once with brine (10 mL), dried over Na_2SO_4,

and concentrated under reduced pressure. Column chromatography (hexanes/ethyl acetate 70:30) gave desired product.

4.5.12 Synthesis of Intermediate I2:

To a round-bottomed flask containing thiophene-2-carboxylic acid was slowly added chlorosulfonic acid (10 mL) at 0°C. After addition, the reaction was stirred at room temperature overnight. Then, the mixture was slowly poured over ice and extracted with ethyl acetate (3 x 30 mL). The combined organic layer was dried over Na_2SO_4 and concentrated under reduced pressure to give chlorosulfonyl containing intermediate I2 which was proceeded to the next step without further purification or characterization.

4.5.13 Synthesis of Intermediate I7:

To a round-bottom flask containing I6 (1 eq) in anhydrous DCM (10 mL) under argon gas was slowly added BBr_3 (5 eq) at -78°C. The mixture was stirred at -78°C for 1 hour and then warmed to room temperature to continue stirring for 12 hours. After, the reaction was cooled to 0°C and quenched slowly with iced water (10 mL). Next, the two layers were separated, and the water layer extracted twice with DCM (10 mL). The organic layers were combined and washed once with $NaHCO_3$ (10 mL), once with brine (10 mL), dried over Na_2SO_4, and concentrated under reduced pressure to give a crude mixture which was purified via column chromatography (hexanes: ethyl acetate (95:5) to give intermediate I7 as an off-white solid.

4.5.14 Synthesis of Analog 17:

To a solution of HSGN-94 (1 eq) in dry DMF (5 mL), sodium hydride, NaH (3 eq), was added, and the reaction mixture was allowed to stir for 30 min at room temperature. Then, methyl iodide (2 eq) was added dropwise, and the mixture was stirred for 2 h at room temperature. The reaction mixture was concentrated under reduced pressure and the residue was treated with aqueous NH_4OH (30% in water, 10 mL). The crude product was extracted with Et_2O (3 × 15 mL) and purified by silica gel column chromatography using hexanes: ethyl acetate (70:30) to give desired product.

4.5.15 Synthesis of HSGN-Probe:

To a solution of I11 (14 mg, 31.1 µmol) and biotin-PEG_3-N_3 (20 mg, 45 µmol, 1.5 eq) in DMF (2 mL) was added a mixture of $CuSO_4 \cdot 5H_2O$ (3 mg) and sodium ascorbate (3 mg) in water (0.2 mL). The solution was allowed to stir at 60°C for 12 hours. The solvents were evaporated, and the product was purified by column chromatography using DCM/MeOH (90/10) as eluent to obtain HSGN-Probe (77% yield) as a clear oil.

4.5.16 Characterization Data:

4-(Piperidin-1-ylsulfonyl)benzoic acid (S1):
Off-white solid (190 mg, 71% yield). ^{1}H NMR (500 MHz, DMSO-*d*6) δ 8.1 (d, *J* = 8.3 Hz, 2H), 7.8 (d, *J* = 8.2 Hz, 2H), 2.9 (d, *J* = 5.4 Hz, 4H), 1.5 (t, *J* = 5.7 Hz, 4H), 1.4 (d, *J* = 3.7 Hz, 2H). ^{13}C NMR (126 MHz, DMSO-*d*6) δ 166.7, 139.8, 135.1, 130.6, 128.1, 47.0, 25.1, 23.2. HRMS (ESI) m/z calcd for $C_{12}H_{16}NO_4S$ $[M + H]^+$ 270.0794, found 270.0793.

4-(Pyrrolidin-1-ylsulfonyl)benzoic acid (S2):
Off-white solid (154 mg, 44% yield). ^{1}H NMR (800 MHz, DMSO-d_6) δ 8.2 – 8.1 (m, 2H), 7.9 – 7.9 (m, 2H), 3.2 – 3.1 (m, 4H), 1.7 (q, *J* = 3.7 Hz, 4H). ^{13}C NMR (201 MHz, DMSO-d_6) δ 166.5, 140.8, 135.1, 130.5, 127.8, 48.2, 25.1. HRMS (ESI) m/z calcd for $C_{11}H_{14}NO_4S$ $[M + H]^+$ 256.0644, found 256.0646.

4-(*N*-Cyclopropylsulfamoyl)benzoic acid (S3):
Off-white solid (166 mg, 51% yield). ^{1}H NMR (800 MHz, DMSO-d_6) δ 8.1 (d, *J* = 8.0 Hz, 2H), 7.9 – 7.9 (m, 3H), 2.2 – 2.1 (m, 1H), 0.5 (dd, *J* = 7.0, 2.1 Hz, 2H), 0.4 (t, *J* = 3.1 Hz, 2H). ^{13}C NMR (201 MHz, DMSO-d_6) δ 166.6, 144.6, 134.7, 130.3, 127.4, 24.5, 5.5. HRMS (ESI) m/z calcd for $C_{10}H_{12}NO_4S$ $[M + H]^+$ 242.0487, found 242.0484.

4-(*N*,*N*-Dimethylsulfamoyl)benzoic acid (S4):
Off-white solid (177 mg, 57% yield). ^{1}H NMR (800 MHz, DMSO-d_6) δ 8.2 (dd, *J* = 8.4, 1.8 Hz, 2H), 7.9 (dd, *J* = 8.4, 1.7 Hz, 2H), 2.7 (s, 6H). ^{13}C NMR (201 MHz, DMSO-d_6) δ 166.5, 139.4, 135.2, 130.5, 128.0, 37.8. HRMS (ESI) m/z calcd for $C_9H_{12}NO_4S$ $[M + H]^+$ 230.0487, found 230.0488.

4-((2-Azabicyclo[2.2.1]heptan-2-yl)sulfonyl)benzoic acid (S5):
Off-white solid (210 mg, 55% yield). ^{1}H NMR (800 MHz, DMSO-d_6) δ 8.1 – 8.1 (m, 2H), 7.9 – 7.9 (m, 2H), 4.1 (s, 1H), 3.1 – 3.0 (m, 1H), 3.0 (d, *J* = 9.0 Hz, 1H), 2.5 (s, 1H), 1.6 – 1.5 (m, 3H), 1.3 – 1.3 (m, 1H), 1.2 (d, *J* = 9.9 Hz, 1H), 0.8 (d, *J* = 10.0 Hz, 1H). ^{13}C NMR (201 MHz, DMSO-d_6) δ 166.5, 142.5, 134.9, 130.5, 127.7, 60.3, 54.7, 37.4, 36.6, 31.2, 27.1. HRMS (ESI) m/z calcd for $C_{13}H_{16}NO_4S$ $[M + H]^+$ 282.0800, found 282.0801.

4-((4-Methylpiperidin-1-yl)sulfonyl)benzoic acid (S6):
Off-white solid (235 mg, 61% yield). ^{1}H NMR (800 MHz, DMSO-d_6) δ 8.2 – 8.1 (m, 2H), 7.9 – 7.8 (m, 2H), 3.6 (d, *J* = 12.1 Hz, 2H), 2.3 (td, *J* = 12.1, 2.7 Hz, 2H), 1.7 – 1.6 (m, 2H), 1.4 – 1.3 (m, 1H), 1.1 (qd, *J* = 12.2, 4.0 Hz, 2H), 0.9 (d, *J* = 6.5 Hz, 3H). ^{13}C NMR (201 MHz, DMSO-d_6) δ 166.5, 140.4, 135.2, 130.5, 127.9, 46.3, 33.3, 29.6, 21.5. HRMS (ESI) m/z calcd for $C_{13}H_{18}NO_4S$ $[M + H]^+$ 284.0957, found 284.0956.

4-((3-Methylpiperidin-1-yl)sulfonyl)benzoic acid (S7):
Off-white solid (227 mg, 59% yield). ^{1}H NMR (800 MHz, DMSO-d_6) δ 8.2 – 8.1 (m, 2H), 7.9 – 7.7 (m, 2H), 3.5 (ddd, *J* = 16.2, 11.9, 6.1 Hz, 2H), 2.3 (td, *J* = 11.5, 3.2 Hz, 1H), 2.1 – 2.0 (m, 1H), 1.7 – 1.6 (m, 3H), 1.5 (dt, *J* = 12.9, 3.9 Hz, 1H), 0.9 – 0.9 (m, 1H), 0.8 (d, *J* = 6.4 Hz, 3H). ^{13}C NMR (201 MHz, DMSO-d_6) δ 166.5, 140.4, 135.1, 130.5, 127.9, 52.9, 46.4, 31.6, 30.5, 24.5, 18.9. HRMS (ESI) m/z calcd for $C_{13}H_{18}NO_4S$ $[M + H]^+$ 284.0957, found 284.0959.

4-((2-Methylpiperidin-1-yl)sulfonyl)benzoic acid (S8):
Off-white solid (247 mg, 64% yield). ^{1}H NMR (800 MHz, DMSO-d_6) δ 8.1 – 8.1 (m, 2H), 7.9 – 7.9 (m, 2H), 4.1 (d, *J* = 4.8 Hz, 1H), 3.6 (dt, *J* = 13.2, 3.2 Hz, 1H), 3.0 (td, *J* = 13.1, 2.7 Hz, 1H), 1.6 – 1.5 (m, 2H), 1.5 – 1.4 (m, 3H), 1.2 (qt, *J* = 12.5, 4.2 Hz, 1H), 1.0 (d, *J* = 7.0 Hz, 3H). ^{13}C NMR (201 MHz, DMSO-d_6) δ 166.5, 145.1, 134.7, 130.6, 127.2, 48.8, 40.5, 30.2, 25.1, 18.0, 15.8. HRMS (ESI) m/z calcd for $C_{13}H_{18}NO_4S$ $[M + H]^+$ 284.0957, found 284.0957.

5-(3,5-Dimethylpiperidin-1-yl)sulfonyl)nicotinic acid (S9):
Off-white solid (173 mg, 53% yield). ^{1}H NMR (800 MHz, DMSO-d_6) δ 9.3 (s, 1H), 9.1 (s, 1H), 8.4 (d, *J* = 1.8 Hz, 1H), 3.7 – 3.6 (m, 2H), 1.9 (t, *J* = 11.3 Hz, 2H), 1.7 (tdd, *J* = 17.8, 15.2, 7.5, 3.8 Hz, 3H), 0.8 (d, *J* = 6.5 Hz, 6H), 0.6 (q, *J* = 12.1 Hz, 1H). ^{13}C NMR (201 MHz, DMSO-d_6) δ 165.3,

153.9, 151.1, 135.7, 133.8, 127.9, 52.3, 40.9, 31.0, 18.9. HRMS (ESI) m/z calcd for $C_{13}H_{19}N_2O_4S$ $[M + H]^+$ 299.1066, found 299.1067.

4-(3,5-Dimethylpiperidin-1-yl)sulfonyl)thiophene-2-carboxylic acid (S10):
Off-white solid (220 mg, 66% yield). ^{1}H NMR (500 MHz, DMSO-*d*6) δ = 8.5 (d, *J* = 1.6, 1H), 7.7 (d, *J* = 1.6, 1H), 3.7 – 3.5 (m, 2H), 1.8 (t, *J* = 11.2, 2H), 1.7 – 1.6 (m, 3H), 0.8 (d, *J* = 6.4, 6H), 0.6 – 0.5 (m, 1H). ^{13}C NMR (126 MHz, DMSO-*d*6) δ = 162.4, 137.7, 137.6, 136.7, 130.7, 52.5, 40.9, 31.0, 19.2. HRMS (ESI) m/z calcd for $C_{12}H_{18}NO_4S_2$ $[M + H]^+$ 304.0677, found 304.0676.

3-((3,5-Dimethylpiperidin-1-yl)sulfonyl)thiophene-2-carboxylic acid (S11):
Off-white solid (121 mg, 59% yield). ^{1}H NMR (800 MHz, DMSO-d_6) δ 7.8 (d, *J* = 5.1 Hz, 1H), 7.4 (d, *J* = 5.2 Hz, 1H), 3.8 – 3.7 (m, 2H), 2.1 (t, *J* = 11.8 Hz, 2H), 1.7 (d, *J* = 12.9 Hz, 1H), 1.6 – 1.5 (m, 2H), 0.8 (d, *J* = 6.7 Hz, 6H), 0.6 (q, *J* = 12.2 Hz, 1H). ^{13}C NMR (201 MHz, DMSO-d_6) δ 161.4, 139.7, 136.3, 130.3, 130.2, 130.1, 130.0, 52.5, 41.3, 31.0, 19.0. HRMS (ESI) m/z calcd for $C_{12}H_{18}NO_4S_2$ $[M + H]^+$ 304.0677, found 304.0678.

5-((3,5-Dimethylpiperidin-1-yl)sulfonyl)furan-2-carboxylic acid (S12):
Off-white solid (171 mg, 60% yield). ^{1}H NMR (800 MHz, DMSO-d_6) δ 7.3 – 7.3 (m, 1H), 7.2 (d, *J* = 3.6 Hz, 1H), 3.7 – 3.6 (m, 2H), 2.2 (t, *J* = 11.7 Hz, 2H), 1.7 – 1.7 (m, 1H), 1.6 – 1.6 (m, 2H), 0.8 (d, *J* = 6.8 Hz, 6H), 0.6 (q, *J* = 12.3 Hz, 1H). ^{13}C NMR (201 MHz, DMSO-d_6) δ 158.8, 149.8, 148.1, 118.0, 117.6, 52.2, 40.9, 30.9, 18.9. HRMS (ESI) m/z calcd for $C_{12}H_{18}NO_5S$ $[M + H]^+$ 288.0906, found 288.0907.

4-((3,5-Dimethylpiperidin-1-yl)sulfonyl)-3-nitrobenzonitrile (I5):
Yellow solid (280 mg, 61% yield). ^{1}H NMR (500 MHz, DMSO-d_6) δ 8.3 (d, *J* = 2.1 Hz, 1H), 7.8 (dd, *J* = 8.9, 2.2 Hz, 1H), 7.3 (d, *J* = 8.9 Hz, 1H), 3.3 – 3.2 (m, 2H), 2.5 – 2.5 (m, 2H), 1.8 (d, *J* = 12.1 Hz, 1H), 1.7 – 1.6 (m, 2H), 0.8 (d, *J* = 6.5 Hz, 6H), 0.8 (q, *J* = 12.2 Hz, 1H). ^{13}C NMR (126 MHz, DMSO-d_6) δ 147.8, 138.7, 136.7, 131.8, 121.6, 118.4, 99.6, 57.3, 41.4, 31.1, 19.1. HRMS (ESI) m/z calcd for $C_{14}H_{18}N_3O_4S$ $[M + H]^+$ 324.1018, found 324.1015.

4-((3,5-dimethylpiperidin-1-yl)sulfonyl)-3-methoxybenzonitrile (I6):
Off-white solid (273 mg, 51% yield). ^{1}H NMR (500 MHz, DMSO-d_6) δ 7.9 (d, *J* = 8.1 Hz, 1H), 7.8 (d, *J* = 1.5 Hz, 1H), 7.5 (dd, *J* = 8.1, 1.4 Hz, 1H), 3.9 (s, 3H), 3.6 (dd, *J* = 12.1, 4.0 Hz, 2H),

2.2 – 2.0 (m, 2H), 1.7 (ddt, *J* = 13.2, 4.1, 2.2 Hz, 1H), 1.5 (dq, *J* = 11.0, 3.6 Hz, 2H), 0.8 (d, *J* = 6.6 Hz, 6H), 0.6 (q, *J* = 12.0 Hz, 1H). ^{13}C NMR (126 MHz, DMSO-*d*$_6$) δ 157.0, 131.8, 131.4, 124.7, 118.1, 117.4, 117.0, 57.2, 52.3, 41.3, 31.4, 19.1. HRMS (ESI) m/z calcd for $C_{15}H_{21}N_2O_3S$ $[M + H]^+$ 309.1273, found 309.1270.

4-((3,5-Dimethylpiperidin-1-yl)sulfonyl)-3-hydroxybenzonitrile (I7):
Off-white solid (158 mg, 72% yield). ^{1}H NMR (500 MHz, Chloroform-*d*) δ 9.1 (s, 1H), 7.6 (d, *J* = 8.2 Hz, 1H), 7.3 (d, *J* = 1.6 Hz, 1H), 7.3 (dd, *J* = 8.2, 1.6 Hz, 1H), 3.8 – 3.6 (m, 2H), 1.9 – 1.8 (m, 2H), 1.8 – 1.7 (m, 3H), 0.9 (d, *J* = 6.5 Hz, 6H), 0.6 – 0.4 (m, 1H). ^{13}C NMR (126 MHz, Chloroform-*d*) δ 155.4, 129.4, 129.4, 124.3, 123.2, 123.2, 122.8, 122.7, 118.2, 117.0, 52.4, 41.0, 30.9, 18.9. HRMS (ESI) m/z calcd for $C_{14}H_{19}N_2O_3S$ $[M + H]^+$ 295.1116, found 295.1116.

3,5-Dimethyl-1-((4-nitrophenyl)sulfonyl)piperidine (I8):
Yellow solid (214 mg, 53% yield). ^{1}H NMR (800 MHz, DMSO-*d*$_6$) δ 8.4 (d, *J* = 8.4 Hz, 2H), 8.0 (d, *J* = 8.4 Hz, 2H), 3.8 – 3.6 (m, 2H), 1.9 (t, *J* = 11.4 Hz, 2H), 1.8 – 1.5 (m, 3H), 0.8 (d, *J* = 6.6 Hz, 6H), 0.5 (q, *J* = 12.0 Hz, 1H). ^{13}C NMR (201 MHz, DMSO-*d*$_6$) δ 150.4, 142.6, 129.2, 129.1, 125.0, 124.9, 52.4, 41.0, 30.9, 18.9. HRMS (ESI) m/z calcd for $C_{13}H_{19}N_2O_4S$ $[M + H]^+$ 299.1066, found 299.1065.

4-((3,5-Dimethylpiperidin-1-yl)sulfonyl)aniline (I9):
Off-white solid (115 mg, 64% yield). ^{1}H NMR (800 MHz, DMSO-*d*$_6$) δ 7.4 (d, *J* = 9.1 Hz, 2H), 6.7 (d, *J* = 8.3 Hz, 2H), 5.8 (s, 2H), 3.5 (dd, *J* = 11.1, 3.3 Hz, 2H), 1.7 – 1.5 (m, 5H), 0.8 (d, *J* = 6.1 Hz, 6H), 0.5 (q, *J* = 11.9 Hz, 1H). ^{13}C NMR (201 MHz, DMSO-*d*$_6$) δ 153.3, 129.6, 129.5, 121.6, 113.3, 113.2, 52.8, 41.3, 30.8, 19.2. HRMS (ESI) m/z calcd for $C_{13}H_{21}N_2O_2S$ $[M + H]^+$ 269.1324, found 269.1326.

4-(*N*-(Prop-2-yn-1-yl)sulfamoyl)benzoic acid (I10):
Off-white solid (173 mg, 63% yield). ^{1}H NMR (800 MHz, DMSO-*d*$_6$) δ 8.2 (t, *J* = 6.0 Hz, 1H), 8.1 – 8.1 (m, 2H), 7.9 – 7.9 (m, 2H), 3.8 (d, *J* = 3.6 Hz, 2H), 2.9 (s, 1H). ^{13}C NMR (201 MHz, DMSO-*d*$_6$) δ 166.6, 144.8, 134.7, 130.3, 127.3, 79.6, 75.0, 32.3. HRMS (ESI) m/z calcd for $C_{10}H_{10}NO_4S$ $[M + H]^+$ 240.0331, found 240.0328.

4-(*N*-(Prop-2-yn-1-yl)sulfamoyl)-*N*-(5-(4-(trifluoromethyl)phenyl)-1,3,4-oxadiazol-2-yl)benzamide (I11):

Off-white solid (45 mg, 24% yield). ^{1}H NMR (800 MHz, DMSO-d_6) δ 8.4 (t, J = 5.9 Hz, 1H), 8.2 – 8.1 (m, 4H), 8.0 – 7.9 (m, 4H), 3.8 (dd, J = 5.9, 2.5 Hz, 2H), 3.0 (t, J = 2.5 Hz, 1H). ^{13}C NMR (201 MHz, DMSO-d_6) δ 164.5, 160.3, 158.7, 144.8, 136.1, 132.0 (q, J = 34.2 Hz), 129.5, 127.5, 127.4, 127.3, 127.1, 126.9, 126.8, 126.6, 126.2, 124.8 (q, J = 273.4 Hz), 79.6, 75.0, 32.4. ^{19}F NMR (471 MHz, DMSO-d_6) δ -62.7 (s, 3F). HRMS (ESI) m/z calcd for $C_{19}H_{14}F_3N_4O_4S$ $[M + H]^+$ 451.0688, found 451.0690.

4-((3,5-Dimethylpiperidin-1-yl)sulfonyl)-*N*-(5-(4-(trifluoromethyl)phenyl)-1,3,4-oxadiazol-2-yl)benzamide (HSGN-94):

The synthesis and characterization of HSGN-94 was demonstrated in our previous report[134]. For *in vivo* analysis, the compound was scaled up. Purity by HPLC was found to be 98%.

4-(Piperidin-1-ylsulfonyl)-*N*-(5-(4-(trifluoromethyl)phenyl)-1,3,4-oxadiazol-2-yl)benzamide (1):

Off-white solid (53 mg, 30% yield). ^{1}H NMR (800 MHz, DMSO-d_6) δ 8.3 – 8.2 (m, 2H), 8.2 – 8.2 (m, 2H), 8.0 – 8.0 (m, 2H), 7.9 – 7.9 (m, 2H), 3.0 (t, J = 5.5 Hz, 4H), 1.6 (q, J = 5.8 Hz, 4H), 1.4 (t, J = 5.9 Hz, 2H). ^{13}C NMR (201 MHz, DMSO-d_6) δ 165.3, 159.9, 159.0, 140.3, 137.0, 132.0 (q, J = 32.2 Hz), 129.7, 127.9, 127.5, 127.3, 126.7, 124.8 (q, J = 271.4 Hz), 46.9, 25.1, 23.3. ^{19}F NMR (471 MHz, DMSO-d_6) δ -62.8 (s, 3F). HRMS (ESI) m/z calcd for $C_{21}H_{20}F_3N_4O_4S$ $[M + H]^+$ 481.1157, found 481.1155. Purity by HPLC was found to be 98%.

4-(Pyrrolidin-1-ylsulfonyl)-*N*-(5-(4-(trifluoromethyl)phenyl)-1,3,4-oxadiazol-2-yl)benzamide (2):

Off-white solid (32 mg, 18% yield). ^{1}H NMR (800 MHz, DMSO-d_6) δ 8.4 – 8.3 (m, 2H), 8.2 – 8.1 (m, 2H), 7.9 – 7.7 (m, 4H), 3.3 – 3.0 (m, 4H), 1.7 (d, J = 6.5 Hz, 4H). ^{13}C NMR (201 MHz, DMSO-d_6) δ 171.4, 168.7, 156.8, 141.8, 139.4, 131.4 (q, J = 32.2 Hz), 129.8, 128.2, 127.5, 126.9, 126.6, 124.9 (q, J = 271.4 Hz), 48.2, 25.1. ^{19}F NMR (471 MHz, DMSO-d_6) δ -62.7 (s, 3F). HRMS (ESI) m/z calcd for $C_{20}H_{18}F_3N_4O_4S$ $[M + H]^+$ 467.1001, found 467.1000. Purity by HPLC was found to be 99%.

4-(*N*-cyclopropylsulfamoyl)-*N*-(5-(4-(trifluoromethyl)phenyl)-1,3,4-oxadiazol-2-yl)benzamide (3):

Off-white solid (41 mg, 22% yield). ^{1}H NMR (800 MHz, DMSO-d_6) δ 8.2 – 8.2 (m, 2H), 8.2 – 8.2 (m, 2H), 8.0 – 7.9 (m, 4H), 2.2 (tq, *J* = 6.8, 3.3 Hz, 1H), 0.5 (dd, *J* = 7.1, 2.2 Hz, 2H), 0.5 – 0.3 (m, 2H). ^{13}C NMR (201 MHz, DMSO-d_6) δ 165.2, 160.0, 158.9, 144.6, 136.5, 132.0 (q, *J* = 32.2 Hz), 129.6, 127.5, 127.3, 126.8, 126.2, 124.8 (q, *J* = 273.4 Hz), 24.6, 5.5. ^{19}F NMR (471 MHz, DMSO-d_6) δ -62.8 (s, 3F). HRMS (ESI) m/z calcd for $C_{19}H_{16}F_3N_4O_4S$ $[M + H]^+$ 453.0844, found 453.0844. Purity by HPLC was found to be 95%.

4-(*N*,*N*-Dimethylsulfamoyl)-*N*-(5-(4-(trifluoromethyl)phenyl)-1,3,4-oxadiazol-2-yl)benzamide (4):

Off-white solid (49 mg, 26% yield). ^{1}H NMR (800 MHz, DMSO-d_6) δ 8.3 – 8.2 (m, 2H), 8.2 – 8.1 (m, 2H), 8.0 – 8.0 (m, 2H), 8.0 – 7.9 (m, 2H), 2.7 (s, 6H). ^{13}C NMR (201 MHz, DMSO-d_6) δ 165.3, 160.0, 158.9, 139.4, 137.0, 132.0 (q, *J* = 32.2 Hz), 129.7, 128.0, 127.5, 127.3, 126.8, 124.8 (q, *J* = 271.4 Hz), 37.9. ^{19}F NMR (471 MHz, DMSO-d_6) δ -62.8 (s, 3F). HRMS (ESI) m/z calcd for $C_{18}H_{16}F_3N_4O_4S$ $[M + H]^+$ 441.0844, found 441.0847. Purity by HPLC was found to be 99%.

4-((2-Azabicyclo[2.2.1]heptan-2-yl)sulfonyl)-*N*-(5-(4-(trifluoromethyl)phenyl)-1,3,4-oxadiazol-2-yl)benzamide (5):

Off-white solid (26 mg, 15% yield). ^{1}H NMR (800 MHz, DMSO-d_6) δ 8.3 – 8.2 (m, 2H), 8.2 – 8.2 (m, 2H), 8.0 – 7.9 (m, 4H), 4.2 (s, 1H), 3.1 (dd, *J* = 9.0, 2.8 Hz, 1H), 3.0 (d, *J* = 9.1 Hz, 1H), 2.5 (s, 1H), 1.7 – 1.5 (m, 3H), 1.4 – 1.3 (m, 1H), 1.2 (d, *J* = 9.9 Hz, 1H), 0.9 (dt, *J* = 9.9, 2.0 Hz, 1H). ^{13}C NMR (201 MHz, DMSO-d_6) δ 165.3, 160.0, 159.0, 142.4, 136.8, 132.0 (q, *J* = 32.2 Hz), 129.7, 127.7, 127.5, 127.3, 126.8, 124.8 (q, *J* = 271.4 Hz), 60.3, 54.7, 37.4, 36.6, 31.3, 27.1. ^{19}F NMR (471 MHz, DMSO-d_6) δ -62.7 (s, 3F). HRMS (ESI) m/z calcd for $C_{22}H_{20}F_3N_4O_4S$ $[M + H]^+$ 493.1157, found 493.1156. Purity by HPLC was found to be 98%.

4-((4-Methylpiperidin-1-yl)sulfonyl)-*N*-(5-(4-(trifluoromethyl)phenyl)-1,3,4-oxadiazol-2-yl)benzamide (6):

Off-white solid (40 mg, 23% yield). ^{1}H NMR (800 MHz, DMSO-d_6) δ 8.3 – 8.2 (m, 2H), 8.2 – 8.1 (m, 2H), 8.0 – 8.0 (m, 2H), 7.9 – 7.9 (m, 2H), 3.7 (d, *J* = 11.9 Hz, 2H), 2.4 – 2.3 (m, 2H), 1.7 – 1.6 (m, 2H), 1.4 – 1.3 (m, 1H), 1.1 (qd, *J* = 12.1, 3.9 Hz, 2H), 0.9 (d, *J* = 6.6 Hz, 3H). ^{13}C NMR (201

MHz, DMSO-d_6) δ 165.2, 159.9, 159.0, 140.4, 137.0, 132.0 (q, *J* = 32.2 Hz), 129.7, 127.9, 127.5, 127.3, 126.8, 124.8 (q, *J* = 273.4 Hz), 46.3, 33.3, 29.6, 21.5. ^{19}F NMR (471 MHz, DMSO-d_6) δ -62.8 (s, 3F). HRMS (ESI) m/z calcd for $C_{22}H_{22}F_3N_4O_4S$ $[M+H]^+$ 495.1310, found 495.1306. Purity by HPLC was found to be 97%.

4-((3-Methylpiperidin-1-yl)sulfonyl)-*N*-(5-(4-(trifluoromethyl)phenyl)-1,3,4-oxadiazol-2-yl)benzamide (7):

Off-white solid (36 mg, 21% yield). ^{1}H NMR (800 MHz, DMSO-d_6) δ 8.3 – 8.2 (m, 2H), 8.2 – 8.2 (m, 2H), 8.0 – 8.0 (m, 2H), 7.9 – 7.9 (m, 2H), 3.5 (ddd, *J* = 16.2, 11.9, 5.7 Hz, 2H), 2.4 (td, *J* = 11.6, 2.8 Hz, 1H), 2.1 – 2.0 (m, 1H), 1.7 (dt, *J* = 13.5, 3.6 Hz, 1H), 1.7 – 1.6 (m, 2H), 1.5 – 1.4 (m, 1H), 0.9 (dtd, *J* = 14.8, 11.5, 3.7 Hz, 1H), 0.9 (d, *J* = 6.4 Hz, 3H). ^{13}C NMR (201 MHz, DMSO-d_6) δ 165.2, 159.9, 159.1, 140.4, 137.1, 131.9 (q, *J* = 32.2 Hz), 129.7, 127.8, 127.6, 127.3, 126.8, 124.8 (q, *J* = 271.4 Hz), 53.0, 46.5, 31.7, 30.5, 24.5, 18.9. ^{19}F NMR (471 MHz, DMSO-d_6) δ -62.7 (s, 3F). HRMS (ESI) m/z calcd for $C_{22}H_{22}F_3N_4O_4S$ $[M+H]^+$ 495.1310, found 495.1312. Purity by HPLC was found to be 98%.

4-((2-Methylpiperidin-1-yl)sulfonyl)-*N*-(5-(4-(trifluoromethyl)phenyl)-1,3,4-oxadiazol-2-yl)benzamide (8):

Off-white solid (24 mg, 14% yield). ^{1}H NMR (800 MHz, DMSO-d_6) δ 8.2 – 8.2 (m, 2H), 8.2 – 8.2 (m, 2H), 8.0 – 7.9 (m, 4H), 4.2 – 4.1 (m, 1H), 3.7 – 3.6 (m, 1H), 3.0 (td, *J* = 13.1, 2.7 Hz, 1H), 1.7 – 1.5 (m, 2H), 1.4 (dq, *J* = 9.2, 5.6, 5.0 Hz, 3H), 1.2 (dt, *J* = 12.8, 4.3 Hz, 1H), 1.1 (d, *J* = 6.9 Hz, 3H). ^{13}C NMR (201 MHz, DMSO-d_6) δ 165.2, 160.0, 159.0, 145.0, 136.6, 132.0 (q, *J* = 32.2 Hz), 129.8, 127.5, 127.3, 127.2, 126.8, 126.8, 124.8 (q, *J* = 273.4 Hz), 48.8, 30.3, 25.1, 18.0, 15.9. ^{19}F NMR (471 MHz, DMSO-d_6) δ -62.8 (s, 3F). HRMS (ESI) m/z calcd for $C_{22}H_{22}F_3N_4O_4S$ $[M+H]^+$ 495.1310, found 495.1311. Purity by HPLC was found to be 99%.

5-((3,5-Dimethylpiperidin-1-yl)sulfonyl)-*N*-(5-(4-(trifluoromethyl)phenyl)-1,3,4-oxadiazol-2-yl)nicotinamide (9):

Off-white solid (37 mg, 22% yield). ^{1}H NMR (800 MHz, DMSO-d_6) δ = 9.4 (d, *J*=2.1, 1H), 9.1 (d, *J*=2.1, 1H), 8.7 (s, 1H), 8.2 (d, *J*=8.1, 2H), 8.0 (d, *J*=8.2, 2H), 3.7 (dd, *J*=11.4, 3.8, 2H), 1.9 (t, *J*=11.3, 2H), 1.6 (d, *J*=10.8, 3H), 0.8 (d, *J*=6.4, 6H), 0.6 – 0.5 (m, 1H). ^{13}C NMR (201 MHz, DMSO-d_6) δ 164.1, 159.6, 159.0, 153.3, 150.9, 135.1, 133.7, 132.0 (q, *J* = 32.2 Hz), 129.8, 127.4,

127.3, 126.8, 124.8 (q, *J* = 273.4 Hz), 52.3, 41.0, 31.0, 19.0. ^{19}F NMR (471 MHz, DMSO-d_6) δ -62.8 (s, 3F). HRMS (ESI) m/z calcd for $C_{22}H_{23}F_3N_5O_4S$ $[M+H]^+$ 510.1417, found 510.1415. Purity by HPLC was found to be 99%.

4-((3,5-Dimethylpiperidin-1-yl)sulfonyl)-*N*-(5-(4-(trifluoromethyl)phenyl)-1,3,4-oxadiazol-2-yl)thiophene-2-carboxamide (10):
Off-white solid (49 mg, 29% yield). ^{1}H NMR (800 MHz, DMSO-d_6) δ 8.54 (s, 1H), 8.35 (s, 1H), 8.15 (d, *J* = 8.0 Hz, 2H), 7.98 (d, *J* = 8.0 Hz, 2H), 3.59 (dd, *J* = 11.2, 3.8 Hz, 2H), 1.85 (t, *J* = 11.2 Hz, 2H), 1.68 – 1.61 (m, 3H), 0.83 (d, *J* = 6.4 Hz, 6H), 0.64 – 0.44 (m, 1H). ^{13}C NMR (201 MHz, DMSO-d_6) δ 160.0, 159.6, 159.0, 141.0, 137.5, 131.9 (q, *J* = 32.2 Hz), 129.4, 127.6, 127.3, 126.8, 126.2, 124.8 (q, *J* = 271.4 Hz), 52.5, 41.1, 31.0, 19.1. ^{19}F NMR (471 MHz, DMSO-d_6) δ -62.7 (s, 3F). HRMS (ESI) m/z calcd for $C_{21}H_{22}F_3N_4O_4S_2$ $[M+H]^+$ 515.1029, found 515.1029. Purity by HPLC was found to be 96%.

3-((3,5-Dimethylpiperidin-1-yl)sulfonyl)-*N*-(5-(4-(trifluoromethyl)phenyl)-1,3,4-oxadiazol-2-yl)thiophene-2-carboxamide (11):
Off-white solid (30 mg, 18% yield). ^{1}H NMR (800 MHz, DMSO-d_6) δ 8.2 – 8.1 (m, 2H), 8.0 – 7.9 (m, 2H), 7.9 (d, *J* = 5.2 Hz, 1H), 7.4 (d, *J* = 5.2 Hz, 1H), 3.7 (dd, *J* = 12.2, 4.0 Hz, 2H), 2.1 (t, *J* = 11.7 Hz, 2H), 1.7 (d, *J* = 13.1 Hz, 1H), 1.6 – 1.5 (m, 2H), 0.8 (d, *J* = 6.6 Hz, 6H), 0.6 (q, *J* = 12.1 Hz, 1H). ^{13}C NMR (201 MHz, DMSO-d_6) δ 159.6, 158.3, 139.5, 136.7, 131.9 (q, *J* = 32.2 Hz), 129.5, 127.9, 127.5, 127.3, 126.8, 126.7, 124.8 (q, *J* = 273.4 Hz), 52.4, 41.2, 30.9, 19.0. ^{19}F NMR (471 MHz, DMSO-d_6) δ -62.7 (s, 3F). HRMS (ESI) m/z calcd for $C_{21}H_{22}F_3N_4O_4S_2$ $[M+H]^+$ 515.1029, found 515.1026. Purity by HPLC was found to be 96%.

5-((3,5-Dimethylpiperidin-1-yl)sulfonyl)-*N*-(5-(4-(trifluoromethyl)phenyl)-1,3,4-oxadiazol-2-yl)furan-2-carboxamide (12):
Off-white solid (38 mg, 22% yield). ^{1}H NMR (800 MHz, DMSO-d_6) δ 8.2 – 8.1 (m, 2H), 8.0 – 7.9 (m, 2H), 7.6 (d, *J* = 3.8 Hz, 1H), 7.3 (d, *J* = 3.6 Hz, 1H), 3.7 (dd, *J* = 12.0, 4.1 Hz, 2H), 2.2 (t, *J* = 11.7 Hz, 2H), 1.7 (d, *J* = 13.4 Hz, 1H), 1.6 – 1.6 (m, 2H), 0.9 (d, *J* = 6.6 Hz, 6H), 0.7 (q, *J* = 12.3 Hz, 1H). ^{13}C NMR (201 MHz, DMSO-d_6) δ 159.5, 158.9, 156.3, 150.0, 149.5, 132.0 (q, *J* = 30.2 Hz), 127.5, 127.3, 126.8, 124.8 (q, *J* = 273.4 Hz), 117.9, 117.7, 117.3, 52.3, 40.9, 30.9, 18.9. ^{19}F

NMR (471 MHz, DMSO-d_6) δ -62.8 (s, 3F). HRMS (ESI) m/z calcd for $C_{21}H_{22}F_3N_4O_5S$ $[M+H]^+$ 499.1263, found 499.1262. Purity by HPLC was found to be 97%.

4-((3,5-Dimethylpiperidin-1-yl)sulfonyl)-3-nitro-*N*-(5-(4-(trifluoromethyl)phenyl)-1,3,4-oxadiazol-2-yl)benzamide (13):
Yellow solid (42 mg, 26% yield). ^{1}H NMR (800 MHz, DMSO-d_6) δ 8.5 (s, 1H), 8.2 – 8.1 (m, 2H), 8.1 – 8.1 (m, 1H), 8.0 – 7.9 (m, 2H), 7.4 (d, *J* = 8.8 Hz, 1H), 3.4 – 3.2 (m, 2H), 2.5 (t, *J* = 12.0 Hz, 2H), 1.8 (d, *J* = 13.0 Hz, 1H), 1.8 – 1.7 (m, 1H), 0.9 (d, *J* = 6.6 Hz, 6H), 0.8 (q, *J* = 12.0 Hz, 1H). ^{13}C NMR (201 MHz, DMSO-d_6) δ 163.4, 160.1, 159.0, 148.2, 139.1, 133.6, 131.9 (q, *J* = 32.2 Hz), 127.6, 127.4, 127.2, 126.8, 126.7, 124.8 (q, *J* = 271.4 Hz), 120.7, 57.7, 41.5, 31.0, 19.0. ^{19}F NMR (471 MHz, DMSO-d_6) δ -62.8 (s, 3F). HRMS (ESI) m/z calcd for $C_{23}H_{23}F_3N_5O_6S$ $[M+H]^+$ 554.1321, found 554.1322. Purity by HPLC was found to be 95%.

4-((3,5-Dimethylpiperidin-1-yl)sulfonyl)-3-methoxy-*N*-(5-(4-(trifluoromethyl)phenyl)-1,3,4-oxadiazol-2-yl)benzamide (14):
Off-white solid (31 mg, 19% yield). ^{1}H NMR (500 MHz, DMSO-d_6) δ 8.2 – 8.1 (m, 2H), 8.0 – 8.0 (m, 2H), 7.9 – 7.9 (m, 1H), 7.8 (d, *J* = 1.6 Hz, 1H), 7.7 – 7.7 (m, 1H), 4.0 (s, 3H), 3.6 (dd, *J* = 12.1, 4.0 Hz, 2H), 2.2 – 2.1 (m, 2H), 1.7 (d, *J* = 13.0 Hz, 1H), 1.5 (ddt, *J* = 14.5, 11.3, 4.6 Hz, 2H), 0.8 (d, *J* = 6.6 Hz, 6H), 0.6 (q, *J* = 12.2 Hz, 1H). ^{13}C NMR (126 MHz, DMSO-d_6) δ 164.0, 158.7, 156.9, 137.9, 131.3 (q, *J* = 32.2 Hz), 127.4, 127.0, 125.3, 123.1 (q, *J* = 271.4 Hz), 120.7, 113.3, 56.8, 52.5, 41.4, 31.4, 19.1. ^{19}F NMR (471 MHz, DMSO-d_6) δ -62.7 (s, 3F). HRMS (ESI) m/z calcd for $C_{24}H_{26}F_3N_4O_5S$ $[M+H]^+$ 539.1576, found 539.1577. Purity by HPLC was found to be 95%.

3-Amino-4-((3,5-dimethylpiperidin-1-yl)sulfonyl)-*N*-(5-(4-(trifluoromethyl)phenyl)-1,3,4-oxadiazol-2-yl)benzamide (15):
Off-white solid (34 mg, 73% yield). ^{1}H NMR (800 MHz, DMSO-d_6) δ 8.2 – 8.1 (m, 2H), 8.0 – 7.9 (m, 2H), 7.4 (d, *J* = 2.2 Hz, 1H), 7.3 – 7.3 (m, 1H), 7.0 (d, *J* = 8.1 Hz, 1H), 3.1 (dd, *J* = 11.3, 3.5 Hz, 2H), 2.1 (t, *J* = 11.0 Hz, 2H), 1.9 – 1.7 (m, 3H), 0.9 (d, *J* = 6.8 Hz, 6H), 0.7 (q, *J* = 12.0 Hz, 1H). ^{13}C NMR (201 MHz, DMSO-d_6) δ 165.8, 160.3, 159.2, 143.6, 142.4, 131.8 (q, *J* = 32.2 Hz), 127.7, 127.5, 127.2, 126.7, 124.8 (q, *J* = 271.4 Hz), 119.1, 117.9, 114.6, 58.3, 42.3, 31.5, 19.5. ^{19}F

NMR (471 MHz, DMSO-d_6) δ -62.8 (s, 3F). HRMS (ESI) m/z calcd for $C_{23}H_{25}F_3N_5O_4S$ $[M+H]^+$ 524.1579, found 524.1579. Purity by HPLC was found to be 95%.

4-((3,5-Dimethylpiperidin-1-yl)sulfonyl)-3-hydroxy-*N*-(5-(4-(trifluoromethyl)phenyl)-1,3,4-oxadiazol-2-yl)benzamide (16):

Off-white solid (38 mg, 23% yield). ^{1}H NMR (800 MHz, DMSO-d_6) δ 8.2 – 8.1 (m, 2H), 8.0 (d, *J* = 8.4 Hz, 2H), 7.9 (d, *J* = 8.1 Hz, 1H), 7.8 – 7.7 (m, 1H), 7.6 – 7.5 (m, 2H), 3.7 – 3.6 (m, 2H), 2.2 – 2.0 (m, 2H), 1.7 (d, *J* = 13.0 Hz, 1H), 1.6 (q, *J* = 8.8, 7.7 Hz, 2H), 0.8 (d, *J* = 6.6 Hz, 6H), 0.6 – 0.5 (m, 1H). ^{13}C NMR (201 MHz, DMSO-d_6) δ 165.3, 160.2, 158.7, 155.8, 138.3, 132.1 (q, *J* = 32.2 Hz), 131.1, 128.5, 127.4, 126.7, 123.3 (q, *J* = 271.4 Hz), 118.6, 117.7, 52.5, 41.3, 31.1, 18.9. ^{19}F NMR (471 MHz, DMSO-d_6) δ -62.7 (s, 3F). HRMS (ESI) m/z calcd for $C_{23}H_{24}F_3N_4O_5S$ $[M+H]^+$ 525.1420, found 525.1419. Purity by HPLC was found to be 95%.

4-((3,5-Dimethylpiperidin-1-yl)sulfonyl)-*N*-methyl-*N*-(5-(4-(trifluoromethyl)phenyl)-1,3,4-oxadiazol-2-yl)benzamide (17):

Off-white solid (29 mg, 57% yield). ^{1}H NMR (800 MHz, DMSO-d_6) δ 8.4 – 8.4 (m, 2H), 8.1 – 8.1 (m, 2H), 8.0 – 8.0 (m, 2H), 7.9 – 7.8 (m, 2H), 3.8 (s, 3H), 3.7 (dd, *J* = 11.3, 3.8 Hz, 2H), 1.8 (t, *J* = 11.4 Hz, 3H), 1.7 – 1.6 (m, 3H), 0.8 (d, *J* = 6.6 Hz, 6H), 0.5 (q, *J* = 12.1, 11.5 Hz, 1H). ^{13}C NMR (201 MHz, DMSO-d_6) δ 170.1, 156.0, 154.3, 140.9, 132.3 (q, *J* = 32.2 Hz), 130.3, 128.8, 128.0, 127.1, 126.9, 126.8, 124.7 (q, *J* = 271.4 Hz), 52.6, 41.1, 34.9, 30.9, 19.0. ^{19}F NMR (471 MHz, DMSO-d_6) δ -62.8 (s, 3F). HRMS (ESI) m/z calcd for $C_{24}H_{26}F_3N_4O_4S$ $[M+H]^+$ 523.1627, found 523.1629. Purity by HPLC was found to be 95%.

N-(4-((3,5-Dimethylpiperidin-1-yl)sulfonyl)phenyl)-5-phenyl-1,3,4-oxadiazole-2-carboxamide (18):

Off-white solid (90 mg, 39% yield). ^{1}H NMR (800 MHz, DMSO-d_6) δ 8.2 – 8.1 (m, 2H), 8.1 – 8.1 (m, 2H), 7.8 – 7.8 (m, 2H), 7.7 – 7.7 (m, 1H), 7.7 – 7.6 (m, 2H), 3.7 – 3.5 (m, 2H), 1.8 (t, *J* = 11.4 Hz, 2H), 1.7 – 1.6 (m, 3H), 0.8 (d, *J* = 6.5 Hz, 6H), 0.6 – 0.4 (m, 1H). ^{13}C NMR (201 MHz, DMSO-d_6) δ 165.9, 158.8, 152.3, 141.9, 133.2, 132.4, 129.9, 128.8, 127.6, 123.1, 121.3, 52.7, 41.1, 30.9, 19.1. HRMS (ESI) m/z calcd for $C_{22}H_{25}N_4O_4S$ $[M+H]^+$ 441.1591, found 441.1592. Purity by HPLC was found to be 96%.

N-(5-cyclohexyl-1,3,4-oxadiazol-2-yl)-4-((3,5-dimethylpiperidin-1-yl)sulfonyl)benzamide (19): Off-white solid (45 mg, 32% yield). ^{1}H NMR (800 MHz, DMSO-d_6) δ 8.2 – 8.2 (m, 2H), 7.9 – 7.9 (m, 2H), 3.7 (dd, *J* = 11.6, 3.9 Hz, 2H), 2.9 (ddd, *J* = 10.8, 7.0, 3.8 Hz, 1H), 2.0 (dd, *J* = 13.2, 4.0 Hz, 2H), 1.8 (t, *J* = 11.4 Hz, 2H), 1.8 (dt, *J* = 13.3, 4.1 Hz, 2H), 1.7 – 1.6 (m, 4H), 1.6 (qd, *J* = 11.4, 3.5 Hz, 2H), 1.4 (tdd, *J* = 15.4, 11.8, 3.6 Hz, 2H), 1.3 – 1.2 (m, 1H), 0.8 (d, *J* = 6.5 Hz, 6H), 0.5 (q, *J* = 12.0 Hz, 1H). ^{13}C NMR (201 MHz, DMSO-d_6) δ 166.3, 165.7, 158.2, 140.3, 137.5, 129.7, 127.8, 52.6, 41.1, 34.6, 30.9, 29.7, 25.6, 24.9, 19.0. HRMS (ESI) m/z calcd for $C_{22}H_{31}N_4O_4S$ $[M+H]^+$ 447.2066, found 447.2062. Purity by HPLC was found to be 95%.

N-(5-cyclopropyl-1,3,4-oxadiazol-2-yl)-4-((3,5-dimethylpiperidin-1-yl)sulfonyl)benzamide (20): Off-white solid (30 mg, 24% yield). ^{1}H NMR (800 MHz, DMSO-d_6) δ 8.2 – 8.2 (m, 2H), 7.9 – 7.8 (m, 2H), 3.7 – 3.6 (m, 2H), 2.2 – 2.1 (m, 1H), 1.8 (t, *J* = 11.3 Hz, 2H), 1.7 – 1.6 (m, 3H), 1.2 – 1.1 (m, 2H), 1.0 – 1.0 (m, 2H), 0.8 (dd, *J* = 6.6, 1.3 Hz, 6H), 0.5 (q, *J* = 12.0 Hz, 1H). ^{13}C NMR (201 MHz, DMSO-d_6) δ 164.8, 157.8, 140.3, 137.2, 129.6, 128.7, 127.8, 52.6, 41.1, 30.9, 19.0, 7.8, 6.2. HRMS (ESI) m/z calcd for $C_{19}H_{25}N_4O_4S$ $[M+H]^+$ 405.1597, found 405.1596. Purity by HPLC was found to be 97%.

4-(*N*-((1-(13-Oxo-17-(2-oxohexahydro-1H-thieno[3,4-*d*]imidazol-4-yl)-3,6,9-trioxa-12-azaheptadecyl)-1H-1,2,3-triazol-4-yl)methyl)sulfamoyl)-*N*-(5-(4-(trifluoromethyl)phenyl)-1,3,4-oxadiazol-2-yl)benzamide (HSGN-Probe):
Clear oil (21 mg, 77% yield). ^{1}H NMR (800 MHz, Methanol-d_4) δ 8.3 – 8.1 (m, 4H), 8.1 – 7.9 (m, 2H), 7.9 – 7.9 (m, 2H), 7.8 (s, 1H), 4.5 (d, *J* = 4.2 Hz, 2H), 4.3 (dd, *J* = 7.8, 4.3 Hz, 1H), 4.2 (s, 2H), 3.8 (t, *J* = 4.7 Hz, 2H), 3.6 – 3.6 (m, 8H), 3.5 (t, *J* = 5.4 Hz, 2H), 3.2 (dt, *J* = 9.5, 4.9 Hz, 1H), 2.9 – 2.9 (m, 1H), 2.7 – 2.7 (m, 1H), 2.3 – 2.1 (m, 2H), 1.8 – 1.5 (m, 5H), 1.5 – 1.4 (m, 3H), 1.3 – 1.2 (m, 2H). ^{13}C NMR (201 MHz, Methanol-d_4) δ 174.7, 165.1, 164.6, 159.4, 158.8, 144.4, 143.6, 136.4, 132.8 (q, *J* = 34.2 Hz), 128.8, 126.9, 126.0, 124.4 (q, *J* = 271.4 Hz), 123.9, 70.1, 70.0, 69.9, 69.8, 69.1, 68.8, 61.9, 60.1, 55.5, 49.8, 39.6, 38.8, 37.7, 35.3, 28.3, 28.0, 25.4. ^{19}F NMR (471 MHz, Methanol-d_4) δ -65.7 (s, 3F). HRMS (ESI) m/z calcd for $C_{37}H_{46}F_3N_{10}O_9S_2$ $[M+H]^+$ 895.2843, found 895.2846. Purity by HPLC was found to be 91%.

4.5.17 Biological Analysis

4.5.18 Bacterial strains media, cell lines and reagents

Clinical isolates used in this study (Appendix A, Table A.7) were obtained from the Biodefense and Emerging Infections Research Resources Repository (BEI Resources) and the American Type Culture Collection (ATCC). Cation-adjusted Mueller Hinton broth (CAMHB), tryptic soy broth (TSB) and tryptic soy agar (TSA) were purchased from Becton, Dickinson and Company (Cockeysville, MD, USA). Human keratinocyte cell line (HaCaT) was obtained from AddexBio (San Diego, CA, USA). Dulbecco's Modified Eagle Medium (DMEM) was obtained from Sigma-Aldrich (St. Louis, MO, USA). Fetal bovine serum (FBS) and phosphate-buffered saline (PBS) were purchased from Corning (Manassas, VA, USA). Linezolid and vancomycin were purchase from Chem-Impex International (Wood Dale, IL, USA). Compounds were synthesized from commercial sources in our laboratory and prepared in stock solutions in DMSO.

4.5.19 Determination of the MICs

MICs of 1,3,4-oxadiazol-2-yl benzamides were determined using the broth microdilution method as outlined previously[212]. Briefly, a bacterial solution equivalent to 0.5 McFarland standard was prepared and diluted in CAMHB to achieve a bacterial concentration of about 5×10^5 CFU/mL and seeded in 96-well plates. Streptococci, enterococci and *Listeria* were diluted in TSB. Serial dilutions of tested agents were incubated with the bacteria aerobically at 37° C for 18-20 hours (except for *S. pneumoniae* which was incubated in presence of 5% CO_2). MICs were determined as the lowest concentration of the each test agent that completely inhibited the bacterial growth as determined visually.

4.5.20 *In vitro* cytotoxicity analysis of HSGN-94 against human keratinocytes (HaCat) cells

Cytotoxicity assessment for HSGN-94 was determined as previously described[213-214]. HSGN-94 was assayed (at concentrations of 16, 32, 64 and 128 µg/mL) against human keratinocyte cells (HaCat) to determine its potential toxic effect to mammalian skin cells *in vitro*. Briefly, cells were incubated with the compound (in sextuplicate) at 37 ºC with 5% CO_2 for 2 hours. DMSO was included as a control to determine the baseline measure of the cytotoxic impact of the compound. MTS 3-(4, 5-dimethylthiazol-2-yl)-5-(3-carboxymethoxyphenyl)-2-(4-

sulfophenyl)-2H-tetrazolium) (Promega, Madison, WI, USA) was subsequently added and the plate was incubated for three hours before the absorbance readings (at OD_{490}) were recorded.

4.5.21 Multi-step Resistance Selection:

To assess if MRSA USA300 could form resistance to HSGN-94, a multi-step serial passaging experiment was conducted for 65 days, as described previously[117, 215-216]. Resistance was considered as a greater than four-fold increase in the MIC as compared to the initial MIC.

4.5.22 Global Proteomics Analysis:

Exponentially growing *S. aureus* ATCC 25923 was treated with 0.25 µg/mL HSGN-94 or an equivalent amount of DMSO for 2 hours. After, the cells were pelleted by centrifugation and washed twice with PBS. Sample preparation for LC/MS/MS and data acquisition was performed as described previously[217]. Data was analyzed using the MaxQuant software (v. 1.6.0.16)[218-220] while bioinformatics analysis was done using the Perseus software[174], as outlined previously[217].

4.5.23 Total RNA isolation and RT-PCR:

Exponentially growing *S. aureus* ATCC 25923 was incubated with 0.25 µg/mL HSGN-94 or DMSO for 2 hours at 37 °C in triplicates. The cells were then pelleted by centrifugation. RNA isolation, cDNA synthesis, and RT-PCR analysis was performed following a previously reported procedure[217]. A BioRad CFX96™ Touch Real-Time PCR Detection System was used. PCR primers were either designed using Primer-BLAST or obtained from the referenced literature (Appendix A, Table A.8). The data were normalized against 16S rRNA, as an internal control, and the P-values from student's *t*-test showed * ≤ 0.05.

4.5.24 Pull-Down Assay:

The pull down assay and proteomic analysis was performed following a previously reported procedure[185]. Concisely, streptavidin resin and reagents were equilibrated at room temperature and then 100 µL of settled resins were added to spin columns and centrifuged at 500 xg for 5 minutes. The beads were washed twice with PBS and incubated at room temperature for 30 minutes. Then, the beads were again washed twice with PBS, and collected. Next, to exponentially growing *S.*

aureus ATCC 25923 was added 50 µL beads and 50 µL of 10 mg/mL HSGN-Probe or an equivalent amount of DMSO (control) and this was incubated at room temperature for 4 hours. After, the cells were pelleted by centrifugation and resuspended in PBS. The cells were then lysed with freeze-thawed using liquid N_2 and cells were then collected via centrifugation. Next, protein concentration was determined using BCA Protein Assay Kit (ThermoFisher Scientific, Waltham, MA, USA) and normalized. Then, SDS-PAGE was performed using a 12% gel, stained with coomassie blue, and gel bands were excised. The gel was then washed with 1:1 100 mM ammonium bicarbonate :acetonitile for 10 minutes and dreid in a vacuum centrifuge for 5-10 minutes. After, the gel was treated with DTT followed by trypsin solution so as to perform alkylation and digestion as described in a previous section above. The sample was then extracted using 1% formic acid solution in acetonitrile and then collected and transferred to new centrifuge tube. This solution then underwent LC/MS/MS analysis using a reverse-phase HPLC-ESI-MS/MS system composed of an UltiMate™ 3000 RSLCnano system coupled to a Q-Exactive (QE) High Field (HF) Hybrid Quadrupole-Orbitrap™ mass spectrometer (Thermo Fisher Scientific, Waltham, MA) and a Nano-spray Flex™ ion source (Thermo Fisher Scientific) was used to analyze the samples standard data-dependent mode. Data aqusition was performed using MaxQuant and bioinformatic analysis using Perseus as mentioned above.

4.5.25 Membrane Lipid Extraction and TLC Analysis:

Exponential growing *S. aureus* ATCC 25923 was treated with DMSO, 0.0625 µg/mL (1/4X MIC) HSGN-94, 0.25 µg/mL (1X MIC) HSGN-94, or 2 µg/mL (8X MIC) HSGN-94 for 5 hours at 37°C. The samples were normalized to OD_{600} 0.9 and then centrifuged at 10,000 rpm for 10 minutes. The cells were collected and washed twice with 0.1 M sodium acetate (pH 4.7). Next, lipids were extracted following the Bligh-Dyer method[221] and lipids were isolated and dried over nitrogen stream. Detection of glycolipids was performed via TLC using a previously reported procedure[187]. MALDI-TOF analysis was used to identify glycolipids on TLC. See Appendix A for MALDI mass spectra.

4.5.26 Multiple Reaction Monitoring Profiling (MRM-Profiling) of Lipids

Exponential growing *S. aureus* ATCC 25923 was treated with DMSO, 0.25 µg/mL (1X MIC) HSGN-94, or 2 µg/mL (8X MIC) HSGN-94 for 5 hours at 37°C. The samples were normalized to OD_{600} 0.9 and then centrifuged at 10,000 rpm for 10 minutes. The cells were collected and washed twice with 0.1 M sodium acetate (pH 4.7). Next, lipids were extracted following the Bligh-Dyer method[221] and lipids were isolated and dried over nitrogen stream. Experiments were carried out following a previously reported procedure[189]. PCA plots were constructed using MetaboAnalyst 5.0.

4.5.27 Macromolecular Biosynthesis Assay:

The inhibition of macromolecules by HSGN-94 at (0.125–4X MIC) were assayed in triplicate via scintillation counting using the previously reported procedure[222].

4.5.28 MRSA Murine Skin Infection Model:

The mice study was approved by the Purdue Animal Care and Use Committee and conducted in accordance with the National Institutes of Health Guide for the Care and Use of Laboratory Animals. Twelve-week-old female Balb/c mice (Jackson laboratories, ME, USA), weighing on average 20 grams, were used for this study. Mice were housed in ventilated cages with access to water and food ad libitum. MRSA murine skin infection model was performed as described in previous reports[223-225]. One day prior to formation of skin wounds, the fur along the dorsal region of mice was shaved and disinfected with 70% ethanol. Thereafter, the dorsal skin just caudal to the scapulae was pinched and two excisional 6-mm diameter wounds were made in each mouse using a 6 mm-diameter sterile biopsy punch (Sklar instruments, PA, USA) in the shaved dorsal regions under isoflurane anesthesia. Mice received a subcutaneous injection of 0.03 mg/kg buprenorphine immediately before application of biopsy punches to reduce pain. Excisional wounds were infected with 20 µL (per each wound) of 4.2×10^9 CFU/mL MRSA USA300 and covered with Tegaderm film (3M, MN, USA) that is fixed with Uro-Bond V silicone adhesive (Urocare, CA, USA). The infection was allowed to proceed for two days before initiating treatment. On the first day of treatment, mice were randomly divided into groups of five mice, and they subsequently received treatments. One group was injected clindamycin I.P. (25 mg/kg once daily).

The formed wounds for the remaining groups were treated topically twice daily with either 2% HSGN-94, 2% mupirocin, or the vehicle alone (petroleum jelly). Tegaderm was applied over the wounds after each treatment to prevent mice from biting, scratching, or grooming the area around the wounds. After five days, mice were humanely euthanized, 12 hours after the last dose, via CO_2 asphyxiation and the skin tissue of each wound was harvested aseptically. For each mouse, the left wound was fixed in 10% formalin for histopathological analysis (H&E staining) and the right wound was homogenized in sterile PBS using an Omni tissue homogenizer (Omni International, GA, USA). To determine the bacterial load in the wounds, the homogenate was serially diluted in PBS and aliquots of each dilution were plated on mannitol salt agar plates (to select for MRSA colonies). The plates were incubated for at least 18 hours at 37°C before bacterial colonies were enumerated.

4.5.29 Expression of Proinflammatory Cytokines:

Skin homogenates obtained from the right wound of each mouse were centrifuged (10,000 rpm for 10 minutes) and the supernatant was transferred to a separate tube. For each treatment group, 100 µL aliquots from each sample (from all five mice) were pooled together. The total protein content for each sample was measured via the bicinchoninic acid assay, standardized, and expression of cytokines and growth factors was subsequently determined via the Quantibody Mouse cytokine array 4000 kit (RayBiotech Life, Norcross, GA). The concentrations of cytokines (pg/mL) in each treatment group was calculated and presented as a bar graph using GraphPad Prism 8.0 (La Jolla, CA).

4.5.30 Evaluation of Inflammation via Histopathology:

The left wound of infected mice in all the four three groups of diabetic mice (vehicle, HSGN-94, mupirocin and clindamycin) were aseptically harvested after mice were euthanized and evaluated histologically. Sections of affected skin were removed and placed in 10% neutral-buffered formalin for 24 hours. Tissues were processed over 10 hours using a Sakura Tissue-Tek VIP6 tissue processor. Tissues were processed sequentially in 70%, 80%, 95%, and 100% ethanol, followed by xylene and paraffin, and were embedded in Surgipath Paraplast Plus (Leica Biosystems, Wetzlar, Germany). Tissue sections, 4-µm thickness, were placed on charged slides,

stained with hematoxylin and eosin (H & E), and cover- slipped using a Leica ST5010-CV5030 integrated workstation.All stained slides were scanned using Aperio® VERSA is a whole glass slide scanner. All slides were analyzed by a board certified veterinary pathologist.

4.6 Acknowledgments

G. Naclerio synthesized all compounds in study. G. Naclerio and N. Abutaleb performed MIC assays. G. Naclerio performed TLC of lipid extracts, MALDI mass spectrometry, and RT-qPCR. C. Karanja performed global proteomics, pull-down assay, and MRM experiments. N. Abutaleb did *in vivo* experiment, cytokine expression assay, and histopathology. K. Onyedibe did macromolecular synthesis assay. G. Naclerio and H. Sintim wrote the manuscript.

CHAPTER 5. POTENT TRIFLUOROMETHOXY, TRIFLUOROMETHYLSULFONYL, TRIFLUOROMETHYLTHIO AND PENTAFLUOROSULFANYL CONTAINING (1,3,4-OXADIAZOL-2-YL)BENZAMIDES AGAINST DRUG-RESISTANT GRAM-POSITIVE BACTERIA

This chapter was reproduced from *RSC Med. Chem.*, **2020**, *11*, 102-110 with permission from the Royal Society of Chemistry.

5.1 Abstract

According to the Centers for Disease Control and Prevention (CDC), methicillin-resistant *Staphylococcus aureus* (MRSA) affects about 80,000 patients in the US annually and directly causes about 11,000 deaths. Therefore, despite the fact that there are several drugs available for the treatment of MRSA, there is a need for new chemical entities. We previously reported that a 1,3,4-oxadiazolyl sulfonamide F6, was bacteriostatic and inhibited MRSA strains with a minimum inhibitory concentration (MIC) of 2 μg/mL. Here, we report the discovery of trifluoromethoxy (OCF_3), trifluoromethylsulfonyl (SO_2CF_3), trifluoromethylthio (SCF_3) and pentafluorosulfanyl (SF_5) containing (1,3,4-oxadiazol-2-yl)benzamides exhibiting potent antibacterial activities against MRSA. Interestingly, whereas the OCF_3 and SO_2CF_3 containing oxadiazoles were bacteriostatic, the SCF_3 and SF_5 containing oxadiazoles were bactericidal. They exhibited a wide spectrum of activity against an extensive panel of Gram-positive bacterial strains, including MRSA, vancomycin resistant *Staphylococcus aureus* (VRSA), vancomycin resistant *enterococcus* (VRE) and *Streptococcus pneumoniae*. Furthermore, compounds 6 and 12 outperformed vancomycin in clearing intracellular MRSA in infected macrophages. Moreover, the tested compounds behaved synergistically or additively with antibiotics used for treatment of MRSA infections.

5.2 Introduction

On February 27, 2017, the World Health Organization (WHO) published a list of bacteria for which new antibiotics are urgently needed. This first ever list of antibiotic-resistant "priority pathogens", comprises 12 families of bacteria that pose the greatest threat to human health[226]. Methicillin-resistant, vancomycin-intermediate and vancomycin-resistant *Staphylococcus aureus*

were listed as high priority category that requires development of new antibiotics. *S. aureus*, a Gram-positive bacterial pathogen, is one of the leading causes of community- and hospital-acquired infection[107]. The rise in antimicrobial resistant strains partly contributes to the increasing death rate associated with *S. aureus* infection[108]. For instance, methicillin-resistant *S. aureus* (MRSA) bacteremia is accompanied by higher mortality rates compared to methicillin-sensitive *S. aureus* (MSSA) bacteremia[109]. Moreover, deadly staphylococcal infections are still a global threat. According to the Centers for Disease Control and Prevention (CDC), more than 119,000 people suffered from bloodstream *S. aureus* infections in the United States in 2017, and nearly 20,000 died. Therefore, the need for novel anti-MRSA therapies cannot be overemphasized.

Despite the availability of drugs that are effective against MRSA, such as vancomycin, trimethoprim-sulfamethoxazole, clindamycin, tetracycline, doxycycline, minocycline, daptomycin, rifampin or linezolid[151], about 14% of patients who get serious MRSA infections die[132]. The majority of the aforementioned drugs used to treat MRSA have limitations that preclude certain patient class. For example, vancomycin is not appropriate for patients with reduced kidney function (such as elderly or diabetic patients)[152]. Additionally, *S. aureus* strains, which are resistant to the most commonly used antibiotics such as vancomycin[152], trimethoprim-sulfamethozole[153], linezolid[227], clindamycin[228] and daptomycin[229] has also been well documented. Therefore, the increase in resistance to commonly used drugs for MRSA infections, along with growths in both hospital and community acquired MRSA infections demonstrate the vital need for new entities that are active against MRSA.

We previously reported that F6 was active against MRSA with a minimum inhibitory concentration (MIC) of 2 μg/mL[117]. F6 was found to be bacteriostatic, non-toxic and efficacious in a mouse wound infection model. It was determined in the previous report that the 3,5-dimethylpiperidinyl sulfonamide moiety was essential for antibacterial activity. In this report, we revealed that whereas substitution of the 3,5-dimethylpiperidinyl sulfonamide moiety with most groups abrogated antibacterial activity, substitution with the trifluoromethylsulfonyl, trifluoromethoxy, trifluoromethylthio and pentafluorosulfanyl groups afforded analogs that were more potent than F6.

A few bioactive compounds, which also bear the trifluoromethoxy, trifluoromethylsulfonyl, trifluoromethylthio and pentafluorosulfanyl groups have been reported (Figure 5.1). DSM265 (a new antimalarial drug) completed phase IIa clinical trials (NCT02123290)[230]. DSM265 is orally

bioavailable with favorable pharmacokinetics, revealing that the pentafluorosulfanyl group is appropriate to append to potential drugs. Likewise, the pentafluorosulfanyl containing COX-2 inhibitor has been shown to reduce inflammation and pain *in vivo*[231]. As for trifluoromethylthio-containing compounds, Triflorex is an FDA approved drug for the treatment of anorexia[232]. Triflorex is given orally, demonstrating that the trifluoromethylthio group can be adequately substituted on potentially bioactive compounds. The trifluoromethylsulfonyl and trifluoromethoxy groups are increasingly being introduced into bioactive compounds. For example, Rilutek (FDA approved for the treatment of amyotrophic lateral sclerosis (ALS)) and Saprisartan (approved for hypertension) contain the trifluoromethoxy and trifluoromethylsulfonyl groups respectively (Figure 5.1)[233-234].

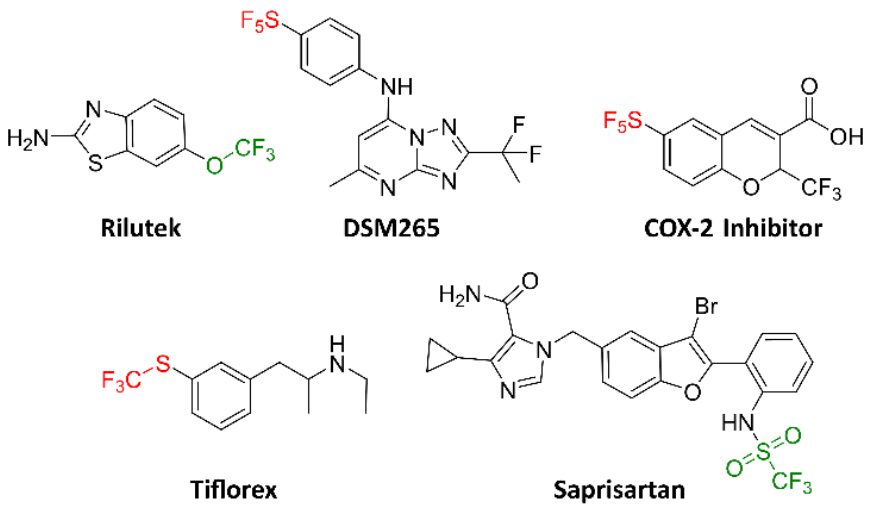

Figure 5.1 Trifluoromethoxy, trifluoromethylsulfonyl, trifluoromethylthio, and pentafluorosulfanyl containing bioactive molecules.

5.3 Results and Discussion

5.3.1 Synthesis of (1,3,4-oxadiazol-2-yl)benzamides and evaluation of their antibacterial activity

Our group has been interested in discovering novel chemotypes that are active against drug-resistant bacteria. F6 and its analogs were readily made in one step via amide coupling. Coupling reagents such as 1-Ethyl-3-(3-dimethylaminopropyl)carbodiimide hydrochloride (EDC·HCl), hydroxybenzotriazole (HOBt), or (2-(1H-benzotriazol-1-yl)-1,1,3,3-tetramethyluronium hexafluorophosphate (HBTU) were either unsuccessful or low-yielding whereas using

benzotriazol-1-yloxytris(dimethylamino)phosphonium hexafluorophosphate (BOP) reagent resulted in product yield up to 43%. Using methylithium to deprotonate the amine, followed by coupling with the acid chloride also afforded products in up to 25% yield. Having developed the methodology to make F6, we applied the BOP reagent to make a series of analogs bearing electron-withdrawing and donating groups (Figure 5.2)[235]. These compounds were initially screened for their ability to inhibit the growth of *S. aureus* at 16 μg/mL (Figure 5.3). For compounds that showed inhibitory activity, we determined the MIC (Table 5.1). From these results, compounds bearing, trifluoromethyl (5), trifluoromethylsulfonyl (6), trifluoromethoxy (11), trifluoromethylthio (12), and pentafluorosulfanyl (13) groups were active but not others (Figure 5.3 and Table 5.1). Interestingly, it appears that electron-withdrawing ability alone did not dictate antibacterial activity. For example, compounds bearing 4-cyano (2) -nitro (3), and -fluoro (4) groups had low to moderate activity. Furthermore, compounds containing hydrophilic electron donating groups (7) were not active (Figure 5.3). The degree of fluorination also had an effect on antibacterial activity for sulfur and oxygen containing compounds. For instance, MICs for methylthio (10), difluoromethylthio (9), trifluoromethylthio (12), and pentafluorosulfanyl (13) were 8 μg/mL, 4 μg/mL, 0.5 μg/mL, and 0.5 μg/mL respectively. MICs for compounds 8 and 11 were 32 μg/mL and 1 μg/mL respectively.

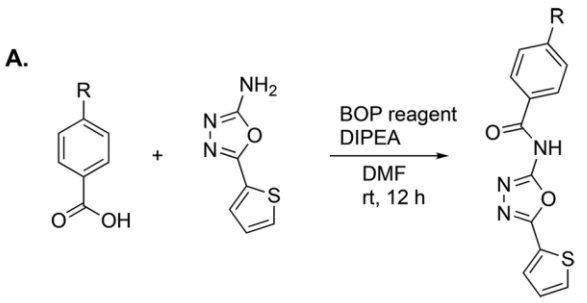

B. Analogs Containing Electron-Withdrawing or Electron-Donating Groups

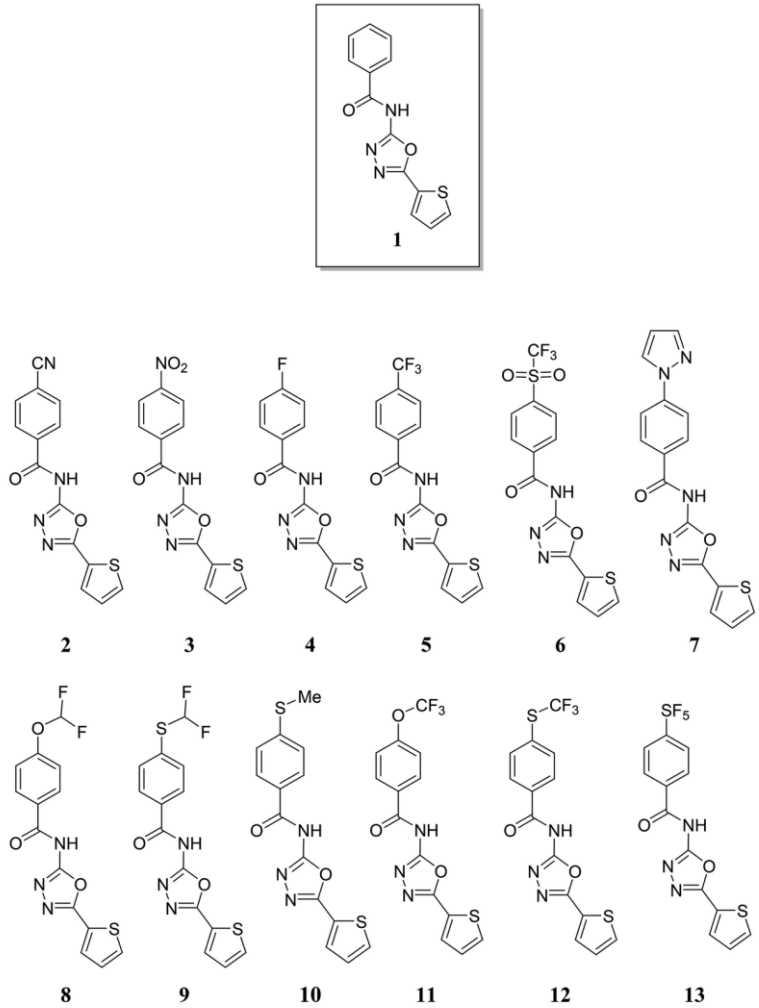

Figure 5.2 A. Synthetic scheme for the synthesis of analogs using BOP reagent. BOP = Benzotriazol-1-yloxy-tris (dimethylamino)phosphonium hexafluorophosphate; DIPEA = *N*,*N*-diisopropylethylamine; DMF = dimethylformamide. B**.** Analogs containing either electron-withdrawing or electron-donating groups.

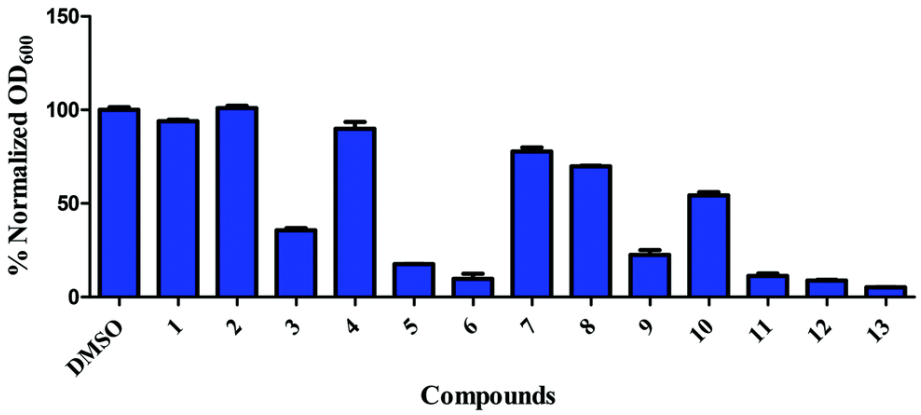

Figure 5.3 Inhibition of growth of *S. aureus* ATCC 25923 by 1,3,4-(oxadiazol-2-yl)benzamides. *S. aureus*, at early exponential growth, was treated with either DMSO or 16 µg/mL of compounds and OD_{600} measured after 24h. Error bars represent standard error of the mean of duplicates.

Table 5.1 Initial screening (MIC, µg/mL) of (1,3,4-oxadiazol-2-yl)benzamides against *Staphylococcus aureus* ATCC 25923 and methicillin-resistant *Staphylococcus aureus* (MRSA) ATCC 33592

Compound/Control Antibiotic	*S. aureus* ATCC 25923	MRSA ATCC 33592
3	4	8
4	32	32
5	2	2
6	0.5	0.5
8	32	32
9	4	4
10	4	4
11	1	1
12	0.5	0.5
13	0.25	0.5
Vancomycin	1	1
Linezolid	2	2

After identifying compounds 5, 6, 11, 12, and 13 as being potent against MRSA, we next investigated other trifluoromethyl-substituted heteroaromatic compounds (Figure 5.4). Unfortunately, this series was not as active as our original hit molecules (compare MICs for 5, 6, 11, 12, and 13, Table 4.1, with compounds 14–17, Table 5.2), demonstrating that the phenyl group is needed for optimal antibacterial activity.

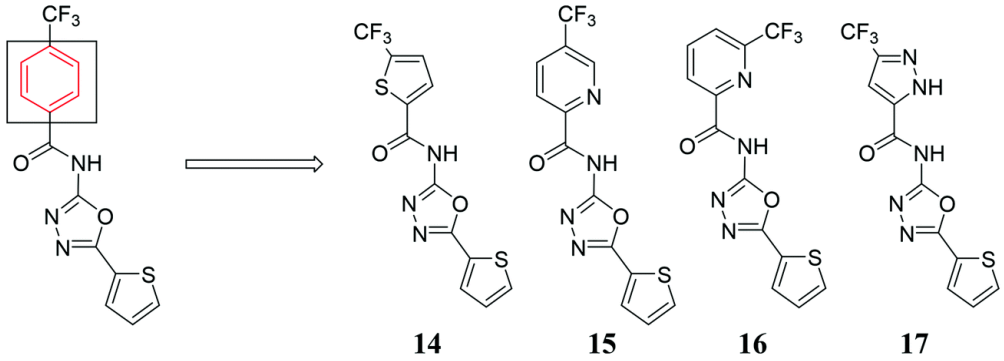

Figure 5.4 Trifluoromethyl-substituted heteroaromatic compounds synthesized.

Table 5.2 Initial screening (MIC, in µg/mL) of other trifluoromethyl-substituted heteroaromatic compounds against *Staphylococcus aureus* ATCC 25923 and MRSA ATCC 33592

Compound	*S. aureus* ATCC 25923	MRSA ATCC 33592
14	4	2
15	64	32
16	16	16
17	>64	>64

5.3.2 Compounds 6, 11, 12, & 13 are not active against Gram-negative bacteria

We next moved to test if compounds 6, 11, 12, and 13 were effective against Gram-negative bacteria. Thus, we tested the compounds viability against clinically relevant Gram-negative bacterial strains. Compounds 6, 11, 12, and 13 did not inhibit the growth of *Escherichia coli* ATCC 25404, *Pseudomonas aeruginosa* ATCC 27853, and *Acinetobacter baumannii* 19606 RW4 at concentrations of 16 µg/mL (Figure 5.5).

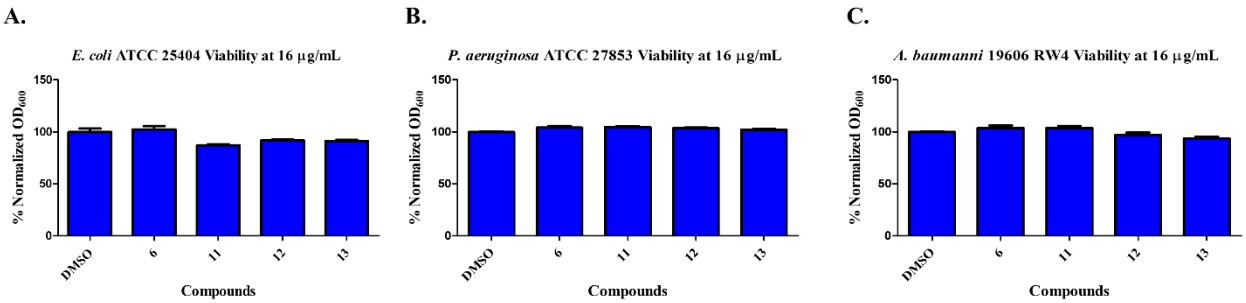

Figure 5.5 Inhibition of growth of A) *E. coli* ATCC 25404; B) *P. aeruginosa* ATCC 27853; C) *A. baumannii* ATCC 19606 by compounds 6, 11, 12, & 13 at 16 µg/mL.

5.3.3 Comprehensive antibacterial profile of compounds 6, 11, 12 and 13 against multidrug-resistant Gram-positive clinical strains

After the initial screening of compounds 6, 11, 12 and 13, we assessed their antibacterial profile against a panel of multidrug-resistant staphylococcal isolates. Compound 6 inhibited growth of the tested strains at concentrations ranging from 4 to 8 µg/mL. Compounds 11, 12 and 13 exhibited a potent activity inhibiting the tested multidrug-resistant staphylococcal strains at concentrations ranging from 0.06 to 2 µg/mL (Table 5.3). Furthermore, compounds 6, 11, 12 and 13 maintained the same potent activity against other clinically relevant Gram-positive bacterial species including vancomycin-resistant enterococci (VRE), multidrug-resistant *Streptococcus pneumoniae* and *Listeria monocytogenes* (Table 5.4). Compounds 11, 12 and 13 exhibited potent activity against *S. epidermidis*, which represents the most common source of infections on implanted medical prosthetic devices due to its huge ability to form strongly adherent biofilms that have intrinsic resistance to antibiotics and the host defense systems[236-237]. Moreover, the compounds kept their superiority over vancomycin against vancomycin-resistant enterococci (VRE). VRE were indicated as the leading cause of nosocomial infections in the USA, causing about 20-30% of hospital-acquired infections and the second major cause of such infections across the world [238]. Moreover, according to the World of Health Organization (WHO), vancomycin-resistant *E. faecium* is categorized as one of twelve bacterial pathogens that urgently need the development of new therapeutics and alternative strategies to combat their infections[239]. Additionally, compounds 6, 11, 12 and 13 exhibited a potent activity against *S. pneumoniae* inhibiting the tested strains at concentrations ranging from 0.125 to 2 µg/mL. *S. pneumoniae* is categorized by CDC as a serious threat bacterium that require prompt and sustained action to overcome its problems. It is associated with 1,200,000 infections yearly with about 7000 deaths in

USA alone. *S. pneumoniae* is responsible for an estimated $96 million in medical costs per year and is the leading cause of bacterial pneumonia and meningitis in the United States. It is also a major cause of bloodstream, ear and sinus infections[240].

Table 5.3 The minimum inhibitory concentration (MIC in μg/mL) of compounds 6, 11, 12 and 13 against methicillin-sensitive Staphylococcus aureus, methicillin-resistant Staphylococcus aureus (MRSA) and vancomycin-resistant Staphylococcus aureus (VRSA) strains.

Bacterial strains	Compounds/ Control antibiotics					
	6	11	12	13	Vancomycin	Linezolid
Methicillin-sensitive *Staphylococcus aureus* ATCC 6538	8	1	0.5	0.5	1	0.5
Methicillin-sensitive *Staphylococcus aureus* NRS 107	4	1	0.25	0.125	1	0.5
MRSA NRS 119	8	1	0.5	0.06	1	>64
MRSA NRS382 (USA100)	8	1	0.5	0.5	2	1
MRSA NRS383 (USA200)	8	2	0.25	1	1	1
MRSA NRS384 (USA300)	4	0.5	0.5	0.5	1	1
MRSA NRS123 (USA400)	4	1	0.5	0.25	1	1
MRSA NRS 385 (USA500)	8	2	2	0.5	2	1
MRSA NRS 386 (USA700)	4	1	0.5	0.125	1	1
MRSA NRS 387 (USA800)	4	2	0.125	0.25	2	1
MRSA NRS 483 (USA1000)	4	1	0.5	0.25	2	1
MRSA NRS 484 (USA1100)	4	0.5	0.5	0.5	2	2
VRSA 10	4	1	0.5	0.25	>64	1
VRSA 12	8	1	0.5	0.125	>64	1

Table 5.4 The minimum inhibitory concentration (MIC in µg/mL) of compounds 6, 11, 12 and 13 against a panel of clinically important Gram-positive bacterial pathogens including *Staphylococcus epidermidis*, *Streptococcus pneumoniae*, *Enterococcus faecalis*, *Enterococcus faecium* and *Listeria monocytogenes*.

Bacterial strains	Compounds/ Control antibiotics					
	6	11	12	13	Vancomycin	Linezolid
Staphylococcus epidermidis NRS101	4	0.5	0.25	0.06	2	1
Cephalosporin- resistant *Streptococcus pneumoniae* ATCC 51916	2	2	0.25	0.25	0.5	1
Methicillin- resistant *Streptococcus pneumoniae* ATCC 700677	1	1	0.25	0.125	1	1
Enterococcus faecalis ATCC 51299 (VRE)1	4	8	4	2	32	1
Enterococcus faecium ATCC 700221 (VRE)	4	4	4	2	>64	1
Listeria monocytogenes ATCC 19111	2	2	0.5	0.125	0.5	0.5

5.3.4 Compounds 6, 11, 12 and 13 are highly tolerable to human cell lines

Selectivity towards prokaryotic cells is an essential attribute for any antibiotic candidate. In this regard, compounds 6, 11, 12 and 13 were assessed for toxicity to mammalian cells, and

they exhibited an excellent safety profile against human colorectal cells (Caco-2) (Figure 5.6). Compounds 6, 11 and 12 were highly tolerable to Caco-2 cells at concentrations higher than 128 µg/mL. This concentration is 256-times higher than the compound's corresponding MIC value against MRSA ATCC 33592 used in the initial screening. Compound **13** was non-toxic to Caco-2 cells up to 64 µg/mL, which is 128-times higher than the compound's MIC against MRSA ATCC 33592.

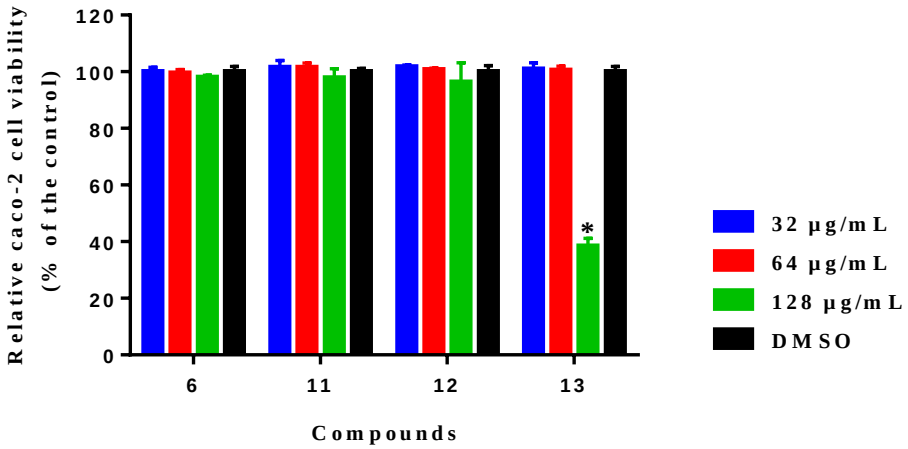

Figure 5.6 Toxicity analysis of compounds 6, 11, 12 and 13 (tested in quadruplicates at 32, 64 and 128 µg/mL) against human colorectal cells (Caco-2) using the MTS 3-(4,5-dimethylthiazol-2-yl)-5-(3-carboxymethoxyphenyl)-2-(4-sulfophenyl)-2H-tetrazolium) assay. Results are presented as percent viable cells relative to DMSO (negative control to determine a baseline measure for the cytotoxic impact of each compound). The absorbance values represent an average of four samples analyzed for each compound. Error bars represent sample standard deviation values. The data were analyzed via two-way ANOVA with post-hoc Dunnett's test for multiple comparisons ($P<0.05$).

5.3.5 Compounds 6, 11, 12, & 13 do not lyse red blood cells

Hemolysis can have serious implications on organ function. For instance, hemolysis has been shown to cause reduced nitrous oxide signaling, resulting in higher systolic, diastolic and mean arterial blood pressure, as well as cardiovascular and renal dysfunction, inflammation, thrombosis, and enhanced susceptibility to infections[241]. Thus, we sought to determine if our compounds would lyse RBCs. All compounds were safe to RBCs at concentration higher than 128 µg/mL as presented by their HC_{50}; the concentration of each compound causing 50% hemolysis to RBCs. Compound 6 caused around 37% hemolysis to RBCs at the concentration of 128 µg/mL (256X MIC). Its hemolytic activity dropped to 35% and 23% at the concentrations of 64 and 32

µg/mL, respectively. Compounds 11, 12, and 13 caused little hemolysis (20%, 19% and 9%, respectively at the concentration of 128 µg/mL) with minimal hemolytic effect at the lower tested concentrations (Figure 5.7). Therefore, these results demonstrate that compounds 6, 11, 12, and 13 will have a minor hemolytic activity to human RBCs when used clinically to treat bacterial infections.

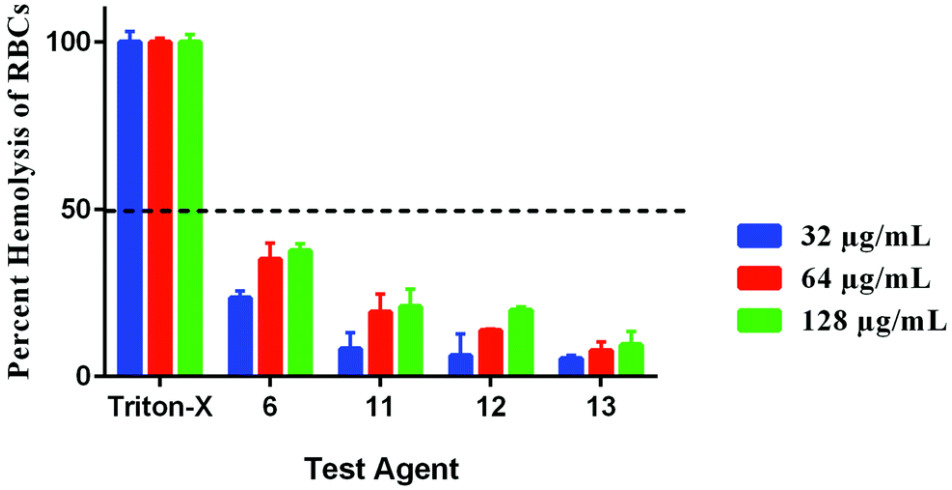

Figure 5.7 Hemolytic activity of compounds 6, 11, 12, and 13 (in triplicate) against human RBCs. The results are presented as percent RBCs hemolysis for each compound relative to triton-X (positive control showing complete hemolysis of RBCs). The absorbance values represent an average of three samples analyzed for each compound. Error bars represent sample standard deviation values.

5.3.6 Compounds 6 & 11 are bacteriostatic, while compounds 12 & 13 are bactericidal against MRSA

With the growing interest in drugs containing trifluoromethoxy, trifluoromethylsulfonyl, trifluoromethylthio, and pentafluorosulfanyl groups[242-243], we proceeded to analyze other aspects of antibacterial activity for compounds 6, 11, 12, and 13. We previously revealed that the 3,5-dimethylpiperidinyl sulfonamide, F6 is bacteriostatic[117]. Thus, we measured the minimum bactericidal concentration (MBC) for 6, 11, 12, and 13 against MRSA strain. Curiously, compounds 12 and 13 were bactericidal, whereas compounds 6 and 11 were bacteriostatic. Compounds' 12 and 13 MBC values were one-fold higher than their corresponding MICs. On the other hand, the MBC values of compounds 6 and 11 were more than 3-folds higher than their corresponding MICs (Table 5.3).

Table 5.5 The minimum bactericidal concentration (MBC, in µg/mL) of compounds 6, 11, 12, & 13 and control antibiotics against MRSA ATCC 33592.

Compounds/ Control antibiotics	MBC (µg/mL)
6	>128
11	>128
12	1
13	1
Vancomycin	1
Linezolid	>128

In order to confirm this mode of killing against MRSA, a time-kill kinetics assay was performed against MRSA ATCC 33592 (Figure 5.8). In concurrence with the previously shown MBC results (Table 5.5), compounds 6 and 11 exhibited a bacteriostatic activity while compounds 11 and 12 exhibited a bactericidal activity. After 24 hours, compounds 6 and 11 caused a 1.04- and 0.69-$\log_{10}$-reduction in the bacterial count, which was similar to linezolid that caused about 1.7-$\log_{10}$-reduction. In contrast, compounds 12 and 13 caused a 4.2- and 3.96-$\log_{10}$-reduction in CFU/mL respectively, which was similar to vancomycin. There are a few examples in the literature whereby researchers have replaced the CF_3, NO_2 or t-Butyl moieties in drugs or lead compounds with the SF_5 unit[244]. Here, we provide a cautionary tale that such replacements are not always conservative and could indeed change the mode of action of or response to a drug or lead compound. Future work, beyond the scope of this manuscript, will investigate the specific modes of actions of these compounds.

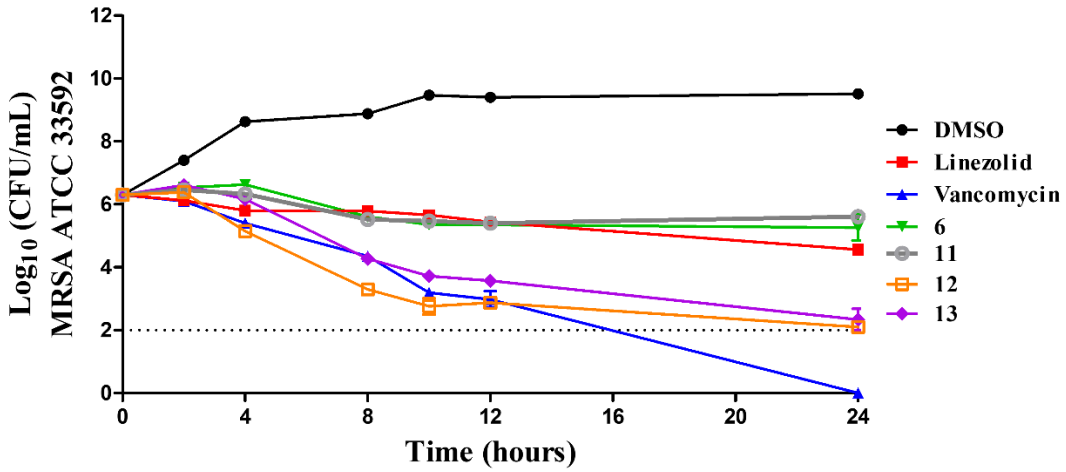

Figure 5.8 Time-kill kinetics analysis of compounds against MRSA ATCC 33592 using vancomycin and linezolid as control antibiotics.

5.3.7 Compounds 6 and 12 significantly kill intracellular MRSA

The rapid and potent antibacterial activity of the (1,3,4-oxadiazol-2-yl)benzamide compounds propelled us to investigate whether these compounds could gain entry inside macrophages infected with MRSA to reduce the burden of intracellular bacteria. *S. aureus* is a highly successful pathogenic bacteria due to extensive release of different virulence factors and its ability to evade host innate immune responses. *S. aureus* produces toxins, like leukocidin A/B, that are able to specifically target and kill phagocytes[245]. Additionally, it has been reported that intracellular MRSA can replicate within the phagolysosome after phagocytosis by macrophages thus permitting the organism to survive, escape from phagocytes, disseminate and cause chronic and persistent infections[246]. Most antibiotics, such as linezolid, β-lactams, vancomycin, aminoglycosides and oritavancin, are unable to target intracellular bacteria[247]. Consequently, antibacterial compounds capable of gaining entry inside infected macrophages are needed. In this regard, we tested the activity of compounds 6 (bacteriostatic compound) and 12 (bactericidal compound) in clearing intracellular MRSA. First, we tested the toxicity profile of compounds 6, 11, 12 and 13 against murine macrophages (J774), used for the intracellular infection experiment, and they showed excellent safety profile (Figure 5.9A) where they were tolerable at a concentration as high as 32 µg/mL. Therefore, we tested two of the compounds at 8 and 16 µg/mL. As depicted in Figure 5.9B, after 24 hours incubation, compound 6 generated a 0.5- and 0.6-$\log_{10}$ reduction of intracellular MRSA at 8 and 16 µg/mL respectively. On the other hand, compound 12 effectively

reduced the intracellular MRSA count where it generated 0.7- and 0.9-$\log_{10}$ reduction of intracellular MRSA at 8 and 16 µg/mL respectively. This activity was superior to vancomycin which was unable to reduce the burden of intracellular MRSA. This result indicates that (1,3,4-oxadiazol-2-yl)benzamides are advantageous over vancomycin in the ability to reduce the burden of intracellular MRSA within infected macrophages.

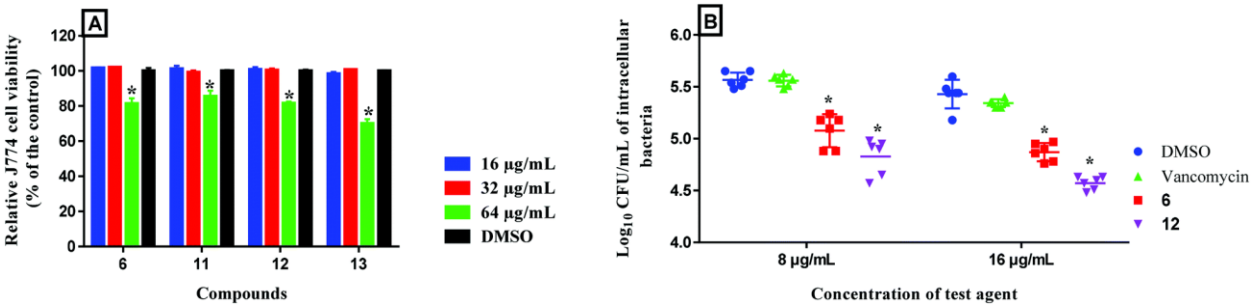

Figure 5.9 A) Toxicity analysis of compounds 6, 11, 12 and 13 (tested in triplicate at 16, 32 and 64 µg/mL) against murine macrophage (J774) cells using the MTS 3-(4,5-dimethylthiazol-2-yl)-5-(3-carboxymethoxyphenyl)-2-(4-sulfophenyl)-2H-tetrazolium) assay. The results are presented as percent viable cells relative to DMSO (negative control to determine a baseline measure for the cytotoxic impact of each compound). The absorbance values represent an average of three samples analyzed for each compound. Error bars represent sample standard deviation values. The data were analyzed via two-way ANOVA with post-hoc Dunnett's test for multiple comparisons to determine statistical difference between the values obtained for each compound and DMSO (*, $P < 0.05$). B) Effect of compounds 6 and 12 and vancomycin to reduce intracellular MRSA present inside murine macrophages (J774). Data are presented as $\log_{10}$ colony forming units of MRSA USA400 per mL inside infected murine macrophages after treatment with 8 and 16 µg/mL of either compounds 6, 12 or vancomycin (tested in triplicates) for 24-hours. Data were analyzed via two-way ANOVA, with post hoc Dunnet's test for multiple comparisons ($P < 0.05$), utilizing GraphPad Prism 6.0 (GraphPad Software, La Jolla, CA). The asterisk (*) represents a significant difference between the treatment of J774 cells with compounds 6 or 12 in comparison to vancomycin.

5.3.8 Synergistic interactions of Compounds 6, 11, 12, & 13 with standard antibiotics

Combination therapy is commonly used in the clinic to treat bacterial infections. For instance, beta-lactams like piperacillin, ceftaroline, and oxacillin are consistently combined with either vancomycin or daptomycin for the treatment of MRSA infections[248]. Therefore, we investigated the synergistic interactions of our compounds with 4 antibiotics. Interestingly, we discovered that compounds 12 and 13 synergize with methicillin, reducing the methicillin's MIC from 128 µg/mL to 32 µg/mL against MRSA 33592 (Table 5.6) with fractional inhibitory concentration index (FICI) of 0.5. Compounds 6 and 11 showed additivity when combined with methicillin, with compound 6 reducing methicillin's MIC to 4 µg/mL. Curiously, the 32-fold

reduction in methicillin's MIC when combined with compound 6 can be later explored in synthesizing analogs that can resensitize MRSA to methicillin. Furthermore, compound 11 demonstrated synergy with daptomycin, reducing its MIC from 0.5 μg/mL to 0.125 μg/mL. Daptomycin can cause nephrotoxicity and hepatotoxicity[249] so the potential to reduce the dosage needed for daptomycin could be clinically important. Compounds 6, 12, and 13 demonstrated additivity with daptomycin but these same compounds did not synergize with either linezolid or vancomycin (Table 5.6). Collectively, the results shed valuable insight into (1,3,4-oxadiazol-2-yl)benzamides that could serve as potential future partners with anti-MRSA agents.

Table 5.6 The cumulative fractional inhibitory concentration index (∑FICI) range of compounds 6, 11, 12, and 13 in combination with antibiotics against MRSA ATCC 33592. ∑FICI was interpreted as follows: ∑FICI of ≤0.5 is considered to demonstrate synergy (SYN). An ΣFICI of >0.5-1.25 was categorized as additive (ADD). ΣFICI of >1.25-4 was considered as indifference (IND), while ΣFICI values of > 4 were categorized as antagonistic.

		MIC alone	Combination MIC		∑FICI	Combination MIC		∑FICI	Combination MIC		∑FICI	Combination MIC		∑FICI
#	Antibiotic	Antibiotic	Antibiotic	6		Antibiotic	11		Antibiotic	12		Antibiotic	13	
1	Linezolid	2	2	0.0625	1.0	2	0.25	1.3	2	0.0625	1.1	2	0.5	1.5
2	Methicillin	128	4	1	0.5	16	0.5	0.6	32	0.25	0.5	32	0.25	0.5
3	Daptomycin	0.5	0.25	0.25	0.6	0.125	0.25	0.5	0.25	0.125	0.6	0.25	0.25	0.8
4	Vancomycin	1	1	0.0625	1.0	1	0.0625	1.1	0.5	0.5	1.0	0.5	0.5	1.0

5.4 Experimental Section

Please see the electronic supplementary information located on the RSC Medicinal Chemistry website for the following: Synthesis and characterization data of compounds (^{1}H, ^{13}C NMR and HRMS). Bacterial strains, media, cell lines and reagents used. Protocols for the determination of the MICs and MBCs against bacteria, synergy of compounds with standard antibiotics, in vitro cytotoxicity analysis of compounds 6, 11, 12 and 13 against human colorectal and murine macrophage cells, hemolysis assay, time-kill kinetics analysis, intracellular infection of J774 cells with MRSA and treatment with compounds 6 and 12. Table of bacterial isolates used in this study.

5.5 Conclusion

We have identified promising trifluoromethoxy, trifluoromethylsulfonyl, trifluoromethylthio, and pentafluorosulfanyl (1,3,4-oxadiazol-2-yl)benzamides with potent antibacterial activity against MRSA, VRSA and *S. pneumoniae*. Additionally, they showed a highly acceptable tolerability to human cell lines and did not lyse RBCs. Furthermore, compounds 6 and 12 outperformed vancomycin in clearing intracellular MRSA in infected macrophages. Moreover, compounds 12 and 13 behaved synergistically when combined with methicillin exhibiting ΣFICI of 0.50 against MRSA ATCC 33592 while compound 11 behaved synergistically with daptomycin exhibiting ΣFICI of 0.50 against the same strain. Consequently, these compounds could be potentially used alone or in combination with antibiotics against multidrug-resistant staphylococci. Overall, this work adds to the increasing number of reports that have attempted to address the anti-bacterial resistance issue with novel small molecules[70, 127-129, 250-256].

5.6 Author Contributions

G. Naclerio synthesized all compounds in study. G. Naclerio and N. Abutaleb performed MIC assays. N. Abutaleb performed cytotoxicity, red blood cell hemolysis, and intracellular clearance assays. G. Naclerio did MBC and time-kill assay. G. Naclerio and K. Onyedibe performed synergy experiments. G. Naclerio and H. Sintim wrote the manuscript. G. Naclerio, N. Abutaleb, H. Sintim, and M. Seleem edited the manuscript.

CHAPTER 6. ULTRAPOTENT INHIBITOR OF *CLOSTRIDIOIDES DIFFICILE* GROWTH, WHICH SUPPRESSES RECURRENCE *IN VIVO*

6.1 Abstract

Clostridioides difficile (*C. difficile*) is the leading cause of healthcare-associated infection in the U.S. and considered an urgent threat by the Centers for Disease Control and Prevention (CDC). Only two antibiotics, vancomycin and fidaxomicin, are FDA-approved for the treatment of *C. difficile* infection (CDI) but these therapies still suffer from high treatment failure and recurrence. Therefore, new chemical entities to treat CDI are needed. Trifluoromethylthio containing *N*-(1,3,4-oxadiazol-2-yl)benzamides displayed very potent activities (sub-μg/mL minimum inhibitory concentration (MIC) values) against Gram-positive bacteria. Here, we report remarkable antibacterial activity enhancement via halogen substitutions, which afforded new anti-*C. difficile* agents with ultrapotent activities (MICs as low as 0.003 μg/mL (0.007 μM)) that surpassed the activity of vancomycin against *C. difficile* clinical isolates. The most promising compound in the series, HSGN-218, was non-toxic to mammalian colon cells and is gut restrictive. In addition, HSGN-218 protected mice from CDI recurrence. Not only does this work provide a potential clinical lead for the development of *C. difficile* therapeutics but also it highlights dramatic drug potency enhancement via halogen substitution.

6.2 Introduction

Clostridioides difficile (*C. difficile*) is a spore-forming Gram-positive anaerobic bacterium and the leading cause of nosocomial infections as well as antibiotic-associated diarrhea in the United States[257]. In 2017, the Centers for Disease Control and Prevention (CDC) determined that in the U.S., 223,900 patients were hospitalized with *C. difficile* infection (CDI), resulting in 12,800 deaths and more than $1 billion in healthcare costs[47]. CDI causes severe diarrhea along with life-threatening complications such as toxic megacolon, pseudomembranous colitis, and systemic

inflammatory response syndrome[258]. Manifestations of the disease are credited to the toxin-mediated damage produced by two major toxins: toxin A (TcdA/enterotoxin) and toxin B (TcdB/cytotoxin), which catalyze the inactivation of Rho GTPases, ultimately causing intense inflammation of the gut, accompanied by necrosis and apoptosis of colonic mucosal cells[259-260]. Furthermore, *C. difficile*'s ability to produce spores hinders the clinical management of CDI because these spores are very resistant to environmental conditions, antibiotics, and disinfection processes. *C. difficile* spores can spread throughout the environment and once ingested by vulnerable hosts, they develop into vegetative cells that colonize the intestines, thereby producing toxins and establishing infection[261-262]. Therefore, *C. difficile* spores serve as the major cause of CDI circulation and recurrence.

CDI is typically caused from the use of antibiotics, which disrupts the reproduction of normal and protective gut microbiota, ultimately allowing *C. difficile* to grow in the colon and produce infectious toxins[263]. Although the overuse of antibiotics is one of the main reasons contributing to CDI, the management of CDI requires antibiotic treatment. Currently, there are only three drugs used to treat CDI: metronidazole, vancomycin, and fidaxomicin. Yet only vancomycin and fidaxomicin are approved by the FDA for treatment of CDI. Although, metronidazole was previously recommended as a first-line therapy for CDI, its use is now only limited to non-severe CDI cases when patients are unable to be treated with vancomycin or fidaxomicin[264]. Moreover, other limitations with metronidazole treatment are its potent activity against a wide spectrum of protective normal microbiota, as well as its high absorption (100% bioavailable) from the intestinal tract, restricting its concentrations in the colon[265-266]. Although oral vancomycin is minimally absorbed into the systemic circulation[267], it has broad spectrum activity against Gram-positive bacteria, leading to a reduction in microbiome diversity[268]. Furthermore, both vancomycin and metronidazole treatments are inadequate due to high treatment failure (14% with vancomycin and 22% with metronidazole) and high recurrence rates (25% to 30%). This is because both antibiotics are ineffective against spores and also they cause disruption of the beneficial gut microbiota[269-270]. Fidaxomicin is the only new drug approved for CDI in the last 30 years. Fidaxomicin has lower recurrence rates compared to vancomycin and metronidazole because of its selectivity towards *C. difficile*; however, its high cost limits its use[271-273]. Even though vancomycin and fidaxomicin are FDA-approved therapies for CDI, emerging resistance or reduced susceptibility are evident to these antibiotics[272, 274]. In addition, one emerging alternative

non-antibiotic therapy for CDI is fecal microbiota transplant (FMT), which restores the disrupted normal microbiome, leading to renovation of the colonization resistance to *C. difficile*[275]. While FMT appeared to be successful in the treatment of some CDI cases, it has many restrictions and poses a serious risk of transmitting infectious pathogens to the patients; especially immunocompromised and elderly patients[276-277]. Therefore, due to the increase in treatment failure and recurrence rates with the commonly used anti-CDI drugs, along with growths of CDI, efforts to develop novel anti-CDI therapeutics have intensified[156].

Our program focuses on the discovery of new *N*-(1,3,4-oxadiazol-2-yl)benzamides to combat the urgent threats of antibiotic-resistant bacteria[117, 134]. We previously reported the trifluoromethylthio-containing (1,3,4-oxadiazol-2-yl)benzamide, compound 12, as a potent anti-MRSA agent[164]. Compound 12 was found to have bactericidal activity as well as being non-toxic to mammalian cells[164]. Compound 12 was however not evaluated *in vivo* as it was not deemed an ideal lead due to the presence of a potential thiophene toxicophore (Figure 6.1). In this report, we describe the generation of a new series of trifluoromethylthio containing (1,3,4-oxadiazol-2-yl)benzamides, which leads to the identification of *N*-(5-(3,5-dichlorophenyl)-1,3,4-oxadiazol-2-yl)-4-((trifluoromethyl)thio)benzamide (HSGN-218), which does not contain a thiophene (Figure 6.1). HSGN-218 was tested for its activity against a panel of clinical pathogenic *C. difficile* strains. Cytotoxicity against mammalian cells, bi-directional Caco-2 permeability and activity against normal gut microbiota were also investigated. Moreover, the activity of HSGN-218 treatment was evaluated in an *in vivo* CDI mouse model and its ability to prevent *C. difficile* recurrence *in vivo* was also investigated.

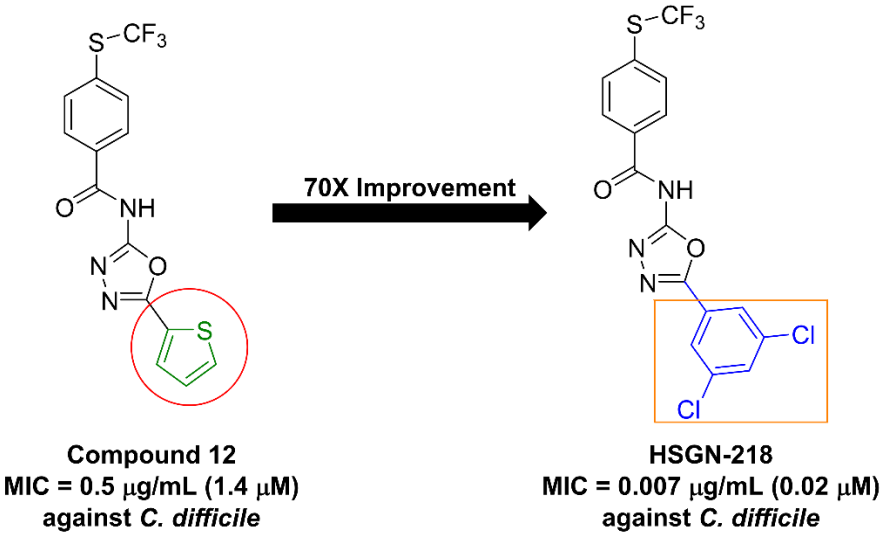

Figure 6.1 Compound 12 contains a potential thiophene toxicophore but was found to be potent against C. difficile. Utilization of halogen substitution led to the discovery of an ultrapotent anti-*C. difficile* agent (HSGN-218**)** with a 70-times imporvement in potency (from 0.5 μg/mL (1.4 μM) to 0.007 μg/mL (0.02 μM).

6.3 Results and Discussion

6.3.1 Halogenation, a High-Level Medicinal Chemistry Design Strategy

Halogens (X = F, Cl, Br, and I) are commonly used substituents in medicinal chemistry and drug discovery[278-281]. For instance, around 40% of the drugs currently FDA-approved or in clinical trials are halogenated and about 25% of the published medicinal chemistry papers and patents contain the late stage addition of halogen atoms[279]. Likewise, 35% of the top-15 selling drugs from 2010 to 2016 are halogenated[282] (Figure 6.2A). Of the halogenated drugs, 57% contain fluorine, 38% contain chlorine, 4% contain bromine, and only 1% contain iodine[279]. The addition of halogen substitutents has been shown to have a major effect on a drug's potency and pharmacological properties. Regarding pharmacological properties, addition of halogen substituents to lead compounds has been shown to increase lipophilicity, permeability, membrane binding and metabolic stability[283-284]. Likewise, insertion of halogen atoms into lead-like compounds also showed enhanced drug metabolism because the carbon-halogen bond is not easily metabolized by cytochrome P450[279]. Concerning potency, halogen atom substitution's effect has been documented. For example, L86-8276, a cyclin-dependent kinase 2 (CDK2) inhibitor was shown to have an IC_{50} value of 2.4 μM (Figure 6.2B)[285]. Yet, the addition of a chlorophenyl group

to give Flavopiridol showed a six-fold improvement in potency to give an IC_{50} of 0.4 μM against CDK2 (Figure 6.2B)[285].

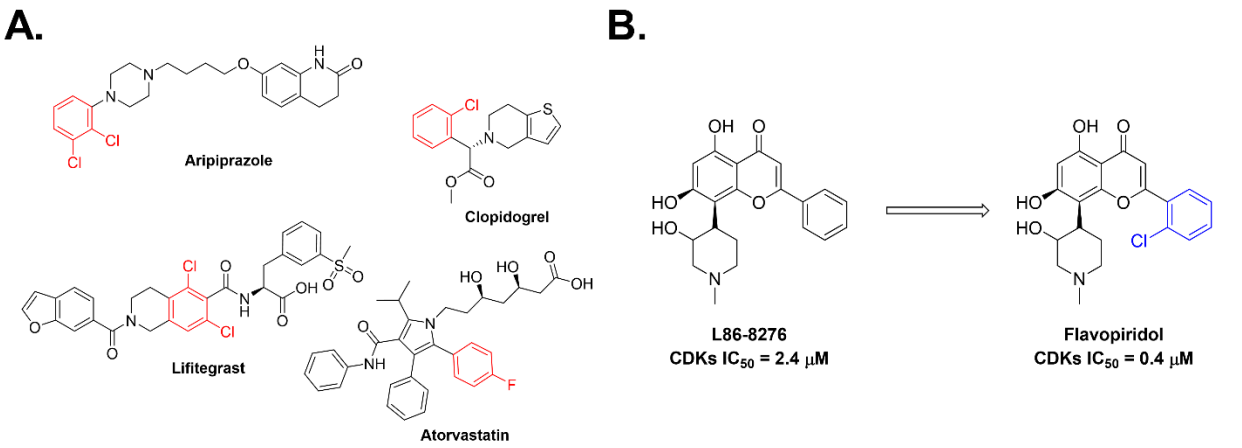

Figure 6.2 Importance of the addition of halogen substituents to lead compounds. A. Examples of the top-15 selling drugs that are halogenated. B. Addition of chlorophenyl to CDK2 inhibitors led to a six-fold enhancement in potency.

6.3.2 Synthesis and Anti-C. difficile Activity of Trifluoromethylthio Containing (1,3,4-oxadiazol-2-yl)Benzamides

We previously reported that compound 12 was potent against a panel of clinically important Gram-positive bacteria[164]. Based on its broad-spectrum Gram-positive activity, we wondered if it would be active against *C. difficile*. Compound 12 inhibited *C. difficile* ATCC BAA 1801 with an MIC of 0.5 μg/mL (1.4 μM) (see Figure 1 and Table 1), which is comparable to vancomycin. However, compound 12 contains an unsubstituted thiophene moiety, which can lead to toxicity concerns (Figure 6.1). For instance, thiophene metabolism, caused by cytochrome P450 mediated oxidation, can lead to the formation of reactive metabolites, thiophene-S oxides[286-287], thiophene epoxides[287], and sulphenic acids[288], which have a high propensity to react with nucleophiles such as water and glutathione[289]. We were however encouraged that compound 12 showed good activity against *C. difficile*, so we proceeded to make new analogs, which did not contain thiophene but instead substituted phenyl groups.

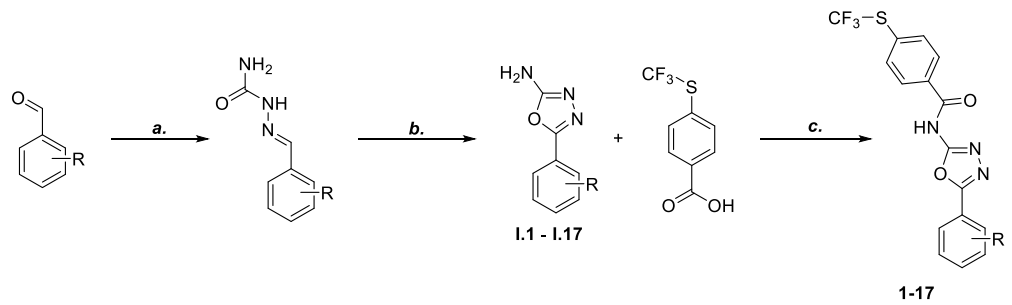

Scheme 6.1 General Route for the Synthesis of trifluoromethylthio-containing *N*-(1,3,4-oxadiazol-2-yl)benzamides[a]. [a]Reagents and Conditions: (*a*) Semicarbazide hydrochloride, NaOAc, MeOH:H_2O (1:1), rt, 30 min, 95% (*b*) Bromine, NaOAc, AcOH, 60 °C, 1 h, 40% - 70% (*c*) BOP Reagent, DIPEA, DMF, rt, 12 h, 16% - 33%.

In our previous report[164], we determined that the 4-(trifluoromethylthio)phenyl group is vital for optimal activity so we kept this constant. The synthesis of the compounds began with a substituted benzaldehyde followed by the addition of semicarbazide and sodium acetate to give the corresponding semicarbazone. Then, using bromine and sodium acetate, the semicarbazone was cyclized into the subsequent 1,3,4-oxadizol-2-amine (Scheme 6.1). Amide coupling between the 1,3,4-oxadiazol-2-amine and 4-trifluoromethylthio benzoic acid using benzotriazol-1-yloxytris(dimethylamino)phosphonium hexafluorophosphate (BOP) reagent gave the desired trifluoromethylthio containing (1,3,4-oxadiazol-2-yl)benzamides (Scheme 6.1).

With the compounds in hand (see Table 6.1), we proceeded to evaluate them against *C. difficile*. Halogen substitutions (especially the Cl, F or CF_3 groups) resulted in the most active compounds. Substitution with OMe, Me, and *i*-propy groups showed only moderate to no actvity (see Table 6.1 for MICs of compounds 6, 11, 12, and 13 against *C. difficile* ATCC BAA 1801). For halogen substituents, the position on the phenyl ring was also important. For example, the MIC for *meta*-Cl (5) was 0.03 µg/mL (0.08 µM), whereas that for the *ortho*- (3) and *para*- (9) analogs were 4 µg/mL (10.0 µM) and 2 µg/mL (5.0 µM) respectively against *C. difficile* ATCC BAA 1801 (Table 6.1). Additionally, for di-substituted halogen containing compounds, the position of the halogens affected actvity. For instance, the 3,5-dichlorophenyl analog (15, HSGN-218) was more than four times more potent than the 2,4-dichlorophenyl (14) analog (MIC = 0.06 µg/mL and 0.007 µg/mL for 14 and 15 respectively). We also proceeded to investigate subsitution of the phenyl group with heteroaromatics, such as pyridinyl (17) which had only moderate activity (Table 6.1) allowing us to conclude that the phenyl ring is needed for optimal activity.

Table 6.1 MICs in µg/mL (µM) of HSGN-218, analogs, and vancomycin, against *C. difficile* ATCC BAA 1801.

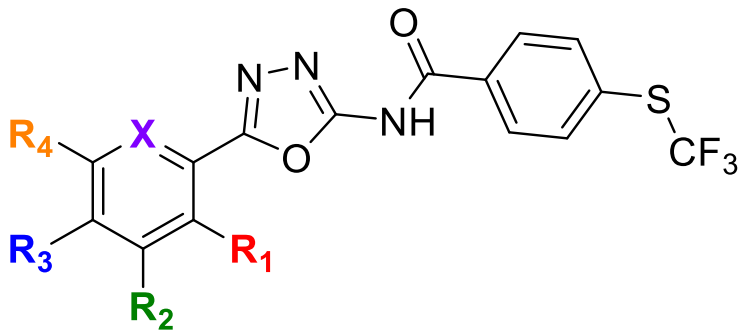

Compound/Control Antibiotic	-R_1	-R_2	-R_3	-R_4	X	MICs in µg/mL (µM)
Compound 12	-	-	-	-	-	0.5 (1.4)
1	H	H	H	H	CH	2 (5.5)
2	F	H	H	H	CH	4 (10.4)
3	Cl	H	H	H	CH	4 (10.0)
4	H	F	H	H	CH	0.03 (0.08)
5	H	Cl	H	H	CH	0.03 (0.08)
6	H	OMe	H	H	CH	4 (10.1)
7	H	CF_3	H	H	CH	0.015 (0.04)
8	H	H	F	H	CH	4 (10.4)
9	H	H	Cl	H	CH	2 (5.0)
10	H	H	CF_3	H	CH	0.125 (0.29)
11	H	H	OMe	H	CH	4 (10.1)
12	H	H	CH_3	H	CH	4 (10.5)
13	H	H	*i*-Propyl	H	CH	128 (314.2)
14	Cl	H	Cl	H	CH	0.03 (0.07)
15; HSGN-218	H	Cl	H	Cl	CH	0.007 (0.02)
16	OMe	H	H	Cl	CH	2 (4.7)
17	H	H	H	H	N	8 (21.8)
Vancomycin	-	-	-	-	-	1 (0.7)
Metronidazole	-	-	-	-	-	0.25 (1.46)
Fidaxomicin	-	-	-	-	-	0.06 (0.06)

6.3.3 Comprehensive antibacterial profile of HSGN-218 against various C. difficile clinical isolates

After the initial screening of HSGN-218, we assessed its antibacterial profile against a panel of *C. difficile* clinical isolates. As depicted in Table 6.2, HSGN-218 exhibited exceptional actvity against *C. difficile* clinical isolates with MICs ranging from 0.003 µg/mL (0.007 µM) to 0.03 µg/mL (0.07 µM). Vancomycin displayed MICs ranging from 0.25 µg/mL (0.2 µM) to 1 µg/mL (0.7 µM) against all the tested strains (Table 6.2). With regard to micromolar concentrations, HSGN-218 is between 2.5 to 100 times more potent than vancomycin in inhibiting clinically relevant *C. difficile* growth *in vitro*. Metronidazole inhibited the growth of the tested *C. difficile* strains at concentrations ranging from 0.125 µg/mL (0.7 µM) to 0.25 µg/mL (1.46 µM). Fidaxomicin displayed MIC values ranging from 0.015 µg/mL (0.01 µM) to 0.06 µg/mL (0.06 µM).

Table 6.2 MICs in µg/mL (µM) of HSGN-218 and vancomycin against various *C. difficile* clinical isolates.

Compound/Control Antibiotic	*C. difficile* NR-13432 (isolate 6)	*C. difficile* NR-13435 (isolate 9)	*C. difficile* NR-32883 (P2)	*C. difficile* NR-32891 (P13)	*C. difficile* NR-32895 (P19)	*C. difficile* NR-32904 (P30)	*C. difficile* ATCC 43255
HSGN-218	0.03 (0.07)	0.003 (0.007)	0.007 (0.02)	0.007 (0.02)	0.007 (0.02)	0.007 (0.02)	0.015 (0.04)
Vancomycin	0.25 (0.2)	1 (0.7)	0.5 (0.4)	0.5 (0.4)	1 (0.7)	1 (0.7)	1 (0.7)
Metronidazole	0.25 (1.46)	0.125 (0.7)	0.125 (0.7)	0.125 (0.7)	0.25 (1.46)	0.25 (1.46)	0.25 (1.46)
Fidaxomicin	0.06 (0.06)	0.06 (0.06)	0.03 (0.03)	0.015 (0.01)	0.03 (0.03)	0.015 (0.01)	0.015 (0.01)

6.3.4 Antibacterial profile of HSGN-218 against vancomycin-resistant enterococci and Gram-negative bacteria

Next, the antibacterial activity of HSGN-218 was assessed against vancomycin-resistant enterococci (VRE) and *Escherichia coli* that are highly common bacteria in the gut. The overgrowth of VRE and colonization of the gut are one of the major issues associated with the vancomycin and metronidazole treatment of CDI[290-291]. Thus, anticlostridial agents capable of inhibiting the growth of VRE are highly desirable. On the other hand, *E. coli* is the predominant aerobic bacteria colonizing in the gut which remains resident throughout the life of the host[292]. As depicted in Table 6.3, HSGN-218 exhibited potent actvity against VRE clinical isolates with MICs ranging from 0.06 µg/mL (0.14 µM) to 0.125 µg/mL (0.29 µM) outperforming vancomycin and metronidazole. When tested against *E. Coli*, HSGN-218 was found to be inactive against *E. coli* BW25113 (wild-type strain). Conversely, the compound showed moderate activity (MIC = 4 µg/mL (9.2 µM)) against *E. coli* JW55031 which is deficient in AcrAB-TolC efflux pump. Thus, the lack of activity against the wild-type *E. coli* could be attributed to that HSGN-218 may be a substrate for AcrAB-TolC efflux pump.

Table 6.3 MICs in µg/mL (µM) of HSGN-218 and control antibiotics against vancomycin-resistant enterococci (VRE) and *Escherichia coli* isolates.

Compound/Control Antibiotic	*E. faecium* ATCC 700221	*E. faecalis* ATCC 51299	*E. coli* JW55031 (TolC Mutant	*E. coli* BW25113 (wild-type strain)
HSGN-218	0.125 (0.29)	0.06 (0.14)	4 (9.2)	>16 (>36.8)
Vancomycin	32 (22.1)	>64 (>44.2)	>64 (>44.2)	>64 (>44.2)
Metronidazole	>64 (>373.9)	>64 (>373.9)	NT[1]	NT
Linezolid	1 (3.0)	1 (3.0)	16 (47.4)	>64 (>189.7)
Gentamicin	NT	NT	0.25 (0.52)	0.25 (0.52)

NT[1], not tested

6.3.5 HSGN-218 is highly tolerable to human cell lines

Prokaryotic cell selectivity is a vital attribute for any antibiotic candidate. Thus, HSGN-218 was assessed for toxicity to mammalian cells. HSGN-218 showed an excellent safety profile against human colorectal cells (Caco-2) (Figure 6.3). It was highly tolerable to Caco-2 cells at concentrations higher than 64 µg/mL. This concentration is more than 9,000-times higher than the compound's corresponding MIC value against *C. difficile* ATCC BAA 1801 used in the initial screening.

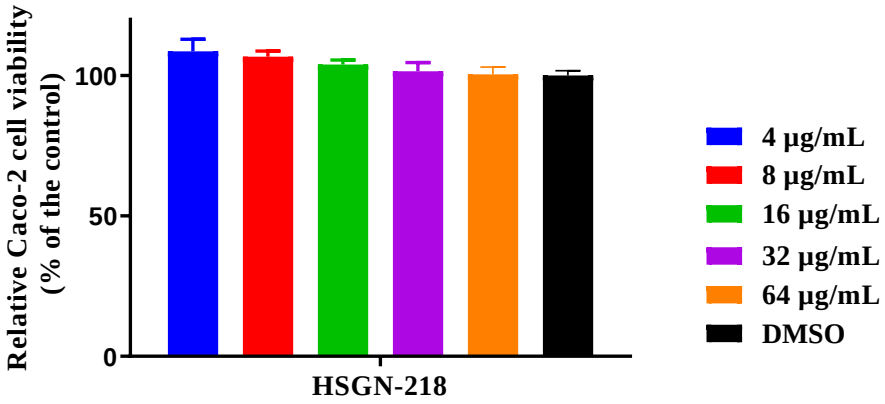

Figure 6.3 *In vitro* cytotoxicity assessment of HSGN-218 (tested in triplicate) against human colorectal cells (Caco-2) using the MTS 3-(4,5-dimethylthiazol-2-yl)-5-(3-carboxymethoxyphenyl)-2-(4-sulfophenyl)-2H-tetrazolium) assay. Results are presented as percent viable cells relative to DMSO (negative control). Error bars represent standard deviation values. A one-way ANOVA, with post hoc Dunnet's multiple comparisons test, determined statistical difference between the values obtained for the compound and DMSO (denoted by the asterisk) ($P < 0.05$).

6.3.6 HSGN-218 demonstrates low Caco-2 permeability

In order to treat CDI, it's vital that a compound does not cross the gastrointestinal tract but instead stays localized in the gut. Thus, we assessed whether HSGN-218 would permeate across the gastrointestinal tract via a Caco-2 bidirectional permeability assay[293]. The assay (performed as a service at Eurofins Panlabs (MO, USA) demonstrated that HSGN-218 showed limited ability to permeate across Caco-2 bilayers ($P_{app} = 0.2 \times 10^{-6}$ cm s^{-1} from the apical to basolateral and $P_{app} = 0.1 \times 10^{-6}$ cm s^{-1} from the basolateral to apical, see Table 6.4). This permeability is comparable to rinitidine ($P_{app} = 0.5 \times 10^{-6}$ cm s^{-1} from the apical to basolateral and $P_{app} = 1.3 \times 10^{-6}$ cm s^{-1} from the basolateral to apical, see Table 6.4), a drug that is known to have low permeability across Caco-

2 bilayers. Propranolol was used as a high permeability control as its $P_{app} = 37.2 \times 10^{-6}$ cm s^{-1} from the apical to basolateral and $P_{app} = 22.7 \times 10^{-6}$ cm s^{-1} from the basolateral to apical (Table 6.4). Therefore, the Caco-2 permeability results indicate that HSGN-218 will not cross the gastrointestinal tract and instead concentrate in the gut, the site for *C. difficile* infections.

Table 6.4 Caco-2 Permeability Analysis for HSGN-218 and Control Drugs.

Compound/Control Drug	Mean A → B P_{app} (cm s^{-1})	Mean B → A P_{app} (cm s^{-1})	Notes
HSGN-218	0.2 x 10^{-6}	0.1 x 10^{-6}	Low Permeability
Ranitidine	0.5 x 10^{-6}	1.3 x 10^{-6}	Low Permeability Control
Propranolol	37.2 x 10^{-6}	22.7 x 10^{-6}	High Permeability Control

6.3.7 *In vitro* antibacterial evaluation of HSGN-218 against normal microflora

Antibiotics administration (especially broad-spectrum ones) causes alteration of the normal intestinal microbial composition, resulting in gut colonization by opportunistic pathogens like *C. difficile*[294]. Consequently, we investigated whether HSGN-218 has a deleterious effect on important representative members of the normal gut microbiota such as *Lactobacillus* spp and *Bacteroides* spp. *Bacteroides* spp comprise a large proportion of the intestinal microbiota, which were reported to contribute to bile acid-mediated inhibition of *C. difficile* and prevent CDI in mouse model[295-296]. Additionally, lactobacilli were reported to interfere with *C. difficile* both *in vitro* and *in vivo*[297-298]. As depicted in Table 6.5, HSGN-218 exhibited weak antibacterial activity against *Lactobacillus* strains (MIC = 16 µg/mL (36.8 µM)) and inhibited growth of species of *Bacteroides* (MIC=1-2 µg/mL (2.3-4.6 µM)). Similarly, vancomycin inhibited *Lactobacillus* strains (MICs = ≤1-2 µg/mL (0.7-1.4 µM)) and exhibited weak activity against *Bacteroides* spp (MICs = 32-64 µg/mL (22.1-44.2 µM)). Although HSGN-218 was similar to vancomycin, the anti-CDI drug of choice, in inhibiting the growth of certain species of the normal microbiota, it must be noted that HSGN-218 inhibits *C. difficile* at concentrations that are 100-times less than what is needed to inhibit *Bacteroides* (compare Table 6.2 with Table 6.5). On the other hand, vancomycin

inhibited both *C. difficile* and *Lactobacillus* strains with comparable MIC values of 1-2 μg/mL. Metronidazole and fidaxomicin (to a lesser extent) also inhibit certain members of the normal intestinal microbiota[299-301].

Table 6.5 MICs in μg/mL (μM) of HSGN-218 and vancomycin against human normal gut microbiota.

Bacterial strains	HSGN-218	Vancomycin	Metronidazole	Fidaxomicin
Lactobacillus gasseri HM-400	16 (36.8)	≤1 (≤0.7)	>64 (>373.9)	>64 (>60.5)
Lactobacillus crispatus HM-103	16 (36.8)	2 (1.4)	>64 (>373.9)	>64 (>60.5)
Lactobacillus crispatus HM-371	16 (36.8)	2 (1.4)	>64 (>373.9)	>64 (>60.5)
Bacteroides fragilis HM-711	2 (4.6)	64 (44.2)	≤1 (5.84)	>64 (>60.5)
Bacteroides fragilis HM-709	1 (2.3)	32 (22.1)	2 (11.68)	>64 (>60.5)
Bacteroides dorei HM-719	2 (4.6)	64 (44.2)	≤1 (5.84)	>64 (>60.5)

6.3.8 Frequency of Mutation

The promising results of HSGN-218 led us to investigate the likelihood of *C. difficile* to develop resistance to HSGN-218. No resistant mutants were isolated at a concentration of 15 × MIC and 20 × MIC in the presence of a high inoculum of *C. difficile* (Table 6.6), indicating that *C. difficle* is unlikely to form rapid resistance to HSGN-218. Likewise, vancomycin exhibited low frequency of mutation ($<1.1\times 10^{-9}$) and no resistant mutants were isolated, in agreement with a previous report[302].

Table 6.6 Frequency of mutation of HSGN-218 against *C. difficile* ATCC 43255.

Test agent	Frequency of mutation	
	15 × MIC	20 × MIC
HSGN-218	$<1.1\times 10^{-9}$	$<1.1\times 10^{-9}$
Vancomycin	$<1.1\times 10^{-9}$	$<1.1\times 10^{-9}$

6.3.9 *In vivo* efficacy of HSGN-218 in a CDI mouse model[303]

The potent antibacterial activities of HSGN-218 against *C. difficile* prompted us to investigate its efficacy in a CDI mouse model and its potential to protect mice from CDI recurrence, as described before. As shown in Figure 6.4, vancomycin (10 mg/kg) protected 100% of mice up to 5 days, as previously reported[304-305]. HSGN-218 (50 mg/kg), was able to significantly protect 66.7% of the mice against *C. difficile* during the 5-days treatment period.

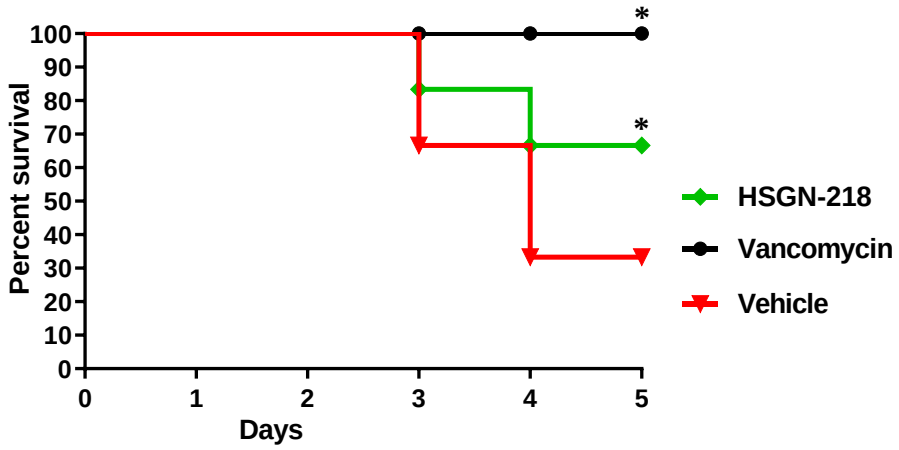

Figure 6.4 *In vivo* efficacy of HSGN-218 in a CDI mouse model. Kaplan–Meier survival curves were analyzed using a log-rank (Mantel–Cox) test. Asterisks (*) denote statistically significant difference between mice treated with either HSGN-218, or vancomycin in comparison with the vehicle-treated mice.

After testing the efficacy of HSGN-218 in the CDI mouse model, we sought to investigate this promising activity of HSGN-218 in preventing *C. difficile* recurrence. *C. difficile* recurrence is challenging to treat. In addition to the subsequent prolongation of *C. difficile* shedding and transmission, 1 out of every 5 patients experienced *C. difficile* recurrence episode died within 30 days of diagnosis[132]. Therefore, we sought to investigate this promising activity of HSGN-218 in

preventing *C. difficile* recurrence. Mice were infected and treated for 5 days and then they were monitored for survival and possible *C. difficile* recurrence until the 21st day. Vancomycin-treated mice survived the first 5 days (similar to prior reports)[304], but in accordance with previous studies[303, 305], mice treated with vancomycin were susceptible to *C. difficile* recurrence and 83.3% of vancomycin-treated mice died after stopping vancomycin treatment. In contrast, HSGN-218 (50 mg/kg), significantly protected mice from CDI recurrence with 100% survival after 5- days treatment period (Figure 6.5).

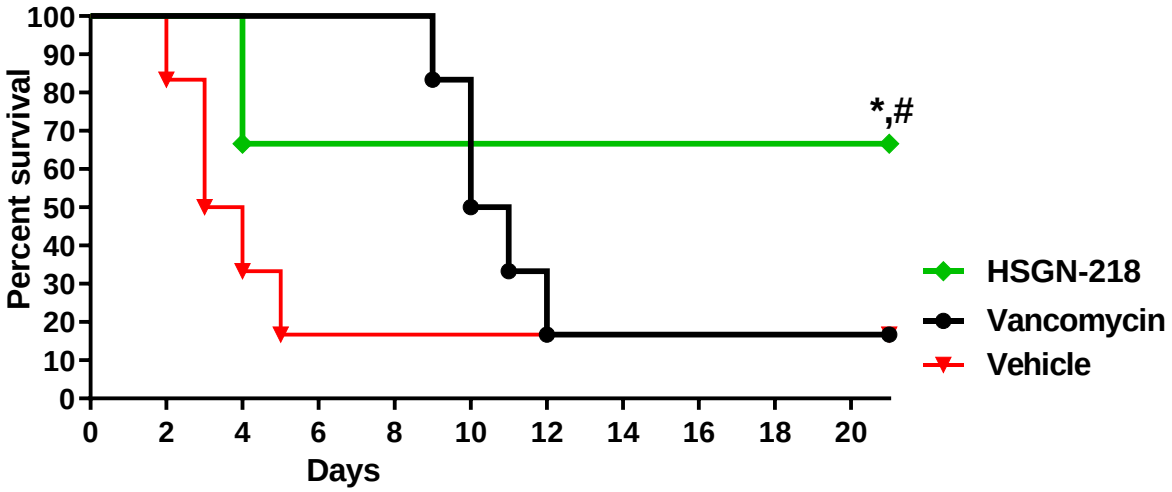

Figure 6.5 *In vivo* efficacy of HSGN-218 against CDI recurrence. Mice were treated with HSGN-218 (50 mg/kg), vancomycin (10 mg/kg) or the vehicle for 5 days and treatments were stopped thereafter. Kaplan–Meier survival curves were analyzed using a log-rank (Mantel–Cox) test. Asterisks (*) denote statistically significant difference between mice treated with either HSGN-218, or vancomycin in comparison with the vehicle-treated mice. Pound (#) denotes statistically significant difference between mice treated with compound HSGN-218 in comparison with vancomycin-treated mice.

6.4 Conclusion

In conclusion, we have identified HSGN-218 as a highly potent small molecule inhibitor of C. difficile growth. HSGN-218 is up to 100-times more active (MICs ranging from 0.003 µg/mL (0.007 µM) to 0.03 µg/mL (0.07 µM)) against C. difficile clinical isolates than vancomycin, the drug of choice for CDI. The compound is also non-toxic to mammalian cells as well as demonstrates low Caco-2 bidirectional permeability, indicating that HSGN-218 would have minimal systemic absorption. Even though HSGN-218 inhibited the growth of certain representative members of normal microbiota, excitingly, HSGN-218 protected mice from CDI as

well as it showed significant efficacy against *C. difficile* recurrence. Therefore, compound HSGN-218 is considered as a lead compound to develop as anti- *C. difficile* therapeutic and deserves serious consideration.

6.5 Experimental Section

6.5.1 Chemistry

General Information: unless noted otherwise, all reagents and solvents were purchased from commercial sources and used as received. The ^{1}H, ^{13}C, and ^{19}F NMR spectra were obtained in DMSO-d_6 as solvent using a 500 MHz spectrometer with Me_4Si as an internal standard. Chemical shifts are reported in parts per million (δ) and are calibrated using residual undeuterated solvent as an internal reference. Data for ^{1}H NMR spectra are reported as follows: chemical shift (δ ppm) (multiplicity, coupling constant (Hz), integration). Multiplicities are reported as follows: s = singlet, d = doublet, t = triplet, q = quartet, m = multiplet, or combinations thereof. High resolution mass spectra (HRMS) were obtained using electron spray ionization (ESI) technique and as TOF mass analyzer. Compounds were characterized by ^{1}H NMR, ^{13}C NMR, ^{19}F NMR, and HRMS data. The purity of compounds was determined to be greater than 95% by measuring the absorbance at 260 nm with high performance liquid chromatography (HPLC) (See supprting information). HPLC spectra were recorded on an Agilent 1260 Infinity system using a ZORBAX RR Eclipse Plus C18 column. The mobile phase gradient went from 50% H_2O : 50% MeOH over 5 minutes and then 40% H_2O : 60% MeOH for 5 minutes, followed by 10% H_2O : 90% MeOH for 2 minues and lastly 50% H_2O : 50% MeOH for 3 minutes at a 1 mL/min flow rate.

6.5.2 Synthesis of 1,3,4-oxadiazol-2-amines [I.1 – I.17]

The synthesis of I.1-I.17 was performed using a literature reported procedure[210]. Obtained ^{1}H, ^{13}C, and ^{19}F spectra were in agreement with literature reported data.

6.5.3 Amide Coupling Procedure for the Synthesis of Compounds 1-17

A 20 mL screw caped vial, charged with the corresponding acid (1 eq.), amine (1 eq.), BOP reagent (2.7 eq.) and diisopropylethylamine (1.5 mL) in DMF solvent (5 mL) was stirred at room temperature for 16 h. After completion, the reaction mixture was concentrated under reduced

pressure, followed by flash column chromatography (hexanes:ethyl acetate 90:10 to 70:30) to give the desired product.

6.5.4 Characterization Data

N-(5-Phenyl-1,3,4-oxadiazol-2-yl)-4-((trifluoromethyl)thio)benzamide (1):

Off-white solid (46 mg, 28%). ^{1}H NMR (500 MHz, DMSO-d_6) δ 8.1 (m, 2H), 8.0 – 7.9 (m, 2H), 7.9 (m, 2H), 7.6 (m, 3H). ^{13}C NMR (126 MHz, DMSO-d_6) δ 165.6, 161.1, 158.6, 136.0, 135.8, 132.2, 131.1 (q, J = 308.7 Hz), 130.1, 129.8, 128.6, 126.6, 123.8. ^{19}F NMR (471 MHz, DMSO-d_6) δ -42.4 (s, 3F). HRMS (ESI) m/z calcd for $C_{16}H_{11}F_3N_3O_2S$ $[M + H]^+$ 366.0524, found 366.0522. Purity by HPLC was found to be 96%.

N-(5-(2-Fluorophenyl)-1,3,4-oxadiazol-2-yl)-4-((trifluoromethyl)thio)benzamide (2):

Off-white solid (38 mg, 22%). ^{1}H NMR (500 MHz, DMSO-d_6) δ 8.1 (m, 2H), 8.0 (td, J = 7.6, 1.8 Hz, 1H), 7.9 (m, 2H), 7.7 (tdd, J = 7.4, 5.1, 1.8 Hz, 1H), 7.5 – 7.4 (m, 2H). ^{13}C NMR (126 MHz, DMSO-d_6) δ 165.6, 160.6 (d, J = 257.0 Hz), 158.7, 157.7, 136.1, 135.7, 134.5 (d, J = 8.82 Hz), 131.1 (q, J = 308.7 Hz), 130.1, 129.7, 128.6, 125.8, 117.6 (d, J = 20.2 Hz), 112.2 (d, J = 11.3 Hz). ^{19}F NMR (471 MHz, DMSO-d_6) δ -42.4 (s, 3F), -112.0 (d, J = 5.7 Hz, 1F). HRMS (ESI) m/z calcd for $C_{16}H_{10}F_4N_3O_2S$ $[M + H]^+$ 384.0430, found 384.0429. Purity by HPLC was found to be 96%.

N-(5-(2-Chlorophenyl)-1,3,4-oxadiazol-2-yl)-4-((trifluoromethyl)thio)benzamide (3):

Off-white solid (41 mg, 23%). ^{1}H NMR (500 MHz, DMSO-d_6) δ 8.1 (m, 2H), 8.0 – 7.9 (m, 1H), 7.9 (m, 2H), 7.7 (m, 1H), 7.6 (td, J = 7.8, 1.6 Hz, 1H), 7.6 (t, J = 7.6 Hz, 1H). ^{13}C NMR (126 MHz, DMSO-d_6) δ 165.2, 159.2, 158.8, 136.1, 135.6, 133.5, 132.3, 131.6, 131.5, 131.1 (q, J = 308.7 Hz), 130.1, 128.7, 128.3, 123.0. ^{19}F NMR (471 MHz, DMSO-d_6) δ -42.4 (s, 3F). HRMS (ESI) m/z calcd for $C_{16}H_{10}ClF_3N_3O_2S$ $[M + H]^+$ 400.0134, found 400.0135. Purity by HPLC was found to be 96%.

N-(5-(3-Fluorophenyl)-1,3,4-oxadiazol-2-yl)-4-((trifluoromethyl)thio)benzamide (4):

Off-white solid (55 mg, 32%). ^{1}H NMR (500 MHz, DMSO-d_6) δ 8.1 (m, 2H), 7.9 (m, 2H), 7.8 (m, 1H), 7.7 – 7.6 (m, 2H), 7.5 (td, J = 8.5, 2.7 Hz, 1H).^{13}C NMR (126 MHz, DMSO-d_6) δ 165.3, 163.7 (d, J = 245.7 Hz), 160.2, 158.7, 136.0, 135.5, 132.4 (d, J = 8.82 Hz), 131.1 (q, J = 308.7 Hz), 130.2, 128.7, 125.9 (d, J = 8.82 Hz), 122.8, 119.3 (d, J = 21.4 Hz), 113.3 (d, J = 25.2 Hz). ^{19}F

NMR (471 MHz, DMSO-d_6) δ -42.4 (s, 3F), -112.5 (q, J = 8.5 Hz, 1F). HRMS (ESI) m/z calcd for $C_{16}H_{10}F_4N_3O_2S$ $[M + H]^+$ 384.0430, found 384.0429. Purity by HPLC was found to be 98%.

N-(5-(3-Chlorophenyl)-1,3,4-oxadiazol-2-yl)-4-((trifluoromethyl)thio)benzamide (5):

Off-white solid (35 mg, 19%). ^{1}H NMR (500 MHz, DMSO-d_6) δ 8.1 (m, 2H), 7.9 – 7.8 (m, 4H), 7.7 (dd, J = 23.9, 7.9 Hz, 2H). ^{13}C NMR (126 MHz, DMSO-d_6) δ 165.4, 159.8, 159.0, 136.1, 134.6, 132.0, 132.0, 131.1 (q, J = 308.7 Hz), 130.2, 128.9, 128.5, 126.0, 125.8, 125.2. ^{19}F NMR (471 MHz, DMSO-d_6) δ -42.4 (s, 3F). HRMS (ESI) m/z calcd for $C_{16}H_{10}ClF_3N_3O_2S$ $[M + H]^+$ 400.0134, found 400.0135. Purity by HPLC was found to be 96%.

N-(5-(3-Methoxyphenyl)-1,3,4-oxadiazol-2-yl)-4-((trifluoromethyl)thio)benzamide (6):

Off-white solid (42 mg, 24%). ^{1}H NMR (500 MHz, DMSO-d_6) δ 8.1 (m, 2H), 7.9 (m, 2H), 7.6 – 7.5 (m, 2H), 7.4 (s, 1H), 7.2 (d, J = 7.9 Hz, 1H), 3.8 (s, 3H). ^{13}C NMR (126 MHz, DMSO-d_6) δ 165.5, 160.9, 160.2, 158.6, 136.0, 135.7, 131.2 (q, J = 308.7 Hz), 130.1, 128.7, 128.6, 125.0, 118.9, 118.3, 111.5, 55.9. ^{19}F NMR (471 MHz, DMSO-d_6) δ -42.4 (s, 3F). HRMS (ESI) m/z calcd for $C_{17}H_{13}F_3N_3O_2S$ $[M + H]^+$ 396.0630, found 396.0632. Purity by HPLC was found to be 98%.

N-(5-(3-Trifluoromethylphenyl)-1,3,4-oxadiazol-2-yl)-4-((trifluoromethyl)thio)benzamide (7):

Off-white solid (53 mg, 27%). ^{1}H NMR (500 MHz, DMSO-d_6) δ 8.2 (d, J = 7.9 Hz, 1H), 8.2 – 8.1 (m, 3H), 8.0 (m, 1H), 7.9 (m, 3H). ^{13}C NMR (126 MHz, DMSO-d_6) δ 165.4, 159.8, 159.1, 136.1, 135.8, 131.4, 131.1 (q, J = 308.7 Hz), 130.8 (q, J = 31.5 Hz), 130.5, 130.4, 130.1, 128.6, 125.2 (q, J = 272.2 Hz), 125.0, 122.8, ^{19}F NMR (471 MHz, DMSO-d_6) δ -42.4 (s, 3F), -62.8 (s, 3F). HRMS (ESI) m/z calcd for $C_{17}H_{10}F_6N_3O_2S$ $[M + H]^+$ 434.0398, found 434.0399. Purity by HPLC was found to be 98%.

N-(5-(4-Fluorophenyl)-1,3,4-oxadiazol-2-yl)-4-((trifluoromethyl)thio)benzamide (8):

Off-white solid (43 mg, 24%). ^{1}H NMR (500 MHz, DMSO-d_6) δ 8.1 (m, 2H), 8.0 (dd, J = 8.7, 5.5 Hz, 2H), 7.9 (m, 2H), 7.4 (t, J = 8.7 Hz, 2H).^{13}C NMR (126 MHz, DMSO-d_6) δ 165.5 (d, J = 250.7 Hz), 160.4, 158.6, 136.1, 135.7, 131.1 (q, J = 308.7 Hz), 130.1, 129.3 (d, J = 8.82 Hz), 128.6, 120.5, 117.2 (d, J = 22.7 Hz). ^{19}F NMR (471 MHz, DMSO-d_6) δ -42.4 (s, 3F), -108.8. (s, 1F).

HRMS (ESI) m/z calcd for $C_{16}H_{10}F_4N_3O_2S$ $[M + H]^+$ 384.0430, found 384.0431. Purity by HPLC was found to be 96%.

N-(5-(4-Chlorophenyl)-1,3,4-oxadiazol-2-yl)-4-((trifluoromethyl)thio)benzamide (9):

Off-white solid (36 mg, 20%). ^{1}H NMR (500 MHz, DMSO-d_6) δ 8.1 (m, 2H), 8.0 – 7.9 (m, 2H), 7.9 (m, 2H), 7.7 – 7.6 (m, 2H). ^{13}C NMR (126 MHz, DMSO-d_6) δ 164.5, 160.4, 158.6, 137.0, 136.1, 135.6, 131.1 (q, J = 308.7 Hz), 130.1, 128.6, 128.4, 127.2, 122.7. ^{19}F NMR (471 MHz, DMSO-d_6) δ -42.4 (s, 3F). HRMS (ESI) m/z calcd for $C_{16}H_{10}ClF_3N_3O_2S$ $[M + H]^+$ 400.0134, found 400.0132. Purity by HPLC was found to be 97%.

N-(5-(4-Trifluoromethylphenyl)-1,3,4-oxadiazol-2-yl)-4-((trifluoromethyl)thio)benzamide (10):

Off-white solid (42 mg, 22%). ^{1}H NMR (500 MHz, DMSO-d_6) δ 8.1 (dd, J = 14.0, 8.0 Hz, 4H), 8.0 (m, 2H), 7.9 (m, 2H). ^{13}C NMR (126 MHz, DMSO-d_6) δ 165.2, 160.0, 159.0, 136.1, 135.6, 132.0 (q, J = 31.5 Hz), 131.1 (q, J = 308.7 Hz), 130.1, 128.7, 127.6, 127.4, 126.9, 125.3 (q, J = 272.2 Hz).^{19}F NMR (471 MHz, DMSO-d_6) δ -42.4 (s, 3F), -62.8 (s, 3F). HRMS (ESI) m/z calcd for $C_{17}H_{10}F_6N_3O_2S$ $[M + H]^+$ 434.0398, found 434.0397. Purity by HPLC was found to be 99%.

N-(5-(4-Methoxyphenyl)-1,3,4-oxadiazol-2-yl)-4-((trifluoromethyl)thio)benzamide (11):

Off-white solid (48 mg, 27%). ^{1}H NMR (500 MHz, DMSO-d_6) δ 8.1 (d, J = 8.0 Hz, 2H), 7.9 – 7.8 (m, 4H), 7.1 (m, 2H), 3.8 (s, 3H). ^{13}C NMR (126 MHz, DMSO-d_6) δ 164.0, 162.5, 161.4, 158.1, 136.1, 131.1 (q, J = 308.7 Hz), 130.1, 128.4, 127.3, 116.1, 115.4, 115.1, 56.0. ^{19}F NMR (471 MHz, DMSO-d_6) δ -42.4 (s, 3F). HRMS (ESI) m/z calcd for $C_{17}H_{13}F_3N_3O_2S$ $[M + H]^+$ 396.0630, found 396.0631. Purity by HPLC was found to be 99%.

N-(5-(4-Methylphenyl)-1,3,4-oxadiazol-2-yl)-4-((trifluoromethyl)thio)benzamide (12):

Off-white solid (35 mg, 21%). ^{1}H NMR (500 MHz, DMSO-d_6) δ 8.1 (m, 2H), 7.9 (m, 4H), 7.4 (m, 2H), 2.4 (s, 3H). ^{13}C NMR (126 MHz, DMSO-d_6) δ 165.7, 161.3, 158.4, 142.5, 136.1, 135.8, 131.1 (q, J = 308.7 Hz), 130.4, 130.1, 128.5, 126.6, 121.1, 21.6. ^{19}F NMR (471 MHz, DMSO-d_6) δ -42.4 (s, 3F). HRMS (ESI) m/z calcd for $C_{17}H_{13}F_3N_3O_2S$ $[M + H]^+$ 380.0681, found 380.0682. Purity by HPLC was found to be 98%.

N-(5-(4-Isopropylphenyl)-1,3,4-oxadiazol-2-yl)-4-((trifluoromethyl)thio)benzamide (13):

Off-white solid (39 mg, 21%). ^{1}H NMR (500 MHz, DMSO-d_6) δ 8.2 – 8.1 (m, 2H), 7.9 (dd, *J* = 8.3, 2.5 Hz, 4H), 7.5 (m, 2H), 3.0 (h, *J* = 6.9 Hz, 1H), 1.2 (d, *J* = 6.9 Hz, 6H). ^{13}C NMR (126 MHz, DMSO-d_6) δ 165.5, 161.2, 158.4, 153.1, 136.1, 135.8, 131.2 (q, *J* = 308.7 Hz), 130.1, 128.5, 127.9, 126.7, 121.4, 33.9, 23.9. ^{19}F NMR (471 MHz, DMSO-d_6) δ -42.4 (s, 3F). HRMS (ESI) m/z calcd for $C_{19}H_{17}F_3N_3O_2S$ $[M + H]^+$ 408.0994, found 408.0993. Purity by HPLC was found to be 97%.

N-(5-(2,4-Dichlorophenyl)-1,3,4-oxadiazol-2-yl)-4-((trifluoromethyl)thio)benzamide (14):

Off-white solid (35 mg, 18%). ^{1}H NMR (500 MHz, DMSO-d_6) δ 8.1 (m, 2H), 8.0 (m, 1H), 7.9 – 7.8 (m, 3H), 7.7 (dd, *J* = 8.5, 2.1 Hz, 1H). ^{13}C NMR (126 MHz, DMSO-d_6) δ 165.1, 158.8, 158.5, 137.5, 136.1, 135.5, 133.3, 132.6, 131.2, 131.1 (q, *J* = 308.7 Hz), 130.1, 128.7, 122.0. ^{19}F NMR (471 MHz, DMSO-d_6) δ -42.4 (s, 3F). HRMS (ESI) m/z calcd for $C_{16}H_9Cl_2F_3N_3O_2S$ $[M + H]^+$ 433.9745, found 433.9747. Purity by HPLC was found to be 99%.

N-(5-(3,5-Dichlorophenyl)-1,3,4-oxadiazol-2-yl)-4-((trifluoromethyl)thio)benzamide (15, HSGN-218):

Off-white solid (37 mg, 19%). ^{1}H NMR (500 MHz, DMSO-d_6) δ 8.1 (m, 2H), 7.9 (m, 5H). ^{13}C NMR (126 MHz, DMSO-d_6) δ 165.4, 159.7, 158.7, 136.1, 135.7, 131.4, 131.2 (q, *J* = 308.7 Hz), 130.1, 128.4, 127.2, 126.3, 124.9. ^{19}F NMR (471 MHz, DMSO-d_6) δ -42.4 (s, 3F). HRMS (ESI) m/z calcd for $C_{16}H_9Cl_2F_3N_3O_2S$ $[M + H]^+$ 433.9745, found 433.9744. Purity by HPLC was found to be 99%.

N-(5-(5-Chloro-2-methoxyphenyl)-1,3,4-oxadiazol-2-yl)-4-((trifluoromethyl)thio)benzamide (16):

Off-white solid (46 mg, 24%). ^{1}H NMR (500 MHz, DMSO-d_6) δ 8.1 (m, 2H), 7.9 (m, 2H), 7.8 (d, *J* = 2.7 Hz, 1H), 7.6 (dd, *J* = 9.0, 2.8 Hz, 1H), 7.3 (m, 1H), 3.9 (s, 3H).^{13}C NMR (126 MHz, DMSO-d_6) δ 165.8, 158.7, 156.8, 136.1, 135.8, 133.3, 131.2 (q, *J* = 308.7 Hz), 130.1, 129.4, 128.6, 126.3, 124.9, 115.4, 114.4, 57.1. ^{19}F NMR (471 MHz, DMSO-d_6) δ -42.4 (s, 3F). HRMS (ESI) m/z calcd for $C_{17}H_{12}ClF_3N_3O_3S$ $[M + H]^+$ 430.0240, found 430.0241. Purity by HPLC was found to be 97%.

N-(5-(Pyridin-2-yl)-1,3,4-oxadiazol-2-yl)-4-((trifluoromethyl)thio)benzamide (17):

Off-white solid (26 mg, 16%). ^{1}H NMR (500 MHz, DMSO-d_6) δ 8.8 (d, J = 4.7 Hz, 1H), 8.1 (dd, J = 8.2, 2.7 Hz, 3H), 8.0 (td, J = 7.8, 1.8 Hz, 1H), 7.9 (m, 2H), 7.6 (ddd, J = 7.6, 4.8, 1.2 Hz, 1H). ^{13}C NMR (126 MHz, DMSO-d_6) δ 164.9, 160.8, 159.0, 150.7, 143.2, 138.3, 136.1, 135.5, 131.1 (q, J = 308.7 Hz), 130.1, 128.7, 126.6, 122.9. ^{19}F NMR (471 MHz, DMSO-d_6) δ -42.4 (s, 3F). HRMS (ESI) m/z calcd for $C_{15}H_{10}F_3N_4O_2S$ $[M + H]^+$ 367.0477, found 367.0475. Purity by HPLC was found to be 98%.

6.5.5 Bacterial strains media, cell lines and reagents

Bacterial strains used in this study (Table 1S) were obtained from the Biodefense and Emerging Infections Research Resources Repository (BEI Resources) and the American Type Culture Collection (ATCC). E. coli BW25113 and JW25113 were obtained from the Coli Genetic Stock Center (CGSC), Yale University, USA. Brain heart infusion broth was purchased from Becton, Dickinson and Company (Cockeysville, MD, USA) and was purchased from Fisher Scientific. Yeast extract, L-cysteine, vitamin K, hemin and phosphate buffered saline (PBS) were all obtained from commercial vendors. Human colorectal adenocarcinoma epithelial cells (Caco-2) (ATCC HTB-37) was obtained from the American Type Culture Collection (ATCC) (Manassas, VA, USA). Dulbecco's Modified Eagle Medium (DMEM), fetal bovine serum (FBS) and phosphate-buffered saline (PBS) was purchased from Corning (Manassas, VA, USA). Vancomycin hydrochloride (Gold Biotechnology, St. Louis, MO, USA), linezolid and gentamicin sulfate (Chem-Impex International, Wood Dale, IL, USA), metronidazole (Alfa Aesar, Ward Hill, MA, USA), and fidaxomicin (Cayman Chemical, Ann Arbor, MI, USA) were purchased commercially. Compounds were synthesized from commercial sources in our laboratory.

6.5.6 Determination of the MICs against *C. difficile* clinical isolates

The minimum inhibitory concentrations (MICs) of tested compounds and control drug; vancomycin, were determined using the broth microdilution method, as previously described[306-309] against *C. difficile* clinical isolates. Briefly, 0.5 McFarland bacterial solution was prepared and diluted in brain heart infusion supplemented (BHIS) broth (to an inoculum size ~5 x 10^5 CFU/mL). Test agents were added and serially diluted before plates were incubated anaerobically at 37°C for

48 hours. MICs reported are the lowest drug concentration that completely suppressed the growth of bacteria, as observed visually.

6.5.7 Determination of the MICs against vancomycin-resistant enterococci (VRE) and *Escherichia coli* strains

The MICs of HSGN-218 and control drugs were determined using the broth microdilution method, according to guidelines outlined by the Clinical and Laboratory Standards Institute (CLSI[212]) against *Enterococcus faecium*, *Enterococcus faecalis* and *Escherichia coli* strains. Bacterial strains were grown aerobically overnight on tryptone soy agar (TSA) plates at 37° C. Afterwards, a bacterial solution equivalent to 0.5 McFarland standard was prepared and diluted in cation-adjusted Mueller-Hinton broth (CAMHB) (for *E. coli*) or tryptone soy broth (TSB) (for enterococcal strains), to achieve a bacterial concentration of about 5×10^5 CFU/mL. Test agents were added in the first row of the 96-well plates and serially diluted along the plates. Plates were then, incubated as previously described. MICs reported in Table 3 are the minimum concentrations of the test agents that completely inhibited the visual growth of bacteria.

6.5.8 *In vitro* cytotoxicity analysis of HSGN-218 against human colorectal cells.

Compounds were assayed for potential cytotoxicity against a human colorectal adenocarcinoma (Caco-2) cell line[310-311304-305304-305304-305304-305304-305304-305304-305304-305304-305304-305304-305301-302299-300299-300299-300299-300297-298297-298297-298297-298297-298297-298297-298296-297289-290289-290289-290289-290290-291]. Briefly, tested compounds were incubated with Caco-2 cells for 2 hours. Then, cells were incubated with MTS (3-(4,5-dimethylthiazol-2-yl)-5-(3-carboxymethoxyphenyl)-2-(4-sulfophenyl)-2H-tetrazolium) reagent for 4 hours before measuring absorbance values (OD_{490}).

6.5.9 Caco-2 permeability assay

Assay and data analysis were performed by Eurofins Panlabs (MO, USA) according to a previously reported protocol[312-313]. The apparent permeability coefficient (Papp) of the tested agents was calculated using the equation below:

$$P_{app}(cm/s) = \frac{V_R * C_{R,end}}{\Delta t} * \frac{1}{A*(C_{D,mid}-C_{R,mid})}$$

where V_R is the volume of the receiver chamber. $C_{R,end}$ is the concentration of the test compound in the receiver chamber at the end time point, Δt is the incubation time and A is the surface area of the cell monolayer. $C_{D,mid}$ is the calculated mid-point concentration of the test compound in the donor side, which is the mean value of the donor concentration at time 0 minute and the donor concentration at the end time point. $C_{R,mid}$ is the mid-point concentration of the test compound in the receiver side, which is one half of the receiver concentration at the end time point. Concentrations of the test compound were expressed as peak areas of the test compound.

6.5.10 *In vitro* antibacterial evaluation of HSGN-218 against normal microflora.

The broth microdilution assay was utilized to determine the MICs of HSGN-218 against commensal organisms that compose the human gut microflora, as described elsewhere[212, 299, 314]. A bacterial solution equivalent to 0.5 McFarland standard was prepared and diluted in BHIS broth (for *Bacteroides*) or in MRS broth (for *Lactobacillus*) to achieve a bacterial concentration of about 5×10^5 CFU/mL. Test agents were added and serially diluted along the plates. Plates were incubated for 48 hours at 37°C before recording the MIC by visual inspection of growth.

6.5.11 Frequency of spontaneous mutation.

HSGN-218 was tested against *C. difficile* to determine the likelihood of development of spontaneous mutation as previously described[302, 315]. Briefly, HSGN-218 and vancomycin were added to BHIS agar to achieve a final concentration of 15 × MIC and 20 × MIC and poured in plates and left to dry out. An inoculum of ~ 10^9 CFU/mL of *C. difficile* ATCC 43255 was spread over the plates and incubated anaerobically at 37°C for 48 hours before plates were checked for the possible bacterial growth.

6.5.12 Preparation of *C. difficile* spores for mice infection

C. difficile spores were prepared as described earlier [316,303]. Briefly, *C. difficile* ATCC 43255 was inoculated onto BHIS agar and incubated anaerobically for 5 days. Spores were collected anaerobically using PBS containing 10% bovine serum albumin, heated at 70°C for 20 minutes to get rid of vegetative cells and counted by dilution and plating onto BHIS supplemented with 0.1% taurocholic acid. Spores were then, stored at 4°C overnight before infecting mice.

6.5.13 *C. difficile* infection (CDI) mouse model

The study was reviewed, approved and performed following the guidelines of the Purdue University Animal Care and Use Committee (PACUC) and according to the recommendations in the Guide for the Care and Use of Laboratory Animals of the National Institutes of Health. Mice were housed in individually ventilated autoclaved cages and received sterile food and water ad libitum throughout the duration of the experiment. CDI mouse model was performed as described previously[303]. Eight-week-old female pathogen-free C57BL/6 mice (Jackson, ME, USA) were pre-treated with an antibiotic cocktail in sterile drinking water to disrupt the mice normal intestinal microflora, reducing the colonization resistance and facilitating infection with the toxigenic strain of *C. difficile*. Afterwards, mice were switched to regular autoclaved water for 2 days and they received a single dose of clindamycin (10 mg/kg) intraperitoneally 1 day prior to *C. difficile* challenge. For infection, mice were restrained and infected via oral gavage with 1.3×10^6 spores of *C. difficile* ATCC 43255. Following infection, mice were randomly allocated into groups (n=6) for treatment. Two hours post-infection, one groups were treated orally with HSGN-218 (50 mg/kg), one group was treated with vancomycin (10 mg/kg) via oral gavage, and one group was treated orally with the vehicle (10% DMSO, 10% tween 80, 80% PBS). Treatments were continued once daily for five days and mice were closely monitored for disease signs (including weight loss, behavioral changes, hunched posture, decreased activity, wet tail and diarrhea).

6.5.14 *In vivo* efficacy of HSGN-218 in *C. difficile* recurrence

In order to investigate the activity of HSGN-218 in preventing *C. difficile* recurrence, mice were infected, as described above and one group was treated orally with HSGN-218 (50 mg/kg), one group was treated with vancomycin (10 mg/kg) via oral gavage, and one group was treated orally with the vehicle for 5 days. Treatments were stopped after 5 days, and mice were monitored for disease signs and recurrence of infection till the 21st day. Then, mice were humanely euthanized using CO_2 asphyxiation.

6.6 Statistical analyses

The survival data were analyzed by Log-rank (Mantel-Cox) test utilizing GraphPad Prism version 6.00 for Windows (GraphPad Software, La Jolla, CA, USA).

6.7 In Silico PAINS Analysis

All synthesized analogs were subjected to PAINS filters by using the SwissADME program[317]. Molecular formula strings of analogs were manually entered into the program, which indicated no PAINS were found.

6.8 Supplementary Information

Please refer to the supplementary information located on the ACS website to see various bacterial strains used in this study, ^{1}H NMR, ^{13}C NMR, and ^{19}F NMR spectra, and HPLC traces of analogs

6.9 Author Contributions

G. Naclerio synthesized all compounds in study. N. Abutaleb performed all *in vitro* and *in vivo* studies. G. Naclerio & H. Sintim wrote the manuscript.

CHAPTER 7. *N*-(1,3,4-OXADIAZOL-2-YL)BENZAMIDES AS ANTIBACTERIAL AGENTS AGAINST *NEISSERIA GONORRHOEAE*

This chapter was reprinted with permission from MDPI. Original article can be found at Naclerio, G. A., Abutaleb, N. S., Alhashimi, M., Seleem, M. N., & Sintim, H. O. *N*-(1,3,4-Oxadiazol-2-yl)Benzamides as Antibacterial Agents against *Neisseria gonorrhoeae*. *Int J Mol Sci* **2021**, *22*(5), 2427.

7.1 Abstract

The Centers for Disease Control and Prevention (CDC) recognizes *Neisseria gonorrhoeae* as an urgent-threat Gram-negative bacterial pathogen. Additionally, resistance to frontline treatment (dual therapy with azithromycin and ceftriaxone) has led to the emergence of multidrug-resistant *N. gonorrhoeae* which has caused a global health crisis. The drug pipeline for *N. gonorrhoeae* has been awfully scant as new antibacterial agents have not been approved by the FDA over the last twenty years. Thus, there is a need for new chemical entities active against drug-resistant *N. gonorrhoeae*. Trifluoromethylsulfonyl (SO_2CF_3), trifluoromethylthio (SCF_3) and pentafluorosulfanyl (SF_5) containing *N*-(1,3,4-oxadiazol-2-yl)benzamides are novel compounds with potent activities against Gram-positive bacterial pathogens. Here, we report the discovery of new *N*-(1,3,4-oxadiazol-2-yl)benzamides (HSGN-237 and -238) with highly potent activity against *N. gonorrhoeae*. Additionally, these new compounds were shown to have activity against clinically important Gram-positive bacteria such as methicillin-resistant *Staphylococcus aureus* (MRSA), vancomycin-resistant enterococci (VRE) and *Listeria monocytogenes* (minimum inhibitory concentrations (MICs) as low as 0.25 μg/mL). Both compounds were highly tolerable to human cell lines. Moreover, HSGN-238 showed outstanding ability to permeate across the gastrointestinal tract, indicating it would have high systemic absorption if used as an anti-gonococcal therapeutic.

7.2 Introduction

Drug-resistant bacterial infections have become a serious global threat. *Neisseria gonorrhoeae* is a Gram-negative bacterial pathogen which causes gonorrhea, a sexually transmitted infection (STI) [318]. *N. gonorrhoeae* infects a variety of mucosal surfaces (i.e. the urethra, endocervix, pharynx, and rectum) [319] and, if left untreated, can cause drastic complications such as pelvic

inflammatory disease, ectopic pregnancy, and increased susceptibility to HIV infections [320]. The Centers for Disease Control and Prevention (CDC) considers *N. gonorrhoeae* an urgent threat as it accounts for 550,000 infections per year and $133.4 million dollars in medical costs in the United States alone [170]. Globally, *N. gonorrhoeae* is also quite devastating. The World Health Organization (WHO) listed *N. gonorrhoeae* as a priority 2 (high) pathogen as it is attributed to 87 million new cases as well as an estimated total treatment cost of $5 billion dollars [321-324].

Efforts to develop novel antibiotics against urgent threat pathogens, especially *N. gonorrhoeae,* have intensified [156]. For instance, former front-line therapies to treat *N. gonorrhoeae* such as penicillin, fluoroquinolones, and cefixime are now resistant to this bacterial pathogen and deemed ineffective as treatment options [325]. This increased resistance rate prompted a global health scare, leading the CDC to recommend treating *N. gonorrhoeae* with dual therapy involving ceftriaxone and azithromycin [318, 326]. Yet, resistance to this dual therapy has been reported, leading to the rise of multidrug-resistant *N. gonorrhoeae* (commonly referred to as super gonorrhea) [319]. To make matters worse, no new classes of antibiotics to treat *N. gonorrhoeae* have been FDA approved over the last two decades warranting the public health concern that once easily treated gonorrhea infections will soon become deadly [327 328-329]. Therefore, the rise in multidrug-resistant *N. gonorrhoeae* infections necessitates intense research efforts to identify and develop new antibiotics.

Our program focuses on the development of *N*-(1,3,4-oxadiazol-2-yl)benzamides to treat drug-resistant bacterial pathogens[117, 134]. We recently reported the discovery of trifluoromethylsulfonyl (SO_2CF_3), trifluoromethylthio (SCF_3) and pentafluorosulfanyl (SF_5) containing *N*-(1,3,4-oxadiazol-2-yl)benzamides that exhibited potent antibacterial activities against clinically important Gram-positive bacterial pathogens [164]. These agents were found to be active against clinical isolates of drug-resistant Gram-positive bacteria, were non-toxic to mammalian cells, and effectively reduced the burden of intracellular methicillin-resistant *Staphylococcus aureus* (MRSA) [164]. Here, we describe a new generation of *N*-(1,3,4-oxadiazol-2-yl)benzamides with potent activity against *N. gonorrhoeae.* The antibacterial activity against *N. gonorrhoeae,* cytotoxicity against mammalian cells and bi-directional Caco-2 permeability were investigated.

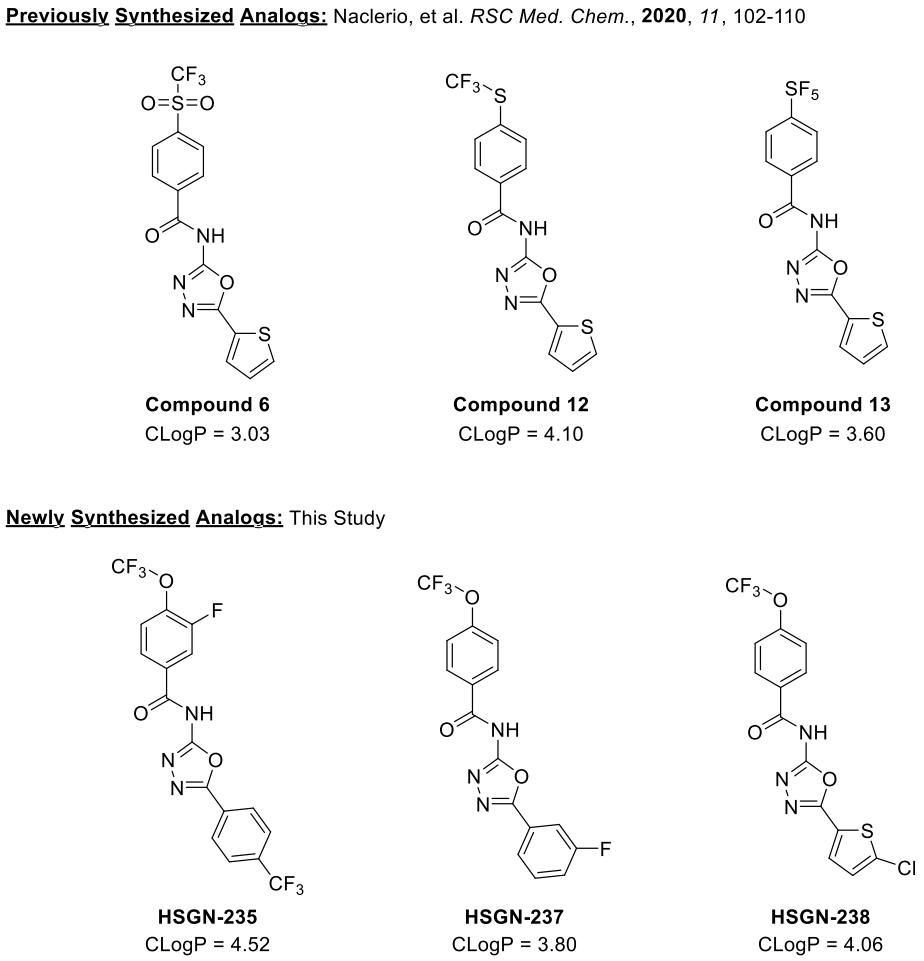

Figure 7.1 Previously reported analogs as well as newly synthesized *N*-(1,3,4-oxiadizol-2-yl)benzamides for this study. Note: CLogP was calculated using SwissADME.

7.3 Results and Discussion

7.3.1 Synthesis and Antigonococcal Activity of N-(1,3,4-oxadiazol-2-yl)benzamides

We previously reported that trifluoromethylsulfonyl (SO_2CF_3), trifluoromethylthio (SCF_3) and pentafluorosulfanyl (SF_5) containing *N*-(1,3,4-oxadiazol-2-yl)benzamides (compounds 6, 12 and 13 respectively) were potent against a panel of drug-resistant Gram-positive bacteria [164]. We wondered if these compounds would be active against *N. gonorrhoeae* and discovered that compounds 6, 12, and 13 have quite potent activity against N. gonorrhoeae strain 181 with minimum inhibitory concentrations (MICs) of 0.5 µg/mL, 0.06 µg/mL, and 0.06 µg/mL respectively (see Table 7.1). While all three compounds have favorable CLogP values, they also contain an unsubstituted thiophene moiety (Figure 7.1) which can cause toxicity. For example, cytochrome P450 mediated oxidation of thiophene moeities can lead to reactive metabolites such

as thiophene epoxides[287], thiophene-S oxides[286-287] and sulphenic acids[288] which can react with nucleophiles like glutathione and/or water[289]. However, since Compounds 6, 12, and 13 showed excellent activities against *N. gonorrhoeae*, as well as adequate CLogP vales we desired to further optimize these compounds via the synthesis of new analogs. We proceeded to use computational methods to guide our synthetic strategy. We began to substitute the benzamide ring with the trifluoromethoxy (OCF_3) group due to its importance in medicinal chemisty[330-331]. For instance, it was reported that the electronegativity of the OCF_3 group allows for enhanced *in vivo* uptake and transport in biological systems[330]. Thus, utilizing this strategy led to the synthesis of HSGN-235 which contained a fluoro atom ortho to the OCF_3 group as well as a trifluoromethyl phenyl. Yet, HSGN-235 was found to contain a much larger CLogP value compared to previously synthesized analogs (Figure 7.1). Since LogP shows a positive correlation between low aqueous solubility and compromising bioavailability (an extremely important attribute when creating antibacterial agents against *N. gonorrhoeae*)[332], we replaced the thiophene moiety with substituted thiophene or phenyl group as unsubstituted thiophene could be a toxicophore, as mentioned above. Considering that the addition of halogens to compounds has been shown to improve drug properties and metabolic stability[278-280, 283-284], our new analogs were made up of compounds with halogen substitutions to a phenyl ring (Figure 7.1).

The synthesis of these compounds started with a substituted aryl aldehyde followed by the addition of semicarbazide and sodium acetate to give the corresponding semicarbazone. Then, using bromine and sodium acetate, the semicarbazone was converted into the subsequent aryl 1,3,4-oxadizol-2-amine. Amide coupling between the aryl 1,3,4-oxadiazol-2-amine and 4-trifluoromethoxy benzoic acid using benzotriazol-1-yloxytris(dimethylamino)phosphonium hexafluorophosphate (BOP) reagent gave the desired *N*-(1,3,4-oxadiazol-2-yl)benzamides (Scheme 7.1).

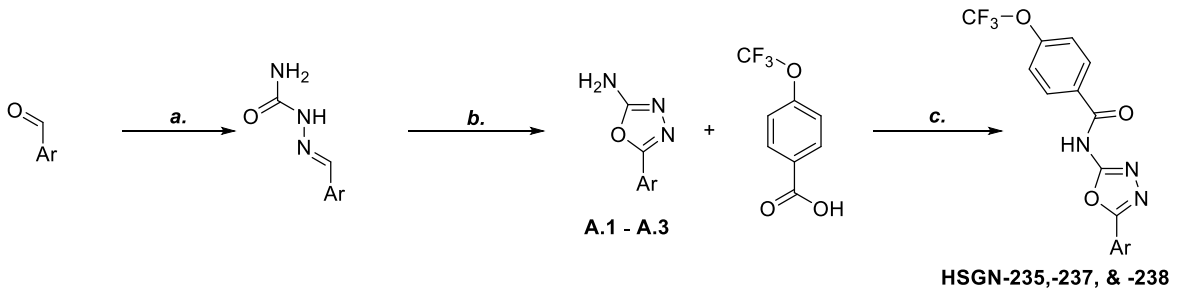

Scheme 7.1 Synthesis of N-(1,3,4-oxadiazol-2-yl)benzamides[a]. [a]Reagents and Conditions: (a) Semicarbazide hydrochloride, NaOAc, MeOH:H_2O (1:1), rt, 30 min. (b) Bromine, NaOAc, AcOH, 60°C, 1 h. (c) BOP Reagent, DIPEA, DMF, rt, 12 h.

Trifluoromethoxy containing (1,3,4-oxadiazol-2-yl)benzamides with substitution of the thiophene moiety with a fluorophenyl (HSGN-237) or chlorothiophenyl (HSGN-238) groups had potent activity against *N. gonorrhoeae* strain 181 with MICs of 0.125 µg/mL (Table 1). Interestingly, substitution of the 4-trifluoromethoxy phenyl group with a fluorine, as well as substitution of the thiophene moiety with trifluoromethylphenyl (HSGN-235) only had moderate activity when tested against *N. gonorrhoeae* strain 181 (Table 7.1).Since both HSGN-237 and HSGN-238 contained aromatic rings bearing a halogen atom, we speculate that the loss of activity for HSGN-235 is due to the addition of the fluorine atom ortho to the trifluoromethoxy group (see Figure 7.1 and Table 7.1 for comparisons).

Table 7.1 MICs (µg/mL) of the previously reported analogs (compounds 6, 12 and 13) and the new compounds (HSGN-235, -237 and -238) against *N. gonorrhoeae* strain 181. The experiment was repeated for 3 independent times.

Compound/Control Drug	*N. gonorrhoeae* strain 181
Compound 6	0.5
Compound 12	0.06
Compound 13	0.06
HSGN-235	16
HSGN-237	0.125
HSGN-238	0.125
Azithromycin	256
Tetracycline	2

After the initial screening against *N. gonorrhoeae* 181, the anti-gonococcal activity of HSGN-235, -237 and -238 was explored against a panel drug-resistant pathogenic N. gonorrhoeae strains including one WHO reference strain (*N. gonorrhoeae* WHO L) which has a well-characterized antibiogram, phenotypic and genetic markers[333]. As depicted in Table 7.2, HSGN-237 and -238 exhibited potent activity against the tested strains inhibiting their growth at concentrations ranging from 0.03 µg/mL to 0.125 µg/mL. Both were superior to azithromycin and tetracycline against the tested isolates. On the other hand, HSGN 235 inhibited the growth of the tested strains at concentrations ranging from 1 µg/mL to 2 µg/mL. Interestingly the minimum bactericidal concentration (MBC) values of HSGN235, -237 and -238 were the same as or one-fold higher than their corresponding MIC values indicating that the compounds exhibit bactericidal activity against the tested *N. gonorrhoeae* strains.

Table 7.2 MICs and MBCs (μg/mL) of HSGN-235, -237 and -238 against *N. gonorrhoeae* clinical isolates. The experiment was repeated for 3 independent times.

Bacterial Strains	HSGN-235		HSGN-237		HSGN-238		Azithromycin		Tetracycline	
	MIC	MBC	MIC	MBC	MIC	MBC	MIC	MBC	MIC	MBC
N. gonorrhoeae 165	2	2	0.06	0.125	0.125	0.25	1	4	4	8
N. gonorrhoeae 166	2	2	0.06	0.06	0.125	0.25	0.5	1	2	8
N. gonorrhoeae 194	1	1	0.03	0.06	0.125	0.125	0.25	0.5	1	4
N. gonorrhoeae 197	1	2	0.03	0.06	0.125	0.125	0.5	2	2	4
N. gonorrhoeae 200	2	2	0.06	0.06	0.125	0.125	0.5	0.5	2	8
N. gonorrhoeae WHO L	1	2	0.06	0.06	0.06	0.125	0.5	1	0.5	2

7.3.2 Antibacterial activity *of N-(*1,3,4-oxadiazol-2-yl)benzamides against other bacterial species

While the focus of these new *N*-(1,3,4-oxadiazol-2-yl)benzamides is towards *N. gonorrhoeae*, we proceeded to test their activity against other Gram-positive and Gram-negative pathogens. Intriguingly, HSGN-235, HSGN-237, and HSGN-238 had potent activity against the tested Gram-positive bacterial pathogens. For instance, all three compounds had potent activity against the staphylococcal strains with MICs ranging from 0.25 μg/mL to 1 μg/mL (Table 7.3). Furthermore, HSGN-235, HSGN-237, and HSGN-238 maintained potent activity against clinically relevant Gram-positive bacterial pathogens like vancomycin-resistant enterococci (VRE) and *Listeria monocytogenes* (Table 7.3). Additionally, we moved to test if HSGN-235, HSGN-237, and HSGN-238 were active against other Gram-negative bacterial pathogens. These compounds were found to be inactive against *E. coli* BW25113. This lack of activity against Gram-negative bacteria appears to be due to HSGN-235, HSGN-237, and HSGN-238 being a substrate for efflux. This can be seen by the shift in the MICs

observed for HSGN-235, HSGN-237, and HSGN-238 against wild-type *E. coli* BW25113 (MIC >8 µg/mL for all compounds; Table 7.3) in comparison to a mutant strain (*E. coli* JW55031) where the AcrAB-TolC multidrug-resistant efflux pump is knocked out (MIC for HSGN-235, HSGN-237, and HSGN-238 improves to 4 µg/mL, 0.25 µg/mL, and 0.06 µg/mL respectively; Table 3). A similar result was observed with linezolid, an antibiotic known to be a substrate for the AcrAB-TolC efflux pump in Gram-negative bacteria, as reported in previous reports[334-335]. Interestingly, HSGN-235, HSGN-237, and HSGN-238 appeared to be bacteriostatic agents as their MBCs were more than three-folds higher than their corresponding MICs against the tested bacterial strains (Table 7.3)

Table 7.3 MICs (μg/mL) and minimum bactericidal concentrations (MBCs, in μg/mL) of HSGN-235, HSGN-237, and HSGN-238 and control drugs (vancomycin, linezolid, and gentamicin) against a panel of clinically important Gram-positive and Gram-negative bacterial pathogens including: *Staphylococcus aureus*, methicillin-resistant *Staphylococcus aureus* (MRSA), *Enterococcus faecalis*, *Enterococcus faecium*, *Listeria monocytogenes*, and *Escherichia coli*. The experiment was repeated for 3 independent times.

	HSGN-235		HSGN-237		HSGN-238		Vancomycin		Linezolid		Gentamicin	
Bacterial Strains	MIC	MBC	MIC	MBC	MIC	MBC	MIC	MBC	MIC	MBC	MIC	MBC
S. aureus ATCC 25923	1	>64	0.25	>64	0.25	>64	1	1	2	64	NT	NT
MRSA USA300	**0.5**	64	0.25	32	0.25	16	1	2	1	16	NT	NT
E. faecalis ATCC 29212	4	32	1	>64	1	32	1	1	2	64	NT	NT
VRE. faecalis ATCC 51575	2	>64	1	>64	1	32	>64	>64	2	64	NT	NT
VRE. faecalis ATCC 51299	1	64	0.5	16	0.25	8	>64	>64	1	32	NT	NT
VRE. faecium ATCC 700221	1	32	0.5	8	0.25	8	32	32	2	64	NT	NT
L. monocytogenes ATCC 19115	1	64	0.5	64	0.5	32	1	1	2	64	NT	NT
E. coli BW25113 (wild-type strain)	>8	>8	>8	>8	>8	>8	>64	>64	>64	>64	0.25	0.25
E. coli JW55031 (TolC Mutant)	4	>64	0.25	16	0.06	32	>64	>64	8	>64	0.25	0.25

[1] NT: Not tested

7.3.3 Antibacterial Activity of *N*-(1,3,4-oxadiazol-2-yl)benzamides against N. gonorrhoeae in presence of serum

An increase in MIC due to antibiotics being highly protein bound has been documented in several classes of antibiotics[336-338]. Therefore, we evaluated our compounds' activity against *N. gonorrhoeae* in presence of different concentrations of fetal bovine serum (FBS). As presented in Table S2, the activity of HSGN-235, -237, and -238 was reduced in presence of FBS. Addition of 1%, 5%, and 10% FBS to the media increased the MIC of HSGN-237 to 0.125 µg/mL, 1 µg/mL, and 4 µg/mL respectively (See Table S2). Similarly, the MIC of HSGN-238 also changed to 0.25 µg/mL and 1 µg/mL in the presence of 1% and 5% FBS respectively but stayed at 1 µg/mL with addition of 10% FBS (Table S2). The MIC of HSGN-235 did not change in the presence of 1% FBS, but increased to 4 µg/mL and 8 µg/mL in the presence of 5% and 10% FBS respectively (Table S2). On the other hand, the MIC values of azithromycin and tetracycline remained the same or one-fold higher than their corresponding MIC values in absence of FBS (Table S2). Yet, hydrophobic antibiotics such as antimicrobial peptides and lipopeptides have been found to show an increase in MIC upon the addition of serum to media[339-340]. Therefore, we predict that the hydrophobicity of these *N*-(1,3,4-oxadiazol-2-yl)benzamides contributes to the rise in MIC in the presence of FBS.

7.3.4 *N*-(1,3,4-oxadiazol-2-yl)benzamides are highly tolerable to human cell lines

Prokaryotic cell selectivity is highly important for an antibiotic candidate. Therefore, since HSGN-237 and -238 were found to be the most potent analogs against *N. gonorrhoeae*, they were assessed for toxicity to mammalian cells over a 24- and 48-hour period (Figure 7.2A & B). Both compounds showed excellent safety profiles against human colorectal cells (Caco-2). For instance, HSGN-237 was non-toxic at concentrations higher than 64 µg/mL which is 512-times higher than the compound's corresponding MIC values against *N. gonorrhoeae* (Figure 7.2A & B). Additionally, HSGN-238 was non-toxic at concentrations up to 16 µg/mL which is 128-times higher than the compound's corresponding MIC values against *N. gonorrhoeae* (Figure 7.2A & B).

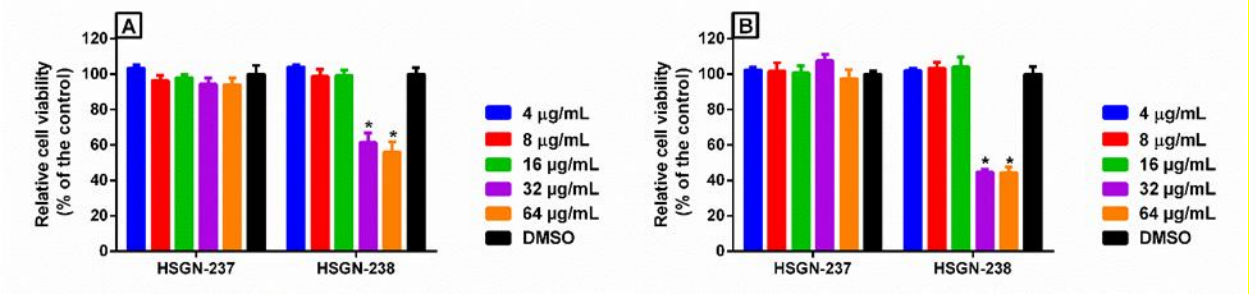

Figure 7.2 *In vitro* cytotoxicity assessment of HSGN-237 and -238 (tested in triplicate) against human colorectal cells (Caco-2) after: A) 24 hours, and B) 48 hours, using the 3-(4,5-dimethylthiazol-2-yl)-5-(3-carboxymethoxyphenyl)-2-(4-sulfophenyl)-2H-tetrazolium (MTS) assay. Results are presented as percent viable cells relative to DMSO (negative control). Error bars represent standard deviation values. A two-way ANOVA, with post hoc Dunnet's multiple comparisons test, determined the statistical difference between the values obtained for the compound and DMSO. Asterisks denote statistically significant difference between treatment of cells with either HSGN-237 or -238 as compared to DMSO-treated cells. The experiment was repeated for 3 independent times.

7.3.5 HSGN-238 demonstrates high intestinal permeability

Oral bioavailability is a highly important consideration when developing bioactive molecules as therapeutic agents[341]. A critical factor of oral bioavailability is human intestinal absorption. The Caco-2 bidirectional permeability assay is the most widely used *in vitro* model for predicting if a bioactive molecule can have adequate systemic absorption [342-343]. Thus, we selected HSGN-238 to act as a model to analyze the drug-like properties of newly synthesized *N*-(1,3,4-oxadiazol-2-yl)benzamides. The assay demonstrated that HSGN-238 showed outstanding ability to permeate across Caco-2 bilayers (apparent permeability, $P_{app} = 82.3 \times 10^{-6}$ cm s^{-1} from the apical to basolateral and $P_{app} = 32.9 \times 10^{-6}$ cm s^{-1} from the basolateral to apical, see Table 7.4). This permeability is comparable to propranolol ($P_{app} = 37.2 \times 10^{-6}$ cm s^{-1} from the apical to basolateral and $P_{app} = 22.7 \times 10^{-6}$ cm s^{-1} from the basolateral to apical (Table 7.4), a drug that is known to have high permeability across Caco-2 bilayers. Ranitidine was used as a low permeability control as its $P_{app} = 0.5 \times 10^{-6}$ cm s^{-1} from the apical to basolateral and $P_{app} = 1.3 \times 10^{-6}$ cm s^{-1} from the basolateral to apical. Therefore, the Caco-2 permeability results indicate that HSGN-238 has a high potential to be strongly absorbed after being administered orally.

Table 7.4 Caco-2 Permeability Analysis for HSGN-238 and control drugs.

Compound/Control Drug	Mean A → B P_{app} (cm s^{-1})	Mean B → A P_{app} (cm s^{-1})	Notes
HSGN-238	82.3 x 10^{-6}	32.9 x 10^{-6}	High Permeability
Ranitidine	0.5 x 10^{-6}	1.3 x 10^{-6}	Low Permeability Control
Propranolol	37.2 x 10^{-6}	22.7 x 10^{-6}	High Permeability Control

7.4 Materials and Methods

7.4.1 Chemistry

General Considerations: All reagents and solvents were purchased from commercial sources. The ^{1}H, ^{13}C, and ^{19}F NMR spectra were acquired in DMSO-d_6 as solvent using a 500 MHz spectrometer with Me_4Si as an internal standard. Chemical shifts are reported in parts per million (δ) and are calibrated using residual undeuterated solvent as an internal reference. Data for ^{1}H NMR spectra are reported as follows: chemical shift (δ ppm) (multiplicity, coupling constant (Hz), integration). Multiplicities are reported as follows: s = singlet, d = doublet, t = triplet, q = quartet, m = multiplet, or combinations thereof. High resolution mass spectra (HRMS) were obtained using electron spray ionization (ESI) technique and as TOF mass analyzer. New compounds were characterized by ^{1}H NMR, ^{13}C NMR, ^{19}F NMR, and HRMS data.

7.4.2 Synthesis of 1,3,4-oxadiazol-2-amines [A.1-A.3]

The synthesis of A.1-A.3 was performed following a literature reported procedure[210]. ^{1}H, ^{13}C, and ^{19}F NMR spectra were in agreement with literature reported data.

7.4.3 Amide Coupling Procedure for Synthesis of Compounds

A 20 mL screw caped vial, charged with the corresponding acid (1 eq.), amine (1 eq.), BOP reagent (2.7 eq.) and diisopropylethylamine (23 eq.) in DMF solvent (3 mL) was stirred at room temperature for 16 h. After completion, the reaction mixture was concentrated under reduced

pressure, followed by flash column chromatography (hexanes:ethyl acetate 80:20 to 60:40) gave the desired product.

7.4.4 Characterization Data

3-Fluoro-4-(trifluoromethoxy)-N-(5-(4-(trifluoromethyl)phenyl)-1,3,4-oxadiazol-2-yl)benzamide (HSGN-235):

Off-white solid (34 mg, 18%). ^{1}H NMR (500 MHz, DMSO-d_6) δ 8.1 (m, 2H), 8.0 (m, 2H), 7.8 (m, 2H), 7.5 (m, 1H). ^{13}C NMR (126 MHz, DMSO-d_6) δ 161.9, 160.1, 158.4, 153.0 (d, J = 258.3 Hz), 136.3 (d, J = 12.6 Hz), 132.0 (q, J = 32.8 Hz), 129.7, 127.5, 127.4, 126.9 (d, J = 3.78 Hz), 126.8, 126.0 (d, J = 5.04 Hz), 125.3, 123.1 (q, J = 288.5 Hz), 121.5 (q, J = 259.6 Hz). ^{19}F NMR (471 MHz, DMSO-d_6) δ -59.0 (s, 3F), -62.9 (s, 3F), -132.1 (s, 1F). HRMS (ESI) m/z calcd for $C_{17}H_9F_7N_3O_3$ $[M + H]^+$ 436.0532, found 436.0531.

N-(5-(3-fluorophenyl)-1,3,4-oxadiazol-2-yl)-4-(trifluoromethoxy)benzamide (HSGN-237):

Off-white solid (42 mg, 24%). ^{1}H NMR (500 MHz, DMSO-d_6) δ 8.2 (dd, J = 8.5, 3.6 Hz, 2H), 7.8 (dd, J = 7.9, 3.6 Hz, 1H), 7.7 – 7.6 (m, 2H), 7.5 (ddd, J = 34.6, 10.1, 6.0 Hz, 3H). ^{13}C NMR (126 MHz, DMSO-d_6) δ 165.0, 163.7 (d, J = 245.7 Hz), 160.2, 158.8, 151.9, 132.4 (d, J = 8.82 Hz), 132.2, 131.3, 125.9 (d, J = 8.82 Hz), 122.8, 121.5 (q, J = 259.6 Hz), 121.1, 119.3 (d, J = 21.4 Hz), 113.3 (d, J = 23.9 Hz). ^{19}F NMR (471 MHz, DMSO-d_6) δ -57.8 (s, 3F), -112.5 (q, J = 8.1 Hz, 1F). HRMS (ESI) m/z calcd for $C_{16}H_{10}F_4N_3O_3$ $[M + H]^+$ 368.0658, found 368.0659.

N-(5-(5-chlorothiophen-2-yl)-1,3,4-oxadiazol-2-yl)-4-(trifluoromethoxy)benzamide (HSGN-238):

Off-white solid (45 mg, 24%). ^{1}H NMR (500 MHz, DMSO-d_6) δ 8.1 (d, J = 8.5 Hz, 2H), 7.6 (d, J = 4.1 Hz, 1H), 7.5 (m, 2H), 7.3 (m, 1H). ^{13}C NMR (126 MHz, DMSO-d_6) δ 164.8, 158.0, 156.5, 151.9, 133.5, 131.9, 131.3, 129.9, 129.1, 123.7, 121.4 (q, J = 258.3 Hz), 121.1. ^{19}F NMR (471 MHz, DMSO-d_6) δ -57.8 (s, 3F). HRMS (ESI) m/z calcd for $C_{14}H_8ClF_3N_3O_3S$ $[M + H]^+$ 389.9927, found 389.9925.

7.4.5 Bacterial strains, media, reagents and cell lines

Neisseria gonorrhoeae clinical isolates (Table 1S) used in this study were obtained from the CDC. *S. aureus*, MRSA, *E. faecalis*, *E. faecium*, and *L. monocytogenes* strains were obtained from the American Type Culture Collection (ATCC). *E. coli* BW25113 and JW25113 were obtained from the Coli Genetic Stock Center (CGSC), Yale University, USA. Media and reagents were purchased from commercial vendors: Brucella broth, chocolate II agar, cation-adjusted Mueller Hinton broth, tryptic soy broth (TSB) and tryptic soy agar (TSA) (Becton, Dickinson and Company, Cockeysville, MD, USA); yeast extract and dextrose (Fisher Bioreagents, Fairlawn, NJ, USA), proteose-peptone, nicotinamide adenine dinucleotide (NAD), agarose and tetracycline (Sigma-Aldrich, St. Louis, MO, USA); hematin, Tween 80, pyridoxal, linezolid and gentamicin sulfate (Chem-Impex International, Wood Dale, IL, USA); Dulbecco's Modified Eagle Medium (DMEM), fetal bovine serum (FBS) and phosphate-buffered saline (PBS) (Corning, Manassas, VA, USA); and azithromycin (TCI America, Portland, OR, USA). Human colorectal adenocarcinoma epithelial cells (Caco-2) (ATCC HTB-37) was obtained from the American Type Culture Collection (ATCC) (Manassas, VA, USA). Compounds were synthesized from commercial sources in our laboratory.

7.4.6 Determination of the MICs of compounds and control drugs against *N. gonorrhoeae* strains

MICs of the tested compounds and control drugs; azithromycin, and tetracycline were determined using the broth microdilution as described previously[344-346]. Briefly, bacteria were grown overnight on chocolate agar II at 37° C in presence of 5% CO_2. Afterwards, a bacterial suspension equivalent to 1.0 McFarland standard was prepared and diluted in brucella broth supplemented with yeast extract, neopeptone, hematin, pyridoxal and NAD. Test agents were added in the first row of the 96-well plates and serially diluted along the plates. Plates were then, incubated at 37° C in the presence of 5% CO_2 for 24 hours. MICs reported in Table 1 are the minimum concentrations of the compounds and control drugs that could completely inhibit the visual growth of bacteria. The minimum bactericidal concentration (MBC) of these drugs was tested by plating 4 µL from wells with no growth onto chocolate agar II plates. Plates were then, incubated at 37° C in the presence of 5% CO_2 for 24 hours. The MBC was categorized as the lowest concentration that reduced bacterial growth by 99.9%[299, 347-348].

7.4.7 Determination of the MICs and MBCs of compounds and control drugs against clinically important Gram-positive and Gram-negative bacteria

The minimum inhibitory concentrations (MICs) of the tested compounds and control drugs; linezolid, vancomycin, and gentamicin were determined using the broth microdilution method, according to guidelines outlined by the Clinical and Laboratory Standards Institute (CLSI)[212] against clinically-relevant bacterial (*Staphylococcus aureus*, MRSA, *Escherichia coli*, *Enterococcus faecalis* and *Enterococcus faecium* strains. *S. aureus*, MRSA, *E. coli*, *Enterococcus faecalis* and *Enterococcus faecium* were grown aerobically overnight on tryptone soy agar (TSA) plates at 37° C. Afterwards, a bacterial solution equivalent to 0.5 McFarland standard was prepared and diluted in cation-adjusted Mueller-Hinton broth (CAMHB) (for *S. aureus*, MRSA, and *E. coli*) to achieve a bacterial concentration of about 5×10^5 CFU/mL. *Enterococcus faecalis* and *Enterococcus faecium* 0.5 McFarland standard solution was diluted in tryptone soy broth (TSB) to achieve a bacterial concentration of about 5×10^5 CFU/mL. Compounds and control drugs were added in the first row of the 96-well plates and serially diluted with the corresponding media containing bacteria. Plates were then, incubated as previously described. MICs reported in Table 2 are the minimum concentration of the compounds and control drugs that could completely inhibit the visual growth of bacteria. The minimum bactericidal concentration (MBC) was tested by spotting 4 µL from wells with no growth onto TSA plates. Plates were incubated at 37 ° C for at least 18 hours before recording the MBC. The MBC was categorized as the lowest concentration that reduced bacterial growth by 99.9%[299, 347-348].

7.4.8 In vitro cytotoxicity analysis of HSGN-237 and -238 against human colorectal cells.

HSGN-237 and -238 were assayed for potential cytotoxicity against a human colorectal adenocarcinoma (Caco-2) cell line, as described previously[117, 349-350]. Briefly, tested compounds were incubated with caco-2 cells for 24 and 48 hours. Then, cells were incubated with MTS (3-(4,5-dimethylthiazol-2-yl)-5-(3-carboxymethoxyphenyl)-2-(4-sulfophenyl)-2H-tetrazolium) reagent for 4 hours before measuring absorbance values (OD_{490}).

7.4.9 Caco-2 permeability assay

Assay and data analysis were performed by Eurofins Panlabs (MO, USA) according to a previously reported protocol[312-313]. The apparent permeability coefficient (P_{app}) of the tested agents was calculated using the equation below:

$$P_{app}(cm/s) = \frac{V_R * C_{R,end}}{\Delta t} * \frac{1}{A*(C_{D,mid}-C_{R,mid})}$$

where V_R is the volume of the receiver chamber. $C_{R,end}$ is the concentration of the test compound in the receiver chamber at the end time point, Δt is the incubation time and A is the surface area of the cell monolayer. $C_{D,mid}$ is the calculated mid-point concentration of the test compound in the donor side, which is the mean value of the donor concentration at time 0 minute and the donor concentration at the end time point. $C_{R,mid}$ is the mid-point concentration of the test compound in the receiver side, which is one half of the receiver concentration at the end time point. Concentrations of the test compound were expressed as peak areas of the test compound.

7.5 Conclusion

We have identified promising *N*-(1,3,4-oxadiazol-2-yl)benzamides with potent antibacterial activity against *N. gonorrhoeae*. Furthermore, HSGN-237 and -238 exhibited highly acceptable tolerability to human colon cells. Moreover, when assessed using a Caco-2 bidirectional permeability assay, HSGN-238 showed remarkable ability to cross Caco-2 bilayers, indicating it would have favorable systemic absorption. Thus, the potent antibacterial profiles of these *N*-(1,3,4-oxadiazol-2-yl)benzamides warrants further investigation and exploration as potential therapeutics to treat drug-resistant *N. gonorrhoeae* infections. OCF_3 modified *N*-(1,3,4-oxadiazol-2-yl)benzamides add to the list of novel antibacterial agents with novel scaffolds that we have reported[163, 217, 222, 252].

7.6 Supplementary Information

For ^{1}H, ^{13}C, ^{19}F, and HRMS data, please see the supplementary information located on *the Int J Mol Sci* website.

7.7 Author Contributions

G. Naclerio synthesized all compounds for study. G. Naclerio and N. Abutaleb performed MIC experiments. N. Abutaleb performed cytotoxicity study. G. Naclerio and H. Sintim wrote the manuscript.

CHAPTER 8. COMPARATIVE STUDIES TO UNCOVER FURTHER MECHANISMS OF ACTION OF *N*-(1,3,4-OXADIAZOL-2-YL)BENZAMIDE CONTAINING ANTIBACTERIAL AGENTS

8.1 Abstract

Drug-resistant bacterial pathogens still cause high levels mortality annually despite the availability of many antibiotics. *Staphylococcus aureus* (MRSA) is especially problematic and the rise in resistance to front line treatments like vancomycin and linezolid calls for new chemical modalities to treat chronic and relapsing *S, aureus* infections. Halogenated *N*-(1,3,4-oxadiazol-2-yl)benzamides are interesting class of antimicrobial agents, which have been described by multiple groups to be effective against different bacterial pathogens. The modes of action of a few *N*-(1,3,4-oxadiazol-2-yl)benzamides have been elucidated. For example, oxadiazoles KKL-35 and MBX-4132, have been described as inhibitors of *trans*-translation (a ribosome rescue pathway) while HSGN-94 was shown to inhibit lipoteichoic acid. However other similarly halogenated *N*-(1,3,4-oxadiazol-2-yl)benzamides neither inhibit *trans*-translation nor LTA but are potent antimicrobial agents. For example, HSGN-220, -218, and -144 are *N*-(1,3,4-oxadiazol-2-yl)benzamides that are modified with OCF_3, SCF_3 or SF_5, and have remarkable minimum inhibitory concentrations (MICs) ranging from 1 μg/mL to 0.06 μg/mL against MRSA clinical isolates and show a low propensity to resistance to MRSA over 30 days. The mechanism of action (MAO) of these highly potent oxadiazoles is however unknown. To provide insights into how these halogenated *N*-(1,3,4-oxadiazol-2-yl)benzamides inhibit bacterial growth, we performed global proteomics and RNA expression analysis of some essential genes of *S. aureus* treated with HSGN-220, -218, and -144. These studies revealed that the oxadiazoles HSGN-220, -218, and -144 are multi-action antibiotics that regulate menaquinone biosynthesis and other essential proteins like DnaX, Pol IIIC, BirA, LexA, and DnaC. In addition, these halogenated *N*-(1,3,4-oxadiazol-2-yl)benzamides were able to depolarize bacterial membranes and regulate siderophore biosynthesis and heme regulation. Iron starvation appears to be part of the MOA that led to bacterial killing. This study demonstrates that *N*-(1,3,4-oxadiazol-2-yl)benzamides are indeed privileged scaffolds for the development of antibacterial agents and that subtle modifications lead to changes to MOA.

8.2 Introduction

Antimicrobial resistance has become a global crisis and it has been estimated that if antimicrobial resistance is not controlled, then by 2050 10 million people each year will die as a result, surpassing annual deaths due to cancer[131]. In the United States, antimicrobial resistance is also a problem. The Centers for Disease Control and Prevention (CDC) recently stated that more than 2.8 million antibiotic-resistant infections occur in the U.S. each year, resulting in more than 35,000 deaths[170]. A Gram-positive bacterial pathogen, *Staphylococcus aureus* (*S. aureus*) is one of the leading causes of community- and hospital- acquired bacteremia, surgical site infections, osteomyelitis, pneumonia, and skin infections[107]. The CDC has designated methicillin-resistant *S. aureus* (MRSA) as a serious threat as it causes 323,700 infections per year resulting in 10,600 deaths[170]. Yet, MRSA's continued rise in both infection and death rate has been attributed to the shortage of newly approved antibiotics with novel mechanisms of action[46]. This lack in development of novel antibiotics is due to the scarce number of pharmaceutical companies with an antibiotic research and development pipeline as it is considered a non-profitable venture because of the high likelihood of resistance emerging[351]. Still, newer antibiotics that have been approved or in clinical trials are derivatives of existing drugs so resistance mechanism that affect the old drugs will also likely affect the newer ones as well[156]. Therefore, the generation of antibiotics with new chemotypes and novel mechanisms of action is of high priority.

Halogenated *N*-(1,3,4-oxadiazol-2-yl)benzamides have emerged as novel compounds with potent activities against several strains of bacteria[117, 134, 163-166, 352-354]. We recently reported that the sulfonamide containing *N*-(1,3,4-oxadiazol-2-yl)benzamide, HSGN-94 (Figure 8.1), inhibits LTA biosynthesis and is a potent inhibitor of MRSA growth (MIC = 0.25 ug/mL)[134, 166]. Keiler and co-workers have also reported that a chloro-substituted acylaminooxadiazole (KKL-35, Figure 8.1) was an inhibitor of *trans*-translation in bacteria. the Gillet et al. have argued that *trans*-translation is not the only target for KKL-35 *in vivo*[355]. While *trans*-translation inhibition or LTA biosynthesis inhibition might partly explain the antibacterial action of some oxadiazole-containing compounds, other halogenated *N*-(1,3,4-oxadiazol-2-yl)benzamides developed by the Gillet group (CT1-115, Figure 8.1)[354] and by our group (HSGN-220, -218, and -144)[163,164] do not inhibit *trans*-translation or LTA biosynthesis. To provide insights into how various halogenated *N*-(1,3,4-oxadiazol-2-yl)benzamides inhibit *S. aureus*, we performed various mechanistic studies, including comparative global proteomics, membrane depolarization and membrane permeation assays, to

identify pathways that are impacted by the oxadiazole-containing compounds and to investigate how subtle modifications affect the biological activities of these interesting antibacterial agents.

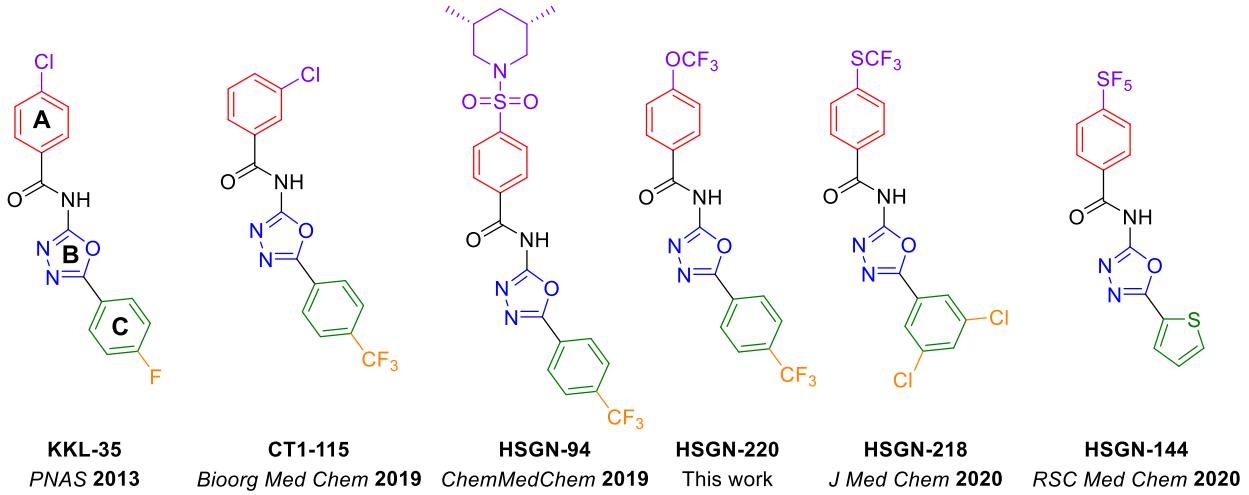

Figure 8.1 Structures of previously reported *N*-(1,3,4-oxadiazol-2-yl)benzamides as potent antibacterial agents against Gram-positive bacteria.

8.3 Results and Discussion

8.3.1 HSGN-220, -218, and -144 demonstrate potent activity against MRSA clinical isolates

To evaluate HSGN-220, -218, and -144's potential as therapeutics against drug-resistant bacteria, we proceeded to evaluate their antibacterial profile against a panel of MRSA clinical isolates. HSGN-218 was previously reported to have highly potent activities against *C. difficile* but its activity against MRSA was not explored[163]. However, our analysis demonstrates that HSGN-218 has remarkable activity against MRSA clinical isolates with MICs ranging from 0.06 µg/mL (0.1 µM) to 0.25 µg/mL (0.6 µM) (See Appendix B for Table B.1). Additionally, HSGN-144 was reported to have activity against MRSA as well as other drug-resistant Gram-positive strains[164]. Here, the compound also demonstrates high potency against MRSA clinical isolates with MICs of 0.5 µg/mL (1.3 µM) (Table B.1). Furthermore, HSGN-220 showed potent antibacterial activity against MRSA clinical isolates as well with MICs ranging from 0.25 µg/mL (0.6 µM) to µg/mL 1 (2.4 µM) (Table B.1). Overall, the compounds performed similarly or better than vancomycin (especially HSGN-218) but significantly outperformed the small molecule antibiotic linezolid against MRSA clinical isolates.

8.3.2 HSGN-220, -218, and -144 have a low propensity to develop resistance to MRSA

Based on HSGN-220, -218, and -144's impressive activity against MRSA, our next step was to determine their mechanism of action against *S. aureus*. A classical method to do this involves obtaining resistant mutants via serial passaging and then using genomic mapping to identify mutations in the target protein(s)[356]. Therefore, we performed the multi-step resistance selection to generate MRSA resistant-mutants for HSGN-220, -218, and -144. However, we failed to generate any resistant mutants after 30 days, indicating that these compounds have a low propensity to develop resistance to MRSA as they performed similarly to known antibiotics vancomycin and linezolid (see Appendix B for Figure B.1). In contrast, the MIC of ciprofloxacin, an antibiotic that targets DNA gyrase, increased four-fold after the fifth passage and continued to increase afterward (Figure B.1). MRSA resistance to ciprofloxacin appeared after the ninth passage (an eight-fold increase in MIC was detected, see Figure B.1). By the fifteenth passage, the MIC of ciprofloxacin increased more than 32-fold from the original MIC value (0.25 μg/mL). The development of MRSA resistance to ciprofloxacin agrees with previously reports[357-359].

8.3.3 Effects of HSGN-220, -218, and -144 on global proteomics in *S. aureus*

Since we could not obtain HSGN-220, -218, or -144 resistant-mutants, we decided to use global proteomics with the aim of assessing the proteins and pathways that are affected by treatment with these compounds. Thus, we treated *S. aureus* with either HSGN-220, -218, or -144 for 2 hours and extracted the total protein for profiling using mass spectrometry. HSGN-220, -218, or -144 treated samples were compared with samples treated with DMSO only (untreated). For each compound, a Venn diagram was constructed to determine the proteins found either in the untreated or treated samples (Figure B.1). A total of 1,000 proteins were identified after *S. aureus* treatment with HSGN-220. Of these 1,000 proteins, 781 proteins (78.1%) were observed to be shared by both DMSO control and HSGN-220 whereas 157 proteins (15.7%) were only identified in DMSO control, and 62 proteins (6.2%) were only identified in HSGN-220 (Figure B.1A). Additionally, a total of 982 proteins were identified after *S. aureus* treatment with HSGN-218. Of these 982 proteins, 736 proteins (74.9%) were observed to be shared by both DMSO control and HSGN-218 while 202 proteins (20.6%) were only identified in DMSO control, and 44 proteins (4.5%) were only identified in HSGN-218 (Figure B.1B). Furthermore, a total of 1,018 proteins

were identified after *S. aureus* treatment with HSGN-144. Of these 1,018 proteins, 825 proteins (81.0%) were observed to be shared by both DMSO control and HSGN-144 whereas 113 proteins (11.1%) were only identified in DMSO control, and 80 proteins (7.9%) were only identified in HSGN-144 (Figure B.1C). Interestingly, heatmap analysis reveals that HSGN-220, -218, and -144 differentially regulate *S. aureus* gene expression (Figure 8.2A).

The proteomics data were then stringently filtered using label-free quantitation (LFQ) intensities and MS/MS counts. Proteins in samples that had LFQs for all three replicates and with at least 2 MS/MS counts were included for further analysis. Proteins found in only treated samples were considered to be highly upregulated while those found in only DMSO control were considered to be highly downregulated.

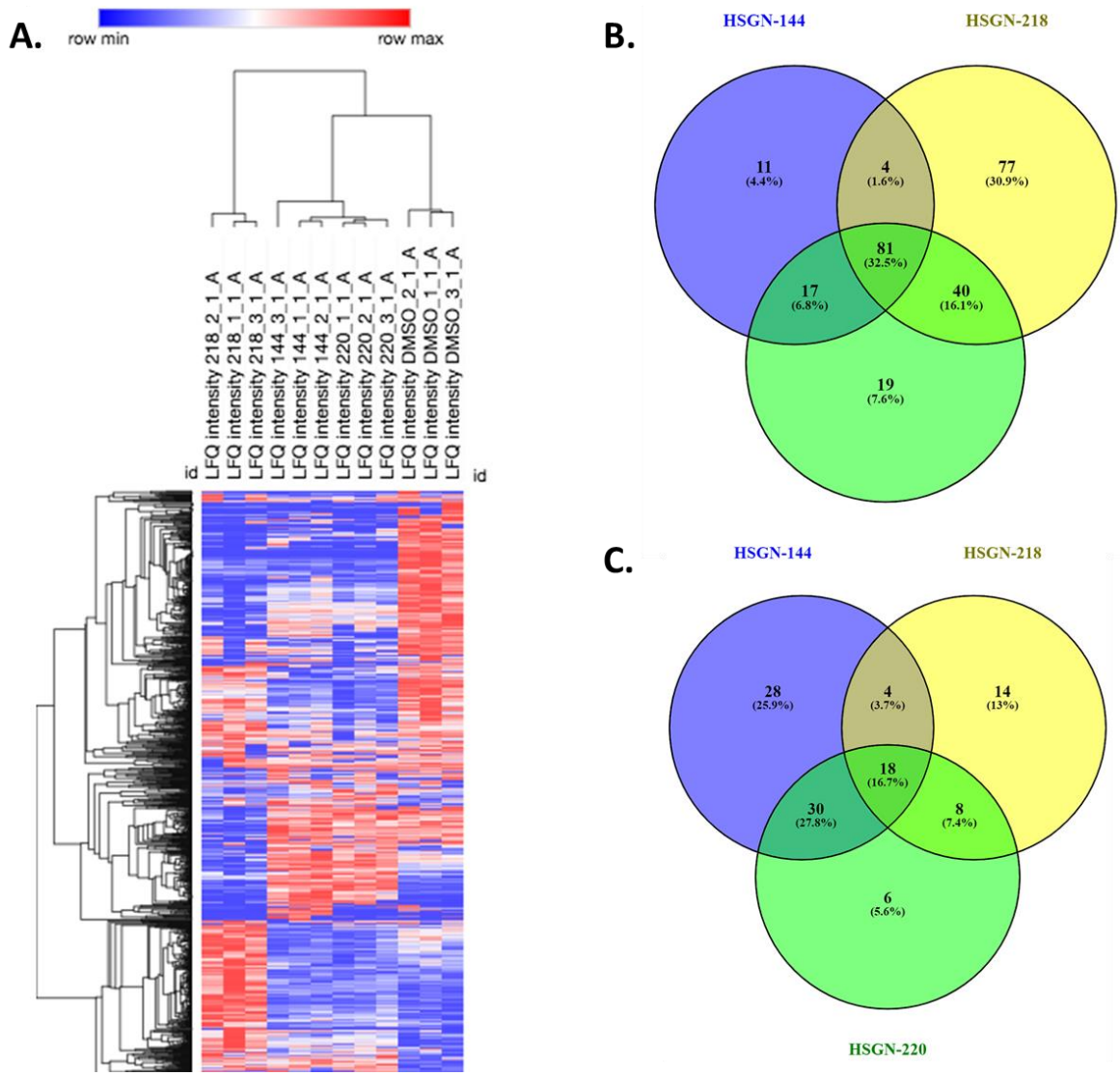

Figure 8.2 Global proteomics analysis of HSGN-220, -218, and -144. (A) Heatmap evaluation of global proteomics data displaying differentially expressed proteins between DMSO- and HSGN-220, -144, or -218-treated *S. aureus*. (B) Venn diagram for comparison of downregulated proteins identified individually, dually, or amongst all three compounds: HSGN-220, -218, and -144. (C) Venn diagram for comparison of upregulated proteins identified individually, dually, or amongst all three compounds: HSGN-220, -218, and -144.

Next, we then sought to compare proteins downregulated by HSGN-220, -218, and -144 via generation of a Venn diagram (Figure 8.2B). After stringent filtration, 249 proteins were identified in DMSO control only when compared to samples treated with HSGN-220, -218, and -144. Of the 249 proteins, 81 (32.5%) were observed to be shared among all three compounds. Individually, 11 proteins (4.4%) were identified in HSGN-144, 77 proteins (30.9%) were detected in HSGN-218, and 19 proteins (7.6%) were found in HSGN-220. Furthermore, 40 proteins

(16.1%) were shared between HSGN-218 and HSGN-220, while 17 proteins (6.8%) were discovered in both HSGN-144 and HSGN-220. Only 4 proteins (1.6%) were detected in both HSGN-218 and HSGN-144.

During our assessment, we first began by analyzing the 81 proteins that were downregulated by all three compounds (see Appendix B for Table B.2). Specifically, we were interested in identifying proteins that were essential to *S. aureus* as these are the most important for the bacteria's growth. We did this by utilizing the comprehensive list of *S. aureus* essential genes developed by Charles et al[180]. We found that all three compounds had a significant impact on DNA synthesis in *S. aureus.* For instance, all three compounds downregulated DNA polymerase III subunit τ/γ (*dnaX*), DNA polymerase III subunit α (*pol IIIC*), and the replicative DNA helicase (*dnaC*) (Table 8.1). Both *dnaX* and *polC* are required for replicative DNA synthesis while *dnaC* participates in initiation and elongation during chromosome replication[360-361]. Additionally, we found that HSGN-220, -218, and -144 also downregulate the essential proteins *birA* and *lexA* (Table 8.1). *birA* is a Group II biotin protein ligase (BPL) which is essential for the catalytic attachment of biotin to biotin-dependent enzymes, resulting in the synthesis of important lipids that make up the cell wall[362]. Furthermore, *lexA* is vital for *S. aureus* to produce the SOS response which modifies transcription in response to environmental stress[363]. Also, this SOS response mediated by *lexA* has been found to play an important role in antibiotic resistance and persistence of *S. aureus* infections[363].

Table 8.1 Select essential proteins that were identified to be downregulated by HSGN-220, -218, and -144.

ID	Protein	Description	Essential in *S. aureus*?
gi|685631628	DnaX	DNA polymerase III τ/γ	Yes
gi|685632359	Pol IIIC	DNA polymerase III α	Yes
gi|685632567	BirA	biotin--acetyl-CoA-carboxylase ligase	Yes
gi|685632450	LexA	XRE family transcriptional regulator	Yes
gi|685631229	DnaC	Replicative DNA helicase	Yes

All three compounds downregulated DNA *pol IIIC,* which has been viewed as a viable new target to combat Gram-positive infections[364]. This is because Pol IIIC is vital for replication of the bacterial chromosome as it makes up a major portion of the DNA Pol III core (see Figure 8.3A). Additionally, Pol IIIC also interacts with other essential proteins necessary for DNA replication like DnaC and DnaX (Figure 8.3B), meaning if Pol IIIC is affected, these other proteins will also be altered, and DNA replication will not take place. Furthermore, Pol IIIC is a highly conserved enzyme and is exclusive to bacteria whose genomes contain less than 50% guanine and cytosine such as: *Streptococcus, Enterococcus, Staphylococcus, Bacillus, Clostridioides, Pneumococcus, Listeria,* and *Lactobacillus*[365]. Moreover, Pol IIIC is not found in Gram-negative bacteria and has little homology with mammalian DNA polymerase, making it specific for Gram-positive pathogens[364]. Because of the uniqueness of Pol IIIC as well as its ability to be a novel drug target to combat Gram-positive bacteria, inhibitors of this enzyme have been developed. For instance, the earliest known inhibitors of Pol IIIC contained the anilino-uracil moiety which showed potent binding to Pol IIIC in *Bacillus subtilis* (*B. subtilis*) but only had moderate activity against Gram-positive bacteria with MICs between 20 µg/mL – 40 µg/mL[366-367]. Ibezapolstat (ACX-362E), which selectively inhibits *C. difficile* Pol IIIC is currently in Phase II clinical trials for *C. difficile* infection[368]. The downregulation of DNA Pol IIIC as well as other proteins essential for DNA replication by HSGN-220, -218, and -144 could explain the potency of these compounds against MRSA.

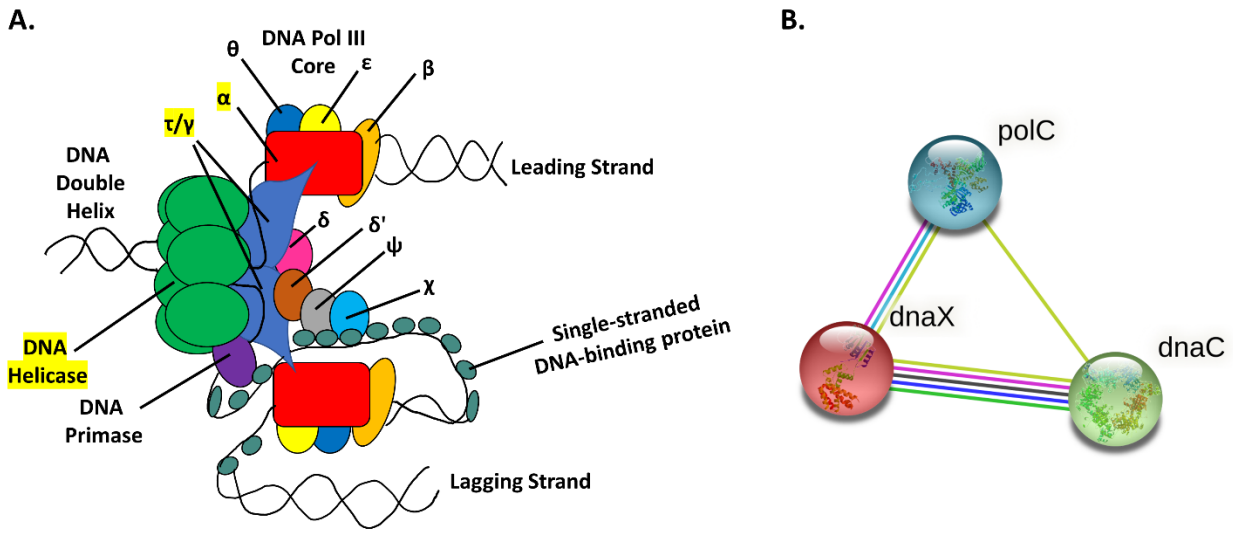

Figure 8.3 **(**A) DNA replication in *S. aureus*. The helicase (DnaC) separates the double-stranded DNA into two single strands. The leading strand is synthesized continuously by the DNA Pol III core, while the lagging strand is synthesized in smaller fragments. Highlighted proteins were found to be downregulated by HSGN-220, -144, and -218. (B**)** Predicted functional protein-protein association networks for Pol IIIC, DnaX, and DnaC. All three proteins interact with one another due to their importance in DNA replication. Predicted interactions showing evidence of gene neighborhood (green lines), gene fusions (red lines) and gene co-occurrences (blue lines) have also been shown. Other interactions showing text mining evidence (yellow lines) as well as co-expression evidence (black lines) are shown. Figures were generated by STRING v 10.5 online database[369].

To investigate if the observed modulations of the aforementioned proteins occurred at the protein or mRNA level, we performed real-time RT-qPCR analysis for *dnaX*, *pol IIIC*, *birA*, *lexA*, and *dnaC* (Figure 8.4). In line with the observations from the global proteomics analysis, we observed decreased *dnaX*, *pol IIIC*, *birA*, *lexA*, and *dnaC* mRNA levels in *S. aureus* treated with either HSGN-220, -144, or -218 (Figure 8.4A). This data suggests that HSGN-220, -144, or -218 modulates the target mRNA expression or stability, which leads to differential protein abundance.

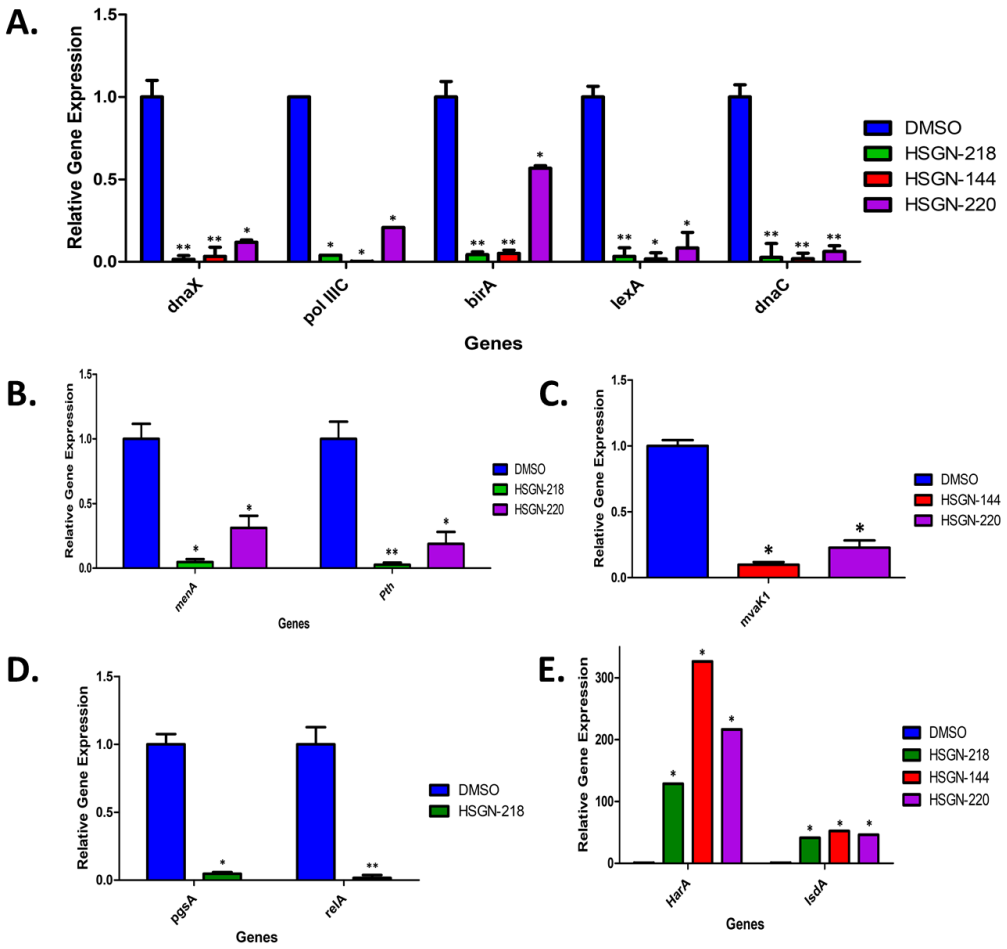

Figure 8.4 The effect of HSGN-220, -144, or -218 treatment on the transcription of proteins identified from global proteomics data. (A) Effect of HSGN-220, -144, or -218 treatment on transcription of *dnaX*, *pol IIIC*, *birA*, *lexA*, and *dnaC*. (B) Effect of HSGN-220 or -218 treatment on the transcription of *menA* and *Pth*. (C) The effect of HSGN-220 or -144 treatment on the transcription of *mvak1*. (D) The effect of HSGN-218 treatment on the transcription of *relA* and *pgsA*. (E) The effect of HSGN-220, -144, or -218 treatment on the transcription of *HarA* and *IsdA*. Total RNA isolated from *S. aureus* treated with either DMSO or 1X MIC HSGN-220 (0.5 µg/mL), -144 (0.5 µg/mL), or -218 (0.06 µg/mL) was reversed transcribed and cDNAs were quantified by RT-qPCR using target-specific primers. The data represents the mean ± SD of triplicate experiments normalized with 16S RNA. Statistically significant differences between DMSO-treatment and HSGN-220, -144, or -218 -treatment was determined by Student's *t*-test analysis (unpaired, two-tailed) and is represented as $*p \leq 0.05$ or $**p \leq 0.01$.

After analyzing the 81 proteins that all three compounds had in common, we then went on to evaluate essential proteins downregulated by only two compounds. For example, both HSGN-218 and HSGN-220 have 40 proteins in common (Figure 8.2B and Table B.3). Yet, both compounds downregulate the essential proteins 1,4-dihydroxy-2-naphthoate octaprenyltransferase (MenA) and peptidyl-tRNA hydrolase (Pth) (Table 8.2). MenA is important in *S. aureus* for the synthesis of menaquinone[370]. Menaquinone plays an important role in electron transport and ATP

generation in Gram-positive and anaerobically respiring Gram-negative bacteria[371-373]. It's been shown that inhibition of MenA, leading to loss of menaquinone, causes cell death, thereby demonstrating the protein's potential as a possible drug target[371, 373]. Pth is an essential enzyme in *S. aureus* as it recycles peptidyl-tRNAs which arise from untimely termination of translation[374]. Pth is found in both Gram-positive and Gram-negative bacteria, and inhibition of this protein leads to the buildup of tRNAs that are toxic to the cell due to impairment of protein synthesis[375-376]. To confirm our global proteomics results, we conducted RT-qPCR analysis for *menA* and *Pth* expression (Figure 8.4B). We detected a decrease of *menA* and *Pth* mRNA levels in *S. aureus* treated with either HSGN-220 or -218 (Figure 8.4B).

Table 8.2 Select essential proteins that were identified to be downregulated by both HSGN-220 and HSGN-218 treatments, as well as with HSGN-144 and HSGN-220 treatment.

Essential Proteins Downregulated by HSGN-218 and HSGN-220			
ID	Protein	Description	Essential in *S. aureus*?
gi|685632127	MenA	1,4-dihydroxy-2-naphthoate octaprenyltransferase	Yes
gi|685631655	Pth	peptidyl-tRNA hydrolase	Yes
Essential Protein Downregulated by HSGN-144 and HSGN-220			
ID	Protein	Description	Essential in *S. aureus*?
gi|685631744	mvak1	mevalonate kinase	Yes

Since HSGN-218 and -220 were found to downregulate *menA* expression (see Figure 8.4B and Table 8.2), we hypothesized that treatment of *S. aureus* with either HSGN-218 or -220 would result in a decrease in menaquinone concentration. Both menaquinone 7 (MK-7) and menaquinone 8 (MK-8) have been found to be the two most abundant menaquinones in *S. aureus*[377-381]. Therefore, to analyze the impact of HSGN-218 and -220 on menaquinone levels in *S. aureus* growing cells, the concentration of MK-7 and -8 by treatment of *S. aureus* with 1X MIC of HSGN-

218 or -220 for 2 hours was quantified by LC/MS/MS using commercially available MK-9 as a standard (Figure 8.5). Interestingly, treatment of *S. aureus* with either HSGN-218 or -220 resulted in a drastic decrease in both MK-7 and MK-8 levels. For instance, *S. aureus* treated with 1% DMSO showed an average concentration for MK-7 and MK-8 equal to 407 µg/µL and 1474 µg/µL respectively. Yet, treatment of *S. aureus* with 1X MIC HSGN-218 demonstrated a reduction in the concentration of MK-7 (38 µg/µL) and MK-8 (105 µg/µL) (see Figure 8.5). Similarly, treatment of *S. aureus* with 1X MIC HSGN-220 also showed a reduction in MK-7 and MK-8 concentrations equal to 36 µg/µL and 79 µg/µL respectively (see Figure 8.5). Therefore, we hypothesize that both HSGN-218's and -220's downregulation of MenA is responsible for the compounds' effect on menaquinone biosynthesis.

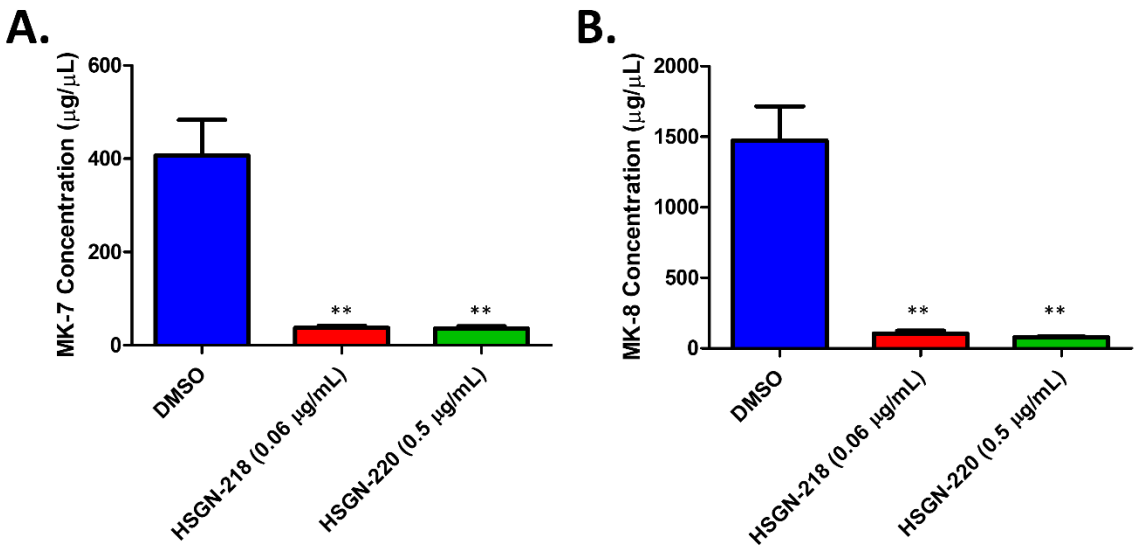

Figure 8.5 Effect of HSGN-218 and -220 on menaquinone biosynthesis. (A) MK-7 concentration (µg/µL) after treatment of *S. aureus* with 1% DMSO, 0.06 µg/mL (1X MIC) HSGN-218, and 0.5 µg/mL (1X MIC) HSGN-220. (B) MK-8 concentration (µg/µL) after treatment of *S. aureus* with 1% DMSO, 0.06 µg/mL (1X MIC) HSGN-218, and 0.5 µg/mL (1X MIC) HSGN-220. Statistically significant differences between DMSO-treatment and HSGN-218 or -220 -treatment was determined by Student's *t*-test analysis (unpaired, two-tailed) and is represented as $**p \leq 0.01$.

Both HSGN-144 and HSGN-220 downregulate 17 similar proteins (Figure 8.2B and Table B.4). However, both compounds only downregulate one essential enzyme, mevalonate kinase (mvak1) (Table 8.2). Mvak1 is essential for isoprenoid biosynthesis in *S. aureus* since it converts coenzyme A to isopentenyl diphosphate[382]. Although humans and plants also contain mevalonate kinase, the bacterial mvak1 is much different, making it an ideal drug target[382]. Additionally,

HSGN-144 and HSGN-218 both share 4 proteins in common (Figure 8.2B and Table B.5), yet none are essential to *S. aureus* and will not be discussed in this manuscript. To verify that HSGN-220 and -144 both downregulate *mvak1*, we did RT-qPCR analysis for *mvak1* expression. The results confirmed our proteomics analysis since we witnessed a decrease of mvak1 mRNA levels in *S. aureus* treated with either HSGN-220 or -144 (Figure 8.4C).

Table 8.3 Select essential proteins that were identified to be downregulated individually by HSGN-218 treatment.

Essential Proteins Downregulated by HSGN-218			
ID	Protein	Description	Essential in *S. aureus*?
gi|685632815	RelA	GTP pyrophosphokinase	Yes
gi|685632378	PgsA	CDP-diacylglycerol--glycerol-3-phosphate 3-phosphatidyltransferase	Yes

Next, we moved to assess essential proteins downregulated by the compounds individually. On its own, HSGN-218 downregulates 77 proteins (Figure 8.2B and Table B.6), yet only 2 are essential in *S. aureus*: GTP pyrophosphokinase (RelA) and CDP-diacylglycerol--glycerol-3-phosphate 3-phosphatidyltransferase (PgsA) (Table 8.3). RelA controls the activation of guanosine 3′, 5′-bis(diphosphate) when bacteria are under stressful conditions making it essential for bacterial survival[383-384]. Moreover, PgsA is highly important for the synthesis of phosphatidyl glycerol (PG), the most abundant membrane phospholipid in bacteria[181]. Reduction of PgsA causes a decrease in PG production and subsequent surface charge alterations, leading to bacterial cell death[385]. To validate that HSGN-218 does indeed downregulate RelA and PgsA, we performed RT-qPCR. Our results demonstrated that *S. aureus* treated with HSGN-218 showed a decrease in mRNA expression levels of both *relA* and *pgsA*, thereby confirming our global proteomics analysis (Figure 8.4D). Furthermore, both HSGN-144 and HSGN-220 independently downregulate 11 and 19 proteins in *S. aureus*, respectively, however none were considered to be essential to the organism (see Table B.7 and Table B.8).

After examining downregulated proteins, we then wanted to compare proteins upregulated by HSGN-220, -218, and -144 via generation of another Venn diagram (Figure 8.2C). After stringent filtration, 108 proteins were identified in HSGN-220, -218, and -144 treated samples only and not in DMSO control. Of the 108 proteins compared, 18 (16.7%) were observed to be shared among all three compounds. Individually, 28 proteins (25.9%) were identified in HSGN-144, 14 proteins (13%) were detected in HSGN-218, and 6 proteins (5.6%) were found in HSGN-220. Furthermore, 8 proteins (7.4%) were shared between HSGN-218 and HSGN-220, while 30 proteins (27.8%) were discovered in both HSGN-144 and HSGN-220. Only 4 proteins (3.7%) were detected in both HSGN-218 and HSGN-144.

HSGN-220, -218, and -144 appear to have a significant effect on iron transportation in *S. aureus*. Particularly, it appears that treatment of *S. aureus* with our *N*-(1,3,4-oxadiazol-2-yl)benzamides increases heme transport. For instance, proteins involved in heme-mediated iron acquisition like IsdA, HarA, HrtA, and SirA are all upregulated by HSGN-220, -218, and -144 (Table 8.4). IsdA and HarA are part of the *S. aureus* Isd system inside the cell wall, which mediates iron acquisition[386]. Heme binds to HarA and is passed across the cell wall through the near iron transporter (NEAT) domains of IsdA and IsdC which then results in the import of heme into the cytoplasm, followed by heme degradation to release free iron to satisfy nutrient needs[386]. HrtA is part of the heme-regulated transport (Hrt) system which regulates the amount of heme being transported into the cell to avoid any toxicity[387]. SirA also controls the amount of free iron throughout the bacterial cell by importing *S. aureus* siderophores staphyloferrin A and staphyloferrin B[388-389].

Table 8.4 Select proteins that were identified to be upregulated by HSGN-220, -218, and -144.

ID	Protein	Description
gi|685632908	HarA	Haptoglobin-binding heme uptake protein
gi|685632217	IsdA	Iron-regulated surface determinant protein A
gi|685631802	SirA	Siderophore compound ABC transporter binding protein
gi|685632219	HrtA	Heme ABC transporter permease

To demonstrate that HSGN-220, -218, and -144 upregulate heme transport in *S. aureus*, we completed RT-qPCR for HarA and IsdA. We witnessed an increase in mRNA levels for both *HarA* and *IsdA* in *S. aureus* treated with either HSGN-220, -218, or -144 (Figure 8.4E), further verifying our global proteomics results.

8.3.4 HSGN-220, -218, and -144 cause iron starvation

In a beautiful work by Huigens and co-workers, they showed that phenazine antibiotics which regulate proteins involved in iron transport, directly bind to iron[199, 390]. Inspired by this work and the fact that HSGN-220, -218, or -144 also regulate proteins involved in iron transport, we evaluated whether HSGN-220, -218, or -144 directly bind to iron (II) using UV-Vis experiments (Figure 8.6A-C), following Huigens' protocol[199]. We found that all three *N*-(1,3,4-oxadiazol-2-yl)benzamides chelate to iron (II) and the chelation intensifies over a 3 hour period.

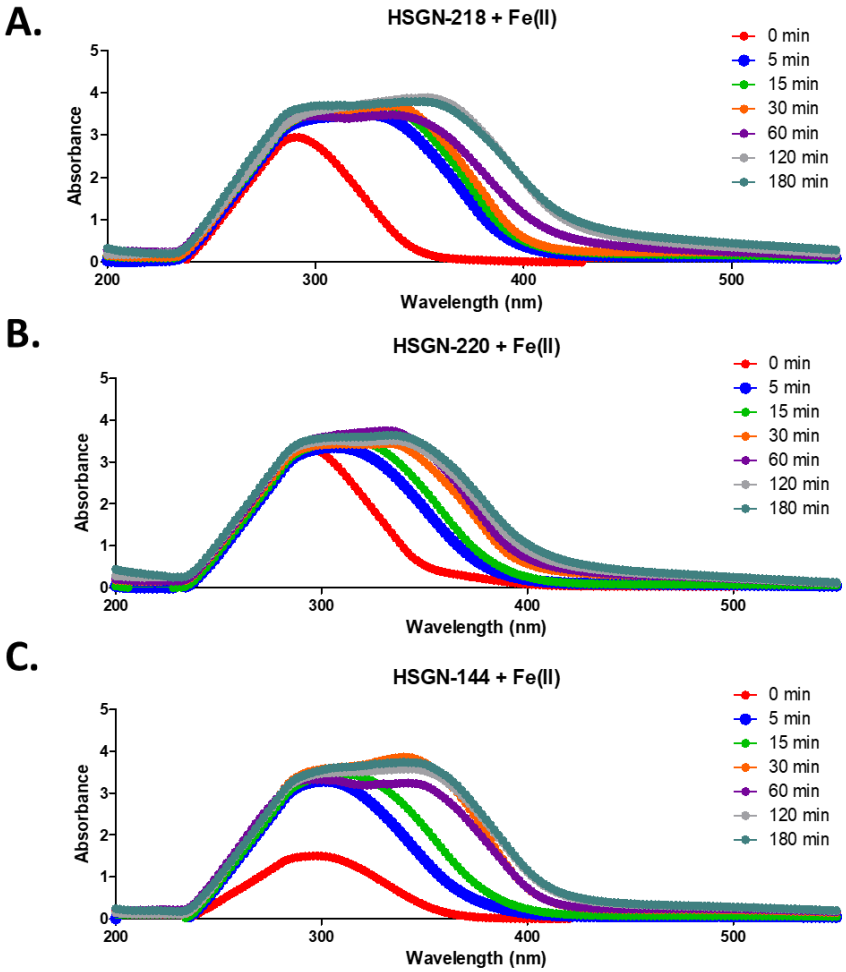

Figure 8.6 HSGN-220, -218, and -144 Chelate to Iron (II). (A) UV–vis spectroscopy of HSGN-218 binding iron (II). (B) UV–vis spectroscopy of HSGN-144 binding iron (II). (C) UV–vis spectroscopy of HSGN-220 binding iron (II).

Additionally, because treatment of *S. aureus* with HSGN-220, -218, or -144 appeared to upregulate SirA and HrtA, two proteins important for siderophore biosynthesis and heme transport respectively, we further evaluated the effect of HSGN-220, -218, and -144 on siderophore biosynthesis and heme regulation in *S. aureus* using plate bioassays[391-392] (see Table 8.5). For these bioassays, we used iron-restricted Tris-minimal succinate (TMS) agar by adding 25 μM of the iron-chelator ethylenediamine-*N*,*N*′-bis(2-hydroxyphenylacetic acid) (EDDHA). 1% DMSO (untreated control) or HSGN-220, -218, or -144 at concentrations of 0.25X MIC, 0.5X MIC, 1X MIC was supplemented into the TMS agar. *S. aureus* (10^9 CFU/mL) was incorporated into plates and 50 μM of siderophore (ferrichrome, defersal, and 2,3-dihydroxy benzoic acid (DHBA)), hemoglobin, or hemin was added onto sterile paper disk and incubated at 37°C for 24 hours.

Interestingly, we found that *S. aureus* treated with 0.5X MIC and 1X MIC of HSGN-220, -218, or -144 showed the inability to utilize siderophores, hemoglobin, or hemin to transport iron and promote growth (see Table 8.5 and Appendix B). However, in the absence of compound, *S. aureus* was able to use siderophores, hemoglobin, or hemin to promote growth (see Table 8.5 and Appendix B). Therefore, we hypothesize that HSGN-220, -218, and -144's effects on both siderophore biosynthesis and heme regulation, which results in up-regulation of SirA and HrtA, starves *S. aureus* of iron and causes bacterial death.

Table 8.5 Utilization of siderophores (ferrichrome, defersal, and 2,3-DHBA), hemoglobin, or hemin by *S. aureus* in the presence and absence of HSGN-220, -218, and -144.

Siderophore	Growth Promotion in:									
	DMSO	HSGN-220			HSGN-218			HSGN-144		
		0.25X MIC	0.5X MIC	1X MIC	0.25X MIC	0.5X MIC	1X MIC	0.25X MIC	0.5X MIC	1X MIC
Ferrichrome	+	-	-	-	+	-	-	-	-	-
Hemoglobin	+	-	-	-	+	-	-	-	-	-
Hemin	+	-	-	-	+	-	-	+	-	-
Desferal	+	-	-	-	+	-	-	+	-	-
2,3-DHBA	+	-	-	-	+	-	-	-	-	-

Note: +, growth; -, no growth.

8.3.5 Effects of HSGN-220, -218, and -144 on membrane depolarization and permeability in *S. aureus*:

We recently reported that the SCF_3 or SF_5 moiety enhances association with bacterial membranes[393]. Thus, we wondered if HSGN-220, -218, and -144 were membrane-targeting agents. Targeting the bacterial membrane has been deemed a potential drug target because it can disrupt the membrane's function and/or physical integrity[394]. The bacterial membrane is essential because it comprises about one third of the proteins in a cell and is the site for highly important processes like respiration, active transport of nutrients and wastes, and the formation of the proton motive force[395]. Additionally, the bacterial cell membrane contains an electrical potential difference which acts as a source of free energy[396]. This energy allows for the bacteria to undergo its essential

functions[396]. For instance, membrane potential has been shown to regulate pH homeostasis[397-398], membrane transport[399], motility[400], antibiotic resistance[401], cell division[402], and environmental sensing[403]. Thus, we began by investigating HSGN-220, -218, and -144's effect on membrane depolarization in *S. aureus* using a fluorescent based assay with DiSC3(5) as a stain. DiSC3(5) is a cationic membrane-permeable dye which accumulates in polarized cells resulting in quenching of overall fluorescence[404]. Upon depolarization, DiSC3(5) is rapidly released into the medium resulting in dequenching. This dequenching triggers a large spike fluorescence intensity[404]. All three compounds showed potent membrane depolarization activity. For instance, at 10x MIC HSGN-220, -218, and -144 showed either equal or greater depolarization when compared to daptomycin (5 μg/mL), a known depolarizer of *S. aureus* membranes[405] (Figure 8.7).

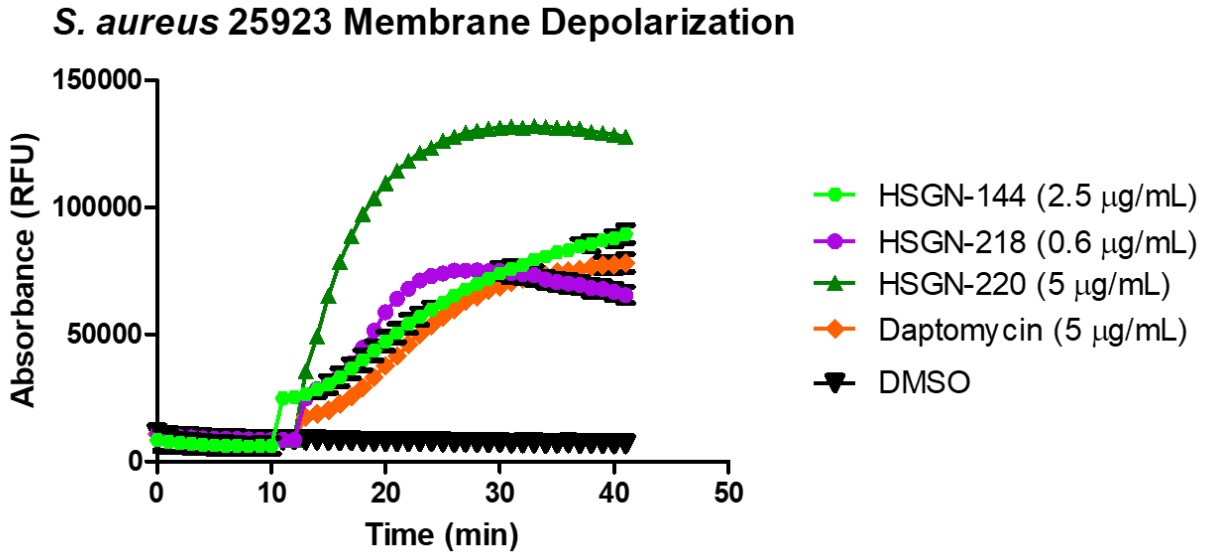

Figure 8.7 Effects of HSGN-220, -218, and -220 on membrane depolarization in *S. aureus* at 10x MIC concentrations using DiSC3(5) dye. Increase in fluorescence indicates depolarization. Daptomycin is used as positive control while 1% DMSO is used as negative control.

Furthermore, disruption of the membrane integrity can lead to leakage of cytosolic content and harmful pleiotropic effects, eventually causing cell death[394]. Therefore, we proceeded to determine the effects of HSGN-220, -218, and -144 on membrane permeability in *S. aureus* via a fluorescent-based assay using sytox green as a dye. Sytox green stain was used as it is a high-affinity nucleic acid stain that does not cross the membranes of live cells but easily penetrates cells with compromised membranes, resulting in strong fluorescence[406]. All three compounds did not

cause membrane permeability in *S. aureus* cells at 10x MIC concentrations as their fluorescence was comparative to the negative control (1% DMSO) (see Appendix B for Figure B.3). However, bithionol, a known antibacterial that affects membrane integrity[69], had a significant influence on membrane permeability (Figure B.3).

8.4 Conclusion

In conclusion, HSGN-220, -218, and -144 are potent antibacterial agents with MICs greater than or equal to those of vancomycin against MRSA clinical isolates. Additionally, HSGN-220, -218, and -144 did not develop resistance to MRSA over 30 days, comparing to FDA approved antibiotics vancomycin and linezolid. Global proteomic analysis demonstrates that HSGN-220, -218, and -144 downregulated essential proteins involved in DNA replication. In particular, the compounds downregulated DNA Pol IIIC, a novel target to combat Gram-positive bacteria. Furthermore, HSGN-218 and -220 downregulated the essential protein MenA and significantly decreased the concentration of menaquinones MK-7 and MK-8 in *S. aureus*. Additionally, HSGN-220, -218, and -144 starve bacteria of iron which we hypothesize is due to their upregulation of proteins involved in heme acquisition and siderophore biosynthesis. We also found that HSGN-220, -218, and -144 had a significant effect on membrane depolarization but did not alter membrane permeability. Therefore, despite their common core, HSGN-220, -218, and -144 showed several similarities and differences in the pathways they affected, demonstrating that subtle changes in a compound's structure can impact their mechanism of action. *N*-(1,3,4-oxadiazol-2-yl)benzamides are interesting new antimicrobials, but it appears that their modes of action are more complicated that initially thought.

Compounds that act on multiple pathways in bacteria have a better chance of clinical utility without bacterial resistance. While the compounds described herein also inhibit multiple pathways in bacteria and recent studies have documented that indeed many approved antibiotics also inhibit multiple pathways[190], medicinal chemists are still not at the stage whereby compounds that are multi-targeting without gross toxicity can be developed *a priori*. Thus far, such compounds are found after the fact. We hope that the studies described herein adds to the database, which would be needed as training set for future modeling for nodes that when targeted lead to potent antimicrobials that resist bacterial resistance.

8.5 Materials and Methods:

8.5.1 Bacterial strains, media, and reagents

Bacterial strains were obtained from various sources as listed in Tables B.10 and B.11. Cation-adjusted Mueller Hinton broth, tryptic soy broth (TSB) and tryptic soy agar (TSA) were purchased from Becton, Dickinson and Company (Cockeysville, MD, USA). Linezolid (Chem-Impex International, Wood Dale, IL, USA), vancomycin hydrochloride (Gold Biotechnology, St. Louis, MO, USA), and ciprofloxacin (Sigma Aldrich, St. Louis, MO, USA), menaquinone-9 (Cayman Chemical, Ann Arbor, MI, USA), deferoxamine mesylate (Cayman Chemical, Ann Arbor, MI, USA), 2,3-Dihydroxybenzoic acid (Sigma Aldrich, St. Louis, MO, USA), ferrichrome (Sigma Aldrich, St. Louis, MO, USA), hemin (Sigma Aldrich, St. Louis, MO, USA), hemoglobin (Sigma Aldrich, St. Louis, MO, USA), ammonium iron(II) sulfate hexahydrate (Sigma Aldrich, St. Louis, MO, USA), and EDDHA (Arctom Chemical, Westlake Village, CA, USA) were purchased commercially. Tris-minimal succinate (TMS) was prepared as previously described[407]. Compounds were previously synthesized from commercial sources in our laboratory.

8.5.2 Determination of the MICs against clinically important Gram-positive bacteria

The broth microdilution method was utilized to test the antibacterial activity of HSGN-220, -218, and -144 against a panel of clinically-important Gram-positive bacteria according to the guidelines outlined by the Clinical and Laboratory Standards Institute (CLSI)[212]. Bacterial strains were grown aerobically overnight on tryptic soy agar (TSA) plates at 37° C. Afterwards, a bacterial solution equivalent to 0.5 McFarland standard was prepared and diluted in CAMHB to achieve a bacterial concentration of about 5×10^5 CFU/mL and seeded in 96-well plates. Compounds and control drugs were added in the first row of the 96-well plates and serially diluted along the plates. Plates were then incubated aerobically at 37° C for 18-20 hours. MICs reported are the minimum concentration of the compounds and control drugs that completely inhibited the visual growth of bacteria.

8.5.3 Multi-step Resistance Selection:

To investigate if MRSA would be capable of forming resistance to HSGN-220, -218, or -144 quickly, a multi-step resistance selection experiment was conducted, as described

previously[117]. The broth microdilution assay was utilized to determine the MIC of HSGN-220, -218, or -144, linezolid, vancomycin, and ciprofloxacin exposed to MRSA USA300 over 30 passages. Resistance was classified as a greater than four-fold increase in the initial MIC.

8.5.4 Global Proteomics Analysis:

Global proteomic analysis was performed as described previously[217]. Briefly, exponentially growing *S. aureus* ATCC 25923 was treated 0.5 µg/mL HSGN-220, 0.0625 µg/mL HSGN-218, 0.5 µg/mL HSGN-144, or an equivalent amount of DMSO for 2 hours. After, the cells were pelleted by centrifugation and washed twice with PBS. The protein was precipitated from the samples through homogenization using 8M urea and the BCA Protein Assay Kit (ThermoFisher Scientific, Waltham, MA, USA) was used to determine the protein concentration. Protein (50 µg) was reduced with 10 mM dithiothreitol (DTT) at 55 °C for 45 min followed by cysteine alkylation with 20 mM iodoacetamide at room temperature under dark for 45 min and an additional 5 mM DTT for 20 min at 37 °C. Trypsin/Lys-C Mix (Promega, Madison, WI, USA) at 1:25 (*w*/w) enzyme-protein ratio was used to digest the protein at 37 °C overnight and passed through C18 silica micro spin columns (The Nest Group Inc., Southborough, MA, USA) to afford eluted peptides. Peptide concentration was determined with the BCA assay as above and adjusted to 0.2 µg/µL. Data acquisition was performed using a reverse-phase HPLC-ESI-MS/MS system composed of an UltiMate™ 3000 RSLCnano system coupled to a Q-Exactive (QE) High Field (HF) Hybrid Quadrupole-Orbitrap™ mass spectrometer (Thermo Fisher Scientific, Waltham, MA) and a Nano-spray Flex™ ion source (Thermo Fisher Scientific) was used to analyze the samples standard data-dependent mode. Acquisition of MS/MS scans were done at a resolution of 15,000 at m/z 200. To avoid repeated scanning of identical peptides, we set the dynamic exclusion at 30 s. Data was analyzed The MaxQuant software (v. 1.6.0.16)[218-220] with the Andromeda search engine. For protein identification and quantification, the spectra were searched against the *S. aureus* sequences downloaded from NCBI database with a minimal length of six amino acids. For bioinformatics analysis, the Perseus software[174] was used. Proteins identified in at least two out of the three replicates and with at least 2 MS/MS counts were processed for further analysis. Differential expression analysis was performed using LFQ intensities. After Log_2 transformation of the intensities and filtering of the data, a two-sample Student's *t*-test was used to determine differentially abundant proteins using a 5% permutation-based FDR filter. Scatter plots were used

to determine the correlation between replicates. The *Z*-score normalized data was used to perform hierarchical clustering and to generate the heat map analysis.

8.5.5 Total RNA isolation and RT-PCR:

RNA isolation and RT-PCR was peformed following a previously reported procedure[217]. Briefly, exponentially growing *S. aureus* ATCC 25923 was incubated with 0.5 µg/mL HSGN-220, 0.0625 µg/mL HSGN-218, 0.5 µg/mL HSGN-144 or 1% DMSO for 2 hours at 37 °C in triplicates. The cells were then pelleted by centrifugation and RNA was isolated using 1 mL TRIzol (Invitrogen, Carlsbad, CA) for total RNA according to the manufacturer's protocol. The Turbo DNA-free kit (Ambion, Austin, TX) was used to remove residual genomic DNA from the isolated RNA. 1 µg of the isolated RNA was then reverse-transcribed using the Superscript II Reverse Transcriptase (ThermoFisher Scientific). The subsequent cDNA were analyzed and quantified using gene-specific primers (Table B.12) and the QuantiTect SYBR Green PCR Kit (Qiagen, Germantown, MD) on a BioRad CFX96™ Touch Real-Time PCR Detection System following the manufacturer's protocol. PCR primers were either designed using Primer-BLAST or obtained from the referenced literature. The data were normalized against 16S rRNA and the *p*-values from student's *t*-test showed * ≤ 0.05 or ** ≤ 0.01.

8.5.6 Quantification of MK Levels

Quantification of MK levels was performed as previously outlined[408]. Briefly, exponentially growing *S. aureus* ATCC 25923 was treated with 0.5 µg/mL HSGN-220, 0.0625 µg/mL HSGN-218, or an equivalent amount of DMSO for 3 hours at 37 °C. Samples were then normalized to OD_{600} 0.8 using sterile saline. Next, the cells were pelleted via centrifugation at 5,000 xg for 10 minutes and washed twice with phosphate buffered saline (PBS). Then, the samples were suspended in 0.5 mL of distilled water by vortexing for 30 s. To denature proteins, 0.75 mL of 2-propanol:hexane (3:2) was added, and the mixture vortexed for 3 min. The mixture was further dispersed by sonicating for 1 min and then vortexed for 3 min. After, the mixture was centrifuged at 4 °C and 1800 g for 5 min. The upper hexane layer was then aspirated and evaporated to dryness under medium heat and nitrogen stream. 5 µL of a suspension of the sample residue in 200 µL methanol:methylene chloride (3:1) was injected into an Agilent 1200 HPLC (Agilent

Technologies)–AB SCIEX Triple Quad 5500 mass spectrometry system for identification and quantification of MKs. MK-7 and MK-8 were detected at the following mass-to-charge ratios: m/z m/z 650 (MK-7) and m/z 718 (MK-8). MK-9 was used as a standard for generating a calibration curve as previously reported[378].

8.5.7 UV–Vis for HSGN-220, -218, and -144 Binding Iron (II):

HSGN-220, -218, or -144–iron(II) complex formation was determined using UV–vis spectrometry as previously reported[199]. Ammonium iron (II) sulfate hexahydrate (0.5 equiv) was added to a stirring solution of HSGN-220, -218, or -144 (10 mM) in dimethyl sulfoxide. Aliquots of 50 μL HSGN-220, -218, or -144 were removed from the resulting mixture and added to 1 mL of dimethyl sulfoxide in a cuvette. Spectral scanning was performed from 200 to 800 nm in 2 nm increments and a loss of absorbance at λ_{max} (free compound) in the UV–vis spectrum, and apparent formation of a *N*-(1,3,4-oxadiazol-2-yl)benzamide–iron(II) complex was observed over time.

8.5.8 Plate Bioassays:

Plate bioassays were performed described previously[392]. Briefly, 10^9 cells/mL was added to molten TMS agar containing 25 μM EDDHA as an iron-chelating agent. 0.25X to 1X MIC concentrations of HSGN-220, -218, or -144 were added to agar. Iron sources to be tested (10 μl of a 50 μM solution) were added to sterile 6-mm-diameter paper disks and placed on the surfaces of the plates. Growth promotion was determined after 24 hours of incubation.

8.5.9 Bacterial membrane depolarization assay:

S. aureus ATCC 25923 was grown in TSB overnight at 37 °C and sub-cultured from the overnight broth to achieve exponential phase (OD_{600} 0.2–0.3). For membrane depolarization, cells were harvested by centrifugation at 3600x*g* at 4 °C for 10 min and washed 3× in membrane assay buffer at pH 7.0 (5 mM glucose + 10 mM HEPES) and pellets were resuspended in the same buffer to OD_{600} 0.2–0.3. Then, DiSC3 was added to a final concentration of 1 μM and incubated in the dark at ambient temperature for 15–30 min to allow the loading of the fluorescent dye into the cell membranes. After the loading period, potassium chloride (KCl) was added to the *S. aureus* cell suspension to a final concentration of 100 mM. The assay was initiated by adding the

antibiotic/compound according to calculated concentrations in triplicate in a black 96 well plate. This was immediately read in a Gen5 fluorescent imager at an excitation wavelength of 615 nm and emission wavelength of 665 nm for a period of 30 min at 30 s intervals. 5 μg/mL daptomycin was used as the positive control while the negative control was suspended cells + DiSC3. The baseline sample was a vial with no drug and no DiSC3.

8.5.10 Bacterial membrane permeability assay:

For membrane permeability, the Sytox green™ fluorescence assay was used. *S. aureus* ATCC 23592 was grown as above, centrifuged, washed in 1× PBS three times and pellets resuspended in 1× PBS + 10% TSB. Sytox green™ (Invitrogen) was added to achieve a final concentration of 5 μM. This was incubated for 15–30 min in the dark for fluorescence to stabilize. 100 μL of the suspension was then aliquoted in triplicate into a 96 well microtiter plate and read inititally at an excitation wavelength of 504 nm and emission wavelength of 522 nm for 10 min before controls and compounds at calculated concentrations were added and absorbance read for another 3 h at 3 min intervals using a Biotek Cytation5 image reader. 4 μg/mL bithionol was used as the positive control while the negative control was 1% DMSO + Sytox green™. The baseline sample was a vial with no drug and no Sytox green™

8.5.11 Author Contributions

G. Naclerio and C. Karanja performed global proteomics. G. Naclerio performed global proteomics data analysis, RT-qPCR, MK-7 and MK-8 quantification, siderophore bioassays, MIC assays, resistance passage, and iron (II) binding assay using UV Vis. K. Onyedibe performed membrane permeability and depolarization assays. G. Naclerio and H. Sintim wrote the manuscript.

CHAPTER 9. POTENT ANTIMICROBIAL ACTIVITIES OF ALKYL OXADIAZOLE BENZAMIDES AGAINST DRUG-RESISTANT GRAM-POSITIVE BACTERIA

9.1 Abstract

Methicillin-resistant *Staphylococcus aureus* (MRSA) and vancomycin-resistant enterococci (VRE) affect around 400,000 patients per year, resulting in almost 20,000 deaths. Therefore, despite the fact that there are FDA-approved therapeutics to combat these pathogens, new effective antimicrobial agents against these pathogens are still needed. Thiophenyl *N*-(1,3,4-oxadiazol-2-yl)benzamides bearing pentafluorosulfanyl (SF_5)-, trifluoromethoxy (OCF_3)- and (trifluoromethyl)thio (SCF_3) groups have been reported as potent inhibitors of drug-resistant Gram-positive bacteria. To make more drug-like analogs, the thiophenyl unit was replaced with hydrogen or alkyl groups and the analogs were tested for antimicrobial activities. HSGN-2143 and -2192, new analogs without the potentially toxic thiophene unit, displayed potent activities against multidrug-resistant Gram-positive pathogens with minimum inhibitory concentration (MIC) values as low as 0.25 μg/mL. HSGN-2143 and -2192 also show high tolerability to mammalian cells and do not lyse human red blood cells.

9.2 Abstract

The ongoing rise in antimicrobial resistance has rendered current antibiotics ineffective. While many drugs exist to treat the majority of infections, the rise of reports detailing infections by multi-drug resistant pathogens[409], which are resistant to most traditional antibiotics could be a warning sign for future pandemics propelled by bacteria. Two Gram-positive pathogens, methicillin-resistant *Staphylococcus aureus* (MRSA) and vancomycin-resistant *Enterococci* (VRE) are particularly problematic as annually MRSA accounts for 323,700 infections resulting in 10,600 deaths, while VRE causes 54,500 infections and 5,400 deaths[170]. Linezolid and vancomycin are two mainstay drugs used to treat *S. aureus* infections but resistance to these drugs have become increasingly prevalent[154, 410-411]. Linezolid and a combination of quinupristin and dalfopristin (QD) are approved by the FDA to treat VRE infections[412]. Unfortunately, the efficacy of linezolid is low and the reported 30-day mortality rate for patients with VRE blood-stream infection is about

30%[413]. Furthermore, both linezolid and QD have toxicity concerns as well, like neuropathy, renal failure, and lactic acidosis[414-415]. New and effective therapeutics against VRE, especially for blood-stream infections, would be welcome.

Our group has demonstrated that *N*-(1,3,4-oxadiazol-2-yl)benzamides are highly potent small molecule antibiotics against drug-resistant bacteria[117, 134, 163-166]. Particularly, we have shown that introduction of pentafluorosulfanyl (SF_5), trifluoromethoxy (OCF_3), or trifluoromethylthio (SCF_3) groups into antibiotics can drastically improve antibacterial activity[163-164, 393]. Previously, we reported the SF_5, OCF_3, and SCF_3 containing *N*-(1,3,4-oxadiazol-2-yl)benzamides, HSGN-144, -145, and -148, as a potent anti-MRSA agents[164]. HSGN-144, -145, and -148 were active against several strains of drug-resistant Gram-positive bacteria, was non-toxic to mammalian cell lines, and cleared intracellular MRSA hidden in macrophages[164]. Still, HSGN-144, -145, and -148 contained an unsubstituted thiophene (a potential toxicophore) (Figure 9.1). In this report, we describe the generation and antimicrobial testing of a new series of SF_5, OCF_3, and SCF_3 containing *N*-(1,3,4-oxadiazol-2-yl)benzamides whereby the potential thiophene toxicophore is replaced with hydrogen or alkyl groups. The most active compounds in this new series, HSGN-2143, HSGN-2192, and HSDP-76 (Figure 9.1), were evaluated for hemolytic activity and cytotoxicity against red blood cells and mammalian cell lines, A549 (lung) and MDA-MB-231 (breast) respectively.

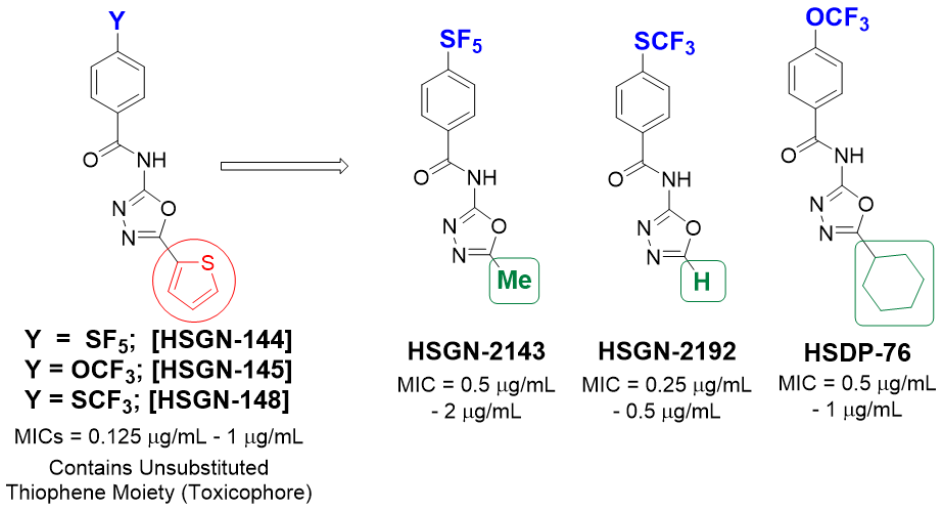

Figure 9.1 HSGN-144, -145, and -148 have antibacterial activity against Gram-positive clinical isolates although they contain an unsubstituted thiophene moiety.

9.3 Results and Discussion

We previously reported that HSGN-144, -145, and -148 showed potent activity against several clinical isolates of Gram-positive bacteria. However, HSGN-144, -145, and -148 contain an unsubstituted thiophene moiety, which can lead to toxicity concerns *in vivo*. For example, cytochrome P450-mediated oxidation can cause thiophene metabolism and lead to the formation of reactive metabolites, thiophene-S oxides[286-287], thiophene epoxides[287], and sulfenic acids[288], which can then react with nucleophiles such as water and glutathione[289]. Thus, we decided to make new oxadiazole analogs whereby the thiophene unit is replaced with alkyl groups

The synthesis of the analogs began with an alkyl or cycloalkyl containing hydrazide which was cyclized into the corresponding 1,3,4-oxadiazol-2-amine (A1-A12) using cyanogen bromide (Scheme 9.1). Next, we converted the substituted benzoic acids into the subsequent acid chlorides S1-S3 using thionyl chloride (Scheme 1). The acid chlorides were then reacted with the 1,3,4-oxadiazol-2-amine using *N*-methylimidazole as a base to give the desired pentafluorosulfanyl or trifluoromethylthio containing alkyl or cycloalkyl *N*-(1,3,4-oxadiazol-2-yl)benzamides (Scheme 9.1).

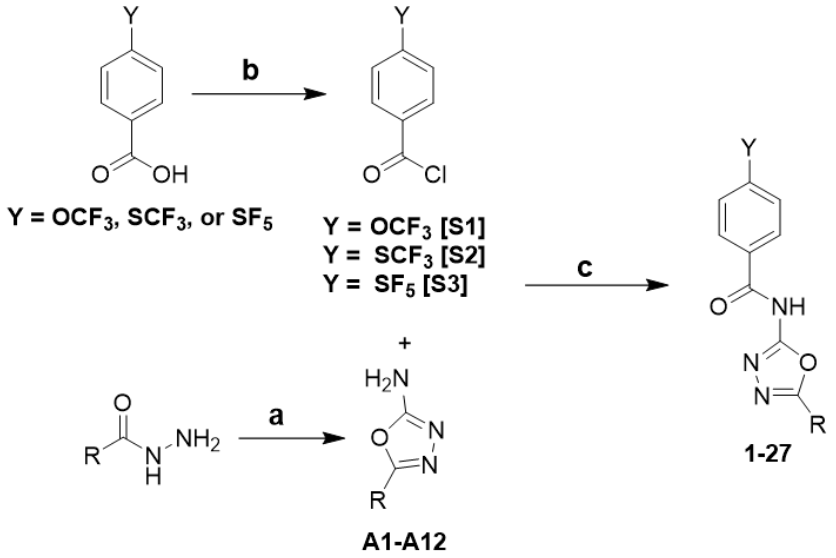

Scheme 9.1 General Route for the Synthesis of Alkyl and Cycloalkyl *N*-(1,3,4-Oxadiazol-2-yl)benzamides[a]. [a]Reagents and Conditions: (a) CNBr, EtOH, 90°C, 2 h (b) $SOCl_2$, 80 °C, 1 h (c) *N*-methylimidazole, 1,4-dioxane, 90°C, 2 h, 6-46%.

With the compounds in hand, we proceeded to evaluate the new analogs against *S. aureus* ATCC 25923. Interestingly, we found that substitution of the phenyl for either an alkyl or

cycloalkyl group did not affect activity. Instead, these compounds were found to have potent activity against *S. aureus* ATCC 25923 Regarding antibacterial activity, we evaluated the effect of replacing an aromatic group for hydrogen (1, HSGN-2192) and other alkyl groups like methyl (2, HSGN-2143 3, and 4), ethyl (5-7), *i*-propyl (8-10), *t*-butyl (11-13), propyl (14 and 15), and butyl (16 and 17). These compounds had a minimum inhibitory concentration (MIC) between 4 μg/mL and 0.5 μg/mL against *S. aureus* ATCC 25923 demonstrating comparable activity to the drugs of choice vancomycin and linezolid. However, for SCF_3 and OCF_3 containing *N*-(1,3,4-oxadiazol-2-yl)benzamides, it appears that addition of a methyl group appeared to result in weak antibacterial activity (Table 1, see MIC for analogs 3 and 4, respectively), but this was the opposite for the SF_5 containing *N*-(1,3,4-oxadiazol-2-yl)benzamide 2 (see Table 9.1). Additionally, it appeared that addition of alkyl groups in OCF_3 containing *N*-(1,3,4,-oxadiazol-2-yl)benzamides (analogs 4, 7, 10, and 13) displayed only weak to moderate antibacterial activity against *S. aureus* (see Table 9.1).

Additionally, we evaluated the addition of cycloalkyl groups like cyclopropyl (18 and 19), cyclobutyl (20), cyclopentyl (21-23), and cyclohexyl (24-26), as well as oxygen heterocycles like tetrahydropyran (27). Antibacterial activity against *S. aureus* ATCC 25923 of these cycloalkyl *N*-(1,3,4-oxadiazol-2-yl)benzamides was assessed and found to be between 4 μg/mL to 1 μg/mL (Table 1). For OCF_3 containing *N*-(1,3,4-oxadiazol-2-yl)benzamides, addition of cycloalkyl groups were more favored as this led to the identification of HSDP-76 (Table 9.1) Interestingly, addition of polar rings like tetrahydropyranyl (27) was found to lead to weak antibacterial activity (see Table 9.1).

Table 9.1 MICs (μg/mL) of HSGN-2143, HSGN-2192, and HSDP-76, Analogs, and Control Antibiotics against *S. aureus* ATCC 25923. Note: cLogP was calculated using the online software SwissADME[317].

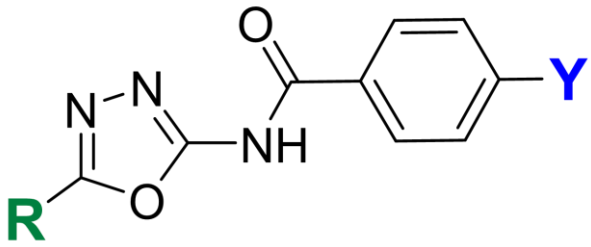

Compound/Control Antibiotic	Y	-R	MIC	cLogP
1, HSGN-2192	SCF_3	H	0.5	2.76
2, HSGN-2143	SF_5	Me	0.5	2.82
3	SCF_3	Me	16	2.82
4	OCF_3	Me	64	2.27
5	SF_5	Et	2	3.08
6	SCF_3	Et	4	3.15
7	OCF_3	Et	8	2.59
8	SCF_3	*i*-propyl	4	3.44
9	SF_5	*i*-propyl	1	3.35
10	OCF_3	*i*-propyl	8	2.90
11	SCF_3	*t*-butyl	2	3.71
12	SF_5	*t*-butyl	1	3.59
13	OCF_3	*t*-butyl	4	3.17
14	SCF_3	propyl	2	3.49
15	SF_5	propyl	1	3.36
16	SCF_3	butyl	1	3.84
17	SF_5	butyl	1	3.67
18	SCF_3	cyclopropyl	2	3.29
19	OCF_3	cyclopropyl	2	2.72
20	SCF_3	cyclobutyl	4	3.63
21	SCF_3	cyclopentyl	2	3.95

Table 9.1 Continued

22	SF_5	cyclopentyl	2	3.80
23	OCF_3	cyclopentyl	2	3.40
24	SCF_3	cyclohexyl	1	4.25
25	SF_5	cyclohexyl	1	4.08
26, HSDP-76	OCF_3	cyclohexyl	1	3.71
27	SF_5	tetrahydropyranyl	8	3.16
HSGN-144	SF_5	thiophenyl	0.25	3.89
HSGN-145	OCF_3	thiophenyl	1	3.40
HSGN-148	SCF_3	thiophenyl	0.5	3.97
Vancomycin	-	-	1	-
Linezolid	-	-	2	-

9.3.1 Comprehensive antibacterial profile of HSGN-2143 and -2192 against multidrug-resistant Gram-positive clinical strains

After the initial screening of HSGN-2143, HSGN-2192, and HSDP-76 we assessed their antibacterial profile against a panel of multidrug-resistant bacterial pathogens. HSGN-2143 inhibited growth of the tested strains at concentrations ranging from 0.5 to 4 μg/mL (Table 2). HSGN-2192 exhibited potent activities, inhibiting the tested multidrug-resistant bacterial strains at concentrations ranging from 0.25 to 1 μg/mL (Table 9.2). Additionally, HSDP-76 displayed potent activity with MICs ranging from 0.5 to 2 μg/mL (Table 2). Furthermore, HSGN-2143, HSGN-2192, and HSDP-76 maintained the same potent activities against other clinically relevant Gram-positive bacterial species including vancomycin-resistant enterococci (VRE) and *Listeria monocytogenes* (Table 9.2). Additionally, we also evaluated HSGN-2143, HSGN-2192, and HSDP-76's activity against Gram-negative bacteria as well. However, these compounds did not inhibit the growth of *E. coli* ATCC 25404 as their MICs were >8 μg/mL.

Table 9.2 The minimum inhibitory concentrations (MICs in μg/mL) of HSGN-2143, HSGN-2192, and HSDP-76 against a panel of clinically important bacterial pathogens including methicillin-resistant *Staphylococcus aureus*, *Enterococcus faecalis*, *Enterococcus faecium*, *Listeria monocytogenes* and *Escherichia coli*.

Bacterial Strain	Compound/Control Antibiotic					
	HSGN-2143	HSGN-2192	HSDP-72	Vancomycin	Linezolid	Colistin
MRSA ATCC 33592	0.5	0.5	1	1	2	NT
MRSA USA300	4	1	1	4	2	NT
MRSA ARLG 1649	4	0.5	1	0.25	4	NT
MRSA ARLG 1644	4	0.25	1	1	4	NT
MRSA ARLG 1663	1	0.5	1	1	2	NT
MRSA ARLG 1570	2	0.5	1	0.5	2	NT
MRSA ARLG 1568	2	0.25	1	1	4	NT
MRSA ARLG 1569	1	0.25	0.5	1	2	NT
MRSA ARLG 1567	1	0.5	1	0.5	4	NT
MRSA ARLG 1561	4	0.25	1	1	2	NT
MRSA ARLG 1665	2	0.25	1	1	2	NT
E. *faecalis* ATCC 29212	0.25	1	1	1	4	NT

Table 9.2 Continued

VRE *faecalis* ATCC 51575	2	0.5	0.5	>128	2	NT
VRE *faecium* ATCC 700221	4	1	2	>128	4	NT
L. monocytogenes ATCC 19115	2	0.25	0.5	1	2	NT
E. coli ATCC 25404	>8	>8	>8	NT	NT	0.5

NT = Not Tested

9.3.2 HSGN-2143, HSGN-2192, and HSDP-76 do not lyse red blood cells

Hemolysis can cause grave effects on organ function. For example, hemolysis has been reported to produce higher systolic, diastolic, and mean arterial blood pressure from reduced nitrous oxide signaling. Additionally, hemolysis can cause cardiovascular and renal dysfunction, thrombosis, and enhanced susceptibility to infections[241]. Thus, we examined whether our compounds would lyse red blood cells (RBCs). HSDP-76 showed around 30% hemolysis at 100 μg/mL (100X MIC) and significantly dropped off at 50 μg/mL, 25 μg/mL, 12.5 μg/mL, and 6.25 μg/mL (Figure 2). Both HSGN-2143 and -2192 showed little to no hemolysis at concentrations up to 100 μg/mL which is 200X their MIC (see Figure 9.2). Therefore, these results demonstrate that HSGN-2143, HSGN-2192, and HSDP-76 will have a minor hemolytic activity to human RBCs when used clinically to treat bacterial infections.

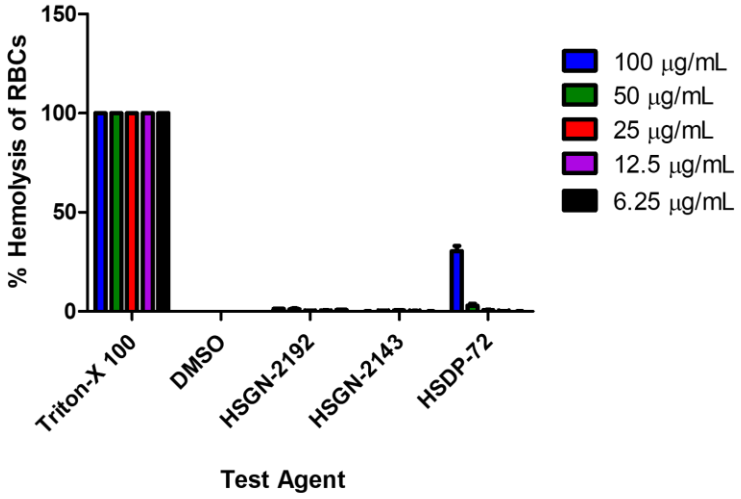

Figure 9.2 Hemolytic activity of HSGN-2143, HSGN-2192, and HSDP-76 (in triplicate) against sheep RBCs. The results are presented as percent RBCs hemolysis for each compound relative to Triton-X-100 (positive control showing complete hemolysis of RBCs) and DMSO (negative control showing no hemolysis of RBCs). The absorbance values represent an average of three samples analyzed for each compound. Error bars represent sample standard deviation values.

9.3.3 HSGN-2143 and -2192 are tolerable to human cell lines

An important attribute of an antibiotic agent is its selectivity for prokaryotic cells. Since HSDP-76 did show some toxicity to RBCs but HSGN-2143 and -2192 showed little to none, we proceeded to evaluate HSGN-2143 and -2192 for toxicity to mammalian cells. HSGN-2143 and -2192 were highly tolerable to A549 and MDA-MB-231 cells at concentrations higher than 32

μg/mL (see Figure 9.3A & B). This concentration is 64-times higher than the compounds' corresponding MIC value against *S. aureus* ATCC 25923 used in the initial screening.

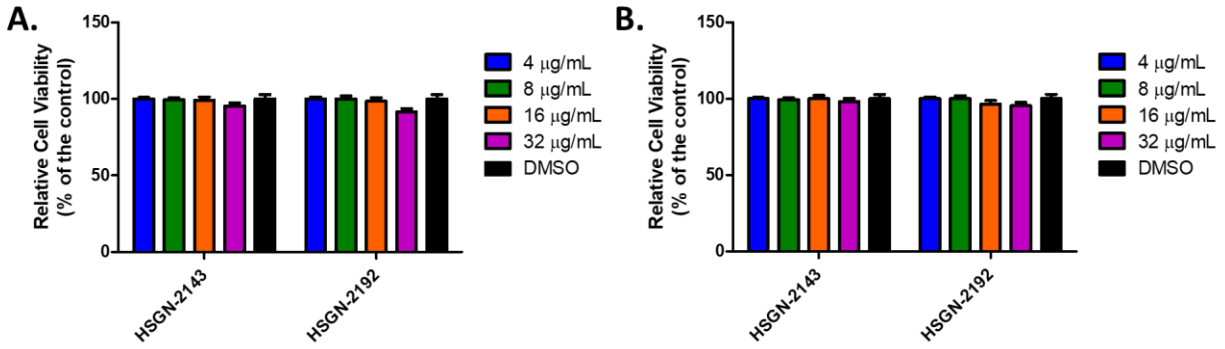

Figure 9.3 *In vitro* cytotoxicity assessment of HSGN-2143 and -2192 (tested in triplicate) against (A) human lung cells (A549) and (B) human breast cells (MDA-MB-231). Results are presented as percent viable cells relative to DMSO (negative control). Error bars represent standard deviation values.

9.4 Conclusion

We have identified promising SF_5, OCF_3, and SCF_3 containing alkyl and cycloalkyl *N*-(1,3,4-oxadiaozl-2-yl)benzamides, HSGN-2143, HSGN-2192, and HSDP-76 with potent antibacterial activity against MRSA, VRE, and *L. monocytogenes*. HSGN-2143, HSGN-2192, and HSDP-76 did not lyse RBCs and HSGN-2143 and -2192 were highly tolerable to human cell lines. In the last few years, the call to action to develop novel antibiotics has been responded to by many academic groups and the anticipation is that compounds reported by others or in this report would progress to further clinical development[200, 202-205, 207-209].

9.5 Materials and Methods

9.5.1 Chemistry

All reagents and solvents were purchased from commercial sources and used as obtained. The ^{1}H, ^{13}C, and spectra were acquired in DMSO-*d*6 solvent using either a 500 MHz or 800 MHz NMR spectrometer with Me_4Si as an internal standard. Chemical shifts are reported in parts per million (δ) and are calibrated using residual undeuterated solvent as an internal reference. Data for ^{1}H NMR spectra are reported as follows: chemical shift (δ ppm) (multiplicity, coupling constant (Hz), integration). Multiplicities are reported as follows: s = singlet, d = doublet, t = triplet, q = quartet, m = multiplet, or combinations thereof. High resolution mass spectra (HRMS) were

obtained using the electron spray ionization (ESI) technique and as a TOF mass analyzer. Compounds were characterized by ^{1}H NMR, ^{13}C NMR, and HRMS data.

9.5.2 General Procedure for Synthesis of Alkyl containing 1,3,4-oxadiazol-2-amines

The synthesis of A1-A12 was performed using a literature-reported procedure[211]. Obtained ^{1}H, and ^{13}C spectra were in agreement with literature-reported data.

9.5.3 General Procedure for the Synthesis of Acid Chlorides

In a round-bottom flask was added the desired benzoic acid in thionyl chloride (5 mL). The reaction mixture was refluxed for 1 hour. After, the reaction mixture was concentrated under reduced pressure and the crude acid chloride was continued onto the next step without purification or characterization.

9.5.4 General Procedure for the Synthesis of Analogs 1-27

In a round-bottom flask was added the corresponding acid chloride (1.3 eq), amine (1 eq), and *N*-methylimidazole (5 eq) in 1,4-dioxane solvent (5 mL). The reaction mixture was stirred at 90°C for 2 h. After completion, the reaction mixture was concentrated under reduced pressure, diluted with ethyl acetate (20 mL), washed twice with water (10 mL), once with brine (10 mL), dried over Na_2SO_4 and then concentrated under reduced pressure. The resulting crude mixture was purified by flash column chromatography (hexanes:ethyl acetate 80:20 to 70:30) to give the desired product.

9.5.5 Characterization Data

N-(1,3,4-Oxadiazol-2-yl)-4-((trifluoromethyl)thio)benzamide (1, HSGN-2192):
Off-white solid (25 mg, 21%). ^{1}H NMR (500 MHz, DMSO-d_6) δ 9.1 (s, 1H), 8.1 – 8.1 (m, 2H), 7.9 – 7.8 (m, 2H). ^{13}C NMR (126 MHz, DMSO-d_6) δ 167.3, 165.1, 158.3, 152.0, 136.2, 131.1 (q, J = 308.7 Hz), 130.1, 128.5. HRMS (ESI) m/z calcd for $C_{10}H_7F_3N_3O_2S$ $[M + H]^+$ 290.0211, found 290.0214.

N-(5-Methyl-1,3,4-oxadiazol-2-yl)-4-(pentafluoro-λ^6-sulfaneyl)benzamide (2, HSGN-2143):
Off-white solid (35 mg, 29%). ^{1}H NMR (800 MHz, DMSO-d_6) δ 8.2 – 8.2 (m, 2H), 8.1 – 8.0 (m, 2H), 2.5 (s, 3H). ^{13}C NMR (201 MHz, DMSO-d_6) δ 165.6, 160.7, 158.4, 155.8, 137.1, 129.8, 126.5, 11.0. HRMS (ESI) m/z calcd for $C_{10}H_9F_5N_3O_2S$ $[M + H]^+$ 330.0336, found 330.0335.

N-(5-Methyl-1,3,4-oxadiazol-2-yl)-4-((trifluoromethyl)thio)benzamide (3):
Off-white solid (22 mg, 18%). ^{1}H NMR (800 MHz, DMSO-d_6) δ 8.1 – 8.1 (m, 2H), 7.9 – 7.8 (m, 2H), 2.5 (s, 3H). ^{13}C NMR (201 MHz, DMSO-d_6) δ 165.6, 161.0, 158.3, 135.9, 130.6 (q, J = 307.5 Hz), 129.9, 128.4, 11.0. HRMS (ESI) m/z calcd for $C_{11}H_9F_3N_3O_2S$ $[M + H]^+$ 304.0368, found 304.0365.

N-(5-Methyl-1,3,4-oxadiazol-2-yl)-4-(trifluoromethoxy)benzamide (4):
Off-white solid (10 mg, 6%). ^{1}H NMR (800 MHz, DMSO-d_6) δ 8.1 – 8.1 (m, 2H), 7.5 (d, J = 8.3 Hz, 2H), 2.5 (s, 3H). ^{13}C NMR (201 MHz, DMSO-d_6) δ 164.4, 161.4, 158.1, 151.6, 132.0, 131.2, 121.1, 119.7 (q, J = 257.3 Hz), 11.1. HRMS (ESI) m/z calcd for $C_{11}H_9F_3N_3O_3$ $[M + H]^+$ 288.0596, found 288.0597.

N-(5-Ethyl-1,3,4-oxadiazol-2-yl)-4-(pentafluoro-λ^6-sulfaneyl)benzamide (5):
Off-white solid (29 mg, 23%). ^{1}H NMR (800 MHz, DMSO-d_6) δ 8.2 (d, J = 8.4 Hz, 2H), 8.1 (d, J = 8.8 Hz, 2H), 2.8 (q, J = 7.6 Hz, 2H), 1.3 (t, J = 7.5 Hz, 3H). ^{13}C NMR (201 MHz, DMSO-d_6) δ 166.1, 164.4, 158.4, 155.7, 137.1, 129.9, 126.5, 18.8, 10.5. HRMS (ESI) m/z calcd for $C_{11}H_{11}F_5N_3O_2S$ $[M + H]^+$ 344.0492, found 344.0492.

N-(5-Ethyl-1,3,4-oxadiazol-2-yl)-4-((trifluoromethyl)thio)benzamide (6):
Off-white solid (29 mg, 22%). ^{1}H NMR (800 MHz, DMSO-d_6) δ 8.1 (d, J = 8.4 Hz, 2H), 7.9 (d, J = 8.2 Hz, 2H), 2.8 (q, J = 7.6 Hz, 2H), 1.3 (t, J = 7.6 Hz, 3H). ^{13}C NMR (201 MHz, DMSO-d_6) δ 166.2, 164.7, 158.3, 135.9, 130.6 (q, J = 307.5 Hz), 129.9, 128.4, 18.8, 10.5. HRMS (ESI) m/z calcd for $C_{12}H_{11}F_3N_3O_2S$ $[M + H]^+$ 318.0524, found 318.0527.

N-(5-Ethyl-1,3,4-oxadiazol-2-yl)-4-(trifluoromethoxy)benzamide (7):
Off-white solid (15 mg, 11%). ^{1}H NMR (500 MHz, DMSO-d_6) δ 8.1 (d, J = 8.1 Hz, 2H), 7.6 – 7.5 (m, 2H), 2.8 (q, J = 7.4 Hz, 2H), 1.3 (t, J = 7.4 Hz, 3H). ^{13}C NMR (126 MHz, DMSO-d_6) δ 164.9,

158.4, 151.7, 132.3, 131.3, 128.8, 123.5, 121.4 (q, *J* = 258.3 Hz), 18.9, 10.7. HRMS (ESI) m/z calcd for $C_{12}H_{11}F_3N_3O_3$ $[M + H]^+$ 302.0753, found 302.0752.

N-(5-Isopropyl-1,3,4-oxadiazol-2-yl)-4-((trifluoromethyl)thio)benzamide (8):
Off-white solid (33 mg, 24%). ^{1}H NMR (800 MHz, DMSO-d_6) δ 8.1 – 8.1 (m, 2H), 7.9 (d, *J* = 8.0 Hz, 2H), 3.2 (p, *J* = 6.9 Hz, 1H), 1.3 (d, *J* = 7.1 Hz, 6H). ^{13}C NMR (201 MHz, DMSO-d_6) δ 167.5, 166.0, 158.3, 135.9, 130.6 (q, *J* = 307.5 Hz), 130.0, 128.3, 26.1, 19.8. HRMS (ESI) m/z calcd for $C_{13}H_{13}F_3N_3O_2S$ $[M + H]^+$ 332.0681, found 332.0684.

N-(5-Isopropyl-1,3,4-oxadiazol-2-yl)-4-(pentafluoro-λ^6-sulfaneyl)benzamide (9):
Off-white solid (22 mg, 17%). ^{1}H NMR (800 MHz, DMSO-d_6) δ 8.2 (d, *J* = 8.4 Hz, 2H), 8.1 – 8.0 (m, 2H), 3.2 (dq, *J* = 14.0, 6.9 Hz, 1H), 1.3 (d, *J* = 7.0 Hz, 6H). ^{13}C NMR (201 MHz, DMSO-d_6) δ 167.3, 158.3, 155.7, 137.1, 129.8, 126.5, 26.1, 19.8. HRMS (ESI) m/z calcd for $C_{12}H_{13}F_5N_3O_2S$ $[M + H]^+$ 358.0649, found 358.0648.

N-(5-Isopropyl-1,3,4-oxadiazol-2-yl)-4-(trifluoromethoxy)benzamide (10):
Off-white solid (64 mg, 46%). ^{1}H NMR (500 MHz, DMSO-d_6) δ 8.2 – 8.1 (m, 2H), 7.6 – 7.4 (m, 2H), 3.2 – 3.1 (m, 1H), 1.3 (d, J = 6.9 Hz, 6H). ^{13}C NMR (126 MHz, DMSO-d_6) δ 167.5, 165.7, 158.6, 151.7, 132.5, 132.2, 131.3, 121.2, 119.4 (q, *J* = 257.0 Hz), 26.1, 19.9. HRMS (ESI) m/z calcd for $C_{13}H_{13}F_3N_3O_3$ $[M + H]^+$ 316.0909, found 316.0907.

N-(5-(Tert-butyl)-1,3,4-oxadiazol-2-yl)-4-((trifluoromethyl)thio)benzamide (11):
Off-white solid (25 mg, 18%). ^{1}H NMR (800 MHz, DMSO-d_6) δ 8.2 – 8.0 (m, 2H), 7.9 – 7.8 (m, 2H), 1.4 (s, 9H). ^{13}C NMR (201 MHz, DMSO-d_6) δ 169.6, 166.3, 158.4, 135.9, 130.6 (q, *J* = 307.5 Hz), 130.0, 128.3, 32.4, 28.0. HRMS (ESI) m/z calcd for $C_{14}H_{15}F_3N_3O_2S$ $[M + H]^+$ 346.0837, found 346.0835.

N-(5-(Tert-butyl)-1,3,4-oxadiazol-2-yl)-4-(pentafluoro-λ^6-sulfaneyl)benzamide (12):
Off-white solid (37 mg, 27%). ^{1}H NMR (800 MHz, DMSO-d_6) δ 8.2 (d, *J* = 8.5 Hz, 2H), 8.1 (d, *J* = 8.8 Hz, 2H), 1.4 (s, 9H). ^{13}C NMR (201 MHz, DMSO-d_6) δ 169.1, 165.6, 158.6, 155.7, 137.4, 129.9, 126.5, 32.4, 27.9. HRMS (ESI) m/z calcd for $C_{13}H_{15}F_5N_3O_2S$ $[M + H]^+$ 372.0805, found 372.0807.

N-(5-(Tert-butyl)-1,3,4-oxadiazol-2-yl)-4-(trifluoromethoxy)benzamide (13):
Off-white solid (9 mg, 6%). ^{1}H NMR (800 MHz, DMSO-d_6) δ 8.1 (d, J = 8.3 Hz, 2H), 7.5 (d, J = 8.3 Hz, 2H), 2.5 (p, J = 1.8 Hz, 1H), 1.3 (s, 9H). ^{13}C NMR (201 MHz, DMSO-d_6) δ 170.0, 164.4, 158.4, 151.6, 131.2, 121.1, 119.7 (q, *J* = 257.3 Hz), 32.3, 27.9. HRMS (ESI) m/z calcd for $C_{14}H_{15}F_3N_3O_3$ $[M + H]^+$ 330.1066, found 330.1063.

N-(5-Propyl-1,3,4-oxadiazol-2-yl)-4-((trifluoromethyl)thio)benzamide (14):
Off-white solid (37 mg, 27%). ^{1}H NMR (800 MHz, DMSO-d_6) δ 8.1 (d, *J* = 7.9 Hz, 2H), 7.9 (d, *J* = 8.0 Hz, 2H), 2.8 (t, *J* = 7.3 Hz, 2H), 1.7 (h, *J* = 7.3 Hz, 2H), 1.0 (t, *J* = 7.4 Hz, 3H). ^{13}C NMR (201 MHz, DMSO-d_6) δ 164.6, 158.0, 135.9, 130.6 (q, *J* = 307.5 Hz), 129.9, 128.4, 26.9, 19.6, 13.5. HRMS (ESI) m/z calcd for $C_{13}H_{13}F_3N_3O_2S$ $[M + H]^+$ 332.0681, found 332.0680.

4-(Pentafluoro-λ^6-sulfaneyl)-*N*-(5-propyl-1,3,4-oxadiazol-2-yl)benzamide (15):
Off-white solid (22 mg, 17%). ^{1}H NMR (800 MHz, DMSO-d_6) δ 8.2 – 8.1 (m, 2H), 8.1 – 8.0 (m, 2H), 2.8 (t, *J* = 7.3 Hz, 2H), 1.7 (h, *J* = 7.3 Hz, 2H), 1.0 (t, *J* = 7.4 Hz, 3H). ^{13}C NMR (201 MHz, DMSO-d_6) δ 165.9, 163.6, 158.4, 155.7, 137.1, 129.9, 126.5, 26.9, 19.5, 13.5. HRMS (ESI) m/z calcd for $C_{12}H_{13}F_5N_3O_2S$ $[M + H]^+$ 358.0649, found 358.0645.

N-(5-Butyl-1,3,4-oxadiazol-2-yl)-4-((trifluoromethyl)thio)benzamide (16):
Off-white solid (28 mg, 20%). ^{1}H NMR (800 MHz, DMSO-d_6) δ 8.2 – 8.1 (m, 2H), 7.9 – 7.8 (m, 2H), 2.8 (t, *J* = 7.4 Hz, 2H), 1.7 (p, *J* = 7.4 Hz, 2H), 1.4 (h, *J* = 7.4 Hz, 2H), 0.9 (t, *J* = 7.4 Hz, 3H). ^{13}C NMR (201 MHz, DMSO-d_6) δ 165.3, 164.1, 158.3, 135.9, 130.6 (q, *J* = 307.5 Hz), 129.9, 128.4, 28.1, 24.7, 21.7, 13.7. HRMS (ESI) m/z calcd for $C_{14}H_{15}F_3N_3O_2S$ $[M + H]^+$ 346.0837, found 346.0835.

N-(5-Butyl-1,3,4-oxadiazol-2-yl)-4-(pentafluoro-λ^6-sulfaneyl)benzamide (17):
Off-white solid (36 mg, 26%). ^{1}H NMR (800 MHz, DMSO-d_6) δ 8.2 (d, *J* = 8.4 Hz, 2H), 8.1 – 8.0 (m, 1H), 2.8 (s, 1H), 1.7 (p, *J* = 7.4 Hz, 2H), 1.4 (p, *J* = 7.4 Hz, 2H), 0.9 (t, *J* = 7.4 Hz, 4H). ^{13}C NMR (201 MHz, DMSO-d_6) δ 165.8, 163.7, 158.6, 155.7, 137.2, 129.8, 126.5, 28.0, 24.7, 21.7, 13.7. HRMS (ESI) m/z calcd for $C_{13}H_{15}F_5N_3O_2S$ $[M + H]^+$ 372.0805, found 372.0808.

N-(5-Cyclopropyl-1,3,4-oxadiazol-2-yl)-4-((trifluoromethyl)thio)benzamide (18):
Off-white solid (26 mg, 19%). ^{1}H NMR (800 MHz, DMSO-d_6) δ 8.1 (d, *J* = 7.9 Hz, 2H), 7.9 – 7.8 (m, 2H), 2.2 (tt, *J* = 8.7, 4.9 Hz, 1H), 1.2 – 1.1 (m, 2H), 1.0 – 1.0 (m, 2H). ^{13}C NMR (201 MHz, DMSO-d_6) δ 165.9, 165.0, 157.3, 135.9, 130.6 (q, *J* = 307.5 Hz), 129.9, 128.4, 7.8, 6.2. HRMS (ESI) m/z calcd for $C_{13}H_{11}F_3N_3O_2S$ $[M + H]^+$ 330.0524, found 330.0523.

N-(5-Cyclopropyl-1,3,4-oxadiazol-2-yl)-4-(trifluoromethoxy)benzamide (19):
Off-white solid (10 mg, 7%). ^{1}H NMR (800 MHz, DMSO-*d*6) δ 8.1 (d, *J* = 8.3 Hz, 2H), 7.5 (d, *J* = 8.4 Hz, 2H), 2.2 (tt, *J* = 8.6, 4.9 Hz, 1H), 1.1 – 1.1 (m, 2H), 1.0 – 0.9 (m, 2H). ^{13}C NMR (201 MHz, DMSO-d_6) δ 165.0, 157.8, 151.6, 132.1, 131.2, 128.7, 121.1, 119.7 (q, *J* = 257.3 Hz), 7.9, 6.2. HRMS (ESI) m/z calcd for $C_{13}H_{11}F_3N_3O_3$ $[M + H]^+$ 314.0753, found 314.0754.

N-(5-Cyclobutyl-1,3,4-oxadiazol-2-yl)-4-((trifluoromethyl)thio)benzamide (20):
Off-white solid (25 mg, 18%). ^{1}H NMR (800 MHz, DMSO-d_6) δ 8.1 – 8.1 (m, 2H), 7.9 – 7.8 (m, 2H), 3.7 (p, *J* = 8.4 Hz, 1H), 2.4 (dtd, *J* = 12.5, 8.7, 3.8 Hz, 2H), 2.3 (dq, *J* = 11.6, 8.8 Hz, 2H), 2.1 (dq, *J* = 11.1, 8.7 Hz, 1H), 2.0 (dtd, *J* = 13.7, 9.0, 4.2 Hz, 1H). ^{13}C NMR (201 MHz, DMSO-d_6) δ 165.9, 164.4, 158.3, 135.9, 130.6 (q, *J* = 307.5 Hz), 130.0, 128.3, 30.1, 26.4, 18.6. HRMS (ESI) m/z calcd for $C_{14}H_{13}F_3N_3O_2S$ $[M + H]^+$ 344.0681, found 344.0680.

N-(5-Cyclopentyl-1,3,4-oxadiazol-2-yl)-4-((trifluoromethyl)thio)benzamide (21):
Off-white solid (40 mg, 27%). ^{1}H NMR (800 MHz, DMSO-d_6) δ 8.1 – 8.1 (m, 2H), 7.9 – 7.8 (m, 2H), 3.3 (p, *J* = 7.8 Hz, 1H), 2.1 (dq, *J* = 12.8, 6.9 Hz, 2H), 1.9 (dq, *J* = 13.5, 7.0 Hz, 2H), 1.7 (dq, *J* = 10.9, 4.8 Hz, 2H), 1.7 – 1.6 (m, 2H). ^{13}C NMR (201 MHz, DMSO-d_6) δ 166.7, 165.4, 158.4, 135.9, 130.6 (q, *J* = 307.5 Hz), 129.9, 128.3, 35.7, 30.6, 25.4. HRMS (ESI) m/z calcd for $C_{15}H_{15}F_3N_3O_2S$ $[M + H]^+$ 358.0837, found 358.0837.

N-(5-Cyclopentyl-1,3,4-oxadiazol-2-yl)-4-(pentafluoro-λ^6-sulfaneyl)benzamide (22):
Off-white solid (30 mg, 21%). ^{1}H NMR (800 MHz, DMSO-d_6) δ 8.2 – 8.2 (m, 2H), 8.1 (d, *J* = 8.4 Hz, 2H), 2.0 (dq, *J* = 12.8, 6.5, 5.7 Hz, 2H), 1.9 – 1.8 (m, 2H), 1.7 – 1.7 (m, *J* = 5.0 Hz, 2H), 1.7 (tdd, *J* = 12.4, 8.0, 3.9 Hz, 2H), 1.2 (t, *J* = 7.3 Hz, 1H). ^{13}C NMR (201 MHz, DMSO-d_6) δ 166.0, 159.0, 155.5, 137.6, 129.9, 128.4, 126.5, 35.6, 30.5, 25.4. HRMS (ESI) m/z calcd for $C_{14}H_{15}F_5N_3O_2S$ $[M + H]^+$ 384.0805, found 384.0808.

N-(5-Cyclopentyl-1,3,4-oxadiazol-2-yl)-4-(trifluoromethoxy)benzamide (23):
Off-white solid (52 mg, 44%). ^{1}H NMR (800 MHz, DMSO-d_6) δ 8.1 (d, *J* = 8.3 Hz, 2H), 7.5 (d, *J* = 8.3 Hz, 2H), 3.3 (d, *J* = 7.9 Hz, 1H), 2.0 (td, *J* = 9.0, 8.2, 4.5 Hz, 2H), 1.8 (dq, *J* = 14.2, 7.2 Hz, 2H), 1.7 (qd, *J* = 11.1, 5.4 Hz, 2H), 1.6 (th, *J* = 8.0, 4.7, 3.9 Hz, 2H). ^{13}C NMR (201 MHz, DMSO-d_6) δ 167.2, 164.5, 158.2, 151.6, 132.1, 131.2, 121.1, 119.7 (q, *J* = 257.3 Hz), 35.6, 30.6, 25.4. HRMS (ESI) m/z calcd for $C_{15}H_{15}F_3N_3O_3$ $[M + H]^+$ 342.1066, found 342.1065.

N-(5-Cyclohexyl-1,3,4-oxadiazol-2-yl)-4-((trifluoromethyl)thio)benzamide (24):
Off-white solid (51 mg, 34%). ^{1}H NMR (800 MHz, DMSO-d_6) δ 8.1 (d, *J* = 7.9 Hz, 2H), 7.9 – 7.8 (m, 2H), 2.9 (t, *J* = 10.8 Hz, 1H), 2.0 (dd, *J* = 13.3, 4.1 Hz, 2H), 1.8 – 1.7 (m, 2H), 1.7 – 1.6 (m, 1H), 1.6 (qd, *J* = 12.6, 11.8, 3.0 Hz, 2H), 1.4 (q, *J* = 12.0 Hz, 2H), 1.3 (q, *J* = 12.1 Hz, 1H). ^{13}C NMR (201 MHz, DMSO-d_6) δ 167.0, 165.3, 158.2, 135.9, 130.6 (q, *J* = 307.5 Hz), 129.9, 128.3, 34.6, 29.8, 25.6, 24.9. HRMS (ESI) m/z calcd for $C_{16}H_{17}F_3N_3O_2S$ $[M + H]^+$ 372.0994, found 372.0992.

N-(5-cyclohexyl-1,3,4-oxadiazol-2-yl)-4-(pentafluoro-λ^6-sulfaneyl)benzamide (25):
Off-white solid (56 mg, 38%). ^{1}H NMR (800 MHz, DMSO-d_6) δ 8.2 – 8.2 (m, 2H), 8.1 – 8.0 (m, 2H), 3.0 – 2.9 (m, 1H), 2.0 (dd, *J* = 12.7, 4.5 Hz, 2H), 1.8 (dt, *J* = 13.3, 4.1 Hz, 2H), 1.7 (dt, *J* = 13.0, 4.2 Hz, 1H), 1.6 – 1.5 (m, 2H), 1.4 (dtd, *J* = 15.6, 11.8, 5.9 Hz, 2H), 1.3 (qt, *J* = 11.6, 3.6 Hz, 1H). ^{13}C NMR (201 MHz, DMSO-d_6) δ 166.1, 158.5, 155.7, 137.4, 129.9, 126.5, 34.6, 29.7, 25.6, 24.9. HRMS (ESI) m/z calcd for $C_{15}H_{17}F_5N_3O_2S$ $[M + H]^+$ 398.0961, found 398.0960.

N-(5-Cyclohexyl-1,3,4-oxadiazol-2-yl)-4-(trifluoromethoxy)benzamide (26, HSDP-72):
Off-white solid (38 mg, 24%). ^{1}H NMR (800 MHz, DMSO-d_6) δ 8.1 (d, J = 8.1 Hz, 2H), 7.5 (d, J = 8.2 Hz, 2H), 2.9 (t, J = 10.9 Hz, 1H), 2.0 (d, J = 12.7 Hz, 2H), 1.8 – 1.1 (m, 8H). ^{13}C NMR (201 MHz, DMSO-d_6) δ 167.2, 164.2, 157.7, 151.6, 131.2, 121.1, 119.7 (q, *J* = 257.3 MHz), 34.5, 29.8, 25.5, 25.0. HRMS (ESI) m/z calcd for $C_{16}H_{17}F_3N_3O_3$ $[M + H]^+$ 356.1222, found 356.1224.

4-(Pentafluoro-λ^6-sulfaneyl)-*N*-(5-(tetrahydro-2H-pyran-4-yl)-1,3,4-oxadiazol-2-yl)benzamide (27):
Off-white solid (28 mg, 19%). ^{1}H NMR (800 MHz, DMSO-d_6) δ 8.2 – 8.2 (m, 2H), 8.1 – 8.0 (m, 2H), 3.9 (dt, *J* = 11.6, 3.7 Hz, 2H), 3.5 (td, *J* = 11.3, 2.4 Hz, 2H), 3.2 (tt, *J* = 10.8, 4.1 Hz, 1H), 2.0 – 1.9 (m, 2H), 1.8 (dtd, *J* = 13.3, 10.9, 4.2 Hz, 2H). ^{13}C NMR (201 MHz, DMSO-d_6) δ 165.6,

165.2, 158.6, 155.7, 137.3, 129.9, 126.5, 66.2, 31.9, 29.5. HRMS (ESI) m/z calcd for $C_{15}H_{17}F_5N_3O_2S$ $[M + H]^+$ 400.0754, found 400.0752.

9.5.6 Bacterial strains media, cell lines and reagents

Bacterial strains were obtained from various sources as listed in Appendix C Table C.1 and Table C.2. Cation-adjusted Mueller Hinton (CAMHB) broth, tryptic soy broth (TSB) and tryptic soy agar (TSA) were purchased from Becton, Dickinson and Company (Cockeysville, MD, USA). Human lung carcinoma epithelial cells (A549) (ATCC CCL-185) and human breast adenocarcinoma epithelial cells (MDA-MB-231) (ATCC HTB-26) were obtained from the American Type Culture Collection (ATCC) (Manassas, VA, USA). Dulbecco's Modified Eagle Medium (DMEM), fetal bovine serum (FBS) and phosphate-buffered saline (PBS) was purchased from Corning (Manassas, VA, USA). Sheep red blood cells (RBCs) were purchased from Innovative Research (MI, USA). Linezolid (Chem-Impex International, Wood Dale, IL, USA), vancomycin hydrochloride (Gold Biotechnology, St. Louis, MO, USA), and colistin (AK Scientific, Union City, CA, USA) were purchased commercially. Compounds were synthesized from commercial sources in our laboratory.

9.5.7 Determination of MICs

The broth microdilution method was utilized as outlined by the Clinical and Laboratory Standards Institute (CLSI)[212]. MICs are reported as the lowest concentration of compound that entirely inhibited the growth of bacteria, as observed visually.

9.5.8 Hemolysis assay

Hemolysis assay was performed following the procedure described previously[164]. Sheep red blood cells were used. 1% DMSO acted as negative control, while Triton-X-100 served as the positive control. Percent hemolysis was determined from absorbance at 540 nm.

9.5.9 *In vitro* cytotoxicity analysis of HSGN-2143 and -2192 against mammalian cell lines

HSGN-2143 and -2192 were assayed for potential cytotoxicity against both human lung carcinoma (A549) and human breast adenocarcinoma (MDA-MB-231) cell lines as described

previously[163]. Briefly, the tested compounds were incubated with A549 or MDA-MB-231 cells for 24 hours. Then, cells were incubated with 3-(4,5-dimethylthiazol-2-yl)-5-(3-carboxymethoxyphenyl)-2-(4-sulfophenyl)-2H-tetrazolium) (MTS) for 4 hours before measuring absorbance values at 490 nm.

9.6 Author Contributions

G. Naclerio, W. Gribble, and D. Pagan synthesized compounds in study. G. Naclerio and W. Gribble performed MIC assays. K. Onyedibe performed cytotoxicity and hemolysis assays. G. Naclerio and H. Sintim wrote manuscript.

CHAPTER 10. MEMBRANE-TARGETING HALOGENATED *N*-(1,3,4-OXADIAZOL-2-YL)BENZAMIDE POTENTLY ERADICATES METHICILLIN-RESISTANT *STAPHYLOCOCCUS AUREUS* BIOFILM

10.1 Abstract

Staphylococcus aureus (*S. aureus*) is a pathogen that can cause chronic or relapsing infections. This is mostly due to the formation of biofilms which are immobile colonies of bacteria attached to cell surfaces or medical devices. Biofilms are highly resistant to antibiotic treatment and cause 80% of chronic bacterial infections. Therefore, new chemical entities to eradicate biofilm is of high priority. We performed a systematic halogenation study on *N*-(1,3,4-oxadiazol-2-yl)benzamides leading to the identification of HSGN-2241. The compound displayed a highly potent activity against multi-drug resistant Gram-positive bacteria with minimum inhibitory concentrations (MICs) ranging from 0.125 μg/mL and 1 μg/mL. Additionally, HSGN-2241 displayed a rapid killing of MRSA cells as well as the ability to eradicate MRSA pre-formed biofilm. Furthermore, HSGN-2241 was non-toxic to mammalian cells and did not lyse human red blood cells. Current mechanistic studies demonstrated that HSGN-2241 depolarizes *S. aureus* membranes triggering potassium ion release. Moreover, lipidomics analysis of *S. aureus* membranes treated with HSGN-2241 reveals that the compound affects the synthesis of phospholipids and free fatty acids. This work further emphasizes incredible drug potency enhancement via halogen substitution.

10.2 Introduction

The increase in antimicrobial-resistant bacteria has become a serious issue as the World Health Organization (WHO) recognizes that globally 700,000 people die annually from drug-resistant infections [409]. Consequently, if antimicrobial resistance is not taken care of, annual deaths can reach 10 million by 2050[131]. The Gram-positive bacterial pathogen, *Staphylococcus aureus* is one of the leading causes of community- and hospital-acquired bacteremia, surgical site infections, osteomyelitis, pneumonia, and skin infections[107]. Methicillin-resistant *S. aureus* (MRSA) bacteremia causes higher mortality rates compared to methicillin-sensitive *S. aureus* (MSSA)[109]. In 2019, the Centers for Disease Control and Prevention (CDC) estimated that bacterial infections

kill more than 35,000 annually in the U.S. alone with MRSA being accountable for about one-third of the mortalities with an estimated 11,000 annual deaths[111, 170].

further complicating the problem, *S. aureus* can form biofilm which leads to infection persistence[65]. Biofilms are immobile populations of bacteria that grow on a variety of surfaces such as medical devices, catheters, sutures, and dental implants[416]. The bacterial population in biofilm is protected by an extra-cellular matrix (ECM) which further possesses bacterial polymers like extracellular DNA (e-DNA), amyloidogenic proteins, and exopolysaccharides (EPS)[138, 417]. Regarding persistent infections, biofilm cause about 80% of chronic and recurrent bacterial infections[418]. These infections are difficult to treat due to the fact that biofilm is highly resistant to antibiotic treatment and immune responses. Specifically, biofilms show approximately 10–10,000 times more resistance to antibiotics than planktonic growing bacteria[418].

Even though antibiotic treatment is the most effective measure for controlling microbial infections, they are almost impossible to eradicate biofilm infections[419]. To combat biofilm infections, several antimicrobial agents have been developed [156, 420], but none of these compounds have proceeded to clinical trials yet. Therefore, the need to develop new potent anti-biofilm agents with low toxicity is of high priority.

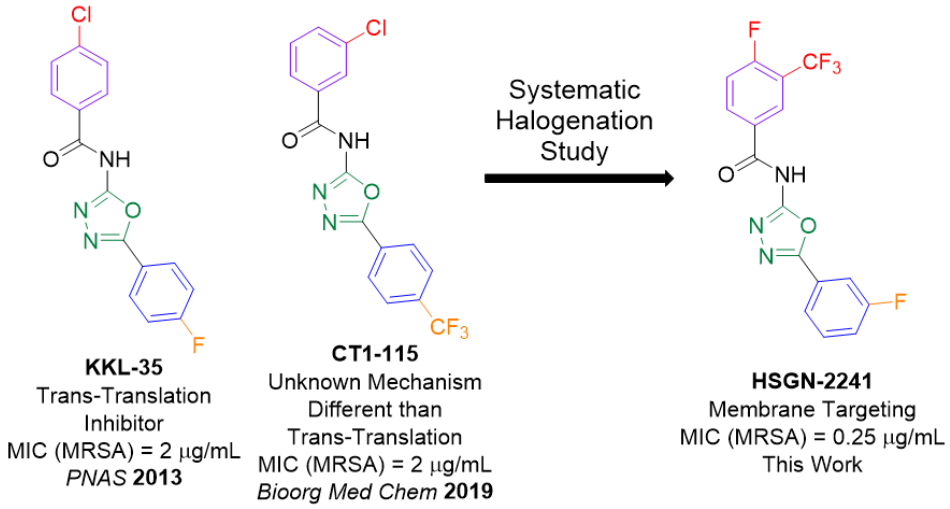

Figure 10.1 KKL-35 has moderate activity against MRSA and has been shown to inhibit trans-translation[353]. CT1-115 also shows moderate activity against MRSA but has an unknown mechanism different than trans-translation[354]. Performance of a systematic halogenation study led to the identification of HSGN-2241 which shows highly potent activity against MRSA and is membrane targeting.

10.3 Materials and Methods

10.3.1 Bacterial strains, media, cell lines and reagents

Bacterial strains were obtained from various sources as listed in Tables D.1 and D.2. Cation-adjusted Mueller Hinton broth (CAMHB), tryptic soy broth (TSB) and tryptic soy agar (TSA) were purchased from Becton, Dickinson and Company (Cockeysville, MD, USA). Dulbecco's Modified Eagle Medium (DMEM), fetal bovine serum (FBS) and phosphate-buffered saline (PBS) were purchased from Corning (Manassas, VA, USA). Human colorectal adenocarcinoma epithelial cell line (Caco-2) (ATCC HTB-37) was obtained from the American Type Culture Collection (ATCC) (Manassas, VA, USA). Single donor human red blood cells (RBCs) were purchased from Innovative Research (Novi, MI, USA). Linezolid (Chem-Impex International, Wood Dale, IL, USA), vancomycin hydrochloride (Gold Biotechnology, St. Louis, MO, USA), ciprofloxacin (Sigma Aldrich, St. Louis, MO, USA), DiSC3(5) (3,3'-Dipropylthiadicarbocyanine Iodide) (Thermo Fisher Scientific, Waltham, MA, USA), potassium chloride (Sigma Aldrich, St. Louis, MO, USA), Potassium-binding benzofuran isophthalate (PBFI) (Sigma Aldrich, St. Louis, MO, USA), sodium acetate (Sigma Aldrich, St. Louis, MO, USA), acetonitrile/methanol/300 mM ammonium acetate (Sigma Aldrich, St. Louis, MO, USA) and daptomycin (AK Scientific, Union City, CA, USA) were purchased commercially. Compounds were synthesized from commercial sources in our laboratory and prepared in stock solutions using dimethyl sulfoxide (DMSO) as a solvent.

10.3.2 Determination of MICs

The MICs were determined using the broth microdilution method following the guidelines of the Clinical and Laboratory Standards Institute (CLSI)[212]. Briefly, a 0.5 McFarland bacterial solution was diluted in CAMHB to reach a bacterial concentration of about 5×10^5 CFU/mL. *Listeria monocytogenes* was diluted in TSB as described. Serial dilutions of test agents were then incubated with bacteria at 37° C for 24 hours. MICs reported are the minimum concentrations of the test agents that entirely inhibited the visual growth of bacteria.

10.3.3 Time-kill analysis

To determine the mode of bacterial inhibition for HSGN-2241, and HSGN-2263, bacterial exponential phase culture was diluted to ~ 2.35×10^6 CFU/mL, in TSB and exposed to HSGN-2241, -2263, linezolid, and vancomycin (5× and 10× MIC, in triplicates), and incubated at 37 °C, as previously described[164, 213]. An aliquot from each treatment was collected after the corresponding times, serially diluted in PBS, and plated onto TSA plates. Plates were incubated at 37 °C for 18-20 hours before enumerating colonies to determine the CFU/mL counts.

10.3.4 *In vitro* cytotoxicity analysis of HSGN-2241 against human colorectal cells

HSGN-2241 was assessed for cytotoxicity against a human colorectal adenocarcinoma (Caco-2) cell line, as described in previous reports[163, 214, 350]. Briefly, HSGN-2241 was incubated with Caco-2 cells for 24 hours. Then, cells were incubated with MTS 3-(4,5-dimethylthiazol-2-yl)-5-(3-carboxymethoxyphenyl)-2-(4-sulfophenyl)-2H-tetrazolium) reagent for 4 hours before measuring absorbance values (OD_{490}).

10.3.5 Hemolysis assay

The hemolytic activity of HSGN-2241 against human red blood cells (RBCs) was assayed following a procedure described previously[164].

10.3.6 Biofilm eradication assay

MRSA USA300 biofilm eradication activity of HSGN-2241, vancomycin, linezolid, and daptomycin was performed using the microtiter plate biofilm formation assay as previously described [166, 421].

10.3.7 Scanning electron microscopy for biofilm

Pre-formed *S. aureus* biofilms were grown in 24 well tissue culture plates with sterile 13 mm glass slides at the base of each well of the culture plates. After 24 hours of treatment with 8 μg/mL of HSGN-2241, media was removed, and wells were washed with PBS twice. Samples were then fixed in chilled 2.5% glutaraldehyde in 0.1M sodium cacodylate buffer and processed

further as previously described[393]. Briefly, samples were post-fixed in 1% osmium tetroxide and dehydrated in a series of ethanol with graded concentrations. Subsequently, sample slides were processed via three changes of hexamethyldisilazane (HMDS), dried overnight and coated with platinum in a Cressington 208HR sputter coater. The coated slides were imaged in the FEI Nova Nano-SEM 200 equipment at 5 kV. DMSO was used as the control in this assay.

10.3.8 RT-PCR on MRSA biofilm genes

MRSA USA300 biofilm was formed in a 24 well plate as described above. The pre-formed biofilm was treated with either HSGN-2241 (8 μg/mL) or DMSO. The plate was incubated at 37 °C for 24 h. Next, medium was carefully discarded, and the plate was washed with PBS to remove the planktonic cells. Afterwards, 5 mL of the RNAprotect bacteria reagent (Qiagen, Germantown, MD) was added to each well of the plate for 5 min, and the biofilm suspension was scraped and transferred into 15 mL tubes. The bacterial cells were then pelleted at 7,000 × *g* for 10 min. RNA isolation, cDNA synthesis, and RT-PCR analysis was performed following a previously reported procedure[217]. A BioRad CFX96™ Touch Real-Time PCR Detection System was used. PCR primers were either created using Primer-BLAST or acquired from the referenced literature (Table D.3). Data were normalized against RNA polymerase subunit β gene (*rpoB*), as an internal control, and the P-values from student's *t*-test showed * ≤ 0.05 or ** ≤ 0.01.

10.3.9 Multi-step resistance selection

To determine if MRSA could form resistance to HSGN-2241 , a multi-step serial passage experiment was used, as described previously[117, 215-216]. Resistance was considered as a greater than four-fold increase in the MIC as compared to the initial MIC.

10.3.10 Bacterial membrane depolarization assay

Membrane depolarization activity of HSGN-2241, at 1×, 5×, and 10× MIC, was assayed in triplicate following a previously reported procedure[393] using DiSC3(5) (3,3'-Dipropylthiadicarbocyanine Iodide) as the fluorometric dye. Daptomycin at 1× and 10× MIC was used as a positive control. 1% DMSO and DiSC3(5) acted as the negative control.

10.3.11 Bacterial membrane permeability assay

Membrane permeability activity of HSGN-2241, at 1×, 5×, and 10× MIC, was assayed in triplicate following a previously reported procedure[393] using Sytox green (Invitrogen, Waltham, MA) as the fluorometric dye. Bithionol (4 µg/mL) was used as the positive control[69]. 1% DMSO and Sytox green served as the negative control.

10.3.12 Potassium ion release assay

The ability of HSGN-2241, at 2.5 µg/mL and 5 µg/mL, to cause potassium ion release in *S. aureus* ATCC 25923 was assayed in triplicate following the previously reported procedure[405]. Potassium-binding benzofuran isophthalate (PBFI) was used as the fluorometric dye. Daptomycin (5 µg/mL) acted as a positive control in the assay. The negative control consisted of 1% DMSO and PBFI.

10.3.13 Flow cytometry

Membrane depolarization activity of HSGN-2241, at 5× and 10× MIC, was performed following a previously reported procedure[393, 405]. To-PRO 3 iodide (Thermo Fisher Scientific, Waltham, MA, USA) (red dye) served as the membrane-permeable dye, while DiOC2 (Thermo Fisher Scientific, Waltham, MA, USA) (green dye) served as the membrane-impermeable dye. Daptomycin acted as a positive control for membrane depolarization. Bithionol was used as the positive control for membrane permeability. Negative control was 1% DMSO with both To-PRO 3 iodide and DiOC2. Bacteria were imaged using a BD Fortessa cell analyzer.

Multiple reaction monitoring profiling (MRM-profiling) of lipids

An overnight culture of *S. aureus* ATCC 25923 was diluted into fresh TSB and incubated at 37°C until reached an OD_{600} of 0.3. Then, the bacterial cells were treated with either 1% DMSO or **HSGN-2241** (2×, 5×, and 10× MIC) for 2 hours at 37°C. Next, lipids were extracted following the Bligh-Dyer method[221], and lipids were isolated and dried over nitrogen stream. MRM experiments were performed following a previously reported procedure[189]. PCA plots were constructed using MetaboAnalyst 5.0.

10.4 Results and Discussion

10.4.1 Synthesis and initial screening of halogen substituted *N*-(1,3,4-oxadiazol-2-yl)benzamides

Previous reported *N*-(1,3,4-oxadiazol-2-yl)benzamides, KKL-35 and CT1-115, were shown to have moderate activity against MRSA with MICs of 2 μg/mL. Yet, halogenation (X = F, Cl, Br, or I) has been shown to enhance drug's potency and pharmacological properties in several instances[278-280, 283-284]. Therefore, we proceeded to explore the effect of halogenation pattern on the antibacterial activity by synthesizing *N*-(1,3,4-oxadiazol-2-yl)benzamides containing mono- or di-substituted halogens.

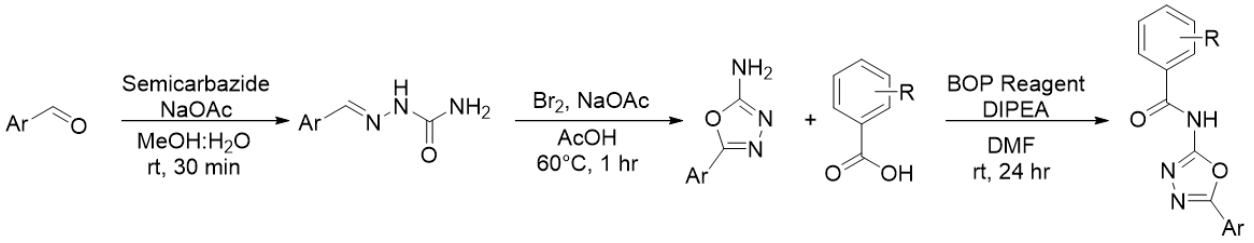

Scheme 10.1 General route for the synthesis of halogen substituted *N*-(1,3,4-oxadiazol-2-yl)benzamides.

To synthesize the *N*-(1,3,4-oxadiazol-2-yl)benzamides, we took an aryl aldehyde and added semicarbazide and sodium acetate to give the subsequent semicarbazone. We then cyclized the semicarbazone into the 1,3,4-oxadiazol-2-amine with bromine and sodium acetate (Scheme 10.1). Next, we performed amide coupling between the halogen substituted benzoic acid and the 1,3,4-oxadiazol-2-amine using benzotriazol-1-yloxytris(dimethylamino)phosphonium hexafluorophosphate (BOP) reagent which gave the halogen substituted *N*-(1,3,4-oxadiazol-2-yl)benzamides (Scheme 10.1).

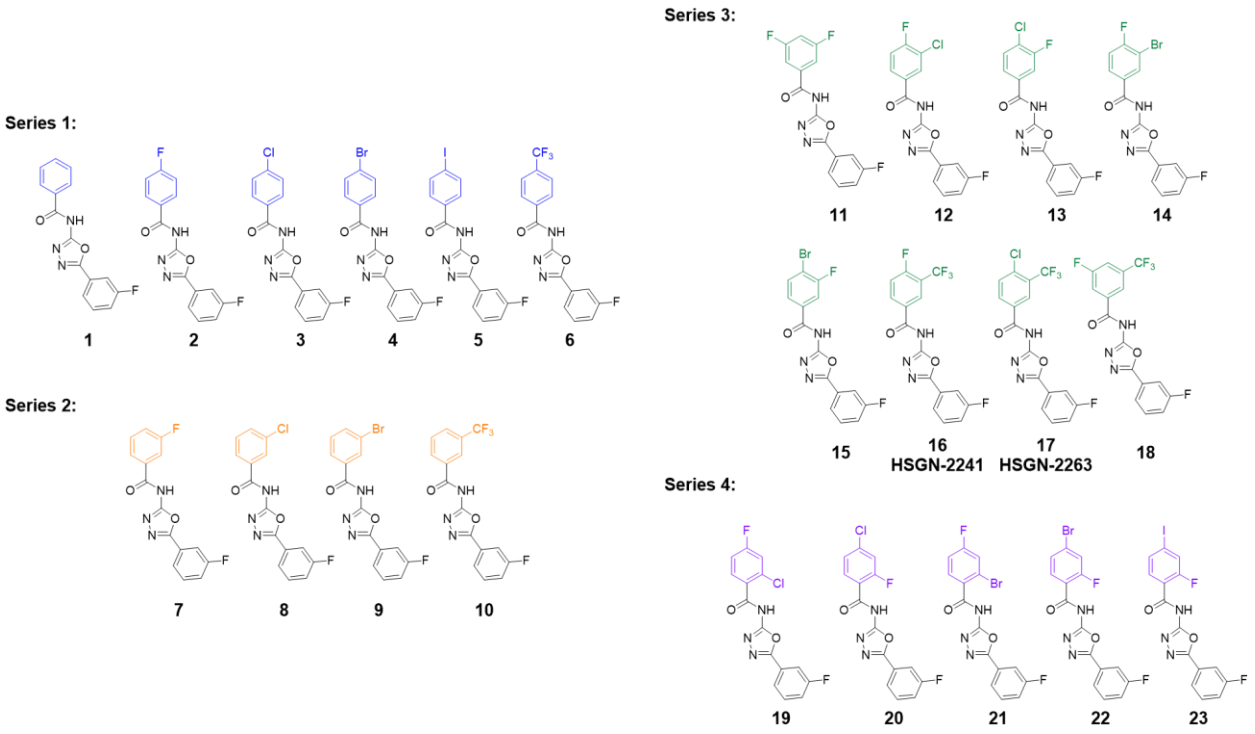

Figure 10.2 New series and halogen-substituted *N*-(1,3,4-oxadiazol-2-yl)benzamides synthesized.

Four types of compounds were synthesized (Series 1-4, Figure 10.2). Series 1 was made up of compounds mono-substituted with a halogen at the 4 position of the benzamide ring (Figure 2; Series 1). No substitution (1) seemed to have a weak activity against *S. aureus* ATCC 25923 and MRSA ATCC 33592 with an MIC of 16 µg/mL (Table 10.1). Addition of fluoro (2), bromo (4), iodo (5), and trifluoromethyl (6) gave compounds with moderate antibacterial activity with MICs ranging from 1 µg/mL to 4 µg/mL (Table 10.1). However, substitution with chloro (3) showed potent activity with MICs = 0.5 µg/mL against *S. aureus* ATCC 25923 and MRSA ATCC 33592 (Table 10.1). Series 2 consisted of compounds with mono-substitution at the 3 position of the benzamide moiety (Figure 10.2; Series 2). In this series, 3-chloro (8) was the most potent (MIC = 0.5 µg/mL; Table 10.1), but antibacterial activity did decrease 2-fold for 3-fluoro (7) and 3-bromo (9) substitutions (Table 10.1). In series 3, we evaluated the effect of di-halogen substitution at either the 3,4 or 3,5 positions of the benzamide ring (Figure 10.2; Series 3). All compounds synthesized in this series showed potent antibacterial activity (MICs = 0.5-1 µg/mL), especially compounds substituted with 4-fluoro-3-triflouromethyl (16, HSGN-2241) and 4-chloro-3-trifluoromethyl (17, HSGN-2263) which displayed MICs of 0.25 µg/mL and 0.125 µg/mL, respectively against *S. aureus* ATCC 25923 and MRSA ATCC 33592 (Table 10.1). In series 4, we

continued investigating di-halogen substitution but at the 2,4 positions. Interestingly, compounds 19-23 showed weak antibacterial activity with MICs ranging from 8 μg/mL to 32 μg/mL (Table 10.1). We suspect that the loss in antibacterial activity may be due to the steric effect from the halogen atom being directly next to the amide bond.

Table 10.1 Initial screening (MICs, in μg/mL) of halogen-substituted *N*-(1,3,4-oxadiazol-2-yl)benzamides against *S. aureus* ATCC 25923 and methicillin-resistant *S. aureus* (MRSA) ATCC 33592

Compound/Control Drug	*S. aureus* ATCC 25923	MRSA ATCC 33592
1	16	16
2	4	4
3	0.5	0.5
4	4	2
5	2	1
6	1	1
7	2	2
8	0.5	0.5
9	2	1
10	1	1
11	1	1
12	0.5	0.5
13	0.5	0.5
14	1	1
15	0.5	0.5
16, HSGN-2241	0.25	0.25
17, HSGN-2263	0.125	0.125
18	0.5	0.5
19	16	16
20	8	8
21	32	16
22	16	16
23	16	8
Vancomycin	1	1
Linezolid	2	2

10.4.2 Comprehensive antibacterial profile of HSGN-2241 and -2263 against MRSA clinical isolates and multidrug-resistant Gram-positive bacteria

After the initial screening of HSGN-2241 and -2263, we assessed their antibacterial profile against a panel of MRSA clinical isolates. Both HSGN-2241 and -2263 exhibited highly potent activities against the tested strains at concentrations ranging from 0.06 μg/mL to 1 μg/mL (Table 10.2). Furthermore, HSGN-2241 and -2263 were also quite potent against additional clinically relevant Gram-positive bacterial species including vancomycin-resistant enterococci (VRE) and *Listeria monocytogenes*, with MIC values ranging from 0.125 μg/mL to 1 μg/mL (Table 10.2). For instance, against these pathogens, the MIC values for HSGN-2241 ranged from 0.25 μg/mL to 1 μg/mL, while HSGN-2263 had MICs ranging from 0.125 μg/mL to 0.5 μg/mL. Interestingly, the antibacterial activity of both compounds was comparable to, one to two-folds more potent than that of the front-line therapeutics, vancomycin and linezolid (Table 10.2).

Table 10.2 MICs (μg/mL) of HSGN-2241 and -2263 against a panel of clinically important Gram-positive bacterial pathogens including MRSA, vancomycin-resistant *Enterococcus faecalis*, vancomycin-resistant *Enterococcus faecium* and *Listeria monocytogenes*

Bacterial Strain	Compound/Control drug			
	HSGN-2241	HSGN-2263	Vancomycin	Linezolid
MRSA USA300	0.5	0.5	1	2
MRSA ARLG 1665	1	1	0.25	2
MRSA ARLG 1663	0.5	1	1	2
MRSA ARLG 1568	0.25	0.125	0.5	1
MRSA ARLG 1664	1	1	1	2
MRSA ARLG 1570	0.25	0.06	0.5	1
MRSA ARLG 1561	0.25	0.125	1	2
MRSA ARLG 1567	0.125	0.125	1	2
MRSA ARLG 1569	0.25	0.125	1	2
MRSA ARLG 1649	0.5	0.125	2	2
E. faecalis ATCC 29212	1	0.5	2	2
VRE *faecalis* ATCC 51575	1	0.25	>128	1
VRE *faecium* ATCC 700221	0.5	0.25	>128	1
L. monocytogenes ATCC 19115	0.25	0.125	2	2

VRE: vancomycin-resistant *Enterococcus*

10.4.3 HSGN-2241 exhibits rapid bactericidal activity, while HSGN-2263 is bacteriostatic against MRSA

After identifying HSGN-2241 and -2263 were highly potent against MRSA clinical isolates as well as other drug-resistant Gram-positive pathogens, we proceeded to identify their mode of inhibition against MRSA. A time-kill kinetics assay was performed against MRSA USA300. HSGN-2263 exhibited a bacteriostatic activity while HSGN-2241 exhibited a bactericidal activity. After 24 hours, HSGN-2263 at concentrations of 2.5 µg/mL (5× MIC) and 5 µg/mL (10× MIC) resulted in a 1.1- and 1.4-$\log_{10}$-reduction in the bacterial count respectively, which was significant reduction as compared to the negative control (DMSO) (Figure 10.3). This reduction was comparable to that of linezolid, at 10 µg/mL (5× MIC) and 20 µg/mL (10× MIC), which caused about a 1.3- and 1.7-$\log_{10}$-reduction respectively. In contrast, HSGN-2241, at concentrations of 2.5 µg/mL (5× MIC) and 5 µg/mL (10× MIC), exhibited a rapid bactericidal activity against MRSA USA300. For instance, 5× MIC of HSGN-2241 completely killed the bacteria after 8 hours of treatment. Similarly, HSGN-2241 (10× MIC) required only 4 hours to completely eradicate the bacterial burden (Figure 10.3). Vancomycin, as reported earlier, displayed a slow bactericidal activity against MRSA as it required 24 hours to generate more than 3-$\log_{10}$-reduction in the bacterial count.

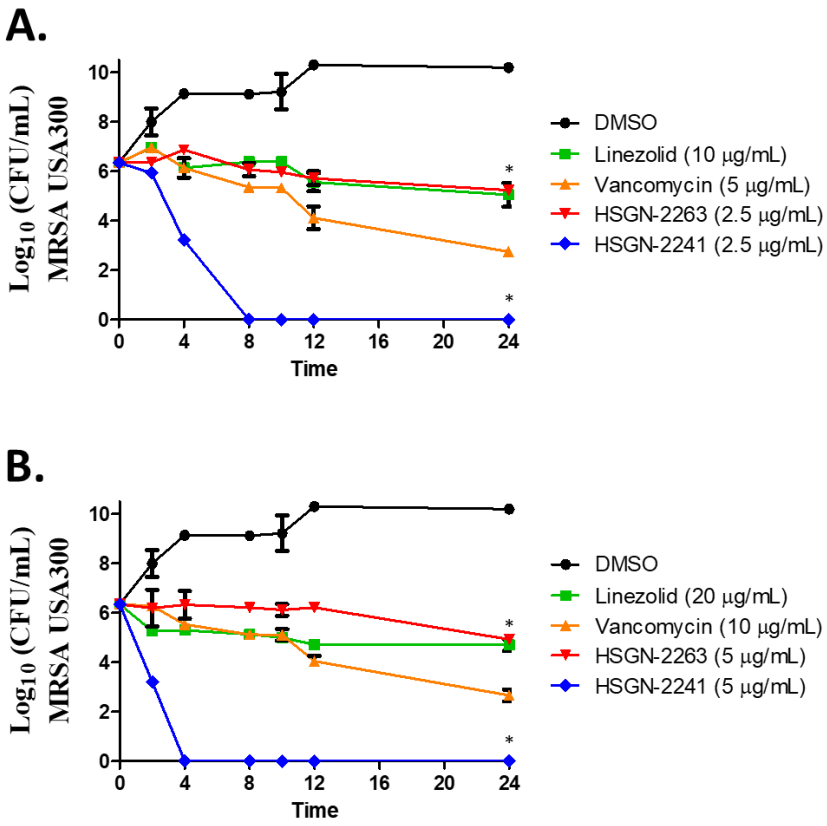

Figure 10.3 Time-kill kinetics analysis of HSGN-2241 and -2263 at: (A) 5× MIC, and (B) 10× MIC. Compounds were tested in triplicate using the corresponding concentrations, against MRSA USA300 using vancomycin and linezolid as control antibiotics. The data are presented as average CFU/mL of MRSA USA300 after treatment with each test agent. Error bars represent standard deviation values for each drug studied. The data were analyzed via a two-way ANOVA with post-hoc Dunnett's test for multiple comparisons. An asterisk (*) indicates a statistically significant difference ($P < 0.05$) between treatments with compounds HSGN-2241 and -2263 compared to DMSO treatment (negative control).

10.4.4 Structure-activity-relationship (SAR) study of HSGN-2241:

Since HSGN-2241 displayed rapid bactericidal activity against MRSA USA300, we decided to further pursue the evaluation of this compound over HSGN-2263. Thus, we proceeded to perform a SAR study on HSGN-2241. Using the same approach outlined in Scheme 10.1, we synthesized a new series of analogs in which we altered the 3-fluorophenyl group in order to assess its importance for antibacterial activity (Figure 10.4). Interestingly, we discovered that the 3-fluorophenyl group was very important for optimal activity against MRSA. For instance, substitution for 4-fluorophenyl (24), 2-fluorophenyl (25), and phenyl (26) did show a decrease in antibacterial activity with MICs of 1 µg/mL, 0.5 µg/mL, and 1 µg/mL respectively (Table 10.3).

Additionally, we investigated addition of other heteroaromatic groups, such as thiophenyl (27), dimethylthiazolyl (28), pyrimidinyl (29), and pyridinyl (30-32). Analogs 27, 28, 30, 31, and 32 all showed moderate activity against MRSA with MICs between 2 µg/mL to 4 µg/mL. Analog 29 displayed weak activity with an MIC value of 16 µg/mL against MRSA (Table 10.3). Thus, this study allowed us to conclude that the 3-fluorophenyl group of HSGN-2241 was important for the compound's highly potent antibacterial activity.

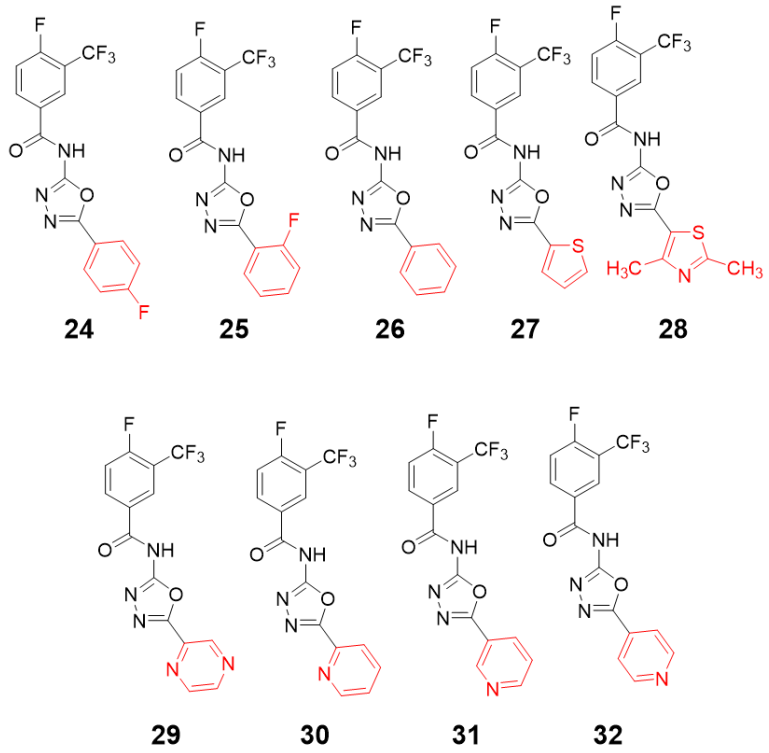

Figure 10.4 Structure-activity-relationship (SAR) study of HSGN-2241 resulting in the synthesis of compounds 24-32.

Table 10.3 MICs (μg/mL) of analogs 24-32 against *S. aureus* ATCC 25923 and methicillin-resistant *S. aureus* (MRSA) ATCC 33592

Compound/Control Drug	*S. aureus* ATCC 25923	MRSA ATCC 33592
24	1	2
25	0.5	0.5
26	1	1
27	2	2
28	2	2
29	16	16
30	4	4
31	4	4
32	4	4
HSGN-2241	0.25	0.25
Vancomycin	1	1
Linezolid	2	2

10.4.5 HSGN-2241 is non-toxic to mammalian cells and does not lyse human red blood cells

Lysis of red blood cells (RBCs) has been shown to have serious repercussions on organ function such as inflammation, cardiovascular and renal dysfunction, thrombosis, and enhanced susceptibility to infections[241]. Thus, we sought to determine if HSGN-2241 would lyse human RBCs. HSGN-2241 did not cause lysis of human RBCs at concentrations as high as 25 μg/mL (Figure 10.5), which is 25 to 100-times higher than the compound's MIC values against MRSA. At 16 μg/mL, HSGN-2241 was also non-toxic to caco-2 cell lines.

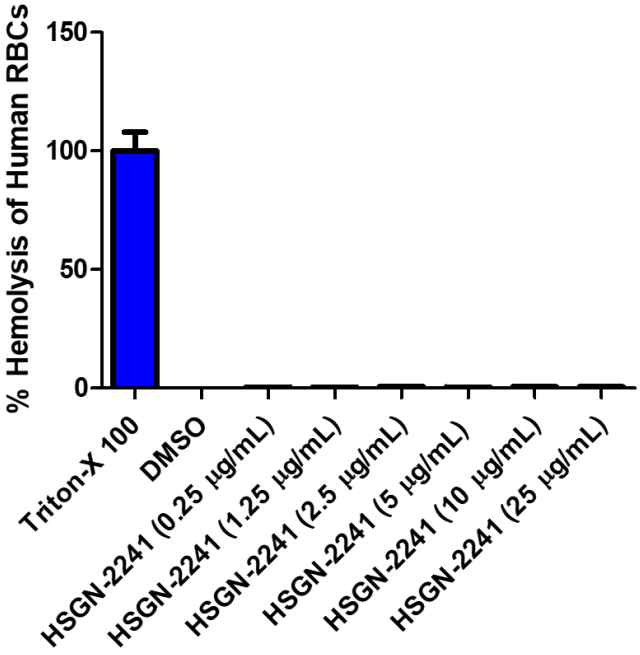

Figure 10.5 Hemolytic activity of HSGN-2241 (in triplicate) against human RBCs. Error bars represent sample standard deviation values.

10.4.6 HSGN-2241 eradicates the pre-formed MRSA biofilm

Since HSGN-2241 showed rapid bactericidal activity against MRSA, we wondered if the compound could also eradicate the pre-formed biofilm. Thus, MRSA USA300 biofilm was treated with HSGN-2241, vancomycin, linezolid, and daptomycin for 24 hours. Interestingly, vancomycin, linezolid, and daptomycin did not eradicate pre-formed biofilms. In contrast, HSGN-2241 did show significant biofilm eradication activity at concentrations as low as 8 μg/mL and 4 μg/mL, that disrupted about 80% and 75% of the pre-formed MRSA biofilm, respectively (Figure 10.6A). To further confirm HSGN-2241's biofilm eradication ability, MRSA biofilm treated with either DMSO, or HSGN-2241 (8 μg/mL) was imaged using the scanning electron microscopy (SEM). From our SEM results, at 8 μg/mL HSGN-2241 could penetrate the biofilm matrix and lyse bacteria in the biofilm as compared to the untreated control (Figure 10.6B).

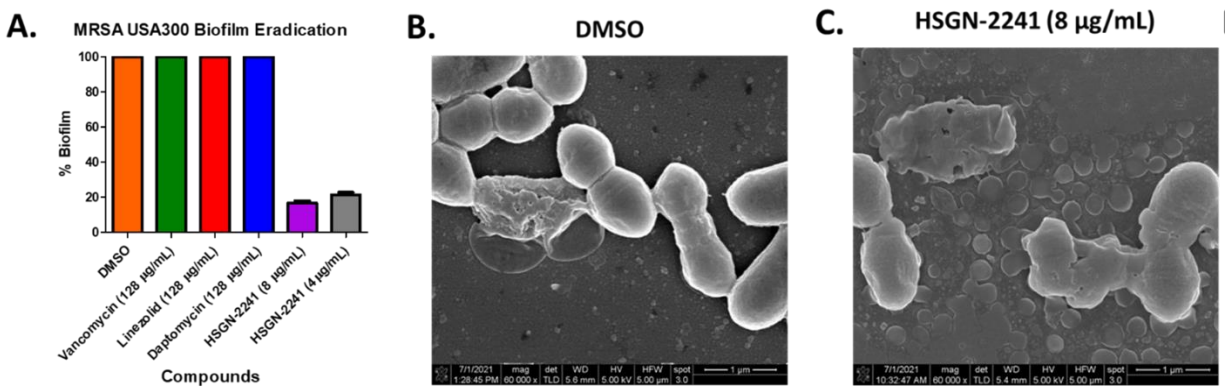

Figure 10.6 Biofilm eradication activity of HSGN-2241. (A) Percent MRSA USA300 biofilm after treatment with vancomycin (128 µg/mL), daptomycin (128 µg/mL), linezolid (128 µg/mL), and HSGN-2241 (8 µg/mL and 4 µg/mL) for 24 hours. Percent biofilm was determined from absorbance at 595 nm. (B) SEM of MRSA USA300 biofilms treated with 1% DMSO (control). (C) SEM of MRSA USA300 biofilms treated with 8 µg/mL HSGN-2241. SEM images are at 60,000× magnification. Images were captured using the FEI Nova Nano-SEM instrument.

10.4.7 HSGN-2241 downregulates expression of important biofilm related genes:

S. aureus expresses microbial surface components recognizing adhesive matrix molecules (MSCRAMMs) which are important for the initial attachment to indigenous tissues and biomaterials[422]. Likewise, the polysaccharide intercellular adhesin (PIA) is the primary adhesin responsible for accumulation and stimulates adhesive interactions between bacterial cells[423]. MSCRAMMs and PIA are essential for biofilm formation in *S. aureus*. Therefore, since HSGN-2241 eradicated biofilm formation, we wondered if it would influence genes (*eno*, *ebps*, *fib*, *cna*) encoding MSCRAMMs as well as genes (*icaA* and *icaD*) encoding PIA. To evaluate this, we treated the pre-formed MRSA USA300 biofilm with 8 µg/mL of HSGN-2241 for 2 hours. Then, we performed real-time RT-qPCR analysis for *eno*, *ebps*, *fib*, *cna*, *icaD*, and *icaA* (Figure 10.7). Interestingly, we discovered that HSGN-2241 significantly downregulated the expression of proteins that are important for biofilm formation. For instance, HSGN-2241 downregulated *eno*, *fib*, *icaD*, and *icaA* (Figure 10.7). On the other hand, HSGN-2241 treatment resulted in upregulation of *ebps*, and had no effect on the expression of *cna* (Figure 10.7).

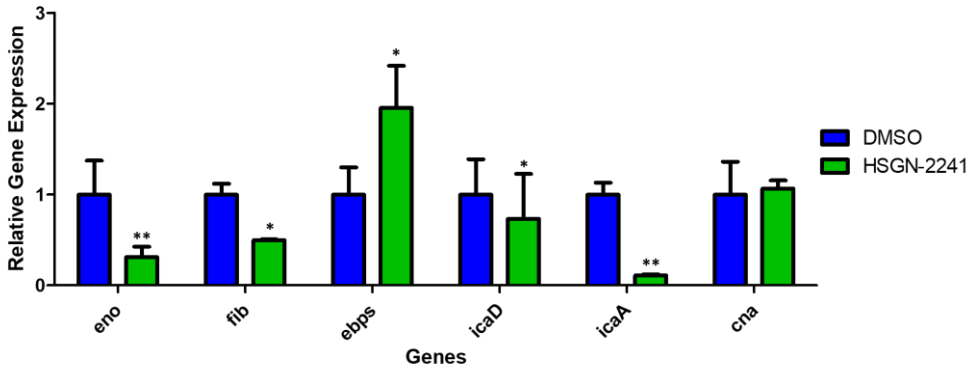

Figure 10.7 The effect of HSGN-2241 treatment on the transcription of genes (*eno*, *ebps*, *fib*, *cna*, *icaA*, and *icaD*), that are important for MRSA biofilm formation. All experiments were performed in triplicates and normalized with *rpoB*. Error bars represent sample standard-deviation. Statistically significant differences between DMSO-treatment and HSGN-2241-treatment were determined by Student's *t*-test analysis (unpaired, two-tailed) and is represented as $*p \leq 0.05$ or $**p \leq 0.01$.

10.4.8 HSGN-2241 does not develop resistance to MRSA

Development of rapid resistance remains a challenge in clinical settings. For instance, antibiotics like ciprofloxacin are not successful at treating MRSA infections because of resistance development[424-425]. To assess MRSA USA300's ability to form resistance to HSGN-2241, we performed the multi-step resistance selection assay. Advantageously, the MIC of HSGN-2241 remained unchanged over thirty passages, keeping up with front-line therapeutics like linezolid and vancomycin (Figure 10.8). Thus, these results suggest that MRSA is doubtful to form rapid resistance to HSGN-2241. However, MRSA did form rapid resistance to ciprofloxacin after the eighth passage (four-fold increase in MIC) which increased to thirty-two-fold by the sixteenth passage.

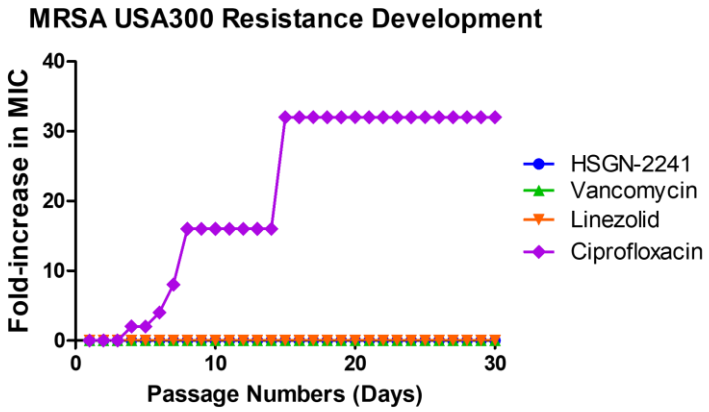

Figure 10.8 Multi-step resistance selection of HSGN-2241, vancomycin, linezolid, and ciprofloxacin against MRSA. MRSA USA300 was serially passaged daily over a 30-day period and the broth microdilution assay was used to determine the MICs of HSGN-2241, vancomycin, linezolid, and ciprofloxacin (control antibiotics) against MRSA after each successive passage. A four-fold shift in the MIC would be indicative of bacterial resistance against the compound.

10.4.9 HSGN-2241 causes depolarization of bacterial membranes and triggers potassium ion release

The bacterial membrane is considered vital for bacteria because it encompasses one third of the proteins in the cell and is the location for vital processes like active transport of nutrients and wastes, respiration, and the development of the proton motive force[395]. Moreover, the bacterial cell membrane contains an electrical potential difference which acts as a source of free energy[396], which allows the bacteria to undergo essential functions like regulation of pH homeostasis[397-398], membrane transport[399], motility[400], antibiotic resistance[401], cell division[402], and environmental sensing[403]. Additionally, disruption of the membrane integrity caused by membrane-targeting agents, can lead to leakage of cytosolic content and harmful pleiotropic effects, eventually causing cell death[394].

Thus, we investigated HSGN-2241's effects on *S. aureus*' cell membrane. First, we assessed HSGN-2241's ability to cause bacterial membrane depolarization or permeabilization. The fluorometric dyes DiSC3(5) and Sytox green were used for membrane depolarization and permeability, respectively. Daptomycin at 5 µg/mL was used as the positive control for the membrane depolarization experiment since it is a known depolarizer of *S. aureus* membranes[405]. Bithionol at 4 µg/mL was used the positive control for the membrane permeability assay since it has been shown to affect membrane integrity [69]. We discovered that HSGN-2241 showed potent

depolarization at 0.25 µg/mL (1× MIC), 1.25 µg/mL (5× MIC), and 2.5 µg/mL (10× MIC) (Figure 10.9A). Additionally, HSGN-2241 did not cause membrane permeability as its fluorescence was comparative to that of the negative control (1% DMSO) (Figure D.1).

Because HSGN-2241 causes depolarization of *S. aureus* membranes and dissipation of membrane potential involves ion movement across the cytoplasmic membrane, we investigated its ability to trigger potassium ion release using the K^+-sensitive fluorescent probe PBFI. HSGN-2241 at both 2.5 µg/mL and 5 µg/mL performed similarly to daptomycin at 5 µg/mL (positive control), triggering potassium ion release from the *S. aureus* membrane (Figure 10.9B).

To further confirm HSGN-2241's potent depolarization activity, we proceeded to use flow cytometry. In this assay, DiOC2 (green dye) served as the membrane-impermeable dye, while To-PRO 3 iodide (red dye) served as the membrane-permeable dye. The positive control for depolarization was daptomycin (5 µg/mL). The ratio of the two dyes (red: green) was assessed and HSGN-2241 displayed an overlying red: green ratio with daptomycin, indicating that HSGN-2241 depolarized *S. aureus* membranes like daptomycin (Figure 10.9C).

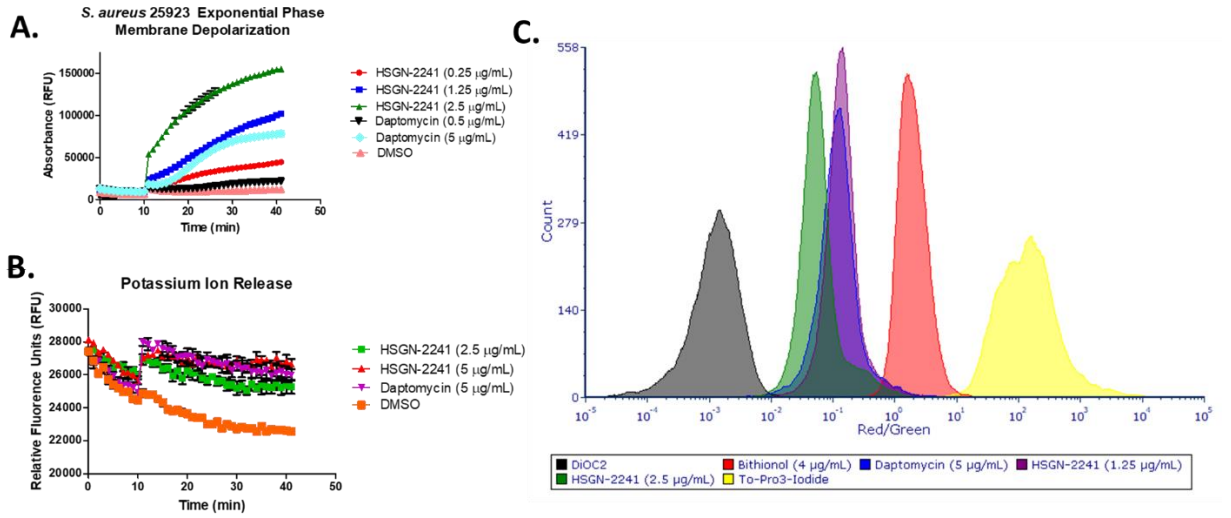

Figure 10.9 Mechanistic studies of HSGN-2241. (A) HSGN-2241 depolarizes *S. aureus* membranes. DiSC3(5) was used as fluorescent probe. (B) HSGN-2241 triggers potassium efflux in *S. aureus*. PBFI was used as the fluorescent probe. (C) Flow cytometry chart demonstrating HSGN-2241 overlaying with daptomycin (5 µg/mL). Charts were constructed using FCS Express software, version 7.0.

10.4.10 Multiple reaction monitoring profiling (MRM-profiling) demonstrates HSGN-2241 effects phospholipids in *S. aureus*

Our initial mechanism of action results indicates that HSGN-2241 is a membrane targeting antibiotic. Yet, to further evaluate HSGN-2241's effects on bacterial membranes, we proceeded to perform multiple reaction monitoring profiling (MRM-Profiling)[189], to differentiate lipid profile differences among *S. aureus* ATCC 25923 treated with either DMSO (control) or HSGN-2241 (2×, 5×, and 10× MIC) for 2 hours. Lipids were extracted and analyzed using electrospray ionization mass spectroscopy (ESI-MS). MRMs were filtered by ion counts and false discovery rate (FDR) adjusted *p*-value in ANOVA, and then analyzed using principal component analysis (PCA). Our experiment focused on comparing differences in glycerophospholipids and free fatty acids in *S. aureus* treated cells. After obtaining this data, PCA scores plots were generated to evaluate HSGN-2241's effects on phosphatidylcholine (PC), phosphatidylglycerol (PG), phosphatidylethanolamine (PE), phosphatidylinositol (PI), and free fatty acids (FFAs). Each point in the PCA plot represents an individual lipid extract sample from staphylococci and the elliptical shaded area is the calculated 95% confidence region for each group. Interestingly, we discovered that HSGN-2241 appears to affect PG (Figure 10.10B), PE (Figure 10.10C), PI (Figure 10.10D) and FFAs (Figure 10.10E), but not PC (Figure 10.10A). Therefore, these results confirm that HSGN-2241 effects the membrane components of *S. aureus*.

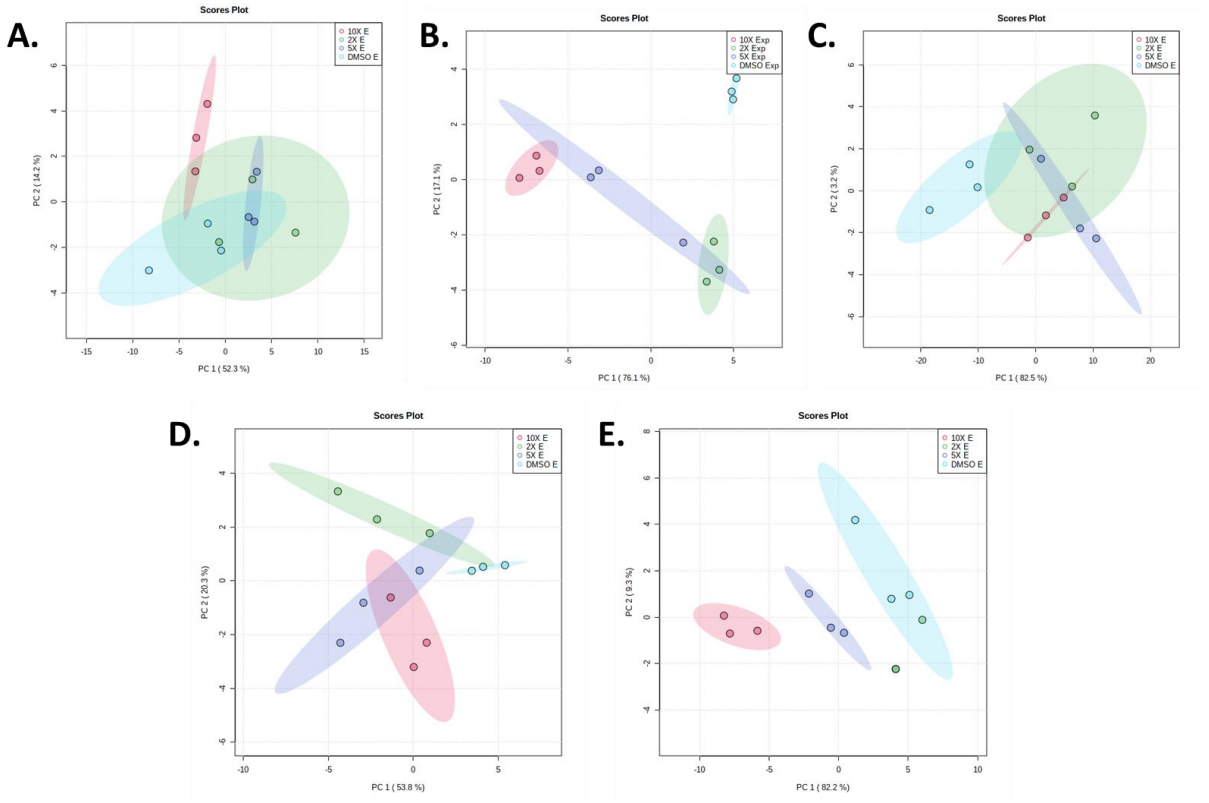

Figure 10.10 PCA scores plots of *S. aureus* treated with either DMSO (control), or HSGN-2241 (2×, 5×, and 10× MIC). (A) Effects on PC synthesis. (B) Effects on PG synthesis. (C) Effects on PE synthesis. (D) Effects on PEI synthesis. (E) Effects on free fatty acids.

10.5 Conclusion:

In conclusion, a systematic halogenation study of *N*-(1,3,4-oxadiazol-2-yl)benzamides led to the identification of HSGN-2241 as a highly potent inhibitor of MRSA growth. HSGN-2241 displayed MICs between 0.125 µg/mL to 1 µg/mL against MRSA clinical isolates and does not form resistance to MRSA. Additionally, HSGN-2241 displayed rapid bactericidal activity against MRSA and eradicates MRSA pre-formed biofilm. In addition, HSGN-2241 showed downregulation of important biofilm related genes such as *eno*, *ebps*, *icaA*, and *icaD*. Furthermore, HSGN-2241 displayed no toxicity to mammalian cells and does not lyse human RBCs. The mechanistic investigation studies of HSGN-2241 on *S. aureus* revealed that the compound depolarizes *S. aureus* membranes causing potassium ion release. Likewise, MRM of lipids in *S. aureus* confirms HSGN-2241 is membrane acting and affects phospholipids and free fatty acid synthesis in *S. aureus*.

10.6 Author Contributions:

G. Naclerio synthesized all analogs in study. G. Naclerio performed MIC assays, time-kill, biofilm eradication assay, multi-step resistance selection, hemolysis assay, membrane permeability, depolarization, and potassium ion release assays, flow cytometry, RT-qPCR, and lipidomics analysis. N. Abutaleb performed cytotoxicity assay. K. Onyedibe performed SEM of biofilm. G. Naclerio and H. Sintim wrote the manuscript.

APPENDIX A. CHAPTER 4 SUPPORTING INFORMATION

I. Chemistry:

i. Synthetic Schemes:

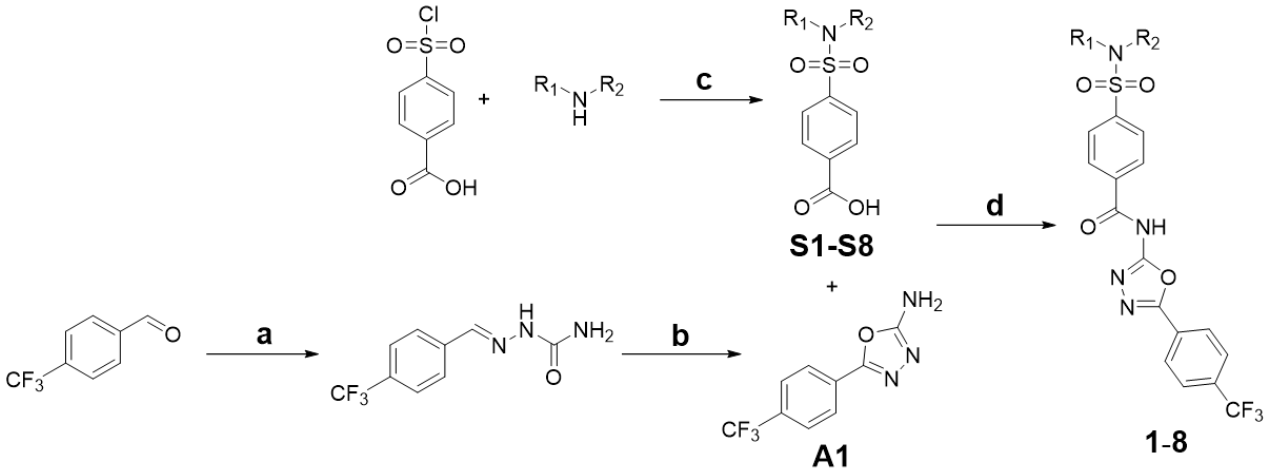

Scheme A.1. General Route for the Synthesis of Analogs 1-8[a]

[a]Reagents and Conditions: (a) Semicarbazide hydrochloride, NaOAc, MeOH/H_2O (1:1), rt, 30 min, 95% (b) Bromine, NaOAc, AcOH, 60 °C, 1 h, 40–70% (c) amine, MeOH, rt, 12 h, 50-60% (d) BOP reagent, DIPEA, DMF, rt, 12 h, 14–30%.

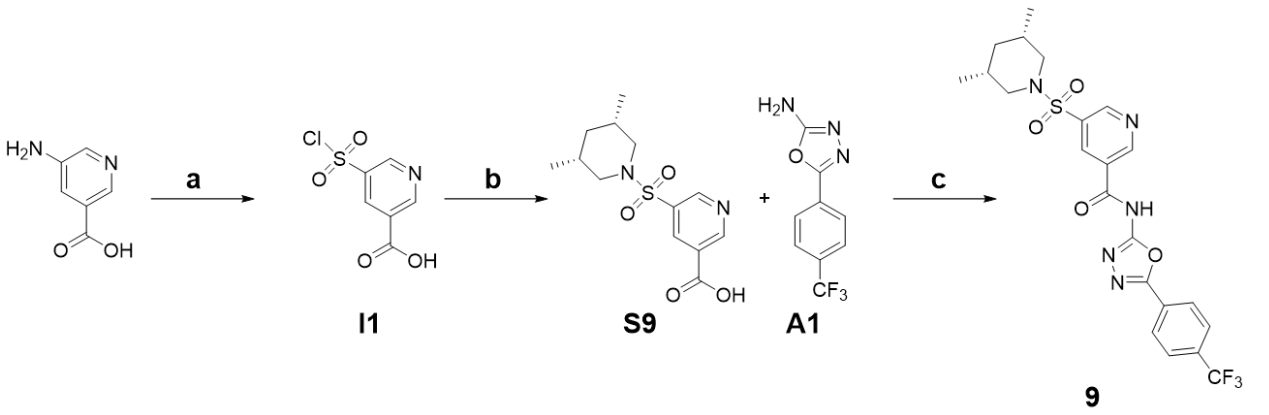

Scheme A.2. General Route for the Synthesis of Analog 9[a]

[a]Reagents and Conditions: (a) i.) $SOCl_2$, H_2O; ii.) $NaNO_2$, HCl, $CuCl_2$, 0°C, 1 h 87% (b) 3,5-dimethylpiperidine, MeOH, rt, 12 h, 53% (c) BOP reagent, DIPEA, DMF, rt, 12 h, 22%.

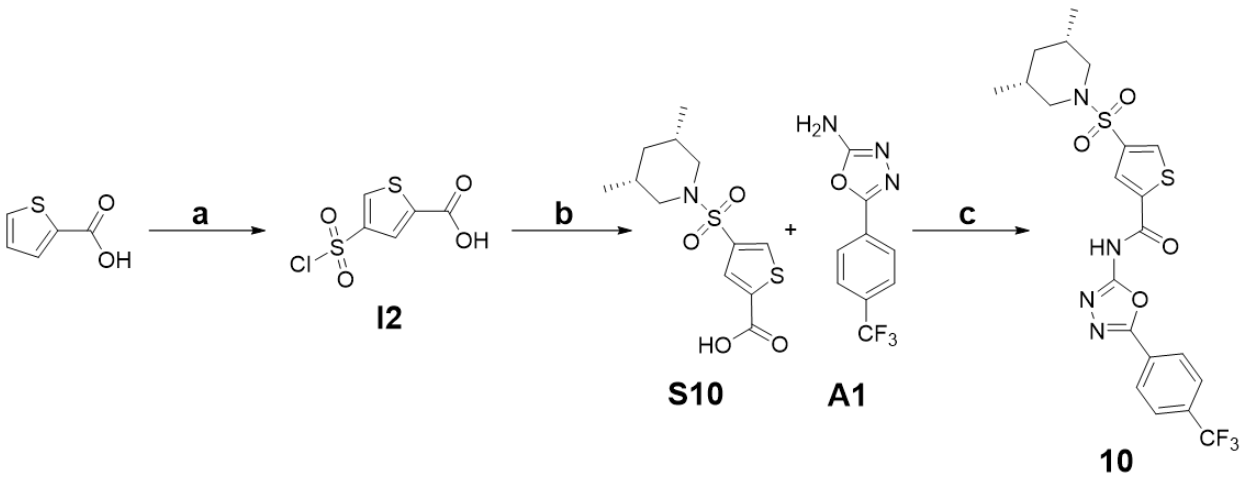

Scheme A.3. General Route for the Synthesis of Analog 10[a]

[a]Reagents and Conditions: (a) HSO_3Cl, rt, 24 h, 69% (b) 3,5-dimethylpiperidine, MeOH, rt, 12 h, 57% (c) BOP reagent, DIPEA, DMF, rt, 12 h, 18%.

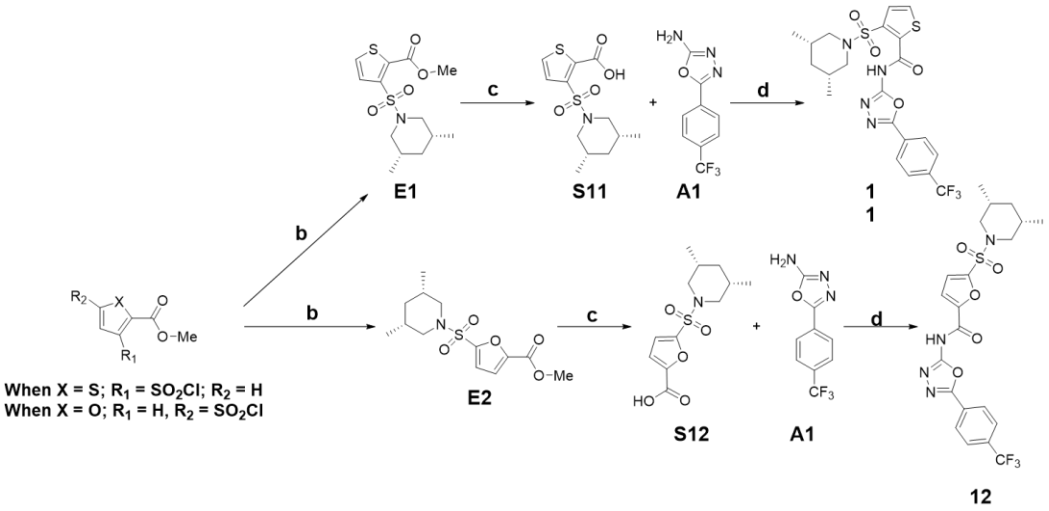

Scheme A.4. General Route for the Synthesis of Analogs 11 and 12[a]

[a]Reagents and Conditions: (a) 3,5-dimethylpiperidine, MeOH, rt, 12 h, 51-55% (b) LiOH, MeOH:H_2O (2:1), rt, 12 h, 59-60% (c) BOP reagent, DIPEA, DMF, rt, 12 h, 15-19%.

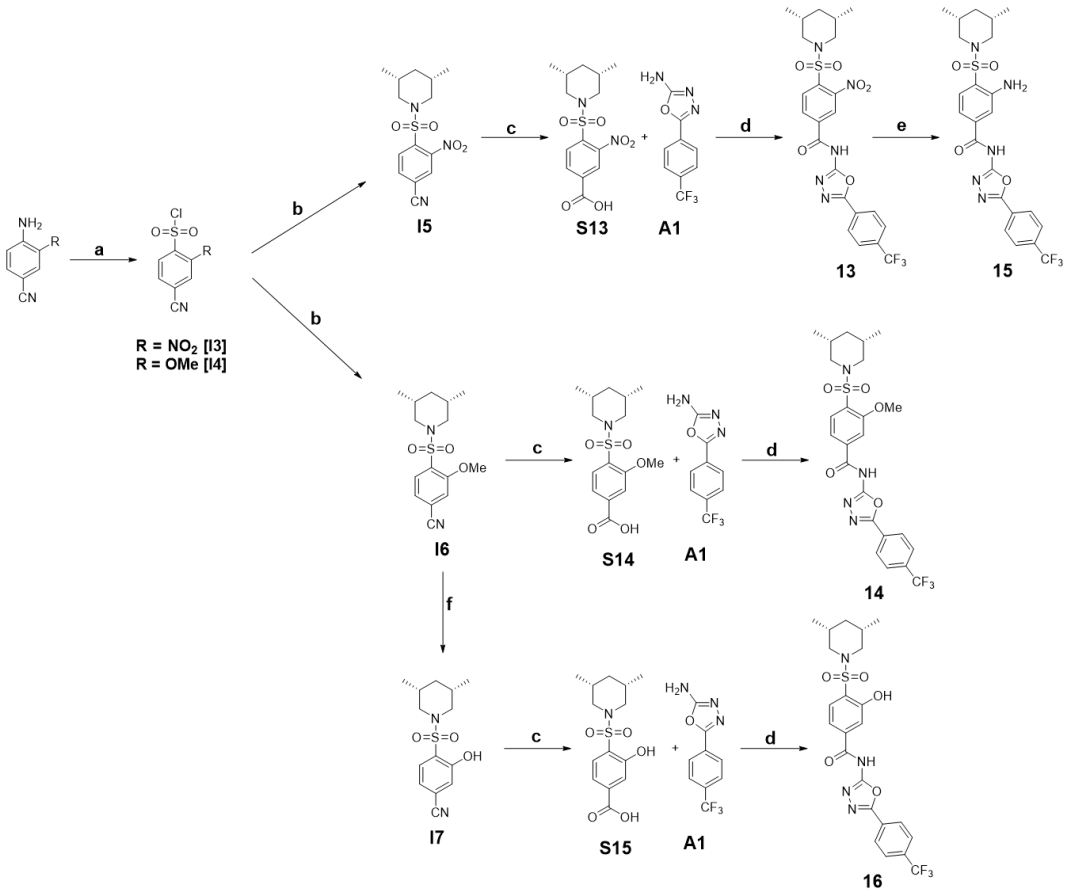

Scheme A.5. General Route for the Synthesis of Analogs 13-16[a]

[a]Reagents and Conditions: (a) i.) $SOCl_2$, H_2O; ii.) $NaNO_2$, HCl, $CuCl_2$, 0°C, 1 h 85-91% (b) 3,5-dimethylpiperidine, MeOH, rt, 12 h, 50-55% (c) 2M NaOH, EtOH, 100°C, 12 h, 52-60% (d) BOP reagent, DIPEA, DMF, rt, 12 h, 31% (e) $Na_2S_2O_4$, DMF:H_2O (9:1), 90°C, 12 h, 73% (f) BBr_3, DCM, rt, 12 h, 61%.

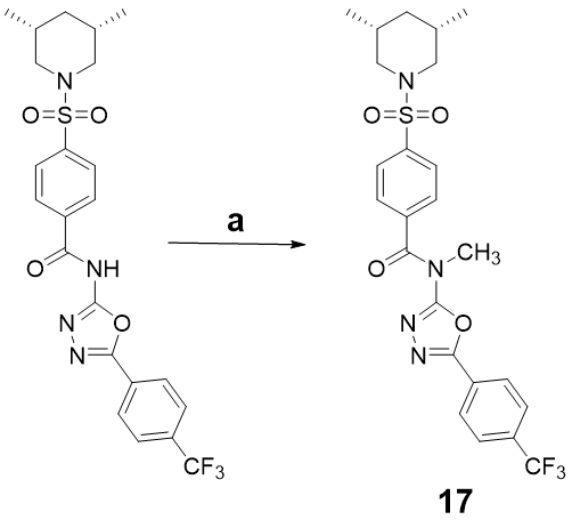

Scheme A.6. General Route for the Synthesis of Analog 17[a]

[a]Reagents and Conditions: (a) MeI, NaH, DMF, rt, 2 h, 57%

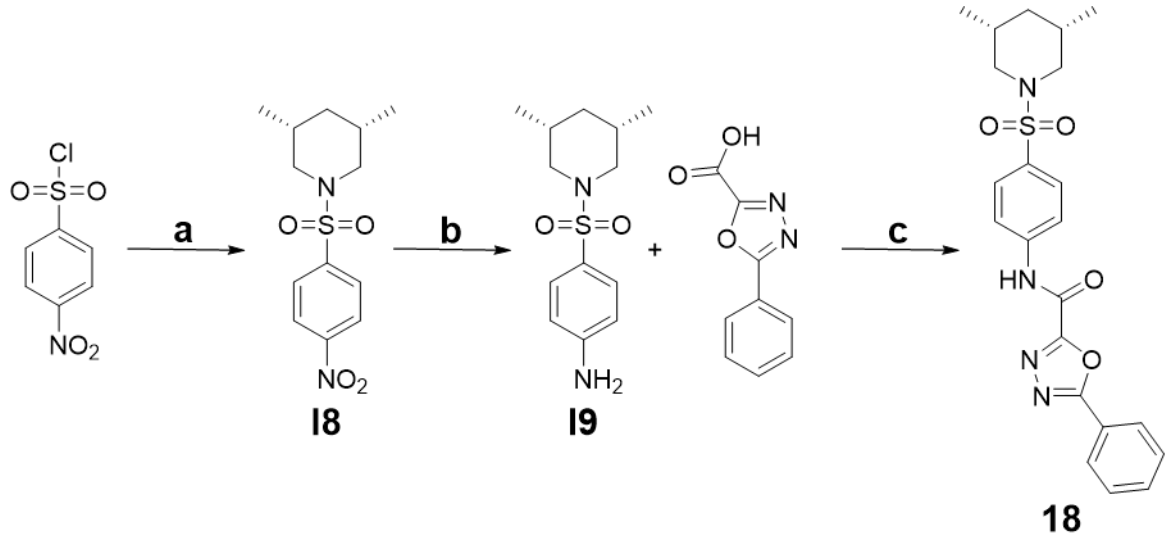

Scheme A.7. General Route for the Synthesis of Analog 18[a]

[a]Reagents and Conditions: (a) 3,5-dimethylpiperidine, MeOH, rt, 12 h, 53% (b) $Na_2S_2O_4$, DMF: H2O (9:1), 90°C, 12 h, 64% (c) BOP reagent, DIPEA, DMF, rt, 12 h, 39%

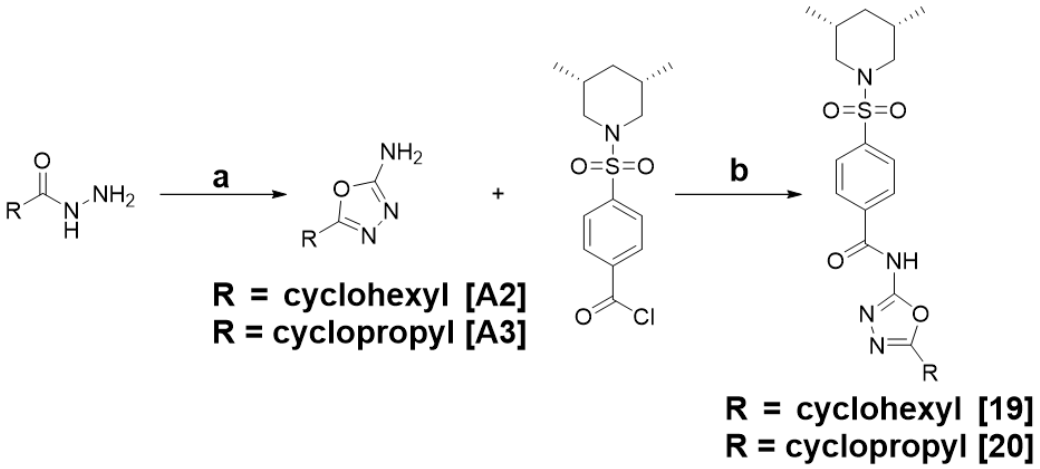

Scheme A.8. General Route for the Synthesis of Analogs 19 and 20[a]

[a]Reagents and Conditions: (a) CNBr, EtOH, 2h, 60°C, 83% (b) *N*-methylimidazole, 1,4-dioxane, 2 h, 90°C, 24-32%

II. Biological Analysis

Table A.1. MICs in µg/mL (µM) of analogs, HSGN-94, vancomycin, and linezolid against *Staphylococcus aureus* ATCC 25923 and methicillin-resistant *Staphylococcus aureus* (MRSA) ATCC 33592

Compound/Control Drug	*S. aureus* ATCC 25923	MRSA ATCC 33592
1	2 (4.2)	2 (4.2)
2	2 (4.3)	2 (4.3)
3	4 (8.8)	4 (8.8)
4	16 (36.3)	16 (36.3)
5	2 (4.1)	2 (4.1)
6	1 (2.0)	1 (2.0)
7	2 (4.0)	2 (4.0)
8	2 (4.0)	2 (4.0)
9	2 (3.9)	2 (3.9)
10	1 (1.9)	1 (1.9)
11	4 (7.8)	4 (7.8)
12	>64 (>128.4)	>64 (>128.4)
13	2 (3.6)	2 (3.6)

14	2 (3.7)	2 (3.7)
15	8 (15.3)	8 (15.3)
16	1 (1.9)	1 (1.9)
17	>64 (>122.5)	>64 (>122.5)
18	>64 (>145.3)	>64 (>145.3)
19	>64 (>143.3)	>64 (>143.3)
20	64 (158.2)	64 (158.2)
HSGN-94	0.25 (0.5)	0.25 (0.5)
Vancomycin	1 (0.7)	1 (0.7)
Linezolid	2 (6.0)	2 (6.0)

Table A.2. MICs in μg/mL (μM) of HSGN-94 against methicillin-sensitive Staphylococcus aureus (MSSA), methicillin-resistant Staphylococcus aureus (MRSA), vancomycin-resistant *Staphylococcus aureus* (VRSA) and *Staphylococcus epidermidis* strains.

Bacterial Strains	HSGN-94	Linezolid	Vancomycin
MSSA ATCC 6538	0.5 (1)	1 (3)	1 (0.7)
MSSA NRS 107	0.25 (0.5)	1 (3)	2 (1.4)
MRSA NRS119	0.5 (1)	32 (96)	2 (1.4)
MRSA NRS123 (USA400)	0.5 (1)	1 (3)	1 (0.7)
MRSA NRS384 (USA300)	0.25 (0.5)	1 (3)	1 (0.7)
MRSA NRS 385 (USA500)	0.5 (1)	2 (6)	1 (0.7)
MRSA NRS 386 (USA700)	0.25 (0.5)	2 (6)	1 (0.7)
VRSA 9	0.25 (0.5)	1 (3)	>64 (>44.8)
VRSA 10	0.5 (1)	2 (6)	>64 (>44.8)
VRSA 12	1 (2)	2 (6)	>64 (>44.8)
S. epidermidis NRS 101	1 (2)	1 (3)	2 (1.4)

Table A.3. MICs in μg/mL (μM) of HSGN-94 against clinically important Gram-positive bacterial pathogens including *Streptococcus pneumoniae*, *Streptococcus pyogenes*, *Enterococcus faecalis*, *Enterococcus faecium*, and *Listeria monocytogenes*

Bacterial Strains	HSGN-94	Linezolid	Vancomycin
Cephalosporin-resistant *Streptococcus pneumoniae* ATCC 51916	0.125 (0.3)	1 (3)	1 (0.7)
Methicillin-resistant *Streptococcus pneumoniae* ATCC 700677	0.06 (0.1)	0.5 (1.5)	1 (0.7)
Streptococcus pyogenes MGAS 1882	0.125 (0.3)	0.5 (1.5)	0.5 (0.4)
Streptococcus pyogenes MGAS 9882	0.25 (0.5)	0.5 (1.5)	0.5 (0.4)
Vancomycin-resistant *Enterococcus faecalis* ATCC 51299	0.25 (0.5)	1 (3)	64 (44.8)
Vancomycin-resistant *Enterococcus faecium* ATCC 700221	0.25 (0.5)	1 (3)	>64 (>44.8)
Listeria monocytogenes ATCC 19111	0.06 (0.1)	1 (3)	1 (0.7)

Table A.4. Functional characterization of proteins downregulated in *S. aureus* after treatment with HSGN-94.

ID	Protein	Classification	Log_2FC	p-value
Virulence				
gi|685631952	Nuc	Thermonuclease	-5.1	0.0010
gi|685633550	LukS-PV	Gamma-hemolysin subunit B	-3.7	0.000026
gi|685631441	EssB	Type VII secretion protein EssB	-3.3	0.024

gi|685631437	EsxA	Type VII secretion protein EsxA	-2.0	0.00063
gi|685631438	EsaA	Type VII secretion protein EsaA	-2.0	0.00011
gi|685631717	SdrD	Hydrolase	-2.0	0.00010
gi|685632604	LukD	Leucotoxin LukD	-2.0	0.013
gi|685633523	NarG	Nitrate reductase subunit alpha	-2.0	0.0021
gi|685631988	LipA	Lipoyl synthase	-2.0	0.000029
Nucleotide metabolism				
gi|685632728	GloB	Hydroxyacylglutathione hydrolase	-2.0	0.000081
gi|685632295	PyrF	Orotidine 5-phosphate decarboxylase	-2.2	0.00010
gi|685632294	CarB	Carbamoyl-phosphate synthase large chain	-2.0	0.000046
Transcription				
gi|685633415	SarR	MarR family transcriptional regulator	-2.0	0.000014
Translation				
gi|685632759	MtaB	30S ribosomal protein S12 methylthiotransferase	-2.0	0.0067
Amino acid biosynthesis				
gi|685633333	Als	Acetolactate synthase	-2.7	0.0031
gi|685633124	DapE	Succinyl-diaminopimelate desuccinylase	-3.3	0.000044
gi|685632550	IlvA	Threonine dehydratase	-2.0	0.0030
Carbohydrate metabolism				
gi|685631305	AdhE	Acetaldehyde dehydrogenase	-2.5	0.0039

Table A.5. Proteins found only in DMSO-treatment Group and Considered Downregulated by HSGN-94 treatment

Protein	Biological process
DNA recombination protein RecF	Homologous recombination
PTS mannose transporter subunit IIABC	Mannose uptake
glycerophosphodiester phosphodiesterase	lipid metabolism

copper-translocating P-type ATPase	copper transport
oxidoreductase	
DNA-binding response regulator	Transcription
molybdenum ABC transporter ATP-binding protein	Molybdate transport
threonine synthase	threonine biosynthesis
nucleoside permease	nucleoside intramembrane transporter
sodium ABC transporter permease	
CDP-diacylglycerol--glycerol-3-phosphate 3-phosphatidyltransferase	Phosphatidylglycerol (PG) synthesis
aureolysin	Virulence factor
carboxylesterase	
type VII secretion protein EsaB	Virulence factor
hydrolase	
signal peptidase II	lipoprotein biosynthesis
peptidase	
sodium ABC transporter ATP-binding protein	sodium transport
MAP domain-containing protein	Virulence factor
protein EssC	Virulence factor
nitrite reductase (NAD(P)H) small subunit	Nitrate assimilation
glutamyl endopeptidase	Virulence factor
50S rRNA methyltransferase	
multifunctional 2,3-cyclic-nucleotide 2-phosphodiesterase/5-nucleotidase/3-nucleotidase	Nucleotide catabolism
site-specific integrase	
holo-ACP synthase	Pantothenate and CoA biosynthesis
uroporphyrinogen-III C-methyltransferase	Porphyrin and chlorophyll metabolism
peptide ABC transporter permease	
orthopoxovirus protein, PF05708 family	hydolase

Table A.6. Proteins identified from Pull-Down Assay with HSGNbeads group

Protein Name	Gene	General Function
tRNA-2-methylthio-*N*(6)-dimethylallyladenosine synthase	miaB	Protein Synthesis
Isocitrate dehydrogenase	idh	Cellular Respiration
50S ribosomal protein L4	rplD	Protein Synthesis
Adenylate kinase	adk	Nucleotide Synthesis
Ribose-5-phosphate isomerase	rpiA	DNA and RNA Synthesis
Transglycosylase	IsaA	Cell-wall Synthesis
S-ribosylhomocysteine lyase	luxS	Quorum Sensing
Nicotinate phosphoribosyltransferase	pncB	NAD Synthesis
RNA polymerase σ factor	SigA	RNA Synthesis
Phosphoglucomutase	PgcA	LTA Biosynthesis
Sucrose-6-phosphate hydrolase	scrB	Sucrose Synthesis
Coproporphyrin III ferrochelatase	cpfC	Heme Biosynthesis
Phenylalanine--tRNA ligase subunit β	PheT	Protein Synthesis
50S ribosomal protein L10	rplJ	Protein Synthesis
Glutamine amidotransferase /GMP synthase	guaA	Nucleotide Synthesis
Xanthine phosphoribosyltransferase	Xpt	DNA and RNA Synthesis
tRNA (uracil-5-)-methyltransferase	trmFO	Protein Synthesis
DNA recombination/repair protein RecA	RecA	DNA Synthesis

Table A.7. Bacterial isolates used in this study

Bacterial isolates	**Isolation**	**Description**
Staphylococcus aureus ATCC 25923	Clinical isolate	Quality control strain for media testing and water testing.
Staphylococcus aureus ATCC 33592	Blood	Used in drug discovery and emerging infectious disease research. Gentamicin-resistant.

		Methicillin-resistant.
Staphylococcus aureus ATCC 6538	Human lesion	Quality control strain for media testing, food testing, drug discovery and water testing.
Staphylococcus aureus NRS 107	human skin, Connecticut, USA, 1991.	Resistant to mupirocin, rifampicin and novobiocin.
MRSA NRS 119	Isolated from a patient with peritonitis, Massachusetts, USA, 2001.	Linezolid, tedizolid and methicillin -resistant
MRSA NRS123 (USA400)	Human abscess, Michigan, 2004.	Community-associated MRSA strain.
MRSA NRS384 (USA300)	Wound, Mississippi, USA	Community-acquired MRSA strain. Resistant to erythromycin and tetracycline.
MRSA NRS 385 (USA500)	From a patient with bloodstream infection, Connecticut, USA.	Hospital-acquired MRSA strain. Resistant to erythromycin, clindamycin, levofloxacin, gentamicin, tetracycline and trimethoprim/sulfamethoxazole.
MRSA NRS 386 (USA700)	From a patient with bloodstream infection, Louisiana, USA.	Associated with infections in both community and healthcare settings. Resistant to erythromycin.
VRSA 9	Left plantar foot wound, Michigan, USA, 2007	Resistant to vancomycin, erythromycin and spectinomycin
VRSA 10	Plantar foot wound, Michigan, USA, 2009.	Resistant to vancomycin, erythromycin and spectinomycin.

VRSA 12	Isolated from a foot wound	Vancomycin-resistant, positive for *vanA*
Staphylococcus epidermidis NRS101	From septicemic patient with colonized intravascular catheters, Tennessee, USA	Resistant to methicillin, erythromycin, kanamycin, gentamicin, clindamycin and trimethoprim.
Streptococcus pneumoniae ATCC 51916	Cerebrospinal fluid, Tennessee, USA.	Cephalosporin-resistant. Representative strain of the Pneumococcal Molecular Epidemiology Network.
Streptococcus pneumoniae ATCC 700677	Human patient, Czechoslovakia, 1987	Resistant to methicillin, erythromycin, penicillin, and tetracycline.
Streptococcus pyogenes MGAS 1882	From a patient with post-streptococcal glomerulonephritis, USA, 1970s.	Serotype M59 Susceptible to penicillin
Streptococcus pyogenes MGAS 9882	From a patient wth with a soft tissue infection, Ontario, Canada, 2000.	Serotype M3
Enterococcus faecalis ATCC 51299	Peritoneal fluid, Missouri, USA.	Resistant to vancomycin. Sensitive to Teicoplanin. Positive for *vanB*
Enterococcus faecium ATCC 700221	Human feces, Connecticut	Resistant to Vancomycin and Teicoplanin. Positive for *vanA*
Listeria monocytogenes ATCC 19111	Poultry, England	Control strain for media testing, enteric research and food testing.

Table A.8. Sequence of primers used in RT-PCR.

Primer Name	Sequence (5'- 3')	Source
pgsA Forward	ATTGGCTTCCCTTAGCGATT	This Study
pgsA reverse	AGAATTGGTTAGTCCTAGTTGCAC	This Study
16S Forward	CGGTCCAGACTCCTACGGGAGGCAGCA	Opoku-Temeng et al.[217]
16S Reverse	GCGTGGACTACCAGGGTATCTAATCC	Opoku-Temeng et al[217].

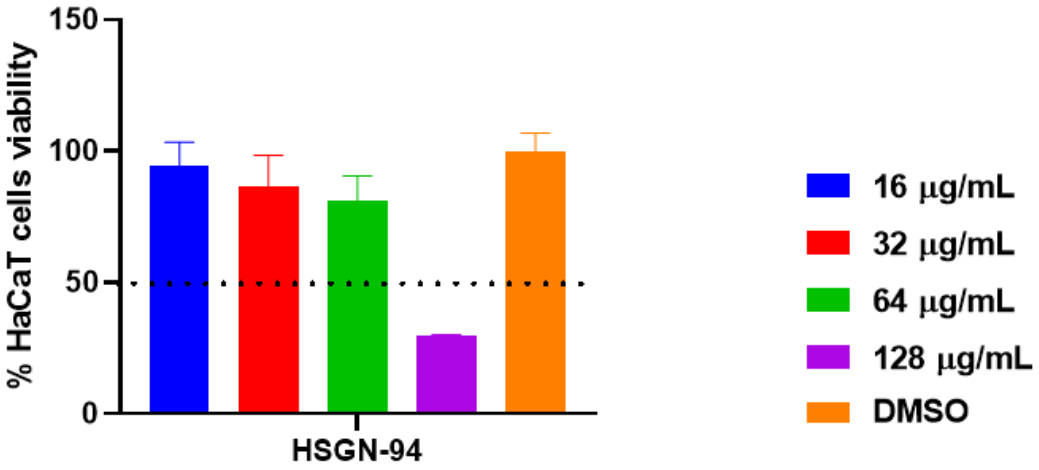

Figure A.1. Analyzing the toxicity of HSGN-94 (tested in sextuplicate at 16, 32, 64 and 128 µg/mL) against human keratinocyte cells (HaCaT) using the MTS; 3-(4,5-dimethylthiazol-2-yl)-5-(3-carboxymethoxyphenyl)-2-(4-sulfophenyl)-2H-tetrazolium) assay. Results are presented as percent viable cells relative to DMSO (negative control to determine a baseline measure for the cytotoxic impact of each compound). The absorbance values represent an average of six samples analyzed for each compound. Error bars represent standard deviation values. Data were analyzed via a one-way ANOVA with post hoc Dunnett's test for multiple comparisons. Asterisks (*) denote a statistical difference ($P<0.05$) between values obtained for the compounds as compared to DMSO.

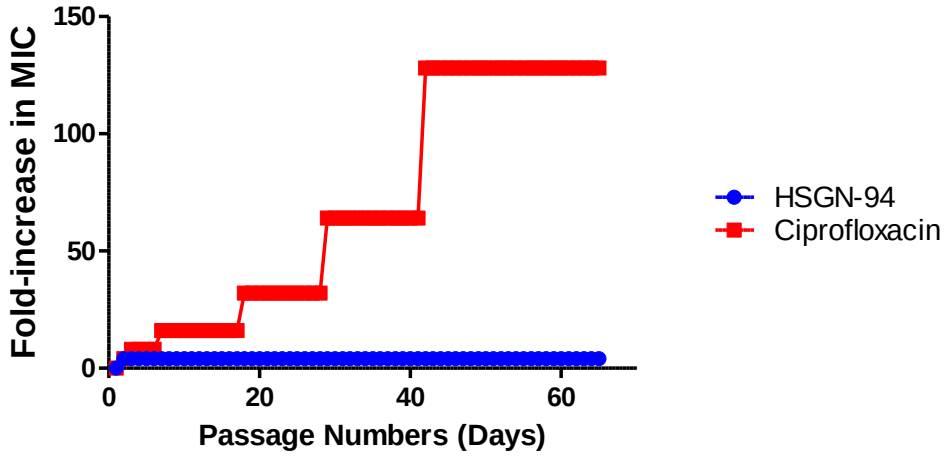

Figure A.2. Multi-step resistance selection of HSGN-94 and ciprofloxacin against MRSA. MRSA USA300 was serially passaged daily over a 65-day period and the broth microdilution assay was used to determine the minimum inhibitory concentration of compounds and control antibiotics against MRSA after each successive passage. An eight-fold shift in MIC would be indicative of bacterial resistance.

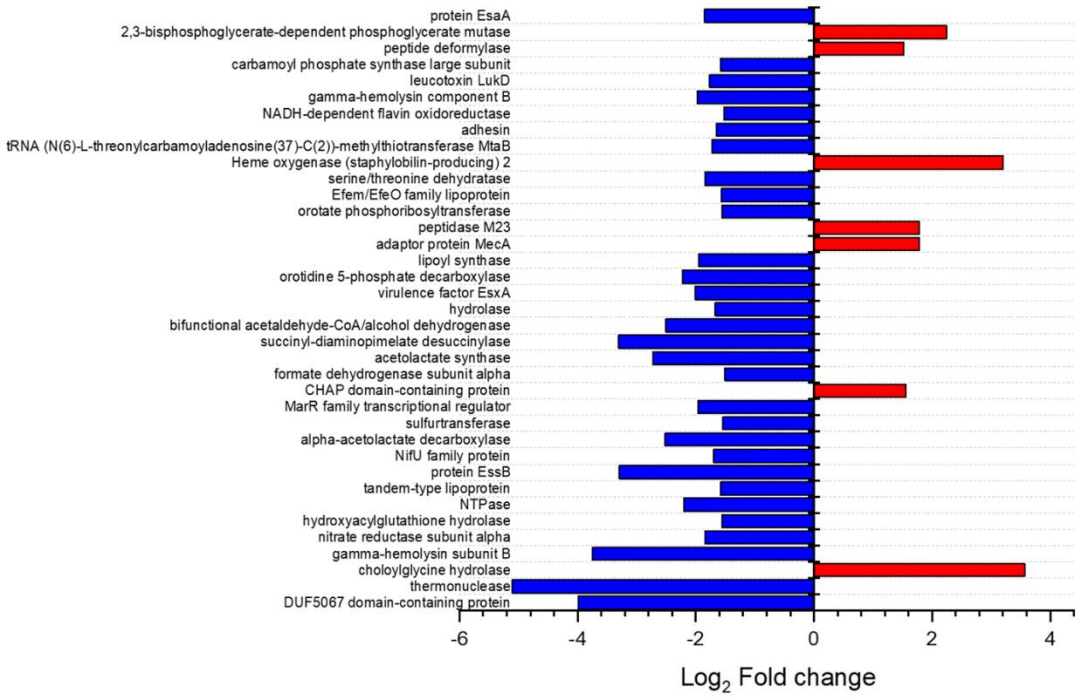

Figure A.3. Bar chart representation of downregulated (blue) and upregulated (red) proteins after *S. aureus* treatment with HSGN-94.

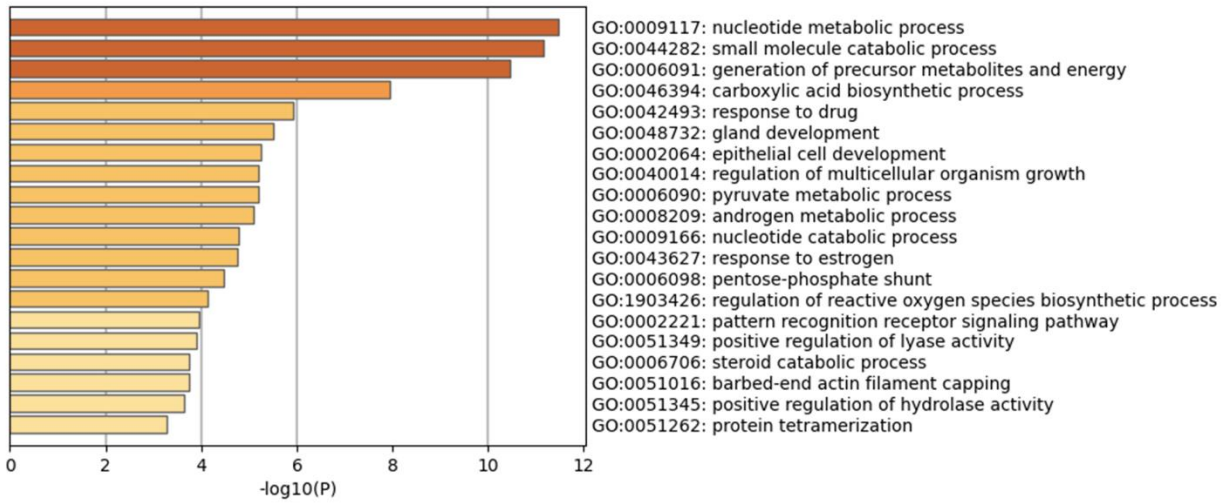

Figure A.4. GO function analysis of significant ($p \leq 0.05$) proteins in *S. aureus* treated with HSGN-94. Analysis was done using Metascape™ software.

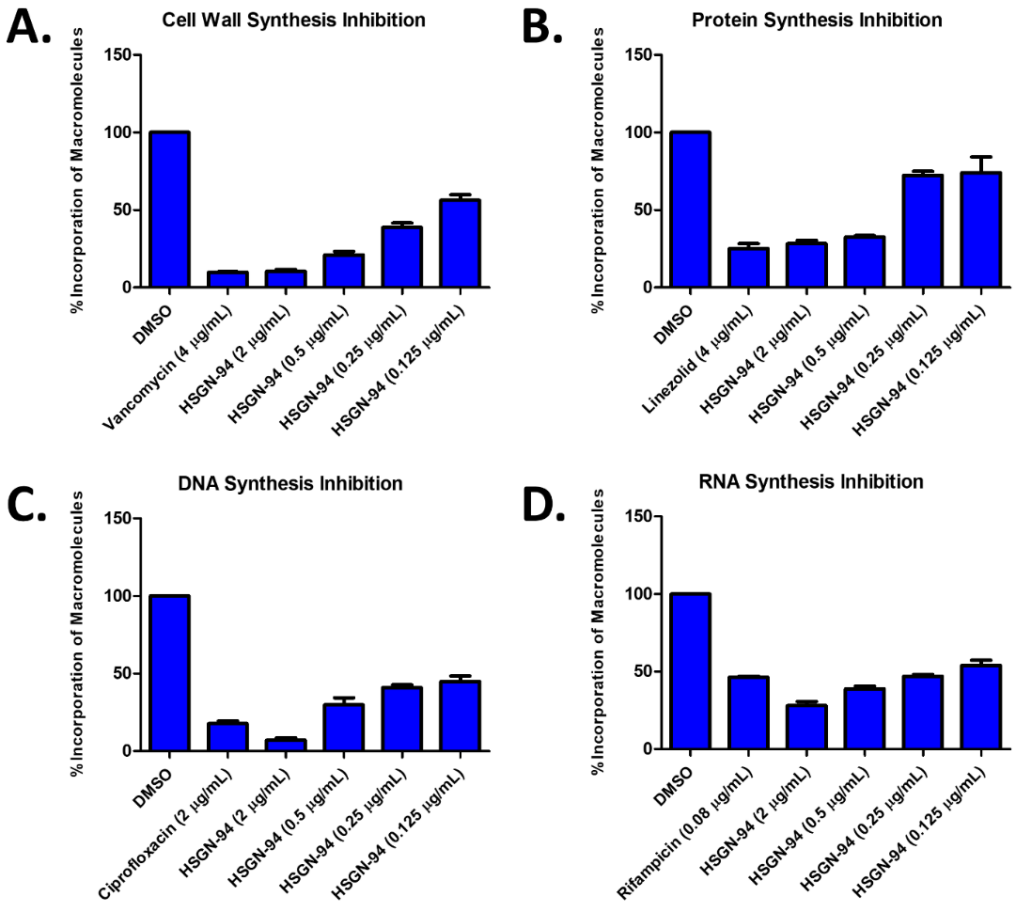

Figure A.5. Effects of HSGN-94 on macromolecular biosynthesis in *S. aureus*. Effects of HSGN-94 at 0.125X to 4X MIC (0.125–2 μg/mL) on relative incorporation of (A) [glucosamine-6-3*H*]-

N-acetyl-d-glucosamine for cell wall synthesis, (B) L-leucine [4,5-3*H*] for protein synthesis. (C) [methyl-]-thymidine for DNA synthesis, and (D) [5-3*H*]-uridine for RNA synthesis. HSGN-94 and control antibiotics were examined by scintillation counting. Experiments were performed in triplicates, and each bar represents the mean ± SD.

III. MALDI Mass Spectra for Glycolipid TLC Samples:

DMSO:

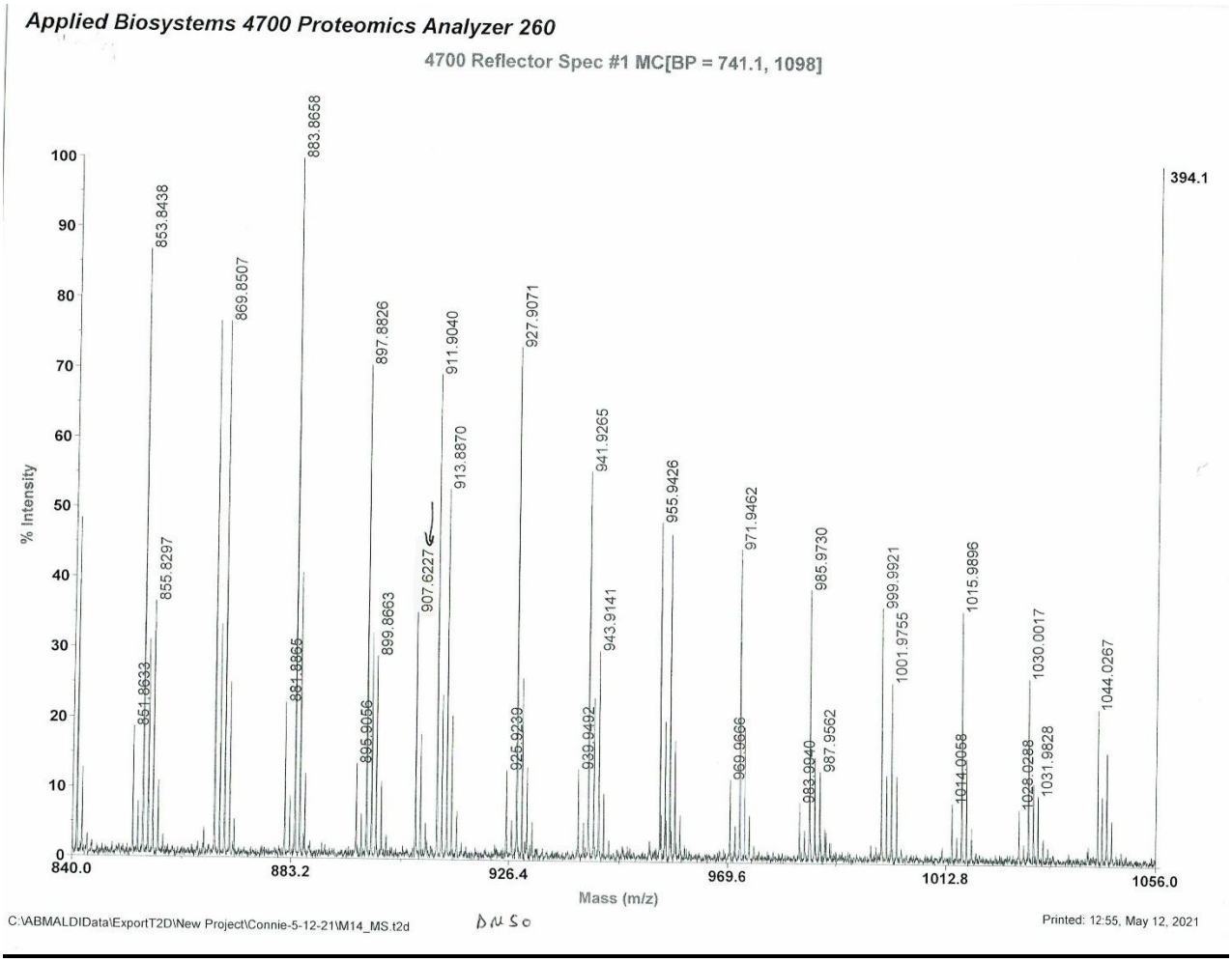

HSGN-94 1/4X MIC:

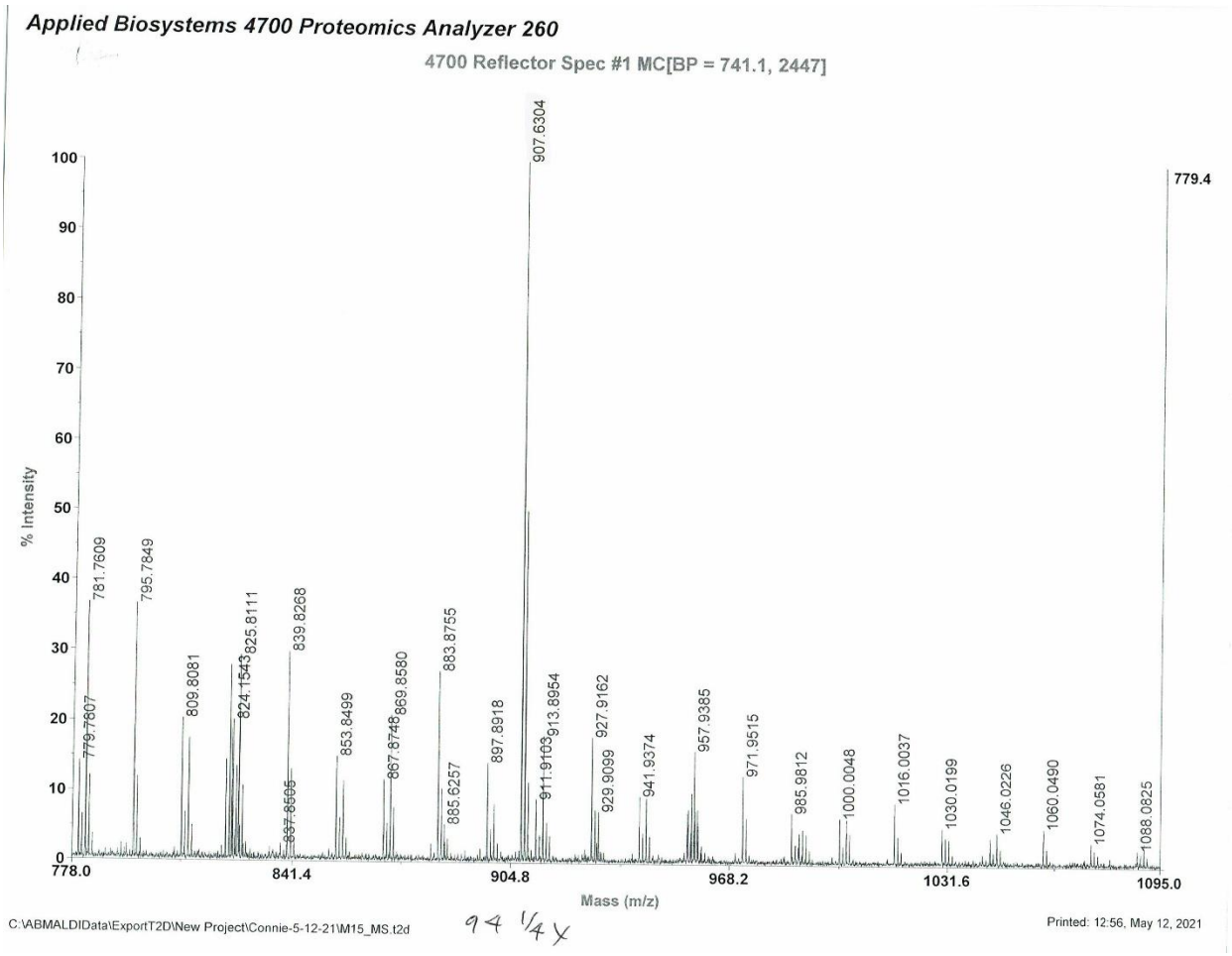

HSGN-94 1X MIC:

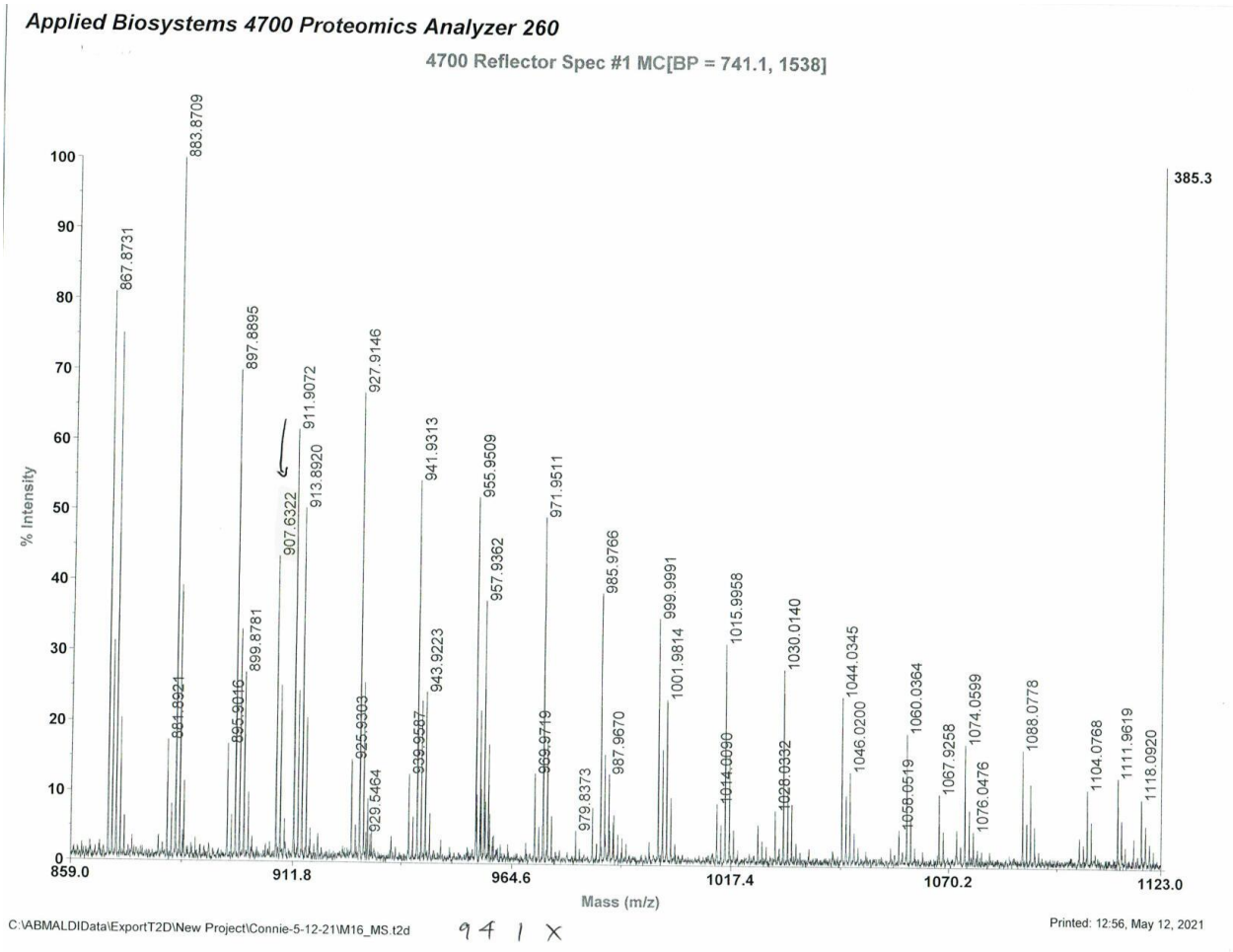

HSGN-94 8X MIC:

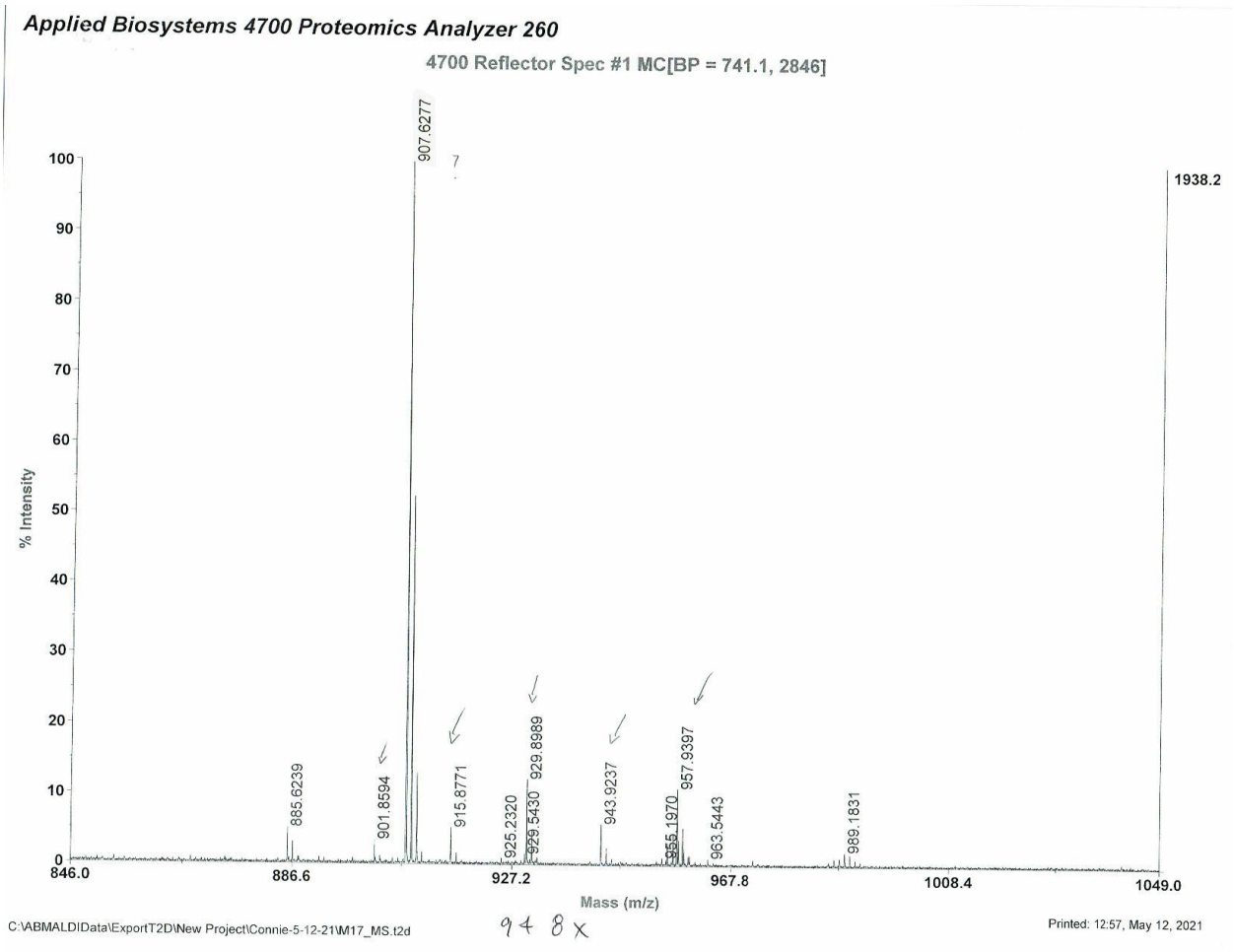

IV. ^{1}H, ^{13}C, and ^{19}F NMR Spectra for Intermediates and Analogs:

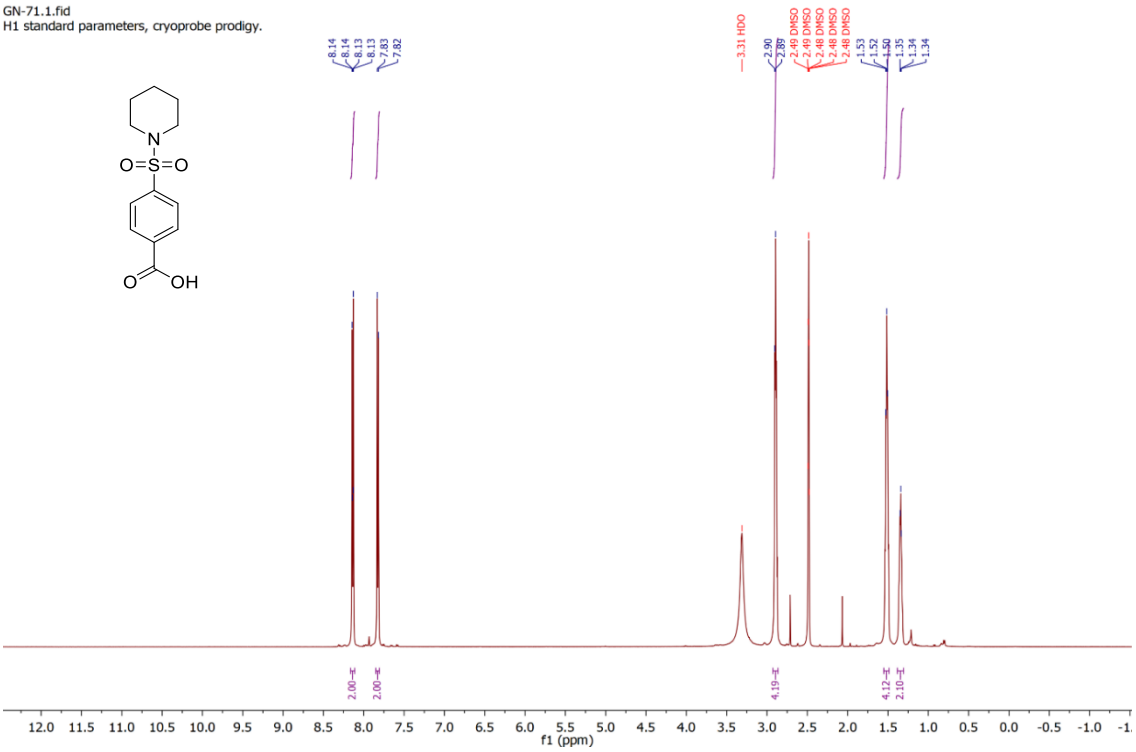

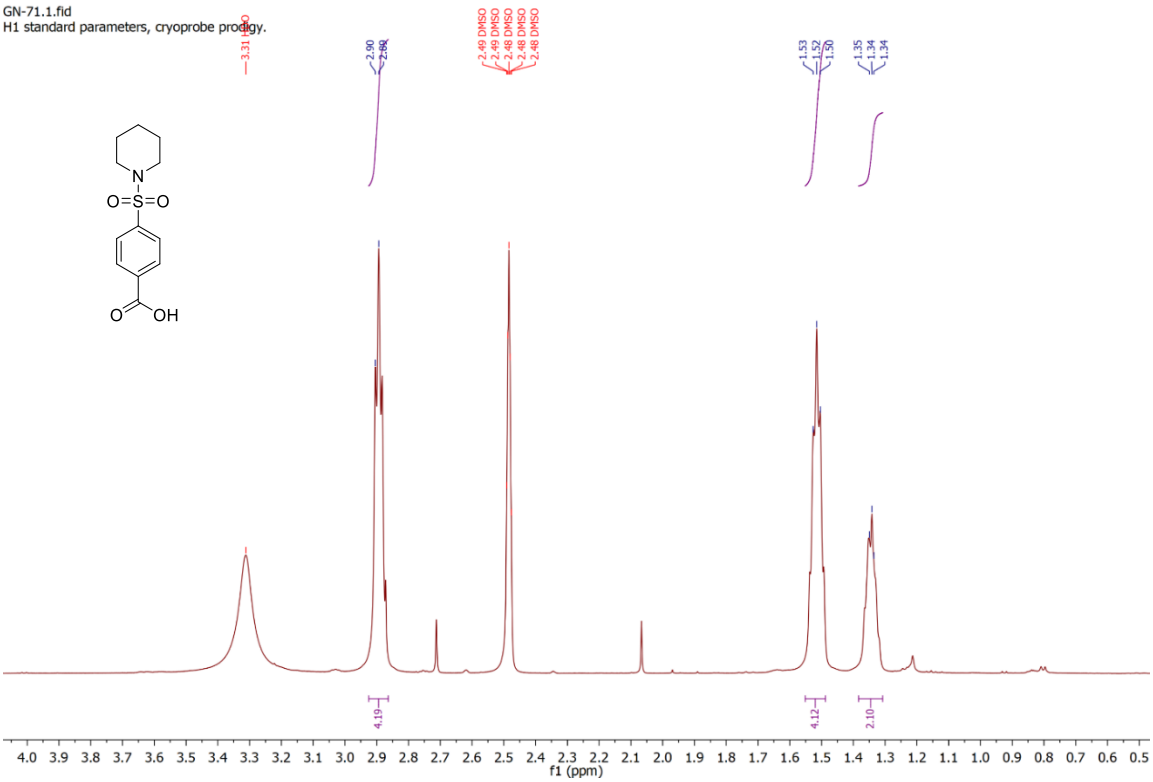

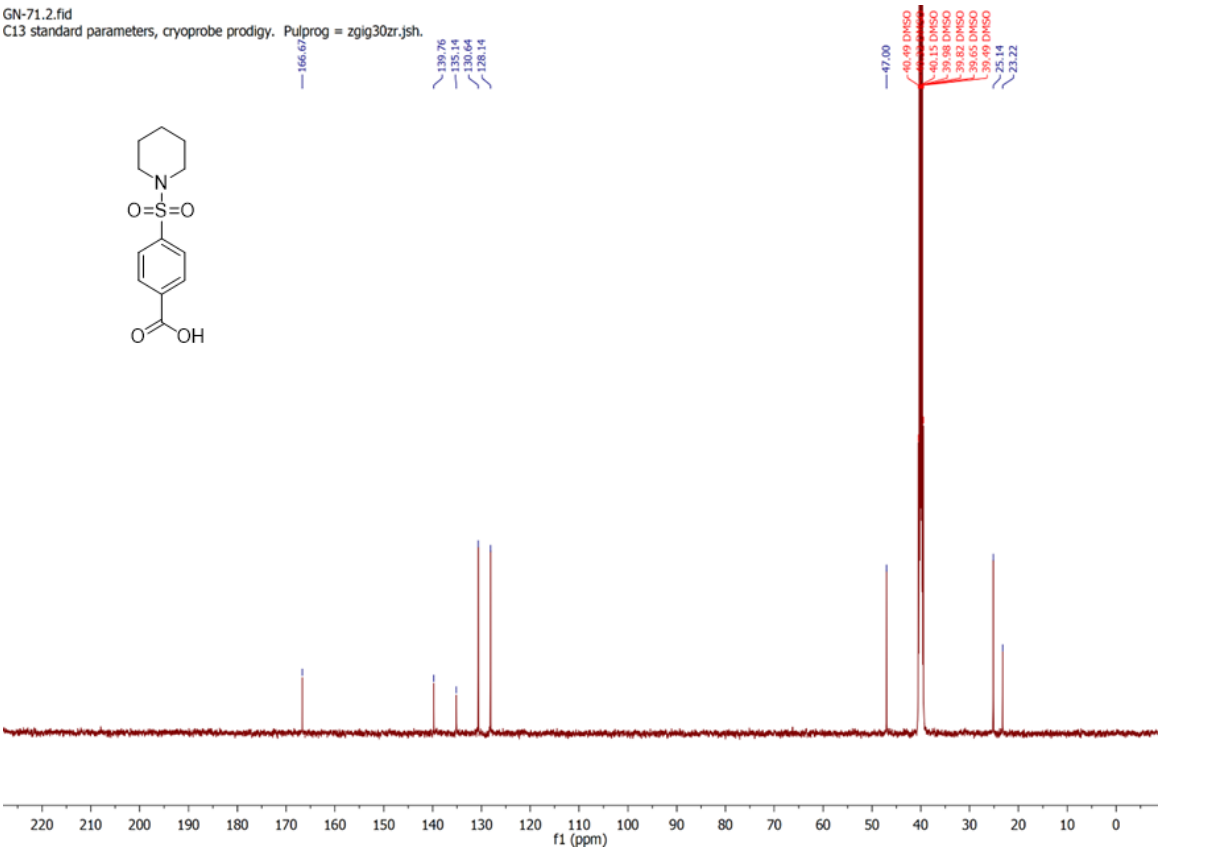
GN-71.2.fid
C13 standard parameters, cryoprobe prodigy. Pulprog = zgig30zr.jsh.
166.67
139.76
135.54
130.64
128.14
47.00
40.49 DMSO
40.32 DMSO
40.15 DMSO
39.98 DMSO
39.82 DMSO
39.65 DMSO
39.49 DMSO
25.14
23.22
N
O=S=O
O
OH
f1 (ppm)

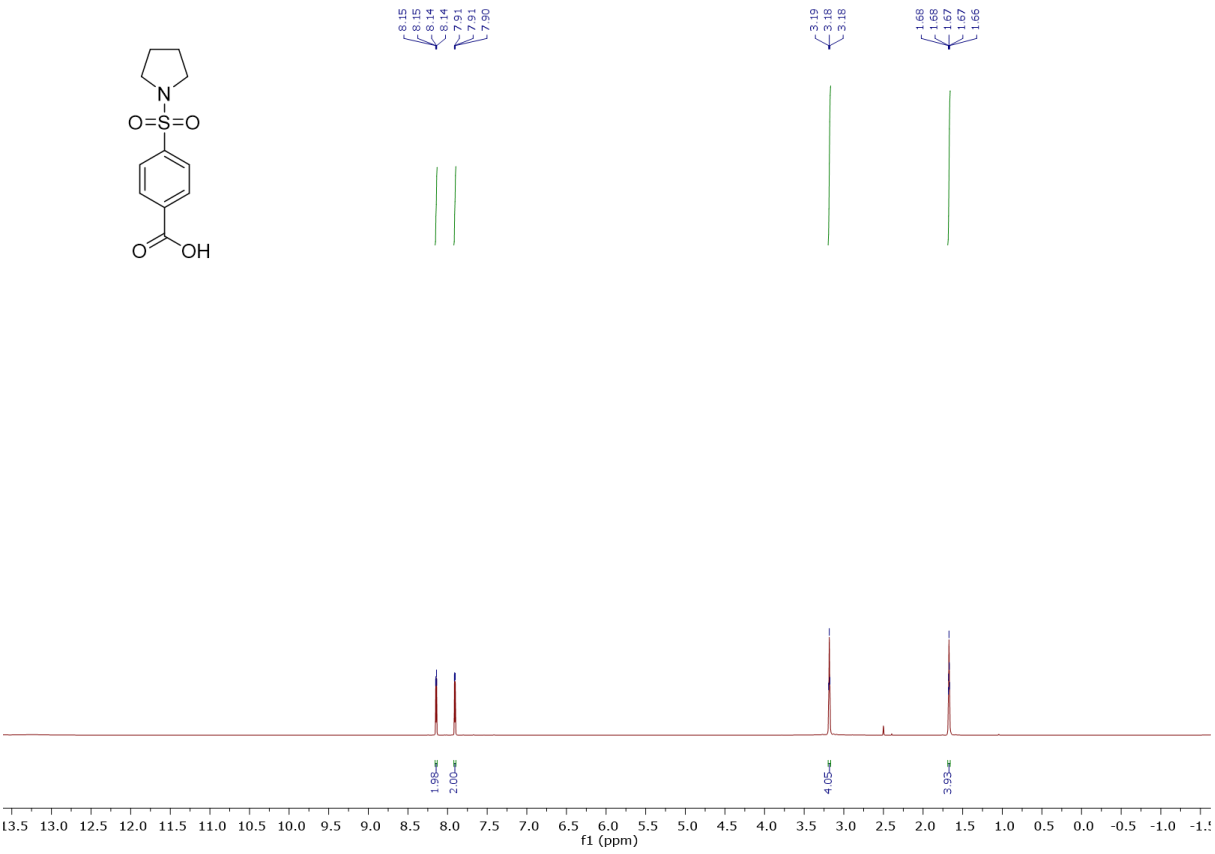
8.15
8.15
8.14
8.14
7.91
7.91
7.90
3.19
3.18
3.18
1.68
1.68
1.67
1.67
1.66
N
O=S=O
O
OH
1.98
2.00
4.05
3.93
f1 (ppm)

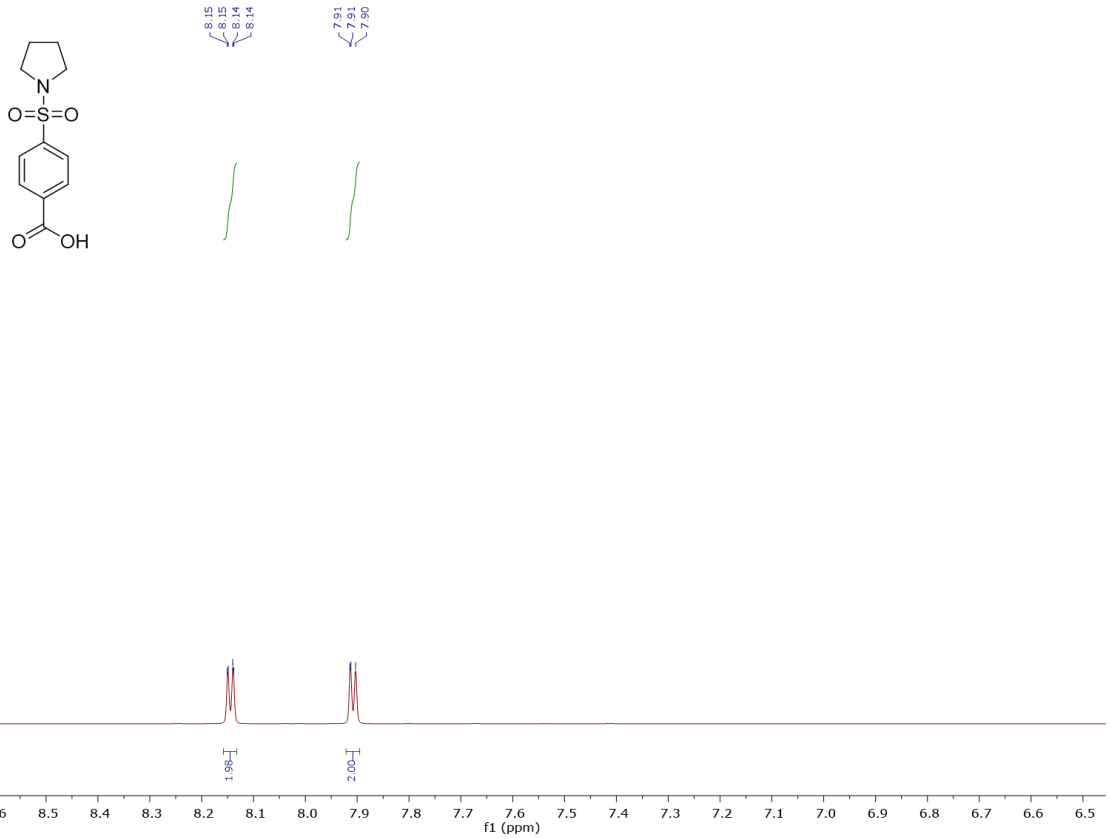
8.15
8.15
8.14
8.14
7.91
7.91
7.90
1.98
2.00
8.7 8.6 8.5 8.4 8.3 8.2 8.1 8.0 7.9 7.8 7.7 7.6 7.5 7.4 7.3 7.2 7.1 7.0 6.9 6.8 6.7 6.6 6.5
f1 (ppm)

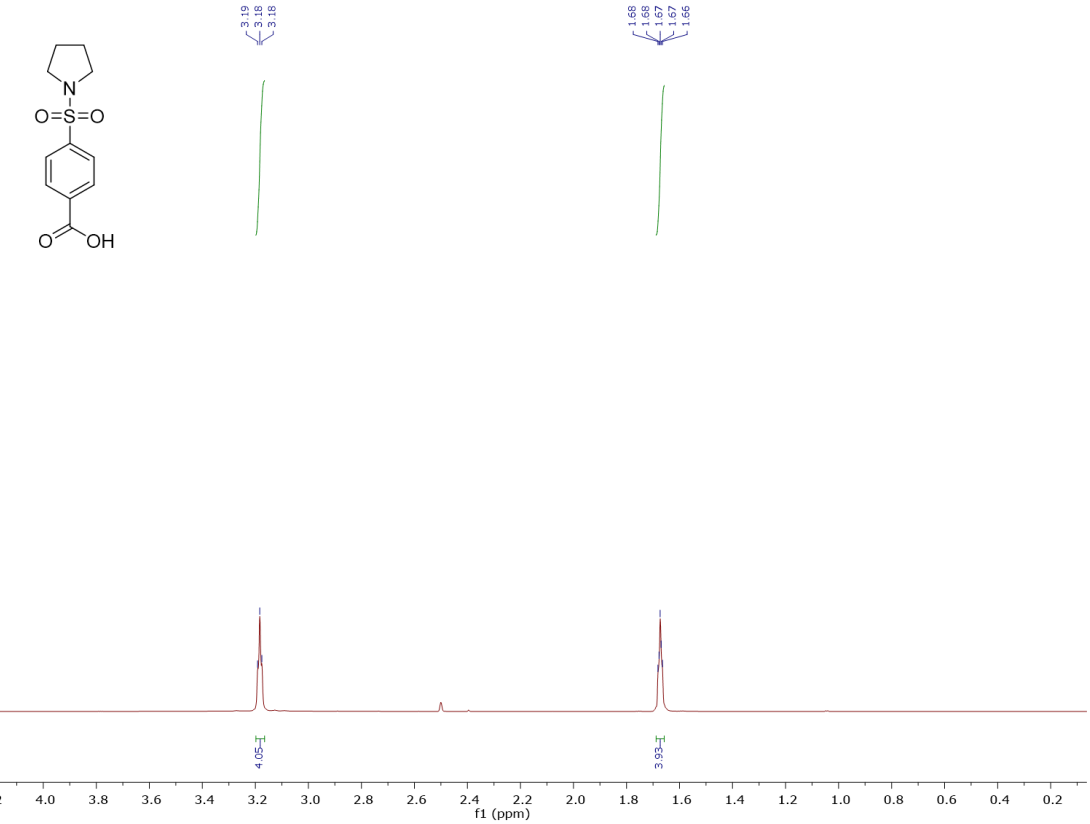
3.19
3.18
3.18
1.68
1.68
1.67
1.67
1.66
4.05
3.93
4.4 4.2 4.0 3.8 3.6 3.4 3.2 3.0 2.8 2.6 2.4 2.2 2.0 1.8 1.6 1.4 1.2 1.0 0.8 0.6 0.4 0.2
f1 (ppm)

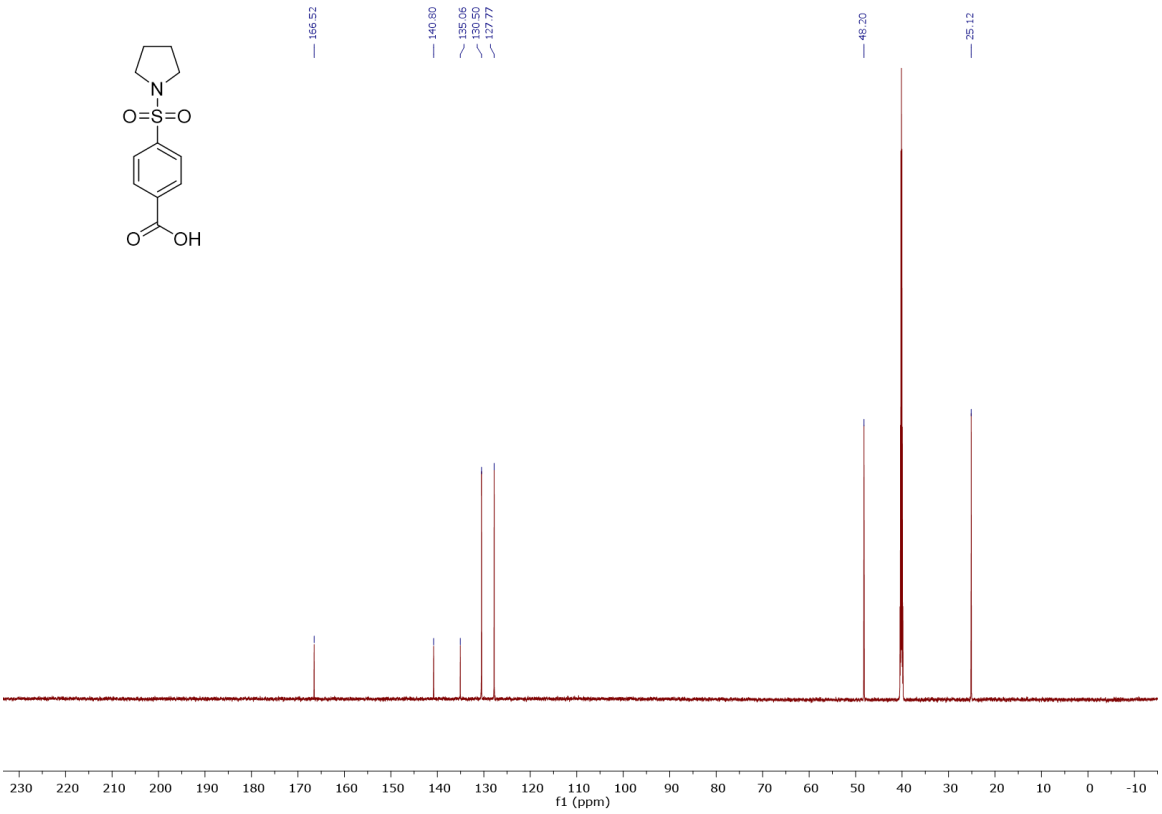
166.52
140.80
135.06
130.50
127.77
48.20
25.12
f1 (ppm)

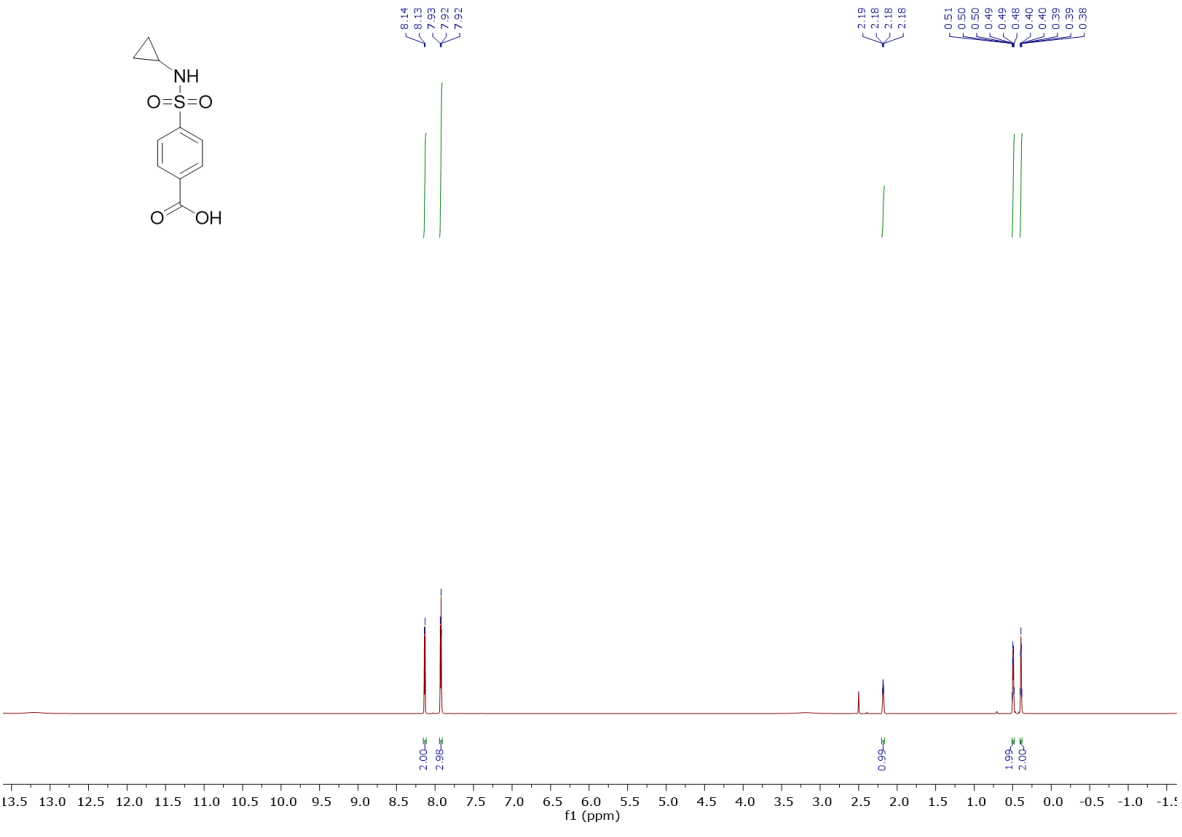
8.14
8.13
7.93
7.92
7.92
2.19
2.18
2.18
2.18
0.51
0.50
0.50
0.49
0.49
0.48
0.40
0.40
0.39
0.39
0.38
2.00
2.98
0.99
1.99
2.00
f1 (ppm)

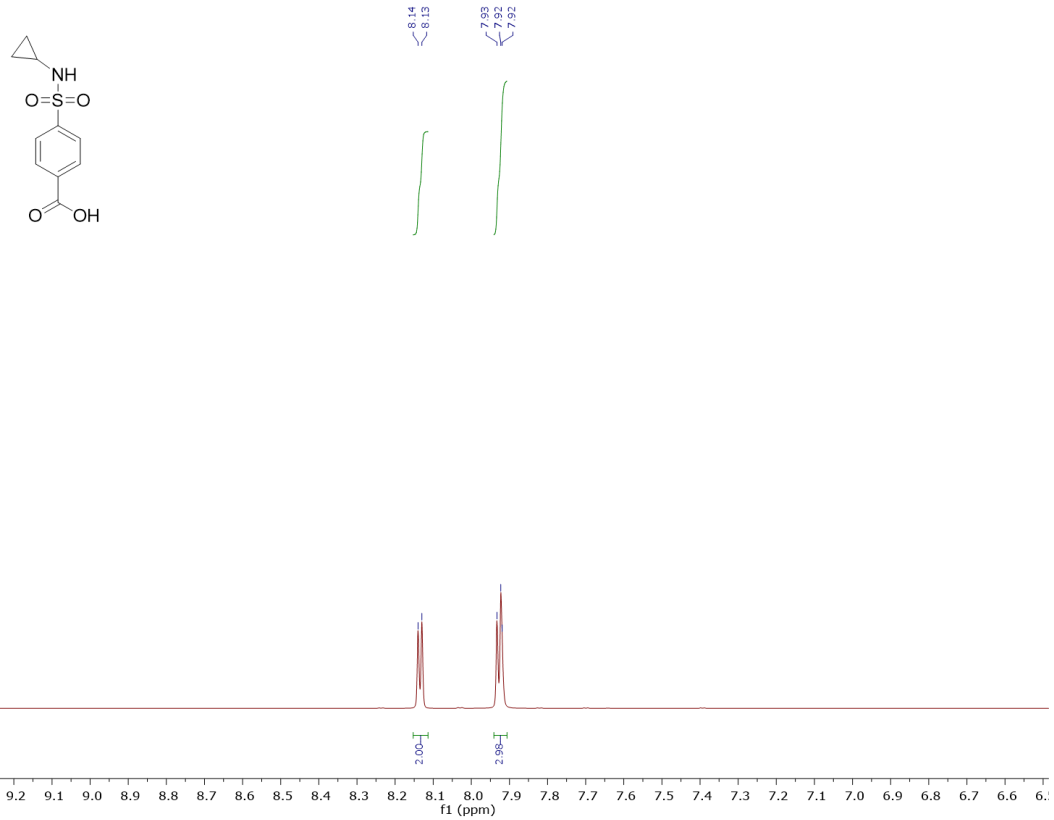
NH
O=S=O
O
OH
8.14
8.13
7.93
7.92
7.92
2.00
2.98
9.5 9.4 9.3 9.2 9.1 9.0 8.9 8.8 8.7 8.6 8.5 8.4 8.3 8.2 8.1 8.0 7.9 7.8 7.7 7.6 7.5 7.4 7.3 7.2 7.1 7.0 6.9 6.8 6.7 6.6
f1 (ppm)

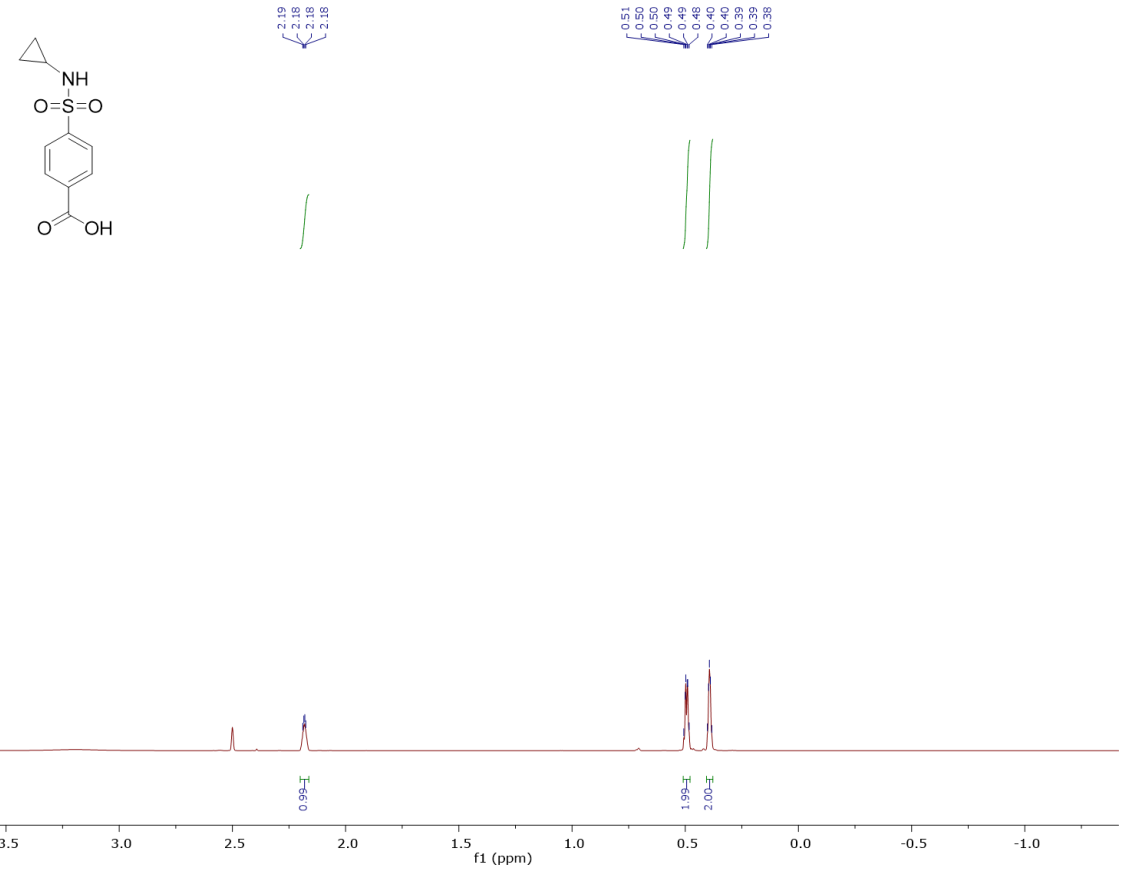
NH
O=S=O
O
OH
2.19
2.18
2.18
2.18
0.51
0.50
0.50
0.49
0.49
0.48
0.40
0.40
0.39
0.39
0.38
0.99
1.99
2.00
4.0 3.5 3.0 2.5 2.0 1.5 1.0 0.5 0.0 -0.5 -1.0
f1 (ppm)

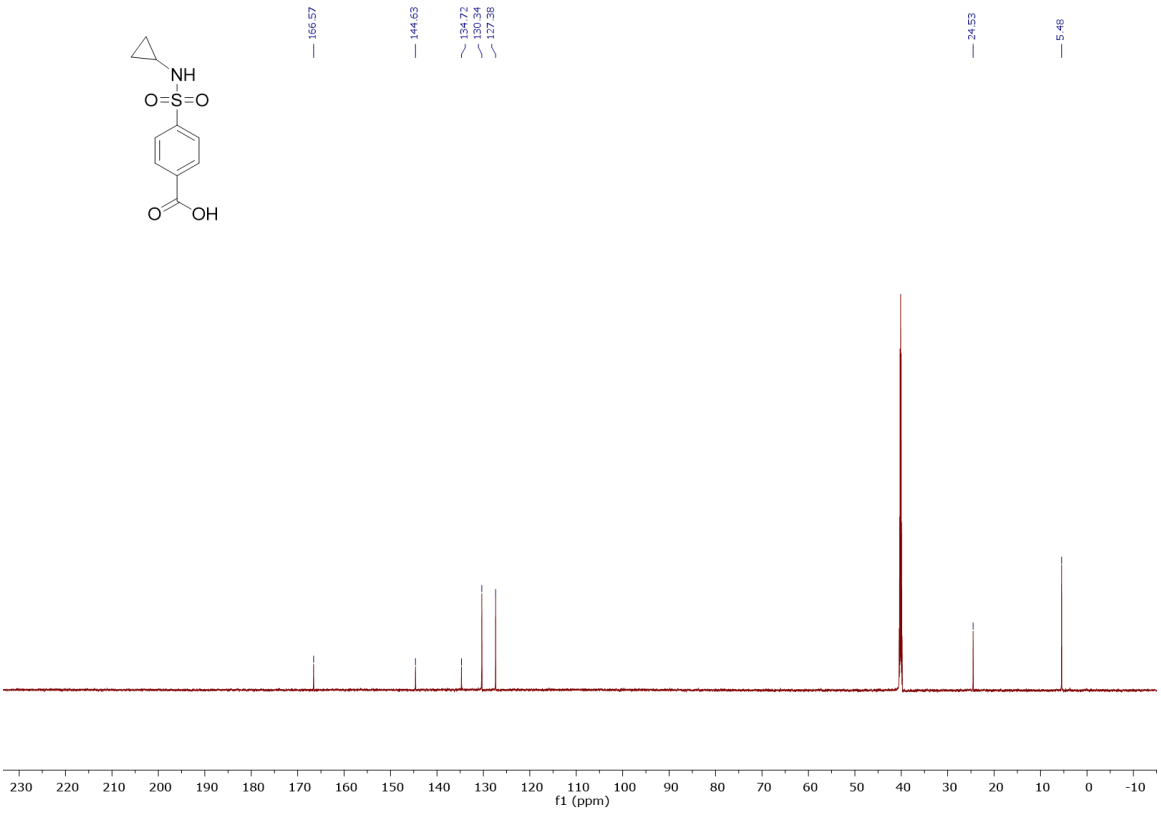
166.57
144.63
134.72
130.34
127.38
24.53
5.48
NH
O=S=O
O
OH
f1 (ppm)

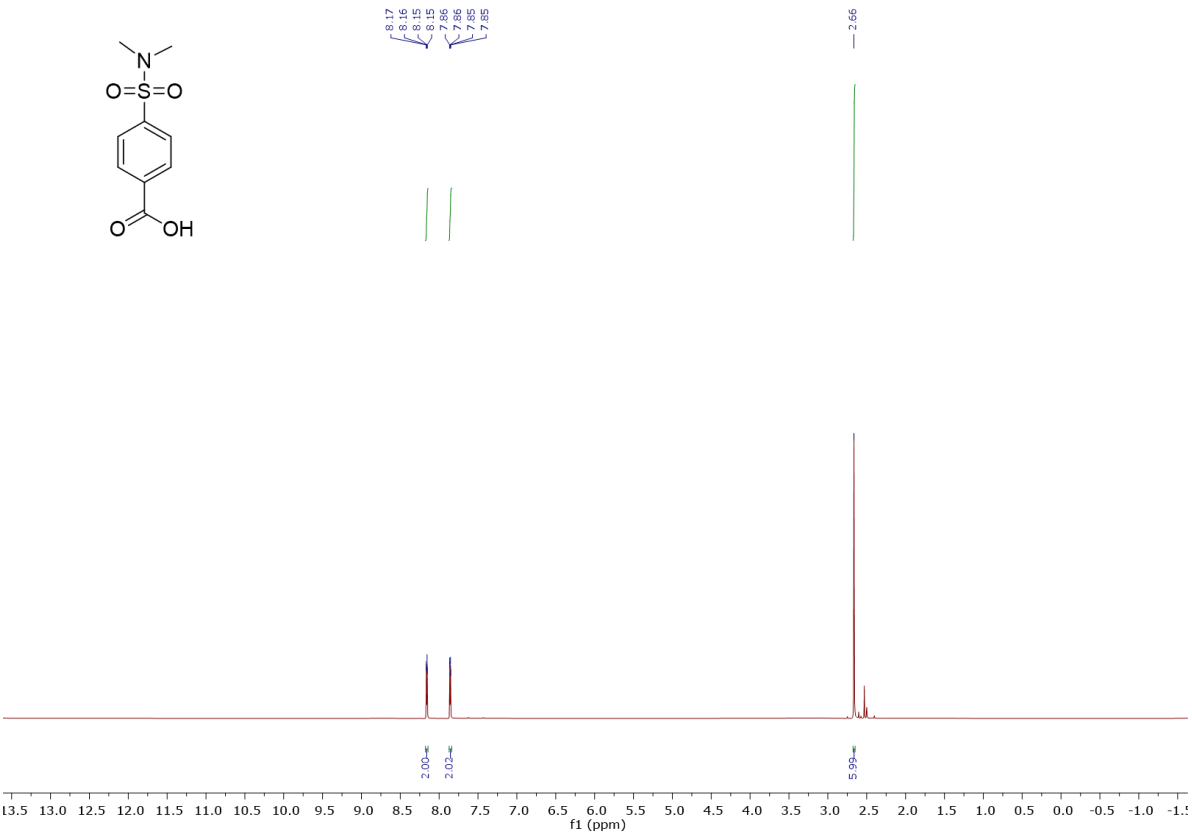
8.17
8.16
8.15
8.15
7.86
7.86
7.85
7.85
2.66
N
O=S=O
O
OH
2.00
2.02
5.99
f1 (ppm)

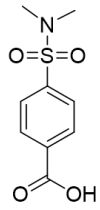
N
O=S=O
O
OH

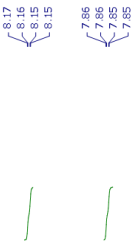
8.17
8.16
8.15
8.15
7.86
7.86
7.85
7.85

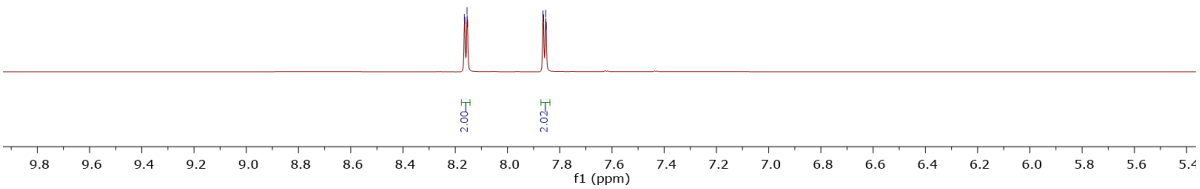
2.00
2.03
9.8
9.6
9.4
9.2
9.0
8.8
8.6
8.4
8.2
8.0
7.8
7.6
7.4
7.2
7.0
6.8
6.6
6.4
6.2
6.0
5.8
5.6
f1 (ppm)

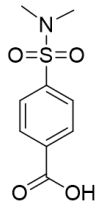
N
O=S=O
O
OH

2.66

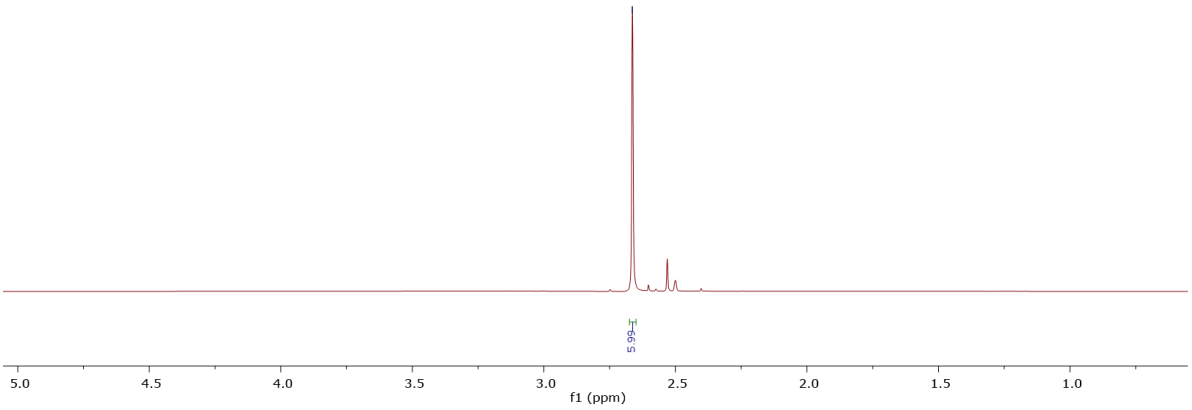
5.99
5.0
4.5
4.0
3.5
3.0
2.5
2.0
1.5
1.0
f1 (ppm)

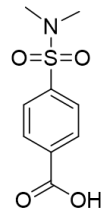

166.48
139.41
135.21
130.49
127.99
37.83
f1 (ppm)

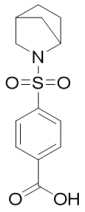

8.14
8.13
7.92
7.91
4.14
3.06
3.06
3.05
3.04
2.99
2.98
2.45
1.56
1.56
1.54
1.32
1.32
1.31
1.30
1.20
1.19
0.84
0.83
1.96
2.00
0.98
1.00
1.00
0.98
2.90
0.92
1.01
0.99
f1 (ppm)

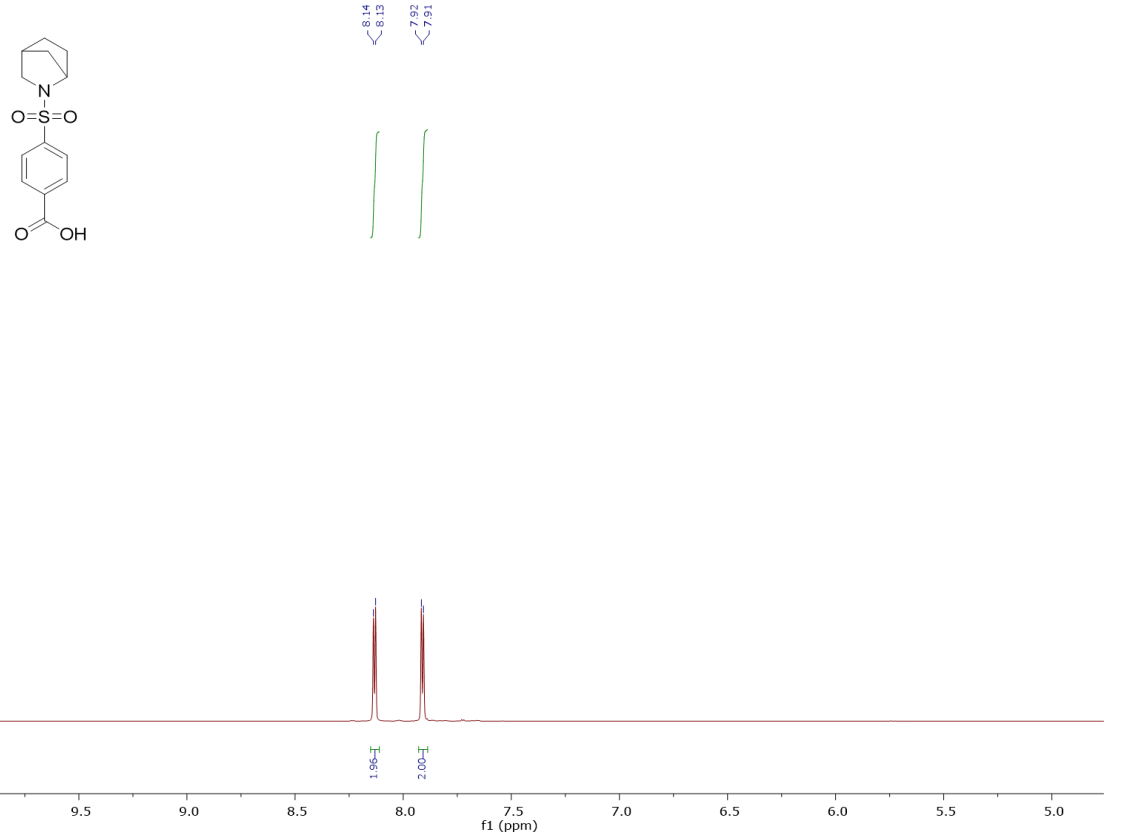
8.14
8.13
7.92
7.91
1.96
2.00
10.0
9.5
9.0
8.5
8.0
7.5
7.0
6.5
6.0
5.5
5.0
f1 (ppm)

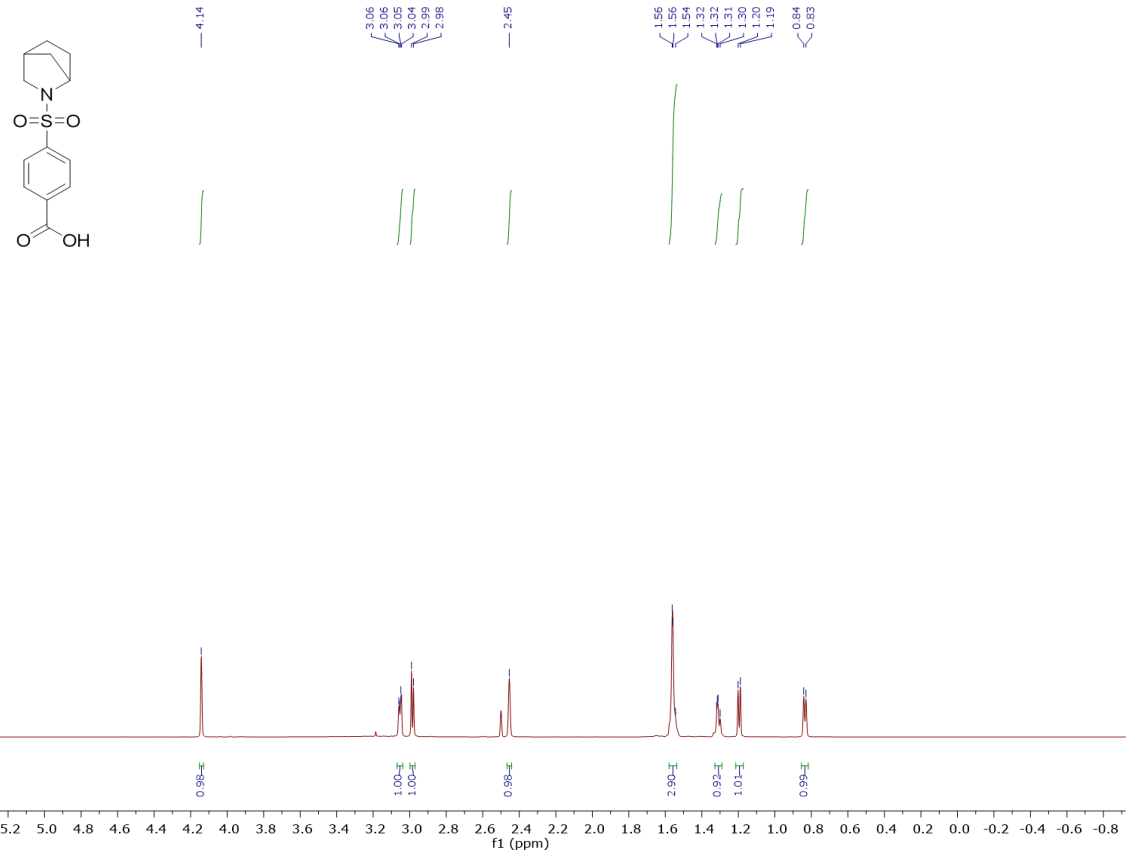
4.14
3.06
3.06
3.05
3.04
2.99
2.98
2.45
1.56
1.56
1.54
1.32
1.32
1.31
1.30
1.20
1.19
0.84
0.83
0.98
1.00
1.00
0.98
2.90
0.92
1.01
0.99
5.6
5.4
5.2
5.0
4.8
4.6
4.4
4.2
4.0
3.8
3.6
3.4
3.2
3.0
2.8
2.6
2.4
2.2
2.0
1.8
1.6
1.4
1.2
1.0
0.8
0.6
0.4
0.2
0.0
-0.2
-0.4
-0.6
-0.8
f1 (ppm)

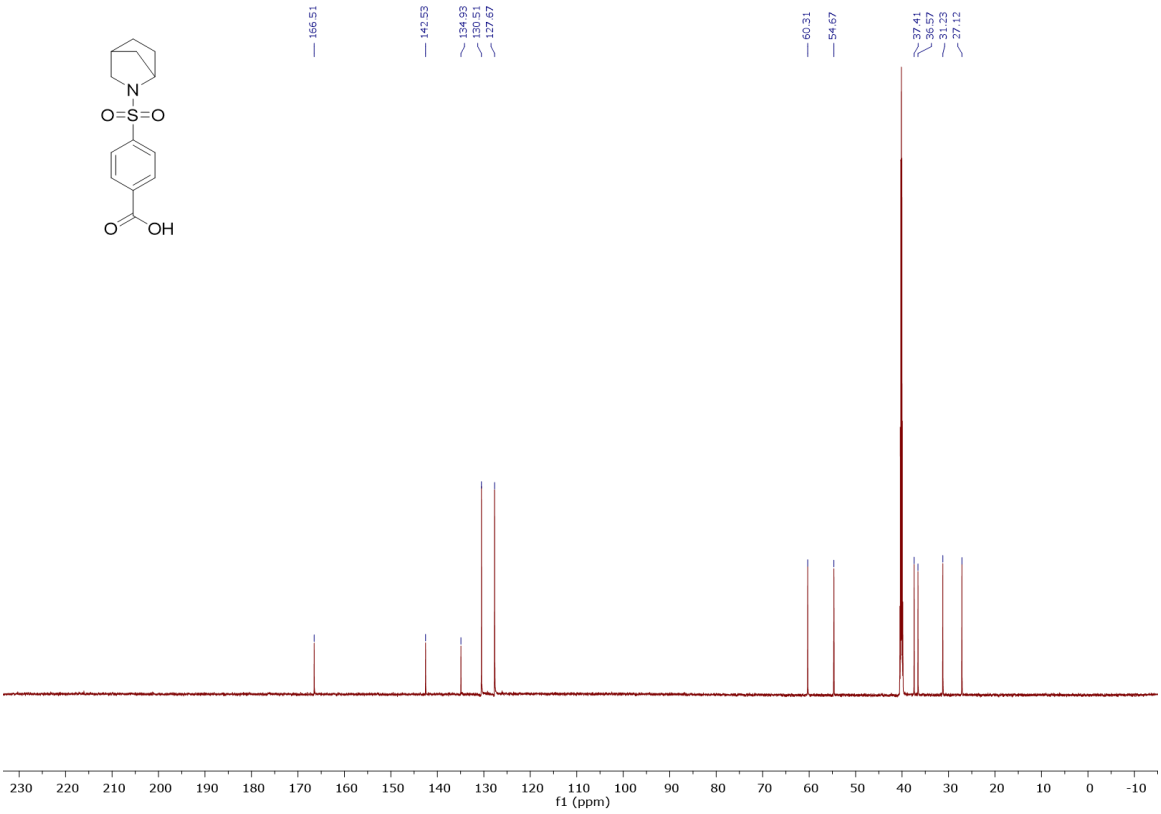
166.51
142.53
134.93
130.51
127.67
60.31
54.67
37.41
36.57
31.23
27.12
f1 (ppm)

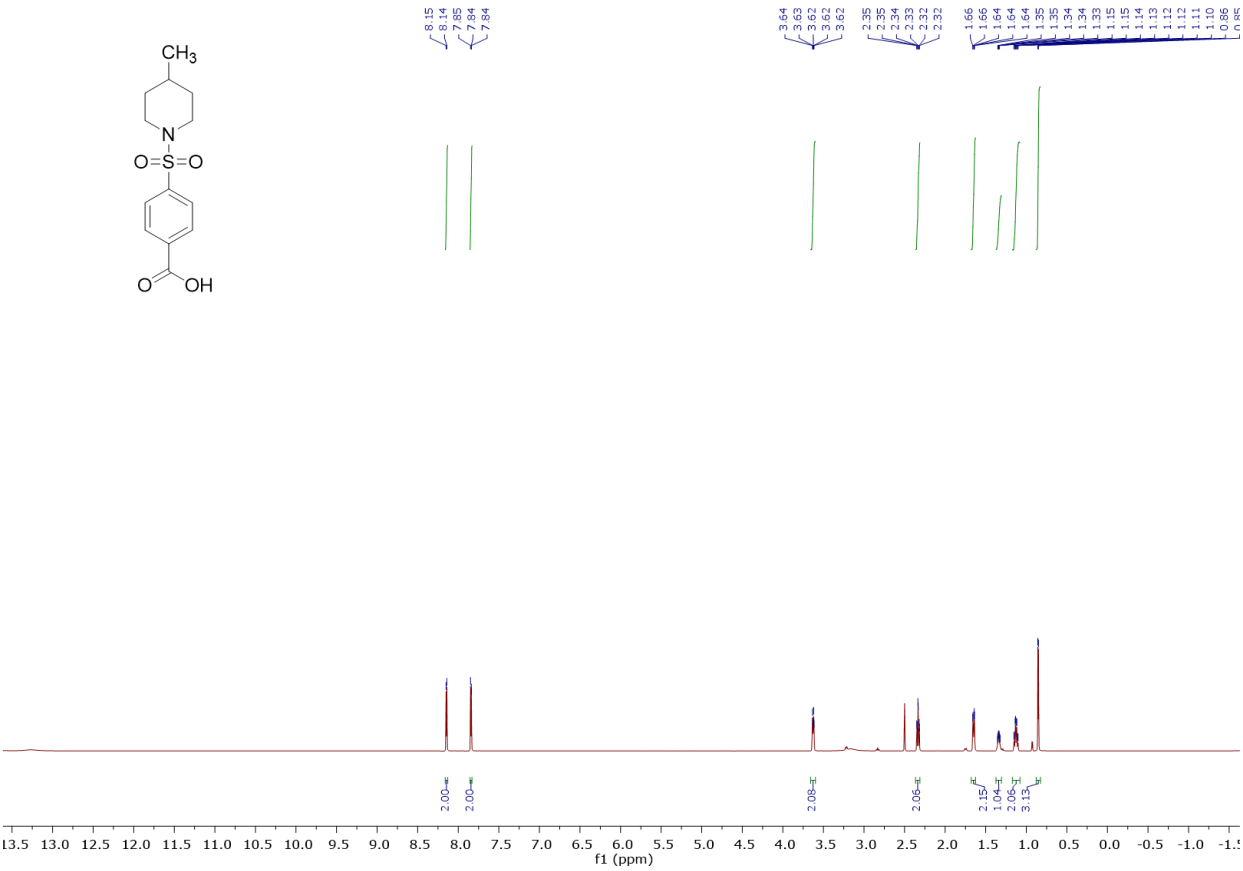
8.15
8.14
7.85
7.84
7.84
3.64
3.63
3.62
3.62
3.62
2.35
2.35
2.34
2.33
2.32
2.32
1.66
1.66
1.64
1.64
1.64
1.35
1.35
1.34
1.34
1.33
1.15
1.15
1.14
1.13
1.12
1.12
1.11
1.10
2.00
2.00
2.08
2.06
2.15
1.04
2.06
3.13
f1 (ppm)

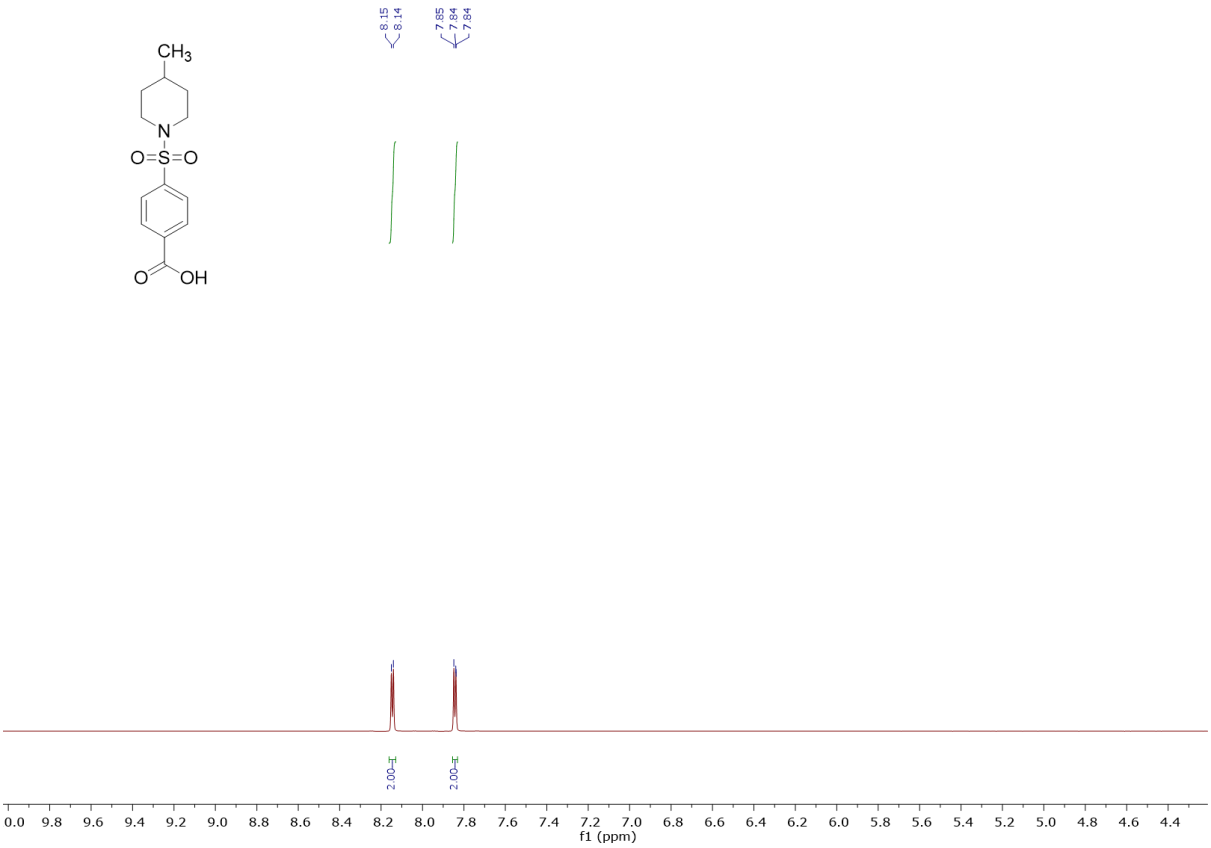
CH3
N
O=S=O
O
OH
8.15
8.14
7.85
7.84
7.84
2.00
2.00
f1 (ppm)

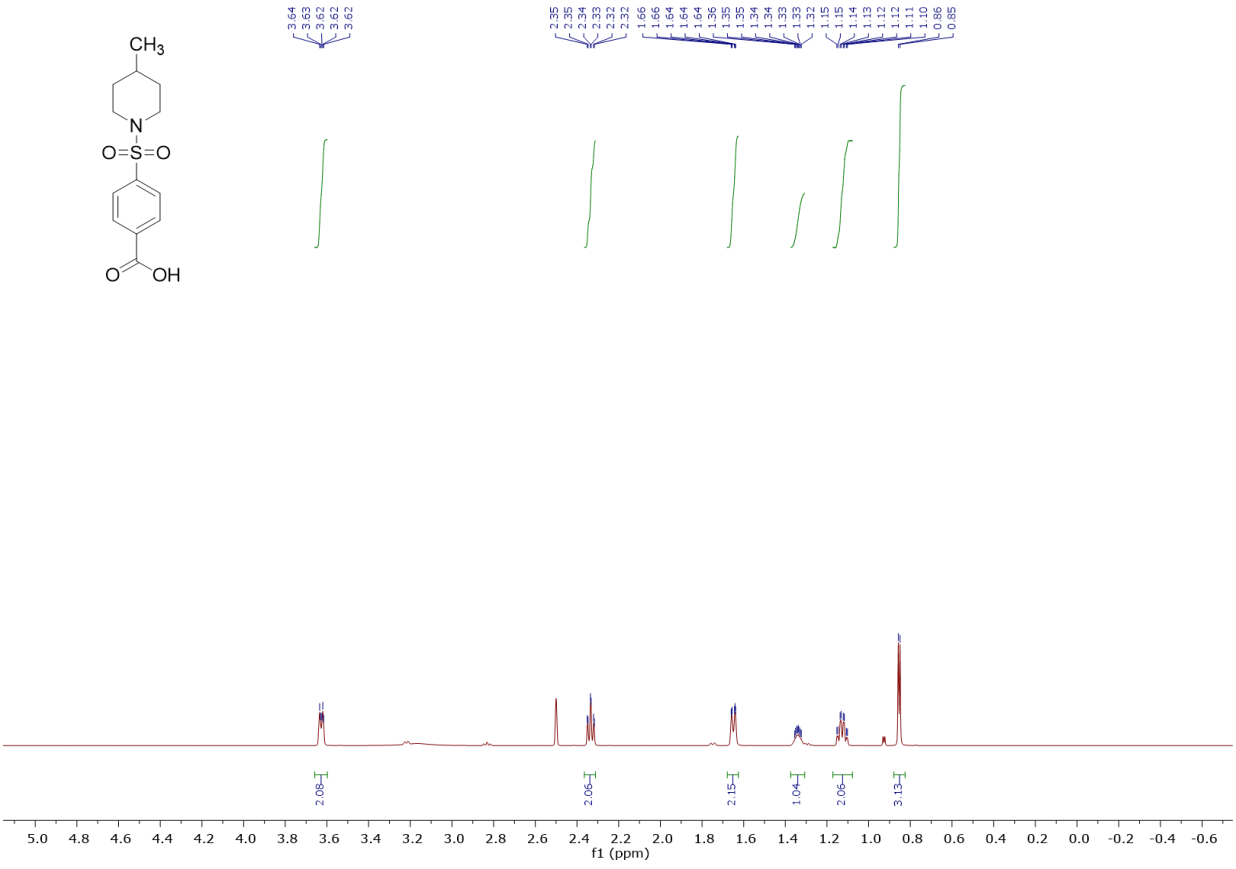
CH3
N
O=S=O
O
OH
3.64
3.63
3.62
3.62
3.62
2.35
2.35
2.34
2.33
2.32
2.32
1.66
1.66
1.64
1.64
1.64
1.36
1.35
1.35
1.34
1.34
1.33
1.33
1.32
1.15
1.15
1.14
1.13
1.12
1.12
1.11
1.10
0.86
0.85
2.08
2.06
2.15
1.04
2.06
3.13
f1 (ppm)

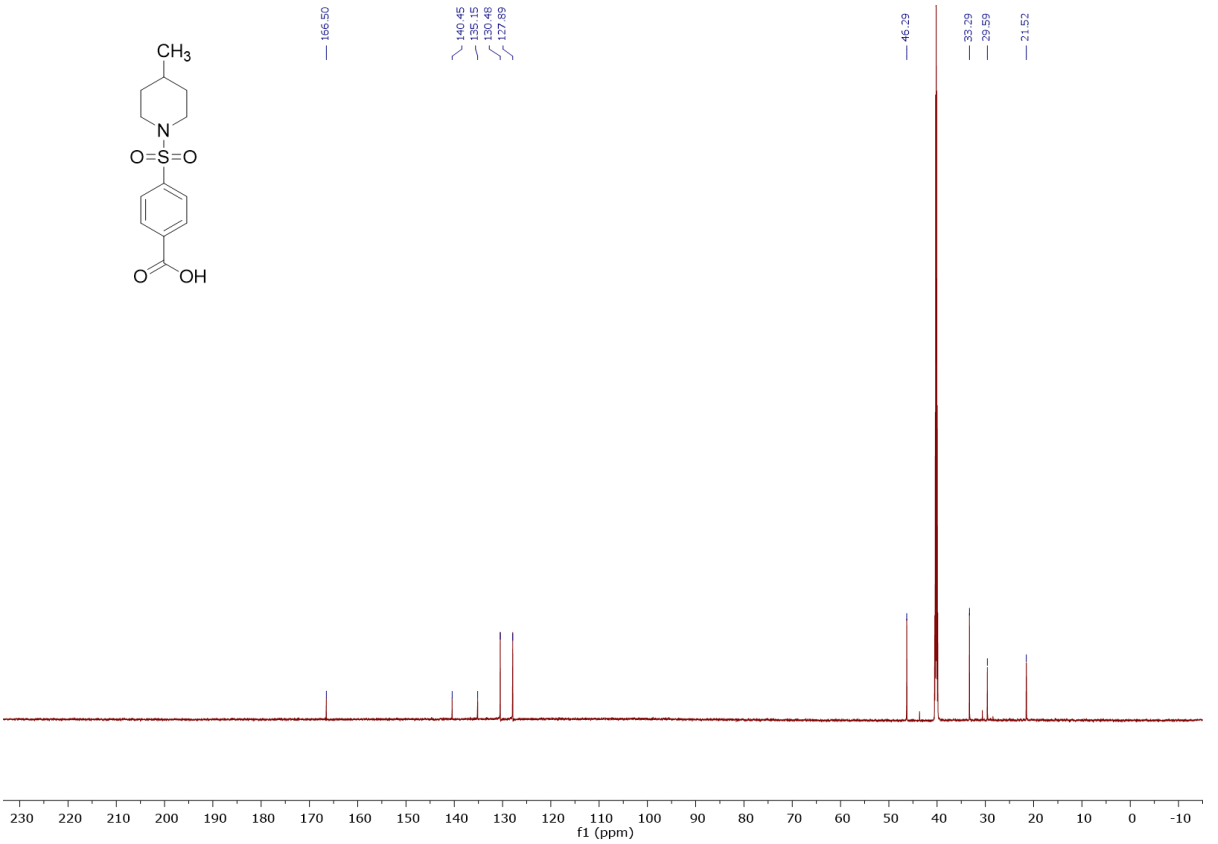
CH3
N
O=S=O
O
OH
166.50
140.45
135.15
130.48
127.89
46.29
33.29
29.59
21.52
f1 (ppm)

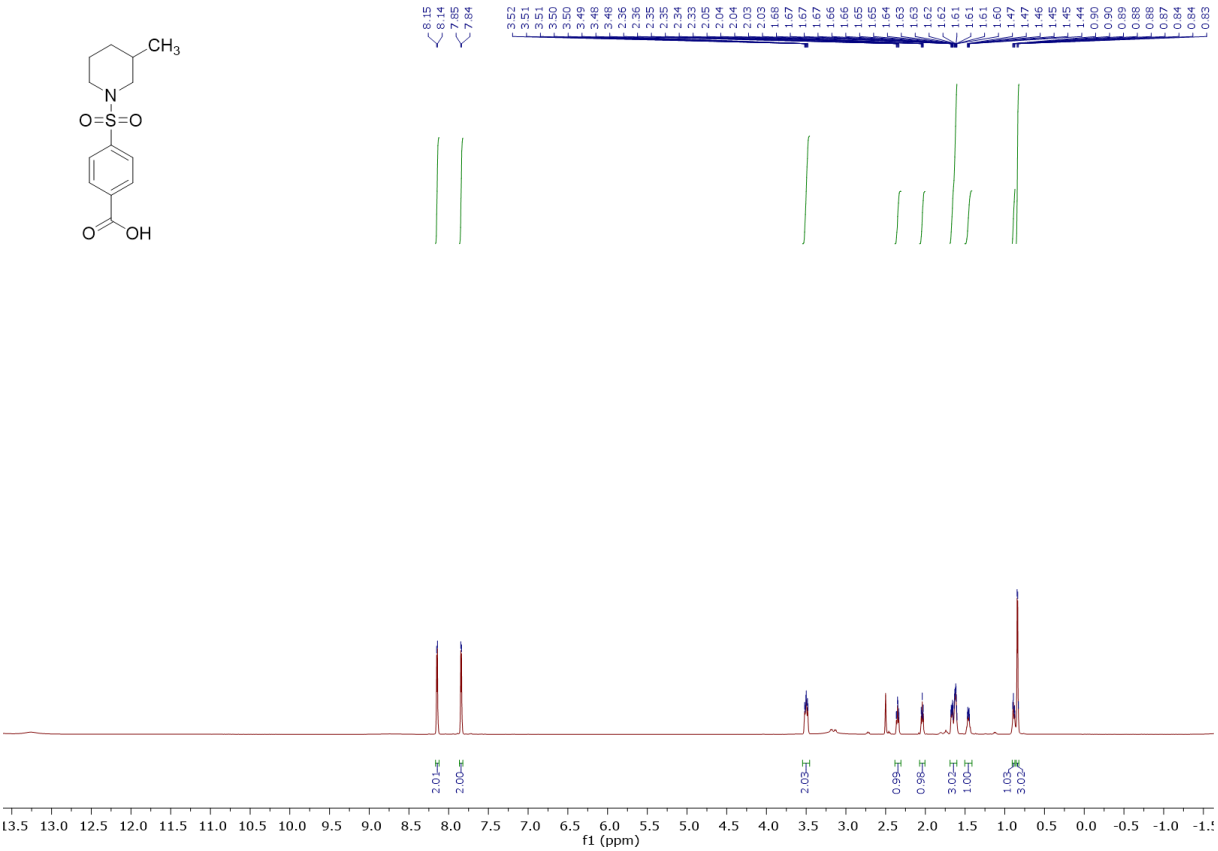
CH3
N
O=S=O
O
OH
8.15
8.14
7.85
7.84
2.01
2.00
2.03
0.99
0.98
3.03
1.00
1.03
3.02
f1 (ppm)

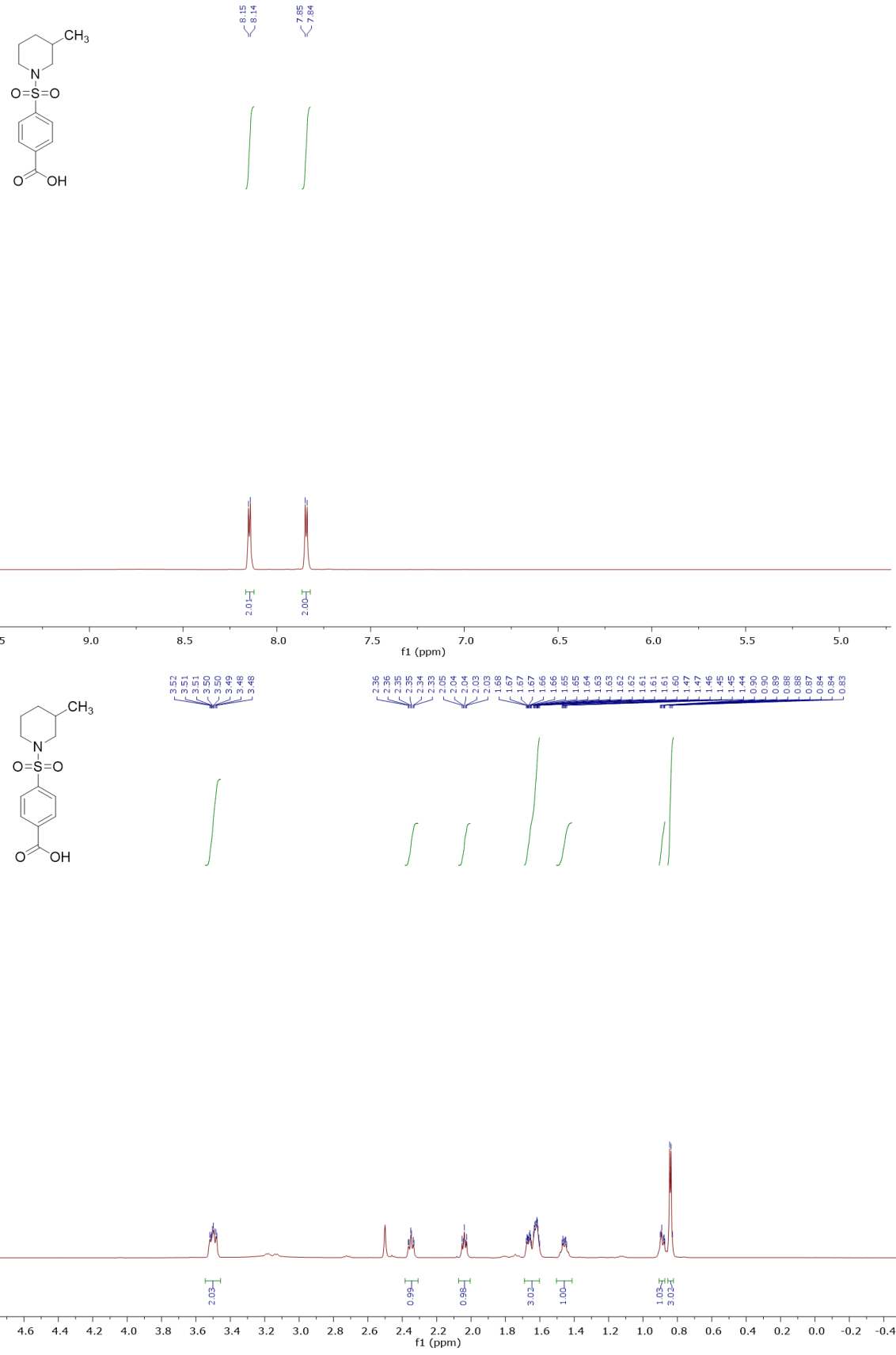
CH3
N
O=S=O
O
OH
8.15
8.14
7.85
7.84
2.01
2.00
9.5
9.0
8.5
8.0
7.5
7.0
6.5
6.0
5.5
5.0
f1 (ppm)
3.52
3.51
3.51
3.50
3.50
3.49
3.48
3.48
2.36
2.36
2.35
2.35
2.34
2.33
2.05
2.04
2.04
2.03
2.03
1.68
1.67
1.67
1.67
1.66
1.66
1.65
1.65
1.64
1.63
1.63
1.62
1.62
1.61
1.61
1.61
1.60
1.47
1.47
1.46
1.45
1.45
1.44
0.90
0.90
0.89
0.88
0.88
0.87
0.84
0.84
0.83
2.03
0.99
0.98
3.02
1.00
1.03
3.02
5.0
4.8
4.6
4.4
4.2
4.0
3.8
3.6
3.4
3.2
3.0
2.8
2.6
2.4
2.2
2.0
1.8
1.6
1.4
1.2
1.0
0.8
0.6
0.4
0.2
0.0
-0.2
-0.4
-0
f1 (ppm)

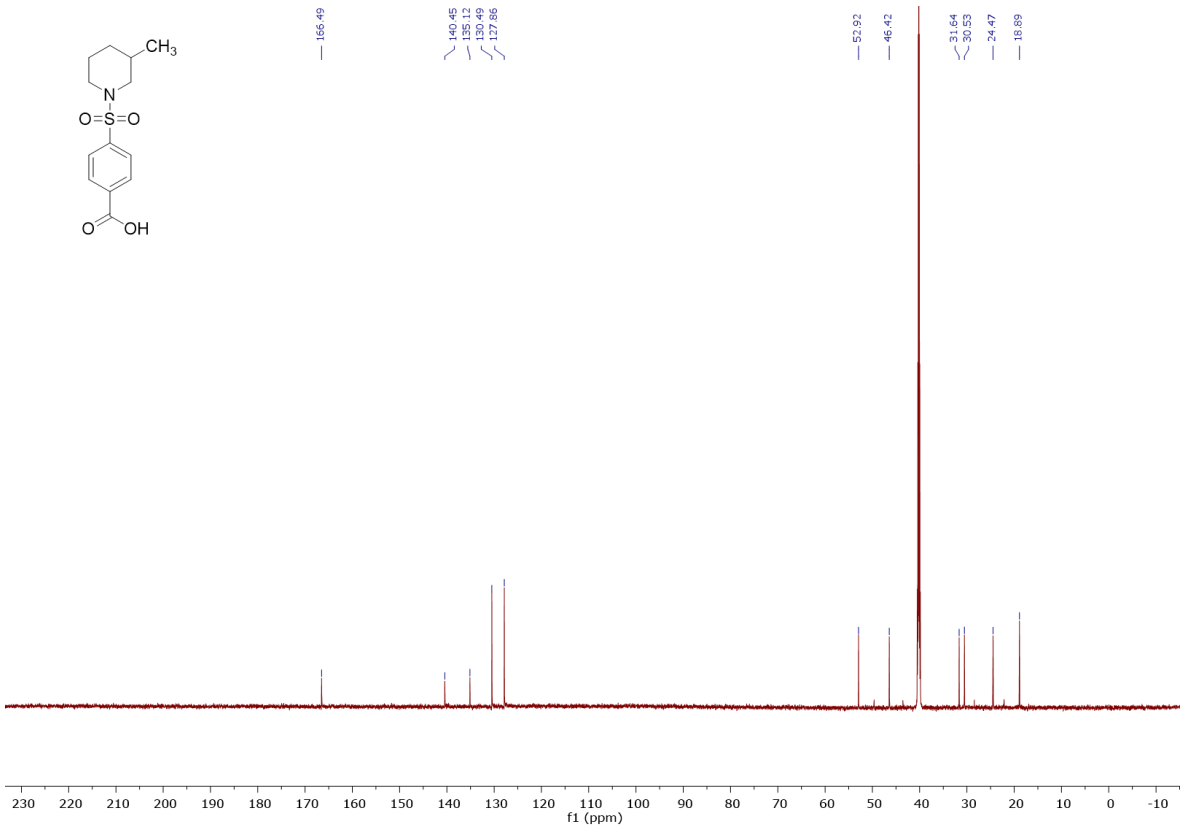
CH3
N
O=S=O
O
OH
166.49
140.45
135.12
130.49
127.86
52.92
46.42
31.64
30.53
24.47
18.89
f1 (ppm)

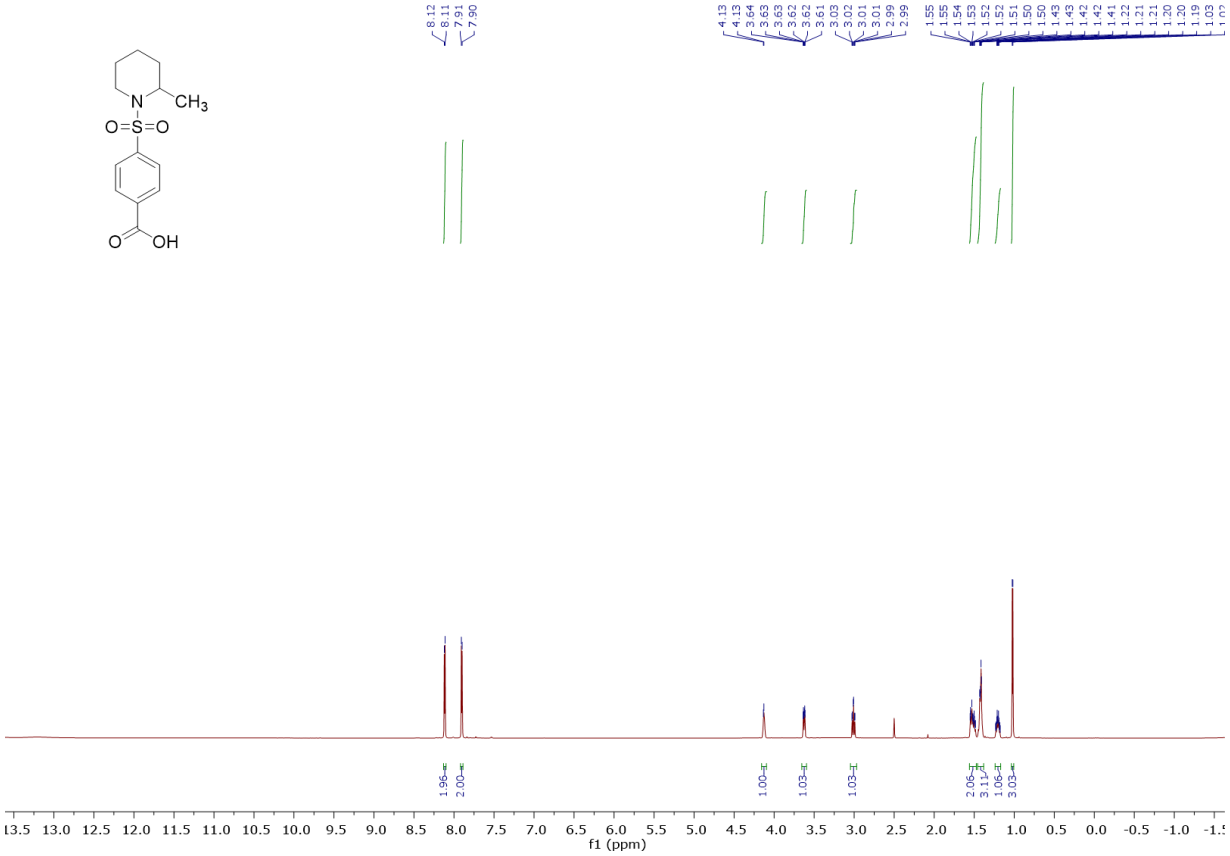
CH3
N
O=S=O
O
OH
8.12
8.11
7.91
7.90
f1 (ppm)

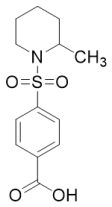
N
CH3
O=S=O
O
OH

8.12
8.11
7.91
7.90
1.96
2.00
f1 (ppm)

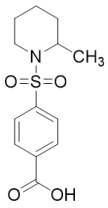
N
CH3
O=S=O
O
OH

4.13
3.64
3.63
3.62
3.61
3.03
3.02
3.01
2.99
1.55
1.54
1.53
1.52
1.51
1.50
1.49
1.43
1.42
1.41
1.23
1.22
1.21
1.20
1.19
1.18
1.03
1.02
1.00
1.03
1.03
2.06
3.11
1.06
3.03
f1 (ppm)

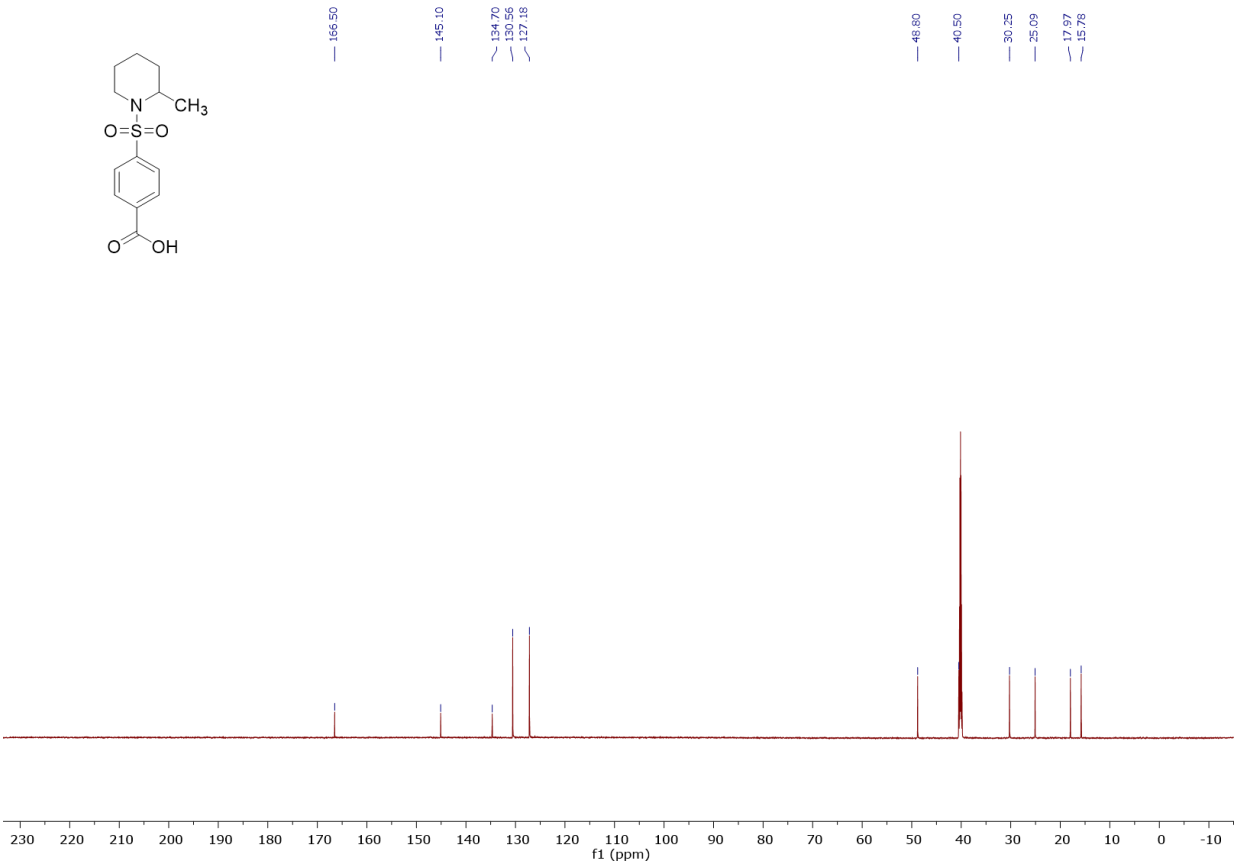
166.50
145.10
134.70
130.56
127.18
48.80
40.50
30.25
25.09
17.97
15.78
f1 (ppm)

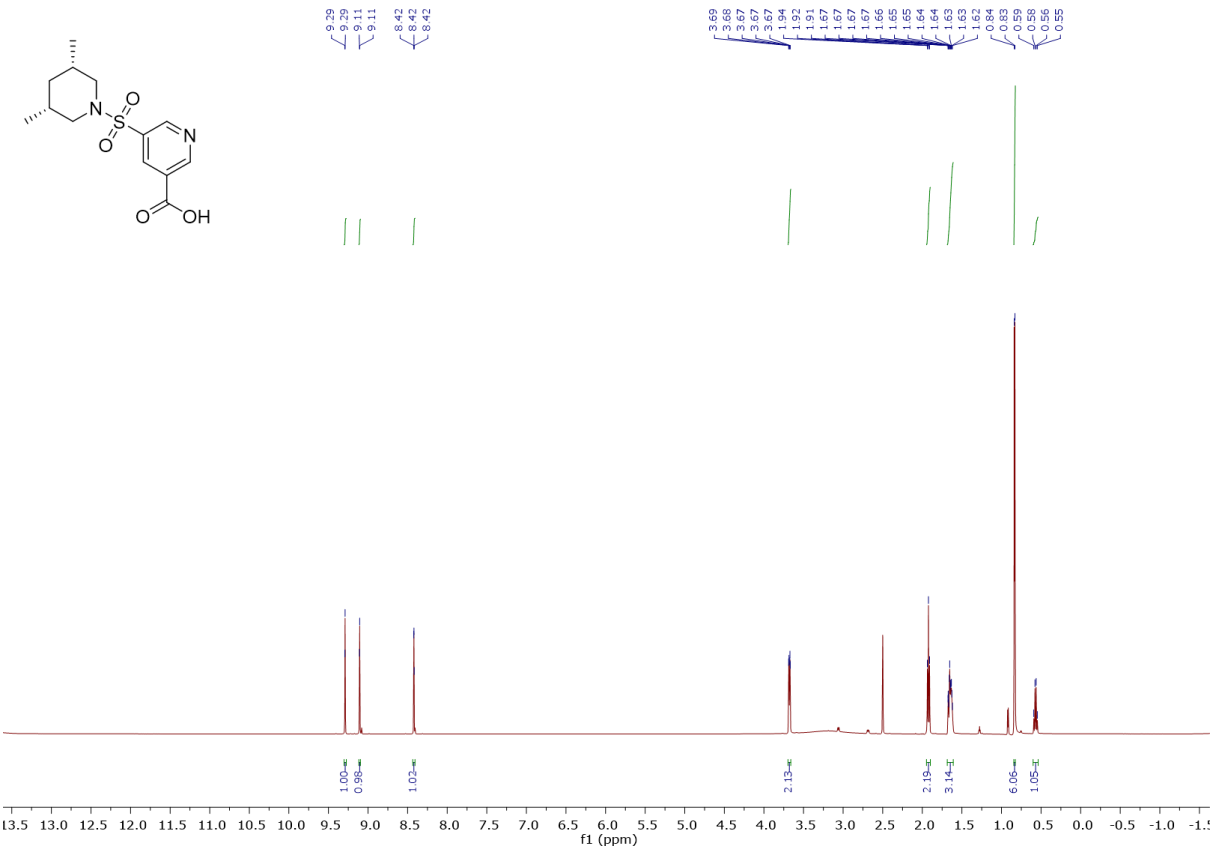
9.29
9.29
9.11
9.11
8.42
8.42
8.42
3.69
3.68
3.67
3.67
3.67
3.67
1.94
1.92
1.91
1.67
1.67
1.67
1.67
1.66
1.65
1.65
1.64
1.64
1.63
1.63
1.62
0.84
0.83
0.59
0.58
0.56
0.55
1.00
0.98
1.02
2.13
2.19
3.14
6.06
1.05
f1 (ppm)

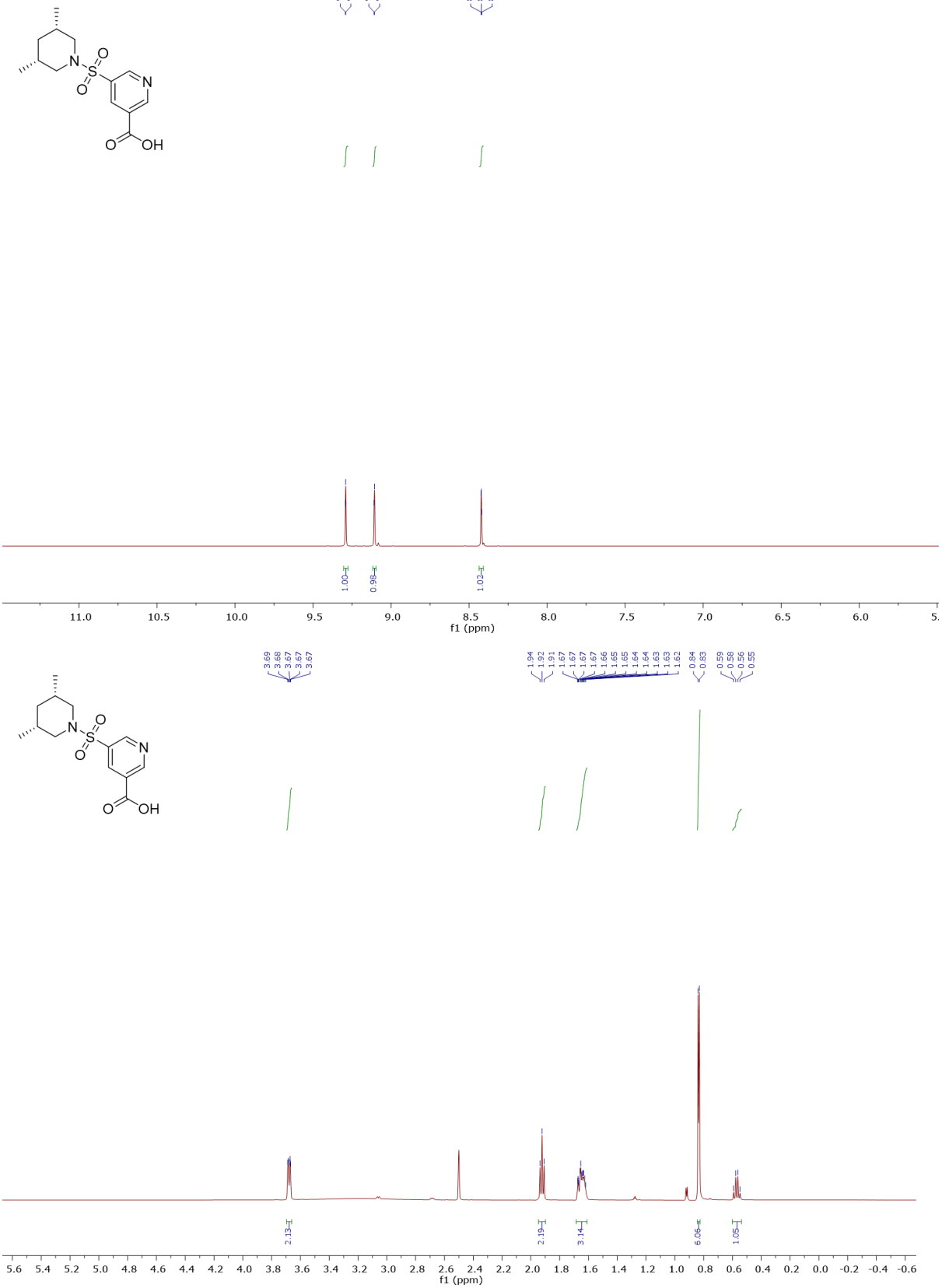
9.29
9.29
9.11
9.11
8.42
8.42
8.42
1.00
0.98
1.02
11.0
10.5
10.0
9.5
9.0
8.5
8.0
7.5
7.0
6.5
6.0
f1 (ppm)
3.69
3.68
3.68
3.67
3.67
3.67
1.94
1.92
1.91
1.67
1.67
1.67
1.67
1.66
1.65
1.65
1.64
1.64
1.63
1.63
1.62
0.84
0.83
0.59
0.58
0.56
0.55
2.13
2.19
3.14
6.06
1.05
5.6
5.4
5.2
5.0
4.8
4.6
4.4
4.2
4.0
3.8
3.6
3.4
3.2
3.0
2.8
2.6
2.4
2.2
2.0
1.8
1.6
1.4
1.2
1.0
0.8
0.6
0.4
0.2
0.0
-0.2
-0.4
-0.6
f1 (ppm)

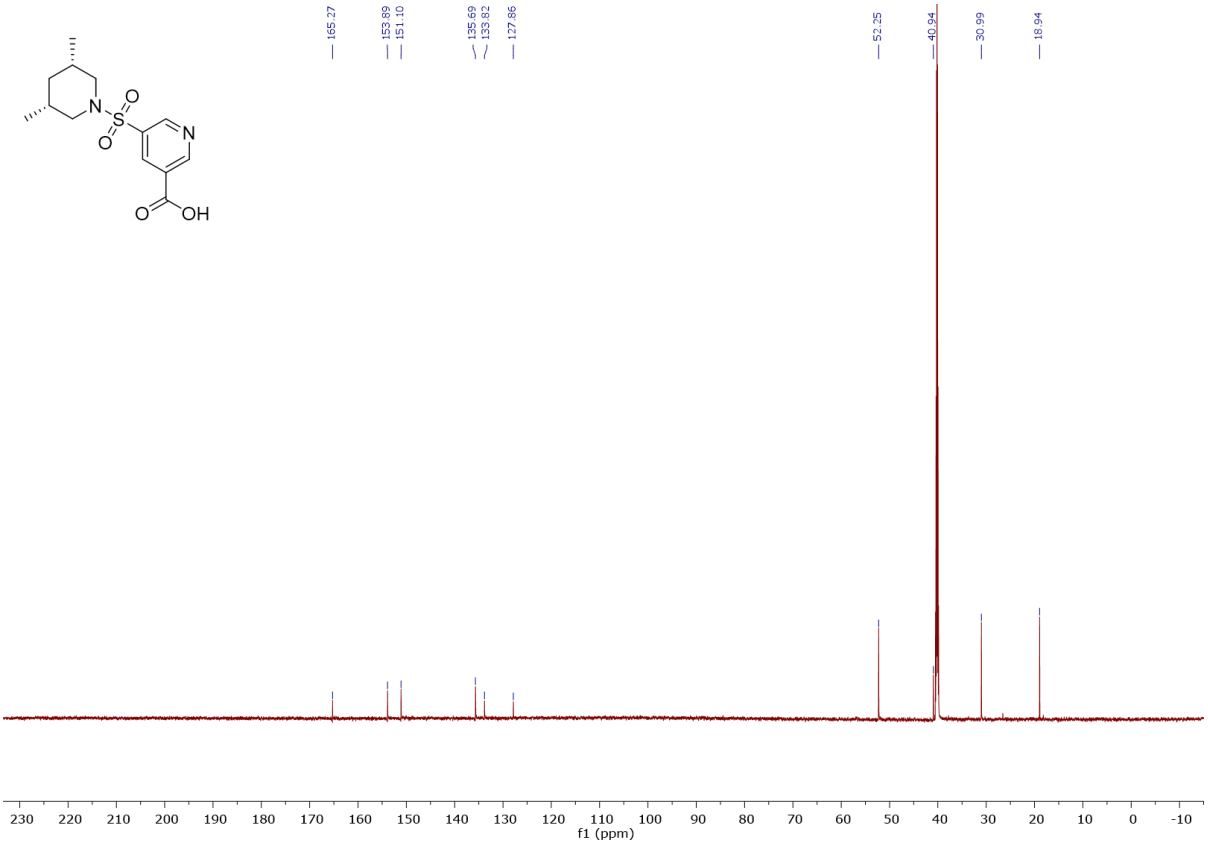

3,5dimethylpiperidinesulfonylthiophene carboxylic acid1.fid
H1 standard parameters, cryoprobe prodigy.

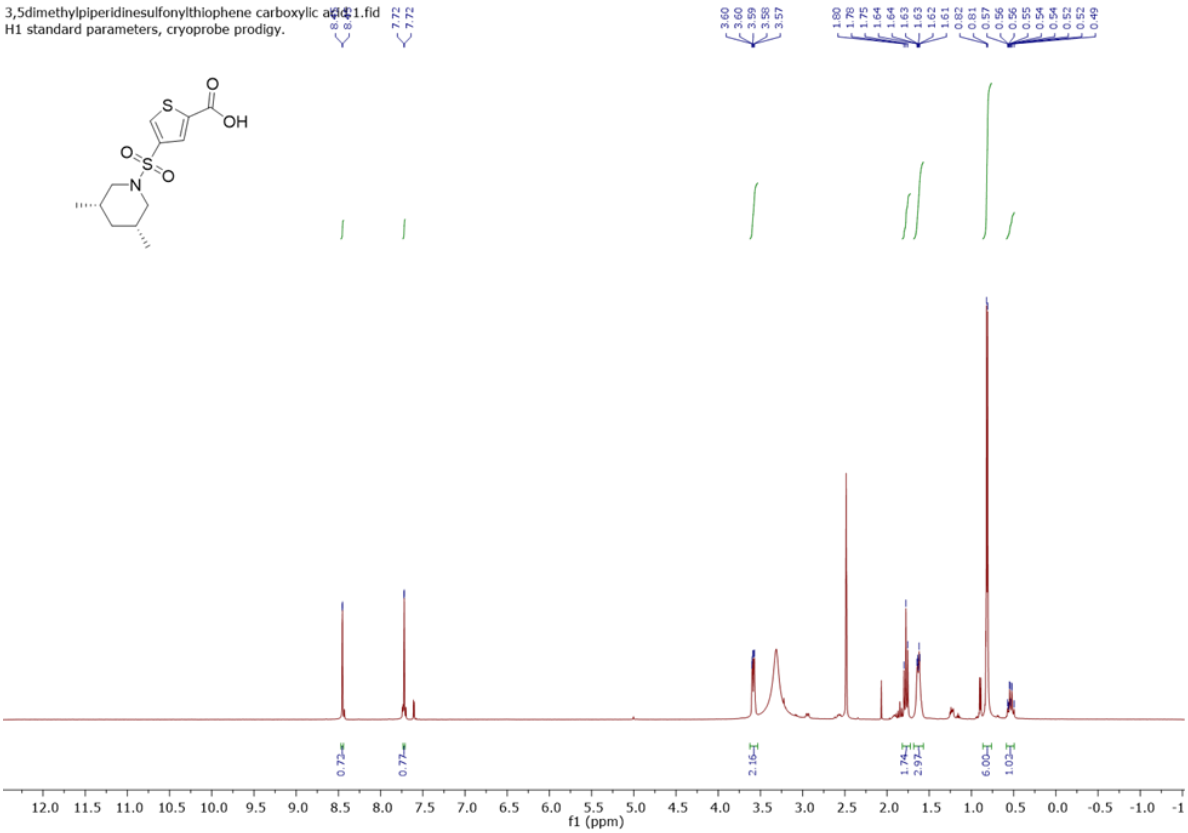

3,5dimethylpiperidinesulfonylthiophene carboxylic acid.1.fid
H1 standard parameters, cryoprobe prodigy.

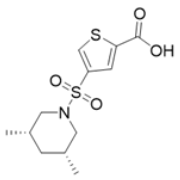

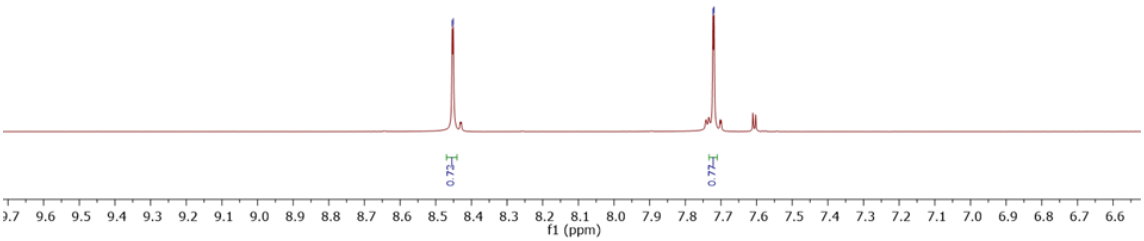

3,5dimethylpiperidinesulfonylthiophene carboxylic acid.1.fid
H1 standard parameters, cryoprobe prodigy.

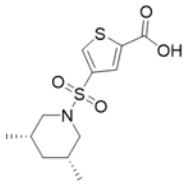

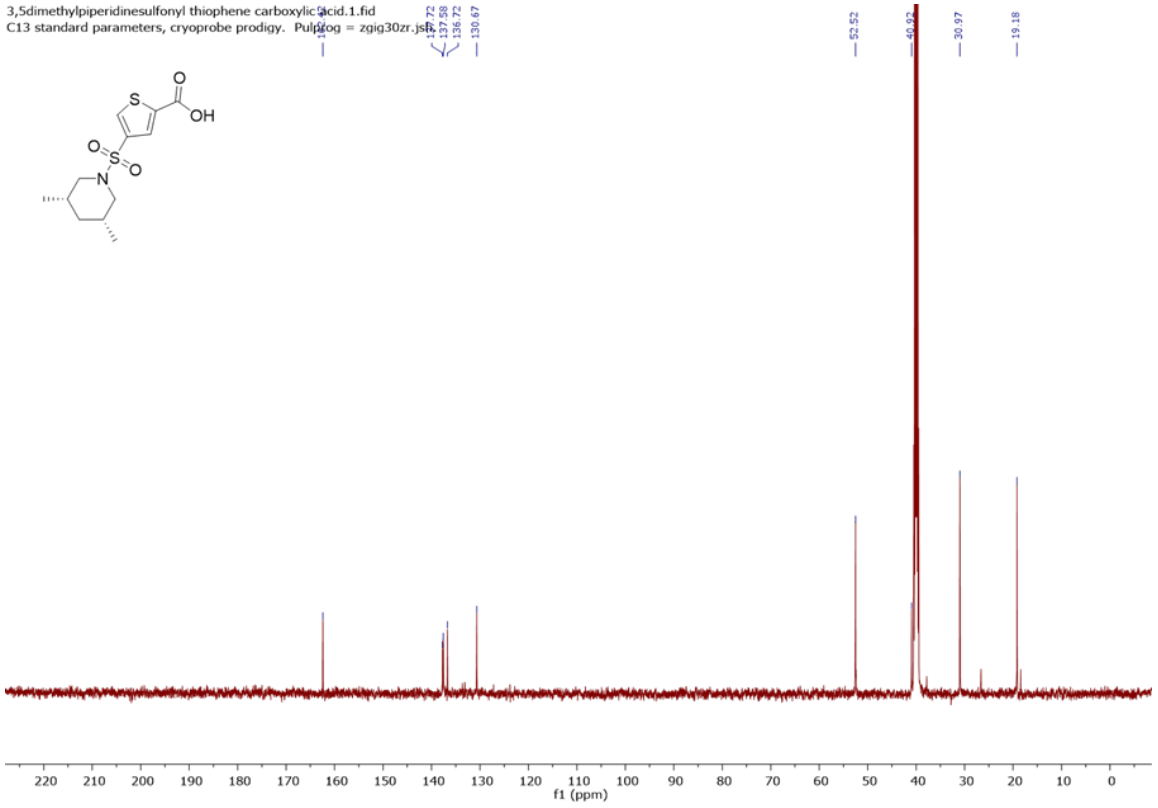
3,5dimethylpiperidinesulfonyl thiophene carboxylic acid.1.fid
C13 standard parameters, cryoprobe prodigy. Pulprog = zgig30zr.jsp
162.72
137.98
136.72
130.67
52.52
40.92
30.97
19.18
f1 (ppm)

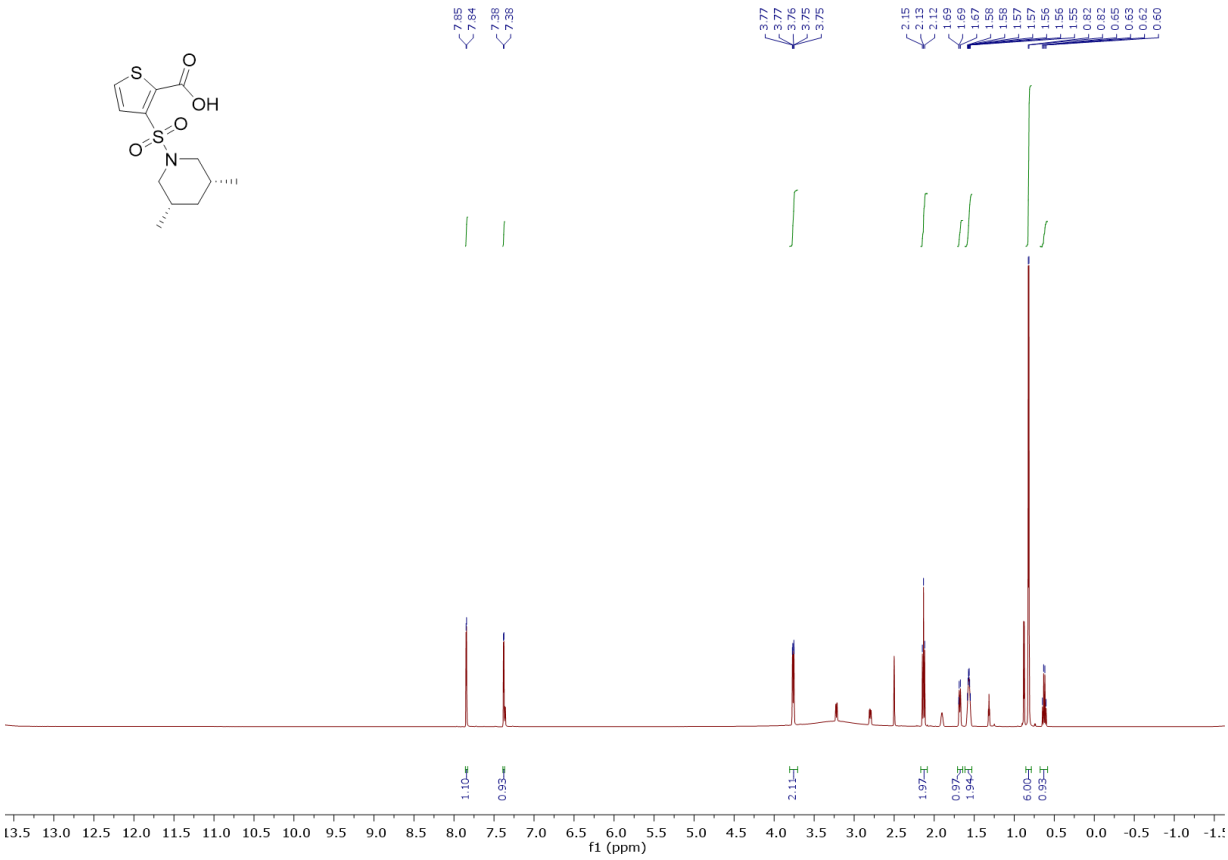
7.85
7.84
7.38
7.38
3.77
3.77
3.76
3.75
3.75
2.15
2.13
2.12
1.69
1.69
1.67
1.58
1.58
1.57
1.57
1.56
1.56
1.55
0.82
0.82
0.65
0.63
0.62
0.60
1.10
0.93
2.11
1.97
0.97
1.94
6.00
0.93
f1 (ppm)

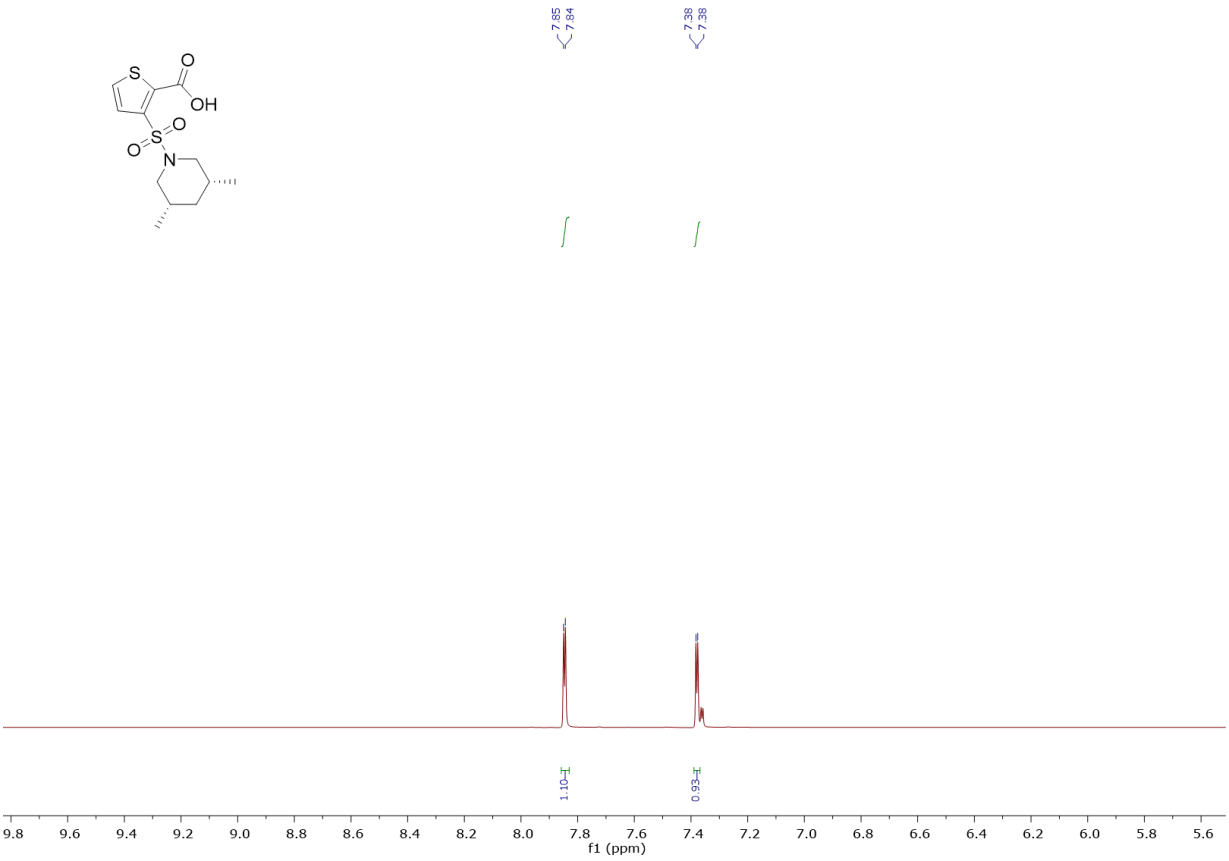
7.85
7.84
7.38
7.38
1.10
0.93
f1 (ppm)

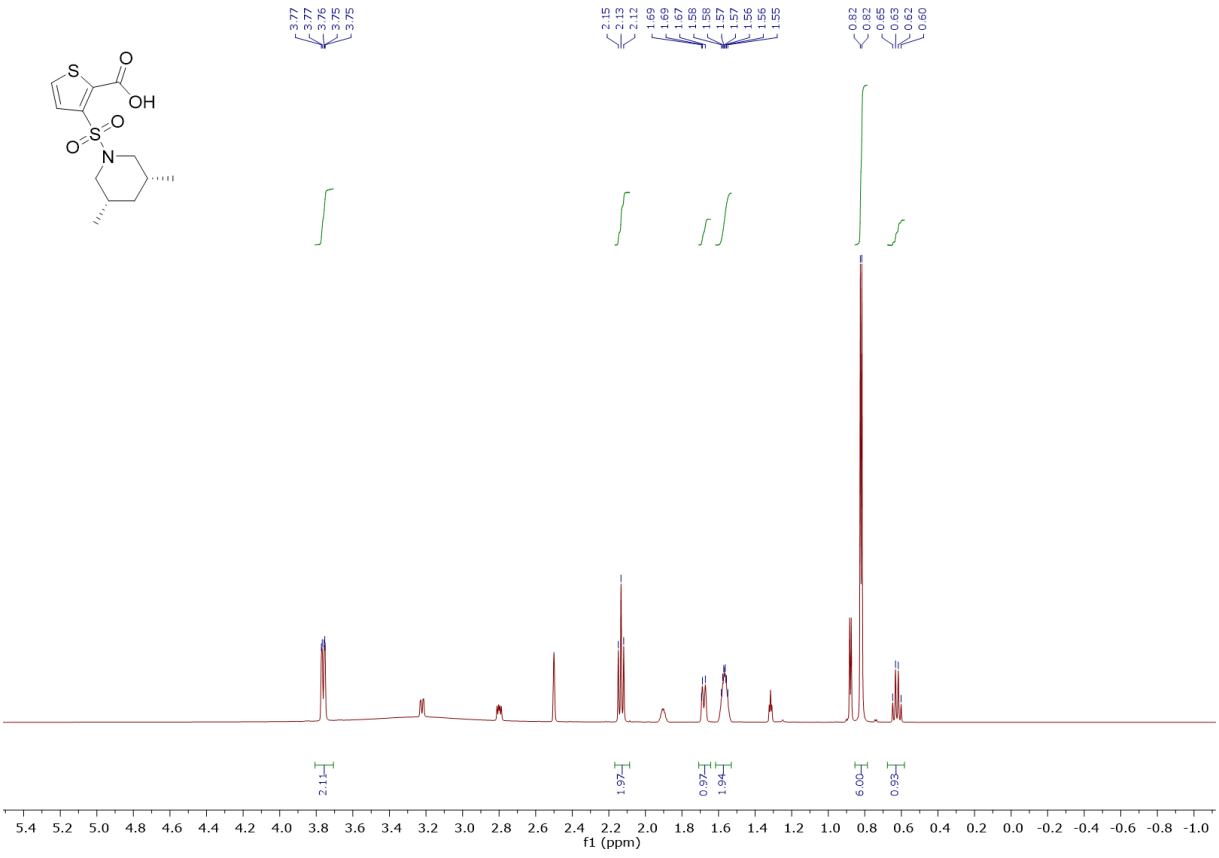
3.77
3.77
3.76
3.75
3.75
2.15
2.13
2.12
1.69
1.69
1.67
1.58
1.58
1.57
1.57
1.56
1.56
1.55
0.82
0.82
0.65
0.63
0.62
0.60
2.11
1.97
0.97
1.94
6.00
0.93
f1 (ppm)

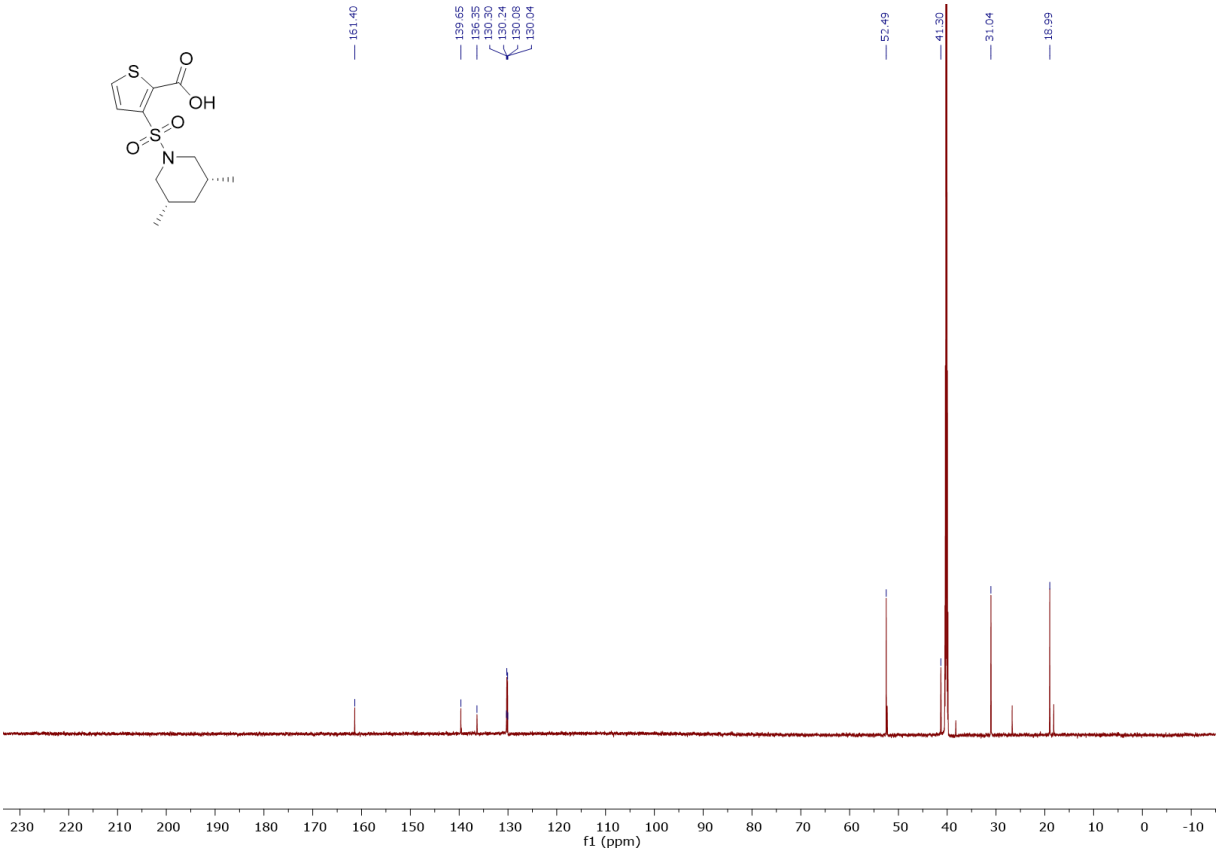
161.40
139.65
136.35
130.30
130.24
130.08
130.04
52.49
41.30
31.04
18.99
f1 (ppm)

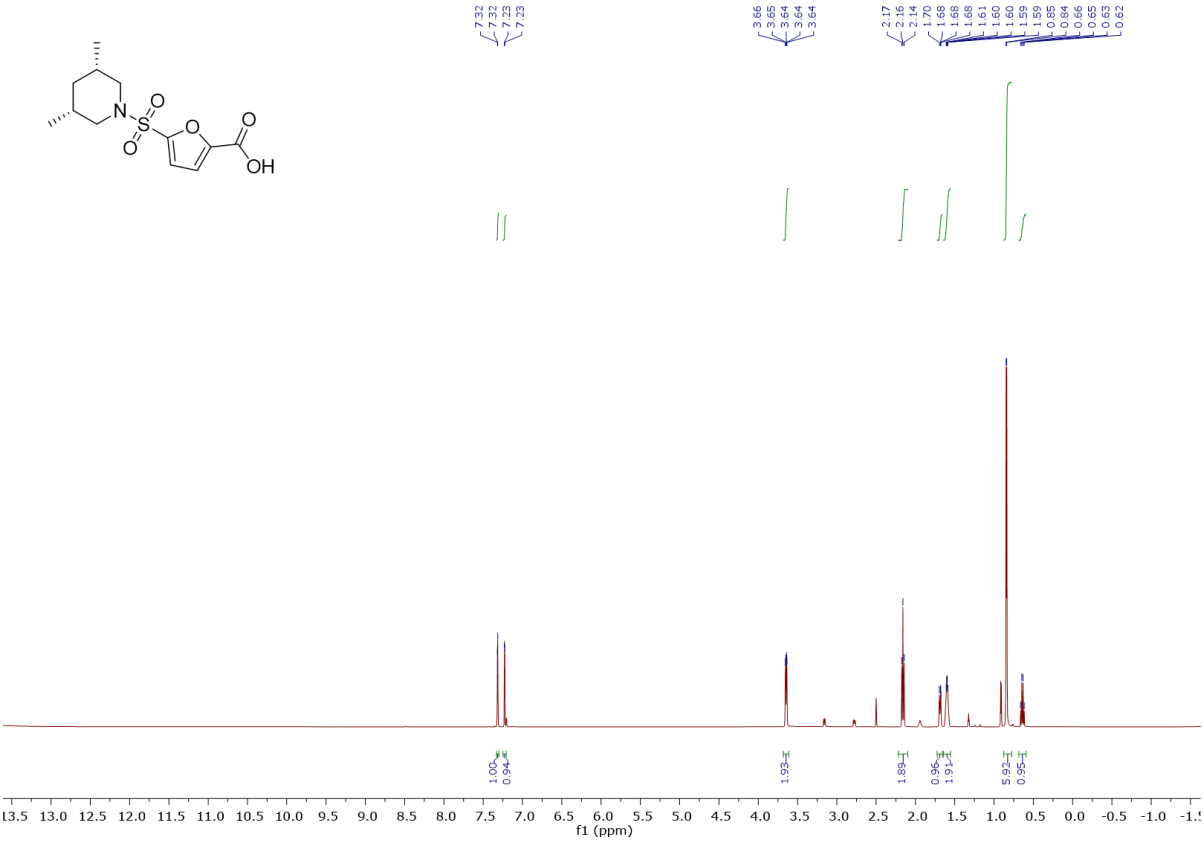
7.32
7.32
7.23
7.23
3.66
3.65
3.64
3.64
3.64
2.17
2.16
2.14
1.70
1.68
1.68
1.68
1.61
1.60
1.60
1.59
1.59
0.85
0.84
0.66
0.65
0.63
0.62
1.00
0.94
1.93
1.89
0.96
1.91
5.93
0.95
f1 (ppm)

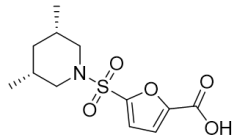
N
S
O
O
O
O
OH

7.32
7.32
7.23
7.23
1.00
0.94
8.3 8.2 8.1 8.0 7.9 7.8 7.7 7.6 7.5 7.4 7.3 7.2 7.1 7.0 6.9 6.8 6.7 6.6 6.5 6.4 6.3 6.2 6.1
f1 (ppm)

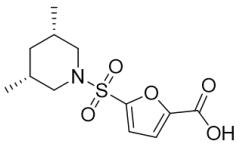
N
S
O
O
O
O
OH

3.66
3.65
3.64
3.64
3.64
2.17
2.16
2.14
1.70
1.68
1.68
1.68
1.61
1.60
1.60
1.59
1.59
0.85
0.84
0.66
0.65
0.63
0.62
1.93
1.89
0.96
1.91
5.92
0.95
5.4 5.2 5.0 4.8 4.6 4.4 4.2 4.0 3.8 3.6 3.4 3.2 3.0 2.8 2.6 2.4 2.2 2.0 1.8 1.6 1.4 1.2 1.0 0.8 0.6 0.4 0.2 0.0 -0.2 -0.4 -0.
f1 (ppm)

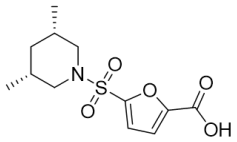

158.78
149.81
148.08
118.04
117.64
52.21
40.92
30.87
18.89
f1 (ppm)

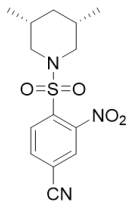

8.26
8.26
7.82
7.81
7.80
7.80
7.36
7.34
3.25
3.24
3.24
3.22
3.22
3.21
2.54
2.52
2.49
1.78
1.77
1.75
1.74
1.70
1.69
1.69
1.68
1.67
1.66
1.66
1.65
1.64
0.83
0.82
0.79
0.76
0.74
0.72
0.98
1.14
1.15
2.06
2.09
1.10
1.97
5.90
1.23
f1 (ppm)

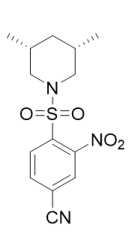
N
O=S=O
NO2
CN

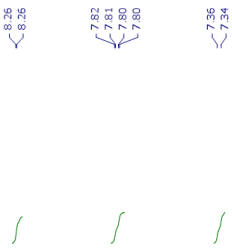
8.26
8.26
7.82
7.81
7.80
7.80
7.36
7.34

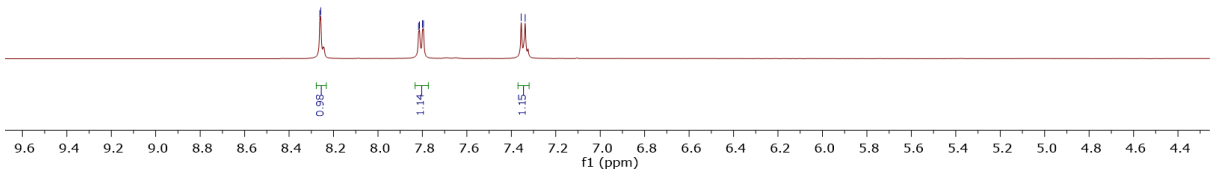
0.98
1.14
1.15
9.6 9.4 9.2 9.0 8.8 8.6 8.4 8.2 8.0 7.8 7.6 7.4 7.2 7.0 6.8 6.6 6.4 6.2 6.0 5.8 5.6 5.4 5.2 5.0 4.8 4.6 4.4
f1 (ppm)

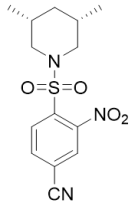
N
O=S=O
NO2
CN

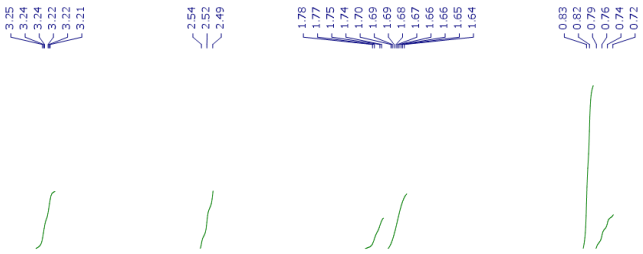
3.25
3.24
3.24
3.22
3.22
3.21
2.54
2.52
2.49
1.78
1.77
1.75
1.74
1.70
1.69
1.69
1.68
1.67
1.66
1.66
1.65
1.64
0.83
0.82
0.79
0.76
0.74
0.72

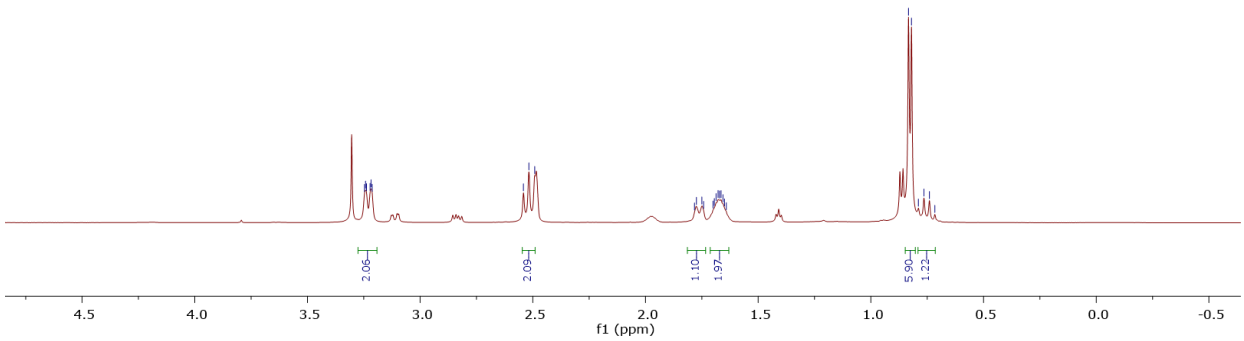
2.06
2.09
1.10
1.97
5.90
1.22
4.5 4.0 3.5 3.0 2.5 2.0 1.5 1.0 0.5 0.0 -0.5
f1 (ppm)

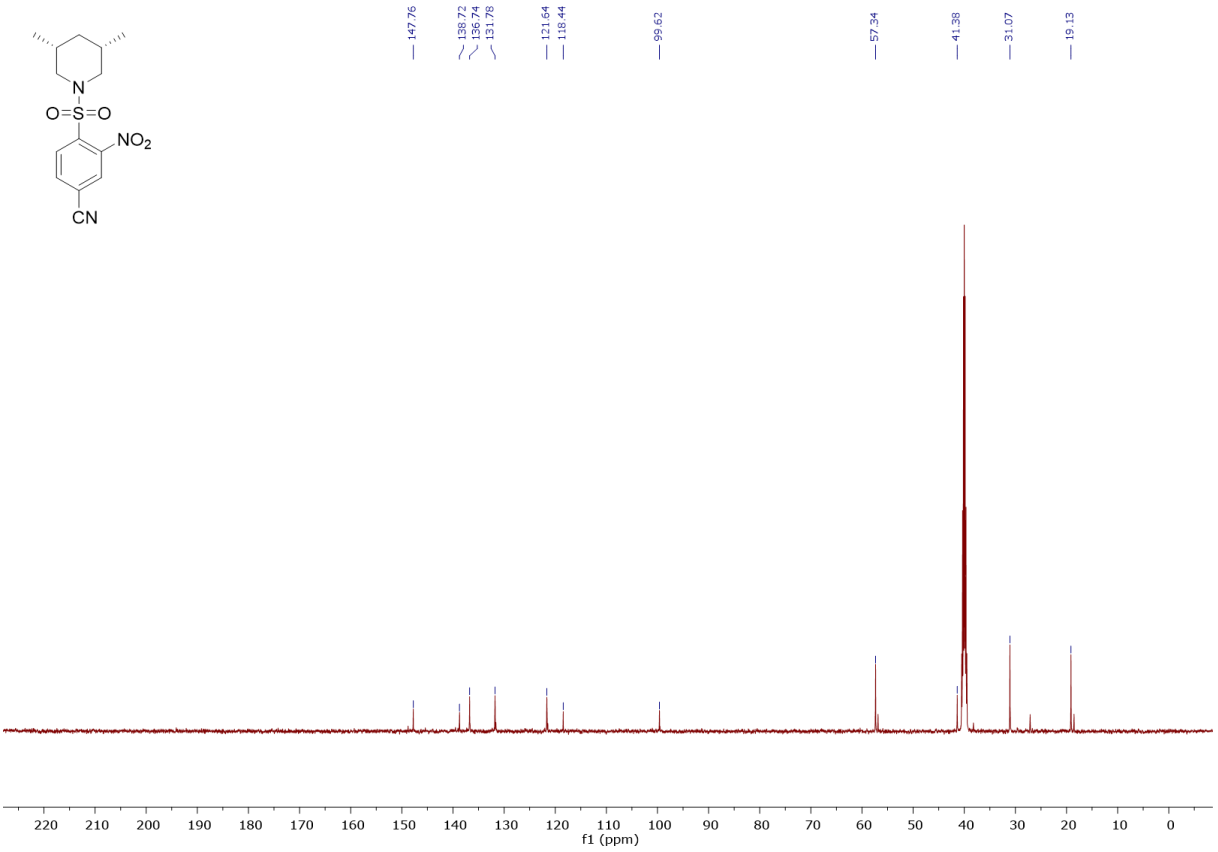
147.76
138.72
136.74
131.78
121.64
118.44
99.62
57.34
41.38
31.07
19.13
O=S=O
NO2
CN
f1 (ppm)

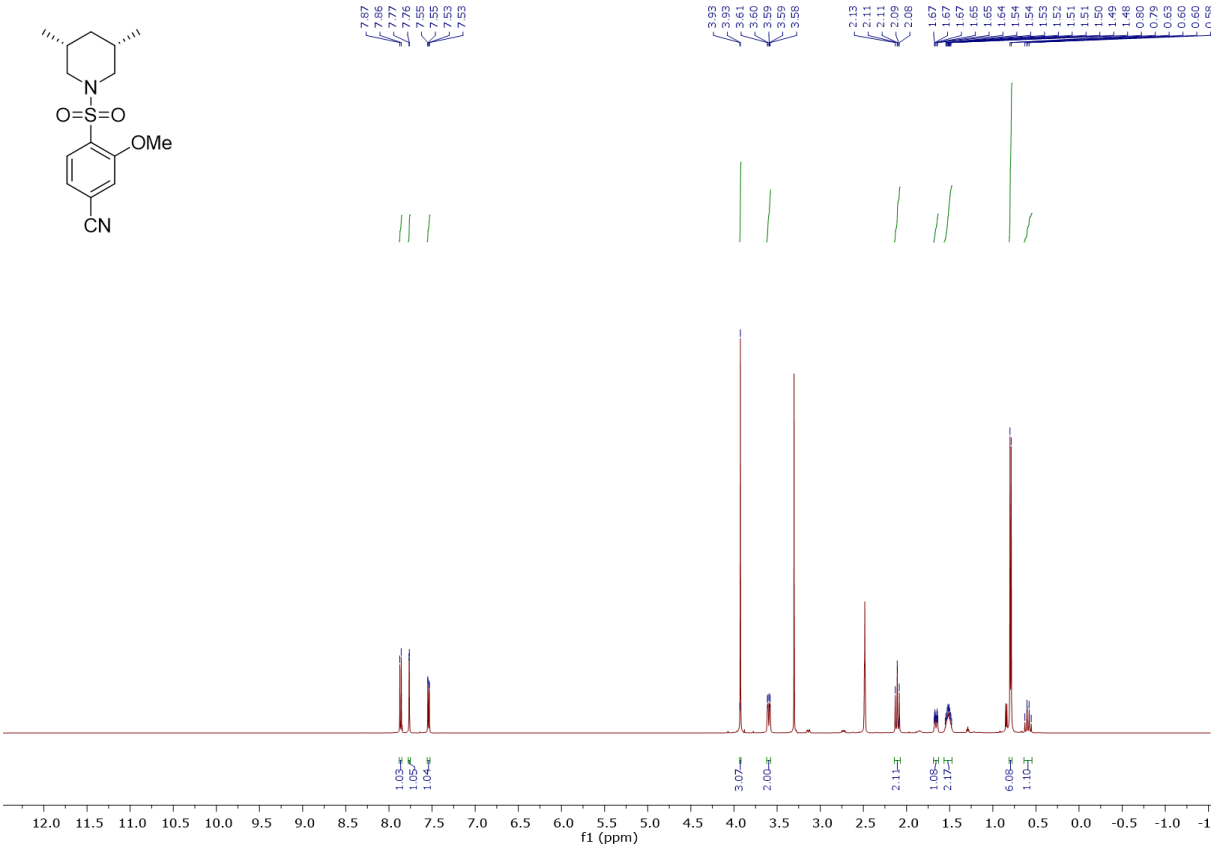
7.87
7.86
7.77
7.76
7.55
7.55
7.53
7.53
3.93
3.93
3.61
3.60
3.59
3.59
3.58
2.13
2.11
2.11
2.09
2.08
1.67
1.67
1.67
1.65
1.65
1.64
1.54
1.54
1.53
1.52
1.51
1.51
1.50
1.48
0.80
0.79
0.63
0.60
0.60
O=S=O
OMe
CN
1.03
1.05
1.04
3.07
2.00
2.11
1.08
2.17
6.08
1.10
f1 (ppm)

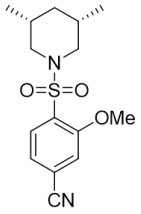
N
O=S=O
OMe
CN

7.87
7.86
7.77
7.76
7.55
7.55
7.53
7.53
1.03
1.05
1.04
f1 (ppm)

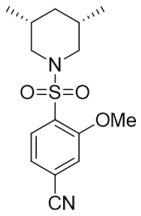
N
O=S=O
OMe
CN

3.93
3.93
3.61
3.60
3.59
3.59
3.59
3.58
2.13
2.11
2.11
2.09
2.08
1.68
1.67
1.67
1.67
1.66
1.65
1.65
1.65
1.64
1.64
1.55
1.54
1.54
1.53
1.52
1.51
1.51
1.50
1.49
1.48
1.48
0.80
0.79
0.63
0.60
0.60
0.60
0.58
0.55
3.07
2.00
2.11
1.08
2.12
6.08
1.10
f1 (ppm)

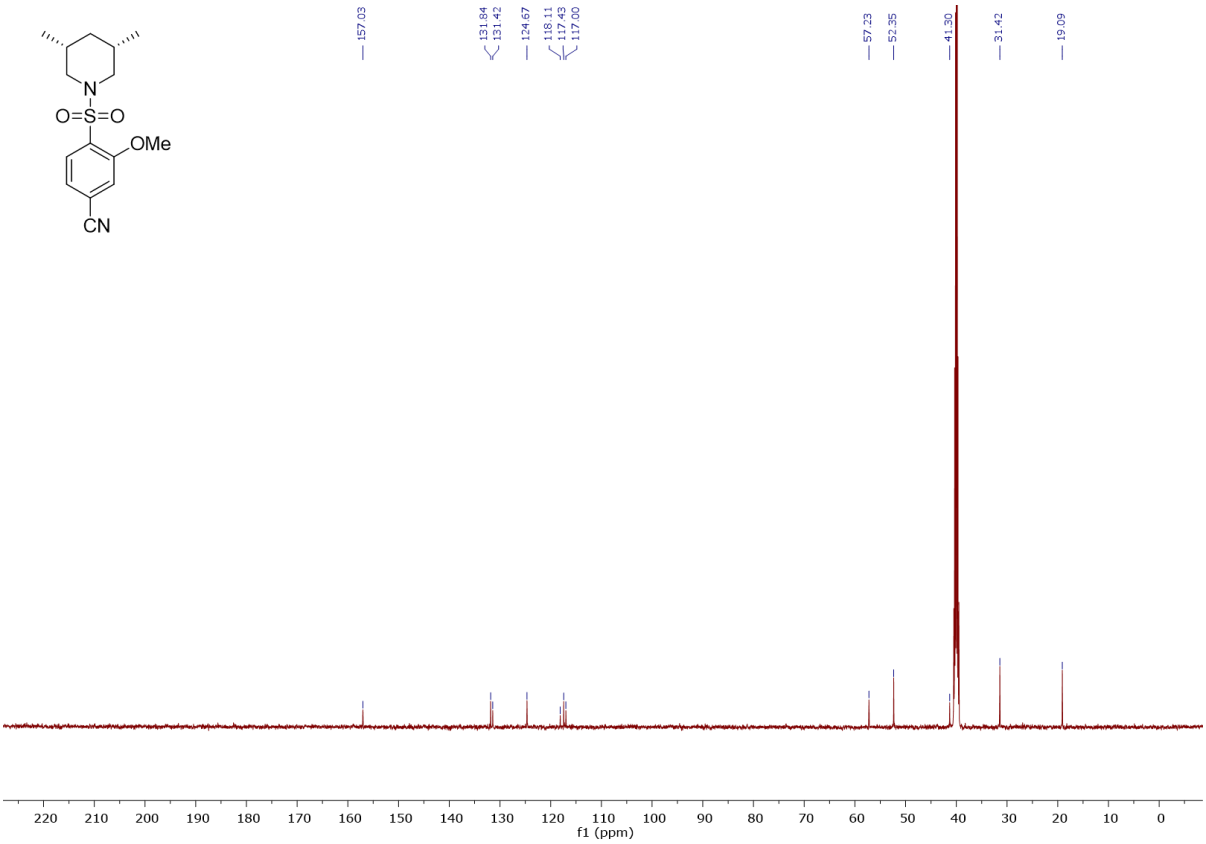
N
O=S=O
OMe
CN
157.03
131.84
131.42
124.67
118.11
117.43
117.00
57.23
52.35
41.30
31.42
19.09
f1 (ppm)

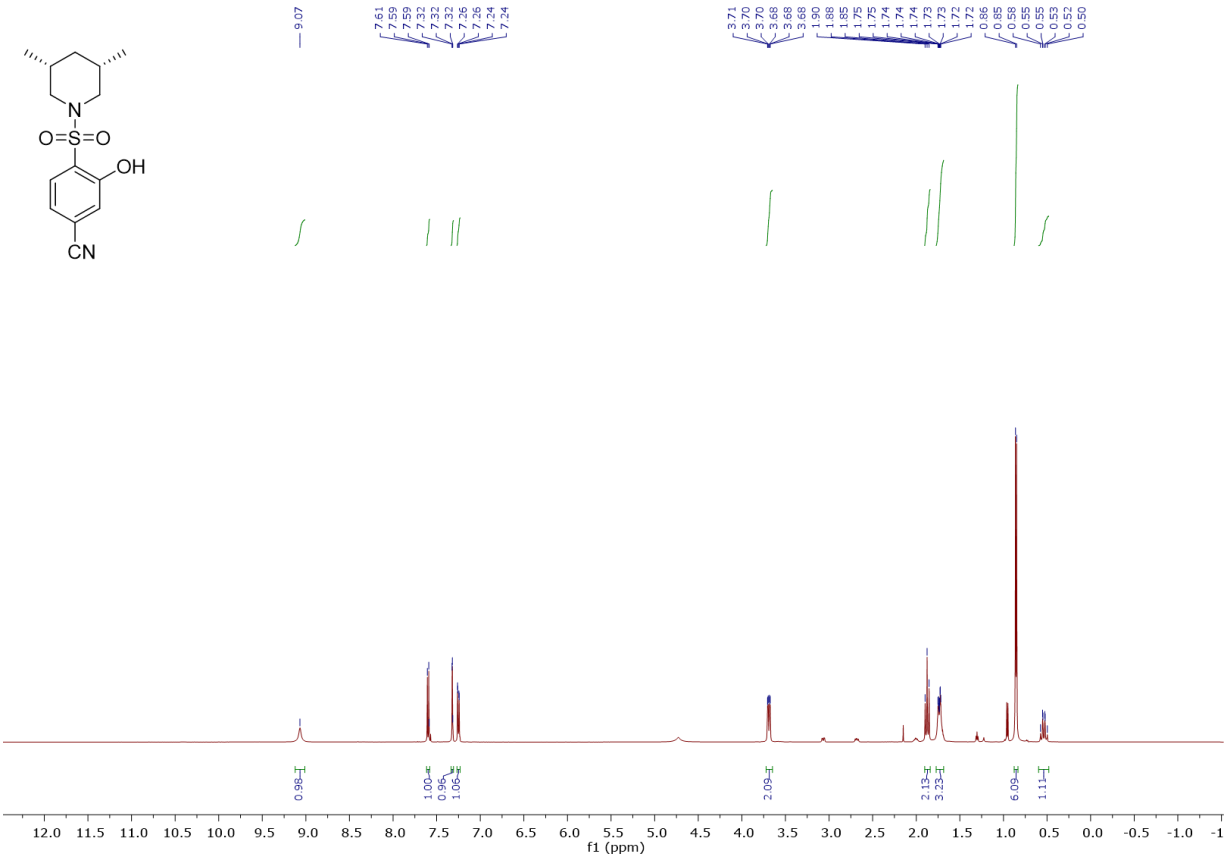
N
O=S=O
OH
CN
9.07
7.61
7.59
7.59
7.32
7.32
7.26
7.26
7.24
7.24
3.71
3.70
3.70
3.68
3.68
3.68
1.90
1.88
1.85
1.75
1.75
1.74
1.74
1.73
1.73
1.72
1.72
0.86
0.85
0.58
0.55
0.55
0.53
0.52
0.50
0.98
1.00
0.96
1.06
2.09
2.13
3.23
6.09
1.11
f1 (ppm)

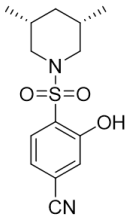
N
O=S=O
OH
CN

9.07
7.61
7.59
7.59
7.32
7.32
7.32
7.26
7.26
7.24
7.24
0.98
1.00
0.96
1.06
f1 (ppm)

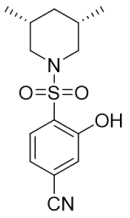
N
O=S=O
OH
CN

3.71
3.70
3.70
3.68
3.68
3.68
1.90
1.88
1.85
1.75
1.75
1.74
1.74
1.74
1.73
1.73
1.72
1.72
0.86
0.85
0.58
0.55
0.55
0.53
0.52
0.50
2.09
2.13
3.23
6.09
1.11
f1 (ppm)

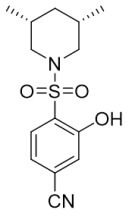
N
O=S=O
OH
CN

155.43
129.44
124.29
123.20
122.78
118.20
117.04
52.44
41.02
30.88
18.87
220 210 200 190 180 170 160 150 140 130 120 110 100 90 80 70 60 50 40 30 20 10 0
f1 (ppm)

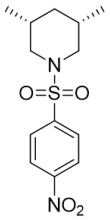
N
O=S=O
NO2

8.42
8.41
8.02
8.01
3.67
3.67
3.67
3.66
3.65
3.65
1.90
1.88
1.87
1.68
1.68
1.68
1.67
1.67
1.67
1.66
1.64
1.64
1.63
1.63
1.62
1.62
1.61
1.61
0.83
0.82
0.57
0.56
0.54
0.53
2.08
1.93
1.94
1.95
2.92
5.96
0.95
13.5 13.0 12.5 12.0 11.5 11.0 10.5 10.0 9.5 9.0 8.5 8.0 7.5 7.0 6.5 6.0 5.5 5.0 4.5 4.0 3.5 3.0 2.5 2.0 1.5 1.0 0.5 0.0 -0.5 -1.0
f1 (ppm)

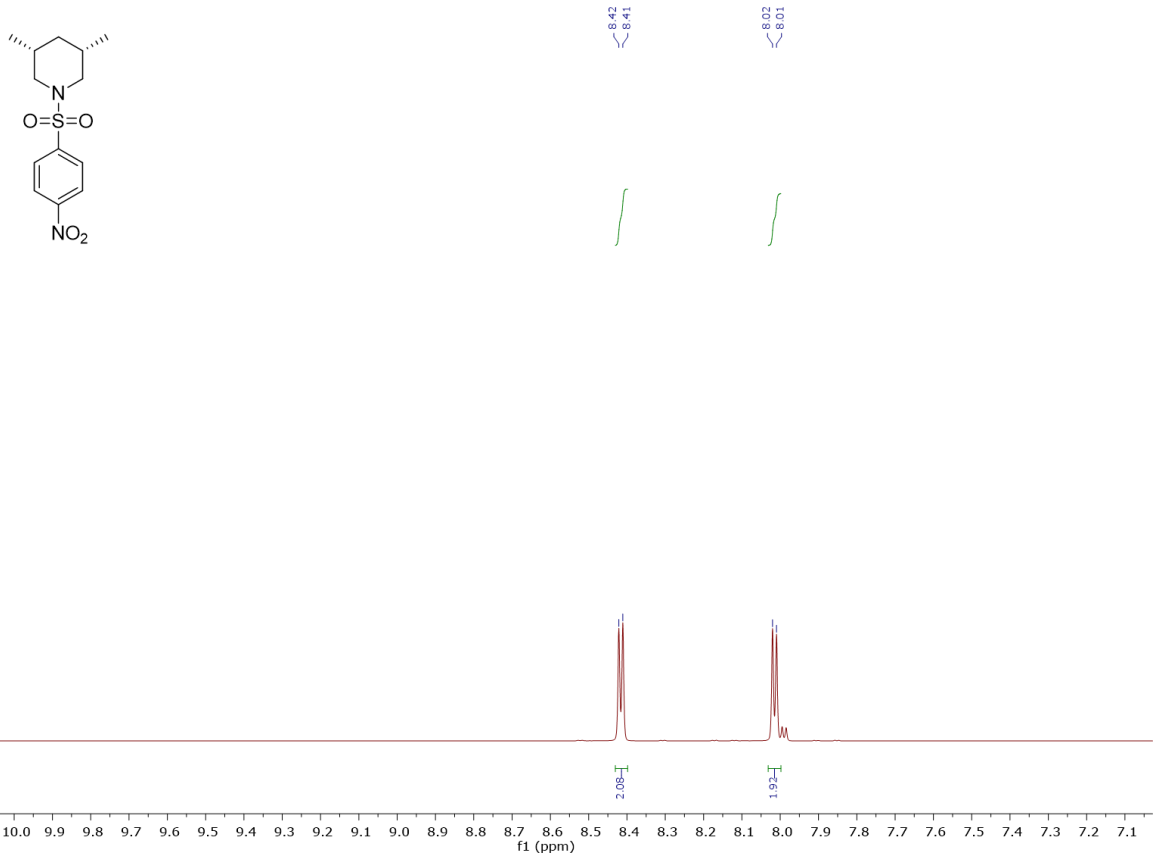
8.42
8.41
8.02
8.01
N
O=S=O
NO2
2.08
1.92
f1 (ppm)

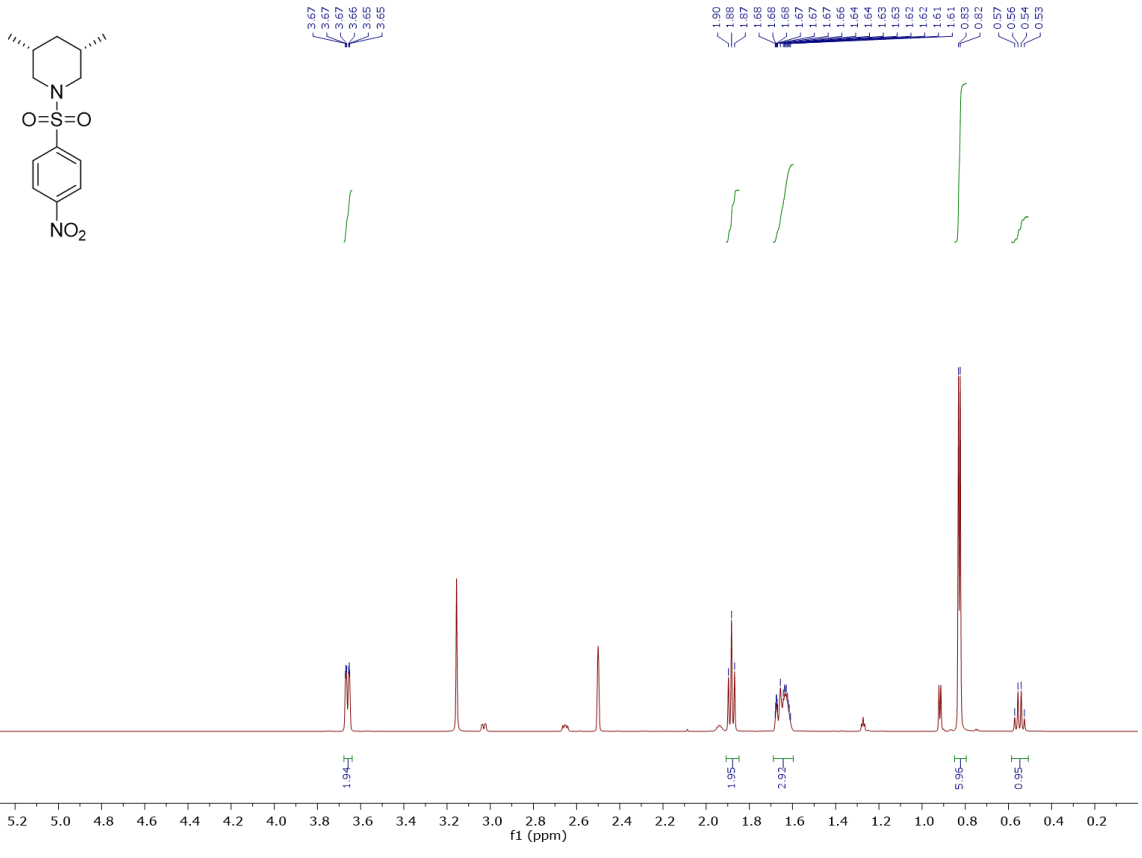
3.67
3.67
3.67
3.66
3.65
3.65
1.90
1.88
1.87
1.68
1.68
1.68
1.67
1.67
1.67
1.66
1.64
1.64
1.63
1.63
1.62
1.62
1.61
1.61
0.83
0.82
0.57
0.56
0.54
0.53
N
O=S=O
NO2
1.94
1.95
2.92
5.96
0.95
f1 (ppm)

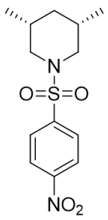
N
O=S=O
NO2

150.39
142.61
129.18
124.96
52.45
40.98
30.94
18.95
230 220 210 200 190 180 170 160 150 140 130 120 110 100 90 80 70 60 50 40 30 20 10 0 -10
f1 (ppm)

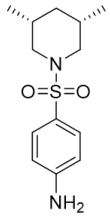
N
O=S=O
NH2

7.37
7.36
7.35
6.67
6.66
5.85
3.54
3.53
3.52
3.52
1.67
1.66
1.65
1.63
1.61
1.61
1.60
0.81
0.80
0.49
0.47
0.46
0.44
1.89
2.10
1.98
1.86
4.89
5.97
0.91
13.5 13.0 12.5 12.0 11.5 11.0 10.5 10.0 9.5 9.0 8.5 8.0 7.5 7.0 6.5 6.0 5.5 5.0 4.5 4.0 3.5 3.0 2.5 2.0 1.5 1.0 0.5 0.0 -0.5 -1.0
f1 (ppm)

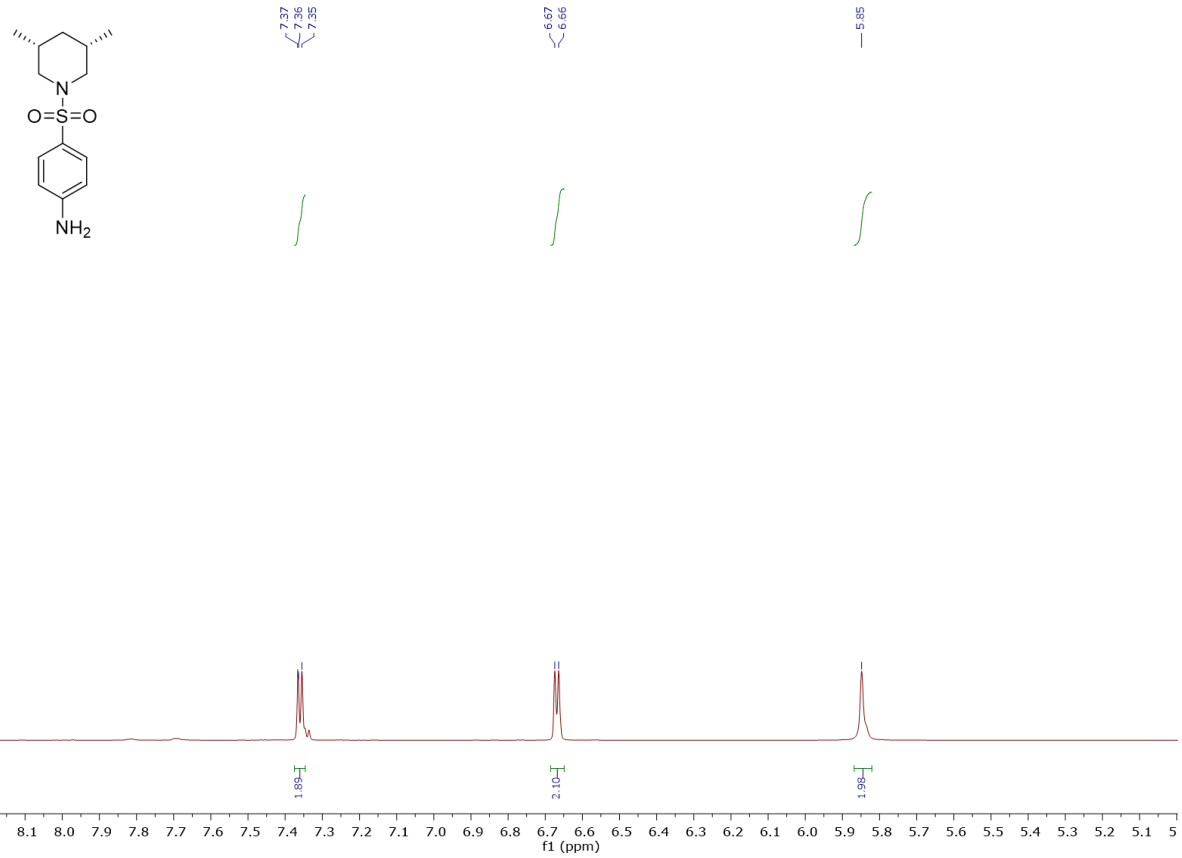
7.37
7.36
7.35
6.67
6.66
5.85
1.89
2.10
1.96
8.2 8.1 8.0 7.9 7.8 7.7 7.6 7.5 7.4 7.3 7.2 7.1 7.0 6.9 6.8 6.7 6.6 6.5 6.4 6.3 6.2 6.1 6.0 5.9 5.8 5.7 5.6 5.5 5.4 5.3 5.2 5.1 5
f1 (ppm)

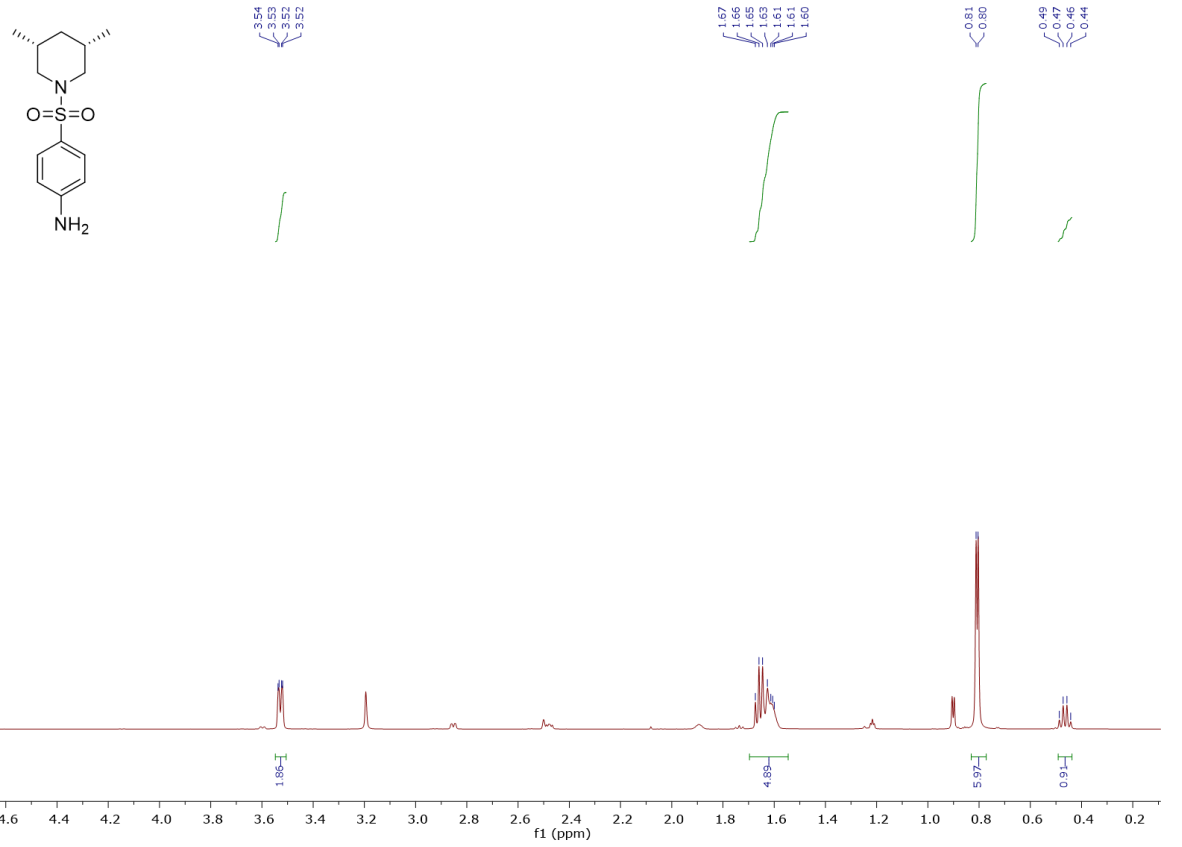
3.54
3.53
3.52
3.52
1.67
1.66
1.65
1.63
1.61
1.61
1.60
0.81
0.80
0.49
0.47
0.46
0.44
1.86
4.89
5.97
0.91
4.6 4.4 4.2 4.0 3.8 3.6 3.4 3.2 3.0 2.8 2.6 2.4 2.2 2.0 1.8 1.6 1.4 1.2 1.0 0.8 0.6 0.4 0.2
f1 (ppm)

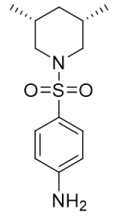
N
O=S=O
NH2

153.26
129.58
121.57
113.27
52.83
41.33
30.82
19.15
230 220 210 200 190 180 170 160 150 140 130 120 110 100 90 80 70 60 50 40 30 20 10 0 -10
f1 (ppm)

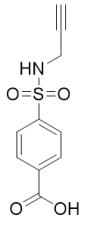
HN
O=S=O
O
OH


8.19
8.18
8.18
8.11
8.11
8.10
7.93
7.93
7.92
3.76
3.75
2.94

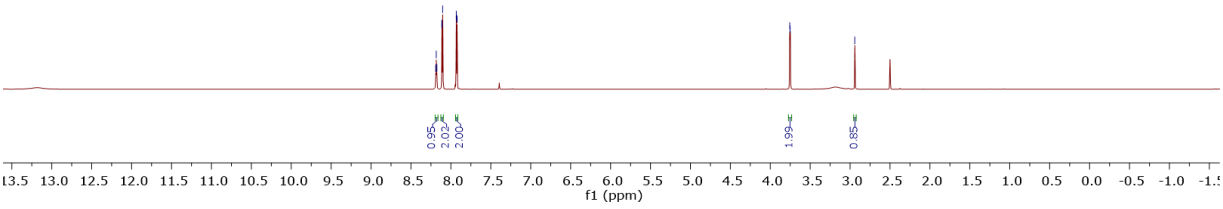
0.95
2.02
2.00
1.99
0.85
13.5 13.0 12.5 12.0 11.5 11.0 10.5 10.0 9.5 9.0 8.5 8.0 7.5 7.0 6.5 6.0 5.5 5.0 4.5 4.0 3.5 3.0 2.5 2.0 1.5 1.0 0.5 0.0 -0.5 -1.0
f1 (ppm)

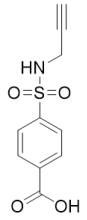
HN
O=S=O
O
OH

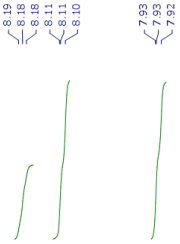
8.19
8.18
8.18
8.11
8.11
8.10
7.93
7.93
7.92

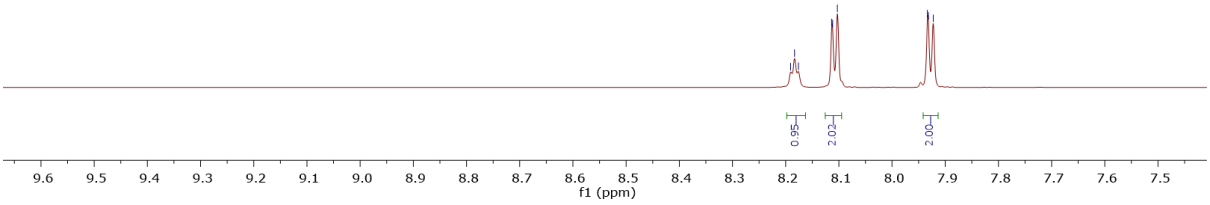
0.95
2.02
2.00
9.6 9.5 9.4 9.3 9.2 9.1 9.0 8.9 8.8 8.7 8.6 8.5 8.4 8.3 8.2 8.1 8.0 7.9 7.8 7.7 7.6 7.5
f1 (ppm)

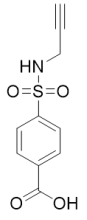
HN
O=S=O
O
OH


3.76
3.75
2.94

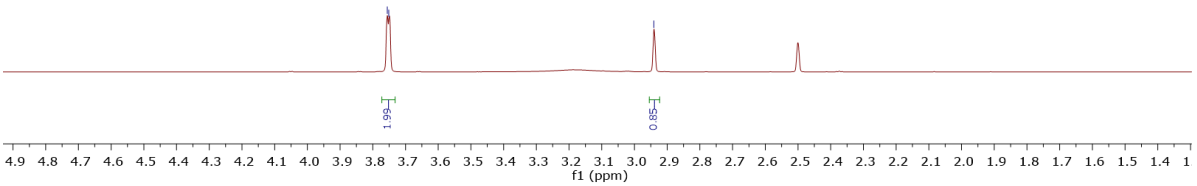
1.99
0.85
4.9 4.8 4.7 4.6 4.5 4.4 4.3 4.2 4.1 4.0 3.9 3.8 3.7 3.6 3.5 3.4 3.3 3.2 3.1 3.0 2.9 2.8 2.7 2.6 2.5 2.4 2.3 2.2 2.1 2.0 1.9 1.8 1.7 1.6 1.5 1.4 1
f1 (ppm)

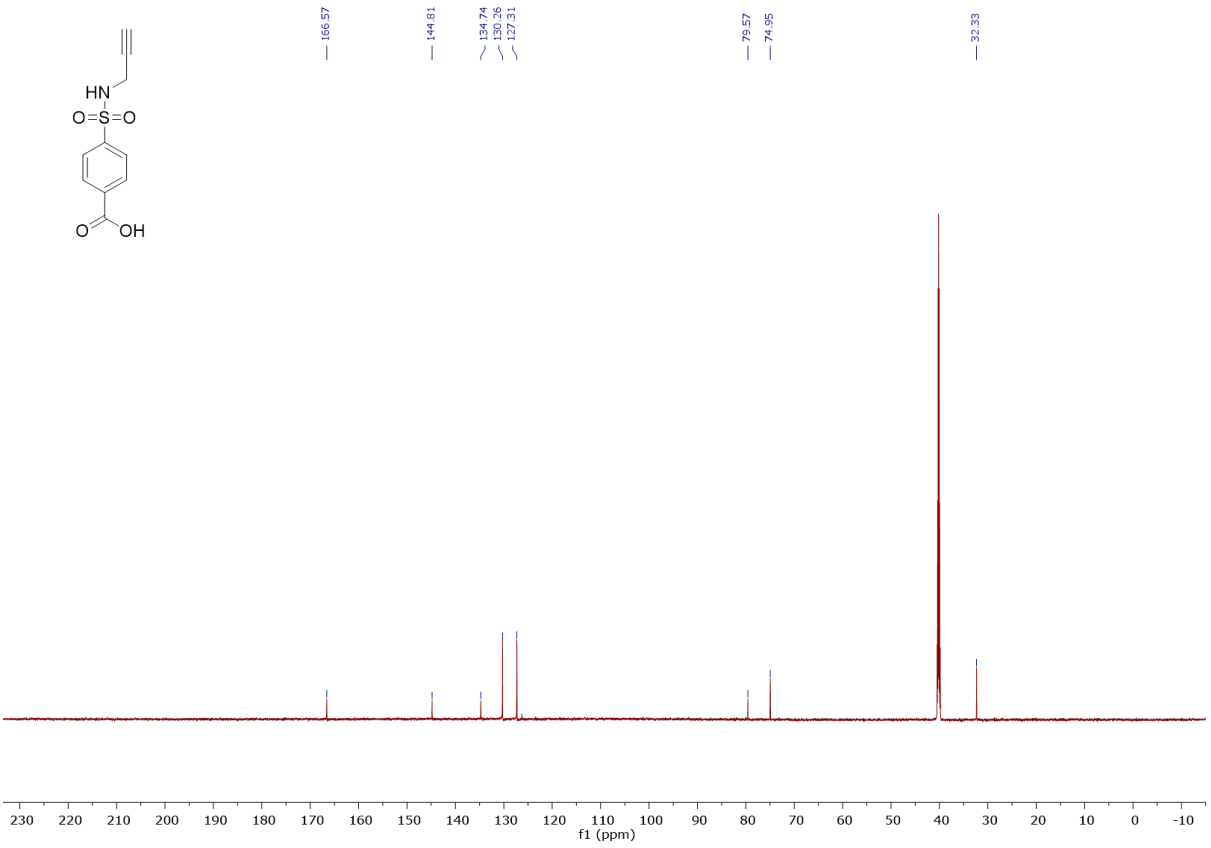
166.57
144.81
134.74
130.26
127.31
79.57
74.95
32.33
HN
O=S=O
O
OH
f1 (ppm)

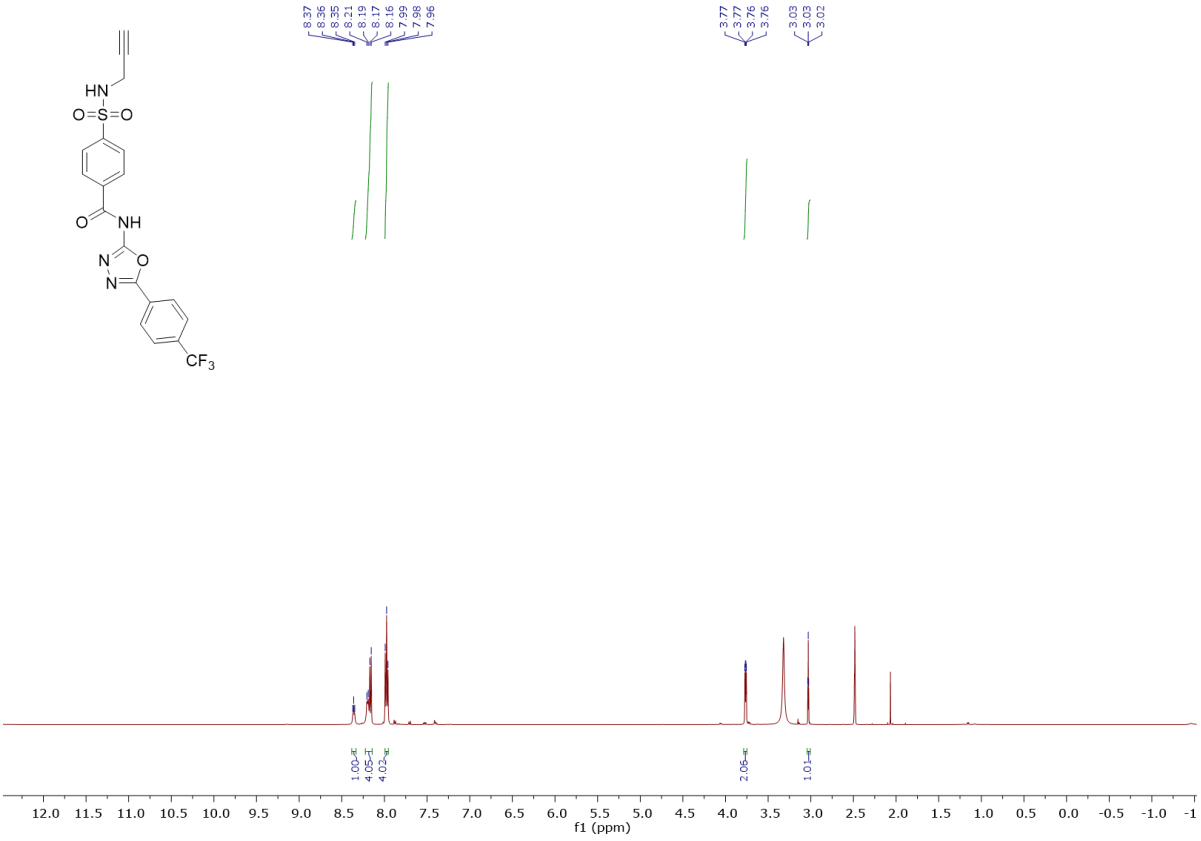
8.37
8.36
8.35
8.21
8.19
8.17
8.16
7.99
7.98
7.96
3.77
3.77
3.76
3.76
3.03
3.03
3.02
HN
O=S=O
O
NH
N
O
N
CF3
1.00
4.05
4.02
2.06
1.01
f1 (ppm)

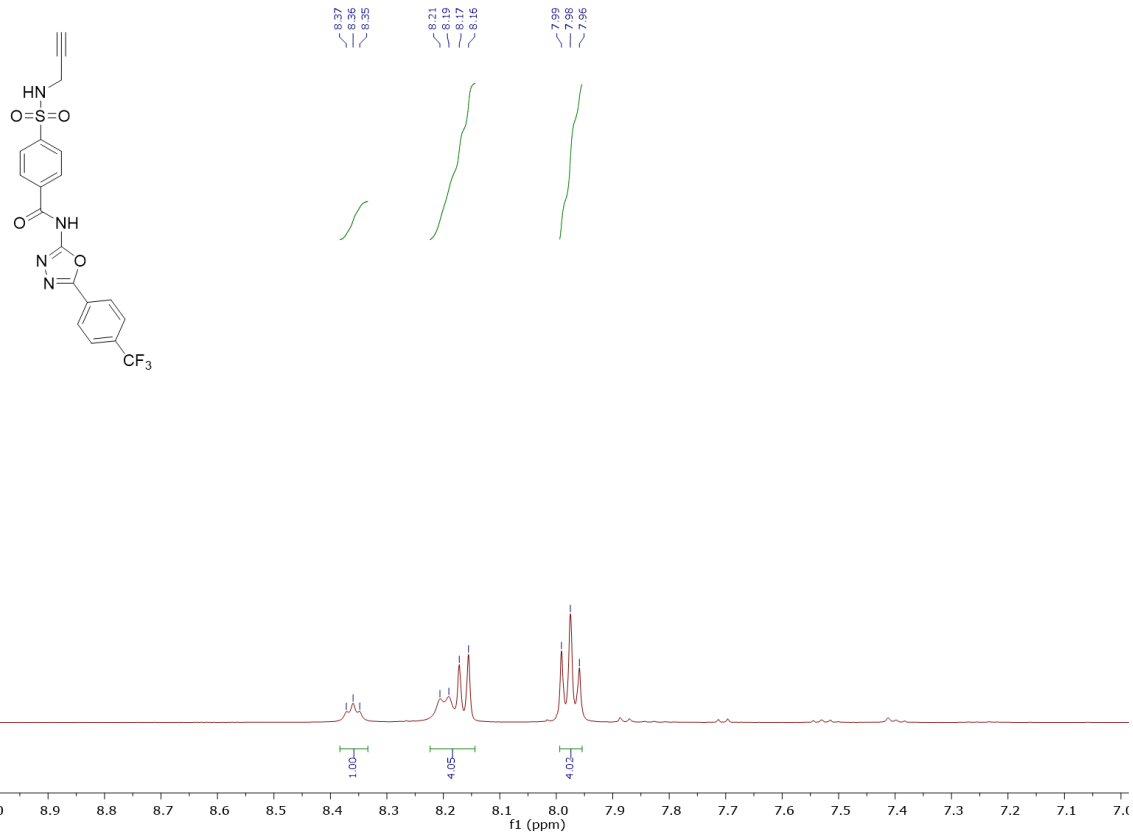
8.37
8.36
8.35
8.21
8.19
8.17
8.16
7.99
7.98
7.96
HN
O=S=O
O
NH
N
O
N
CF3
1.00
4.05
4.02
9.0 8.9 8.8 8.7 8.6 8.5 8.4 8.3 8.2 8.1 8.0 7.9 7.8 7.7 7.6 7.5 7.4 7.3 7.2 7.1
f1 (ppm)

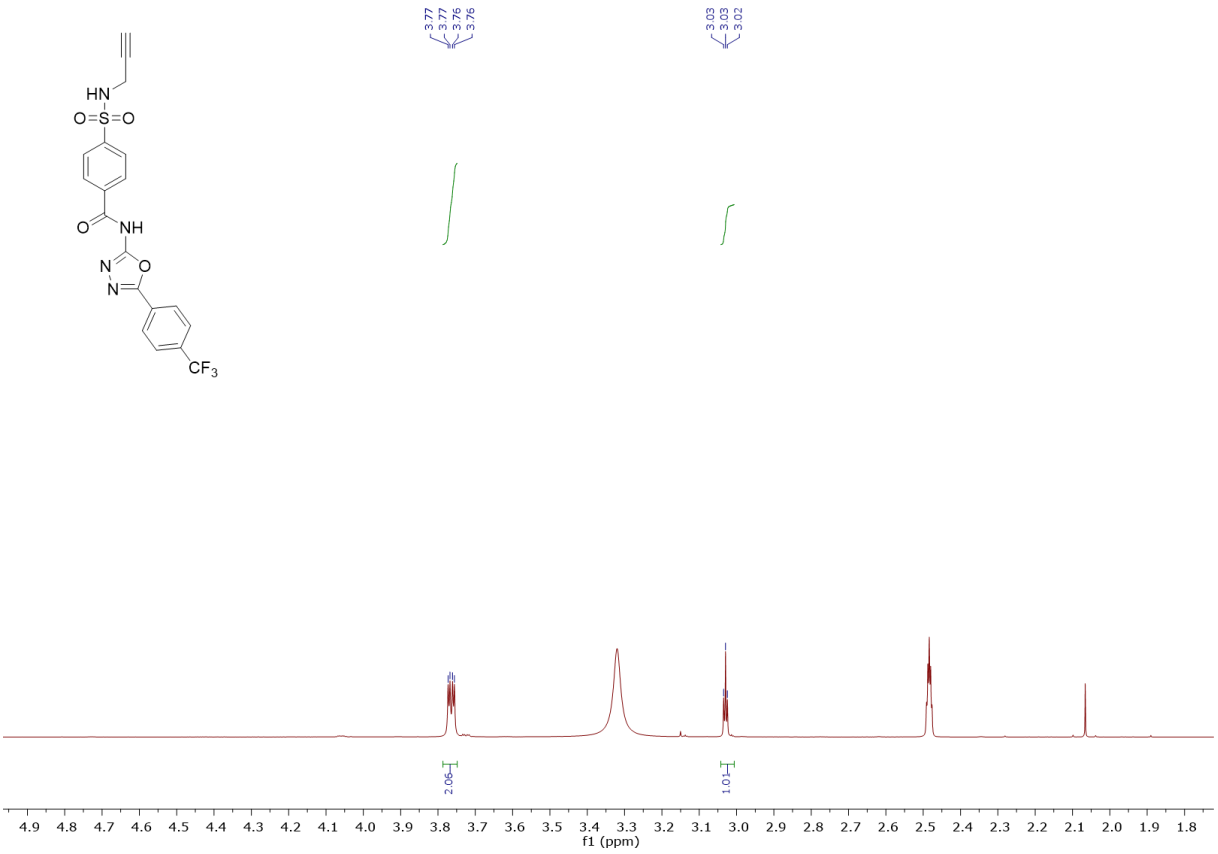
3.77
3.77
3.76
3.76
3.03
3.03
3.02
HN
O=S=O
O
NH
N
O
N
CF3
2.06
1.01
4.9 4.8 4.7 4.6 4.5 4.4 4.3 4.2 4.1 4.0 3.9 3.8 3.7 3.6 3.5 3.4 3.3 3.2 3.1 3.0 2.9 2.8 2.7 2.6 2.5 2.4 2.3 2.2 2.1 2.0 1.9 1.8
f1 (ppm)

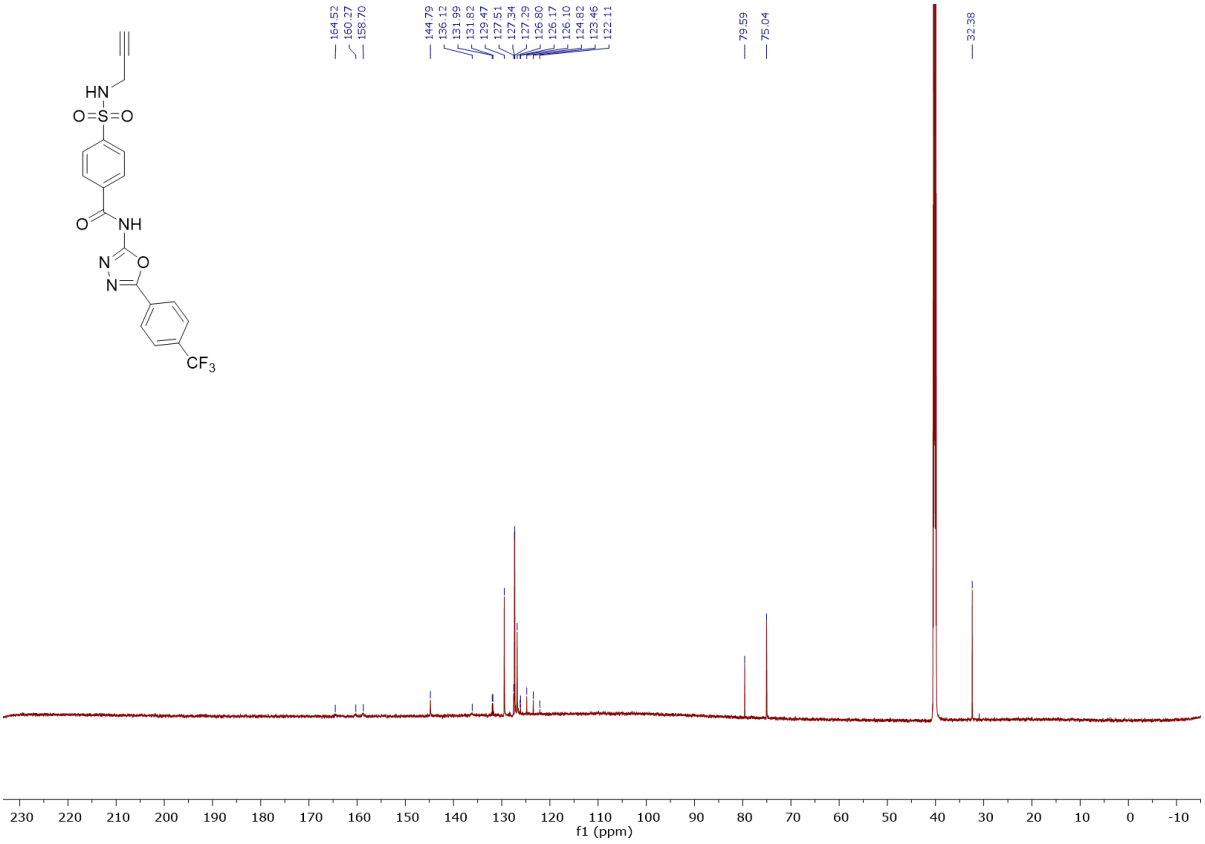
164.52
160.27
158.70
144.79
136.12
131.99
131.82
129.47
127.51
127.34
127.29
126.80
126.17
126.10
124.82
123.46
122.11
79.59
75.04
32.38
HN
O=S=O
O
NH
N
O
N
CF3
230 220 210 200 190 180 170 160 150 140 130 120 110 100 90 80 70 60 50 40 30 20 10 0 -10
f1 (ppm)

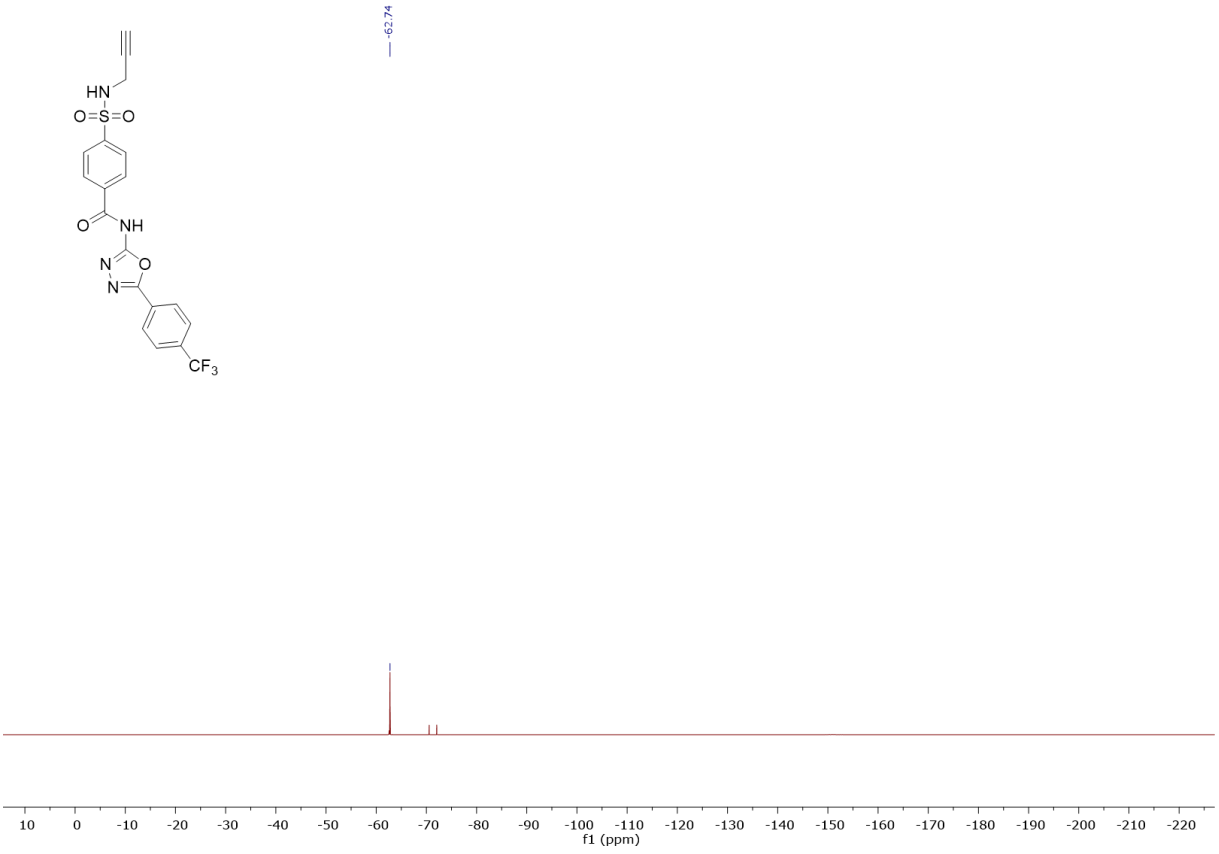
-62.74
HN
O=S=O
O
NH
N
O
N
CF3
10 0 -10 -20 -30 -40 -50 -60 -70 -80 -90 -100 -110 -120 -130 -140 -150 -160 -170 -180 -190 -200 -210 -220
f1 (ppm)

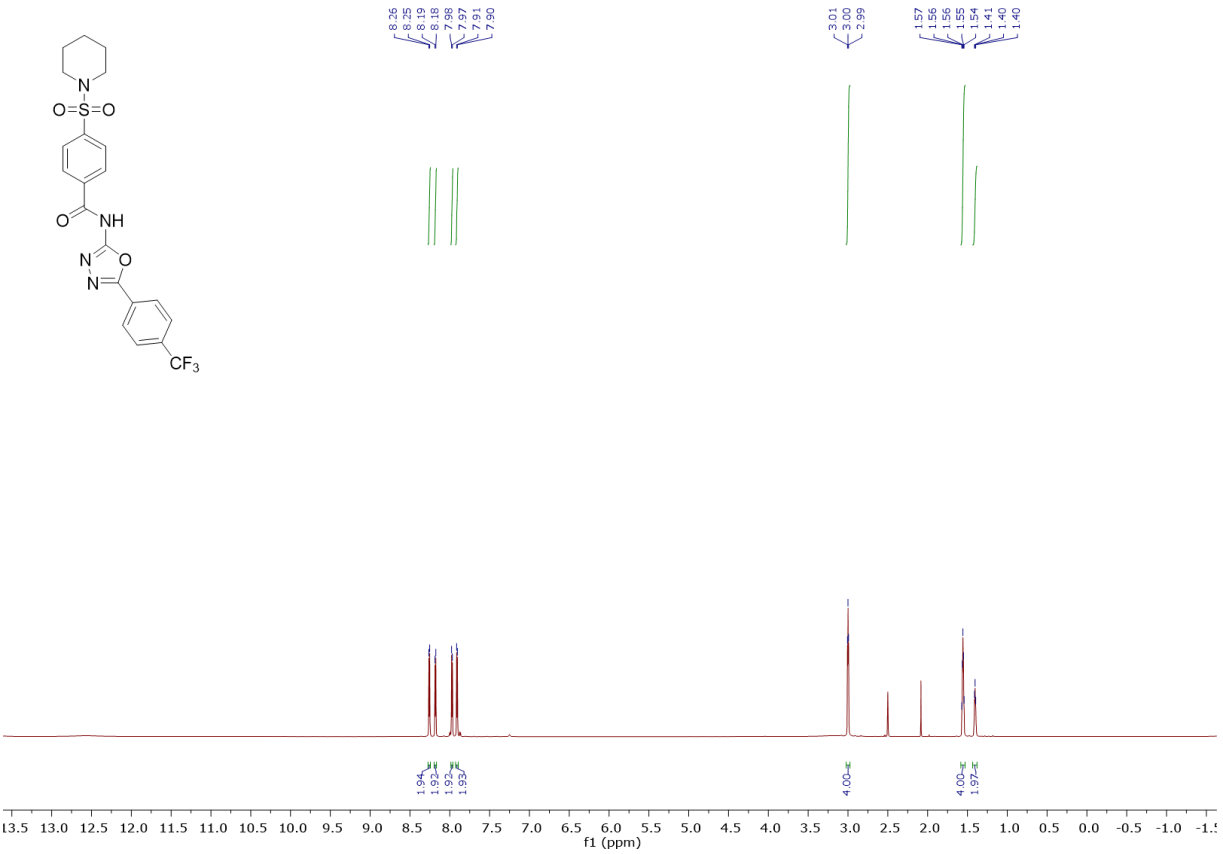
8.26
8.25
8.19
8.18
7.98
7.97
7.91
7.90
3.01
3.00
2.99
1.57
1.56
1.56
1.55
1.54
1.41
1.40
1.40
O=S=O
NH
N
O
CF3
1.94
1.92
1.92
1.93
4.00
4.00
1.97
f1 (ppm)

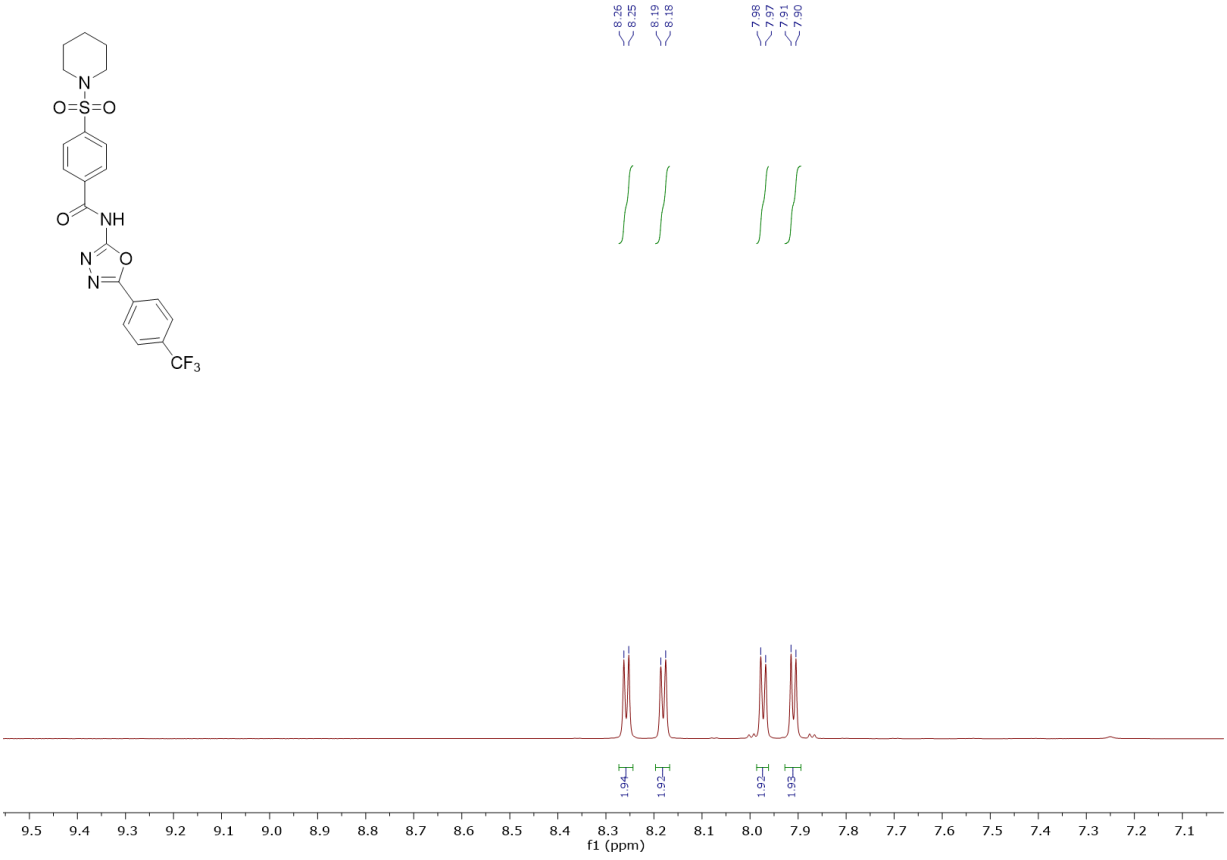
8.26
8.25
8.19
8.18
7.98
7.97
7.91
7.90
O=S=O
NH
N
O
CF3
1.94
1.92
1.92
1.93
f1 (ppm)

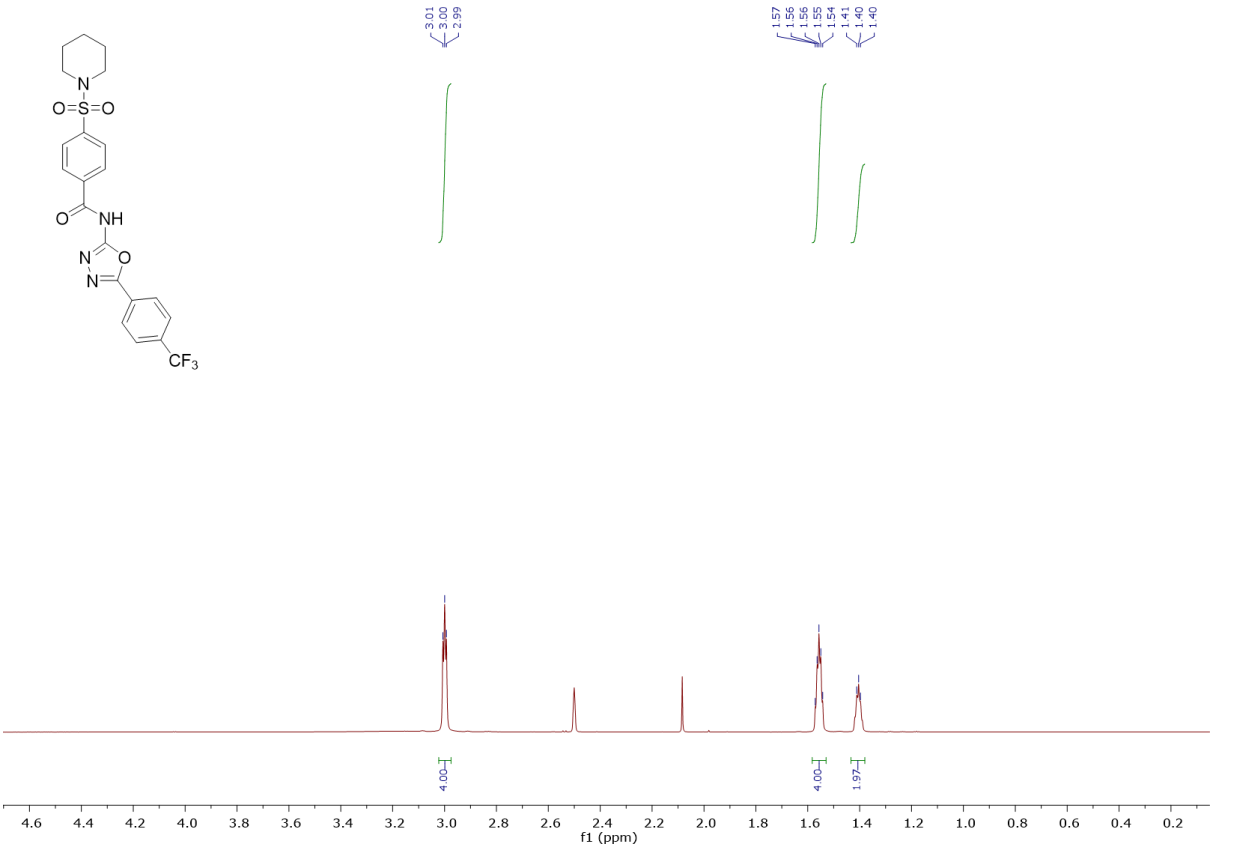
3.01
3.00
2.99
1.57
1.56
1.56
1.55
1.54
1.41
1.40
1.40
4.00
4.00
1.97
f1 (ppm)

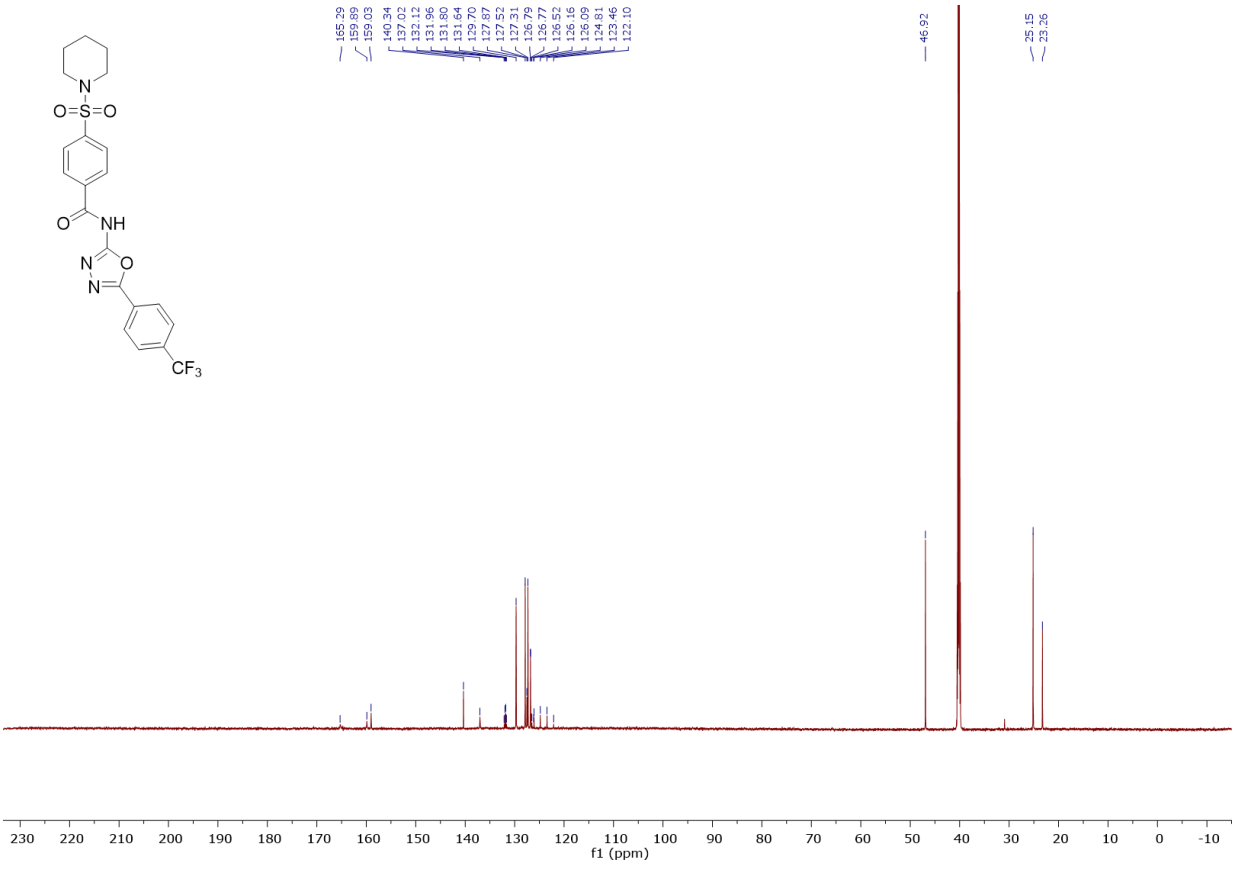
165.29
159.89
159.03
140.34
137.02
132.12
131.96
131.80
131.64
129.70
127.87
127.52
127.31
126.79
126.77
126.52
126.16
126.09
124.81
123.46
122.10
46.92
25.15
23.26
f1 (ppm)

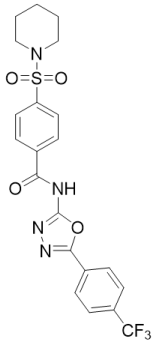
N
O=S=O
O
NH
N
O
N
CF3

-62.78
10 0 -10 -20 -30 -40 -50 -60 -70 -80 -90 -100 -110 -120 -130 -140 -150 -160 -170 -180 -190 -200 -210 -220
f1 (ppm)

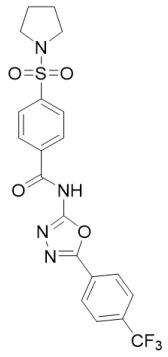
N
O=S=O
O
NH
N
O
N
CF3

8.33
8.32
8.14
8.13
8.12
7.92
7.91
7.89
7.88
3.20
3.19
3.18
1.68
1.68
1.67
1.97
1.95
4.00
3.98
4.04
13.5 13.0 12.5 12.0 11.5 11.0 10.5 10.0 9.5 9.0 8.5 8.0 7.5 7.0 6.5 6.0 5.5 5.0 4.5 4.0 3.5 3.0 2.5 2.0 1.5 1.0 0.5 0.0 -0.5 -1.0
f1 (ppm)

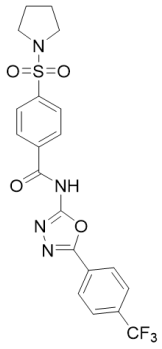

8.33
8.32
8.14
8.13
8.12
7.92
7.91
7.89
7.88
1.97
1.95
4.00
9.4 9.3 9.2 9.1 9.0 8.9 8.8 8.7 8.6 8.5 8.4 8.3 8.2 8.1 8.0 7.9 7.8 7.7 7.6 7.5 7.4 7.3 7.2
f1 (ppm)

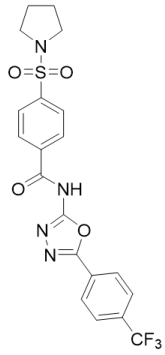

3.20
3.19
3.18
1.68
1.68
1.67
3.99
4.04
5.2 5.0 4.8 4.6 4.4 4.2 4.0 3.8 3.6 3.4 3.2 3.0 2.8 2.6 2.4 2.2 2.0 1.8 1.6 1.4 1.2 1.0
f1 (ppm)

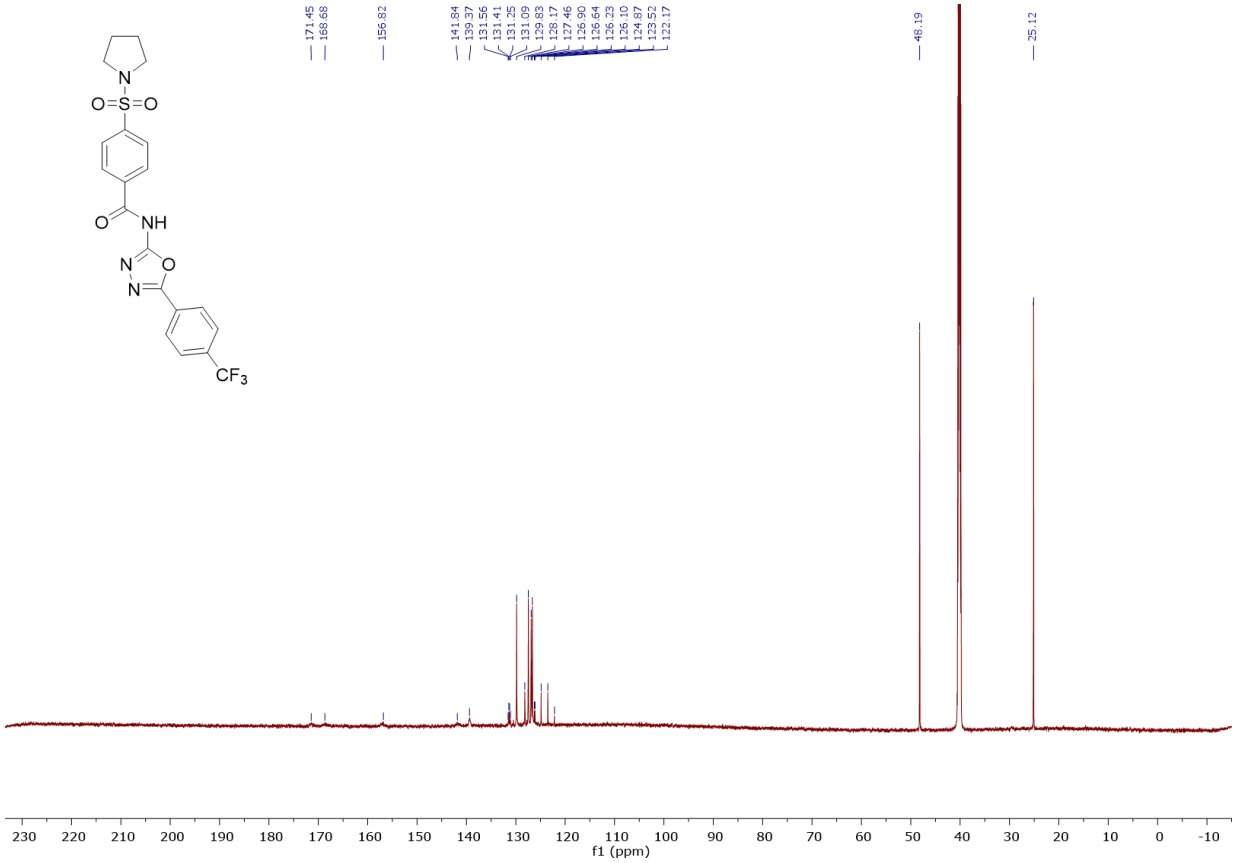
171.45
168.68
156.82
141.84
139.37
131.56
131.41
131.25
131.09
129.83
128.17
127.46
126.90
126.64
126.23
126.10
124.87
123.52
122.17
48.19
25.12
230 220 210 200 190 180 170 160 150 140 130 120 110 100 90 80 70 60 50 40 30 20 10 0 -10
f1 (ppm)


-62.70
10 0 -10 -20 -30 -40 -50 -60 -70 -80 -90 -100 -110 -120 -130 -140 -150 -160 -170 -180 -190 -200 -210 -220
f1 (ppm)

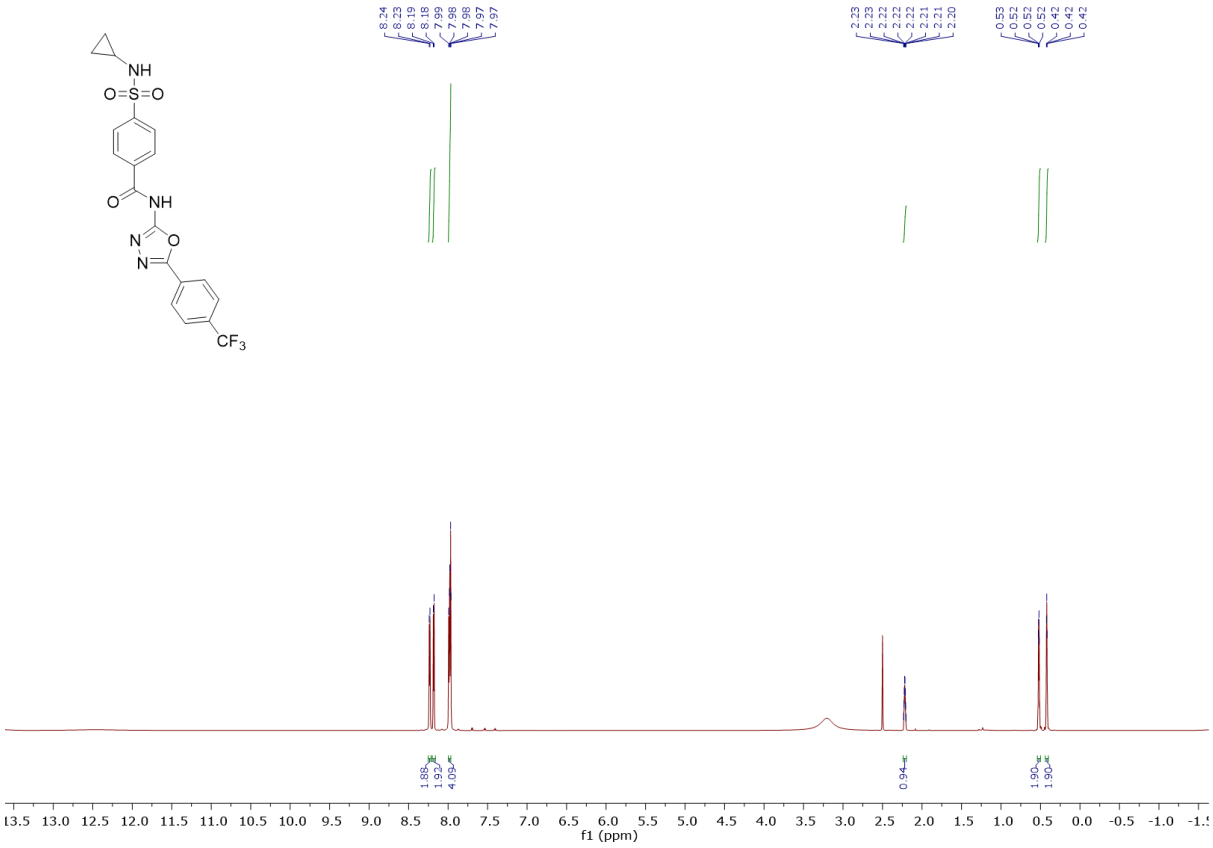
NH
O=S=O
O
NH
N
O
N
CF3
8.24
8.23
8.19
8.18
7.99
7.98
7.98
7.97
7.97
2.23
2.23
2.22
2.22
2.22
2.21
2.21
2.20
0.53
0.52
0.52
0.52
0.42
0.42
0.42
1.88
1.92
4.09
0.94
1.90
1.90
f1 (ppm)

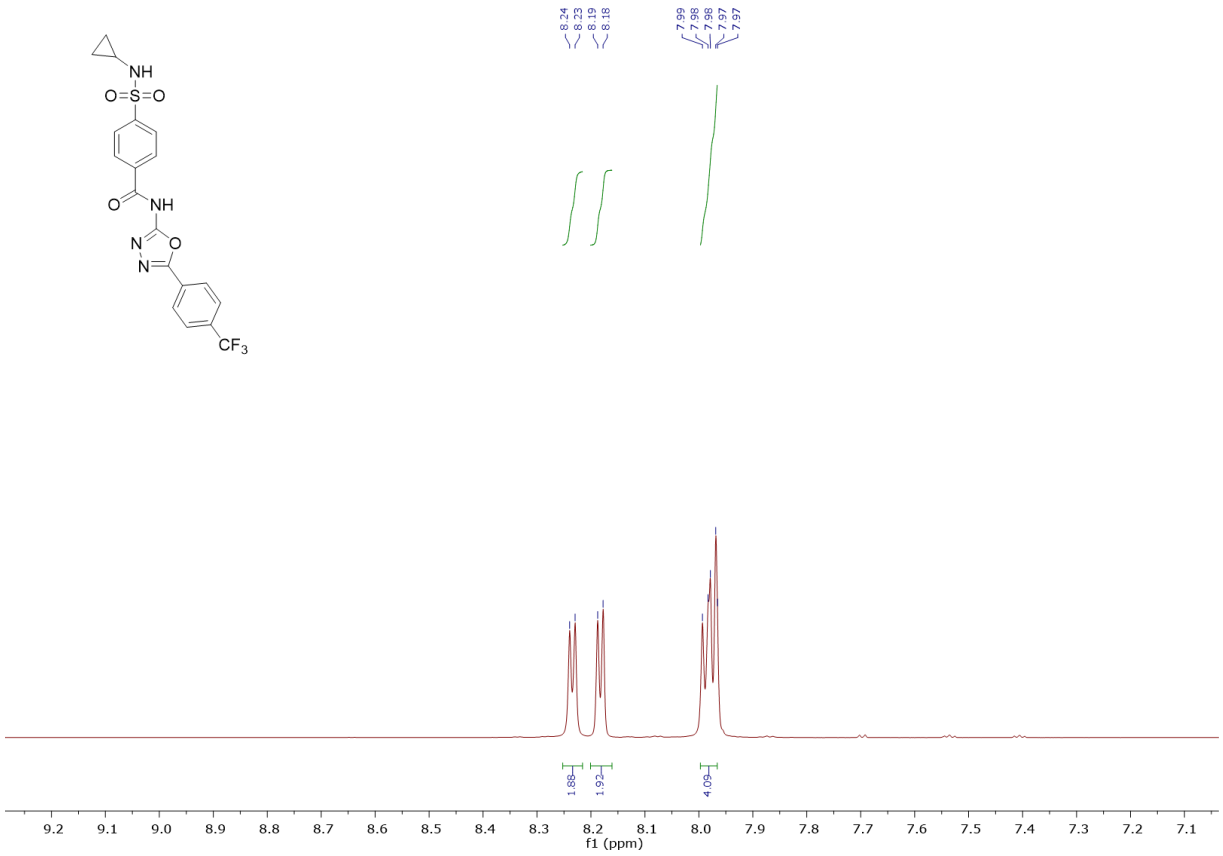
NH
O=S=O
O
NH
N
O
N
CF3
8.24
8.23
8.19
8.18
7.99
7.98
7.98
7.97
7.97
1.88
1.92
4.09
f1 (ppm)

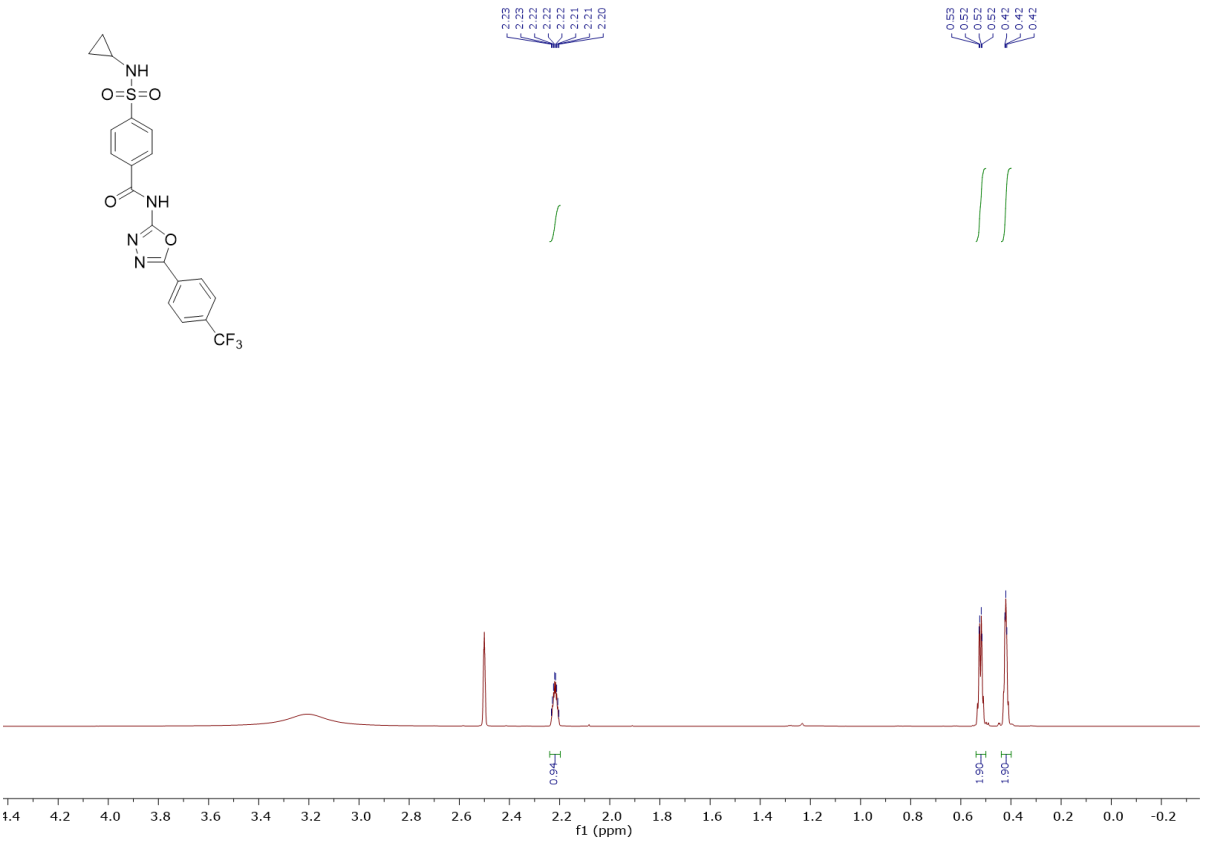
NH
O=S=O
O
NH
N
O
N
CF3
2.23
2.23
2.22
2.22
2.22
2.22
2.21
2.21
2.20
0.53
0.52
0.52
0.52
0.42
0.42
0.42
0.94
1.90
1.90
f1 (ppm)

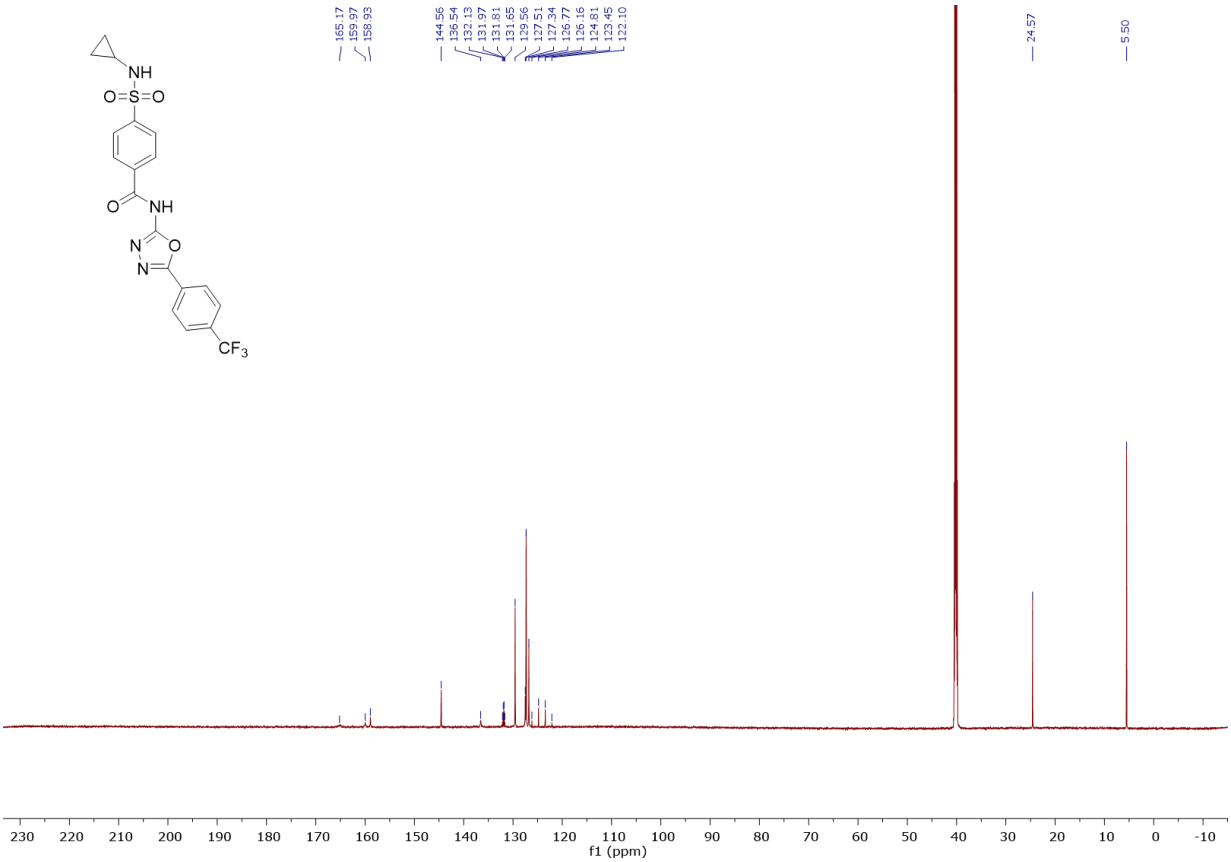
NH
O=S=O
O
NH
N
O
N
CF3
165.17
159.97
158.93
144.56
136.54
132.13
131.97
131.81
131.65
129.56
127.51
127.34
126.77
126.16
124.81
123.45
122.10
24.57
5.50
f1 (ppm)

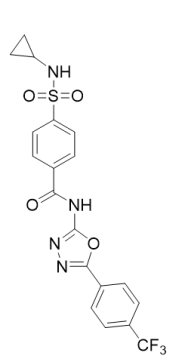
NH
O=S=O
O
NH
N
O
N
CF3

-62.78
10 0 -10 -20 -30 -40 -50 -60 -70 -80 -90 -100 -110 -120 -130 -140 -150 -160 -170 -180 -190 -200 -210 -220
f1 (ppm)

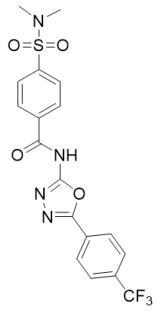
N
O=S=O
O
NH
N
O
N
CF3

8.27
8.26
8.19
8.18
7.98
7.97
7.94
7.93
7.93
2.70
2.00
2.00
2.03
1.97
6.00
13.5 13.0 12.5 12.0 11.5 11.0 10.5 10.0 9.5 9.0 8.5 8.0 7.5 7.0 6.5 6.0 5.5 5.0 4.5 4.0 3.5 3.0 2.5 2.0 1.5 1.0 0.5 0.0 -0.5 -1.0
f1 (ppm)

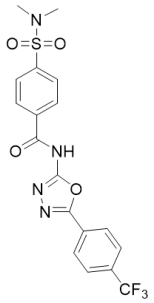
N
O=S=O
O
NH
N
O
N
CF3

8.27
8.26
8.19
8.18
7.98
7.97
7.94
7.93
7.93
2.00
2.00
2.03
1.97
9.6 9.5 9.4 9.3 9.2 9.1 9.0 8.9 8.8 8.7 8.6 8.5 8.4 8.3 8.2 8.1 8.0 7.9 7.8 7.7 7.6 7.5 7.4 7.3 7.2 7.1 7.0
f1 (ppm)

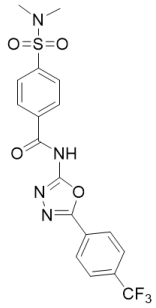
N
O=S=O
O
NH
N
O
N
CF3

2.70
6.00
4.1 4.0 3.9 3.8 3.7 3.6 3.5 3.4 3.3 3.2 3.1 3.0 2.9 2.8 2.7 2.6 2.5 2.4 2.3 2.2 2.1 2.0 1.9 1.8 1.7 1.6 1.5 1.4 1.3 1.2 1.1 1.0 0.9
f1 (ppm)

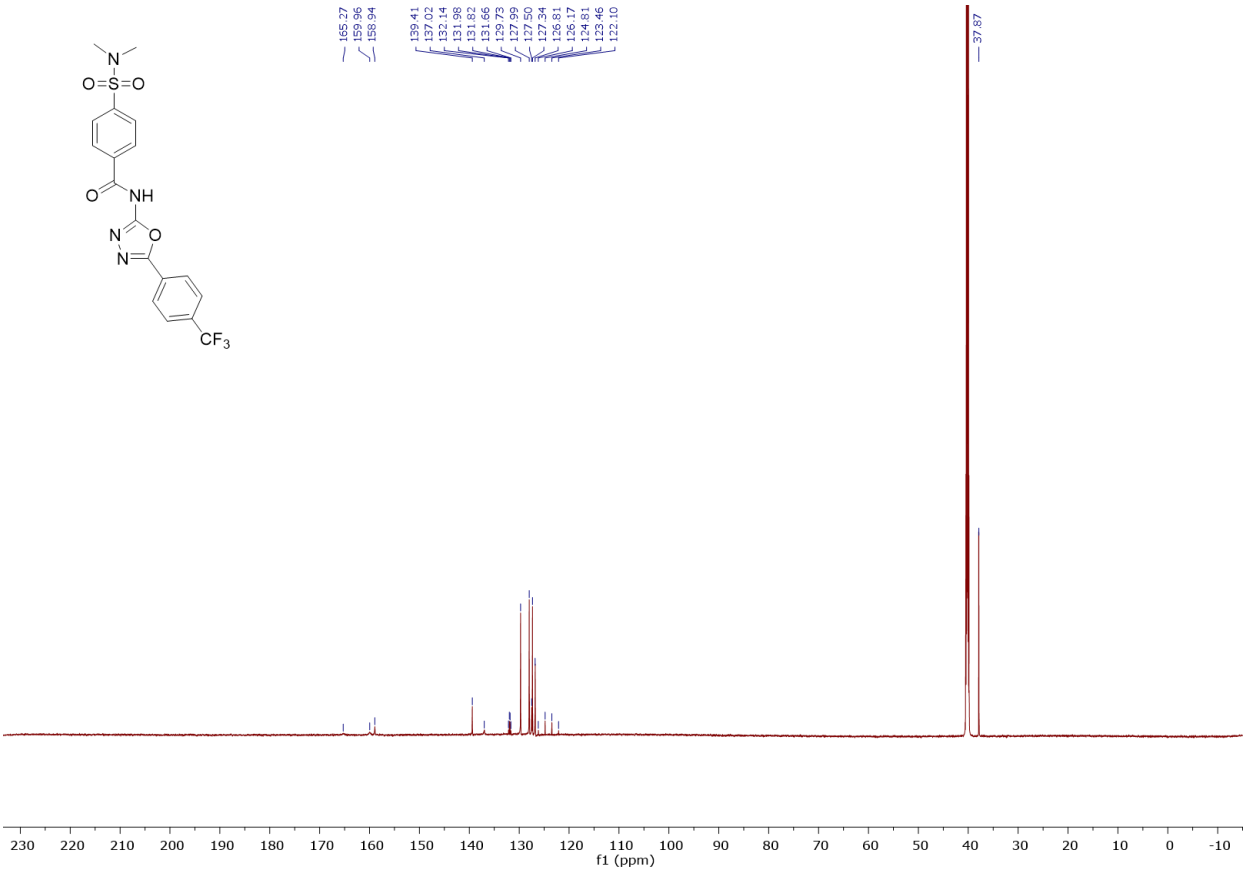
165.27
159.96
158.94
139.41
137.02
132.14
131.98
131.82
131.66
129.73
127.99
127.50
127.34
126.81
126.17
124.81
123.46
122.10
37.87
f1 (ppm)

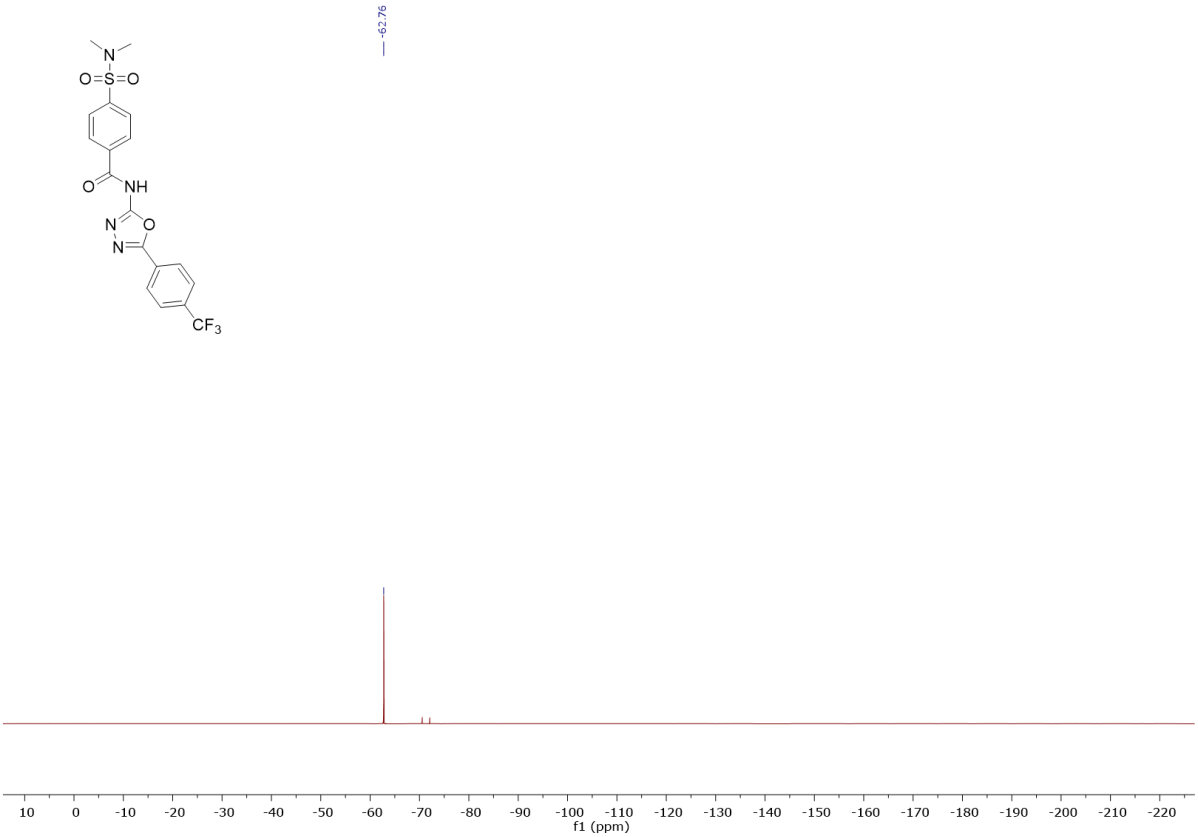
-62.76
f1 (ppm)

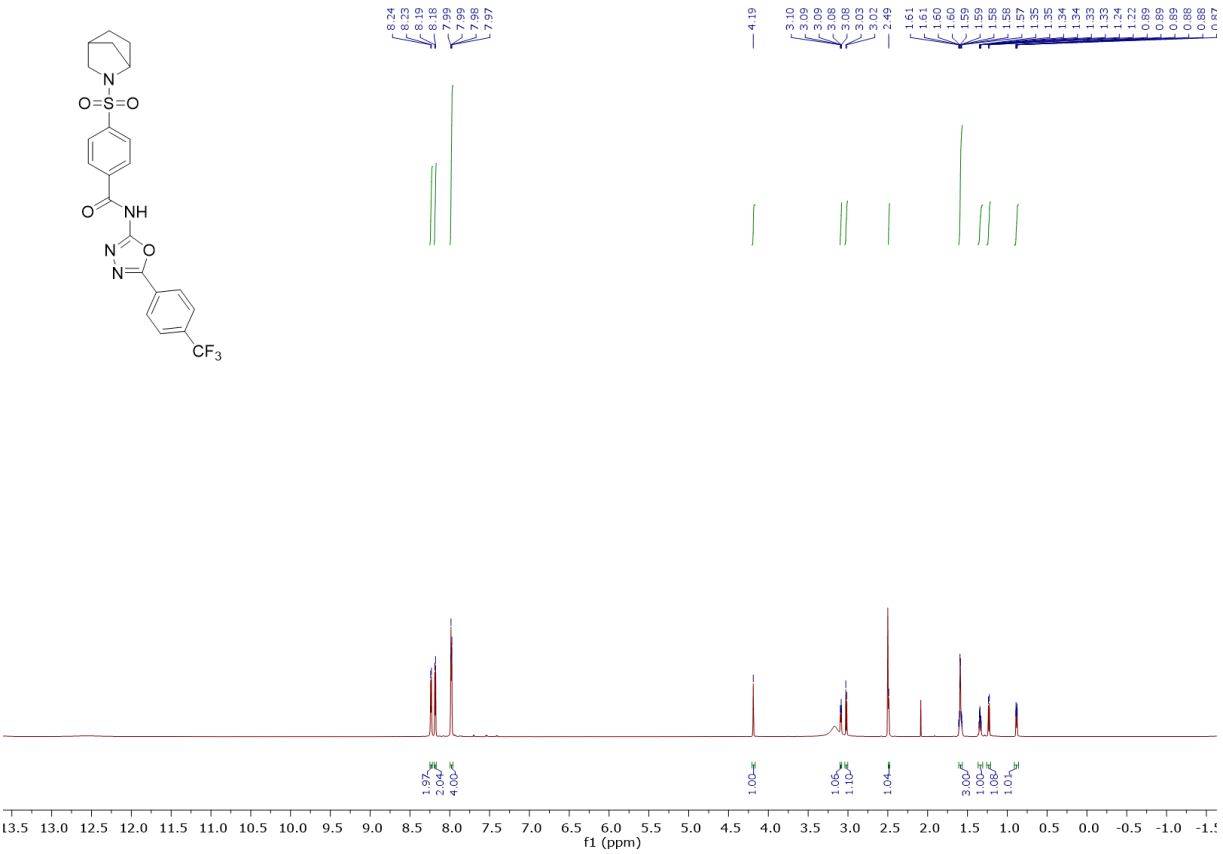
8.24
8.23
8.19
8.18
7.99
7.99
7.98
7.97
4.19
3.10
3.09
3.09
3.08
3.08
3.03
3.02
2.49
1.61
1.61
1.60
1.60
1.59
1.59
1.58
1.58
1.57
1.35
1.35
1.34
1.34
1.33
1.33
1.24
1.22
0.89
0.89
0.89
0.88
0.88
1.97
2.04
4.00
1.00
1.06
1.10
1.04
3.00
1.00
1.08
1.01
f1 (ppm)

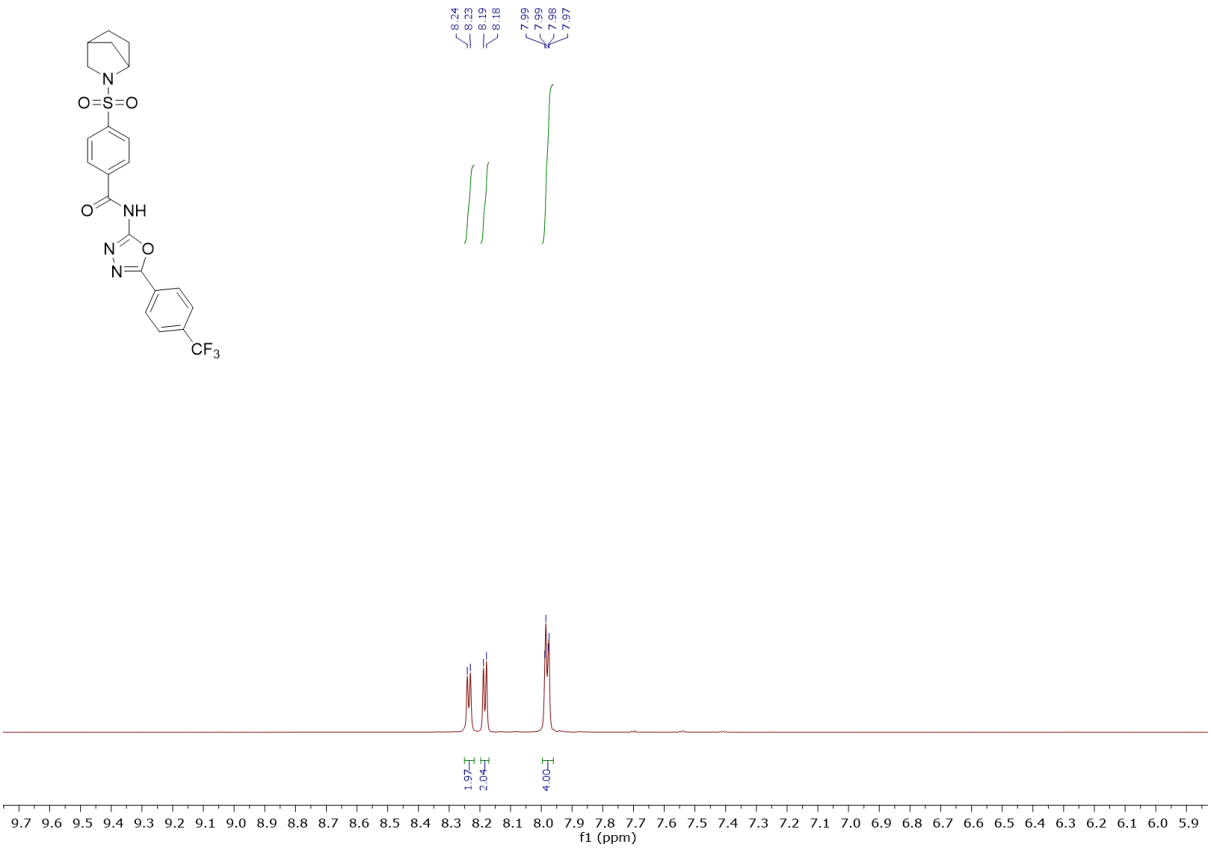
8.24
8.23
8.19
8.18
7.99
7.99
7.98
7.97
1.97
2.04
4.00
f1 (ppm)

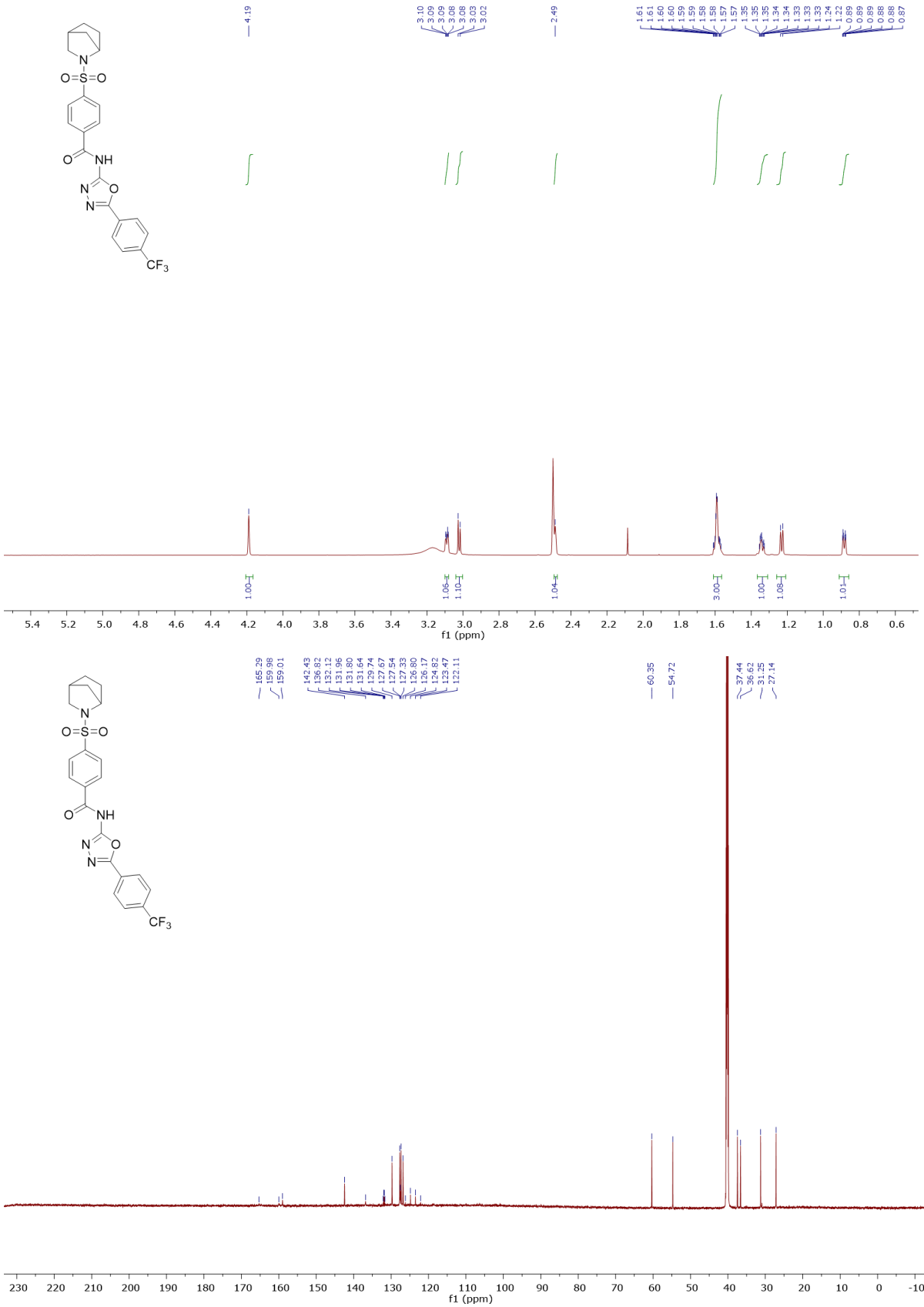
4.19
3.10
3.09
3.09
3.08
3.08
3.03
3.02
2.49
1.61
1.61
1.60
1.60
1.59
1.59
1.58
1.58
1.57
1.57
1.35
1.35
1.34
1.34
1.33
1.33
1.33
1.24
1.22
0.89
0.89
0.89
0.88
0.88
0.87
1.00
1.06
1.10
1.04
3.00
1.00
1.08
1.01
f1 (ppm)
165.29
159.98
159.01
142.43
136.82
132.12
131.96
131.80
131.64
129.74
127.67
127.54
127.33
126.80
126.17
124.82
123.47
122.11
60.35
54.72
37.44
36.62
31.25
27.14
f1 (ppm)

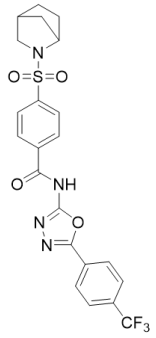
N
O=S=O
O
NH
N
O
N
CF3

-62.75
10 0 -10 -20 -30 -40 -50 -60 -70 -80 -90 -100 -110 -120 -130 -140 -150 -160 -170 -180 -190 -200 -210 -220
f1 (ppm)

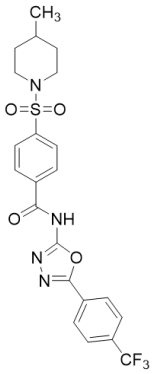
CH3
N
O=S=O
O
NH
N
O
N
CF3

8.26 8.25 8.18 8.17 7.98 7.97 7.92 7.91
3.67 3.66
2.38 2.38 2.37 2.37 2.35 2.35 1.67 1.67 1.66 1.65 1.36 1.36 1.35 1.35 1.34 1.17 1.16 1.15 1.15 1.14 1.13 1.12 1.12 0.87 0.86
2.04 2.15 2.16 2.00 2.07 2.17 2.13 1.17 2.05 3.09
13.5 13.0 12.5 12.0 11.5 11.0 10.5 10.0 9.5 9.0 8.5 8.0 7.5 7.0 6.5 6.0 5.5 5.0 4.5 4.0 3.5 3.0 2.5 2.0 1.5 1.0 0.5 0.0 -0.5 -1.0
f1 (ppm)

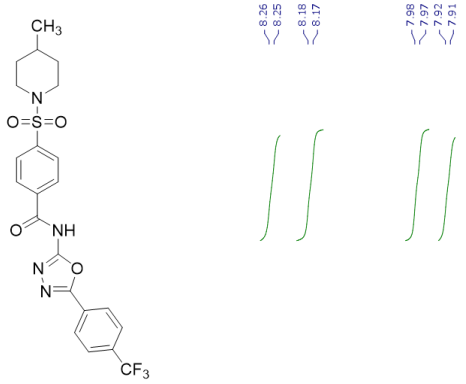
CH3
N
O=S=O
O
NH
N
O
N
CF3

8.26
8.25
8.18
8.17
7.98
7.97
7.92
7.91

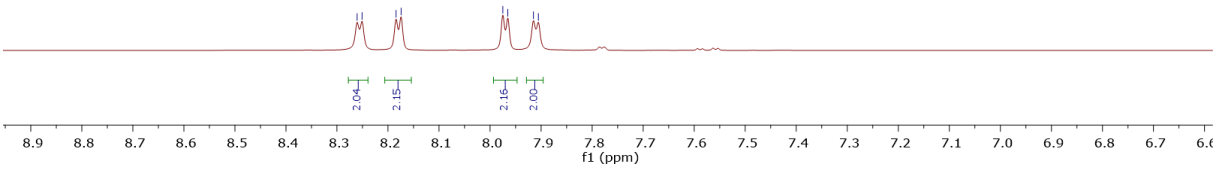
2.04
2.15
2.16
2.00
8.9 8.8 8.7 8.6 8.5 8.4 8.3 8.2 8.1 8.0 7.9 7.8 7.7 7.6 7.5 7.4 7.3 7.2 7.1 7.0 6.9 6.8 6.7
f1 (ppm)

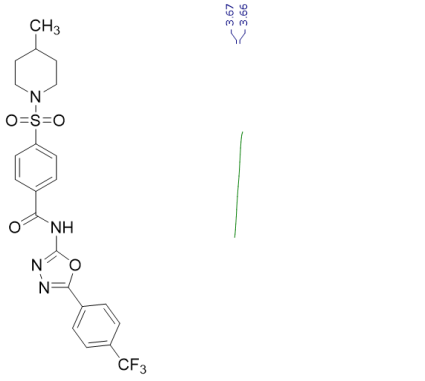
CH3
N
O=S=O
O
NH
N
O
N
CF3

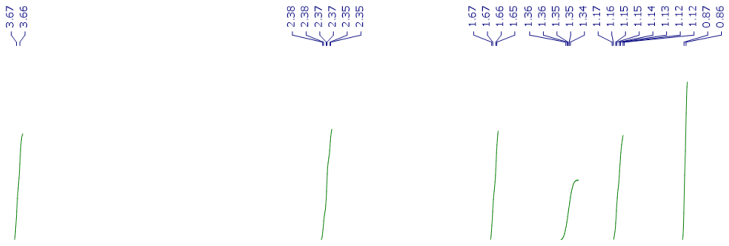
3.67
3.66
2.38
2.38
2.37
2.37
2.35
2.35
1.67
1.67
1.66
1.65
1.36
1.36
1.35
1.35
1.34
1.17
1.16
1.15
1.14
1.13
1.12
1.12
0.87
0.86

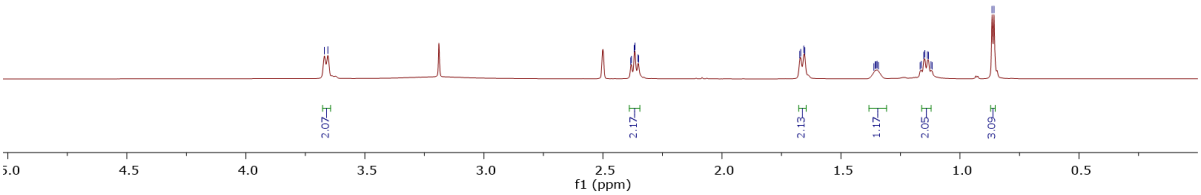
2.07
2.17
2.13
1.17
2.05
3.09
5.0 4.5 4.0 3.5 3.0 2.5 2.0 1.5 1.0 0.5
f1 (ppm)

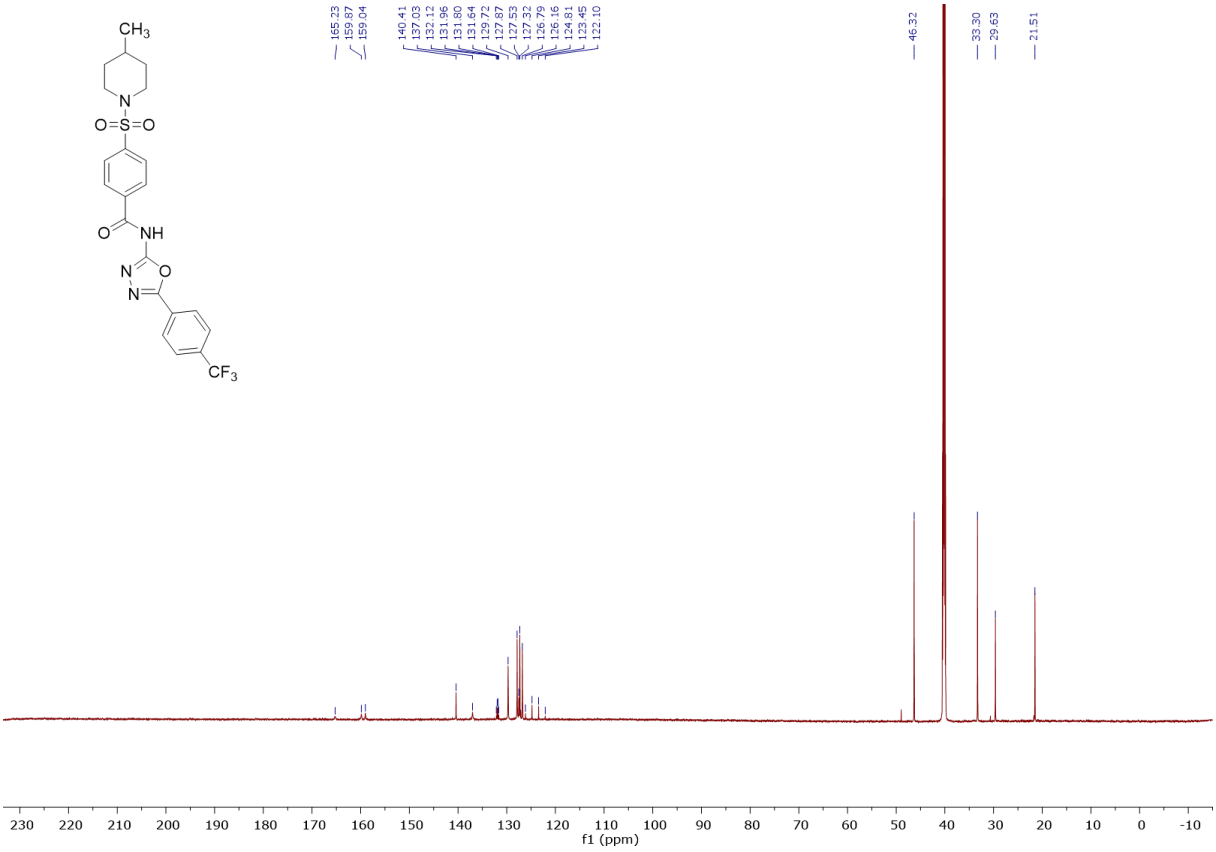
165.23
159.87
159.04
140.41
137.03
132.12
131.96
131.80
131.64
129.72
127.87
127.53
127.32
126.79
126.16
124.81
123.45
122.10
46.32
33.30
29.63
21.51
f1 (ppm)

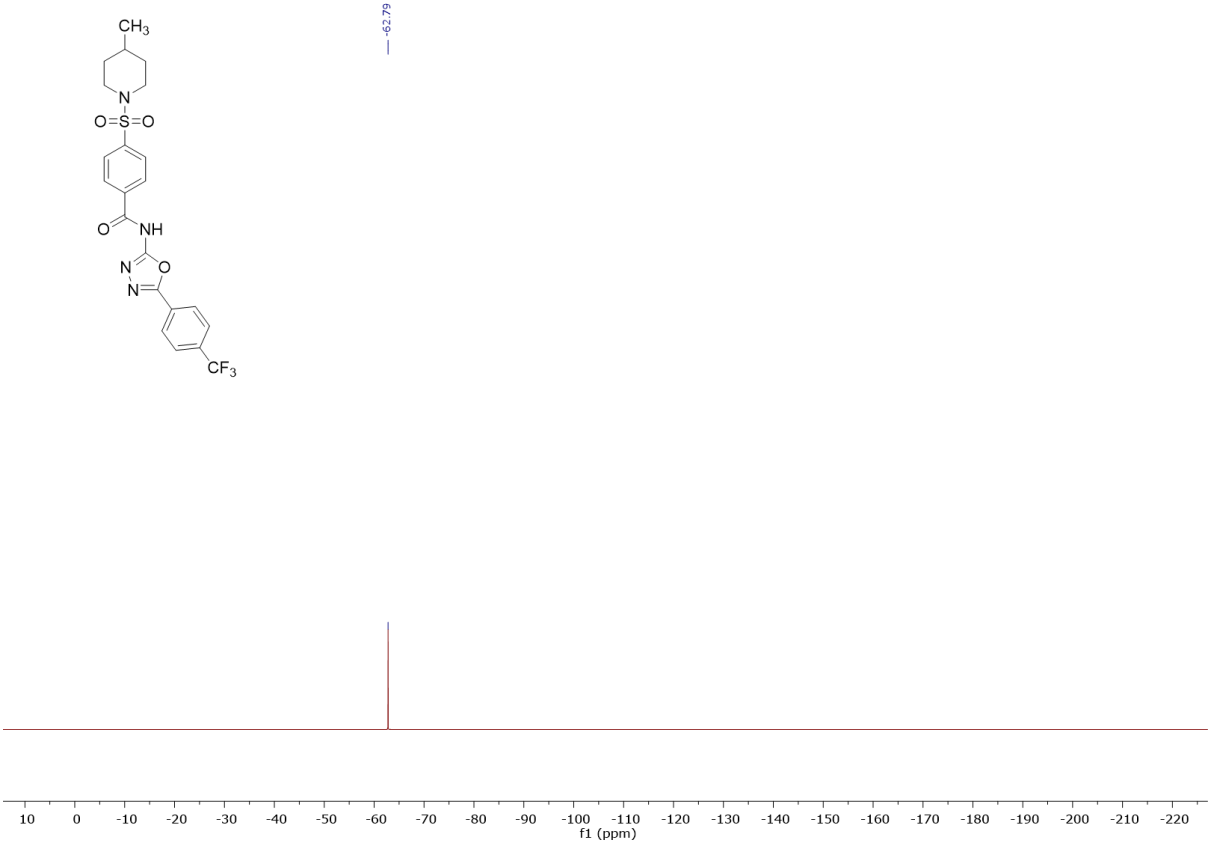
-62.79
f1 (ppm)

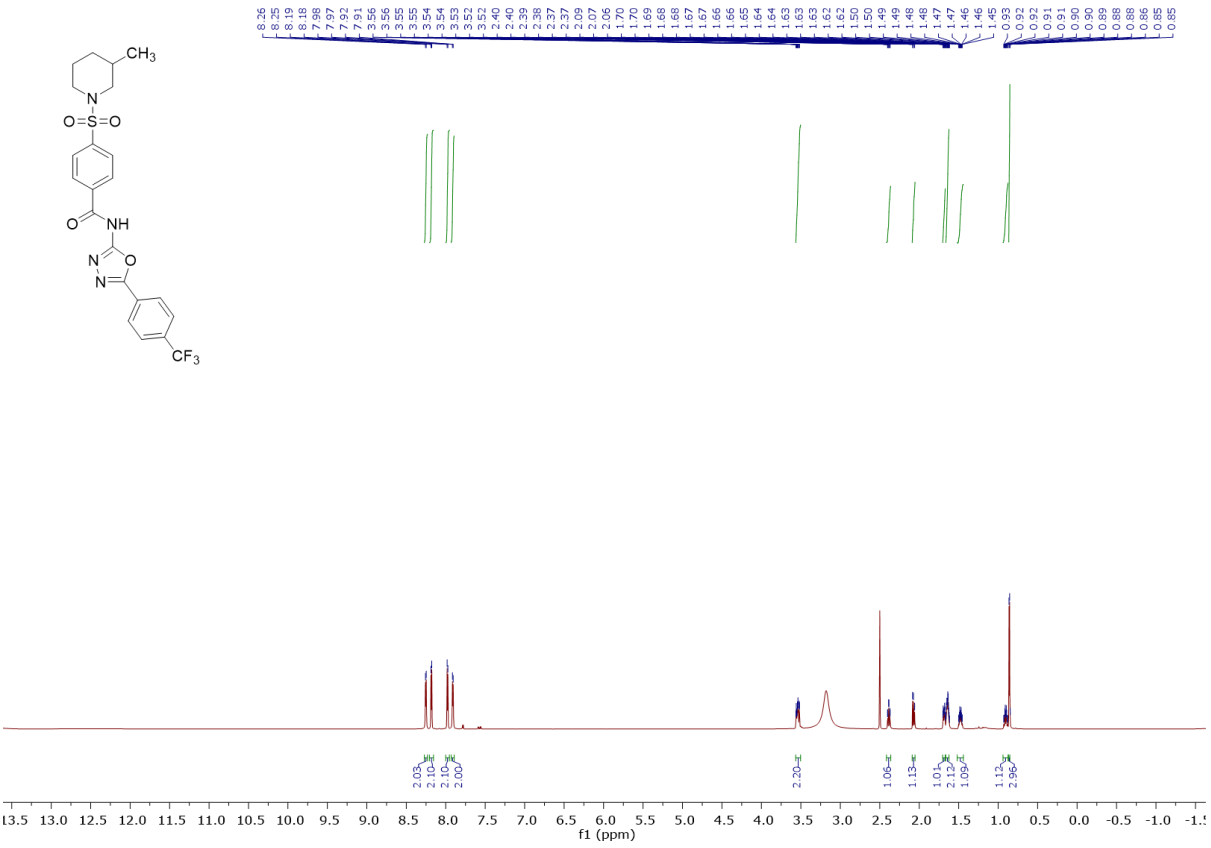
CH3
N
O=S=O
O
NH
N
O
N
CF3
f1 (ppm)

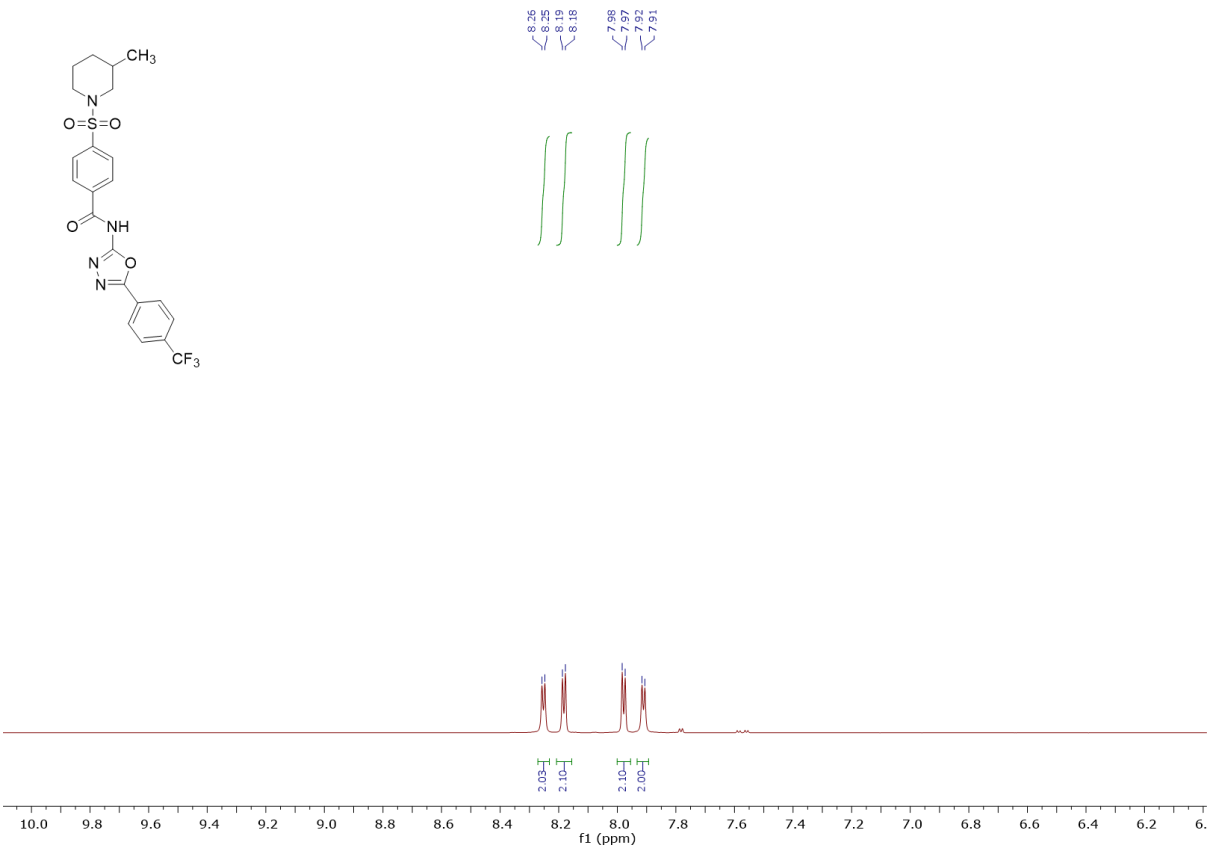
CH3
N
O=S=O
O
NH
N
O
N
CF3
f1 (ppm)

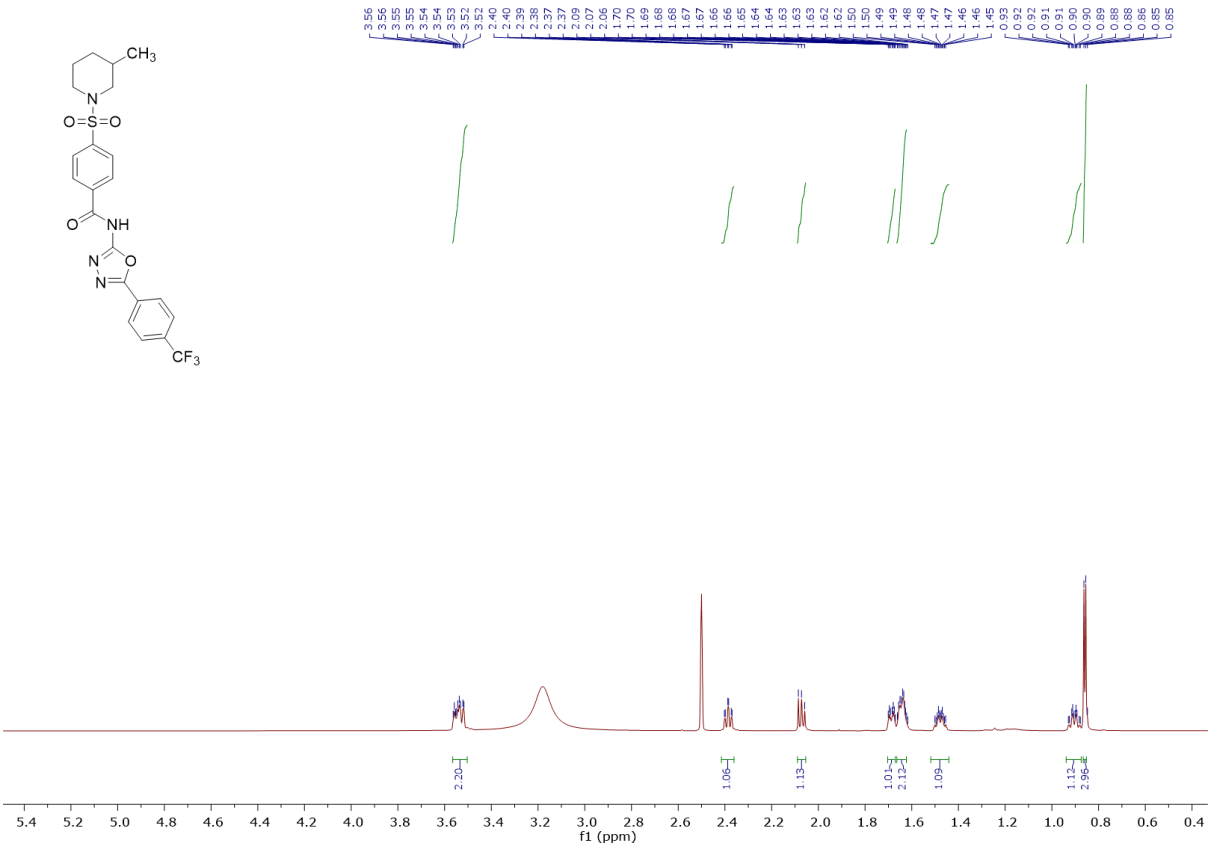
CH3
N
O=S=O
O
NH
N
O
N
CF3
3.56 3.56 3.55 3.55 3.54 3.54 3.53 3.52 3.52 2.40 2.40 2.39 2.38 2.37 2.37 2.09 2.07 2.06 1.70 1.70 1.69 1.68 1.68 1.67 1.67 1.67 1.66 1.66 1.65 1.64 1.64 1.63 1.63 1.63 1.62 1.62 1.50 1.50 1.49 1.49 1.48 1.48 1.47 1.47 1.46 1.46 1.45 0.93 0.92 0.92 0.91 0.91 0.90 0.90 0.89 0.88 0.88 0.86 0.85 0.85
2.20 1.06 1.13 1.01 2.12 1.09 1.12 2.96
5.4 5.2 5.0 4.8 4.6 4.4 4.2 4.0 3.8 3.6 3.4 3.2 3.0 2.8 2.6 2.4 2.2 2.0 1.8 1.6 1.4 1.2 1.0 0.8 0.6 0.4
f1 (ppm)

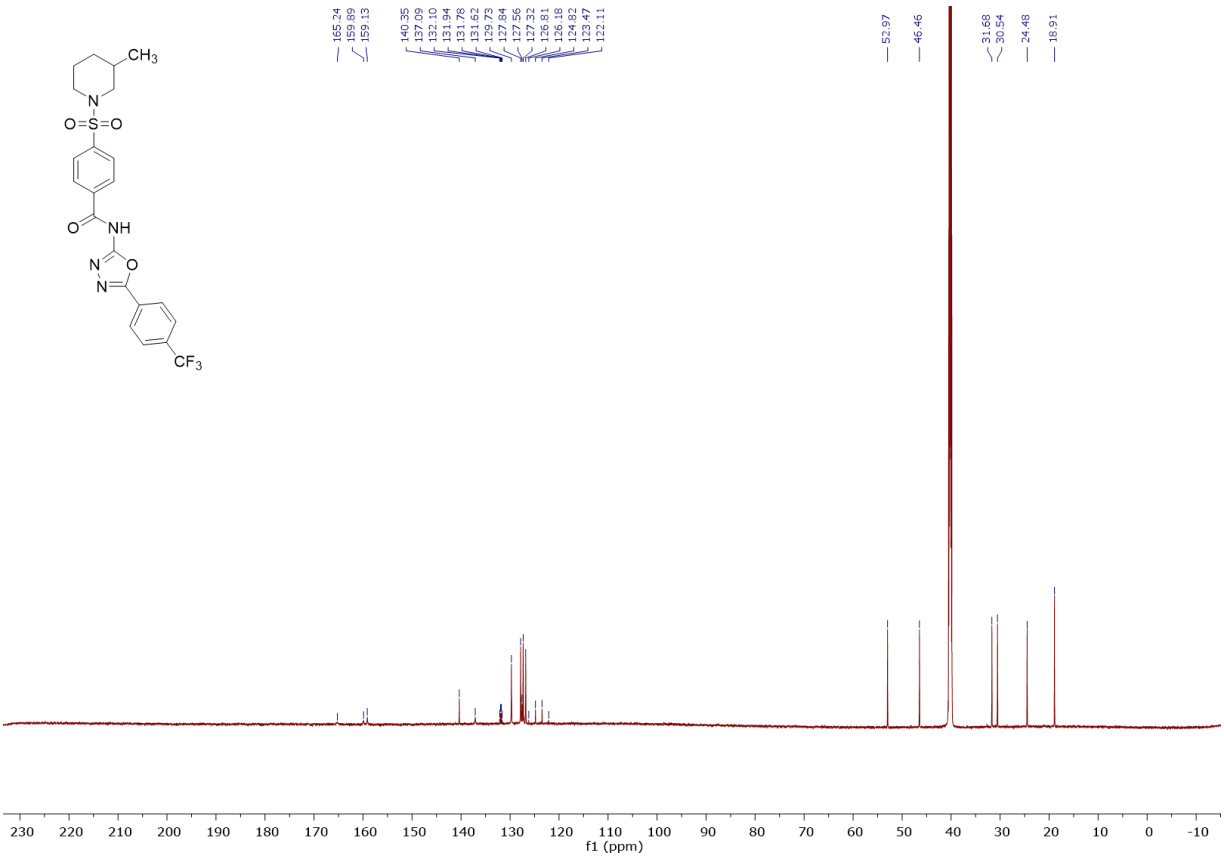
CH3
N
O=S=O
O
NH
N
O
N
CF3
165.24 159.89 159.13 140.35 137.09 132.10 131.94 131.78 131.62 129.73 127.84 127.56 127.32 126.81 126.18 124.82 123.47 122.11 52.97 46.46 31.68 30.54 24.48 18.91
230 220 210 200 190 180 170 160 150 140 130 120 110 100 90 80 70 60 50 40 30 20 10 0 -10
f1 (ppm)

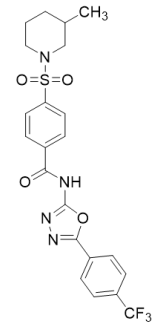
CH3
N
O=S=O
O
NH
N
O
N
CF3

-62.74
10 0 -10 -20 -30 -40 -50 -60 -70 -80 -90 -100 -110 -120 -130 -140 -150 -160 -170 -180 -190 -200 -210 -220
f1 (ppm)

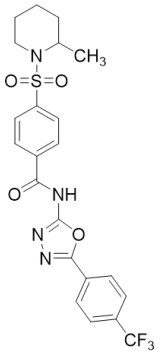
CH3
N
O=S=O
O
NH
N
O
N
CF3

8.22 8.21 8.19 8.18 7.98 7.98 7.97 7.97
4.18 4.17 4.17 4.16 4.16 3.68 3.67 3.67 3.66 3.65 3.06 3.06 3.04 3.04 3.03 3.02
1.58 1.57 1.57 1.56 1.55 1.55 1.55 1.53 1.53 1.47 1.46 1.46 1.45 1.44 1.44 1.43 1.43 1.25 1.24 1.22 1.06
1.97 2.01 4.00 0.98 1.00 1.16 2.02 3.07 1.04 2.98
13.5 13.0 12.5 12.0 11.5 11.0 10.5 10.0 9.5 9.0 8.5 8.0 7.5 7.0 6.5 6.0 5.5 5.0 4.5 4.0 3.5 3.0 2.5 2.0 1.5 1.0 0.5 0.0 -0.5 -1.0
f1 (ppm)

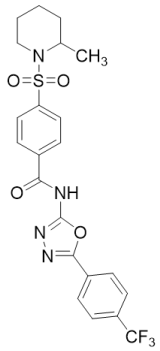

8.22
8.21
8.19
8.18
7.98
7.98
7.97
7.97
1.97
2.01
4.00
f1 (ppm)

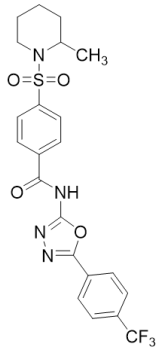

4.18
4.17
4.17
4.16
4.16
3.68
3.67
3.67
3.66
3.65
3.06
3.06
3.04
3.04
3.03
3.02
1.58
1.57
1.57
1.56
1.55
1.55
1.55
1.54
1.54
1.53
1.53
1.51
1.48
1.47
1.46
1.46
1.45
1.44
1.44
1.43
1.43
1.25
1.24
1.24
1.23
1.22
1.22
1.06
1.05
0.98
1.00
1.16
2.02
3.07
1.04
2.98
f1 (ppm)

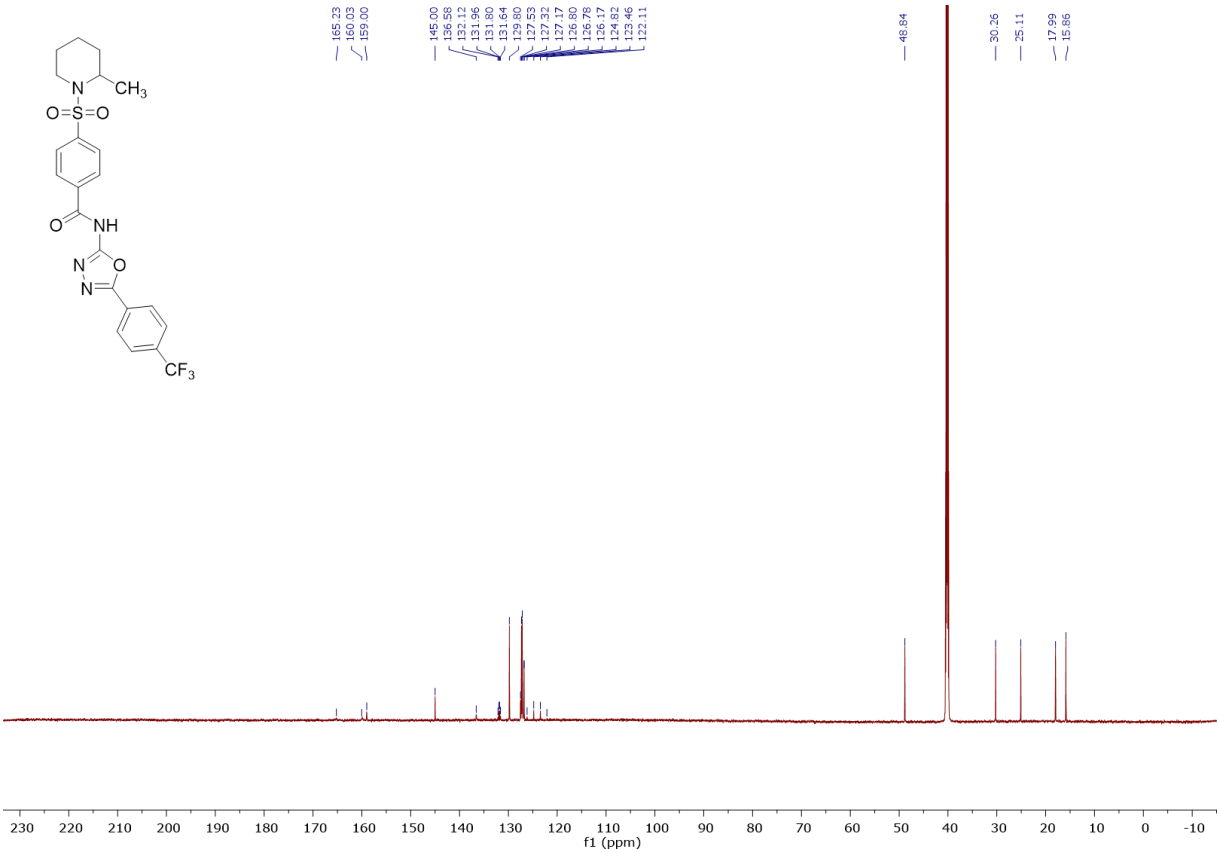
165.23
160.03
159.00
145.00
136.58
132.12
131.96
131.80
131.64
129.80
127.53
127.32
127.17
126.80
126.78
126.17
124.82
123.46
122.11
46.84
30.26
25.11
17.99
15.86
f1 (ppm)

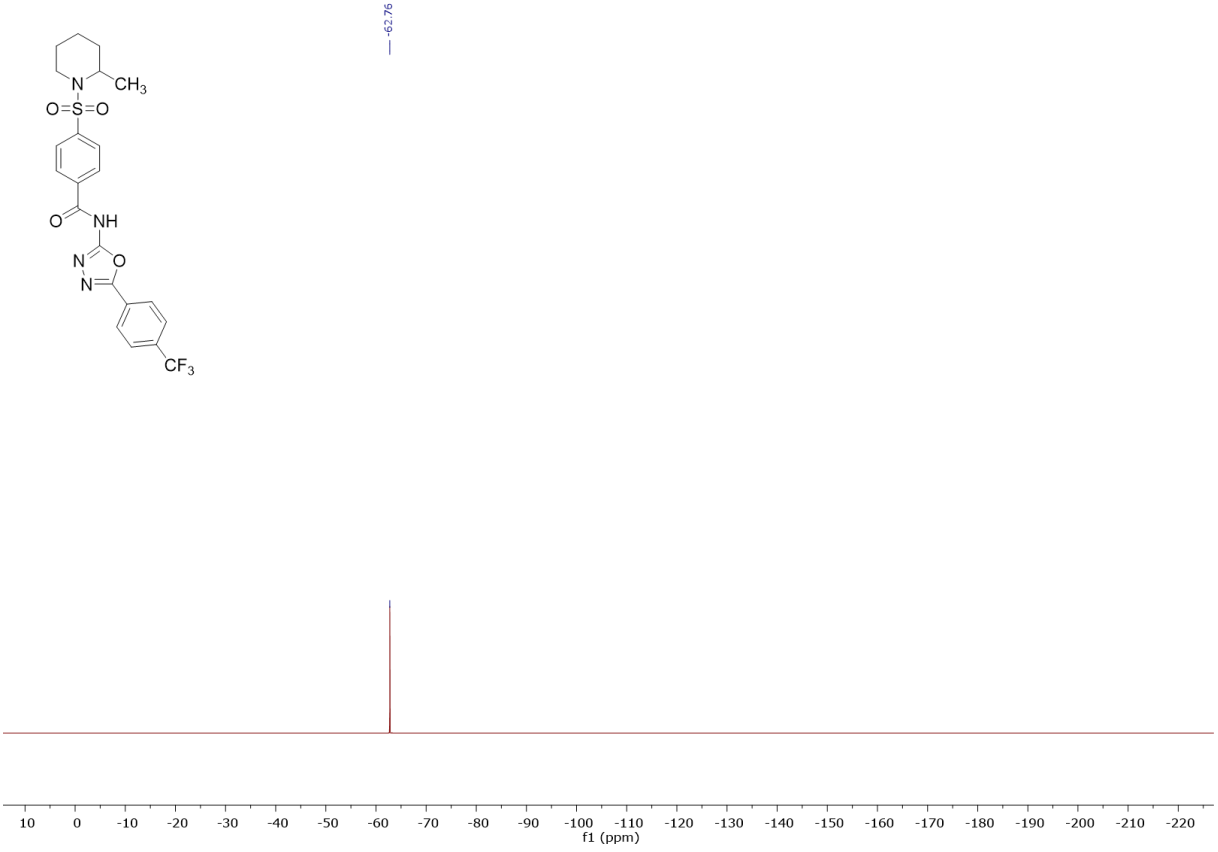
-62.76
f1 (ppm)

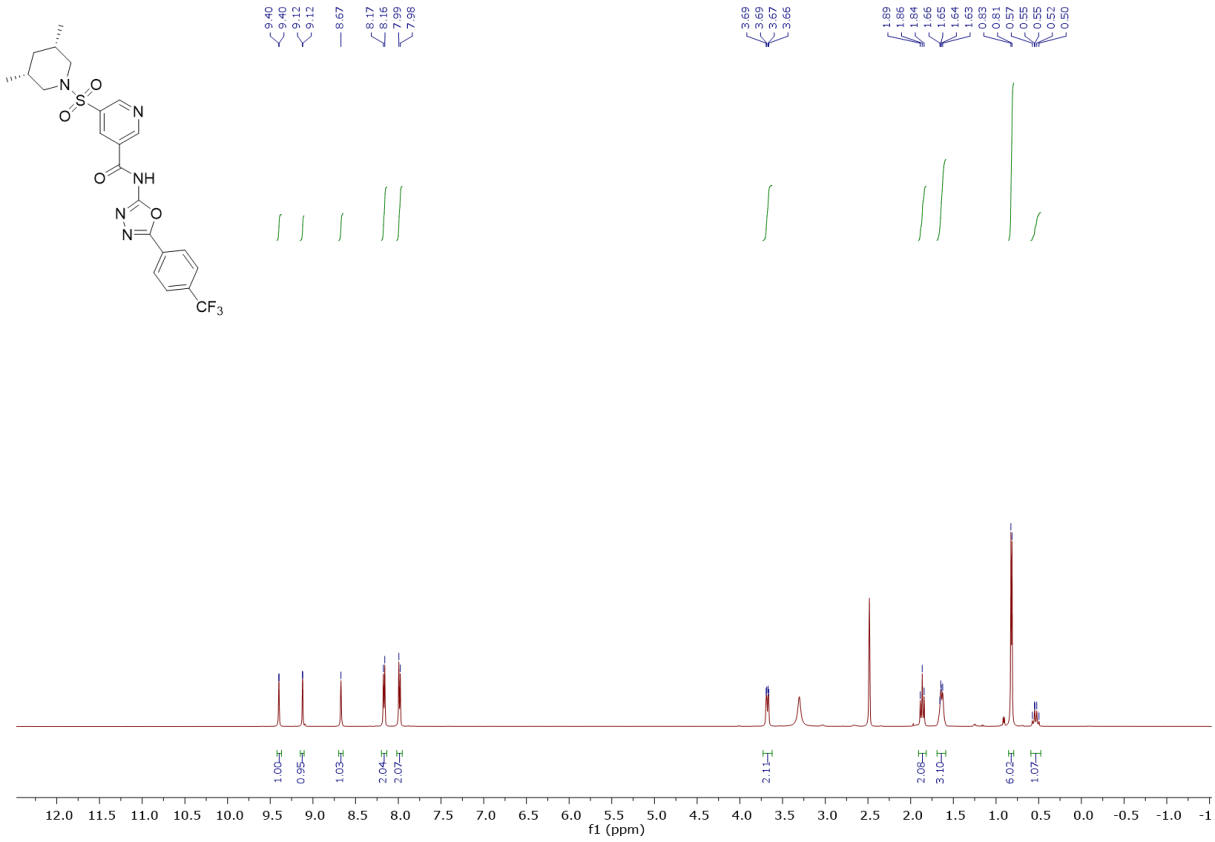
9.40
9.40
9.12
9.12
8.67
8.17
8.16
7.99
7.98
3.69
3.69
3.67
3.66
1.89
1.86
1.84
1.66
1.65
1.64
1.63
0.83
0.81
0.57
0.55
0.55
0.52
0.50
1.00
0.95
1.03
2.04
2.07
2.11
2.08
3.10
6.03
1.07
f1 (ppm)

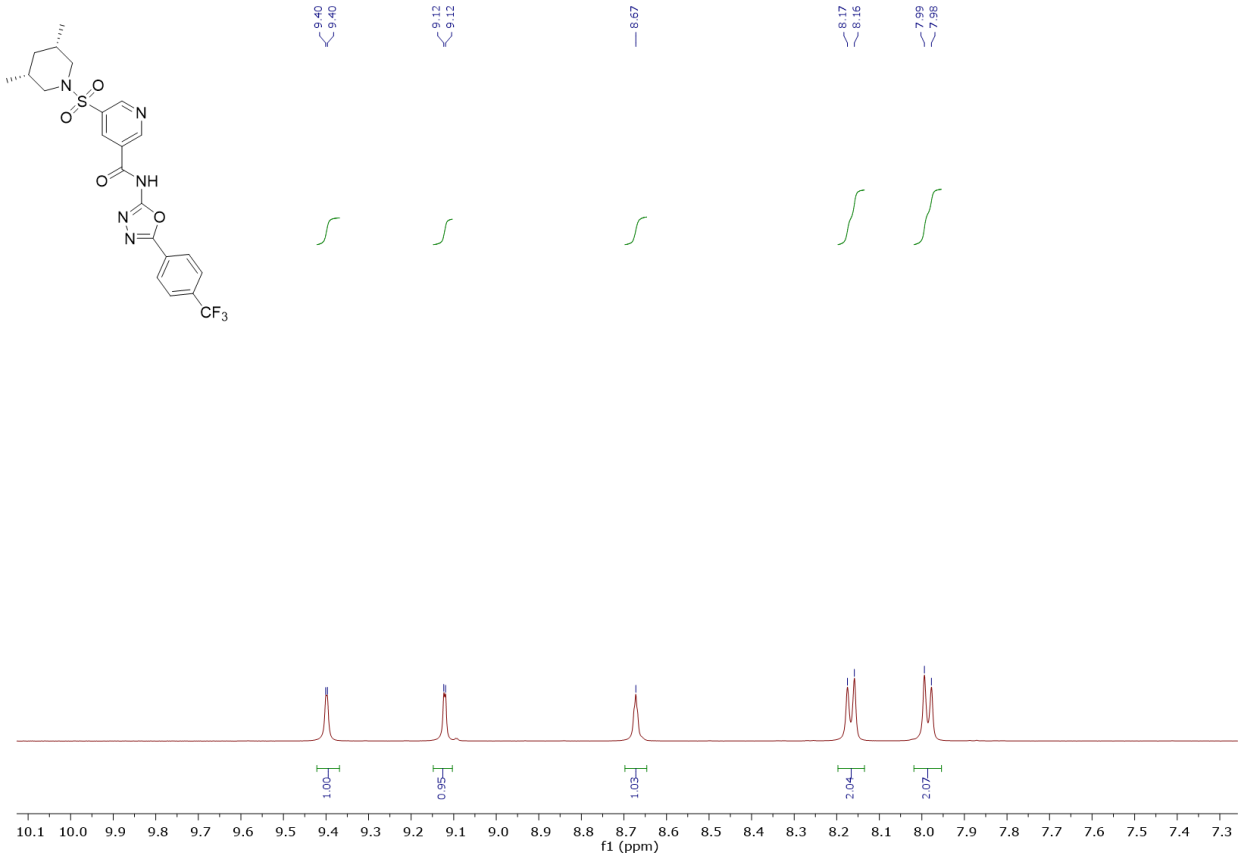
9.40
9.40
9.12
9.12
8.67
8.17
8.16
7.99
7.98
1.00
0.95
1.03
2.04
2.07
f1 (ppm)

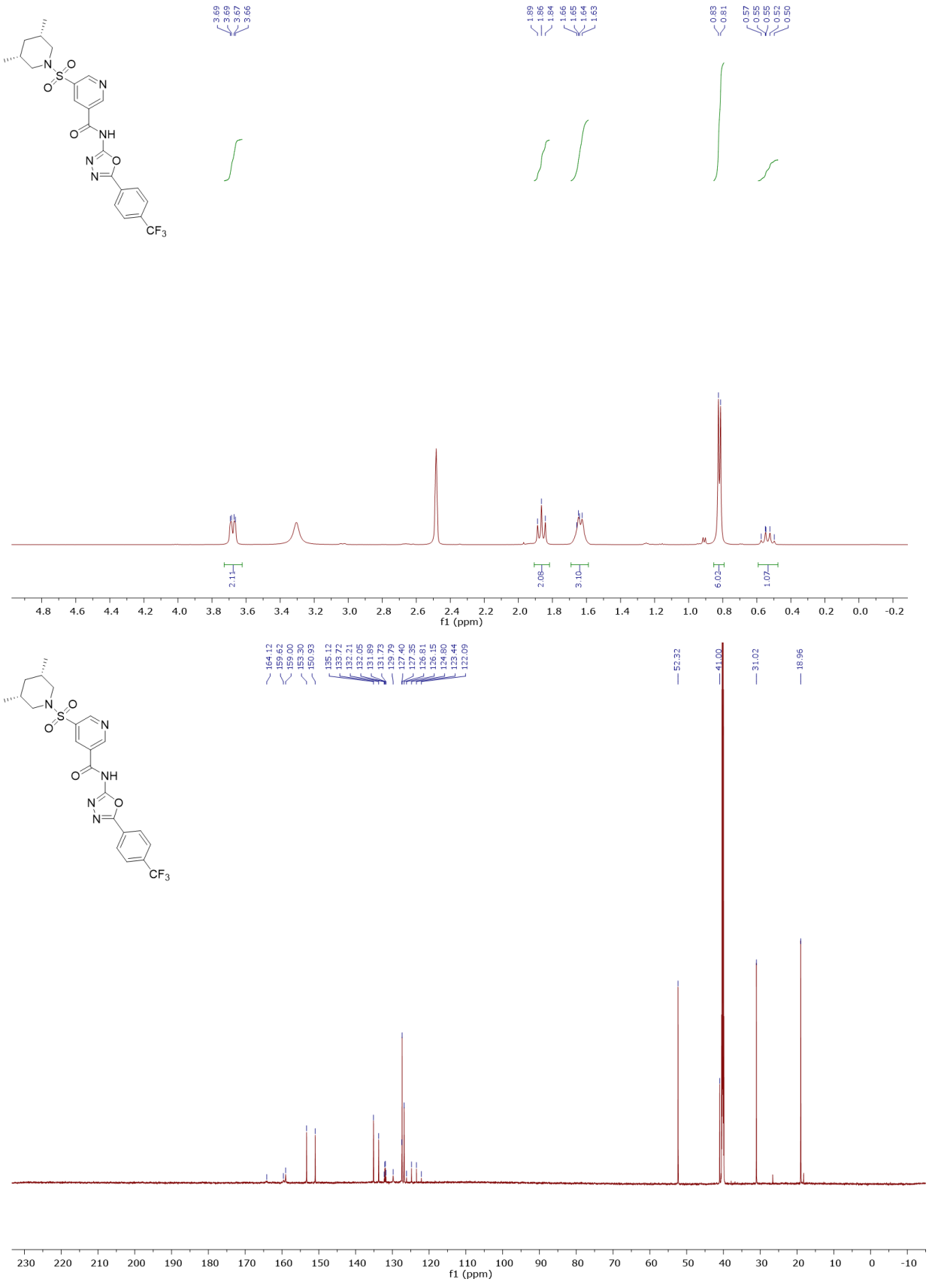
3.69
3.69
3.67
3.66
1.89
1.86
1.84
1.66
1.65
1.64
1.63
0.83
0.81
0.57
0.55
0.55
0.52
0.50
2.11
2.08
3.10
6.03
1.07
f1 (ppm)
164.12
159.62
159.00
153.30
150.93
135.12
133.72
132.21
132.05
131.89
131.73
129.79
127.40
127.35
126.81
126.15
124.80
123.44
122.09
52.32
41.00
31.02
18.96
f1 (ppm)

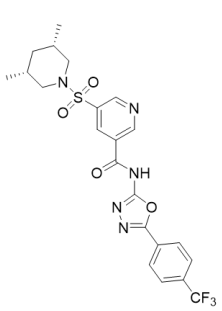

-62.79
10 0 -10 -20 -30 -40 -50 -60 -70 -80 -90 -100 -110 -120 -130 -140 -150 -160 -170 -180 -190 -200 -210 -220
f1 (ppm)

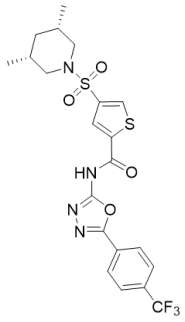

8.54
8.35
8.16
8.14
7.99
7.97
3.61
3.60
3.59
1.87
1.85
1.83
1.67
1.66
1.65
1.64
0.84
0.83
0.60
0.57
0.57
0.55
0.52
1.00
0.77
2.10
2.04
1.99
2.02
3.10
5.98
1.07
12.0 11.5 11.0 10.5 10.0 9.5 9.0 8.5 8.0 7.5 7.0 6.5 6.0 5.5 5.0 4.5 4.0 3.5 3.0 2.5 2.0 1.5 1.0 0.5 0.0 -0.5 -1.0 -1
f1 (ppm)

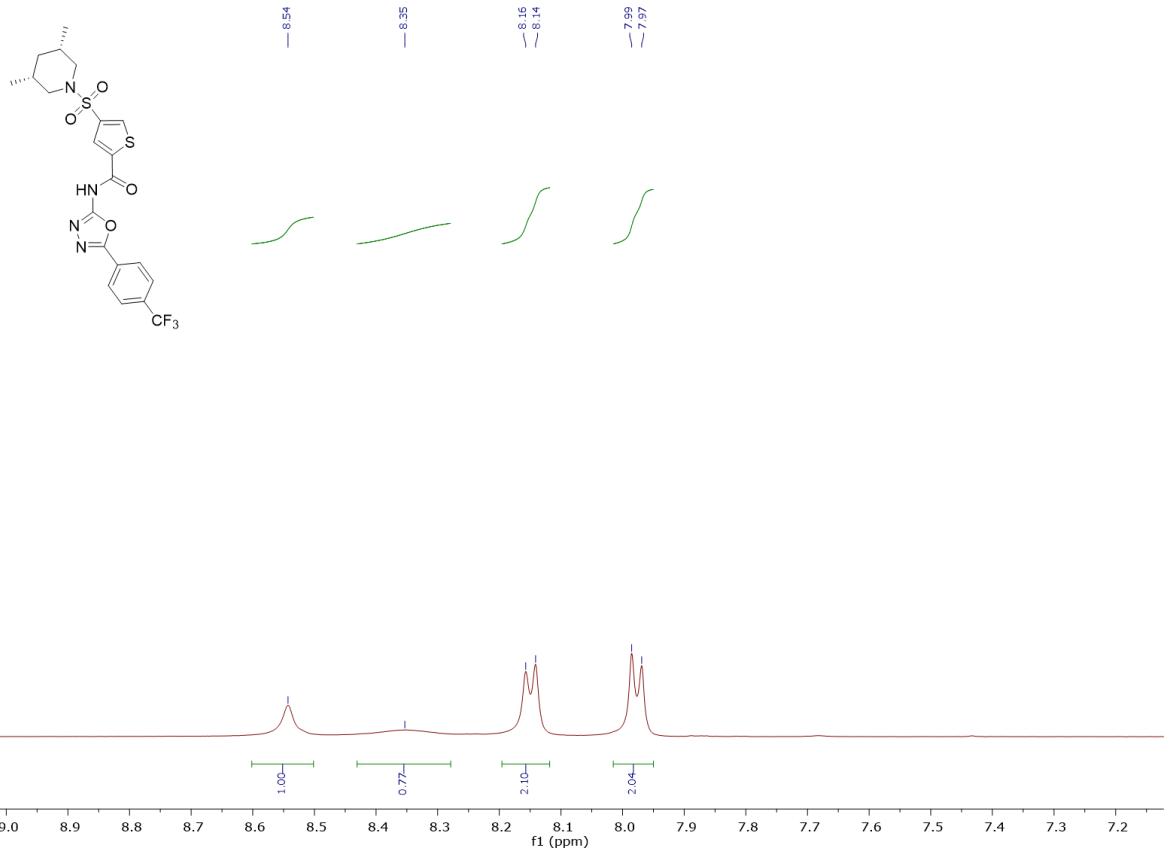
8.54
8.35
8.16
8.14
7.99
7.97
1.00
0.77
2.10
2.04
f1 (ppm)

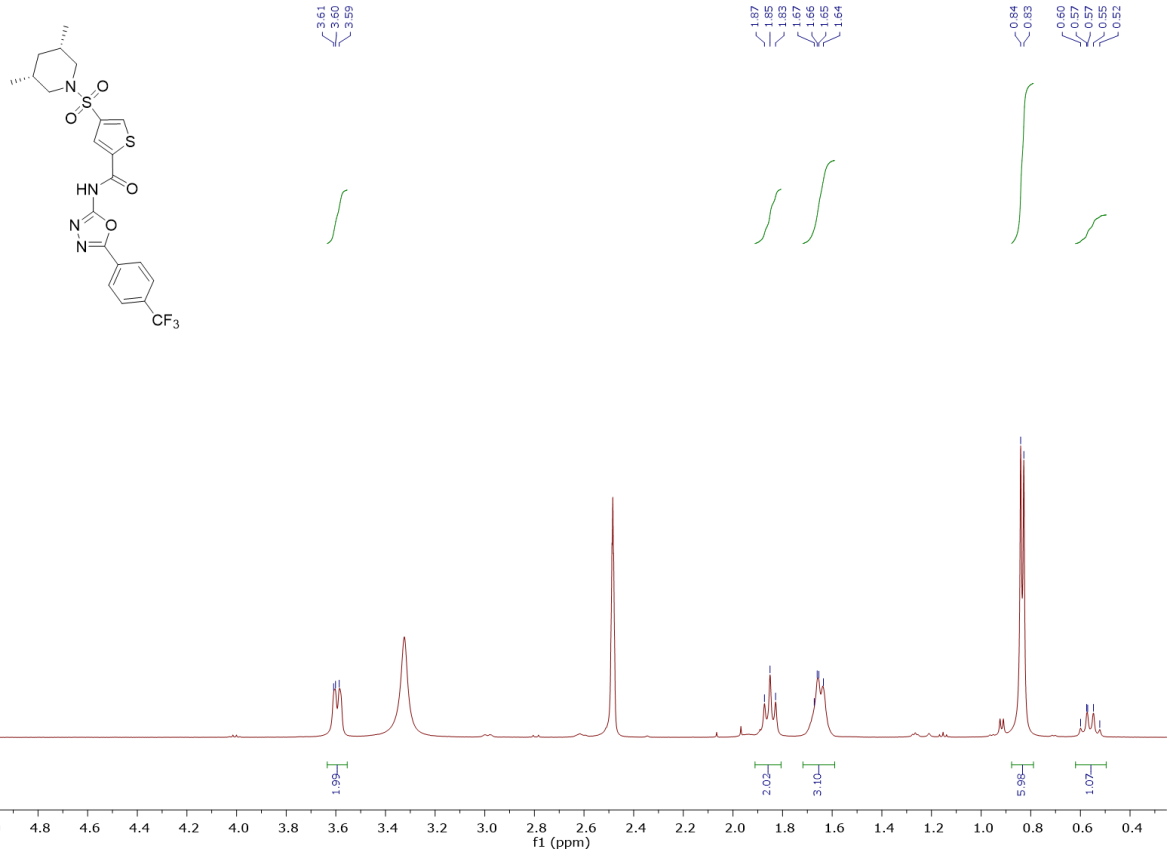
3.61
3.60
3.59
1.87
1.85
1.83
1.67
1.66
1.65
1.64
0.84
0.83
0.60
0.57
0.57
0.55
0.52
1.99
2.02
3.10
5.98
1.07
f1 (ppm)

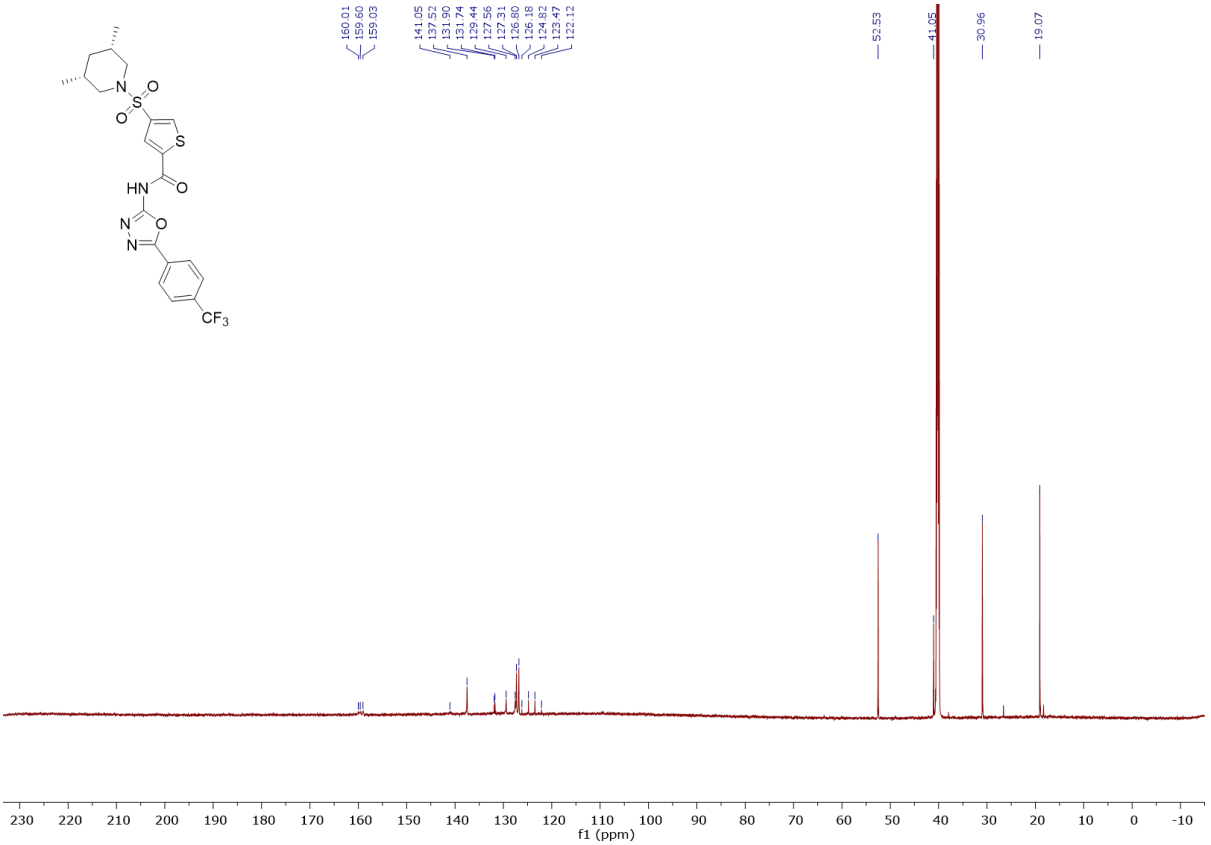
160.01
159.60
159.03
141.05
137.52
131.90
131.74
129.44
127.56
127.31
126.80
126.18
124.82
123.47
122.12
52.53
41.05
30.96
19.07
f1 (ppm)

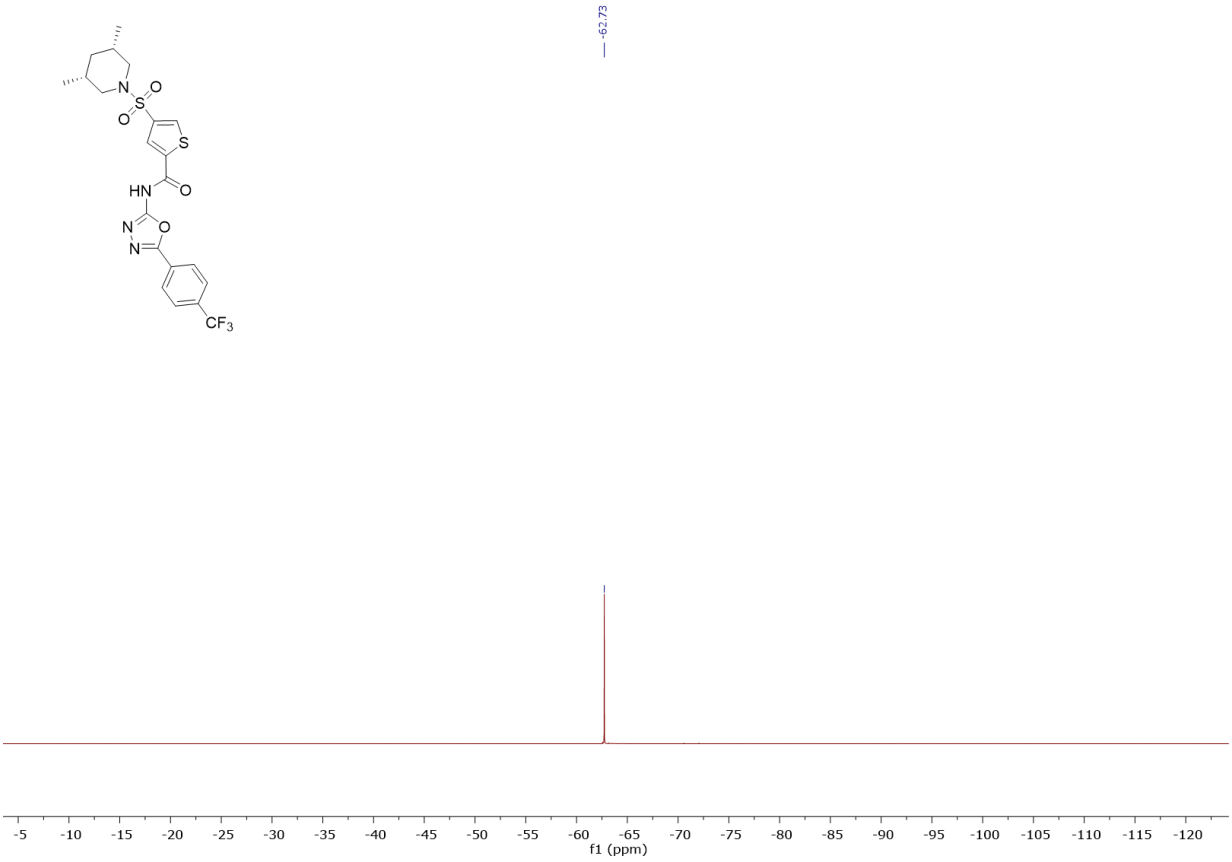
-62.73
f1 (ppm)

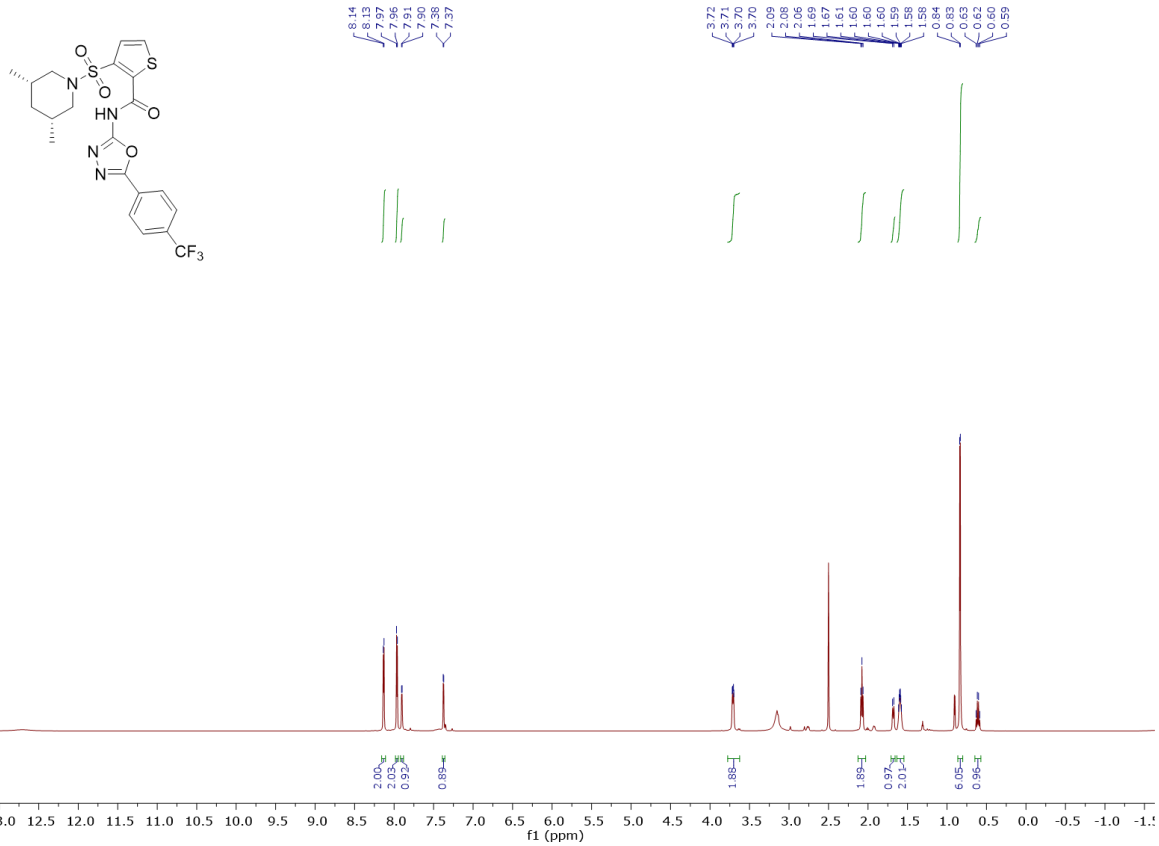
8.14
8.13
7.97
7.96
7.91
7.90
7.38
7.37
3.72
3.71
3.70
3.70
2.09
2.08
2.06
1.69
1.67
1.61
1.60
1.60
1.60
1.59
1.58
1.58
0.84
0.83
0.65
0.62
0.60
0.59
2.00
2.03
0.92
0.89
1.88
1.89
0.97
2.01
6.05
0.96
f1 (ppm)

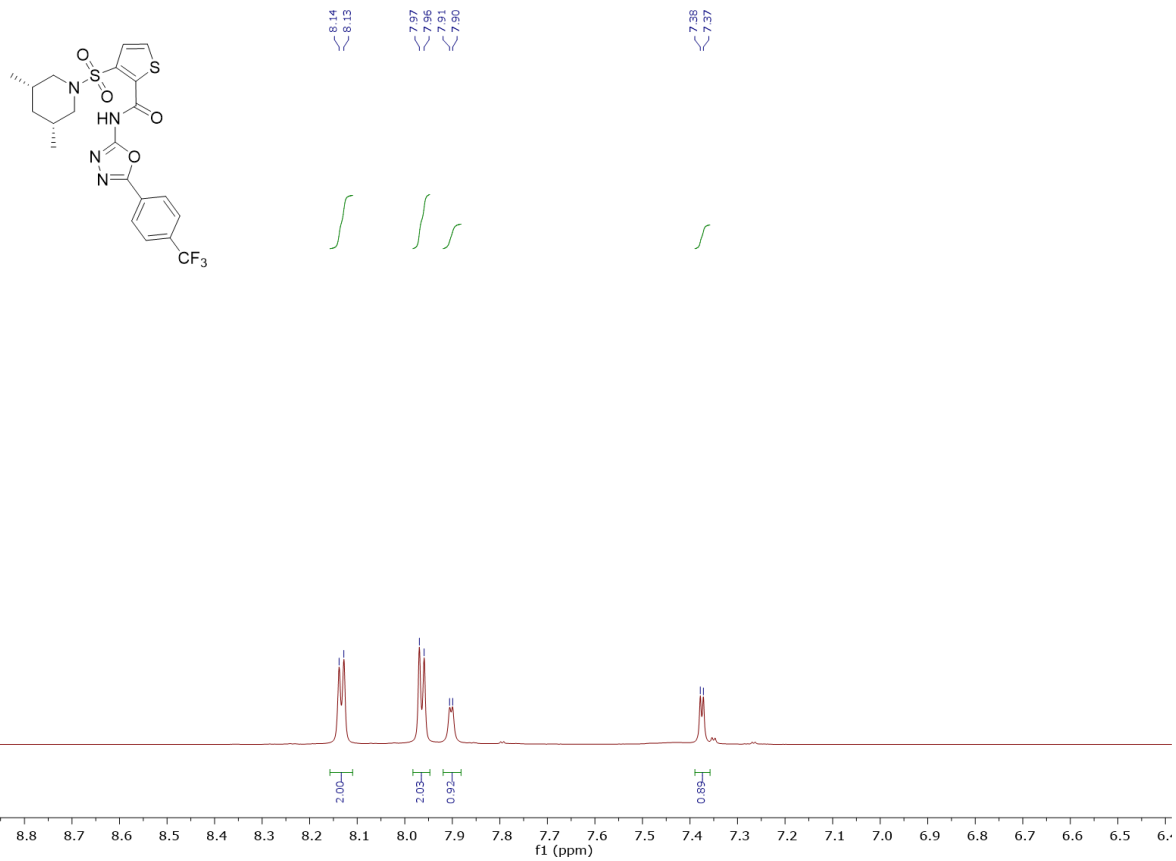
8.14
8.13
7.97
7.96
7.91
7.90
7.38
7.37
2.00
2.03
0.92
0.89
f1 (ppm)

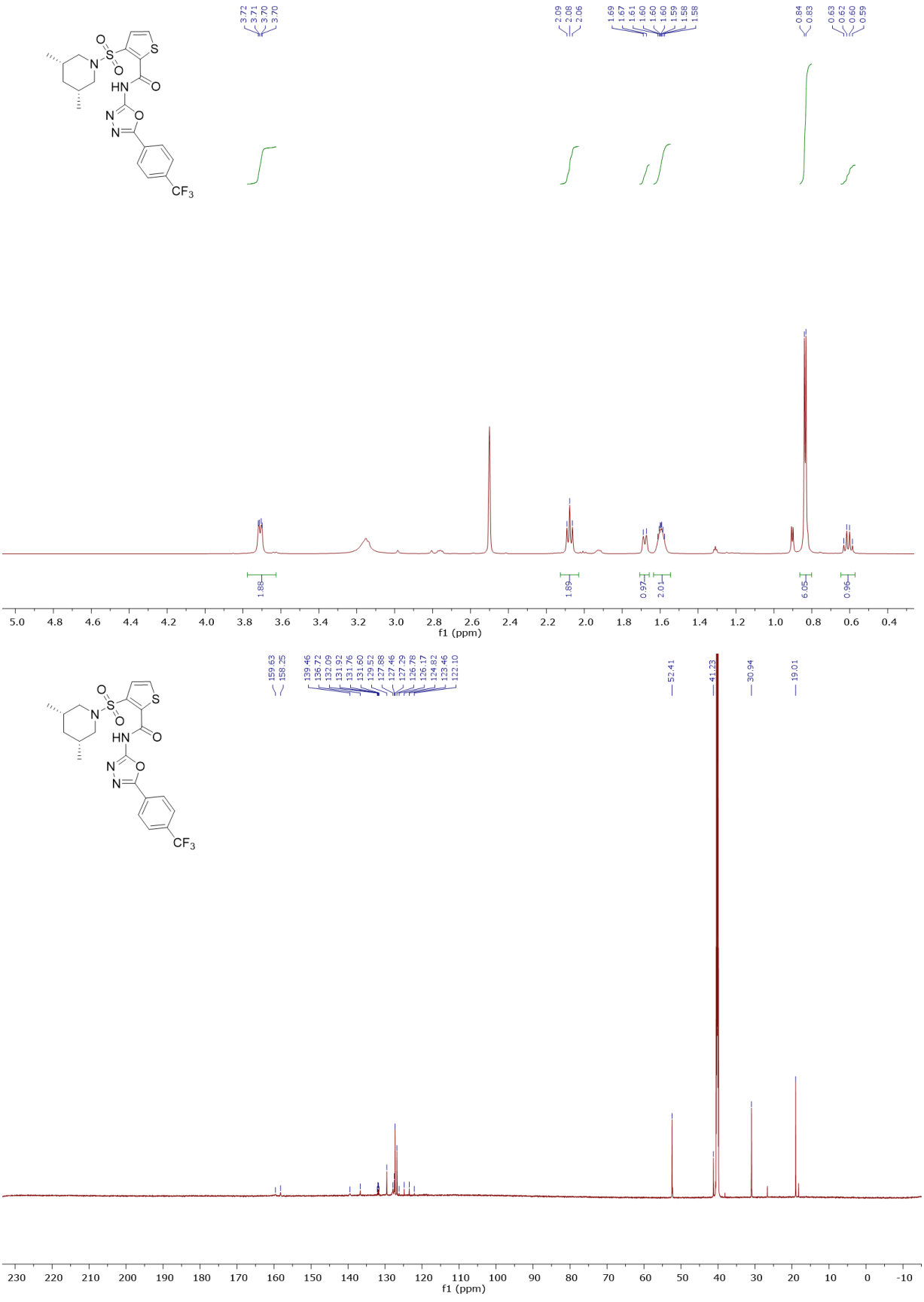
3.72
3.71
3.70
3.70
2.09
2.08
2.06
1.69
1.67
1.61
1.60
1.60
1.60
1.59
1.58
1.58
0.84
0.83
0.63
0.62
0.60
0.59
1.88
1.89
0.97
2.01
6.05
0.96
f1 (ppm)
159.63
158.25
139.46
136.72
132.09
131.92
131.76
131.60
129.52
127.88
127.46
127.39
126.78
126.17
124.82
123.46
122.10
52.41
41.23
30.94
19.01
f1 (ppm)

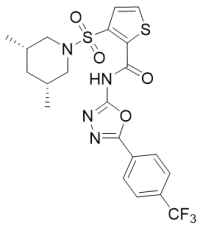
O
S
O
N
S
HN
O
N
O
N
CF3

-62.74
10 0 -10 -20 -30 -40 -50 -60 -70 -80 -90 -100 -110 -120 -130 -140 -150 -160 -170 -180 -190 -200 -210 -220
f1 (ppm)

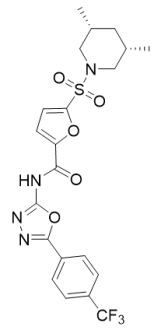
N
O
S
O
O
HN
O
N
O
N
CF3

8.17
8.16
7.98
7.97
7.62
7.62
7.32
7.31
3.70
3.69
3.68
3.68
2.22
2.21
2.19
1.71
1.70
1.69
1.64
1.63
1.62
1.62
1.62
1.61
1.60
0.86
0.85
0.67
0.66
0.64
0.63
2.04
2.07
0.92
0.93
1.93
1.87
0.98
1.92
6.00
0.93
13.5 13.0 12.5 12.0 11.5 11.0 10.5 10.0 9.5 9.0 8.5 8.0 7.5 7.0 6.5 6.0 5.5 5.0 4.5 4.0 3.5 3.0 2.5 2.0 1.5 1.0 0.5 0.0 -0.5 -1.0
f1 (ppm)

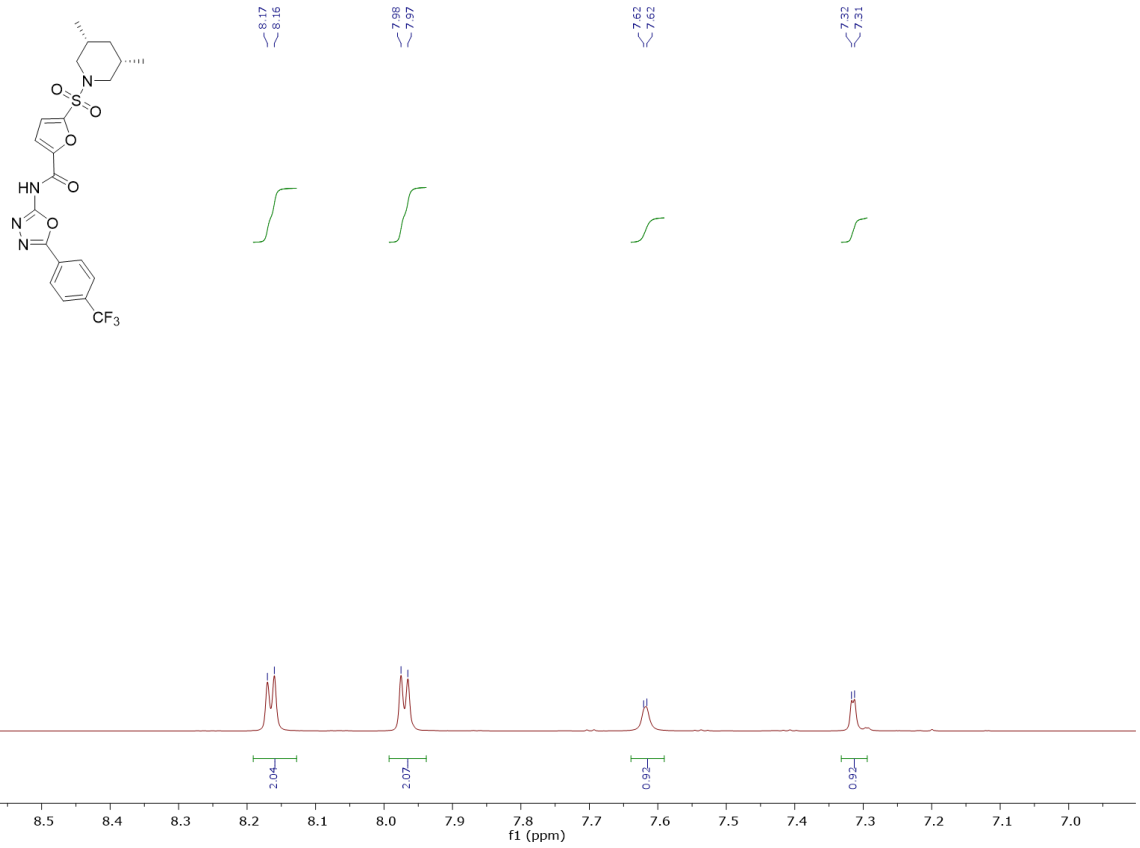
8.17
8.16
7.98
7.97
7.62
7.62
7.32
7.31
2.04
2.07
0.92
0.92
8.6
8.5
8.4
8.3
8.2
8.1
8.0
7.9
7.8
7.7
7.6
7.5
7.4
7.3
7.2
7.1
7.0
f1 (ppm)

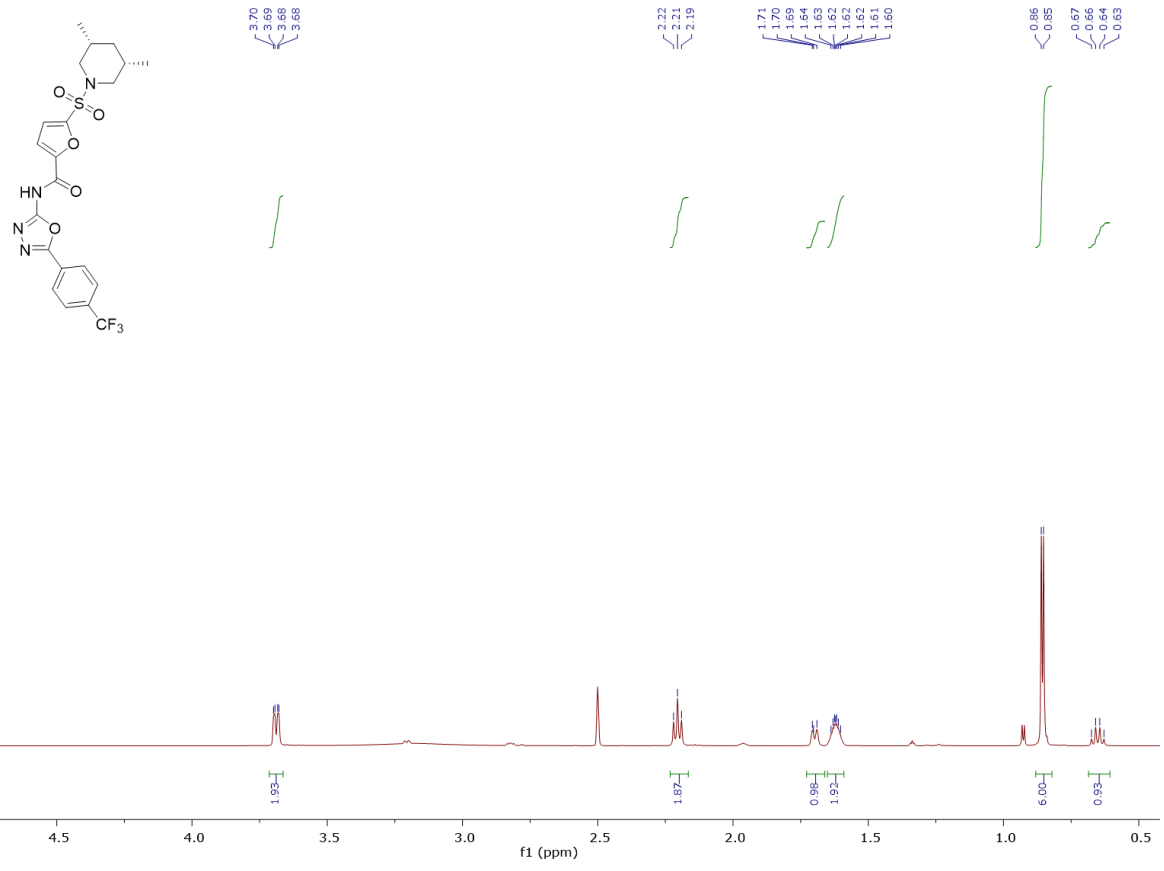
3.70
3.69
3.68
3.68
2.22
2.21
2.19
1.71
1.70
1.69
1.64
1.63
1.62
1.62
1.62
1.61
1.60
0.86
0.85
0.67
0.66
0.64
0.63
1.93
1.87
0.98
1.92
6.00
0.93
4.5
4.0
3.5
3.0
2.5
2.0
1.5
1.0
0.5
f1 (ppm)

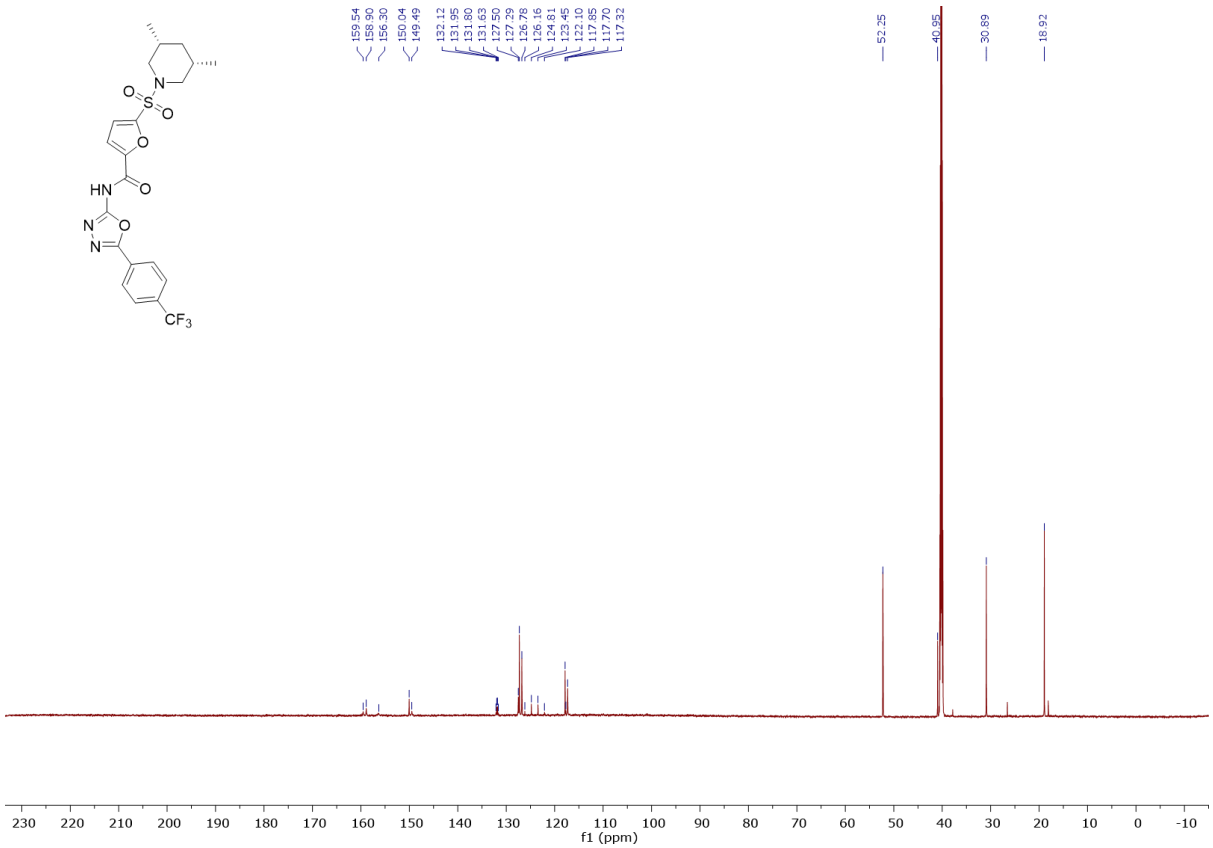
159.54
158.90
156.30
150.04
149.49
132.12
131.95
131.80
131.63
127.50
127.29
126.78
126.16
124.81
123.45
122.10
117.85
117.70
117.32
52.25
40.95
30.89
18.92
230 220 210 200 190 180 170 160 150 140 130 120 110 100 90 80 70 60 50 40 30 20 10 0 -10
f1 (ppm)

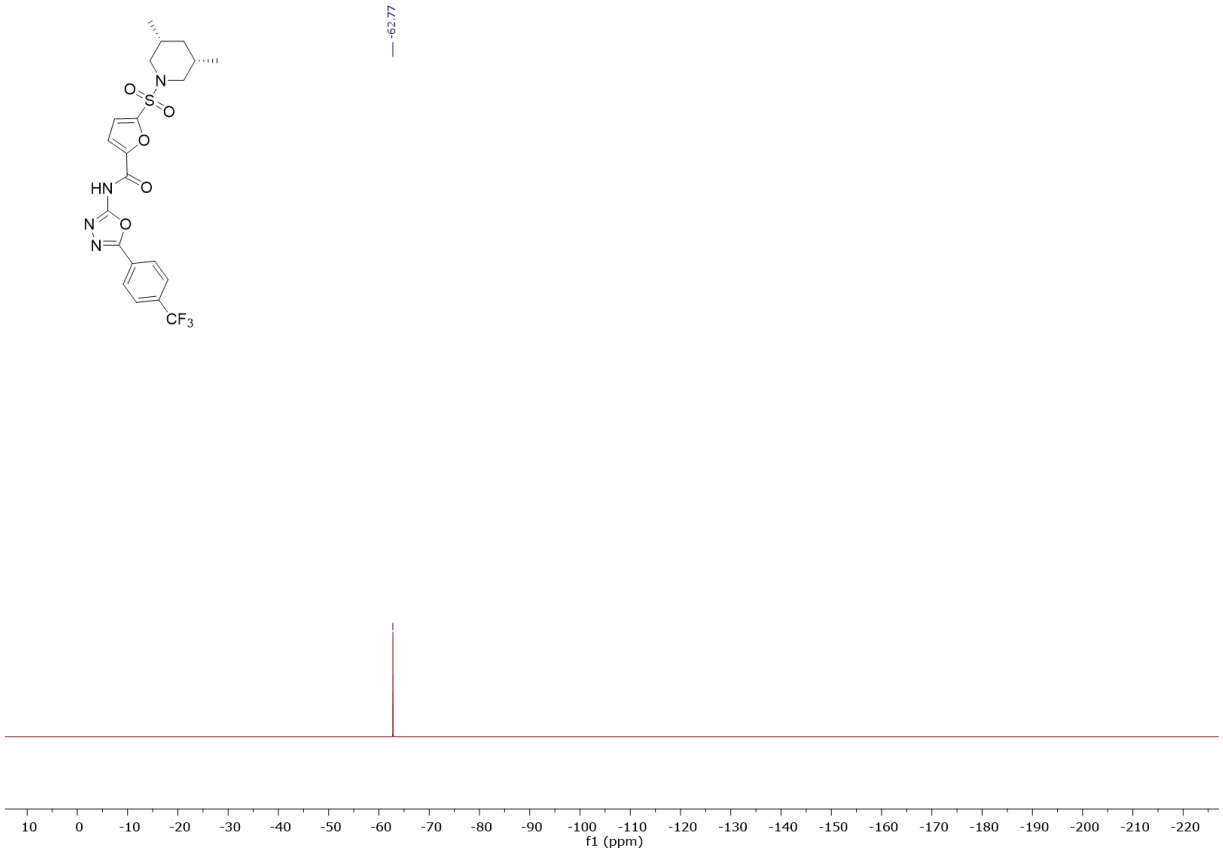
-62.77
10 0 -10 -20 -30 -40 -50 -60 -70 -80 -90 -100 -110 -120 -130 -140 -150 -160 -170 -180 -190 -200 -210 -220
f1 (ppm)

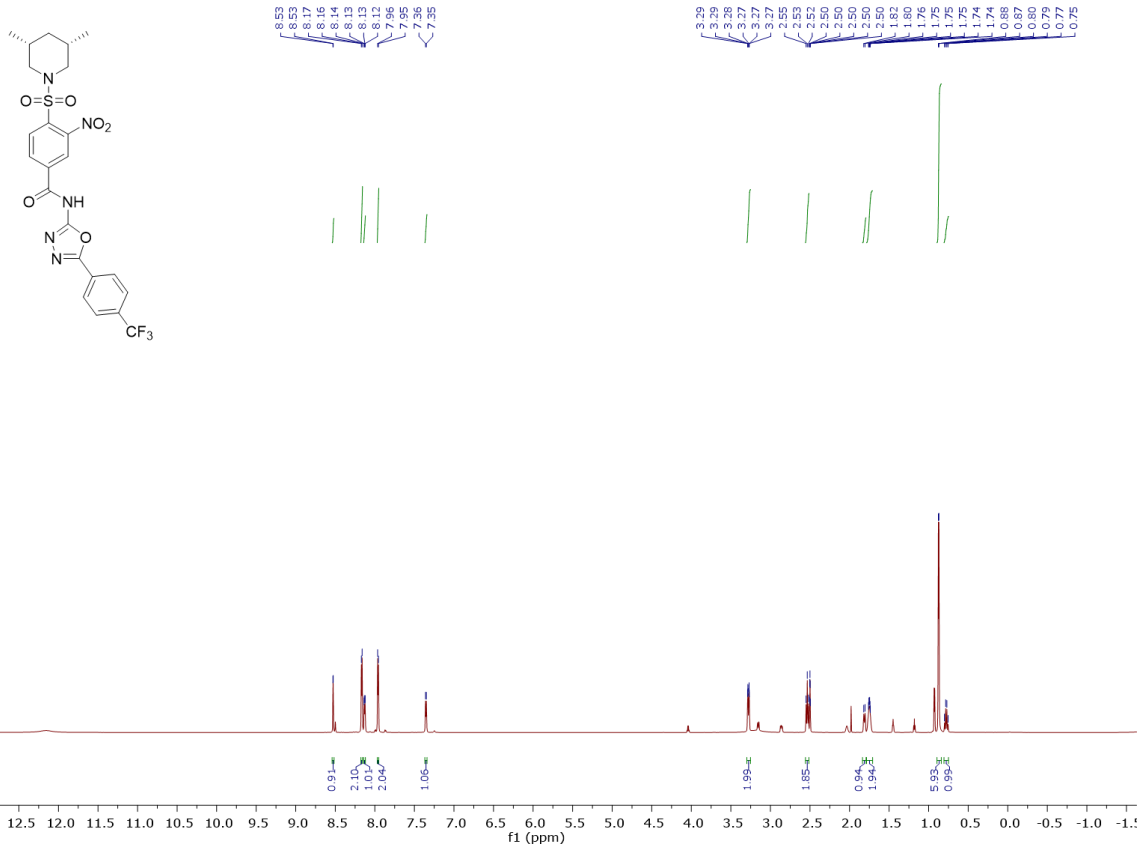
8.53
8.53
8.17
8.16
8.14
8.13
8.13
8.12
7.96
7.95
7.36
7.35
3.29
3.29
3.28
3.27
3.27
3.27
2.55
2.53
2.52
2.50
2.50
2.50
2.50
2.50
1.82
1.80
1.76
1.75
1.75
1.75
1.74
1.74
0.88
0.87
0.80
0.79
0.77
0.75
0.91
2.10
1.01
2.04
1.06
1.99
1.85
0.94
1.94
5.93
0.99
f1 (ppm)

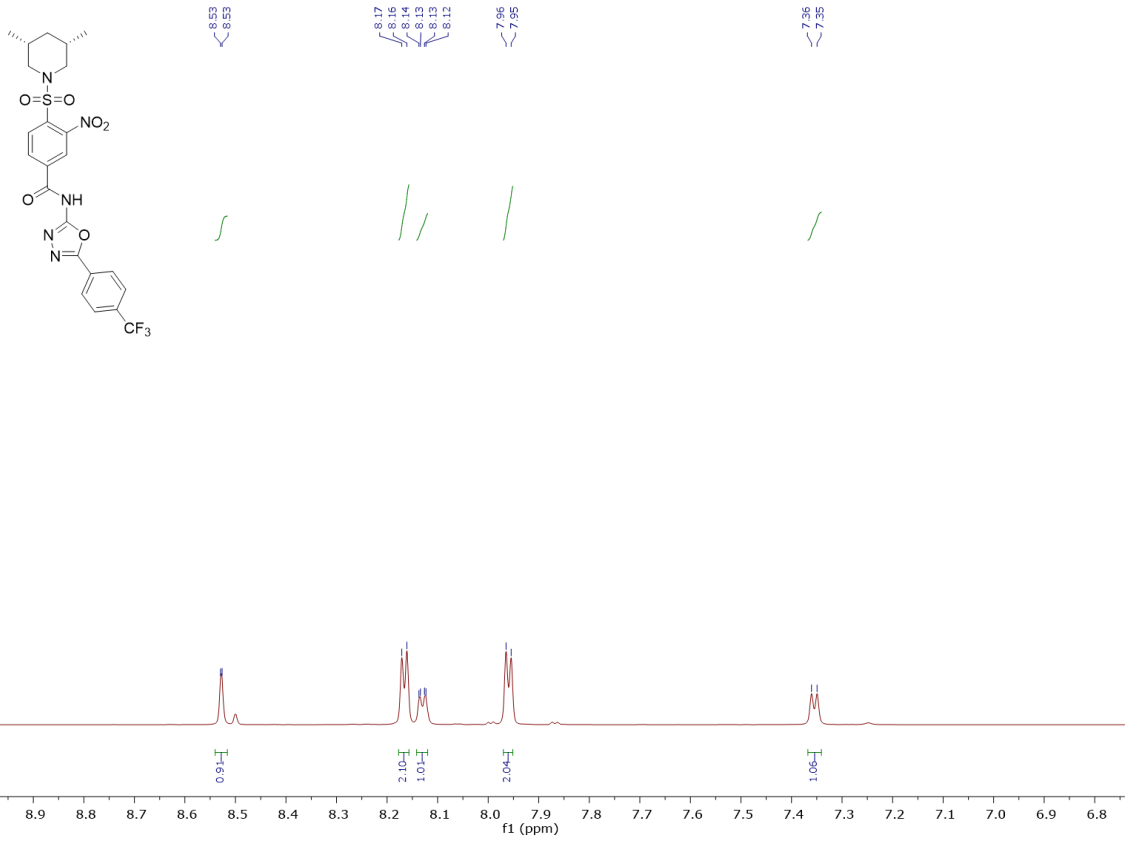
8.53
8.53
8.17
8.16
8.14
8.13
8.13
8.12
7.96
7.95
7.36
7.35
0.91
2.10
1.01
2.04
1.06
f1 (ppm)

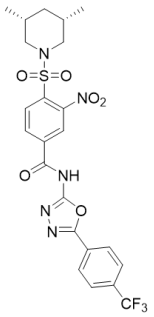

3.29
3.29
3.28
3.27
3.27
3.27
2.55
2.53
2.52
2.50
2.50
2.50
2.50
2.50
1.82
1.80
1.76
1.75
1.75
1.75
1.74
1.74
0.88
0.87
0.80
0.79
0.77
0.75
1.99
1.85
0.94
1.94
5.93
0.99
f1 (ppm)

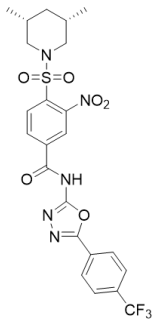

163.41
160.07
159.04
148.24
139.10
133.64
132.05
131.89
131.73
131.57
127.59
127.40
127.25
126.76
126.74
126.08
124.81
123.46
122.10
120.70
57.74
41.55
31.02
19.03
f1 (ppm)

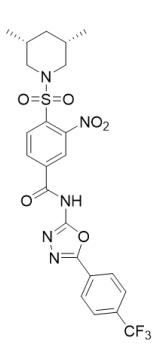

-62.78
10 0 -10 -20 -30 -40 -50 -60 -70 -80 -90 -100 -110 -120 -130 -140 -150 -160 -170 -180 -190 -200 -210 -220
f1 (ppm)

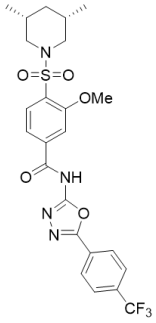

8.17 8.16 7.99 7.98 7.90 7.88 7.81 7.81 7.71 7.71 7.70 7.69
3.97 3.65 3.65 3.63 3.62
2.13 2.11 2.08 2.07 1.69 1.68 1.68 1.66 1.66 1.57 1.56 1.55 1.54 1.54 1.53 1.52 1.51 0.81 0.80 0.63 0.61 0.58 0.56
2.06 2.05 0.95 1.00 1.00
2.91 2.00
2.16 1.02 2.10 5.95 1.06
12.0 11.5 11.0 10.5 10.0 9.5 9.0 8.5 8.0 7.5 7.0 6.5 6.0 5.5 5.0 4.5 4.0 3.5 3.0 2.5 2.0 1.5 1.0 0.5 0.0 -0.5 -1.0 -1
f1 (ppm)

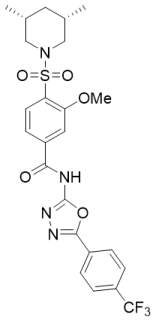
N
O=S=O
OMe
O
NH
N
O
N
CF3

8.17
8.16
7.99
7.98
7.90
7.88
7.81
7.81
7.71
7.71
7.70
7.69
2.08
2.09
0.95
1.00
1.00
8.90 8.85 8.80 8.75 8.70 8.65 8.60 8.55 8.50 8.45 8.40 8.35 8.30 8.25 8.20 8.15 8.10 8.05 8.00 7.95 7.90 7.85 7.80 7.75 7.70 7.65 7.60 7.55 7.50 7.45
f1 (ppm)

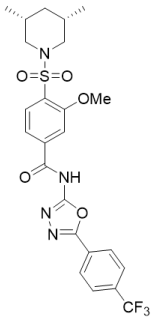
N
O=S=O
OMe
O
NH
N
O
N
CF3

3.97
3.65
3.65
3.63
3.62
2.13
2.11
2.08
2.07
1.69
1.68
1.68
1.66
1.66
1.57
1.56
1.55
1.54
1.54
1.53
1.52
1.51
0.81
0.80
0.63
0.61
0.58
0.56
2.91
2.00
2.16
1.02
2.10
5.95
1.06
5.5 5.0 4.5 4.0 3.5 3.0 2.5 2.0 1.5 1.0 0.5
f1 (ppm)

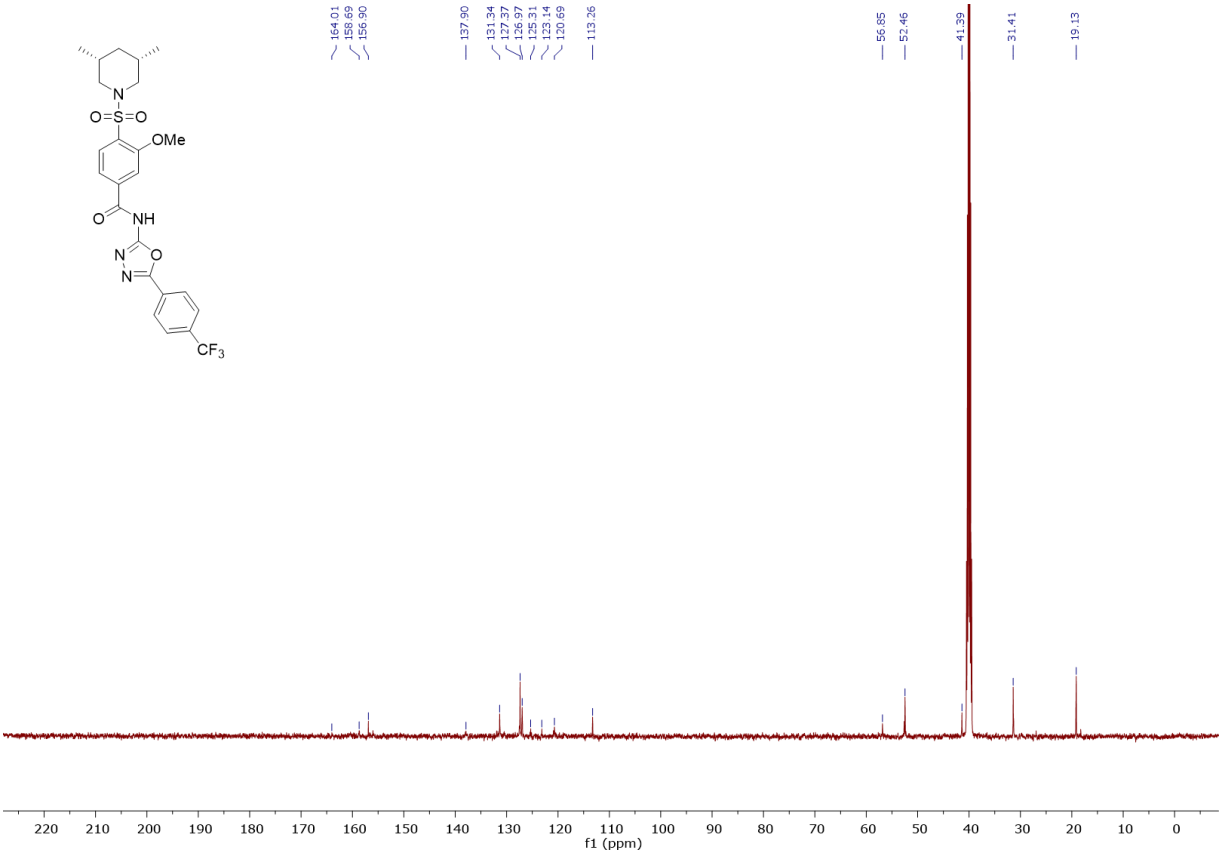
164.01
158.69
156.90
137.90
131.34
127.37
126.97
125.31
123.14
120.69
113.26
56.85
52.46
41.39
31.41
19.13
f1 (ppm)

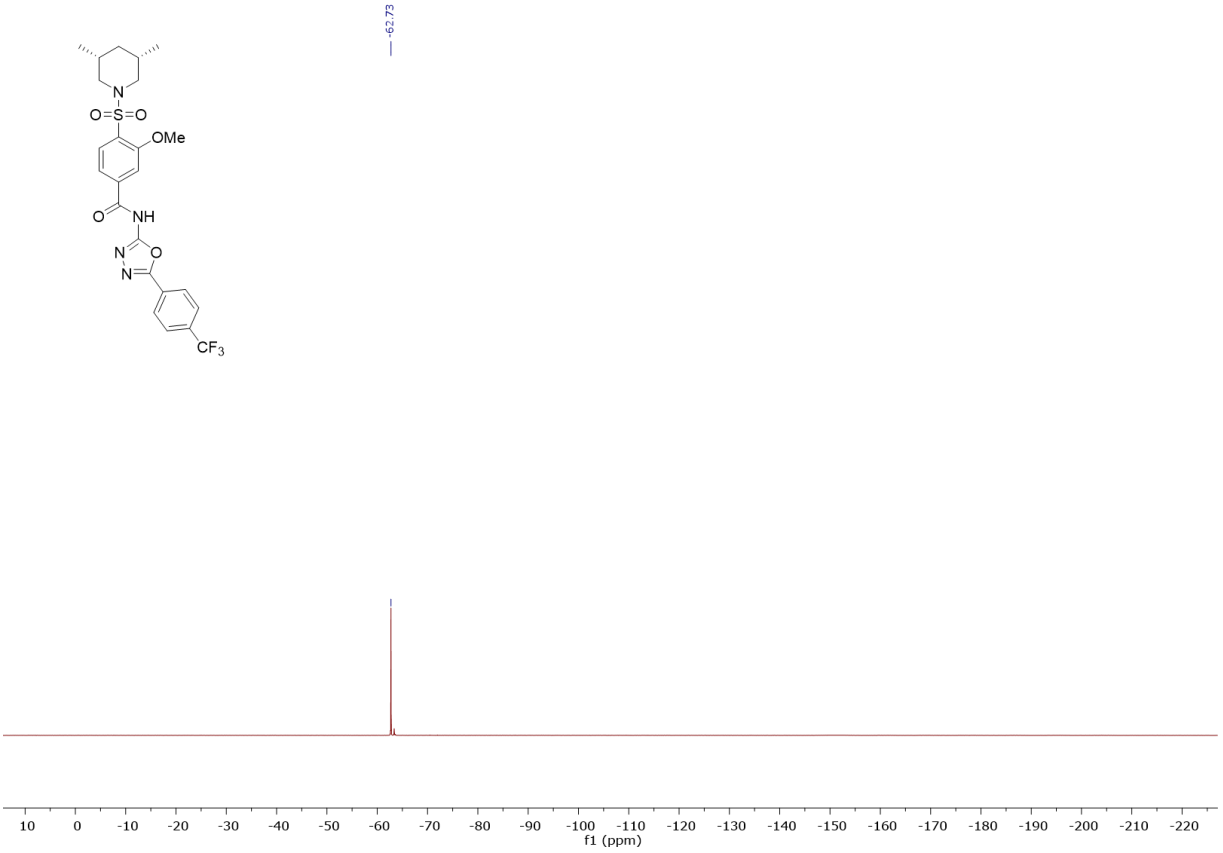
-62.73
f1 (ppm)

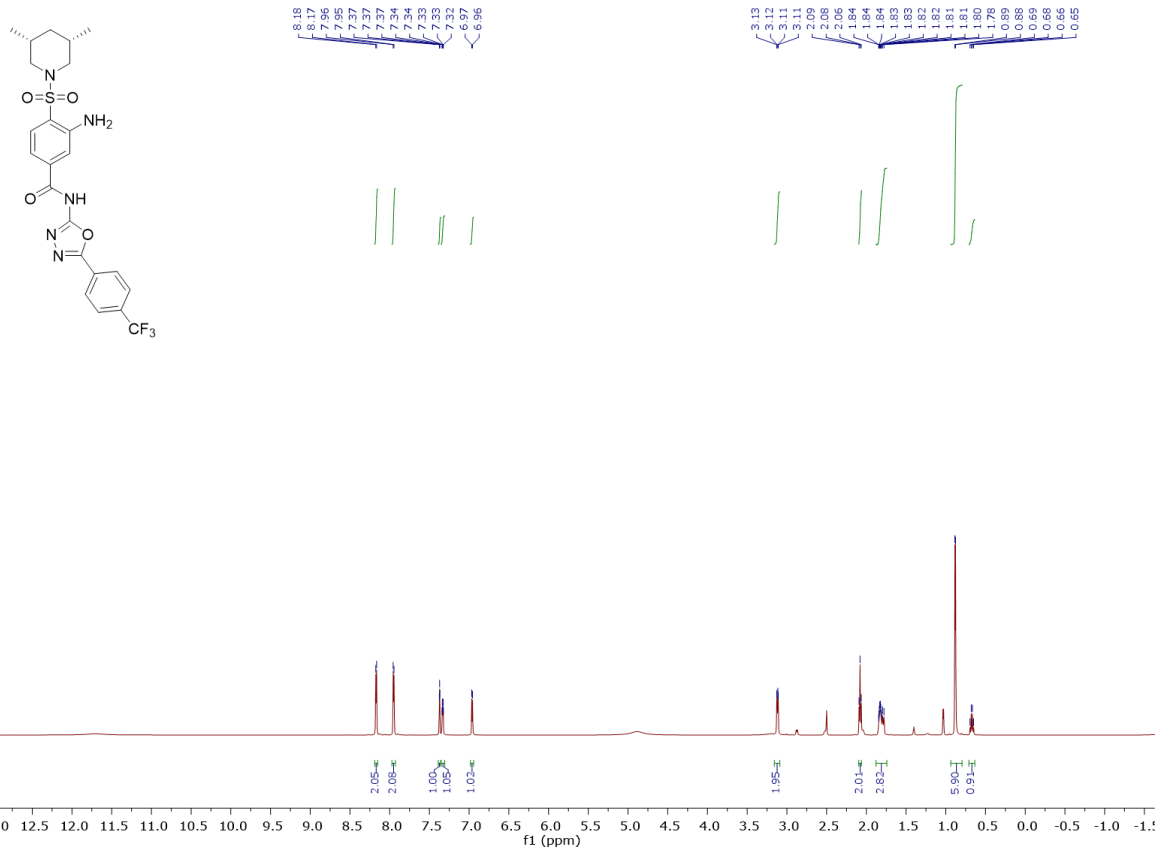
8.18
8.17
7.96
7.95
7.37
7.37
7.34
7.34
7.33
7.33
7.32
6.97
6.96
3.13
3.12
3.11
3.11
2.09
2.08
2.06
1.84
1.84
1.84
1.83
1.83
1.82
1.82
1.81
1.81
1.80
1.78
0.89
0.88
0.69
0.68
0.66
0.65
2.05
2.08
1.00
1.05
1.02
1.95
2.01
2.82
5.90
0.91
f1 (ppm)

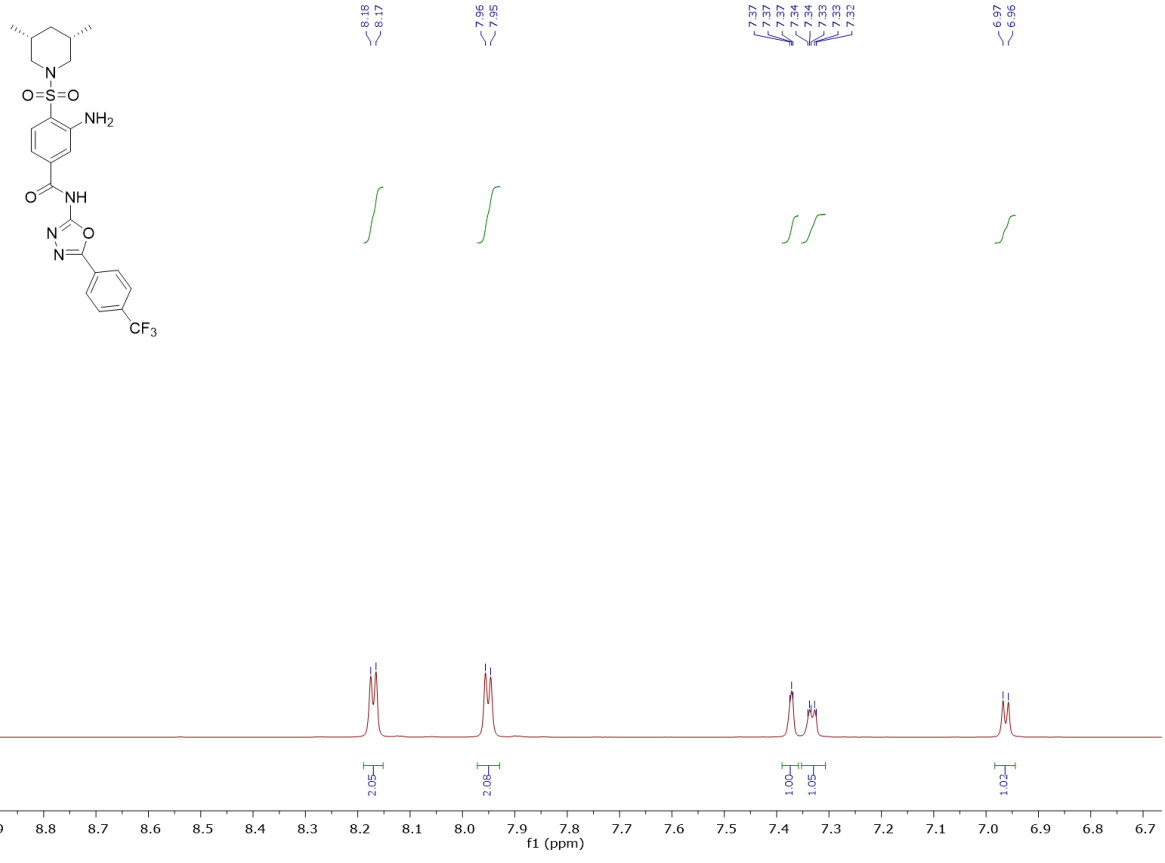
8.18
8.17
7.96
7.95
7.37
7.37
7.37
7.34
7.34
7.33
7.33
7.32
6.97
6.96
2.05
2.08
1.00
1.05
1.02
f1 (ppm)

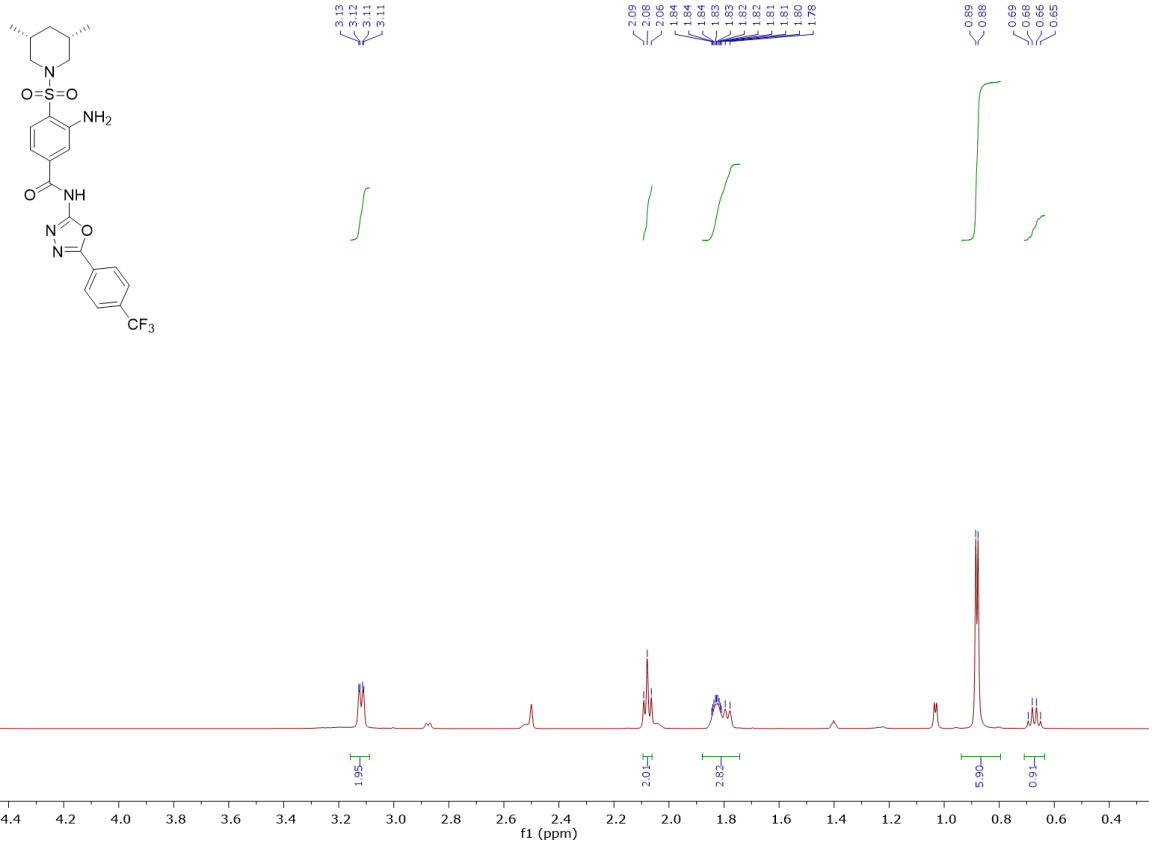
3.13
3.12
3.11
3.11
2.09
2.08
2.06
1.84
1.84
1.84
1.83
1.83
1.82
1.82
1.81
1.81
1.80
1.78
0.89
0.88
0.69
0.68
0.66
0.65
1.95
2.01
2.82
5.90
0.91
4.6 4.4 4.2 4.0 3.8 3.6 3.4 3.2 3.0 2.8 2.6 2.4 2.2 2.0 1.8 1.6 1.4 1.2 1.0 0.8 0.6 0.4
f1 (ppm)

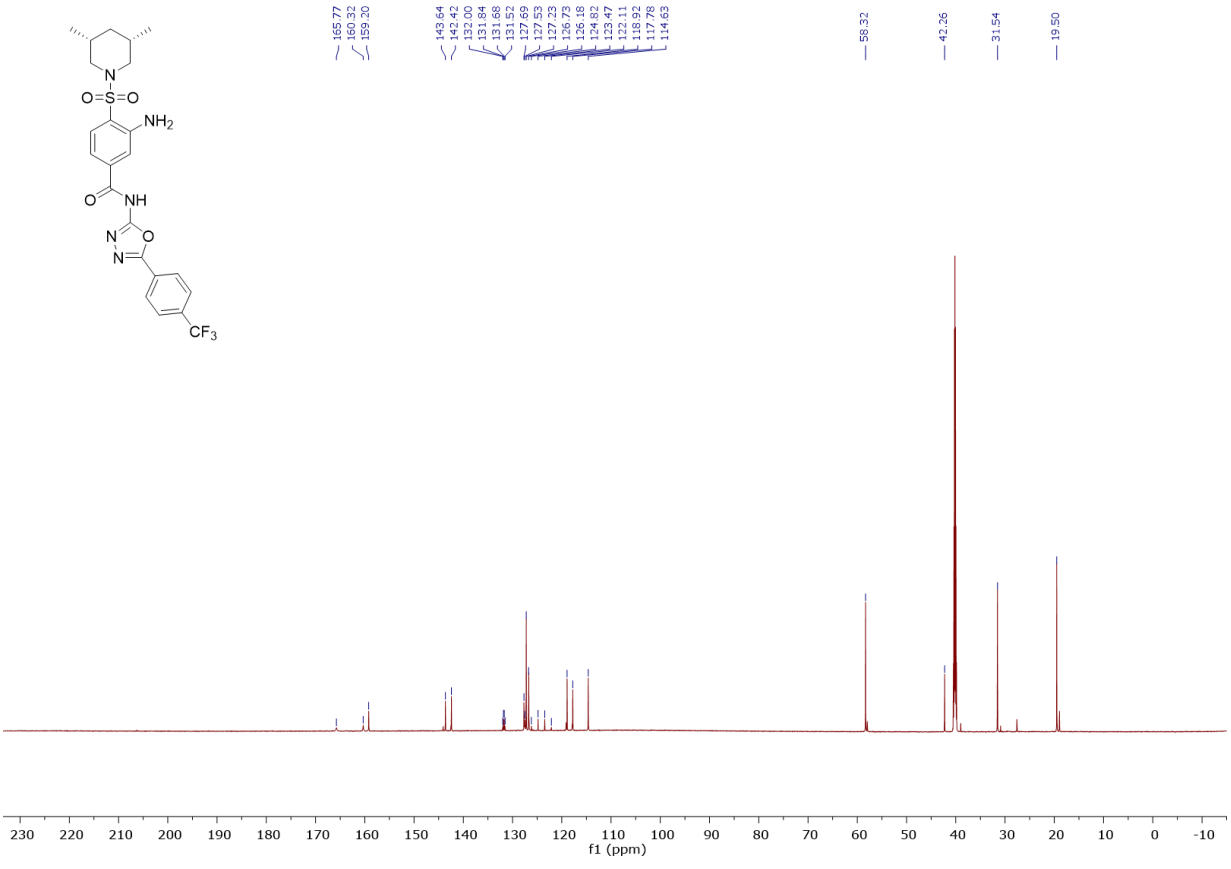
165.77
160.32
159.20
143.64
142.42
132.00
131.84
131.68
131.52
127.69
127.53
127.23
126.73
126.18
124.82
123.47
122.11
118.92
117.78
114.63
58.32
42.26
31.54
19.50
230 220 210 200 190 180 170 160 150 140 130 120 110 100 90 80 70 60 50 40 30 20 10 0 -10
f1 (ppm)

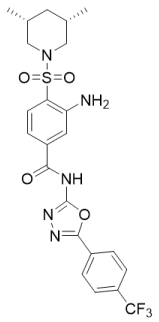
N
O=S=O
NH2
O
NH
N
O
N
CF3

-62.78
10 0 -10 -20 -30 -40 -50 -60 -70 -80 -90 -100 -110 -120 -130 -140 -150 -160 -170 -180 -190 -200 -210 -220
f1 (ppm)

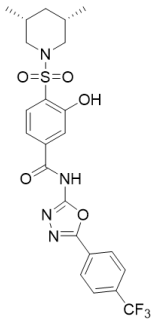
N
O=S=O
OH
O
NH
N
O
N
CF3

8.16 8.16 8.15 7.99 7.97 7.90 7.88 7.81 7.79 7.78 7.71 7.69 7.57 7.56 7.54 7.54
3.67 3.66 3.64 3.64 3.63
2.12 2.11 2.10 2.08 2.07 2.06 1.68 1.65 1.58 1.57 1.56 1.55 1.53 1.52 0.81 0.79 0.62 0.61 0.59 0.58 0.57 0.56 0.54
2.07 2.05 0.80 2.01 1.16
1.93
2.18 1.11 2.04 6.09 1.10
12.0 11.5 11.0 10.5 10.0 9.5 9.0 8.5 8.0 7.5 7.0 6.5 6.0 5.5 5.0 4.5 4.0 3.5 3.0 2.5 2.0 1.5 1.0 0.5 0.0 -0.5 -1.0 -1
f1 (ppm)

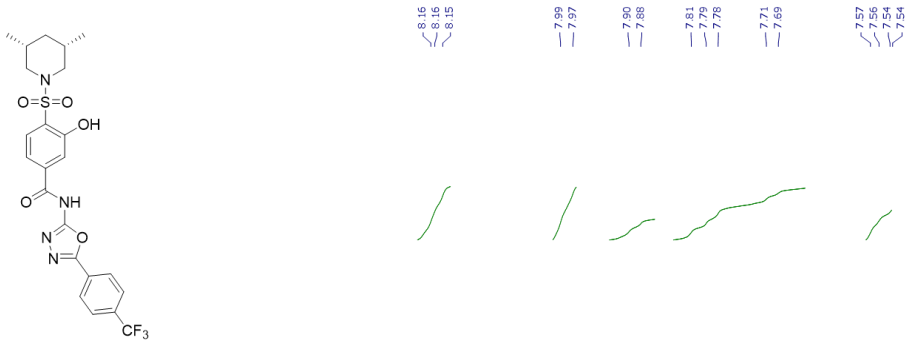
8.16
8.16
8.15
7.99
7.97
7.90
7.88
7.81
7.79
7.78
7.71
7.69
7.57
7.56
7.54
7.54

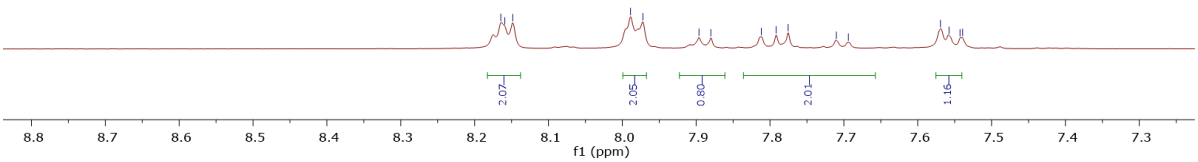
2.07
2.05
0.80
2.01
1.16
8.8
8.7
8.6
8.5
8.4
8.3
8.2
8.1
8.0
7.9
7.8
7.7
7.6
7.5
7.4
7.3
f1 (ppm)

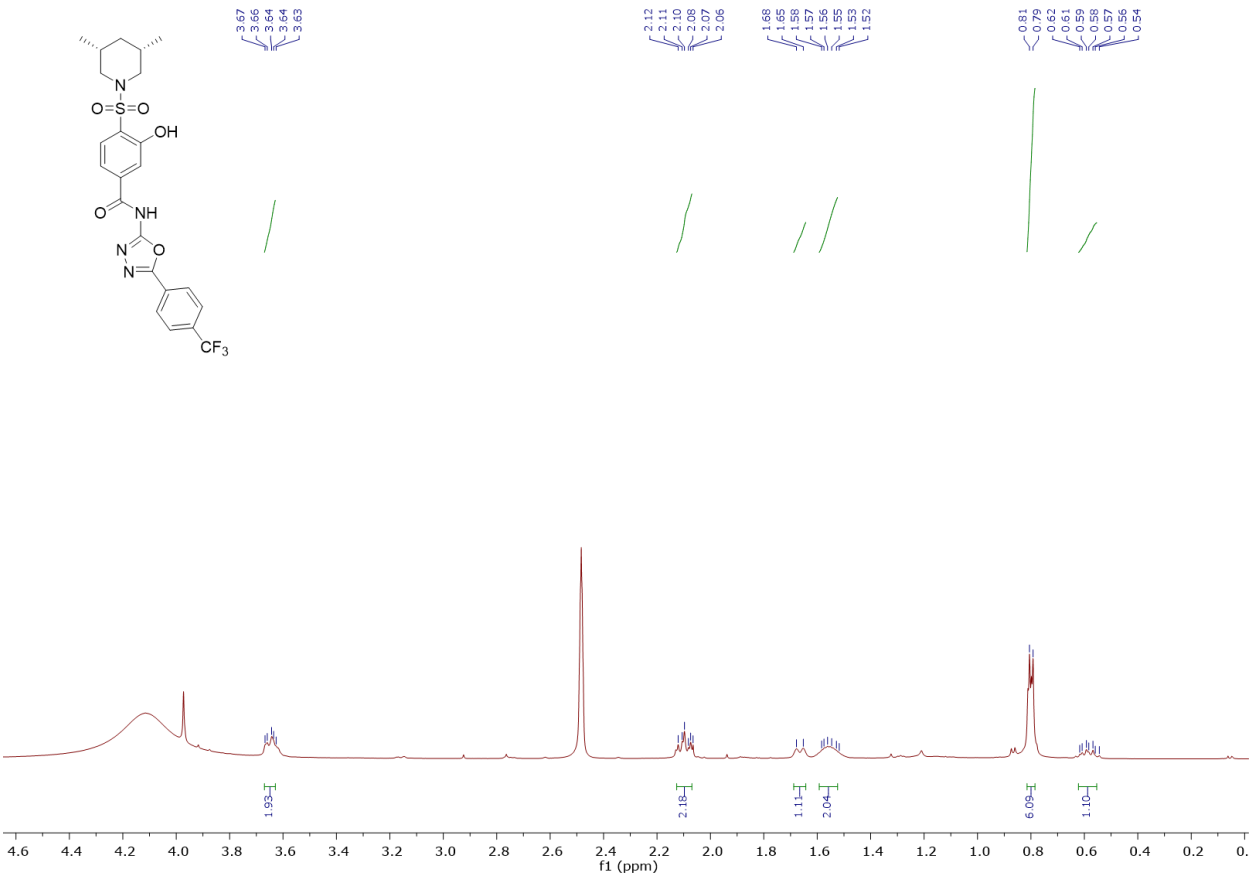
3.67
3.66
3.64
3.64
3.63
2.12
2.11
2.10
2.08
2.07
2.06
1.68
1.65
1.58
1.57
1.56
1.55
1.53
1.52
0.81
0.79
0.62
0.61
0.59
0.58
0.57
0.56
0.54
1.93
2.18
1.11
2.04
6.09
1.10
4.6
4.4
4.2
4.0
3.8
3.6
3.4
3.2
3.0
2.8
2.6
2.4
2.2
2.0
1.8
1.6
1.4
1.2
1.0
0.8
0.6
0.4
0.2
0.
f1 (ppm)

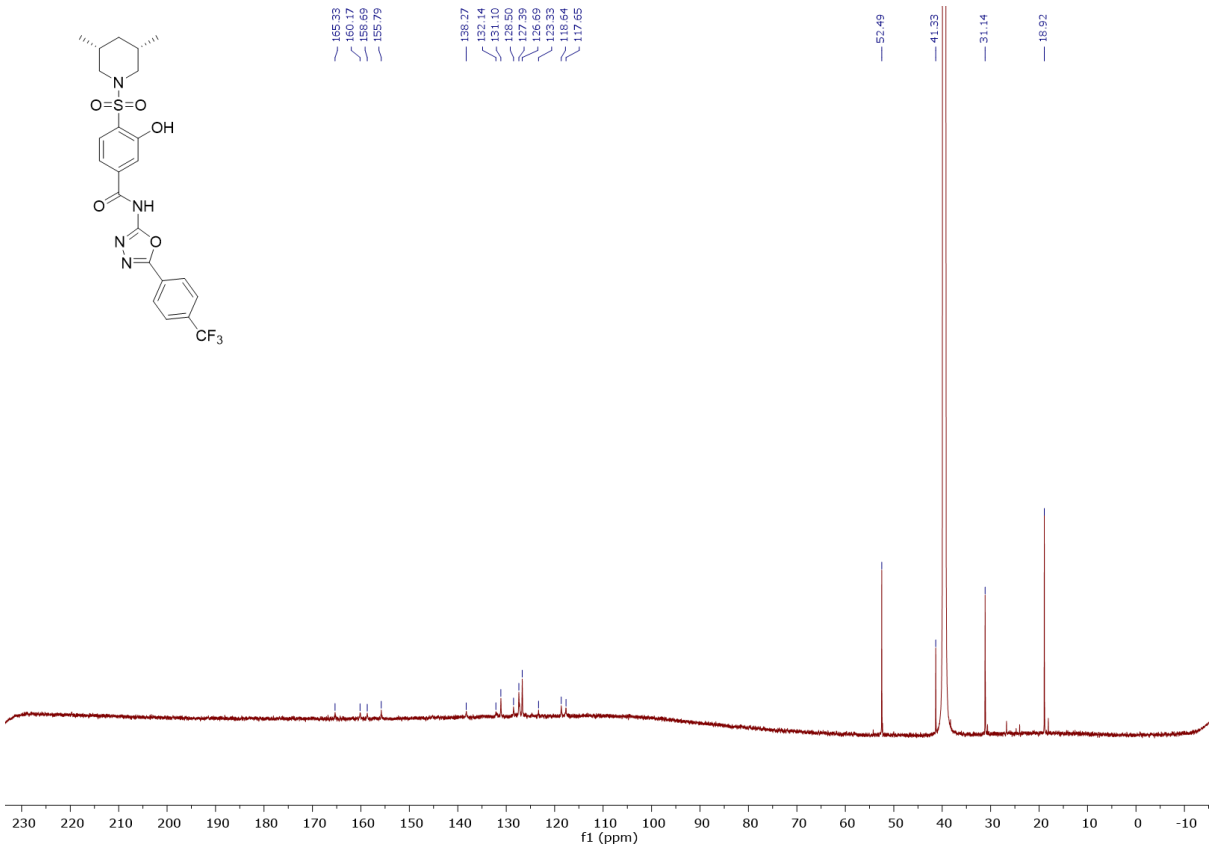
165.33
160.17
158.69
155.79
138.27
132.14
131.10
128.50
127.39
126.69
123.33
118.64
117.65
52.49
41.33
31.14
18.92
f1 (ppm)

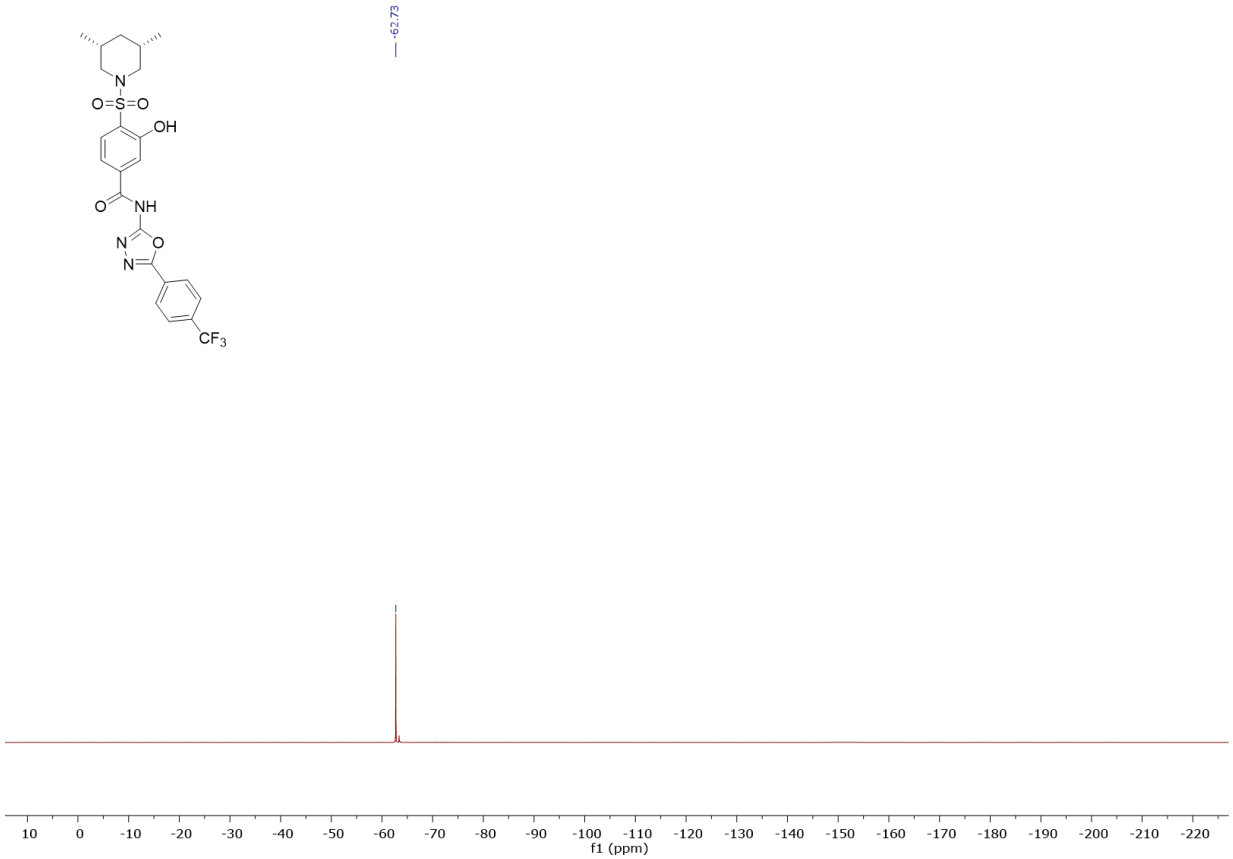
-62.73
f1 (ppm)

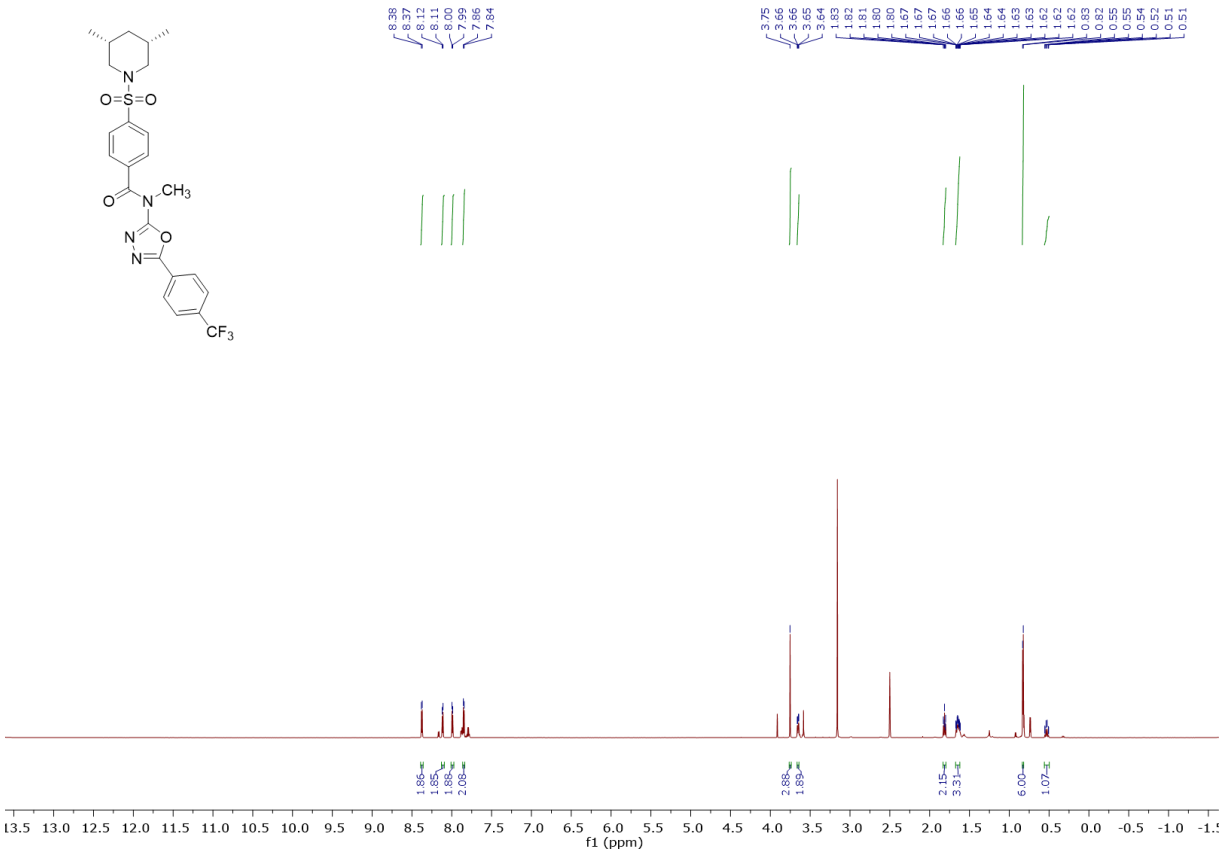
8.38
8.37
8.12
8.11
8.00
7.99
7.86
7.84
3.75
3.66
3.66
3.65
3.64
1.83
1.82
1.81
1.80
1.80
1.67
1.67
1.67
1.66
1.66
1.65
1.64
1.64
1.63
1.63
1.62
1.62
1.62
0.83
0.82
0.55
0.55
0.54
0.52
0.51
0.51
1.86
1.85
1.88
2.08
2.88
1.89
2.15
3.31
6.00
1.07
f1 (ppm)

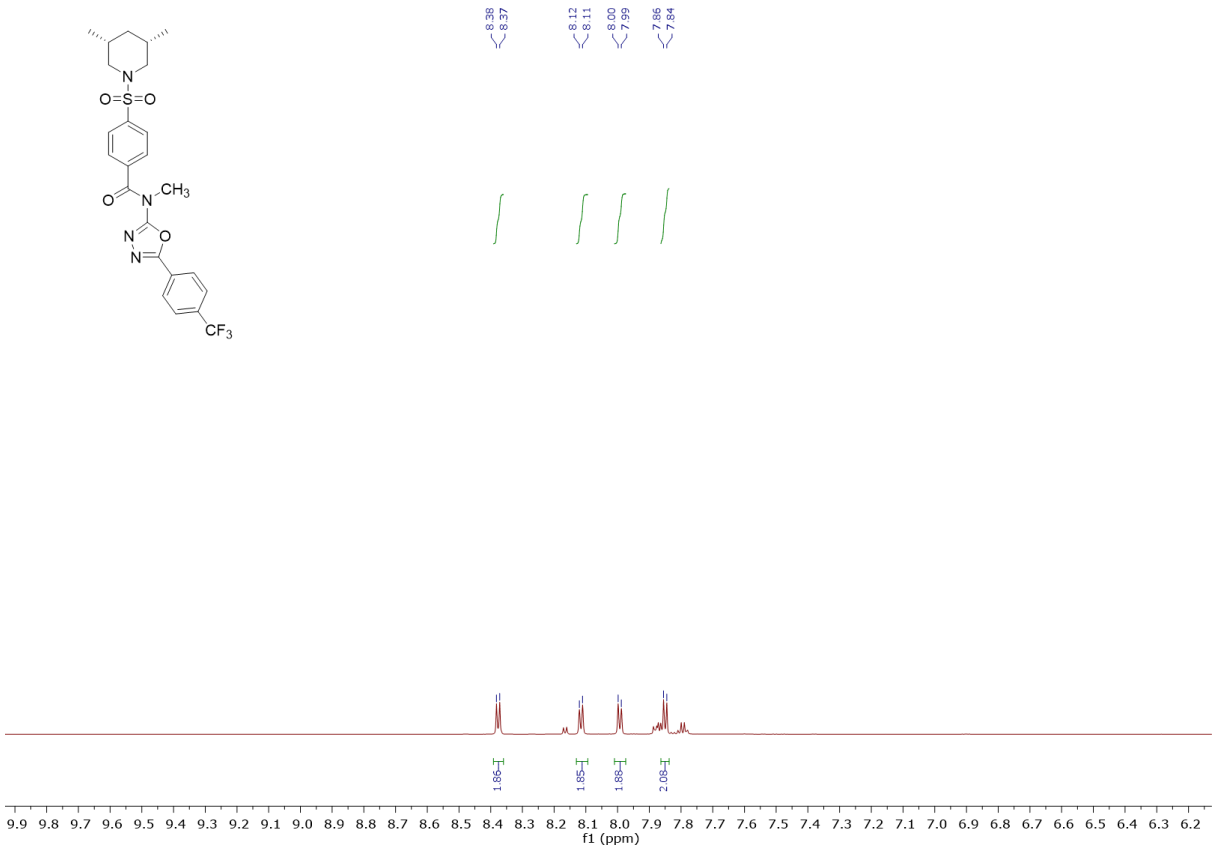
8.38
8.37
8.12
8.11
8.00
7.99
7.86
7.84
1.86
1.85
1.88
2.08
f1 (ppm)

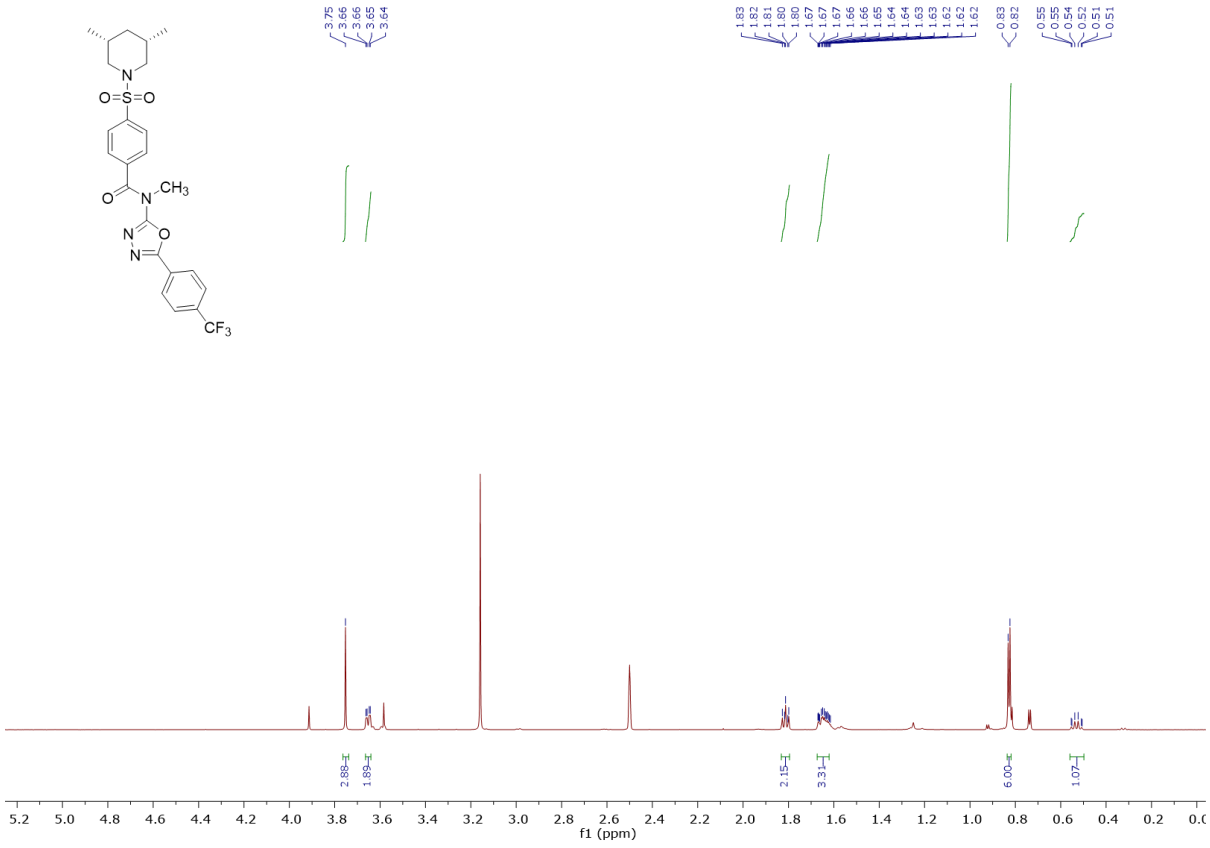
3.75
3.66
3.66
3.65
3.64
1.83
1.82
1.81
1.80
1.80
1.67
1.67
1.67
1.66
1.66
1.65
1.64
1.64
1.63
1.63
1.62
1.62
1.62
0.83
0.82
0.55
0.55
0.54
0.52
0.51
0.51
2.68
1.89
2.15
3.31
6.00
1.07
f1 (ppm)

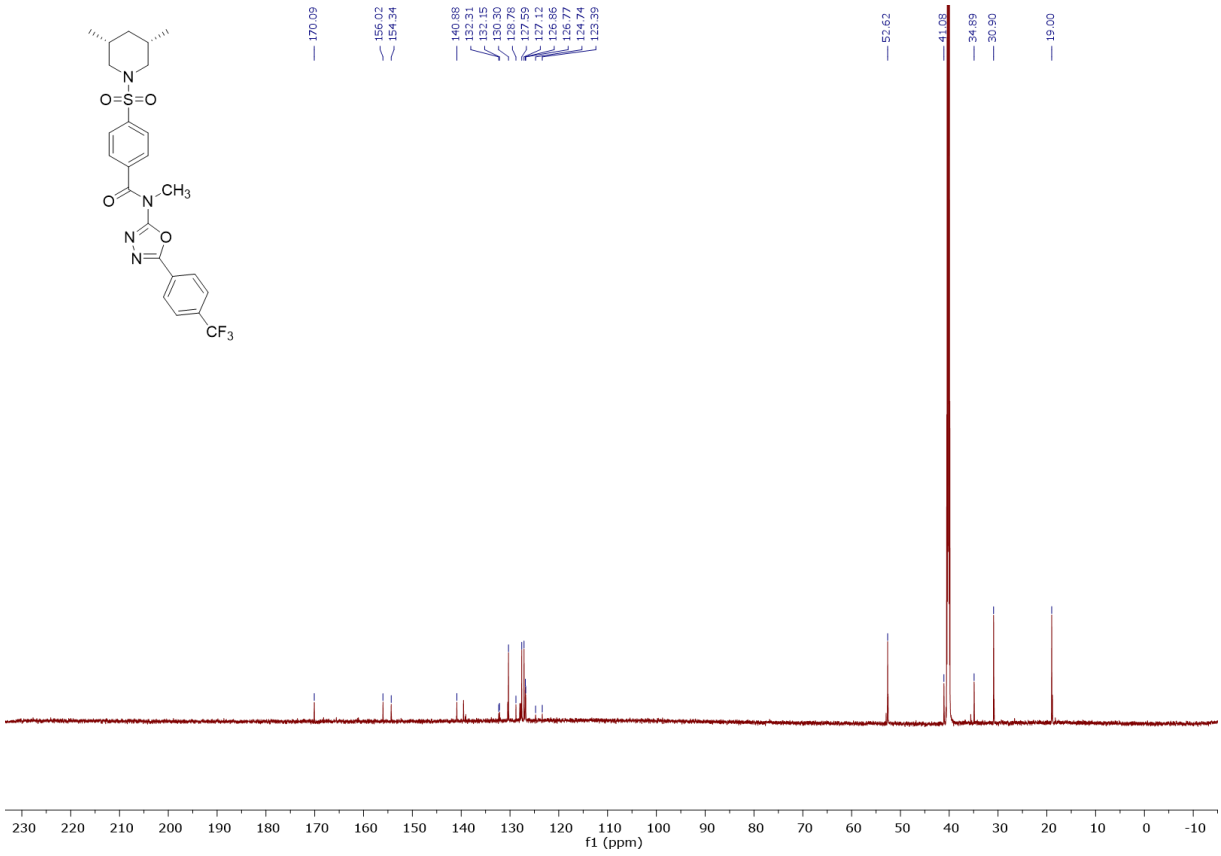
170.09
156.02
154.34
140.88
132.31
132.15
130.30
128.78
127.59
127.12
126.86
126.77
124.74
123.39
52.62
41.08
34.89
30.90
19.00
f1 (ppm)

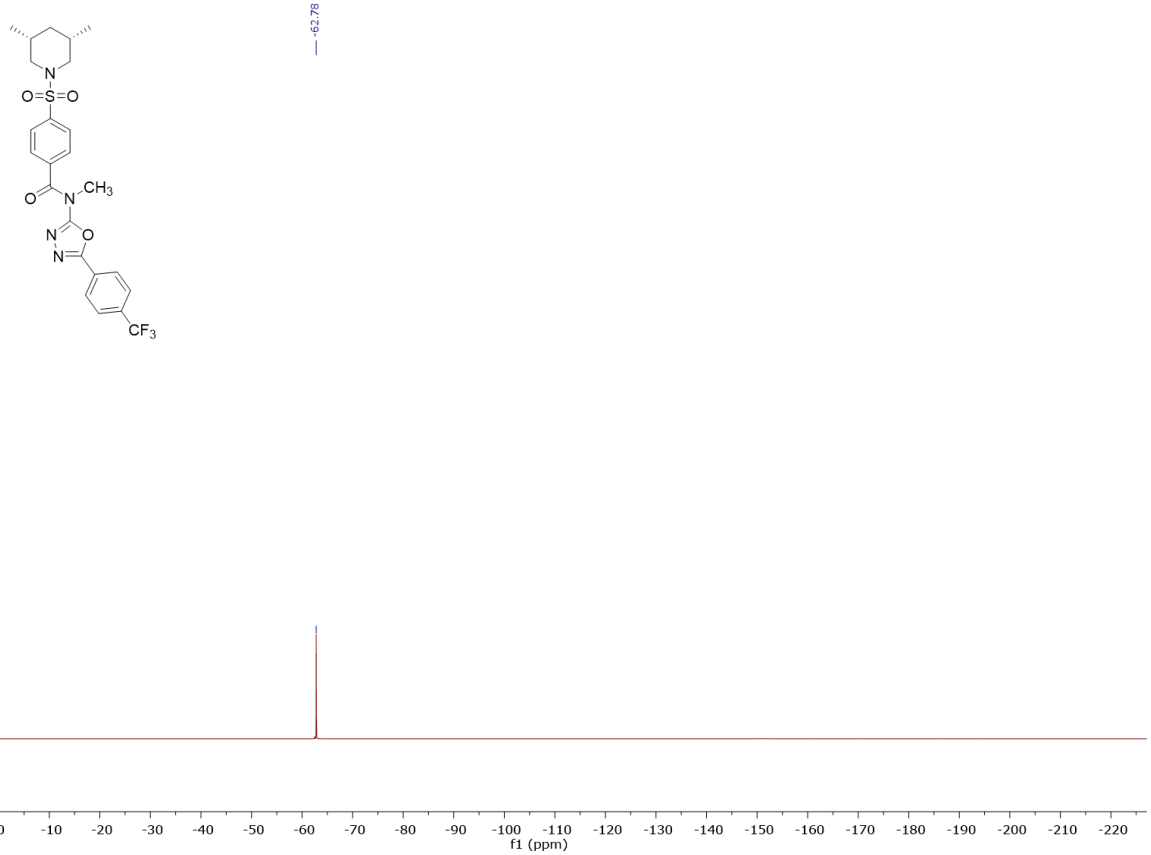
-62.78
f1 (ppm)

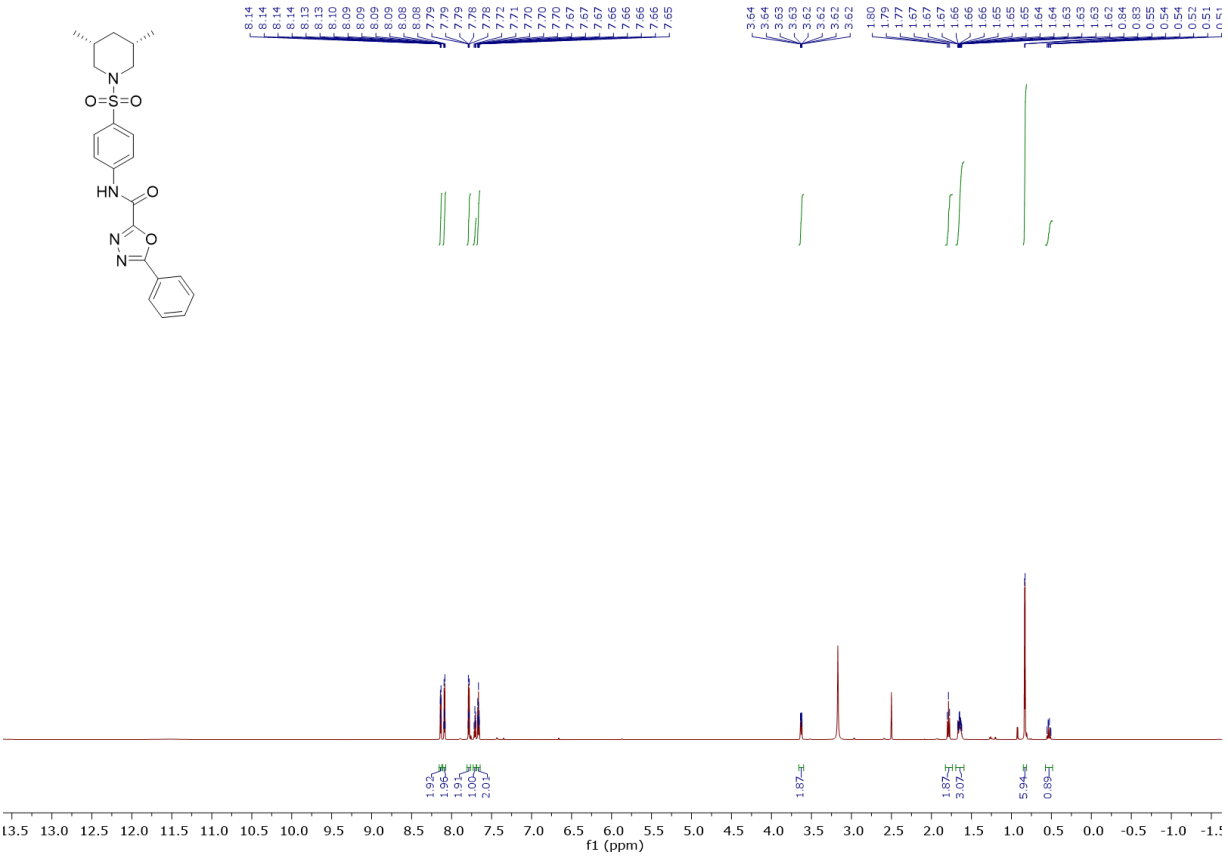
f1 (ppm)

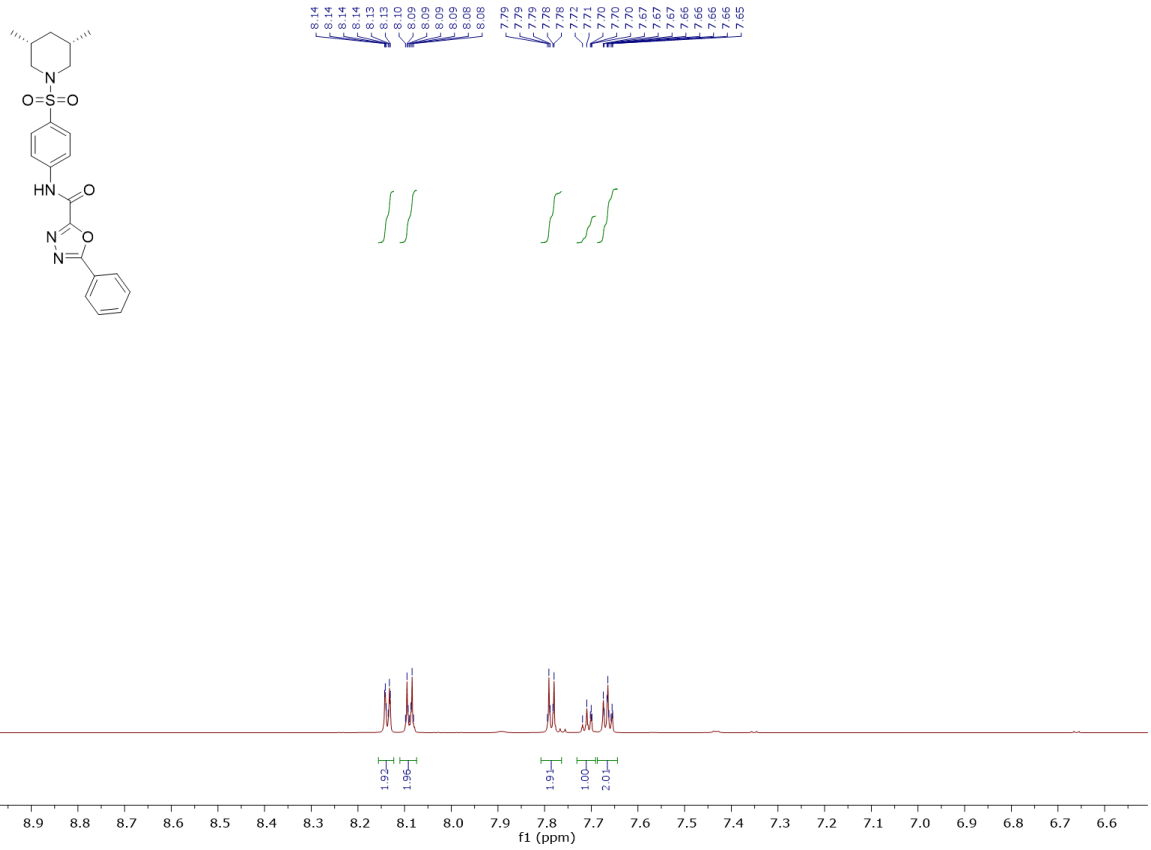

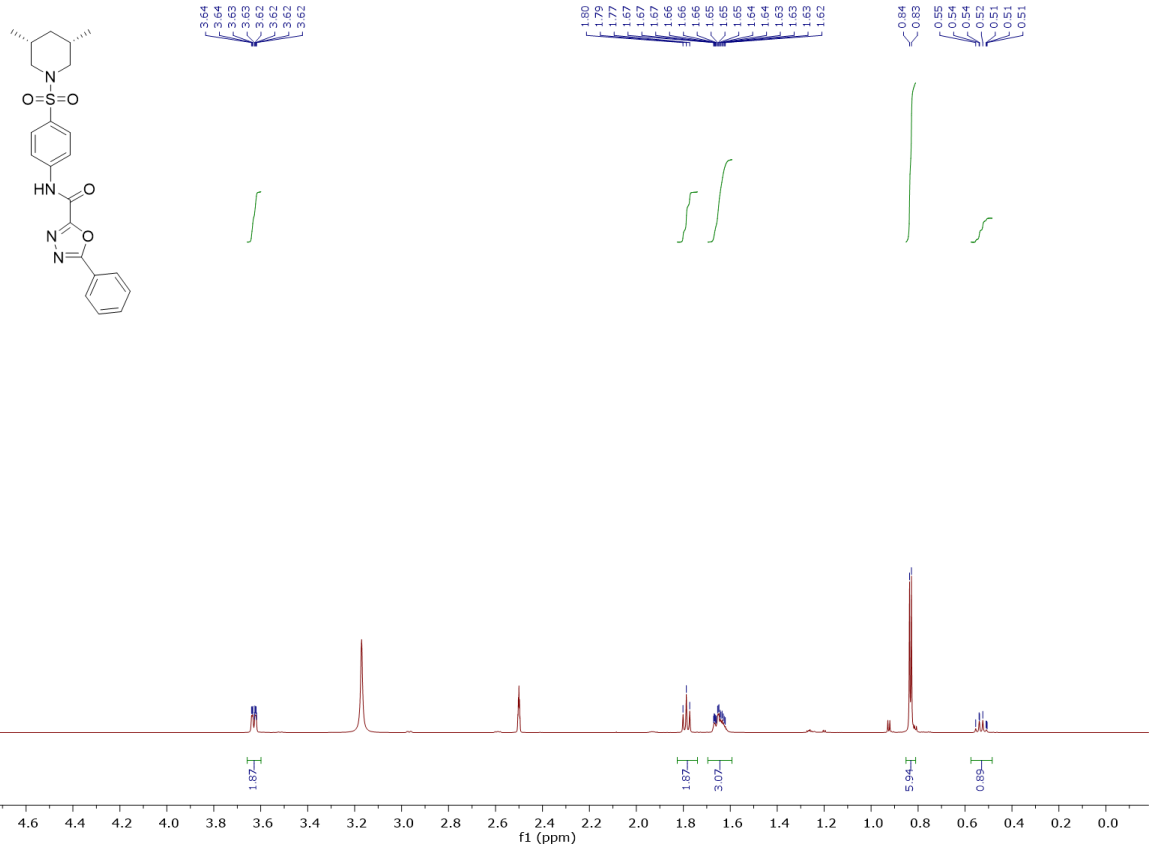

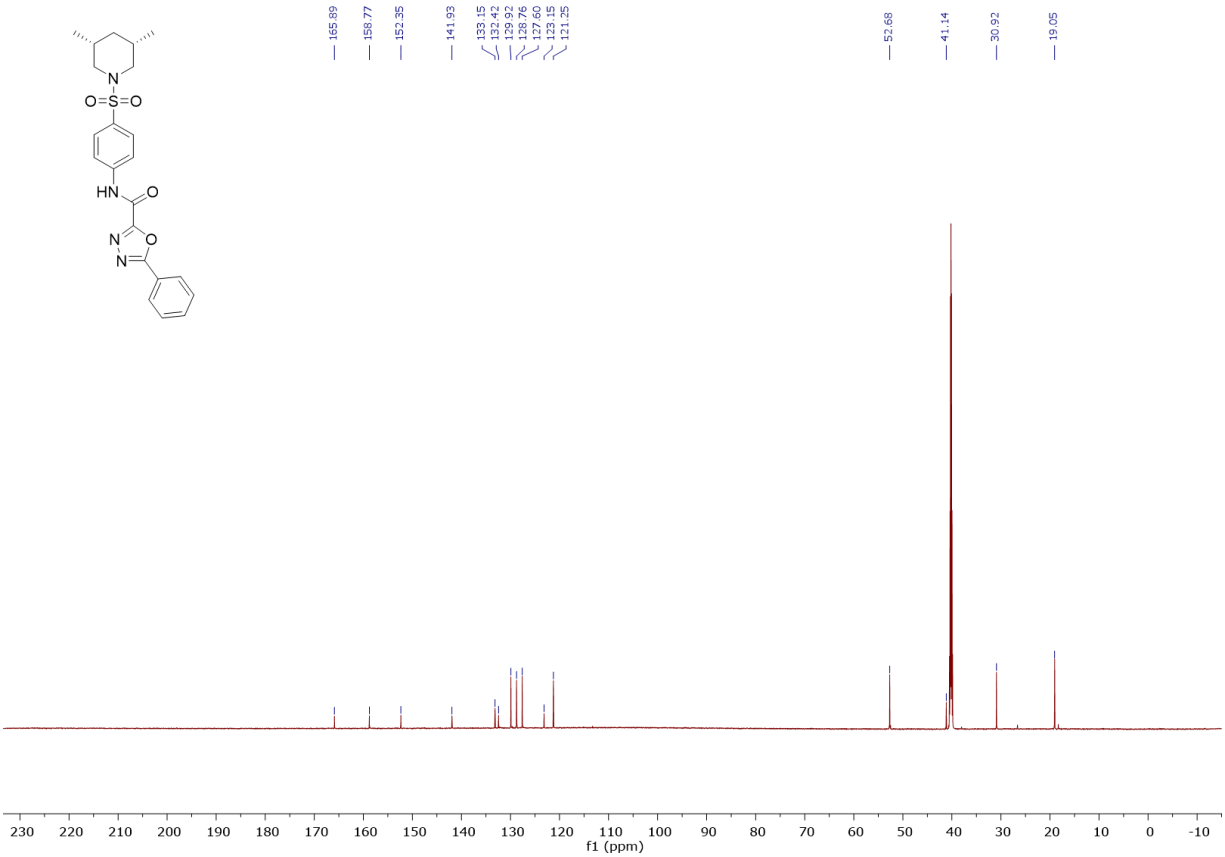
165.89
158.77
152.35
141.93
133.15
132.42
129.92
128.76
127.60
123.15
121.25
52.68
41.14
30.92
19.05
f1 (ppm)

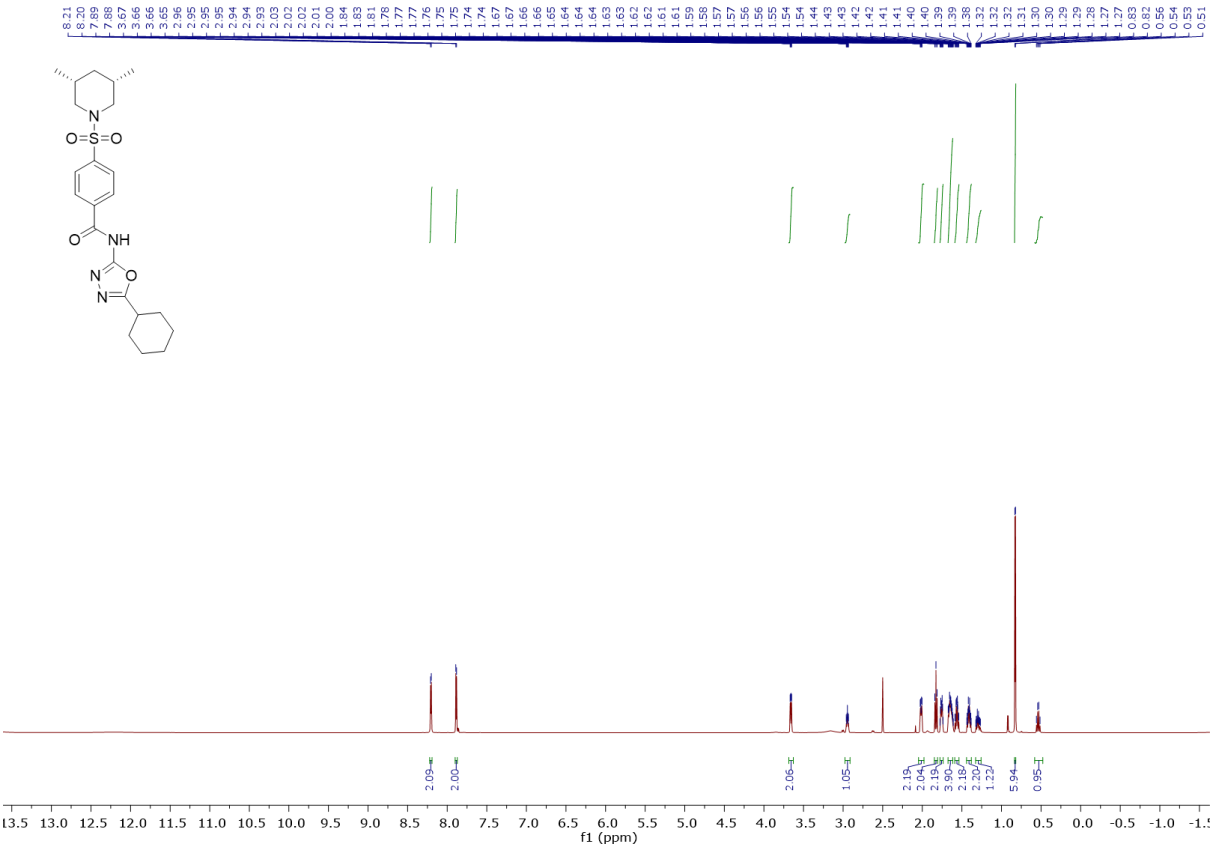
f1 (ppm)

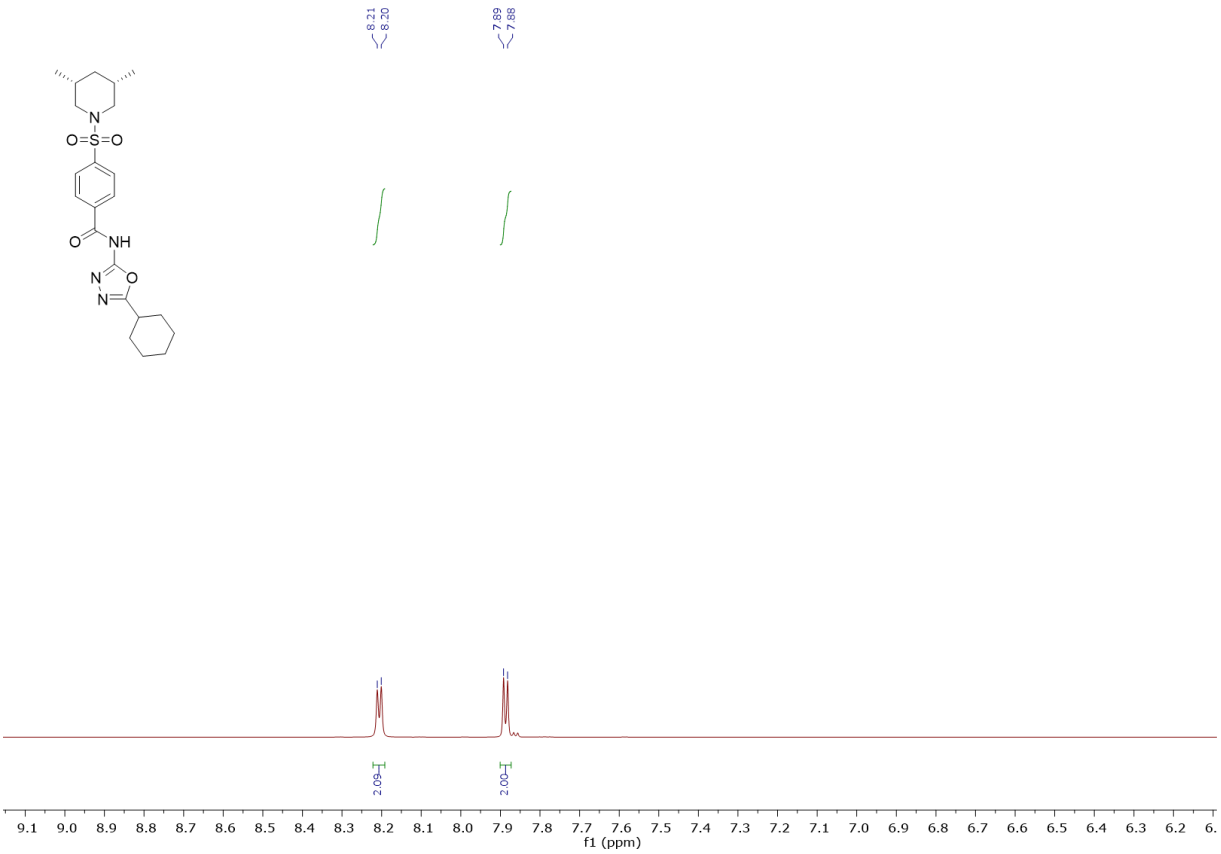
8.21
8.20
7.89
7.88
2.09
2.00
f1 (ppm)

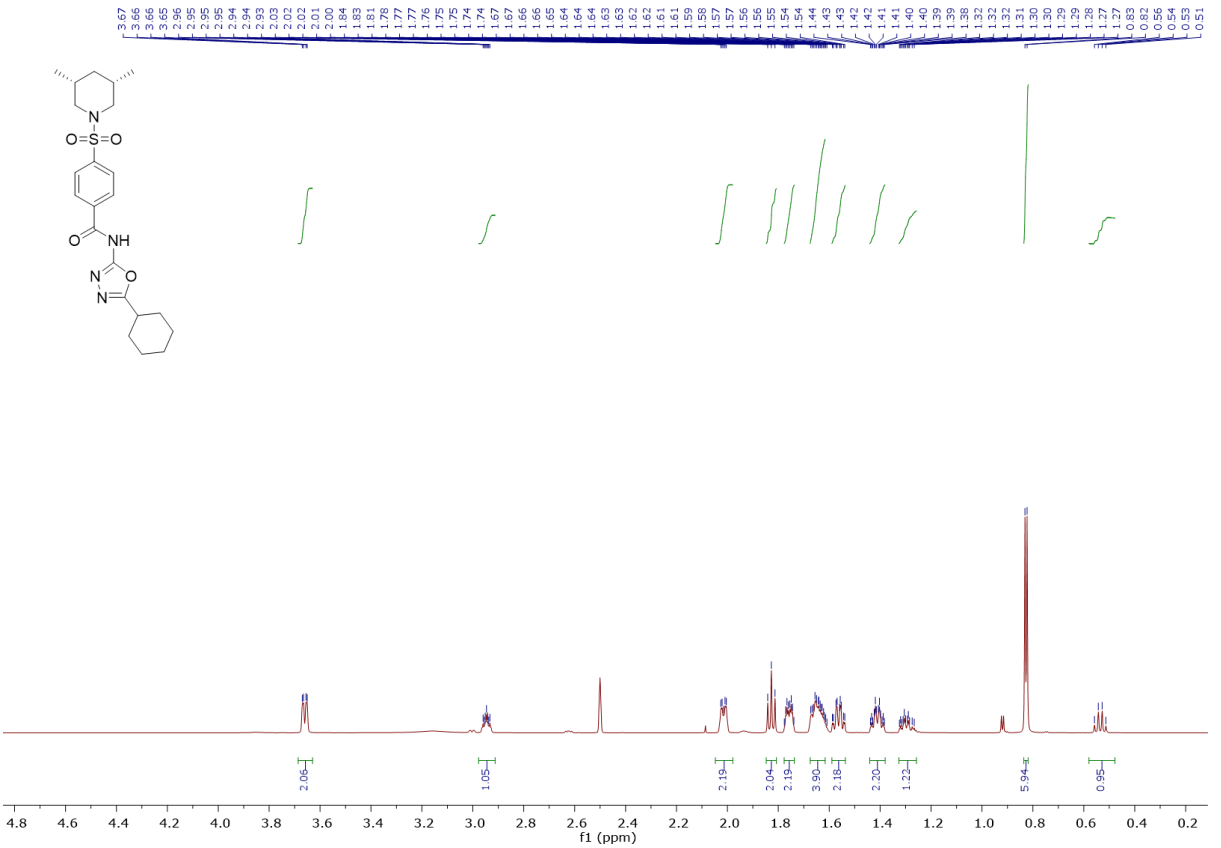
2.06
1.05
2.19
2.04
2.19
3.90
2.18
2.20
1.23
5.94
0.95
f1 (ppm)

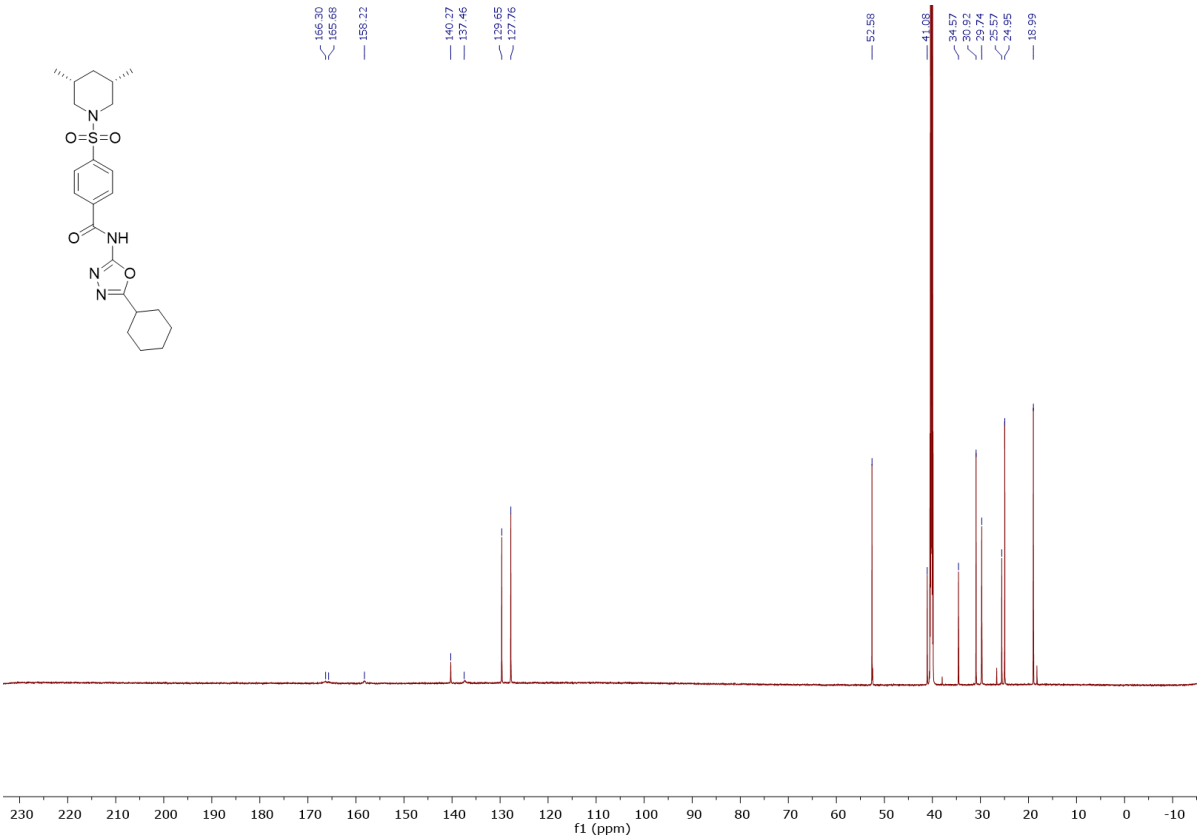
166.30
165.68
158.22
140.27
137.46
129.65
127.76
52.58
41.08
34.57
30.92
29.74
25.57
24.95
18.99
f1 (ppm)

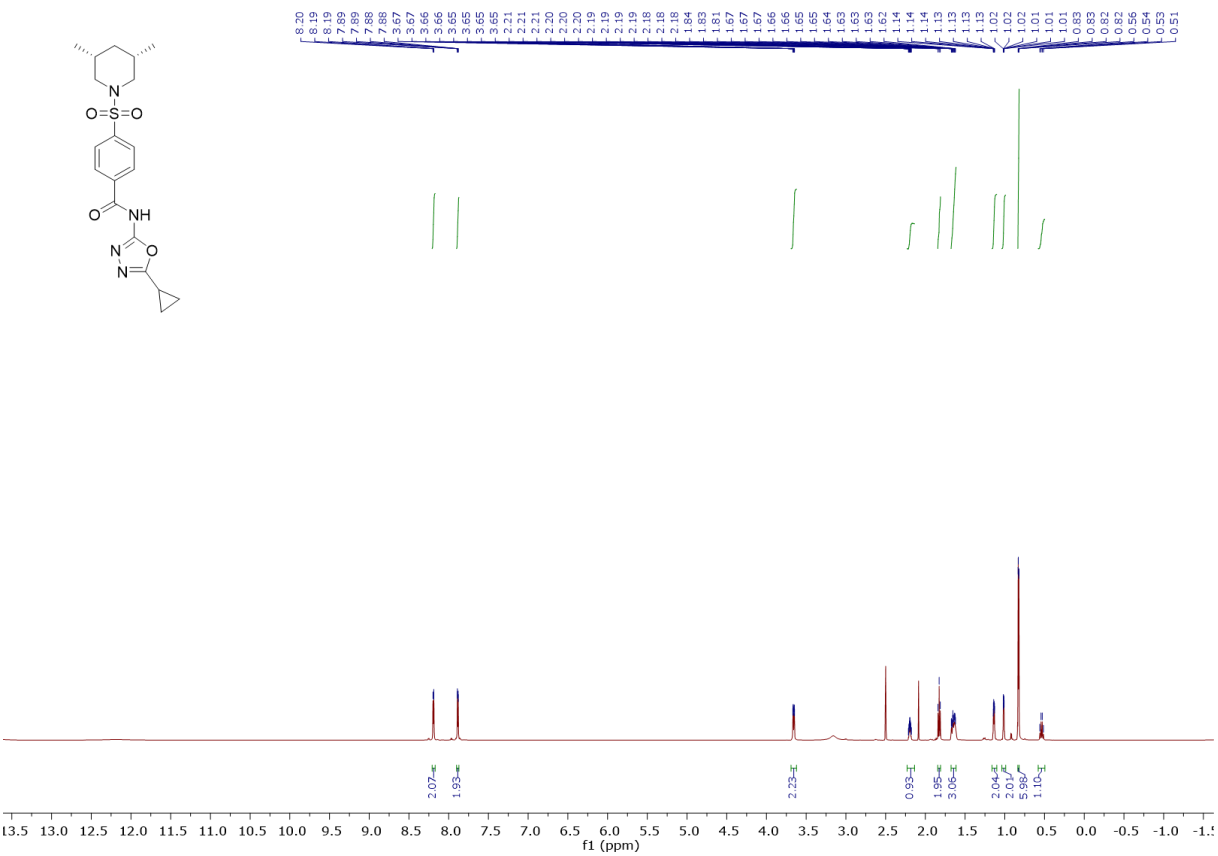
f1 (ppm)

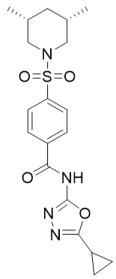

8.20
8.19
8.19
7.89
7.89
7.88
7.88
2.07
1.93
8.9
8.8
8.7
8.6
8.5
8.4
8.3
8.2
8.1
8.0
7.9
7.8
7.7
7.6
7.5
7.4
f1 (ppm)

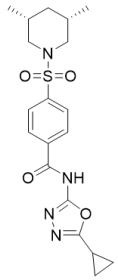

2.23
0.93
1.95
3.06
2.04
2.01
5.98
1.10
5.6
5.4
5.2
5.0
4.8
4.6
4.4
4.2
4.0
3.8
3.6
3.4
3.2
3.0
2.8
2.6
2.4
2.2
2.0
1.8
1.6
1.4
1.2
1.0
0.8
0.6
0.4
0.2
0.0
f1 (ppm)

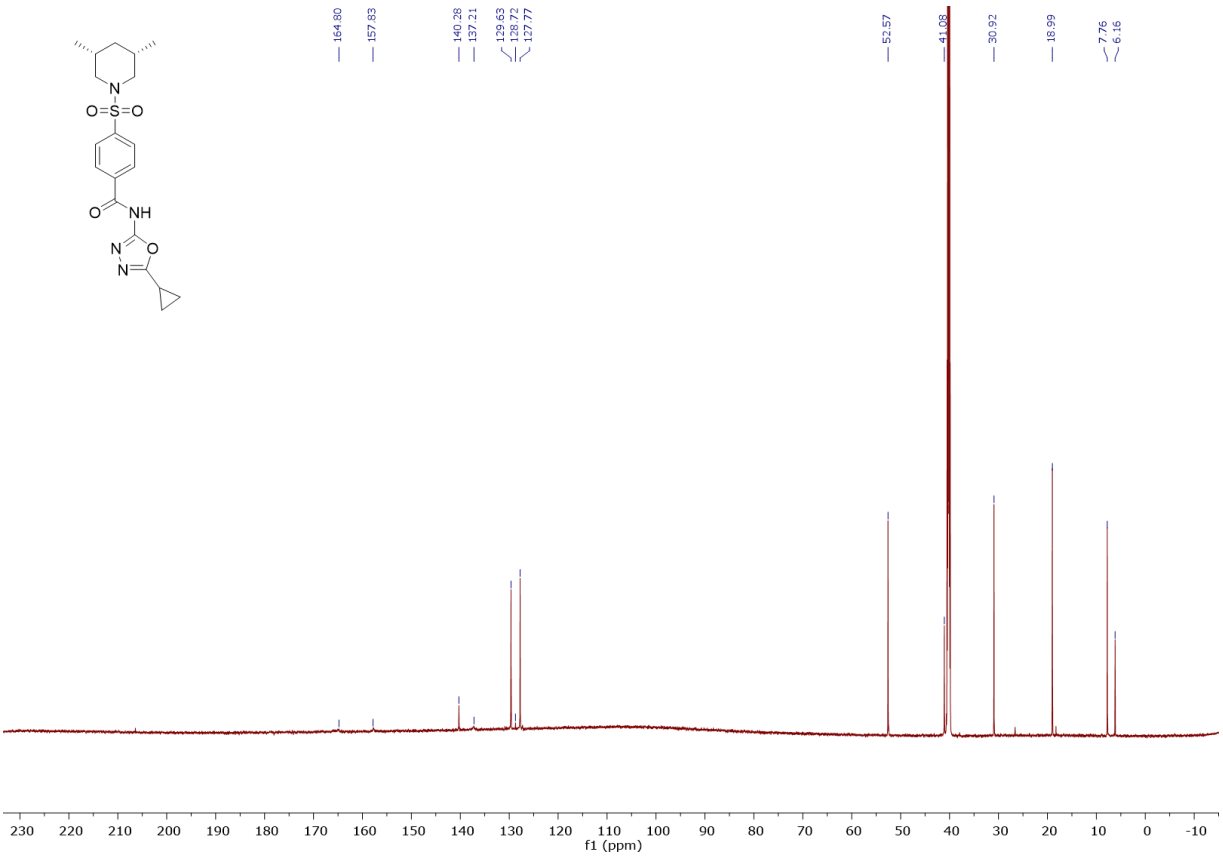
164.80
157.83
140.28
137.21
129.63
128.72
127.77
52.57
41.08
30.92
18.99
7.76
6.16
f1 (ppm)

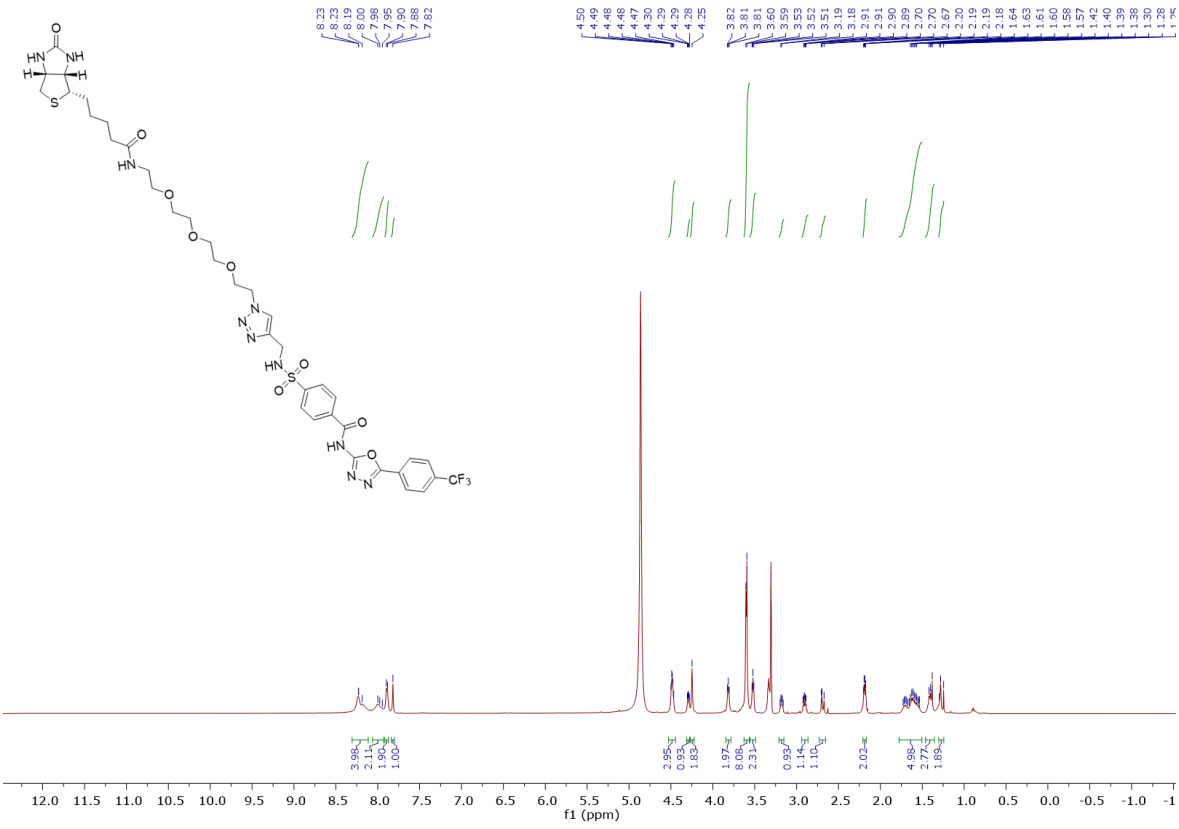
f1 (ppm)

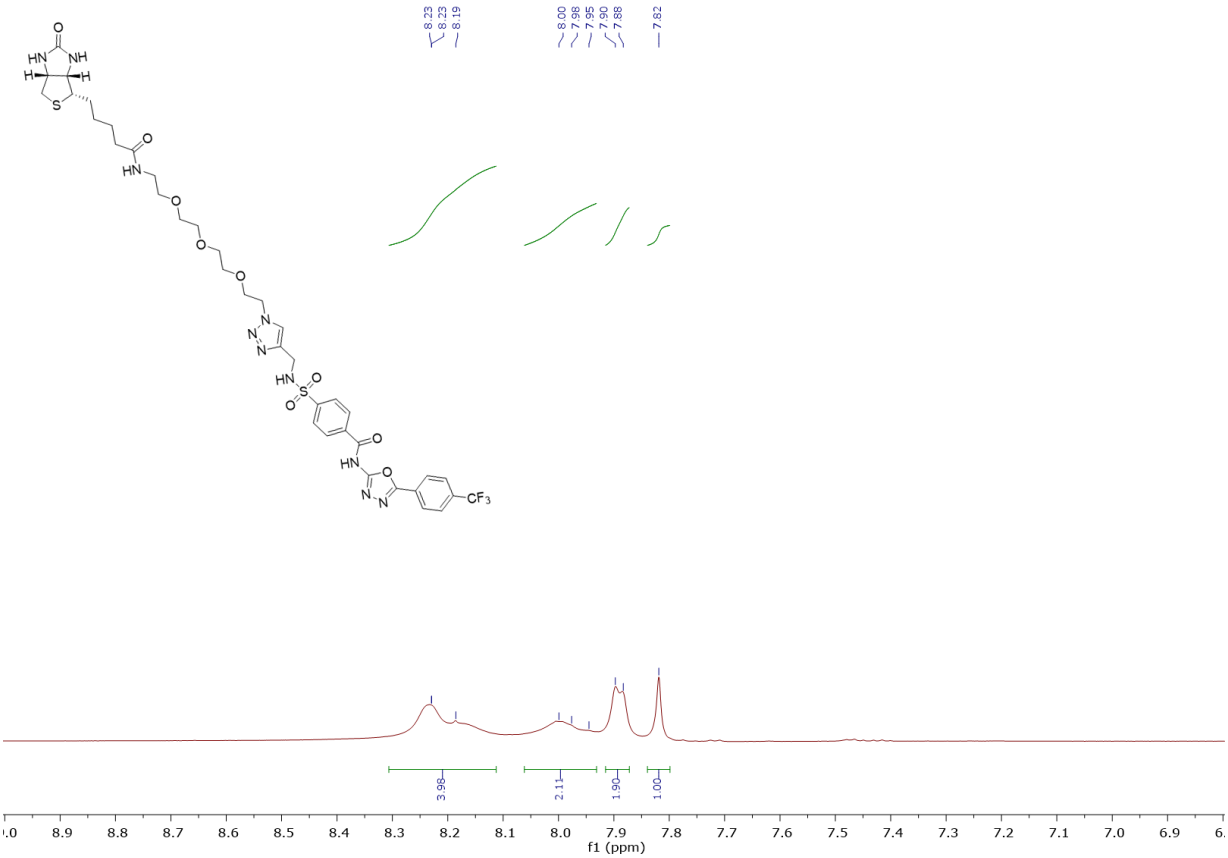
8.23
8.23
8.19
8.00
7.98
7.95
7.90
7.88
7.82
3.98
2.11
1.90
1.00
f1 (ppm)

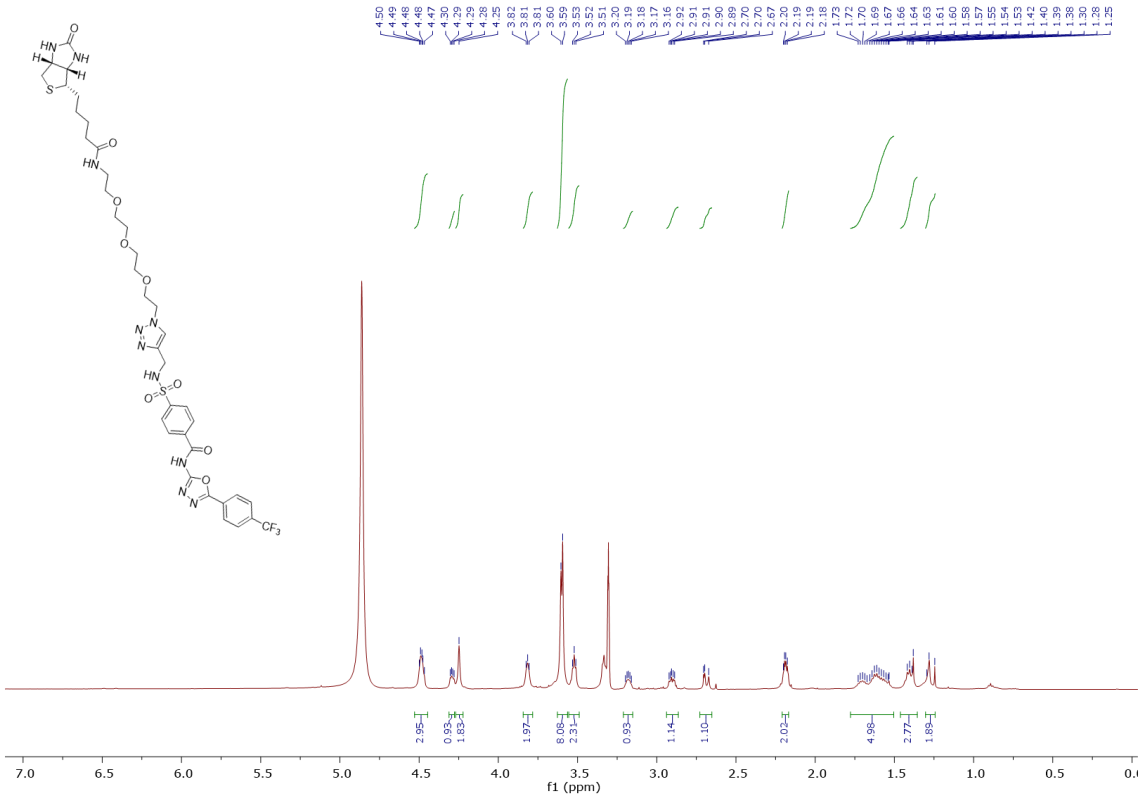
2.95
0.93
1.83
1.97
8.08
2.31
0.93
1.14
1.10
2.02
4.98
2.77
1.89
f1 (ppm)

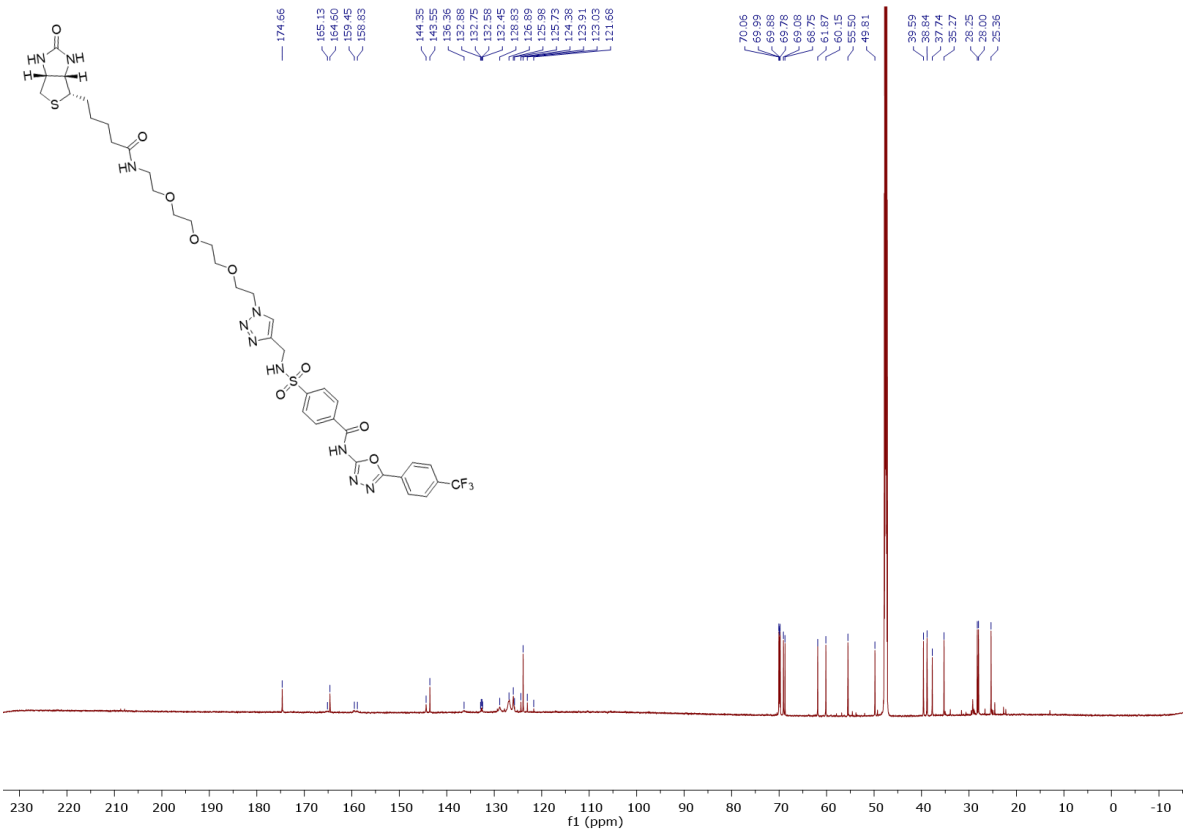
174.66
165.13
164.60
159.45
158.83
144.35
143.55
136.36
132.88
132.75
132.58
132.45
128.83
126.89
125.98
125.73
124.38
123.91
123.03
121.68
70.06
69.99
69.88
69.78
69.08
68.75
61.87
60.15
55.50
49.81
39.59
38.84
37.74
35.27
28.25
28.00
25.36
f1 (ppm)

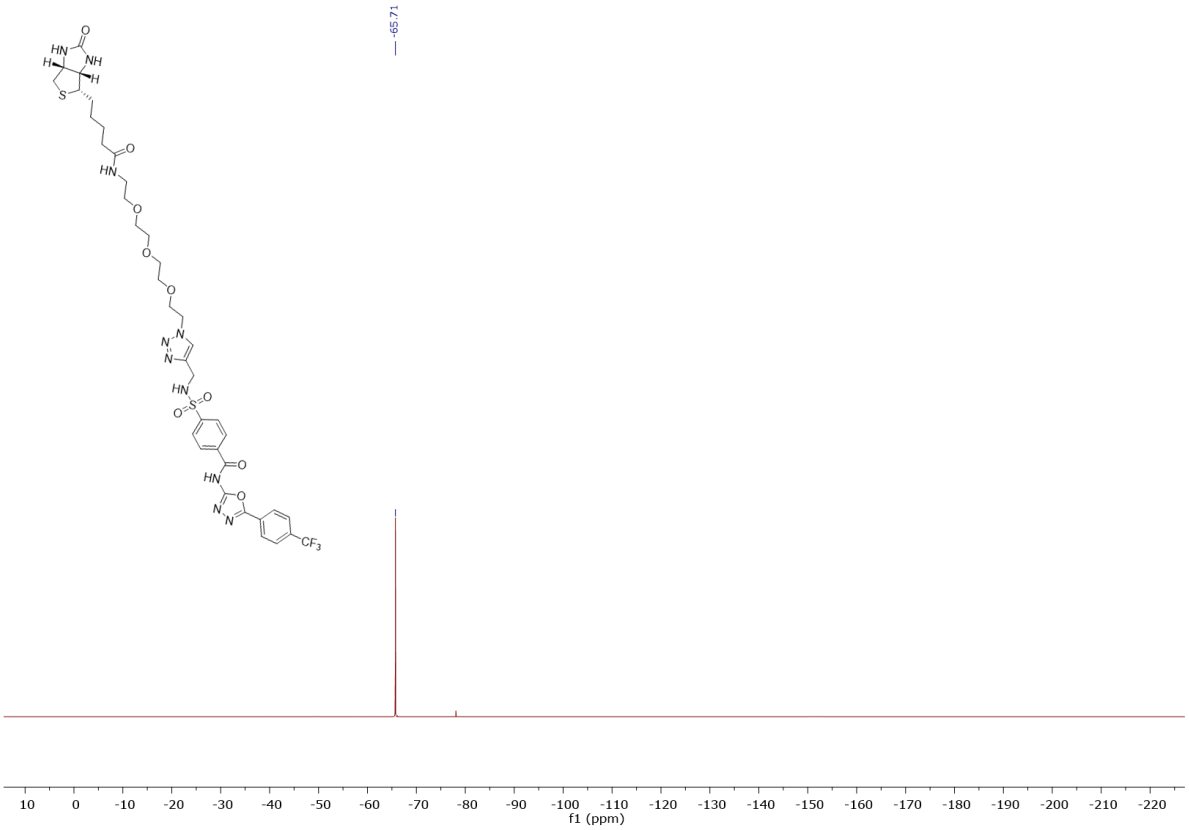
-65.71
f1 (ppm)

V. HPLC Traces:

Table S9: HPLC Retention Times and Percent Purity for HSGN-94, Compounds 1-20, and HSGN-Probe

Compound	Retention Time (min)	Purity
HSGN-94	12.5	98%
1	12.1	98%
2	11.9	99%
3	10.9	95%
4	10.4	99%
5	11.4	95%
6	12.1	97%
7	12.1	98%
8	11.9	99%
9	13.0	96%
10	12.7	96%
11	11.4	96%
12	12.5	97%
13	14.3	95%
14	12.6	95%
15	13.5	95%
16	12.3	95%
17	13.3	95%
18	10.5	96%
19	12.2	95%
20	12.4	97%
HSGN-Probe	9.7	91%

HPLC Trace at 280 nm for 4-((3,5-Dimethylpiperidin-1-yl)sulfonyl)-*N*-(5-(4-(trifluoromethyl)phenyl)-1,3,4-oxadiazol-2-yl)benzamide (HSGN-94):

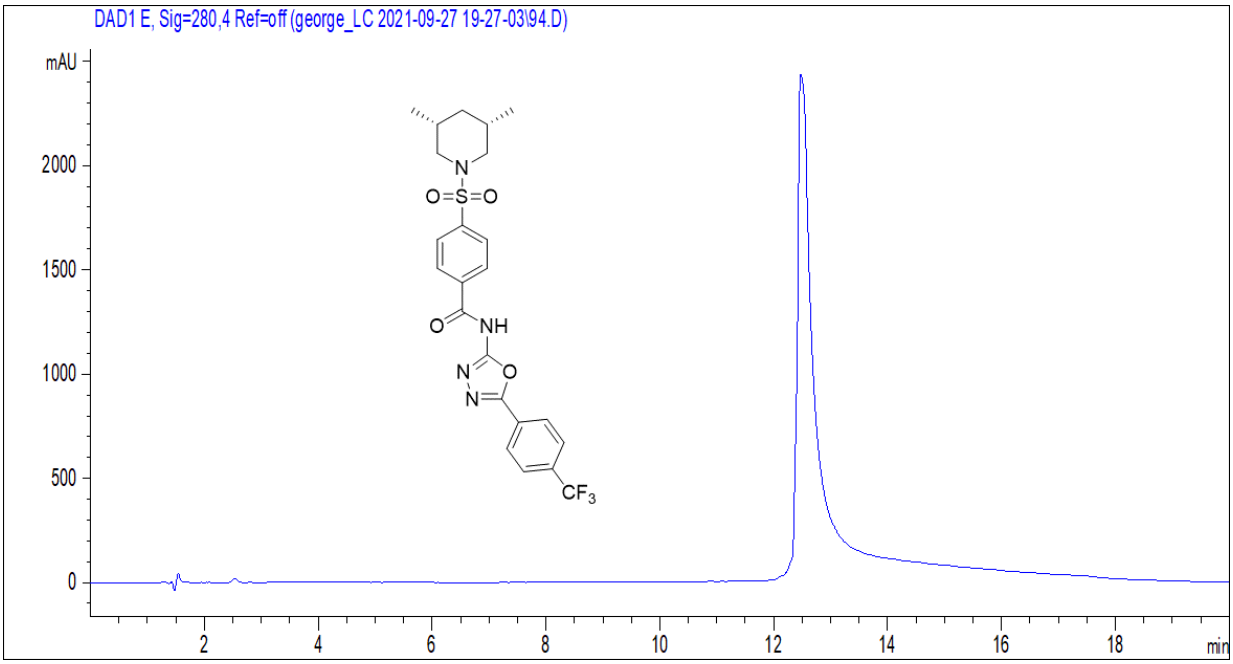

HPLC Trace at 280 nm for 4-(Piperidin-1-ylsulfonyl)-*N*-(5-(4-(trifluoromethyl)phenyl)-1,3,4-oxadiazol-2-yl)benzamide (1):

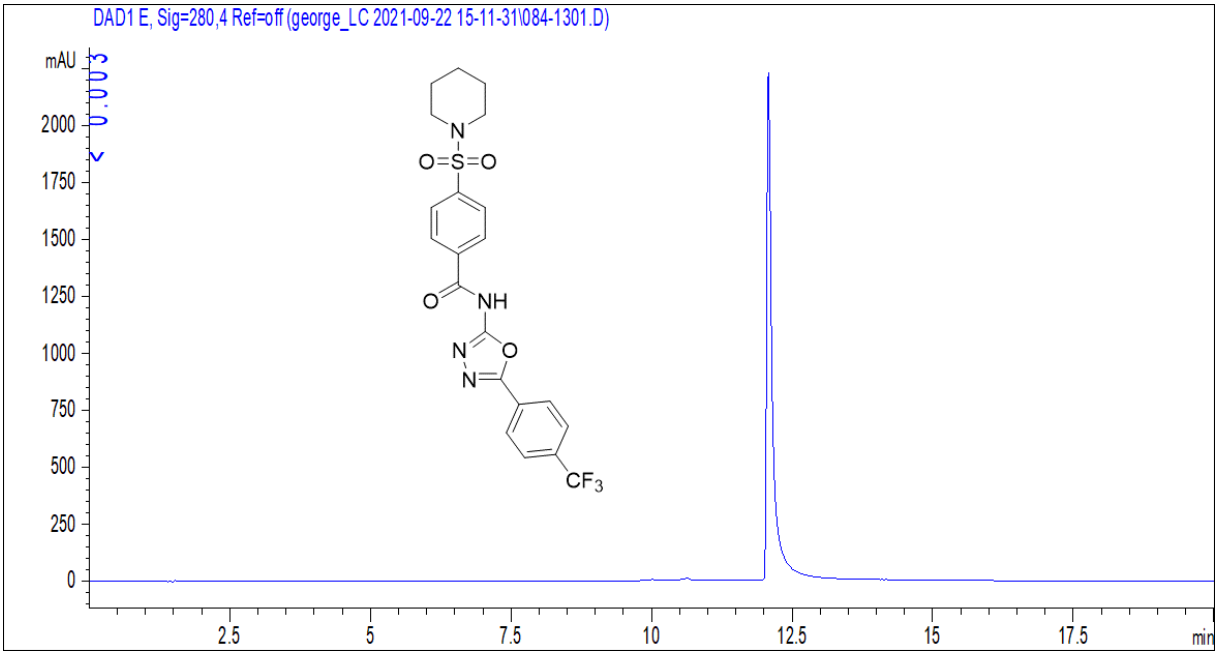

HPLC Trace at 280 nm for 4-(Pyrrolidin-1-ylsulfonyl)-*N*-(5-(4-(trifluoromethyl)phenyl)-1,3,4-oxadiazol-2-yl)benzamide (2):

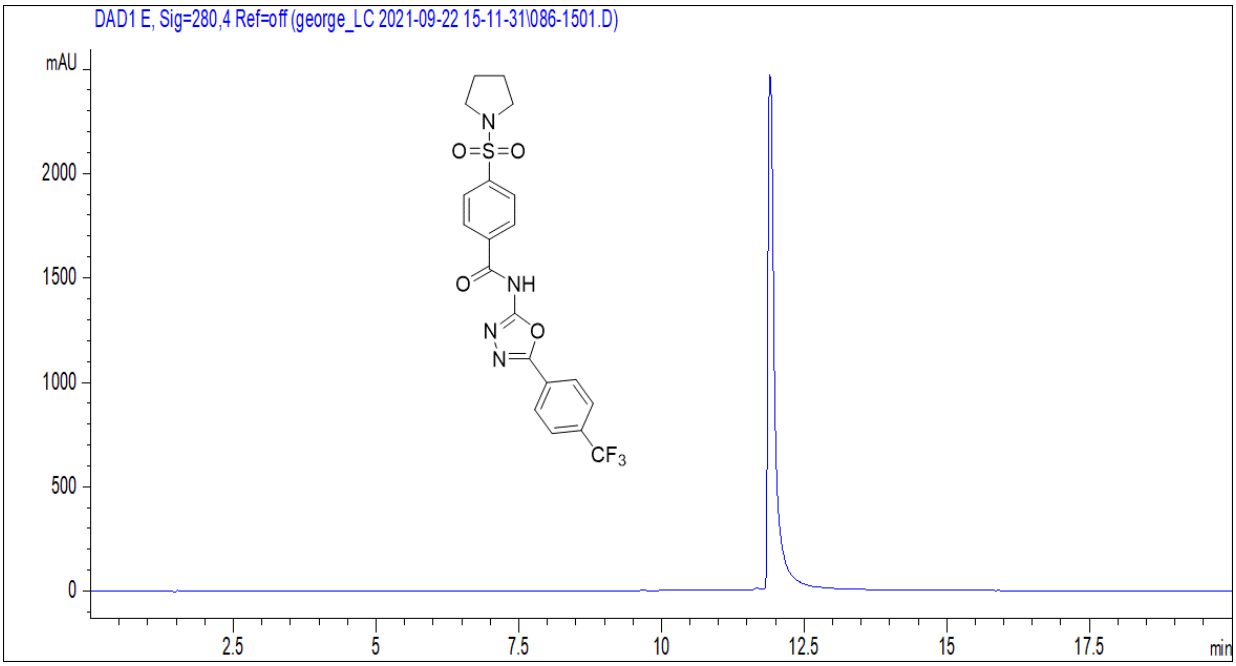

HPLC Trace at 280 nm for 4-(*N*-cyclopropylsulfamoyl)-*N*-(5-(4-(trifluoromethyl)phenyl)-1,3,4-oxadiazol-2-yl)benzamide (3):

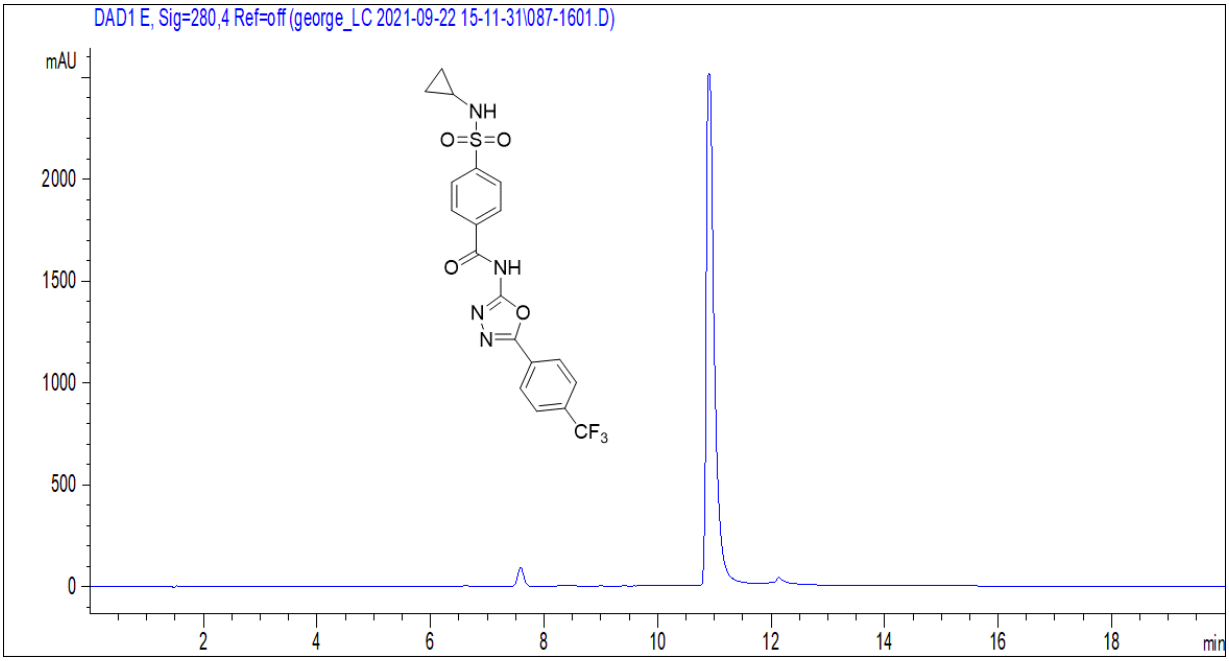

HPLC Trace at 280 nm for 4-(*N*,*N*-Dimethylsulfamoyl)-*N*-(5-(4-(trifluoromethyl)phenyl)-1,3,4-oxadiazol-2-yl)benzamide (4):

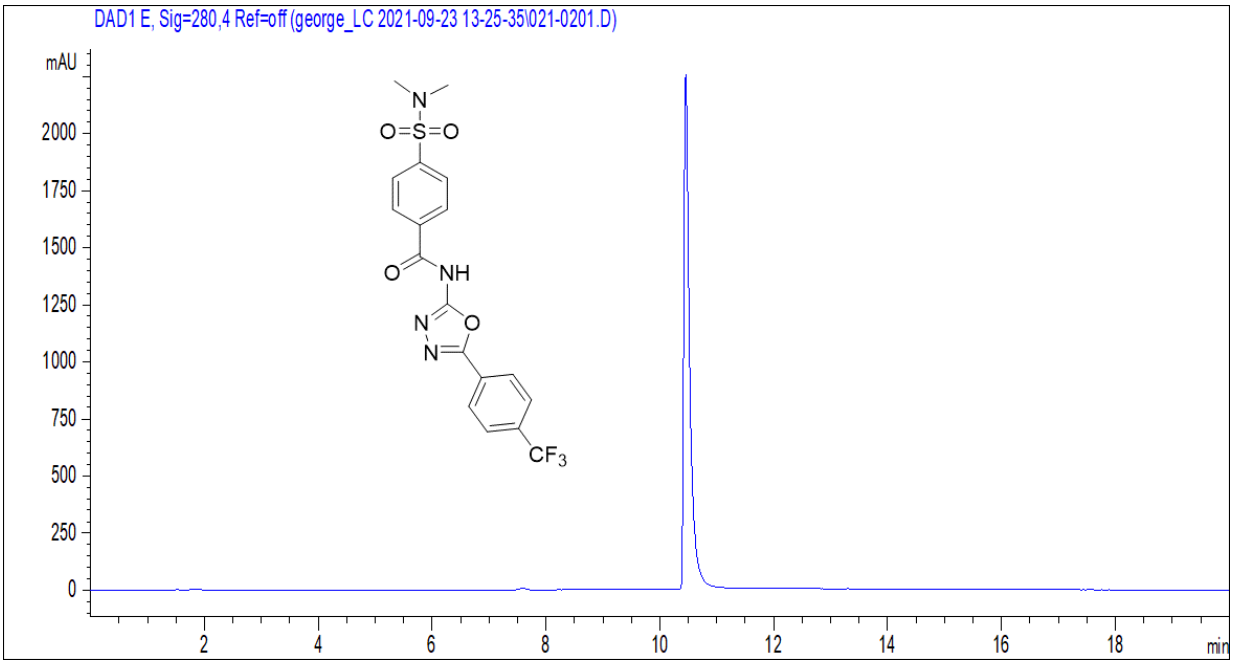

HPLC Trace at 280 nm for 4-((2-Azabicyclo[2.2.1]heptan-2-yl)sulfonyl)-*N*-(5-(4-(trifluoromethyl)phenyl)-1,3,4-oxadiazol-2-yl)benzamide (5):

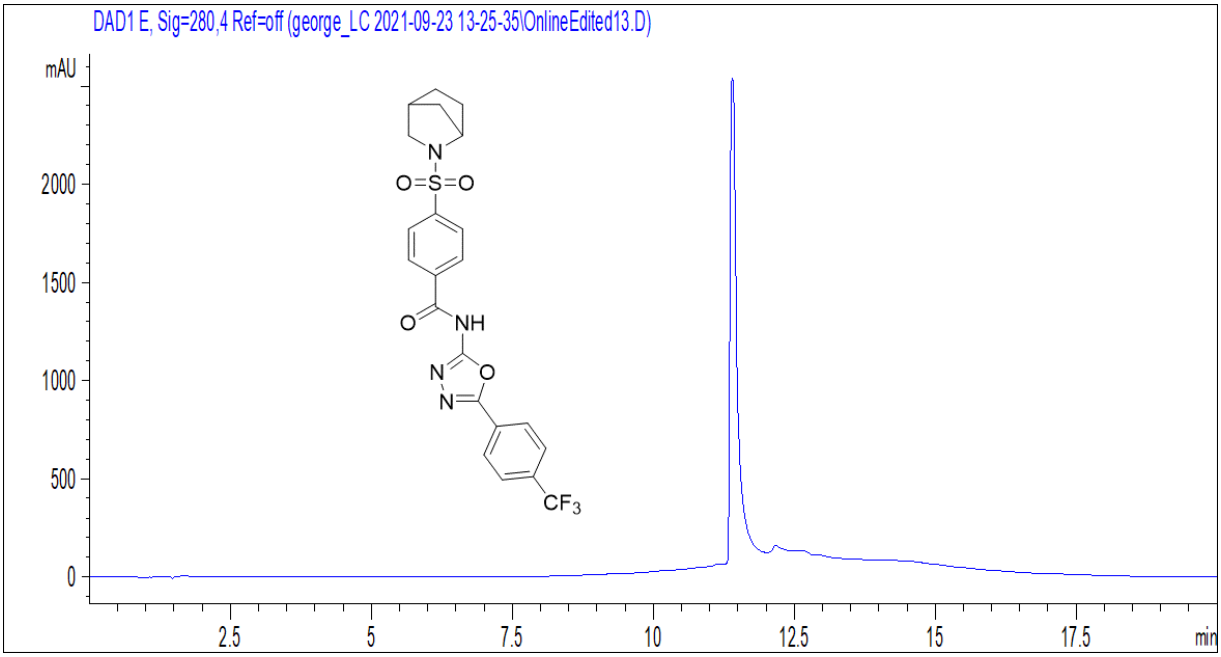

HPLC Trace at 280 nm for 4-((4-Methylpiperidin-1-yl)sulfonyl)-*N*-(5-(4-(trifluoromethyl)phenyl)-1,3,4-oxadiazol-2-yl)benzamide (6):

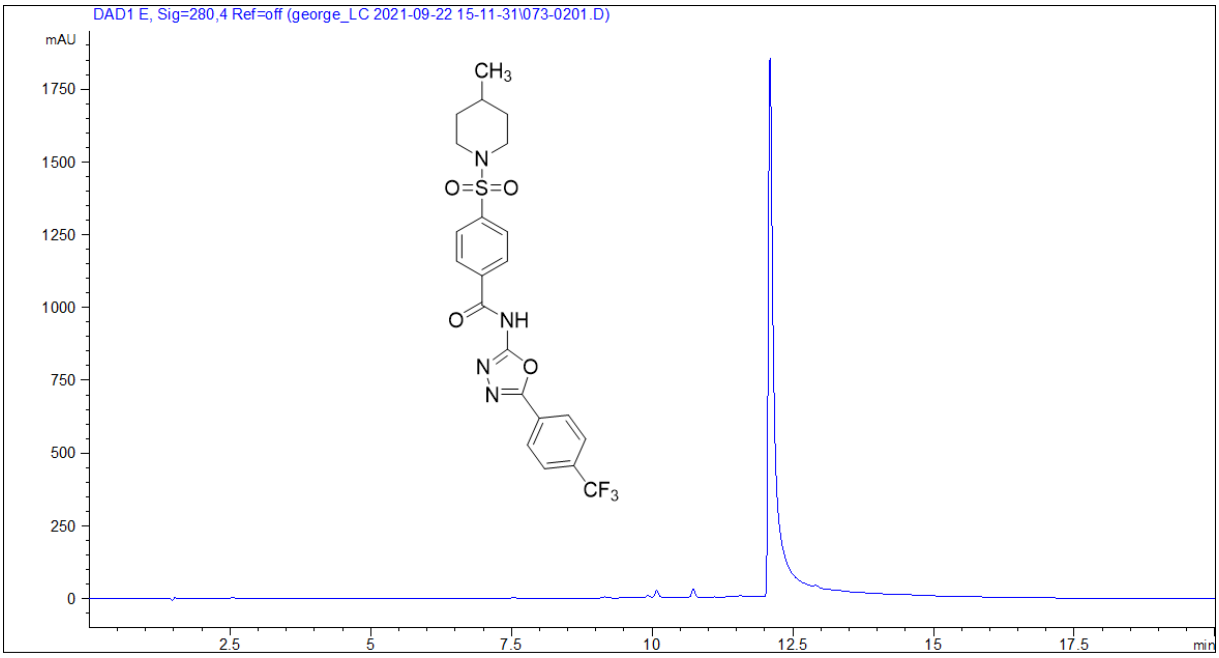

HPLC Trace at 280 nm for 4-((3-Methylpiperidin-1-yl)sulfonyl)-*N*-(5-(4-(trifluoromethyl)phenyl)-1,3,4-oxadiazol-2-yl)benzamide (7):

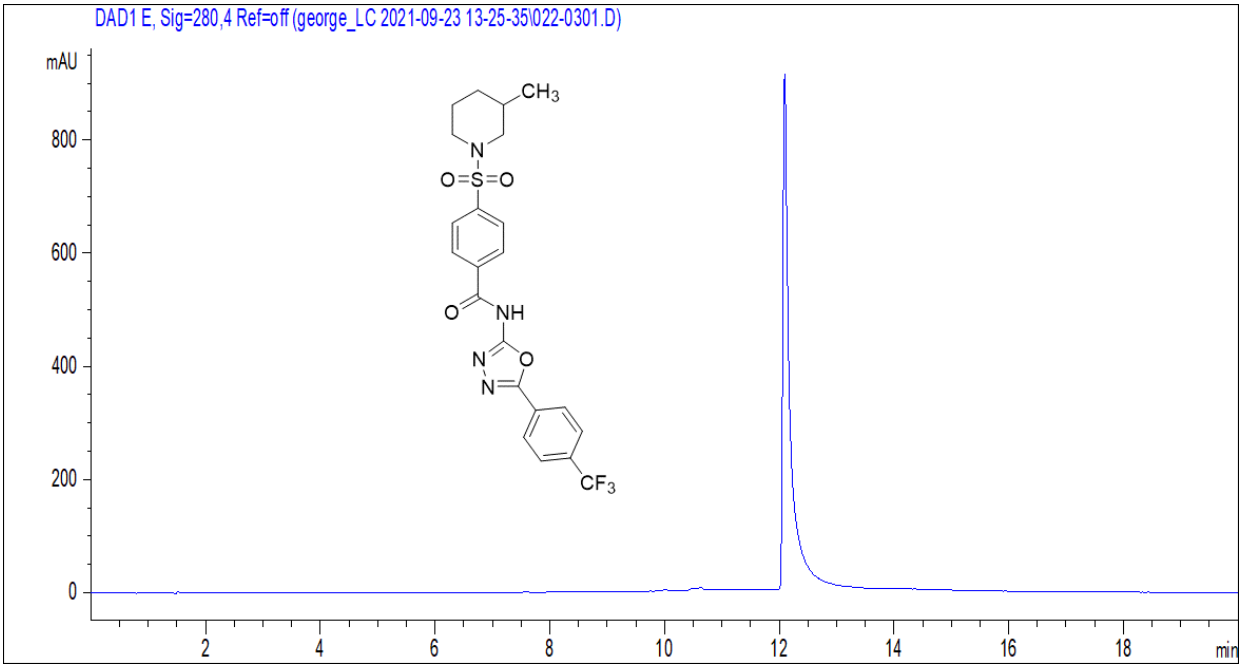

HPLC Trace at 280 nm for 4-((2-Methylpiperidin-1-yl)sulfonyl)-*N*-(5-(4-(trifluoromethyl)phenyl)-1,3,4-oxadiazol-2-yl)benzamide (8):

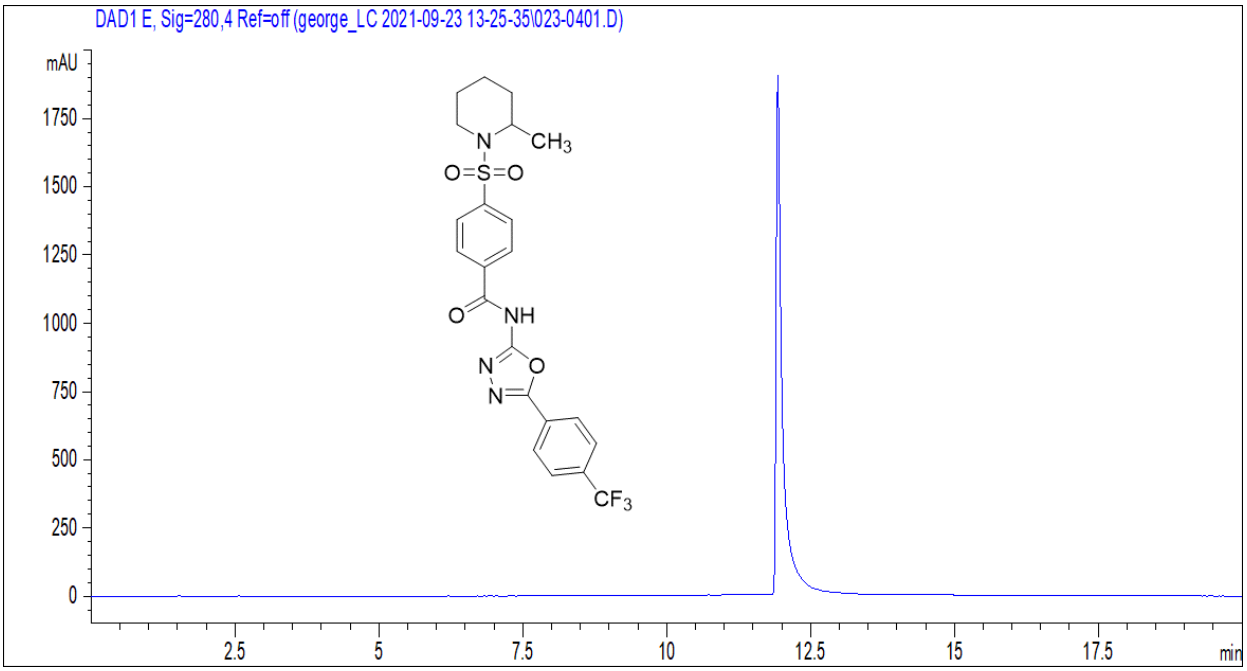

HPLC Trace at 280 nm for 5-((3,5-Dimethylpiperidin-1-yl)sulfonyl)-*N*-(5-(4-(trifluoromethyl)phenyl)-1,3,4-oxadiazol-2-yl)nicotinamide (9):

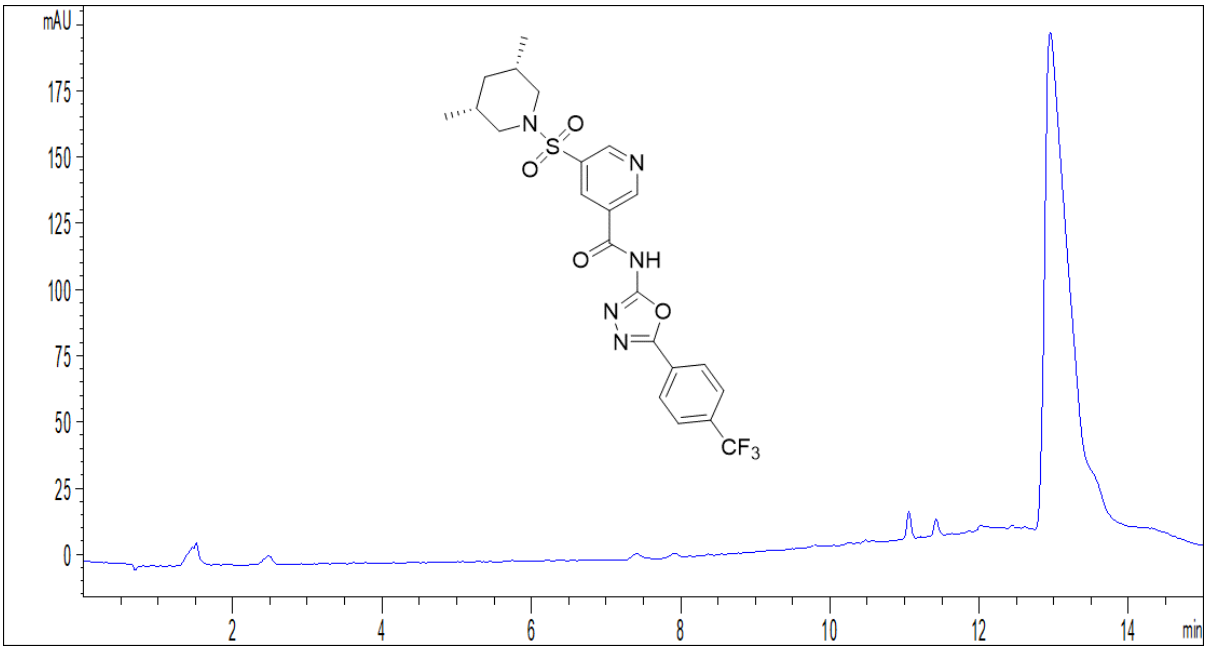

HPLC Trace at 280 nm for 4-((3,5-Dimethylpiperidin-1-yl)sulfonyl)-*N*-(5-(4-(trifluoromethyl)phenyl)-1,3,4-oxadiazol-2-yl)thiophene-2-carboxamide (10):

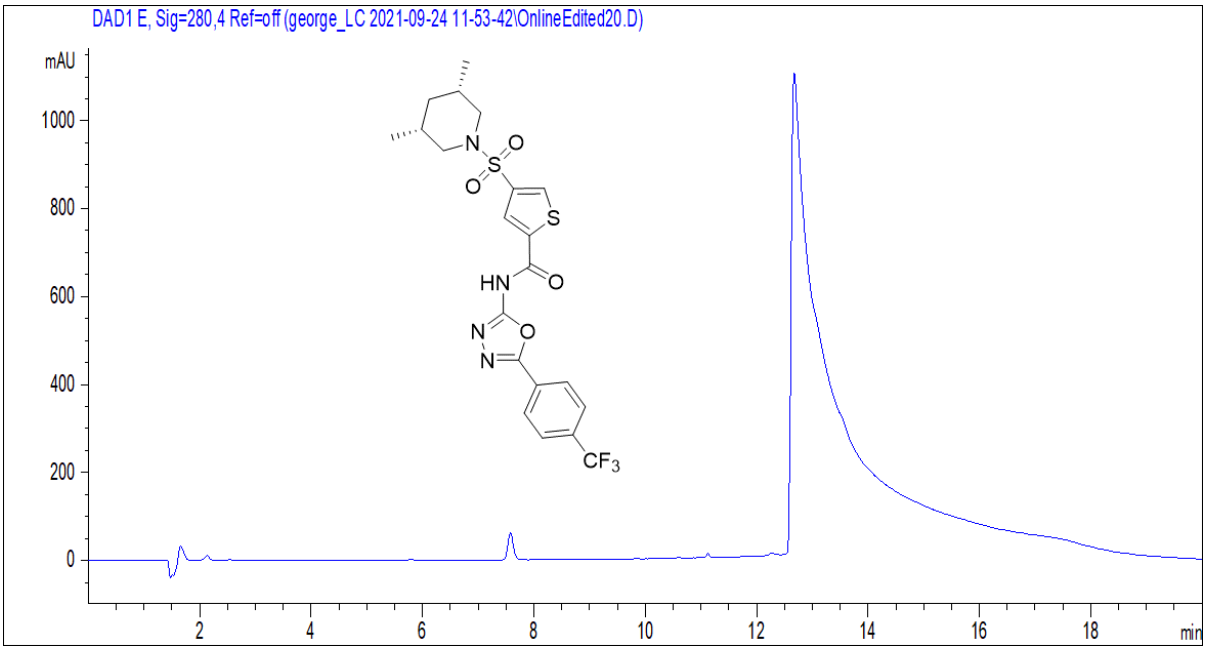

HPLC Trace at 280 nm for 3-((3,5-Dimethylpiperidin-1-yl)sulfonyl)-*N*-(5-(4-(trifluoromethyl)phenyl)-1,3,4-oxadiazol-2-yl)thiophene-2-carboxamide (11):

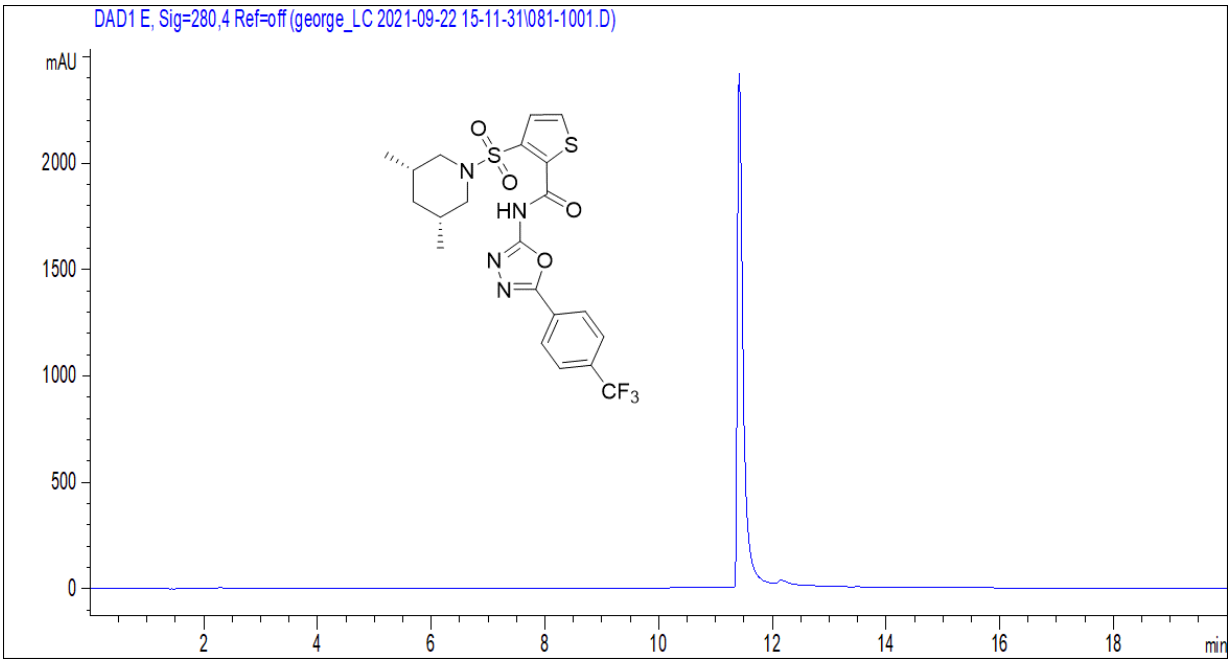

HPLC Trace at 280 nm for 5-((3,5-Dimethylpiperidin-1-yl)sulfonyl)-*N*-(5-(4-(trifluoromethyl)phenyl)-1,3,4-oxadiazol-2-yl)furan-2-carboxamide (12):

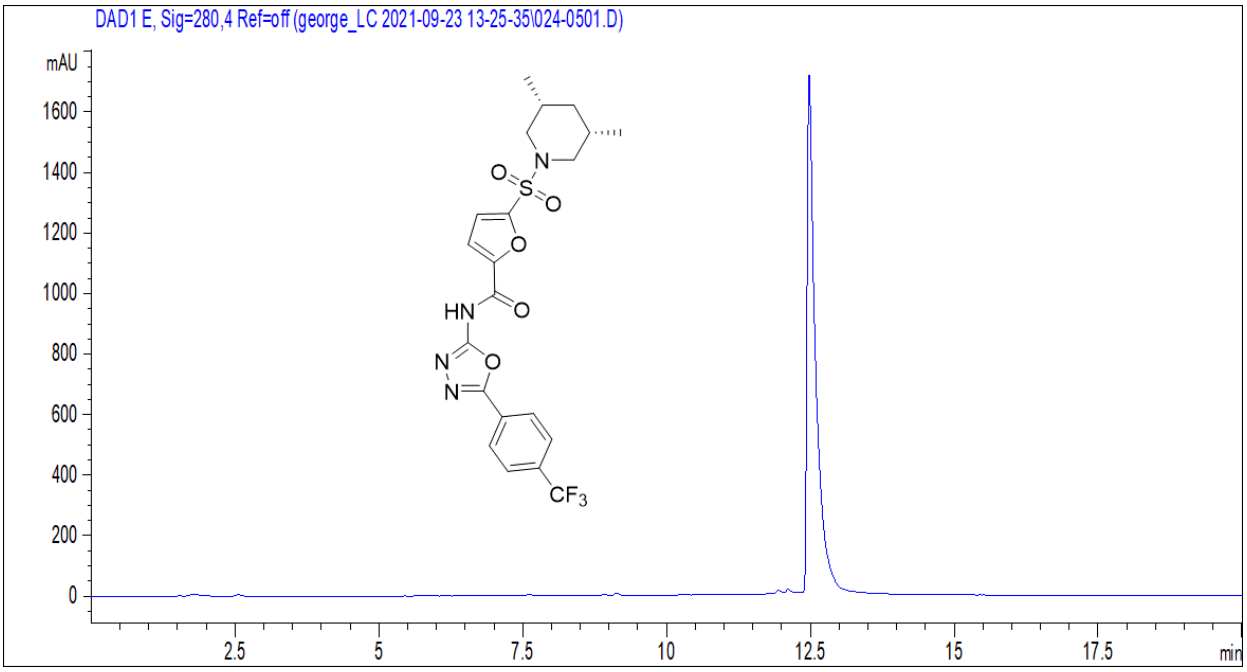

HPLC Trace at 280 nm for 4-((3,5-Dimethylpiperidin-1-yl)sulfonyl)-3-nitro-*N*-(5-(4-(trifluoromethyl)phenyl)-1,3,4-oxadiazol-2-yl)benzamide (13):

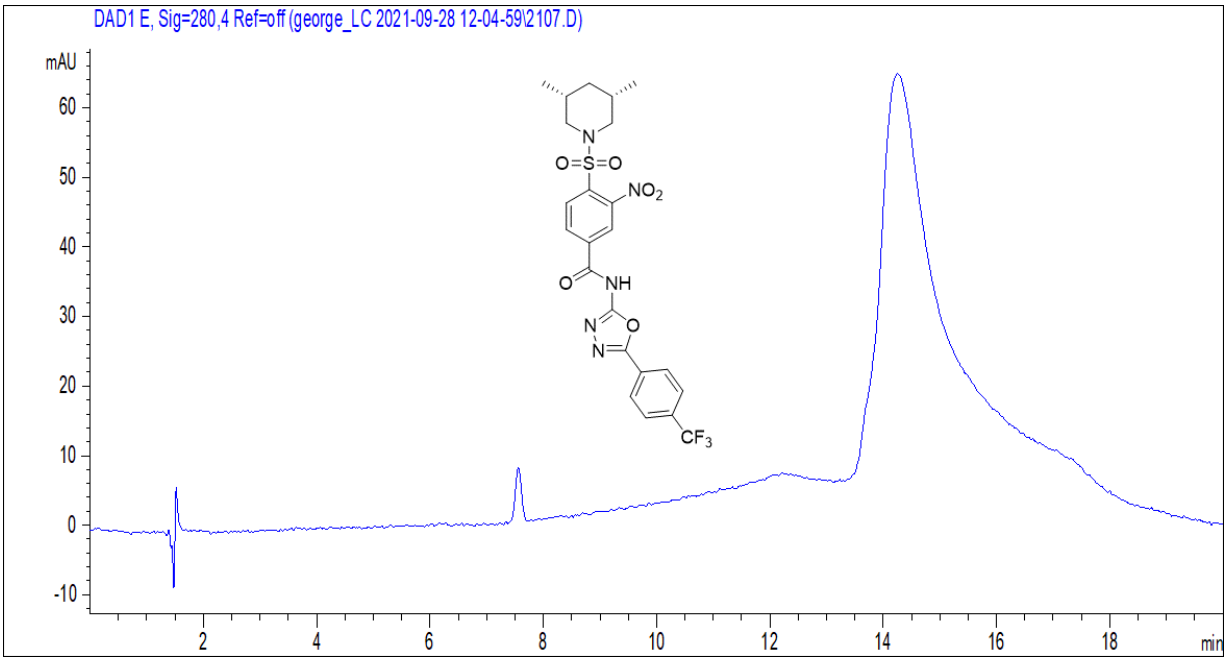

HPLC Trace at 280 nm for 4-((3,5-Dimethylpiperidin-1-yl)sulfonyl)-3-methoxy-*N*-(5-(4-(trifluoromethyl)phenyl)-1,3,4-oxadiazol-2-yl)benzamide (14):

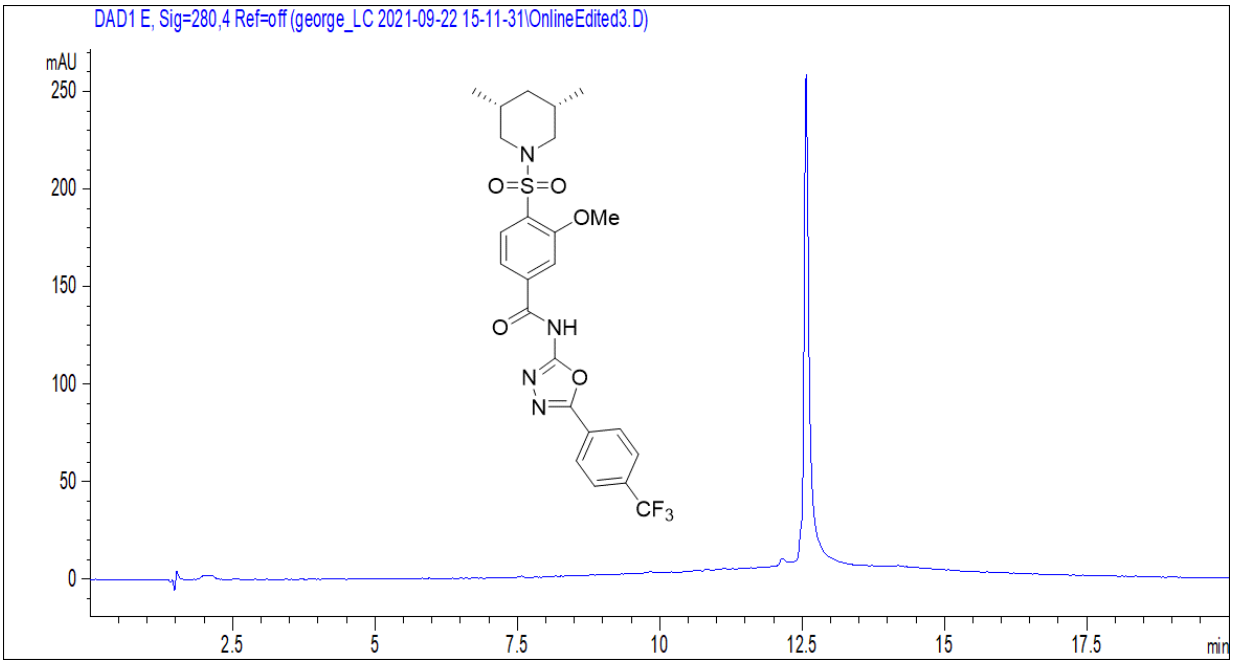

HPLC Trace at 280 nm for 3-Amino-4-((3,5-dimethylpiperidin-1-yl)sulfonyl)-*N*-(5-(4-(trifluoromethyl)phenyl)-1,3,4-oxadiazol-2-yl)benzamide (15):

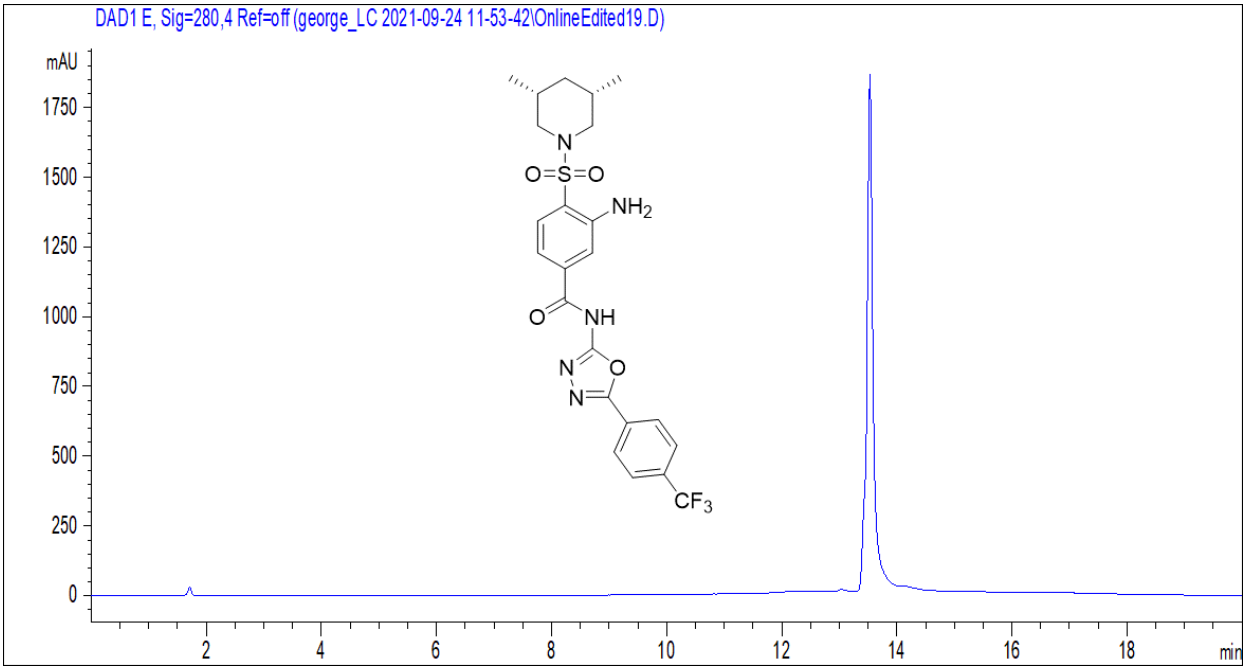

HPLC Trace at 280 nm for 4-((3,5-Dimethylpiperidin-1-yl)sulfonyl)-3-hydroxy-*N*-(5-(4-(trifluoromethyl)phenyl)-1,3,4-oxadiazol-2-yl)benzamide (16):

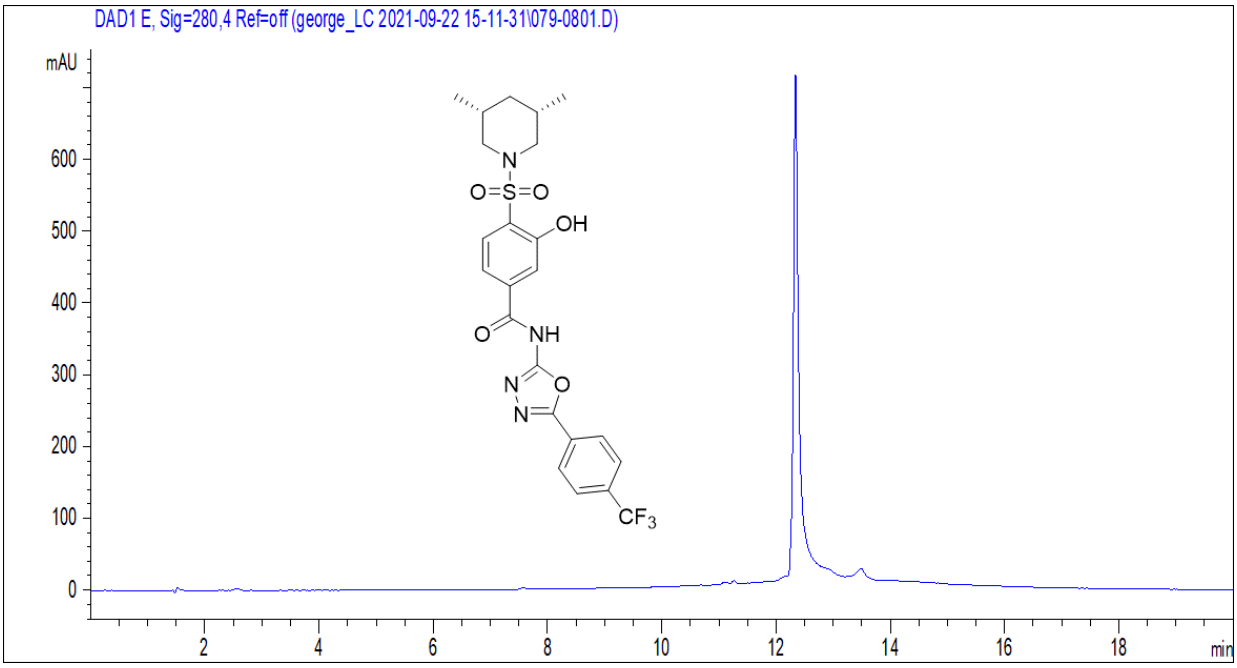

HPLC Trace at 280 nm for 4-((3,5-Dimethylpiperidin-1-yl)sulfonyl)-*N*-methyl-*N*-(5-(4-(trifluoromethyl)phenyl)-1,3,4-oxadiazol-2-yl)benzamide (17):

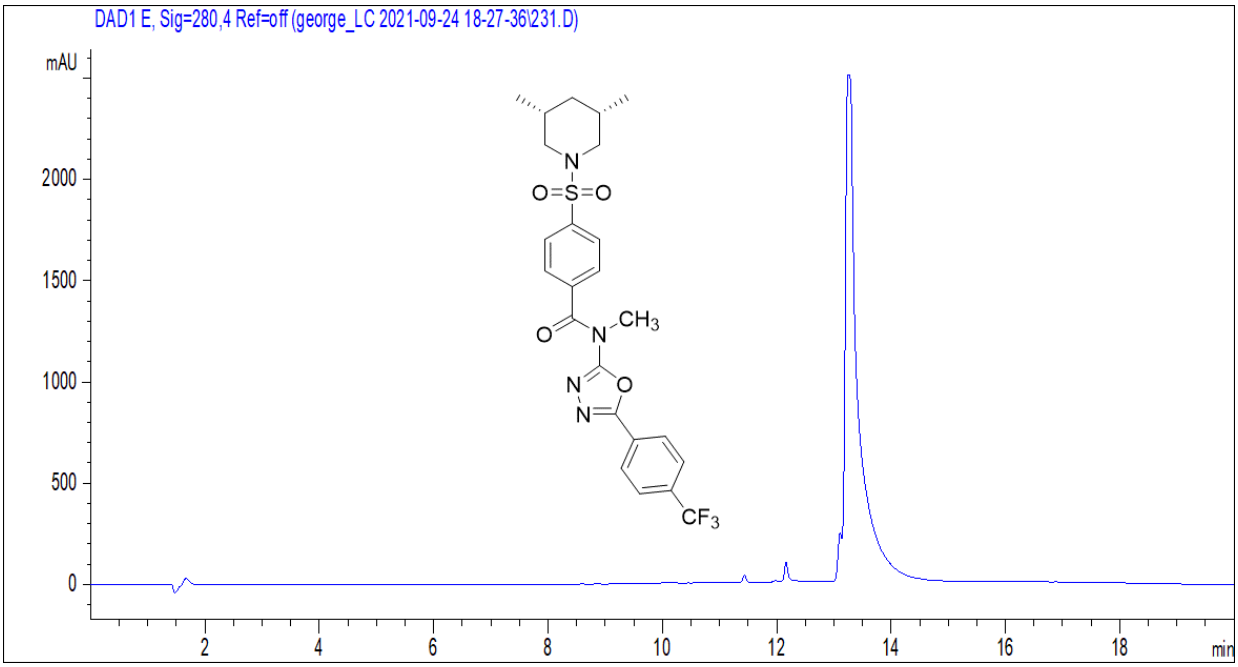

HPLC Trace at 280 nm for *N*-(4-((3,5-Dimethylpiperidin-1-yl)sulfonyl)phenyl)-5-phenyl-1,3,4-oxadiazole-2-carboxamide (18):

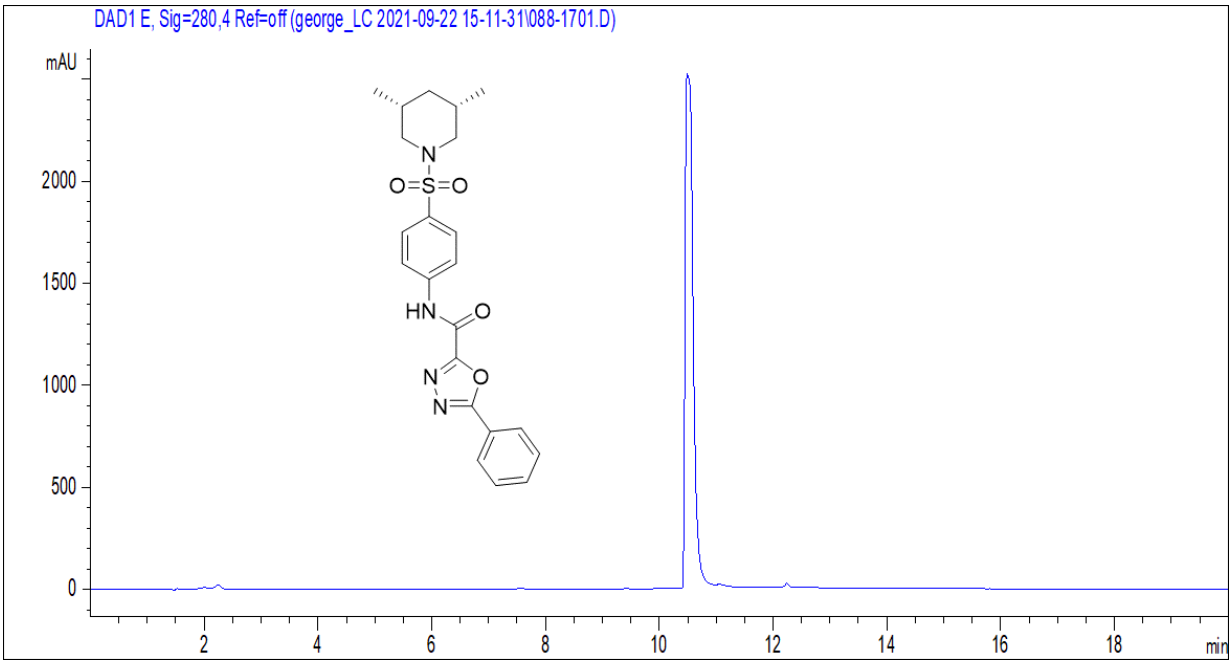

HPLC Trace at 280 nm for *N*-(5-cyclohexyl-1,3,4-oxadiazol-2-yl)-4-((3,5-dimethylpiperidin-1-yl)sulfonyl)benzamide (19):

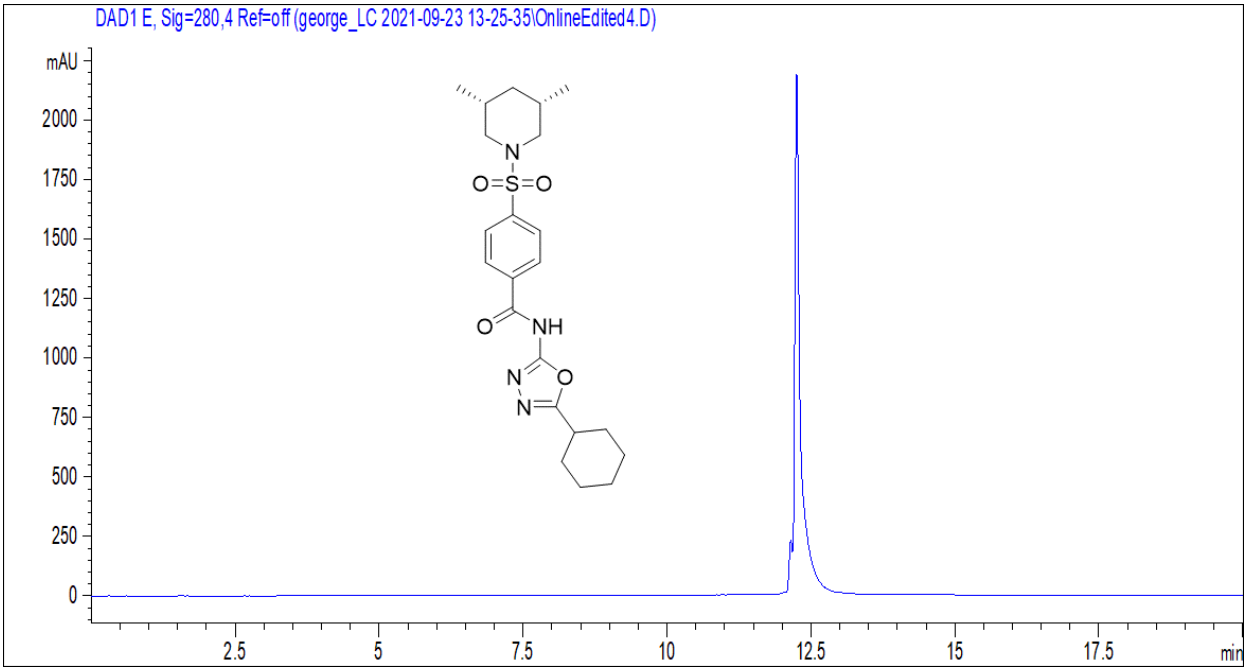

HPLC Trace at 280 nm for *N*-(5-cyclopropyl-1,3,4-oxadiazol-2-yl)-4-((3,5-dimethylpiperidin-1-yl)sulfonyl)benzamide (20):

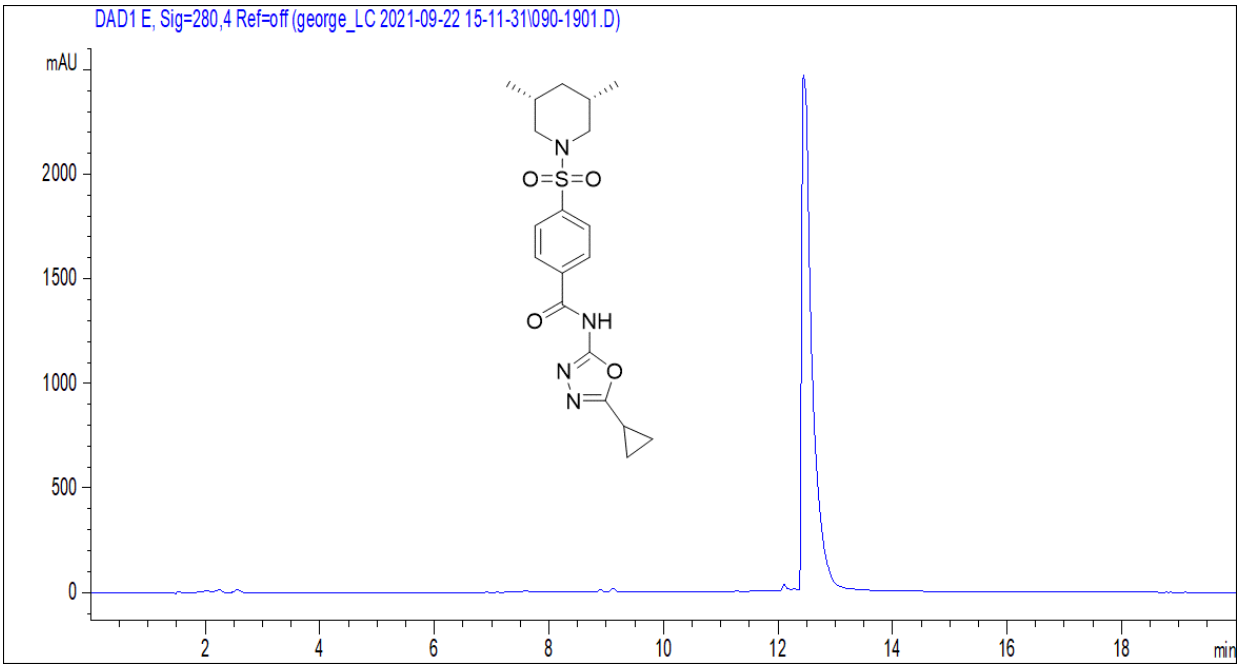

HPLC Trace at 280 nm for 4-(*N*-((1-(13-Oxo-17-(2-oxohexahydro-1H-thieno[3,4-*d*]imidazol-4-yl)-3,6,9-trioxa-12-azaheptadecyl)-1H-1,2,3-triazol-4-yl)methyl)sulfamoyl)-*N*-(5-(4-(trifluoromethyl)phenyl)-1,3,4-oxadiazol-2-yl)benzamide (HSGN-Probe):

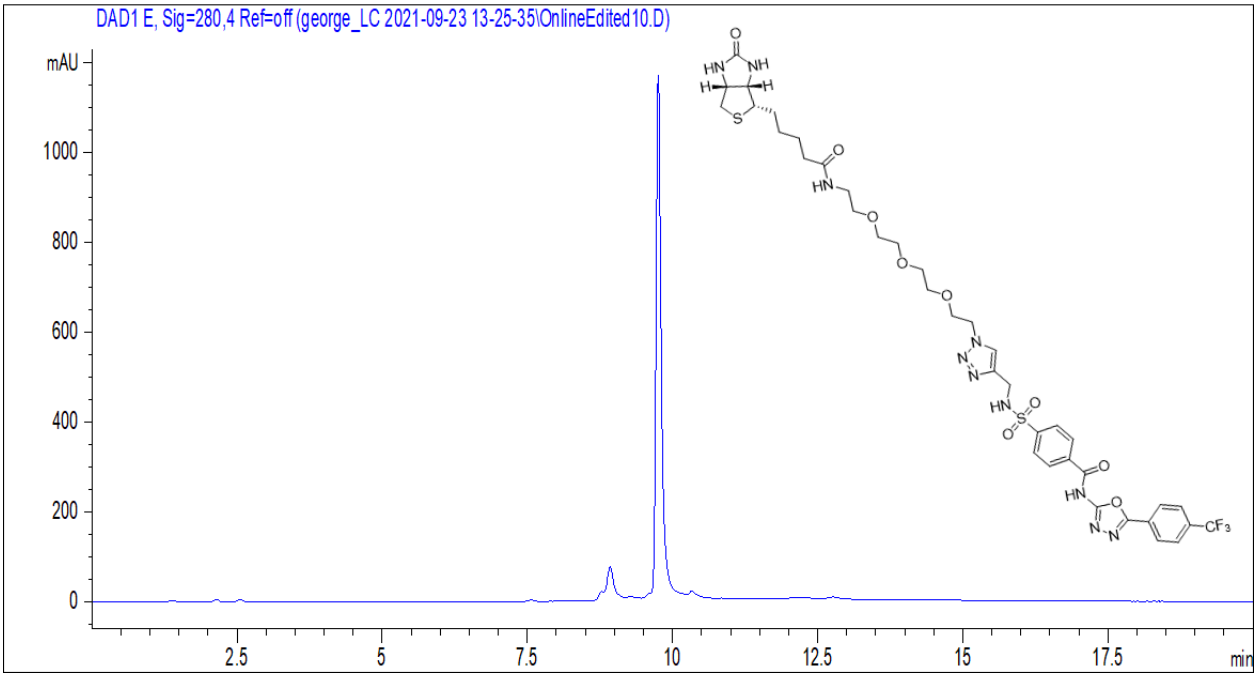

APPENDIX B. CHAPTER 8 SUPPORTING INFORMATION

I. Biological Analysis

Table B.1. MICs in μg/mL (μM) of HSGN-220, -218, -144 and control antibiotics against various MRSA clinical isolates.

Bacterial Strains	Compound/Control Drug				
	HSGN-220	HSGN-218	HSGN-144	Vancomycin	Linezolid
MRSA USA300	0.5 (1.2)	0.25 (0.6)	0.5 (1.3)	1 (0.7)	2 (5.9)
MRSA ARLG 1663	0.5 (1.2)	0.125 (0.3)	0.5 (1.3)	1 (0.7)	2 (5.9)
MRSA ARLG 1568	1 (2.4)	0.06 (0.1)	0.5 (1.3)	0.5 (0.3)	1 (3.0)
MRSA ARLG 1664	1 (2.4)	0.125 (0.3)	0.5 (1.3)	1 (0.7)	2 (5.9)
MRSA ARLG 1570	0.5 (1.2)	0.25 (0.6)	0.5 (1.3)	0.5 (0.3)	1 (3.0)
MRSA ARLG 1561	0.5 (1.2)	0.25 (0.6)	0.5 (1.3)	1 (0.7)	2 (5.9)
MRSA ARLG 1567	1 (2.4)	0.125 (0.3)	0.5 (1.3)	1 (0.7)	2 (5.9)
MRSA ARLG 1569	0.25 (0.6)	0.06 (0.1)	0.5 (1.3)	1 (0.7)	2 (5.9)
MRSA ARLG 1649	0.5 (1.2)	0.25 (0.6)	0.5 (1.3)	2 (1.4)	2 (5.9)

Table B.2. Downregulated proteins shared amongst *S. aureus* treatment with HSGN-220, -218, or -144

ID Number	Protein	Essential in *S. aureus*?
gi|685633647	Glyoxalase	No
gi|685633472	Esterase	No
gi|685632899	Aminotransferase class V	No
gi|1145681322	Nickel ABC transporter substrate-binding protein	No
gi|685632167	Membrane protein	No
gi|685631821	Peptidase M23B	No
gi|685631658	Nucleotide pyrophosphohydrolase	No
gi|685632732	Rhomboid family intramembrane serine protease	No
gi|685632742	Nif3-like dinuclear metal center hexameric protein	No
gi|685633383	Sulfurtransferase	No
gi|685633242	Translation factor Sua5	No
gi|685631402	2-C-methyl-D-erythritol 4-phosphate cytidylyltransferase	No
gi|685633459	Ribose 5-phosphate isomerase	No
gi|685632128	Isochorismate synthase	No
gi|685632794	Peptidase U32	No
gi|685631793	Teichoic acid ABC transporter permease	No
gi|685632458	Nuclease SbcCD subunit C	No
gi|685633050	Hypothetical protein KQ76_09950	No
gi|685631927	Sporulation regulator WhiA	No
gi|685632079	AI-2E family transporter	No
gi|685631939	Protein-export membrane protein SecG	No
gi|685631628	DNA polymerase III subunit gamma/tau	Yes
gi|685632299	Fibronectin-binding protein	No

gi|685633507	AraC family transcriptional regulator	No
gi|685632030	ATP-dependent DNA helicase	No
gi|685633026	LuxR family transcriptional regulator	No
gi|685633532	Zinc ABC transporter substrate-binding protein	No
gi|685633096	Nitric oxide synthase	No
gi|685632325	Ribonuclease III	No
gi|685631783	Sodium:proton antiporter	No
gi|685632992	Restriction endonuclease subunit S	No
gi|685631875	Allophanate hydrolase	No
gi|685633567	Hypothetical protein KQ76_12740	No
gi|685633762	MarR family transcriptional regulator	No
gi|685632359	DNA polymerase III PolC	Yes
gi|685632881	Hypothetical protein KQ76_08855	No
gi|685633443	HAD family hydrolase	No
gi|685633338	tRNA pseudouridine synthase TruA	No
gi|685632541	Virulence factor C	No
gi|685633077	23S rRNA (uracil(1939)-C(5))-methyltransferase RlmD	No
gi|685631627	N-acetyltransferase	No
gi|685633878	Replication protein	No
gi|685631557	Hypothetical protein KQ76_01790	No
gi|685631874	Allophanate hydrolase	No
gi|685633576	2-dehydropantoate 2-reductase	No
gi|685632647	Hypothetical protein KQ76_07650	No
gi|685633063	Two-component sensor histidine kinase	No
gi|685632708	Hypothetical protein KQ76_07970	No
gi|685632126	GNAT family N-acetyltransferase	No
gi|685633581	Glycine/betaine ABC transporter ATP-binding protein	No

gi|685632824	ACT domain-containing protein	No
gi|685632567	Biotin--acetyl-CoA-carboxylase ligase	Yes
gi|685631855	DeoR faimly transcriptional regulator	No
gi|685632379	Damage-inducible protein CinA	No
gi|685632268	Bacillithiol biosynthesis cysteine-adding enzyme BshC	No
gi|685631900	Bacillithiol system protein YtxJ	No
gi|685632450	XRE family transcriptional regulator; LexA repressor	Yes
gi|685631447	DUF5085 domain-containing protein	No
gi|685631419	Aryl-phospho-beta-D-glucosidase	No
gi|685631604	Hypothetical protein KQ76_02045	No
gi|685632862	Transcriptional regulator NrdR	No
gi|685633618	NgoFVII family restriction endonuclease	No
gi|685631561	Sodium:dicarboxylate symporter	No
gi|685631829	LysR family transcriptional regulator	No
gi|685631681	DNA repair protein RadA	No
gi|685633641	Fructose 1,6-bisphosphatase	No
gi|685632472	Phosphatidylglycerol lysyltransferase	No
gi|685632076	Magnesium transporter MgtE	No
gi|685633674	Cysteine methyltransferase	No
gi|685632462	4-hydroxybenzoyl-CoA thioesterase	No
gi|685633451	NAD(P)-dependent oxidoreductase	No
gi|685631229	DNA helicase	Yes
gi|685632989	Lipase	No
gi|685633680	TetR family transcriptional regulator	No
gi|685633431	Hypothetical protein KQ76_12025	No
gi|685631881	Glycine/betaine ABC transporter permease	No
gi|685632642	Hypothetical protein KQ76_07625	No

gi|685631353	ABC transporter ATP-binding protein	No
gi|685631413	DNA-binding response regulator	No

Table B.3. Downregulated proteins shared amongst *S. aureus* treatment with HSGN-220 and -218

ID Number	Protein	Essential in *S. aureus*?
gi|685632552	flap endonuclease	No
gi|685632753	endoribonuclease YbeY	No
gi|685632390	DNA mismatch repair protein MutS	No
gi|685632127	1,4-dihydroxy-2-naphthoate octaprenyltransferase	Yes
gi|685633113	hypothetical protein BWO94_05155	No
gi|685632459	mechanosensitive ion channel protein MscL	No
gi|685631477	alpha/beta hydrolase	No
gi|685631504	hypothetical protein BWO94_03590	No
gi|685632660	hypothetical protein BWO94_12940	No
gi|685632360	ribosome maturation protein RimP	No
gi|685632991	NTPase	No
gi|685631916	hydrolase	No
gi|685632392	glycerol-3-phosphate responsive antiterminator GlpP	No
gi|685631858	N-acetylglucosamine-6-phosphate deacetylase	No
gi|1145683653	CDP-glycerol--poly(glycerophosphate) glycerophosphotransferase	No
gi|685633161	carbohydrate kinase	No
gi|685632658	hypothetical protein BWO94_12930	No
gi|685631815	response regulator GraR	No
gi|685632838	DNA-3-methyladenine glycosylase	No
gi|685632659	hypothetical protein BWO94_12935	No
gi|685632238	succinate dehydrogenase iron-sulfur subunit	No
gi|685633271	mannose-6-phosphate isomerase	No

gi|685633703	NmrA family protein	No
gi|685631659	hypothetical protein BWO94_13090	No
gi|685633020	3-5 exoribonuclease YhaM	No
gi|685632715	octanoyltransferase	No
gi|685633535	protein-disulfide isomerase	No
gi|685632844	hydroxymethylbilane synthase	No
gi|685632210	16S rRNA (guanine(966)-N(2))-methyltransferase RsmD	No
gi|685633237	UDP-N-acetylglucosamine 2-epimerase	No
gi|685633132	CAAX protease	No
gi|685631655	peptidyl-tRNA hydrolase	Yes
gi|1145680072	transcriptional repressor CcpN	No
gi|685632686	oligo-1,6-glucosidase	No
gi|685632205	SCP-like extracellular protein	No
gi|685632031	helicase-exonuclease AddAB subunit AddA	No
gi|685633373	DNA topoisomerase III	No
gi|685632683	ribonuclease Z	No
gi|685632186	spermidine/putrescine import ATP-binding protein PotA	No
gi|685632144	methicillin resistance protein FmtA	No

Table B.4. Downregulated proteins shared amongst *S. aureus* treatment with HSGN-220 and -144

ID Number	Protein	Essential in *S. aureus*?
gi|685632980	ImmA/IrrE family metallo-endopeptidase	No
gi|685631343	pyruvate decarboxylase	No
gi|685632729	hypothetical protein BWO94_08630	No
gi|685631744	mevalonate kinase	Yes
gi|685632072	hypothetical protein BWO94_07345	No
gi|685633258	hypothetical protein BWO94_04500	No
gi|685633330	hydrolase	No

gi|685633508	general stress protein	No
gi|685632574	TPR-repeat-containing protein, component of menaquinone-cytochrome C reductase	No
gi|685632396	lysophospholipase	No
gi|685632025	argininosuccinate synthase	No
gi|685632793	protease	No
gi|685631708	UDP-glucose 4-epimerase	No
gi|685632355	UDP pyrophosphate synthase	No
gi|685632661	transcriptional regulator	No
gi|685632387	tRNA (N6-isopentenyl adenosine(37)-C2)-methylthiotransferase MiaB	No
gi|685632309	23S rRNA (adenine(2503)-C(2))-methyltransferase RlmN	No

Table B.5. Downregulated proteins shared amongst *S. aureus* treatment with HSGN-218 and -144

ID Number	Protein	Essential in *S. aureus*?
gi|68563288	DHH family phosphoesterase	No
gi|685631824	MarR family transcriptional regulator	No
gi|1145678368	laccase	No
gi|685631351	type-1 restriction enzyme R protein	No

Table B.6. Proteins downregulated in *S. aureus* treated with HSGN-218

ID Number	Protein	Essential in *S. aureus*?
gi|685633745	anaerobic ribonucleoside-triphosphate reductase	No
gi|685631513	5-methyltetrahydropteroyltriglutamate--homocysteine methyltransferase	No
gi|685633333	acetolactate synthase	No
gi|685631865	hypothetical protein BWO94_13500	No
gi|685631952	gi|685631952|gb|AIO20463.1| thermonuclease [Staphylococcus aureus subsp.	No

	aureus];gi|1145681598|gb|OOC92195.1| thermonuclease [Staphylococcus aureus]	
gi|685632777	RNA-binding protein	No
gi|685631656	transcription-repair coupling factor	No
gi|685632815	GTP pyrophosphokinase relA	Yes
gi|685633588	peptidase M28	No
gi|685631327	alpha-helical coiled-coil protein	No
gi|685631975	CsbD family protein	No
gi|685633014	multidrug ABC transporter ATP-binding protein	No
gi|685632953	autolysin	No
gi|685632398	glutathione peroxidase	No
gi|685631925	RNase adaptor protein RapZ	No
gi|685633538	amino acid ABC transporter permease	No
gi|685632506	4-hydroxy-tetrahydrodipicolinate synthase	No
gi|685631972	methionine ABC transporter ATP-binding protein	No
gi|685632553	dynamin family protein	No
gi|685633305	IucA/IucC family siderophore biosynthesis protein	No
gi|685631259	1-phosphatidylinositol phosphodiesterase	No
gi|685632437	homoserine dehydrogenase	No
gi|685632817	single-stranded-DNA-specific exonuclease RecJ	No
gi|685633509	DUF4889 domain-containing protein	No
gi|685632121	integrase	No
gi|685633332	alpha-acetolactate decarboxylase	No
gi|685632569	N-acetyl-alpha-D-glucosaminyl L-malate synthase BshA	No
gi|685633380	multidrug transporter	No
gi|685631394	nucleoside hydrolase	No
gi|685632391	DNA mismatch repair protein MutL	No
gi|685631227	DHH family phosphoesterase	No
gi|685633870	hypothetical protein BWO94_04225	No

gi|685631918	excinuclease ABC subunit B	No
gi|685632378	CDP-diacylglycerol--glycerol-3-phosphate 3-phosphatidyltransferase	Yes
gi|1145681323	CDP-glycerol--poly(glycerophosphate) glycerophosphotransferase	No
gi|685631710	HAD family hydrolase	No
gi|685633860	cadmium-transporting ATPase	No
gi|685633008	alpha/beta hydrolase	No
gi|685632190	chitinase	No
gi|685633060	hypothetical protein BWO94_05440	No
gi|685632706	exodeoxyribonuclease VII large subunit	No
gi|685632509	hydrolase	No
gi|685633216	protein translocase component YidC	No
gi|685632804	luciferase family oxidoreductase	No
gi|685631864	DoxX family protein	No
gi|685632225	RNA methyltransferase	No
gi|685632713	lipoprotein	No
gi|685633749	sulfite reductase [NADPH] flavoprotein alpha-component	No
gi|685632566	ATP-dependent helicase DinG	No
gi|685632357	RIP metalloprotease RseP	No
gi|1145681321	protease PrsW	No
gi|685632814	D-tyrosyl-tRNA(Tyr) deacylase	No
gi|685632239	glutamate racemase	No
gi|685633268	hypothetical protein BWO94_04450	No
gi|685632900	D-3-phosphoglycerate dehydrogenase	No
gi|685631882	histidinol-phosphate transaminase	No
gi|685633285	hypothetical protein BWO94_04335	No
gi|685632265	phenol soluble modulin	No
gi|685632000	nitrogen fixation protein NifU	No

gi|685632571	zinc metallopeptidase	No
gi|685631921	prolipoprotein diacylglyceryl transferase	No
gi|685633620	phosphoglucomutase	No
gi|685631759	hypothetical protein BWO94_10685	No
gi|685631616	hypothetical protein BWO94_13915	No
gi|685633476	TetR family transcriptional regulator	No
gi|685632438	threonine synthase	No
gi|685632670	two-component sensor histidine kinase	No
gi|685633214	cardiolipin synthase	No
gi|685632468	sodium:alanine symporter	No
gi|685632281	cell division protein YggT	No
gi|685632473	peptide-methionine (S)-S-oxide reductase	No
gi|685632280	cell division protein SepF	No
gi|685631758	HD domain-containing protein	No
gi|685633000	hypothetical protein BWO94_10060	No
gi|685632452	DUF896 family protein	No
gi|685632194	inositol monophosphatase	No
gi|685633763	tributyrin esterase	No

Table B.7. Proteins downregulated in *S. aureus* treated with HSGN-144

ID Number	Protein	Essential in *S. aureus*?
gi|685632671	DNA-binding response regulator	No
gi|685632300	guanylate kinase	No
gi|685632728	hydroxyacylglutathione hydrolase	No
gi|685631435	hypothetical protein BWO94_03970	No
gi|685631929	malate dehydrogenase	No
gi|685632754	PhoH family protein	No
gi|685632157	phosphoribosylformylglycinamidine synthase subunit PurL	No
gi|685632760	16S rRNA (uracil(1498)-N(3))-methyltransferase	No

gi|685632591	L-asparaginase	No
gi|685633137	pathogenicity island protein	No
gi|685633260	amidohydrolase	No

Table B.8. Proteins downregulated in *S. aureus* treated with HSGN-220

ID Number	Protein	Essential in *S. aureus*?
gi|1145681246	butyryl-CoA dehydrogenase	No
gi|685631724	glucosamine-6-phosphate deaminase	No
gi|685632154	phosphoribosylaminoimidazole-succinocarboxamide synthase	No
gi|685631908	fatty acid-binding protein DegV	No
gi|685632463	hypothetical protein BWO94_11360	No
gi|685632447	guanosine 5-monophosphate oxidoreductase	No
gi|685633168	ABC transporter ATP-binding protein	No
gi|685632923	DUF1444 domain-containing protein	No
gi|685633432	formate dehydrogenase subunit alpha	No
gi|685633010	protoporphyrinogen oxidase	No
gi|685633475	multidrug efflux protein	No
gi|685632372	transcriptional regulator	No
gi|685633257	type II pantothenate kinase	No
gi|685632211	phosphopantetheine adenylyltransferase	No
gi|685632759	30S ribosomal protein S12 methylthiotransferase	No
gi|685632527	response regulator ArlR	No
gi|685631586	restriction endonuclease subunit S	No
gi|685632716	rhodanese	No
gi|685632795	methyltransferase	No

Table B.9. Upregulated proteins shared amongst *S. aureus* treatment with HSGN-220, -218, or -144

ID Number	Protein
gi|685632908	heme transporter HarA
gi|685631274	2,3-diaminopropionate biosynthesis protein SbnB
gi|685632217	iron-regulated surface determinant protein A
gi|685632368	30S ribosomal protein S15
gi|685632219	heme ABC transporter permease
gi|685631802	iron-enterobactin transporter ATP-binding protein
gi|685633225	beta-hydroxyacyl-ACP dehydratase
gi|685633671	CHAP domain-containing protein
gi|685632578	nucleoside-diphosphate kinase
gi|685632267	GNAT family N-acetyltransferase
gi|685632460	choline transporter
gi|1145683298	crystallin
gi|685632331	16S rRNA processing protein RimM
gi|685632310	protein phosphatase
gi|685632096	DUF2187 domain-containing protein
gi|685631997	D-alanyl-lipoteichoic acid biosynthesis protein DltB
gi|685632820	tRNA guanosine(34) transglycosylase Tgt

Table B.10. Bacterial strains, sources and characteristics

Staphylococcus aureus ATCC 25923	ATCC	Methicillin susceptible. Reference strain for antibiotic susceptibility testing
MRSA USA 300	ATCC/BEI resources	Methicillin resistant. Most prevalent MRSA clinical infection strain in the U.S

MRSA ATCC 33592	William Wuest, Emory University	Methicillin resistant, Gentamicin resistant. SCCmec: Type III
Enterococcus faecalis ATCC 29212	ATCC	Reference strain for antibiotic susceptibility testing. Susceptible to most GPC antibiotics
Enterococcus faecalis ATCC 51575 (VRE)	ATCC	Presence of *vanB*. Resistant to gentamicin, streptomycin, and vancomycin. Sensitive to teicoplanin.
Enterococcus faecium ATCC 700221 (VRE)	ATCC	Presence of *vanA*. Resistant to vancomycin and teicoplanin
Listeria monocytogenes ATCC 19115	ATCC	Reference strain for antibiotic susceptibility testing. Susceptible to most GPC antibiotics

ATCC = American Type Culture Collection, GPC = Gram positive cocci, ARLG = Antibacterial Resistance Leadership Group

Table B.11. MRSA clinical isolates used in study

Strain	PFGE Pattern / MLST Type	spa Type eGenomics (Ridom)	SCCmec	Other Genetic Characterization	Additional Non MRSA resistance (dru Type)	Oxacillin MIC in μg/mL
ARLG 1561	USA 300	1	IVa	ACME+, pvl genes+	Ery	NT
ARLG 1567	USA 300	1	IVa	ACME+, pvl genes+	Ery, Cipro	NT
ARLG 1568	USA 300	1	IVa	ACME+, pvl genes+, MupA gene+	Mup, Ery, Cipro	NT

ARLG 1569	USA 300	1	IVa	ACME+, pvl genes+, MupA gene+	Mup, Ery, Cipro, Clinda	NT
ARLG 1570	USA 300	1	IVa	ACME+, pvl genes+, MupA gene+	Mup, Ery, Cipro, Clinda	NT
ARLG-1663	ST239	351 (t030)	3A.1.4	ccrC+, dcs+, Hg-J+, mecl+	(dt10a)	512
ARLG-1649	ST1312	351 (t030)	3A.1.4	ccrC+, dcs+, Hg-J+, mecl+	(dt10g)	256
ARLG-1664	ST239	351 (t030)	16691	ccrC+, Hg-J+, mecl+	(dt9x)	256

* ACME = arginine catabolic mobile element, PFGE = Pulsed field gel electrophoresis, MLST = Multilocus sequence typing, pvl = panton valentin leucocidin, Ery = Erythromycin, Mup = Mupirocin, Cipro = Ciprofloxacin, Clinda = Constitutive clindamycin resistance

Table B.12. Sequence of primers used in RT-PCR.

Primer Name	Sequence (5'- 3')	Source
dnaX Forward	AGAAGAACCTCCAGCACACG	This Study
dnaX Reverse	CATCGCCGAAAGCAATAGCC	This Study
pol IIIC Forward	TATGGGCTTCATCGACACGG	This Study
pol IIIC Reverse	AATACCCGCTGTGTCACCTG	This Study
birA Forward	CCGCGACCTTTCGTTTGTTC	This Study
birA Reverse	ATCTGGACAAAGCATTGCGG	This Study
lexA Forward	GTTCCTATTACCGCAGTA	This Study
lexA Reverse	TACCAGCCTCAATCATAC	This Study
dnaC Forward	TCTTCCGTTGCTTGTTTCGC	This Study
dnaC Reverse	TGAAATGTGAGAGATGTGGAAGTG	This Study
menA Forward	TAGGGAAAGGGCCACCTGTA	This Study
menA Reverse	TGGTGCAATTGTACGCAACG	This Study
Pth Forward	AGCAGTTGCACCGATTATGGA	This Study

Pth Reverse	TCATACCATTGTGACCGCCC	This Study
mvak1 Forward	CAAATTGCACATGGTAAACCAAGT	This Study
mvak1 Reverse	TTCAACGTTTCAGCATGACCTT	This Study
pgsA Forward	ATTGGCTTCCCTTAGCGATT	This Study
pgsA Reverse	AGAATTGGTTAGTCCTAGTTGCAC	This Study
relA Forward	GCACAGCACCATATGGCAAC	This Study
relA Reverse	ATGGAGACCCGCTCGAAATC	This Study
HarA Forward	GCCATCAAGCTTTGCTGCTT	This Study
HarA Reverse	GCAGCACTGCAACAAATCCA	This Study
IsdA Forward	TGCTTTTTCAAATTCCAAATGCGTAGT	This Study
IsdA Reverse	GCAGTTGAACCTGGATATAAGAGCTTA	This Study
16S Forward	CGGTCCAGACTCCTACGGGAGGCAGCA	Opoku-Temeng et al.[217]
16S Reverse	GCGTGGACTACCAGGGTATCTAATCC	Opoku-Temeng et al.[217]

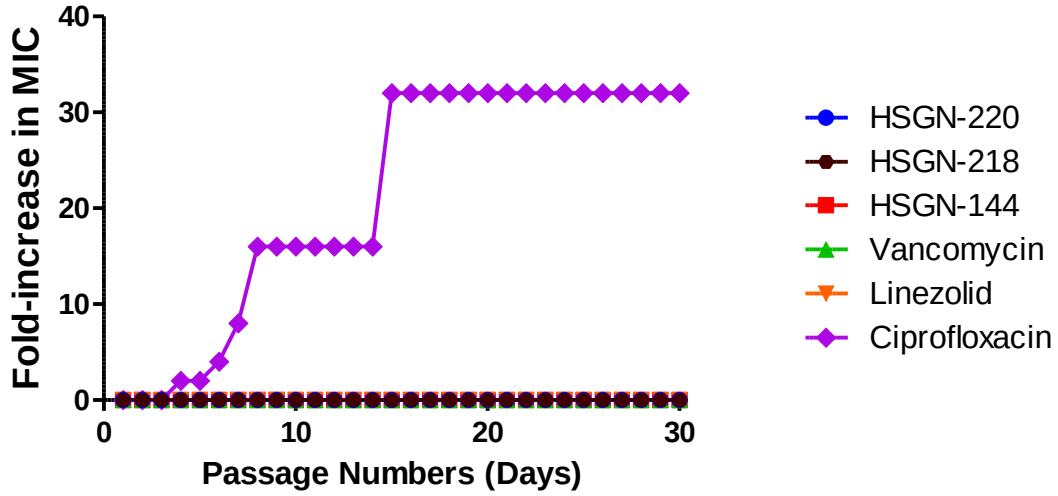

Figure B.1. Multi-step resistance selection of HSGN-220, -218, -144, ciprofloxacin, vancomycin, and linezolid against MRSA. MRSA USA300 was serially passaged daily over a 30-day period and the broth microdilution assay was used to determine the minimum inhibitory concentration of

compounds and control antibiotics against MRSA after each successive passage. A four-fold shift in MIC would be indicative of bacterial resistance.

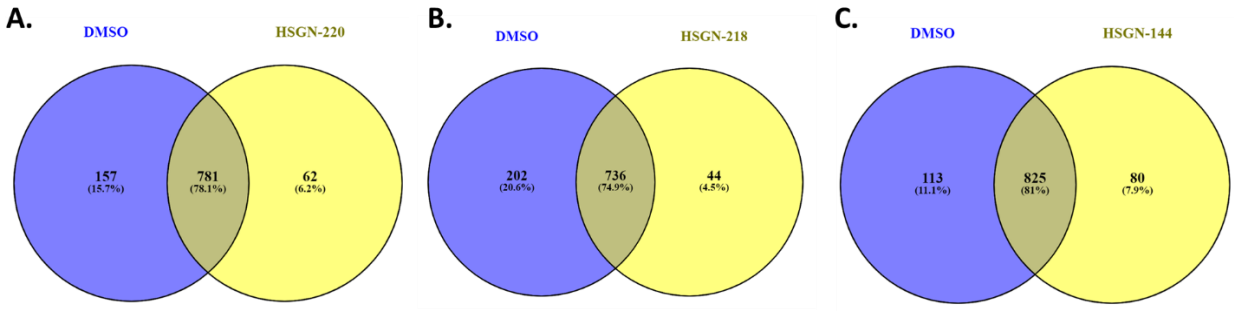

Figure B.2. Venn Diagrams Constructed. (A) Venn diagram for comparison of proteins identified in DMSO-treated cells alone, HSGN-220-treated cells alone and in both treatments. (B) Venn diagram for comparison of proteins identified in DMSO-treated cells alone, HSGN-218-treated cells alone and in both treatments. (C) Venn diagram for comparison of proteins identified in DMSO-treated cells alone, HSGN-144-treated cells alone and in both treatments.

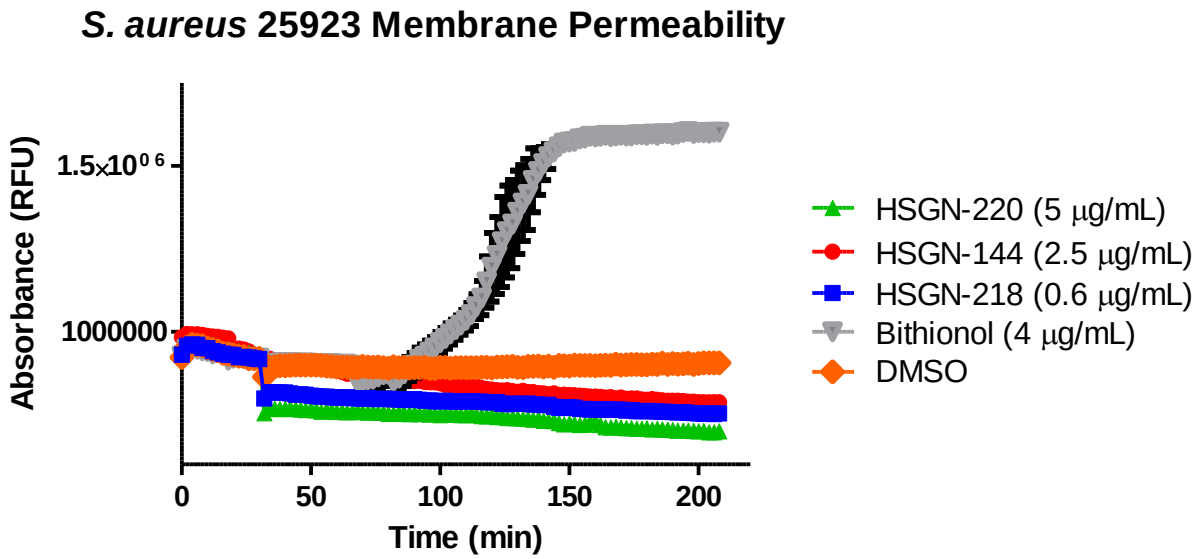

Figure B.3. Effects of HSGN-220, -218, and -220 on membrane permeability in *S. aureus* at 10x MIC concentrations using sytox green dye. Increase in fluorescence indicates permeability. Bithionol is used as positive control while 1% DMSO is used as negative control.

II. Plate Bioassays:

Control (1% DMSO):

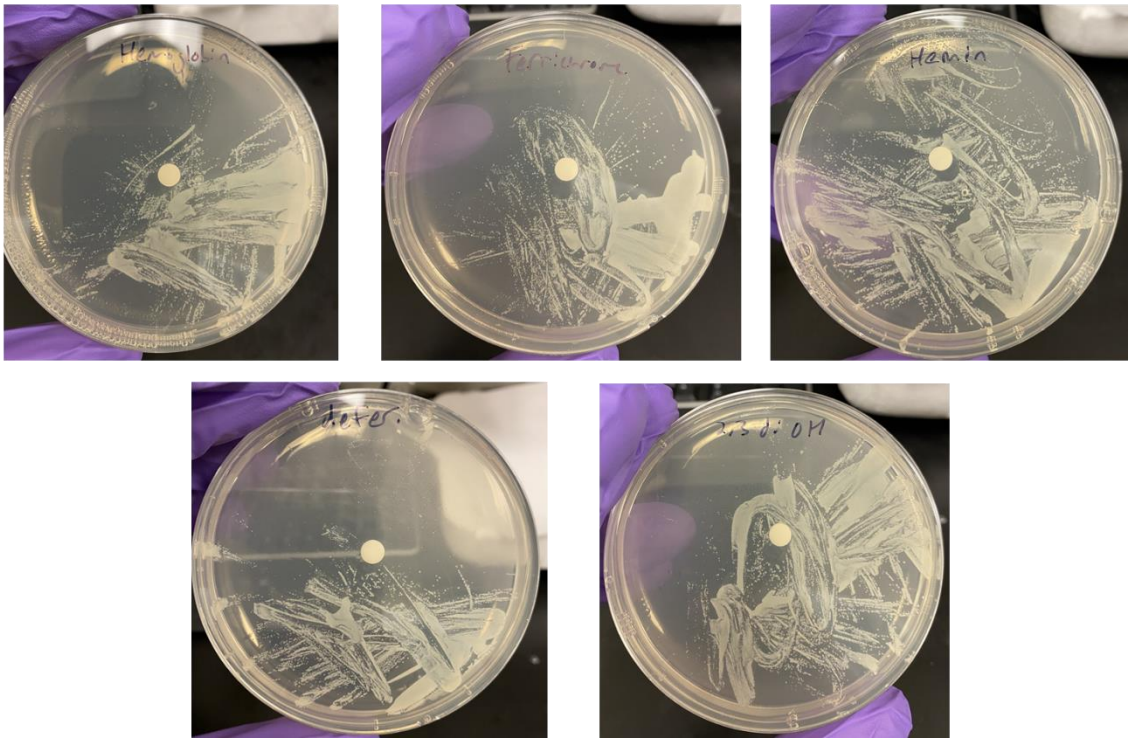

HSGN-218 (1X MIC):

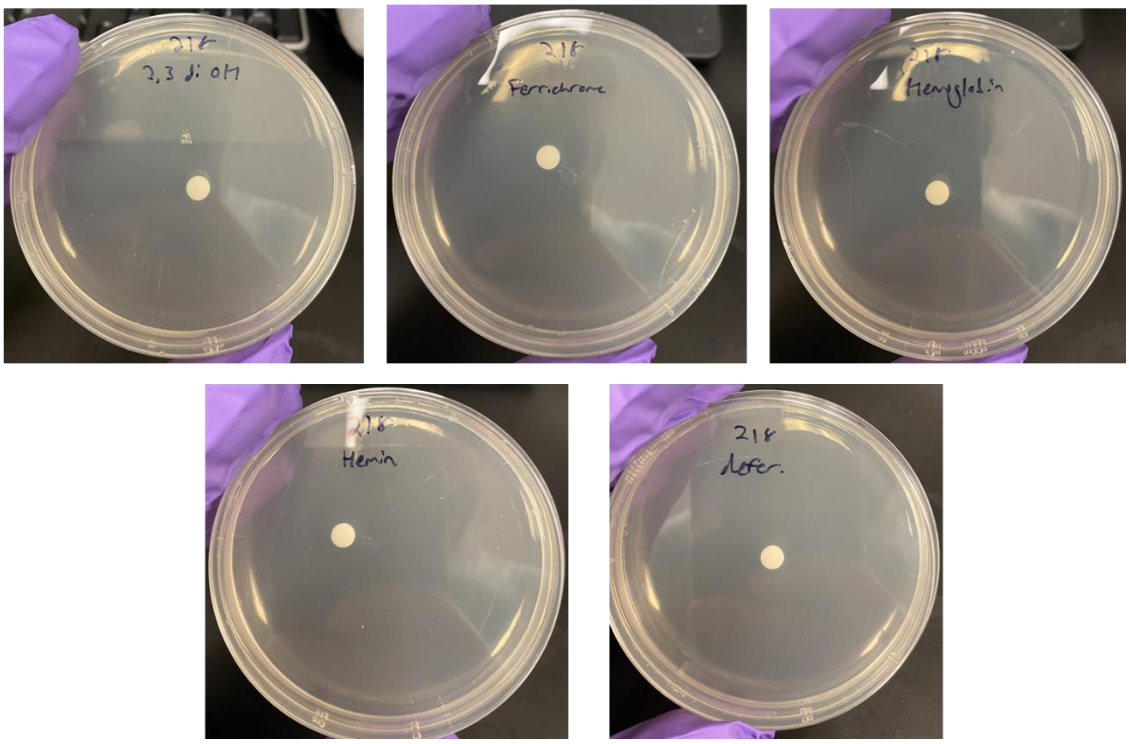

HSGN-218 (0.5X MIC):

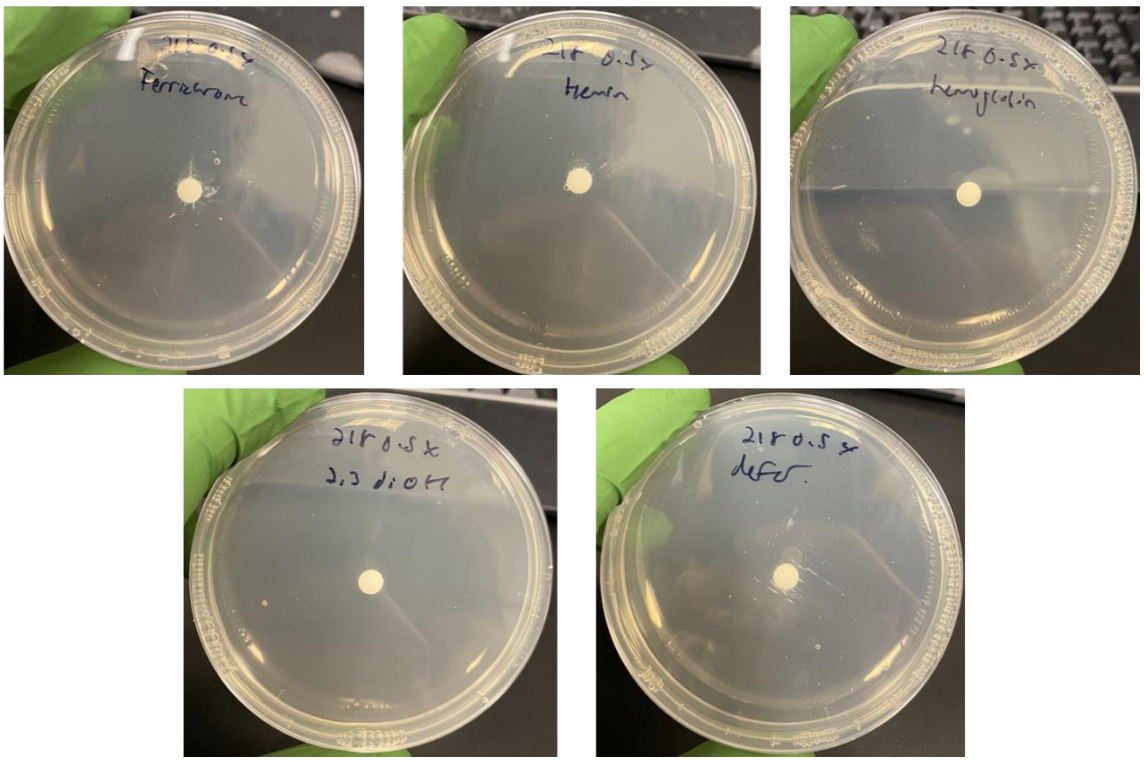

HSGN-218 (0.25X MIC):

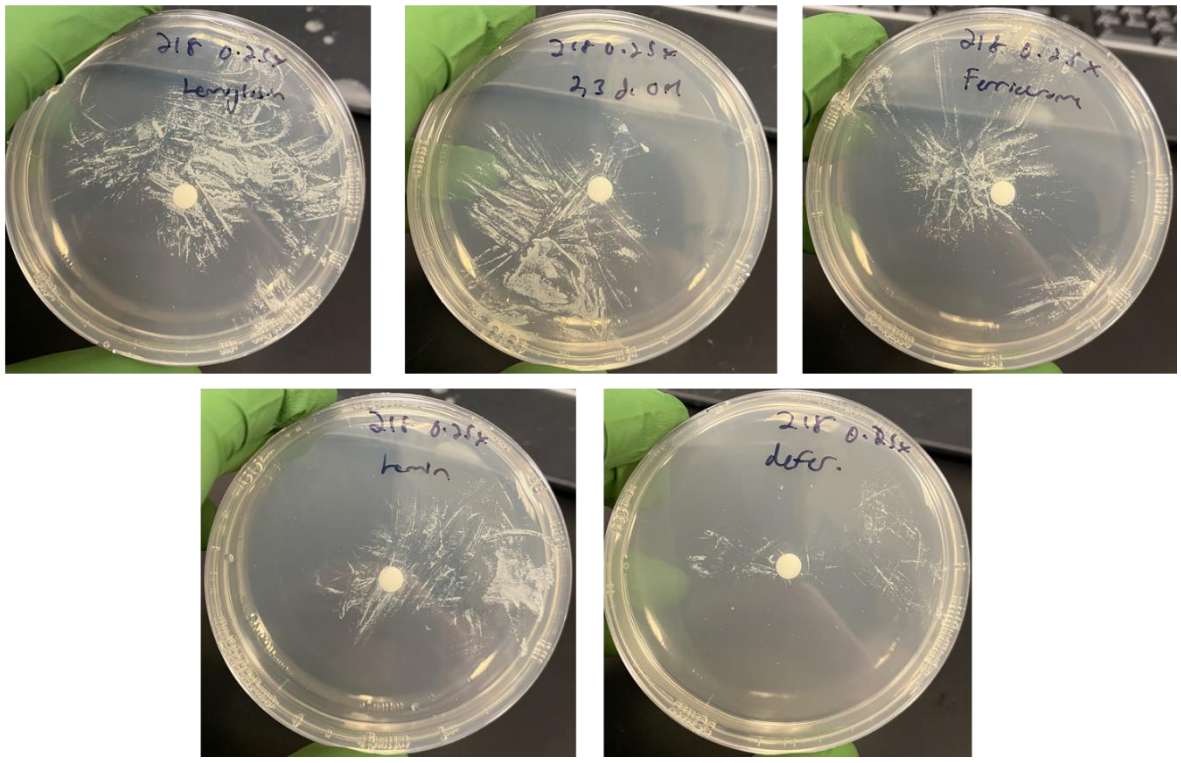

HSGN-220 (1X MIC):

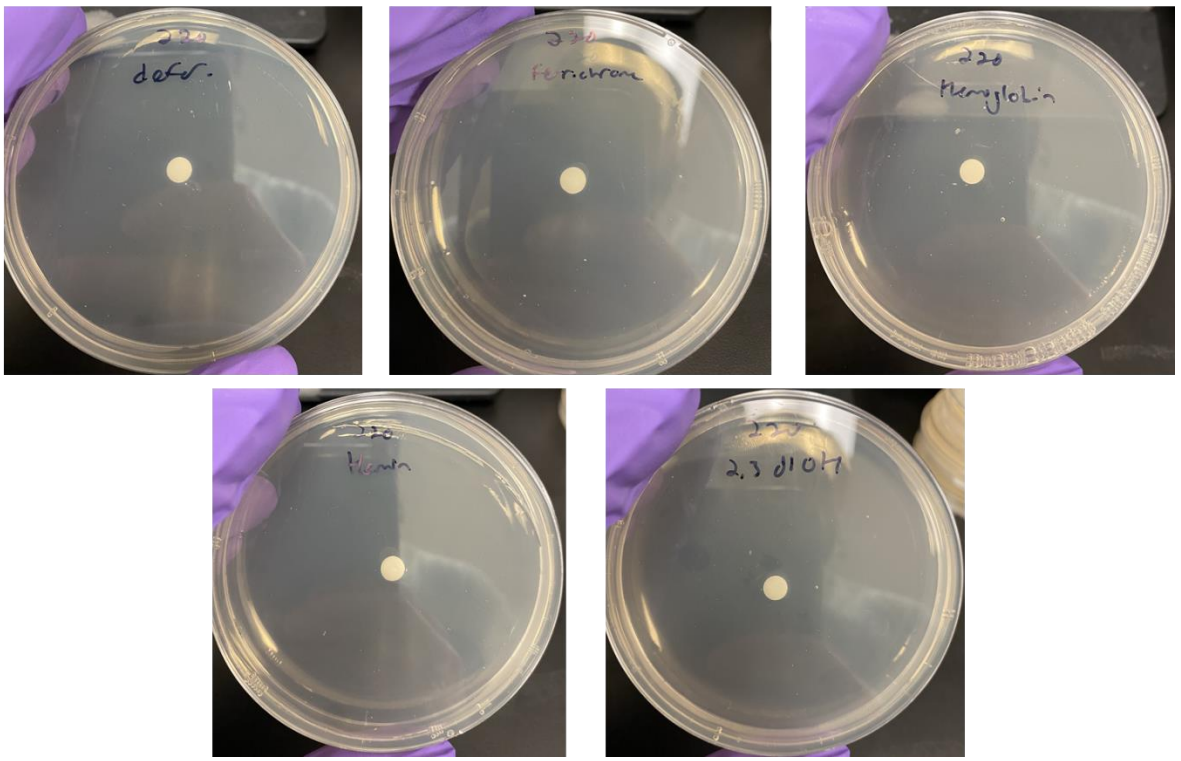

HSGN-220 (0.5X MIC):

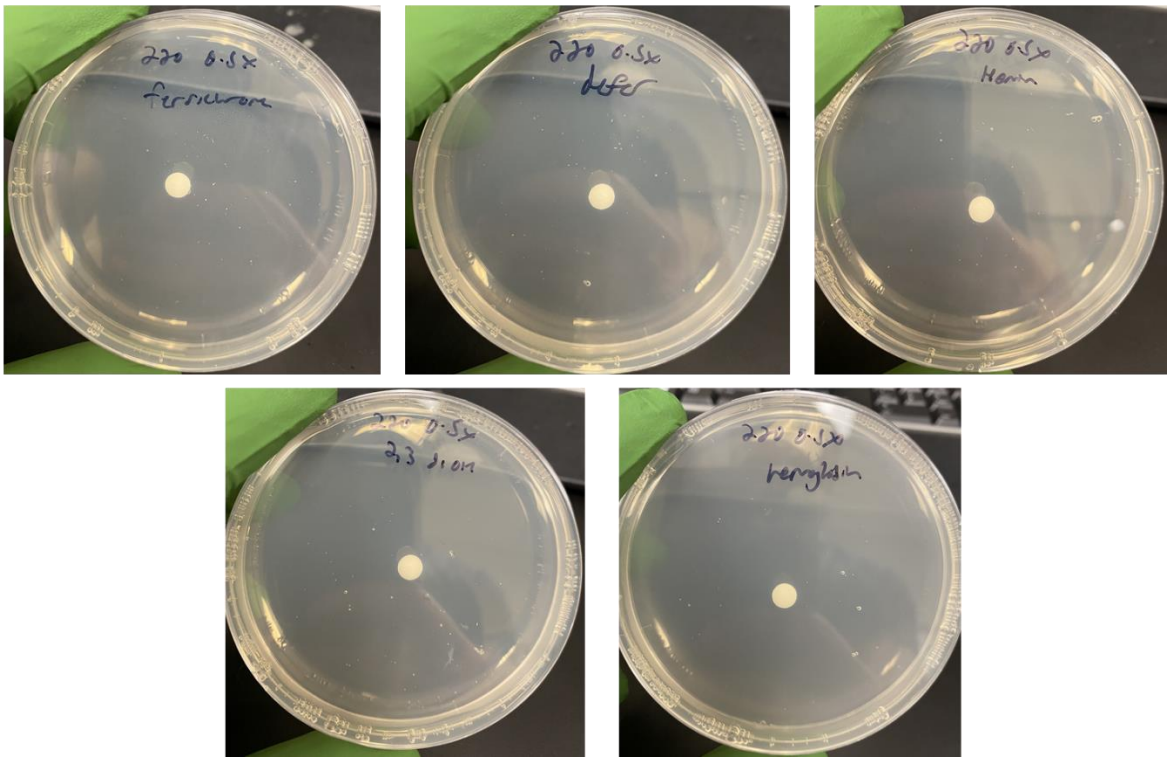

HSGN-220 (0.25X MIC):

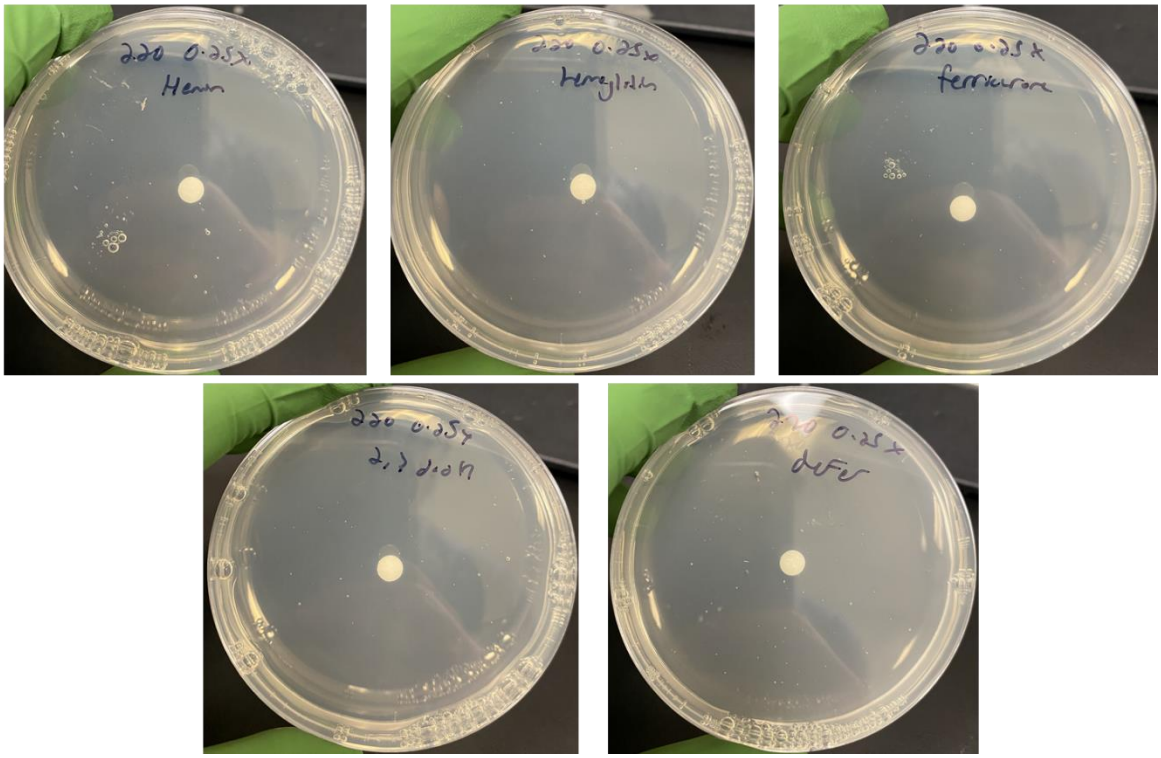

HSGN-144 (1X MIC):

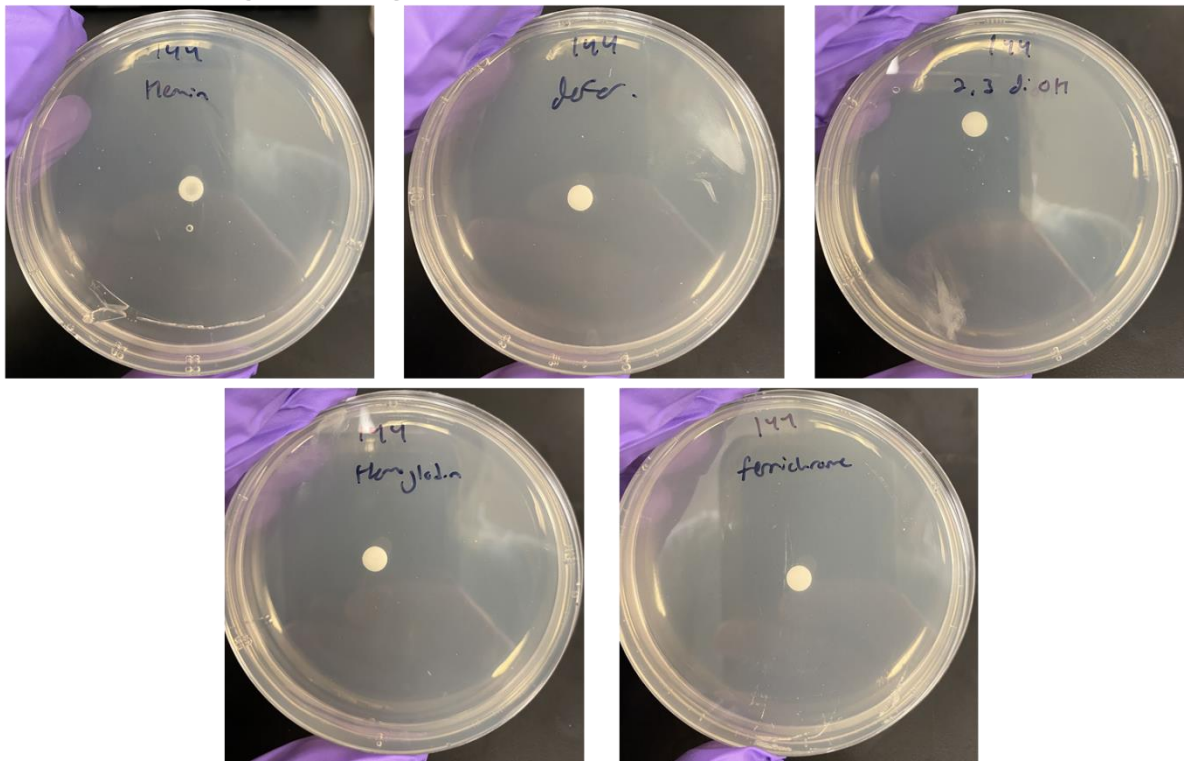

HSGN-144 (0.5X MIC):

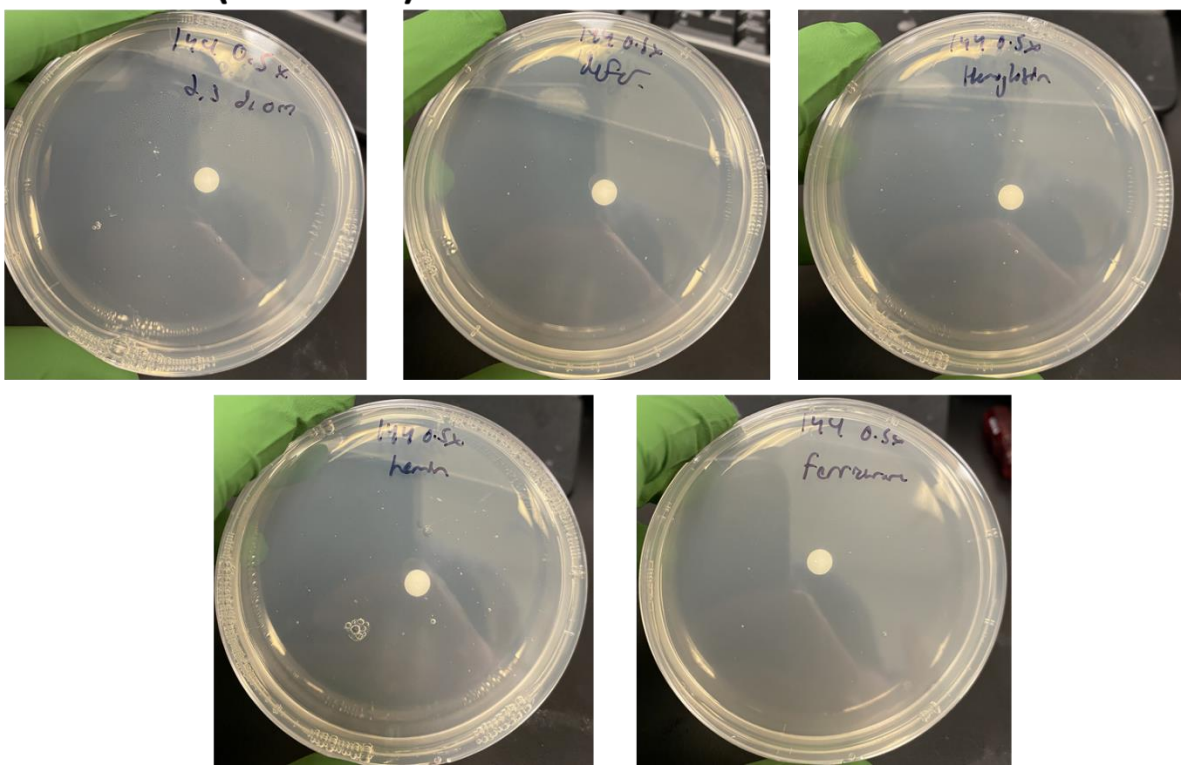

HSGN-144 (0.25X MIC):

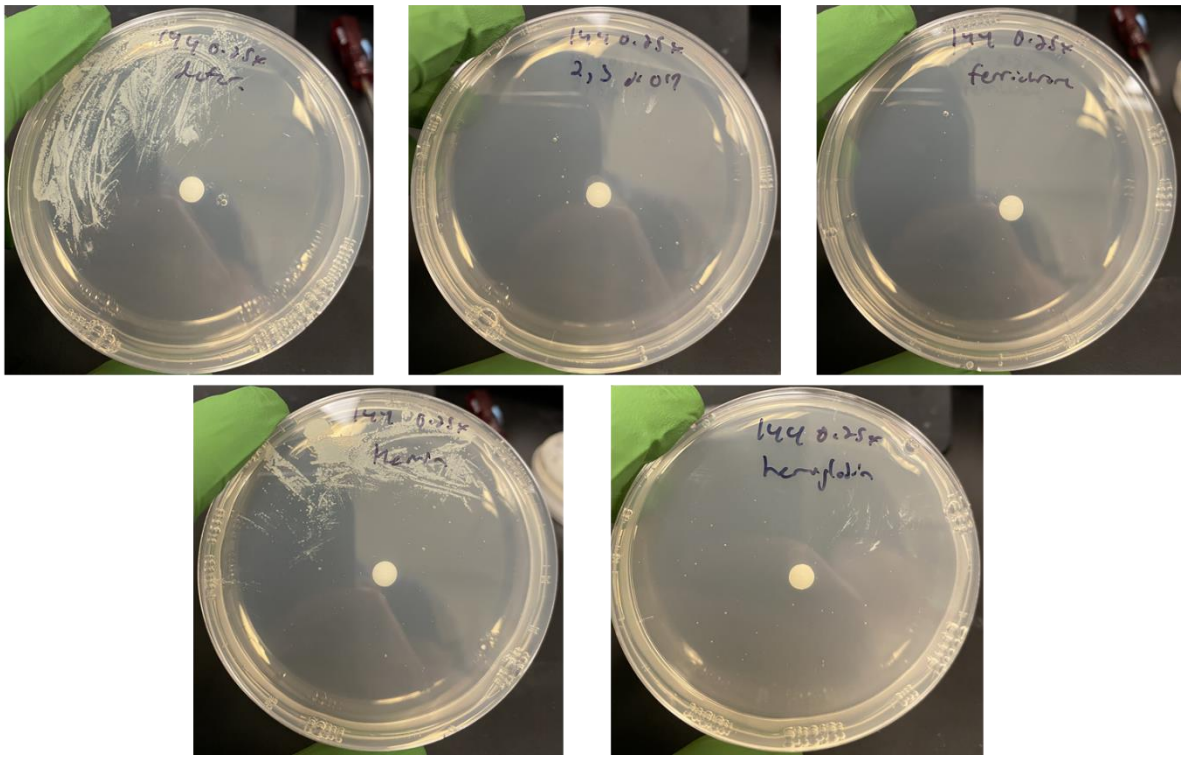

APPENDIX C. CHAPTER 9 SUPPORTING INFORMATION

Table C.1. Bacterial strains, sources and characteristics

Staphylococcus aureus ATCC 25923	ATCC	Methicillin susceptible. Reference strain for antibiotic susceptibility testing
MRSA USA 300	ATCC/BEI resources	Methicillin resistant. Most prevalent MRSA clinical infection strain in the U.S
MRSA ATCC 33592	William Wuest, Emory University	Methicillin resistant, Gentamicin resistant. SCCmec: Type III
Enterococcus faecalis ATCC 29212	ATCC	Reference strain for antibiotic susceptibility testing. Susceptible to most GPC antibiotics
Enterococcus faecalis ATCC 51575 (VRE)	ATCC	Presence of *vanB*. Resistant to gentamicin, streptomycin, and vancomycin. Sensitive to teicoplanin.
Enterococcus faecium ATCC 700221 (VRE)	ATCC	Presence of *vanA*. Resistant to vancomycin and teicoplanin
Listeria monocytogenes ATCC 19115	ATCC	Reference strain for antibiotic susceptibility testing. Susceptible to most GPC antibiotics

ATCC = American Type Culture Collection, GPC = Gram positive cocci, ARLG = Antibacterial Resistance Leadership Group

Table C.2. MRSA clinical isolates used in study

Strain	PFGE Pattern / MLST Type	spa Type eGenomics (Ridom)	SCCmec	Other Genetic Characterization	Additional Non MRSA resistance (dru Type)	Oxacillin MIC in μg/mL
ARLG 1561	USA 300	1	IVa	ACME+, pvl genes+	Ery	NT
ARLG 1567	USA 300	1	IVa	ACME+, pvl genes+	Ery, Cipro	NT
ARLG 1568	USA 300	1	IVa	ACME+, pvl genes+, MupA gene+	Mup, Ery, Cipro	NT
ARLG 1569	USA 300	1	IVa	ACME+, pvl genes+, MupA gene+	Mup, Ery, Cipro, Clinda	NT
ARLG 1570	USA 300	1	IVa	ACME+, pvl genes+, MupA gene+	Mup, Ery, Cipro, Clinda	NT
ARLG-1663	ST239	351 (t030)	3A.1.4	ccrC+, dcs+, Hg-J+, mecl+	(dt10a)	512
ARLG-1649	ST1312	351 (t030)	3A.1.4	ccrC+, dcs+, Hg-J+, mecl+	(dt10g)	256
ARLG-1664	ST239	351 (t030)	16691	ccrC+, Hg-J+, mecl+	(dt9x)	256

* ACME = arginine catabolic mobile element, PFGE = Pulsed field gel electrophoresis, MLST = Multilocus sequence typing, pvl = panton valentin leucocidin, Ery = Erythromycin, Mup = Mupirocin, Cipro = Ciprofloxacin, Clinda = Constitutive clindamycin resistance

^{1}H and ^{13}C NMR Spectra:

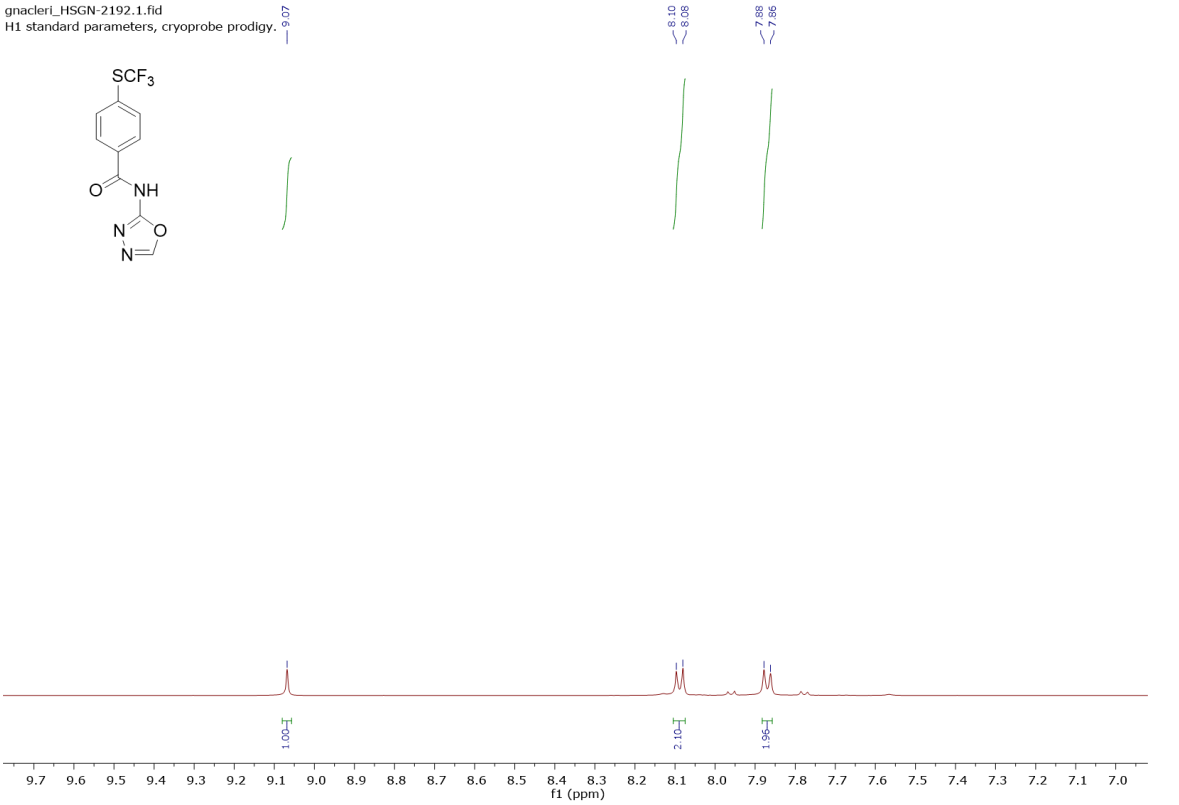

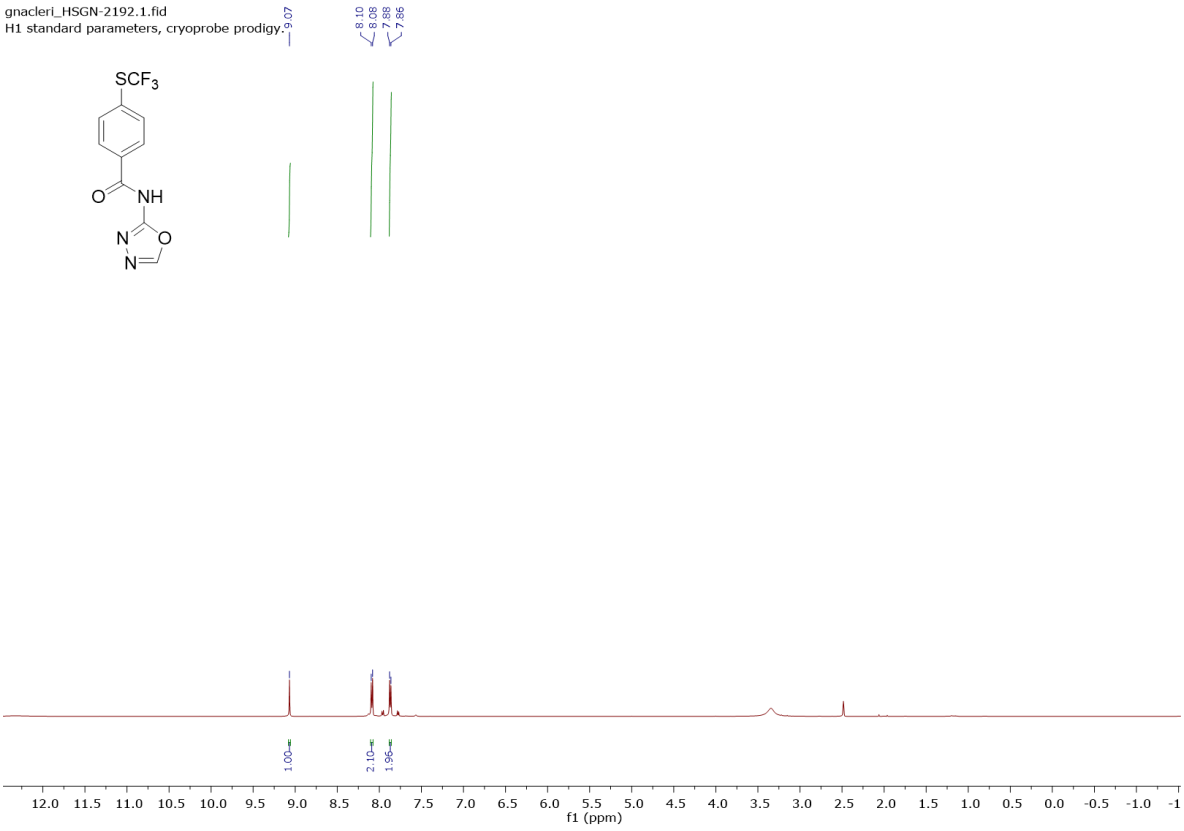

gnacleri_HSGN-2192.2.fid
C13 standard parameters, cryoprobe prodigy. pulprog = zgig30zr.jsh.

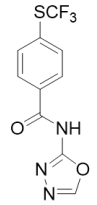

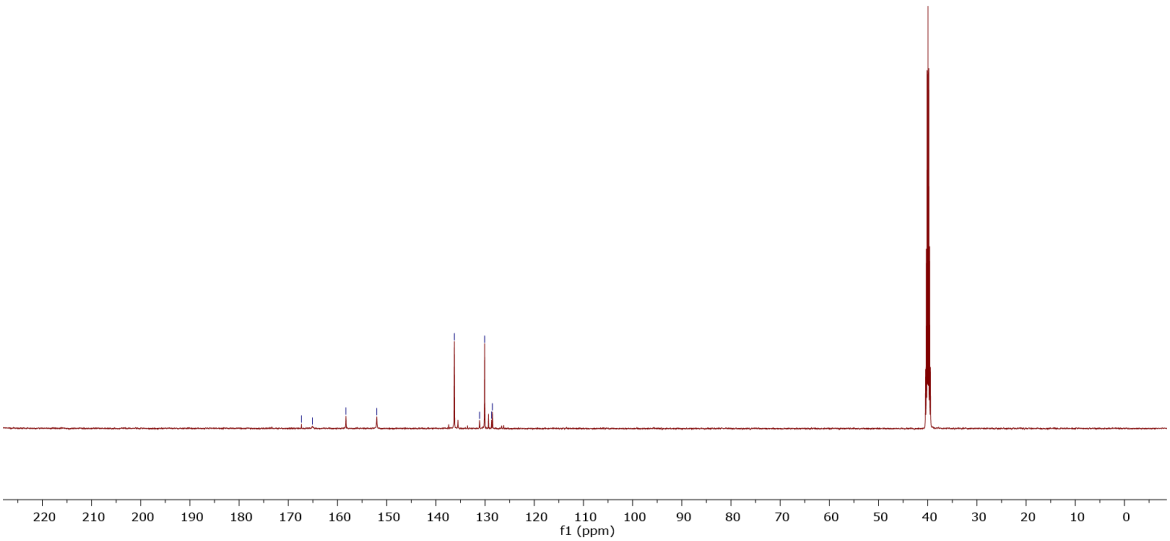

HSGN-2143.1.fid
H1 standard parameters, cryoprobe.

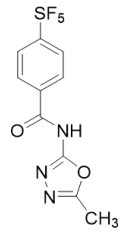

HSGN-2143.1.fid
H1 standard parameters, cryoprobe.

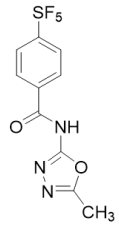

HSGN-2143.1.fid
H1 standard parameters, cryoprobe.

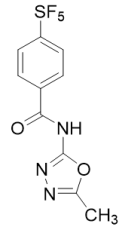

HSGN-2143.2.fid
C13 standard parameters, cryoprobe.
Use "abs13c" to flatten spectrum baseline.

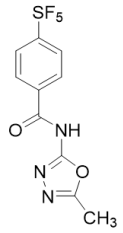

HSGN-2180.1.fid
H1 standard parameters, cryoprobe.

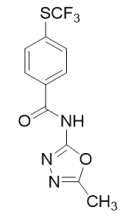

HSGN-2180.1.fid
H1 standard parameters, cryoprobe.

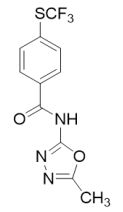

HSGN-2180.1.fid
H1 standard parameters, cryoprobe.

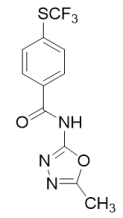

HSGN-2180.2.fid
C13 standard parameters, cryoprobe.
Use "abs13c" to flatten spectrum baseline.

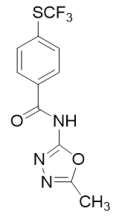

HSWG 133.1.fid
H1 standard parameters, cryoprobe prodigy.

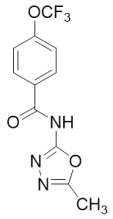

HSWG 133.1.fid
H1 standard parameters, cryoprobe prodigy.

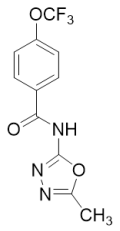

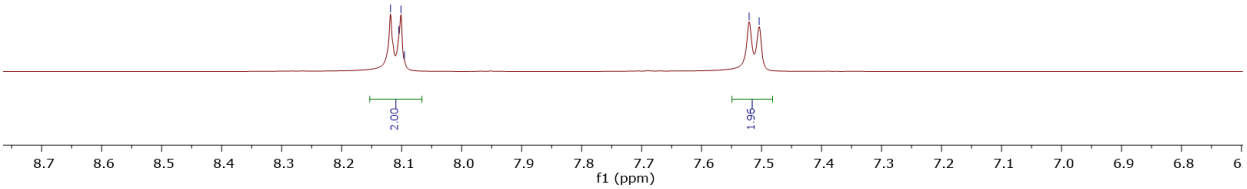

HSWG 133.1.fid
H1 standard parameters, cryoprobe prodigy.

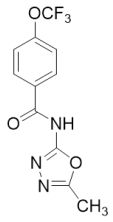

wgribble HSWG 133.2.fid
C13 standard parameters, cryoprobe.
Use "abs13c" to flatten spectrum baseline.

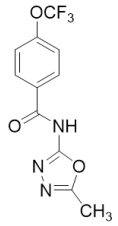

HSGN-2254.1.fid
H1 standard parameters, cryoprobe.

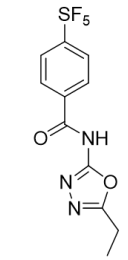

HSGN-2254.1.fid
H1 standard parameters, cryoprobe.

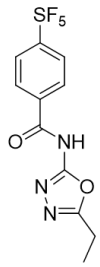

HSGN-2254.1.fid
H1 standard parameters, cryoprobe.

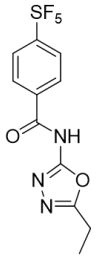

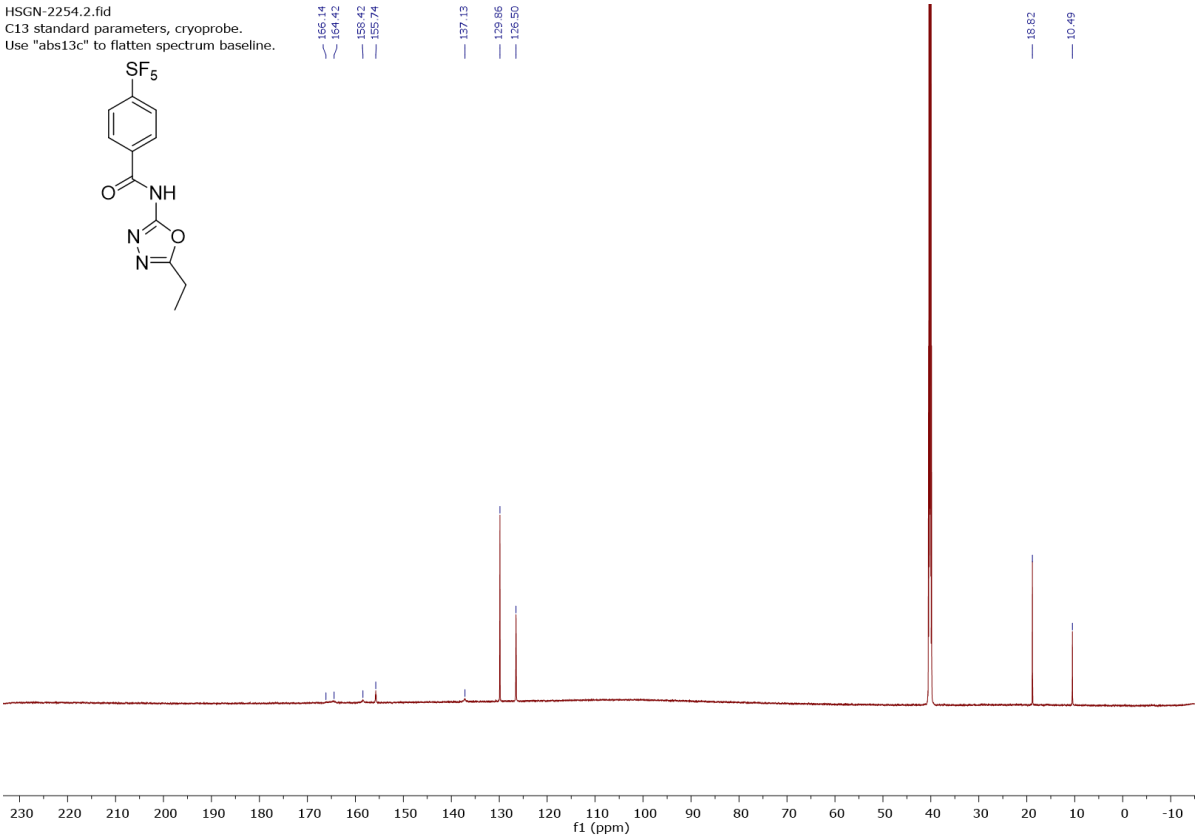
HSGN-2254.2.fid
C13 standard parameters, cryoprobe.
Use "abs13c" to flatten spectrum baseline.
166.14
164.42
158.42
155.74
137.13
129.86
126.50
18.82
10.49
SF5
O
NH
N
O
N
f1 (ppm)

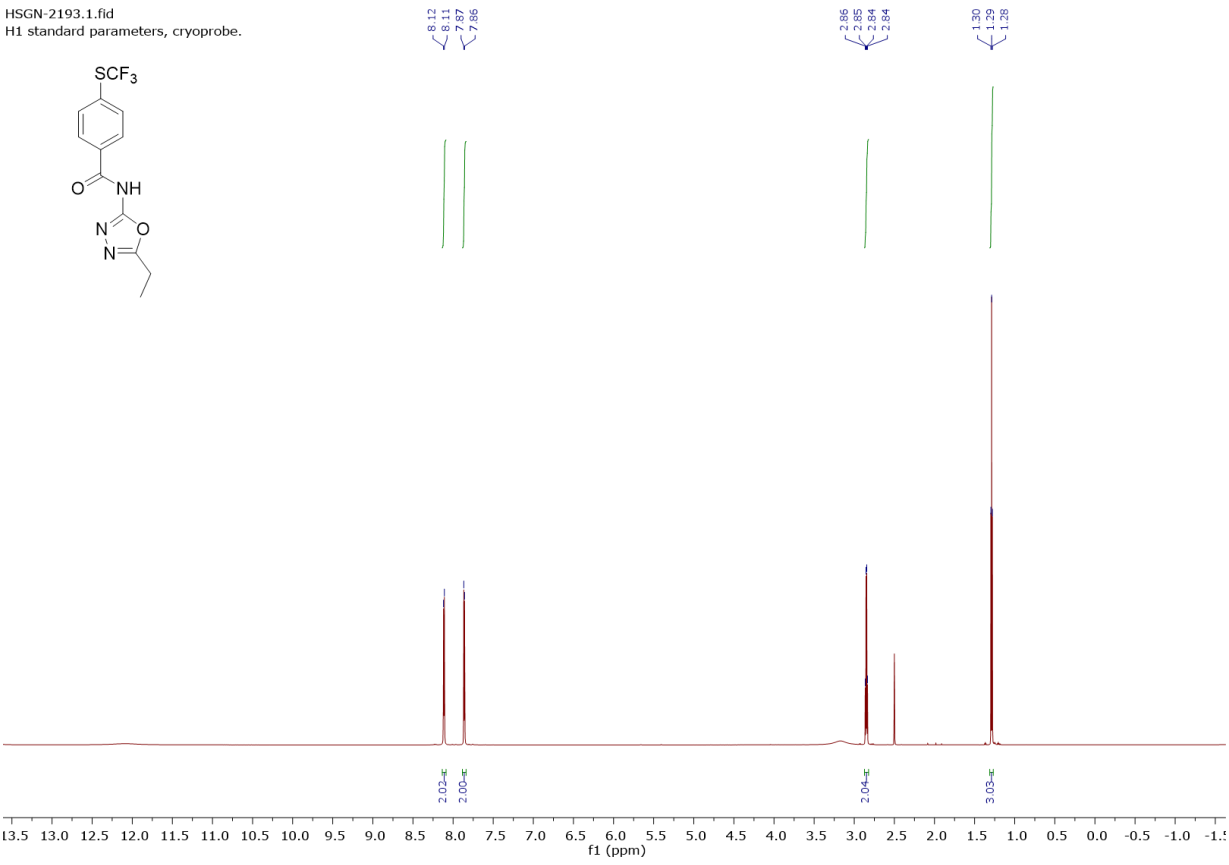
HSGN-2193.1.fid
H1 standard parameters, cryoprobe.
8.12
8.11
7.87
7.86
2.86
2.85
2.84
2.84
1.30
1.29
1.28
SCF3
O
NH
N
O
N
2.02
2.00
2.04
3.03
f1 (ppm)

HSGN-2193.1.fid
H1 standard parameters, cryoprobe.

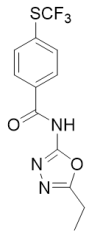

HSGN-2193.1.fid
H1 standard parameters, cryoprobe.

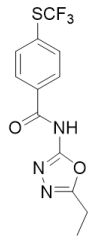

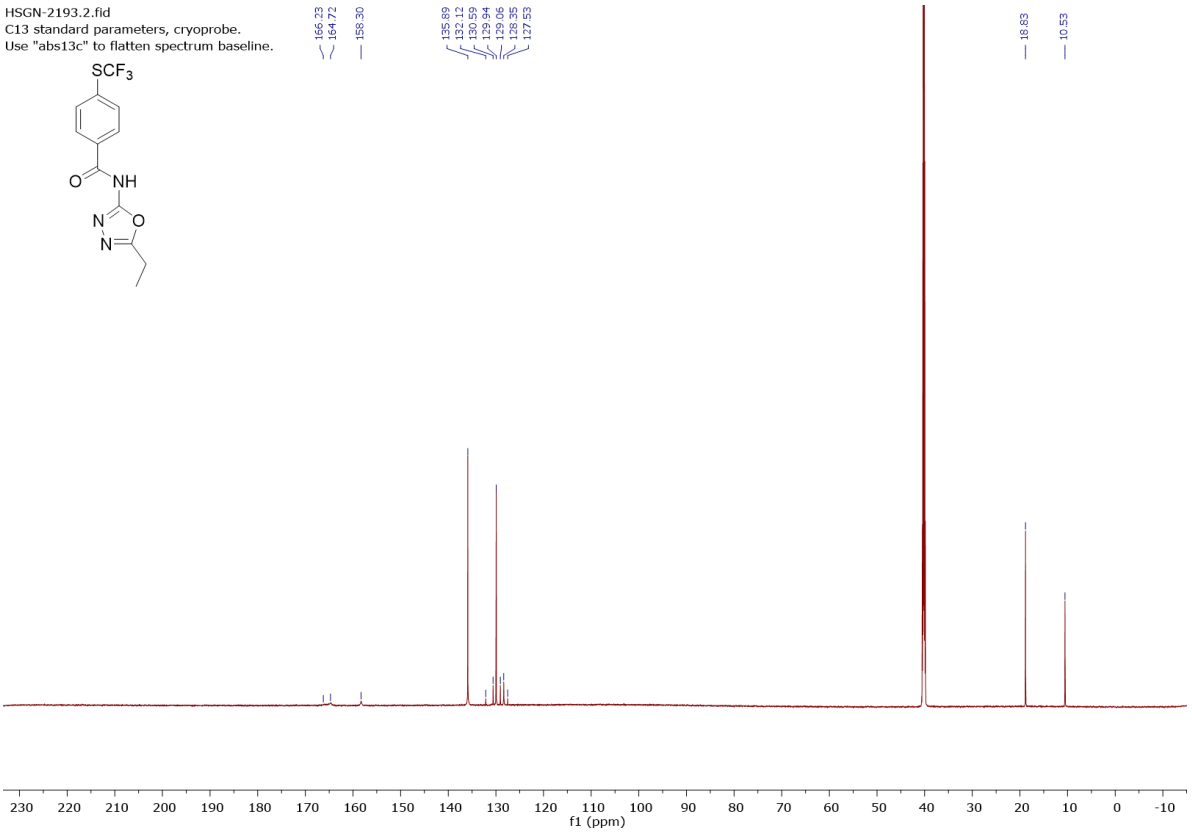
HSGN-2193.2.fid
C13 standard parameters, cryoprobe.
Use "abs13c" to flatten spectrum baseline.
166.23
164.72
158.30
135.89
132.12
130.59
129.94
129.06
128.35
127.53
18.83
10.53
SCF3
O
NH
N
O
N
f1 (ppm)

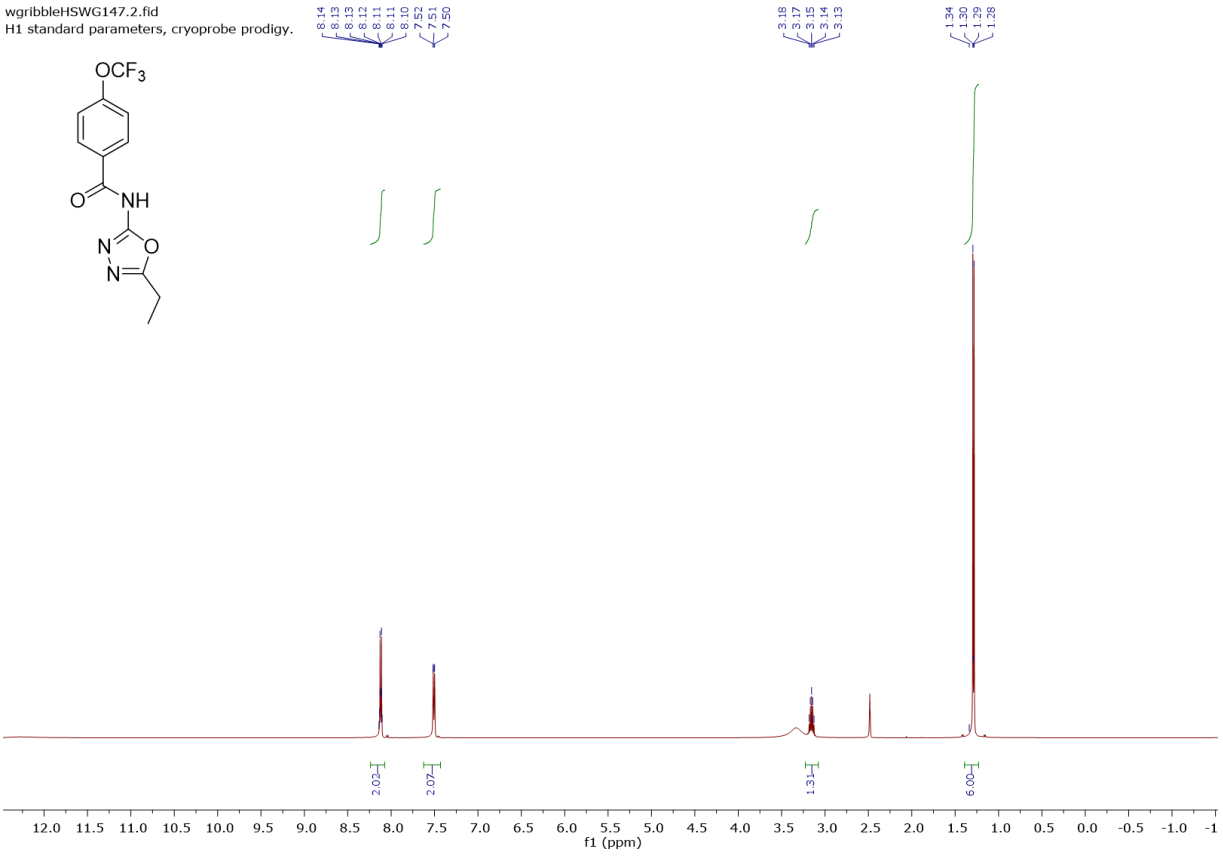
wgribbleHSWG147.2.fid
H1 standard parameters, cryoprobe prodigy.
8.14
8.13
8.13
8.12
8.11
8.11
8.10
7.52
7.51
7.50
3.18
3.17
3.15
3.14
3.13
1.34
1.30
1.29
1.28
OCF3
O
NH
N
O
N
2.02
2.07
1.31
6.00
f1 (ppm)

wgribbleHSWG147.2.fid
H1 standard parameters, cryoprobe prodigy.

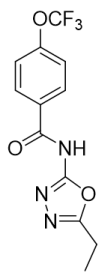

wgribbleHSWG147.2.fid
H1 standard parameters, cryoprobe prodigy

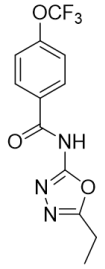

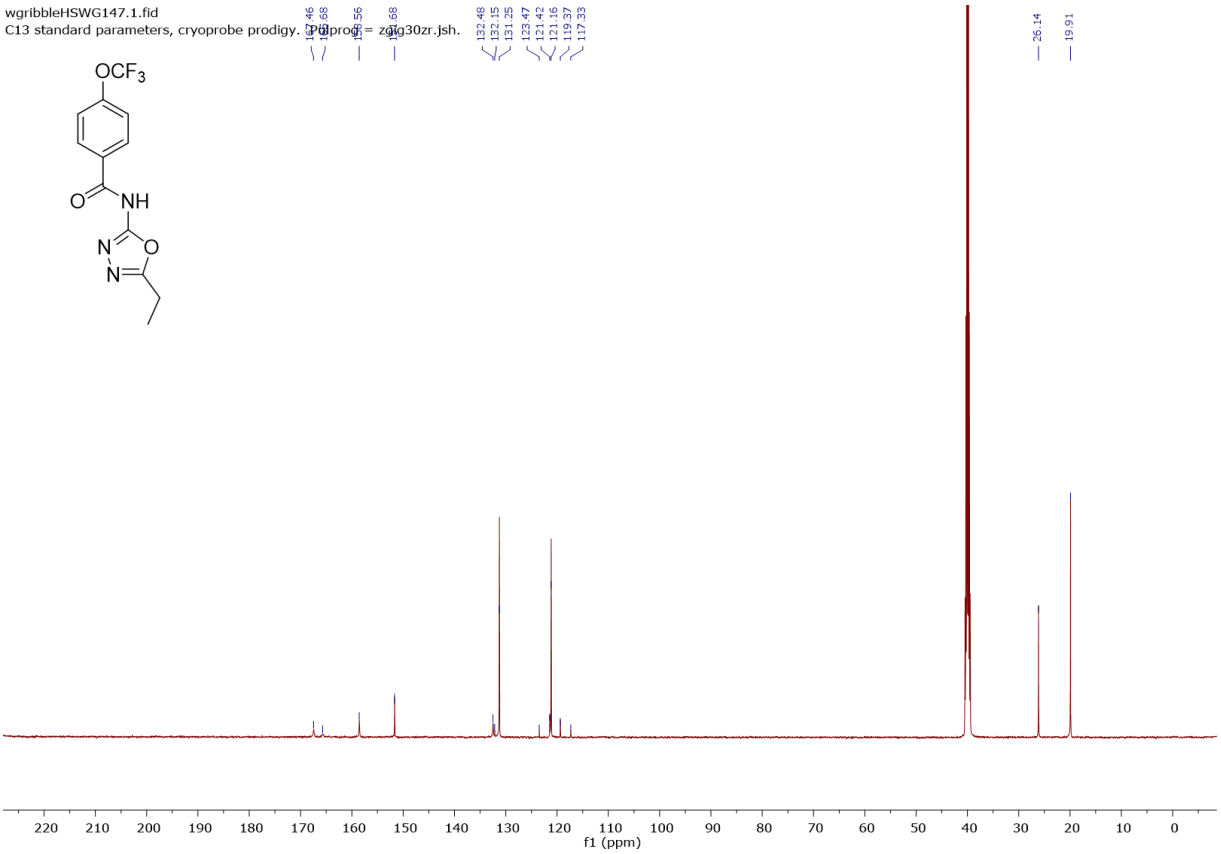
wgribbleHSWG147.1.fid
C13 standard parameters, cryoprobe prodigy. Pulprog = zgig30zr.jsh.
OCF3
O
NH
N
O
N
f1 (ppm)

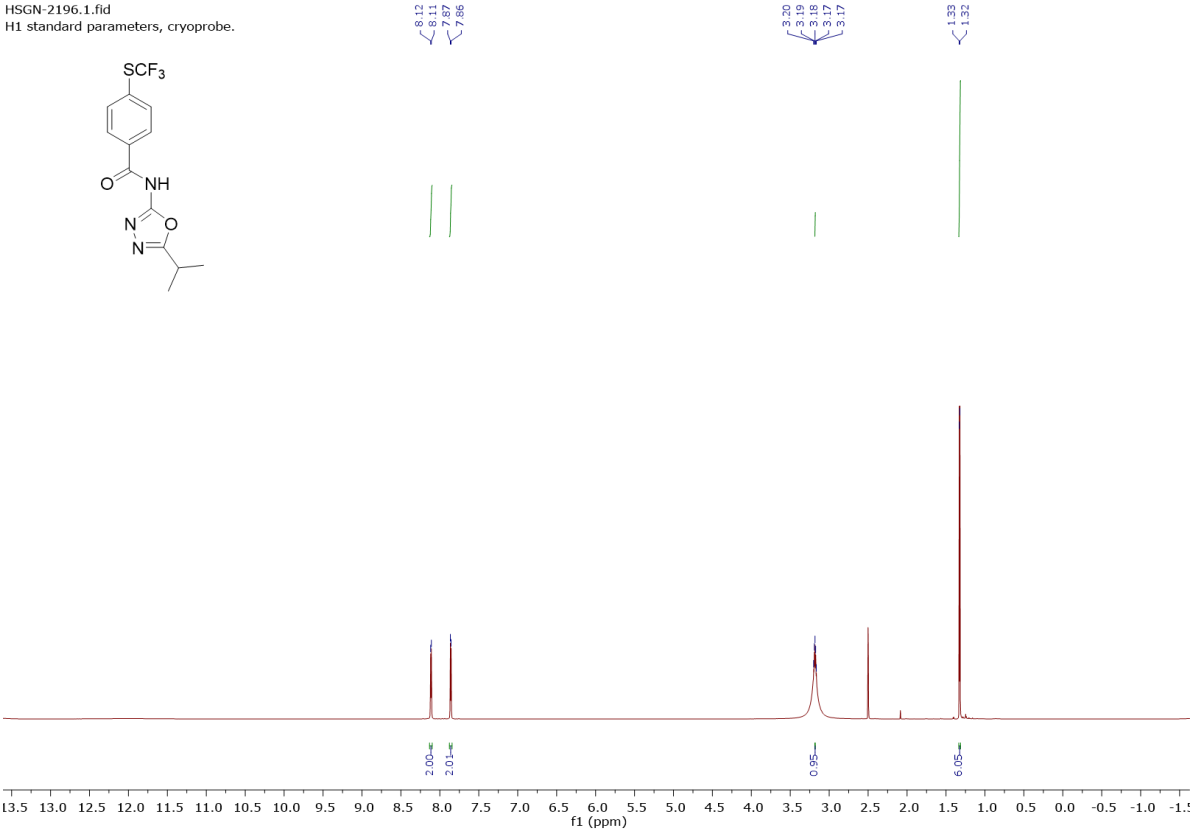
HSGN-2196.1.fid
H1 standard parameters, cryoprobe.
SCF3
O
NH
N
O
N
f1 (ppm)

HSGN-2196.1.fid
H1 standard parameters, cryoprobe.

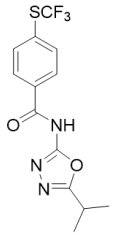

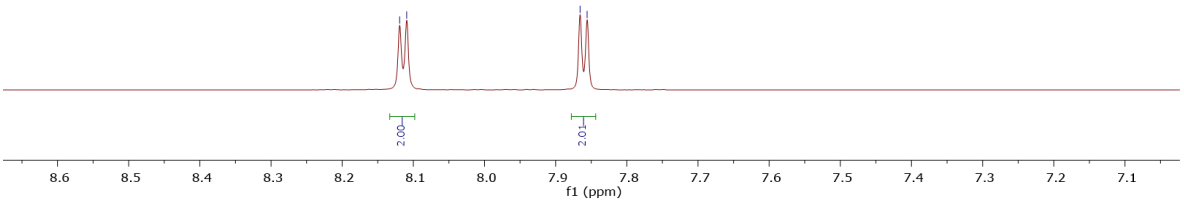

HSGN-2196.1.fid
H1 standard parameters, cryoprobe.

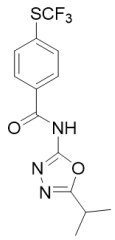

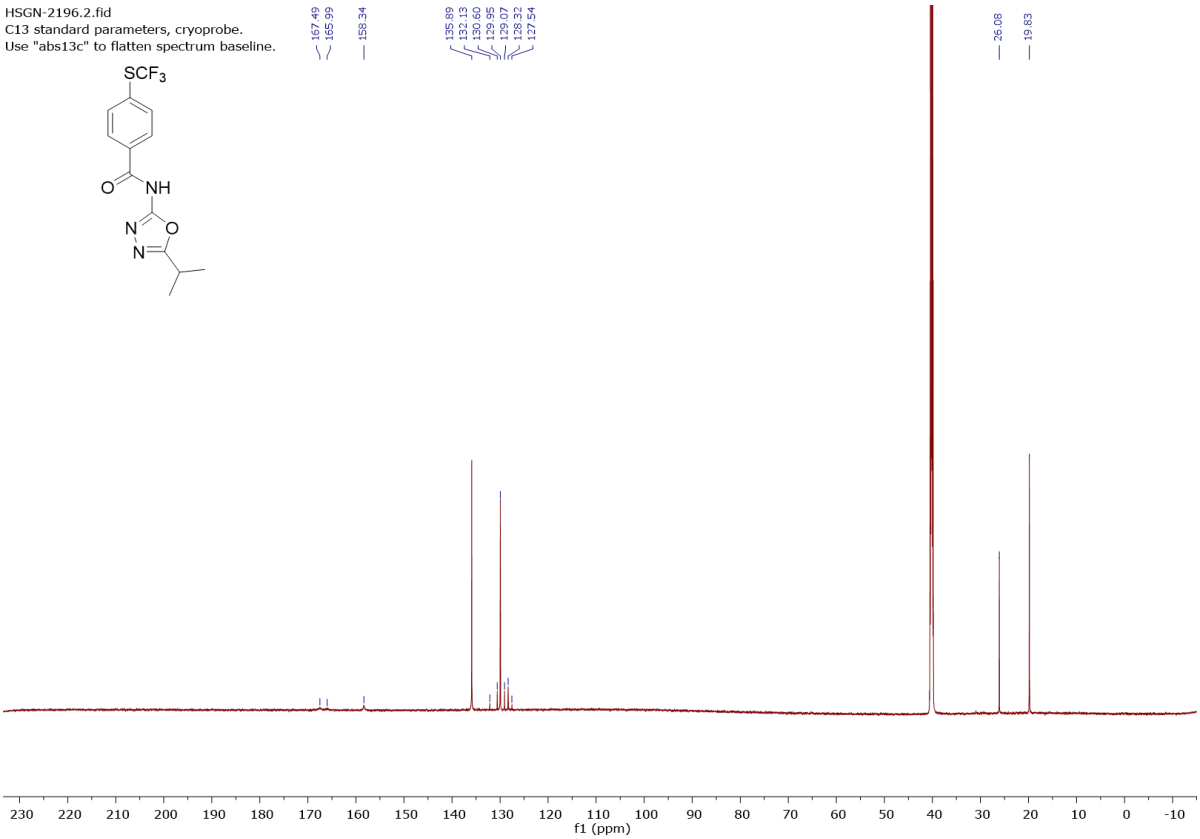
HSGN-2196.2.fid
C13 standard parameters, cryoprobe.
Use "abs13c" to flatten spectrum baseline.
167.49
165.99
158.34
135.89
132.13
130.60
129.95
129.07
128.32
127.54
26.08
19.83
SCF3
O
NH
N
O
N
f1 (ppm)

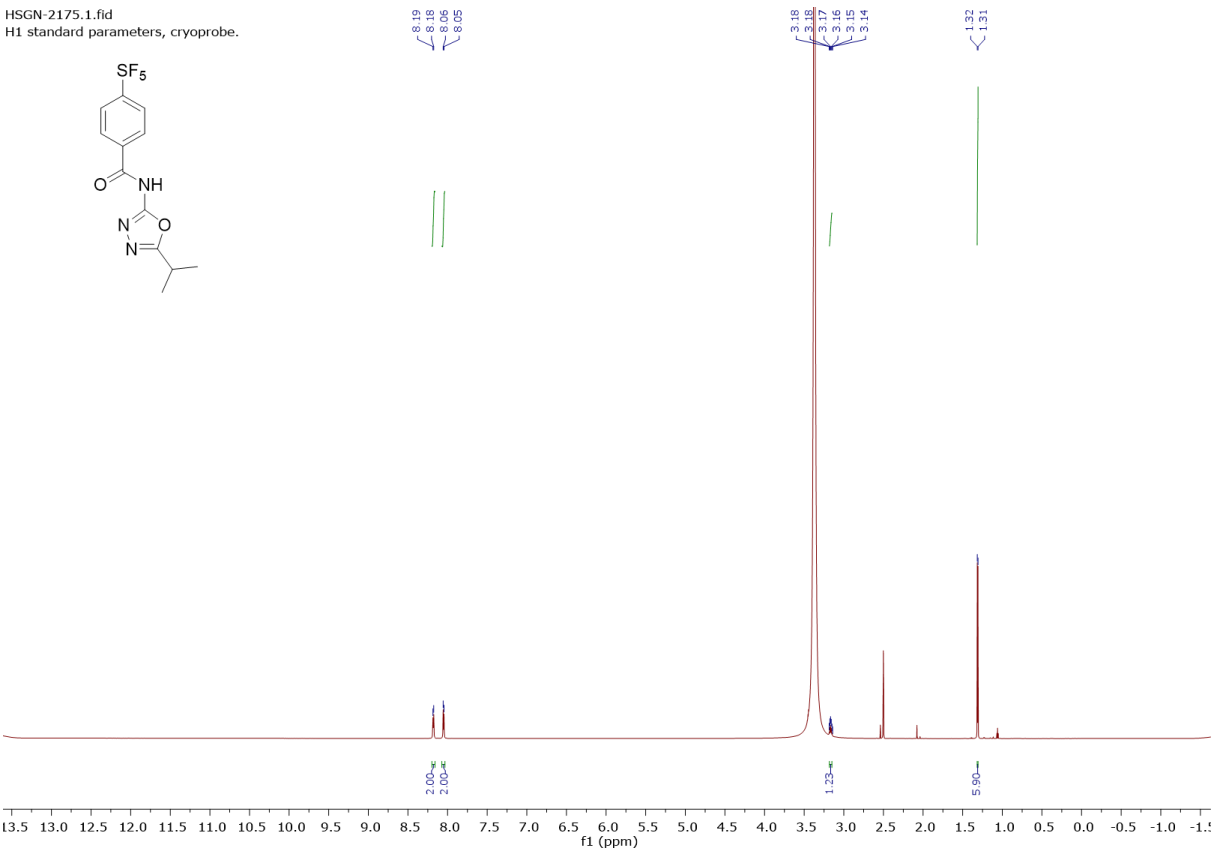
HSGN-2175.1.fid
H1 standard parameters, cryoprobe.
8.19
8.18
8.06
8.05
3.18
3.18
3.17
3.16
3.15
3.14
1.32
1.31
SF5
O
NH
N
O
N
2.00
2.00
1.23
5.90
f1 (ppm)

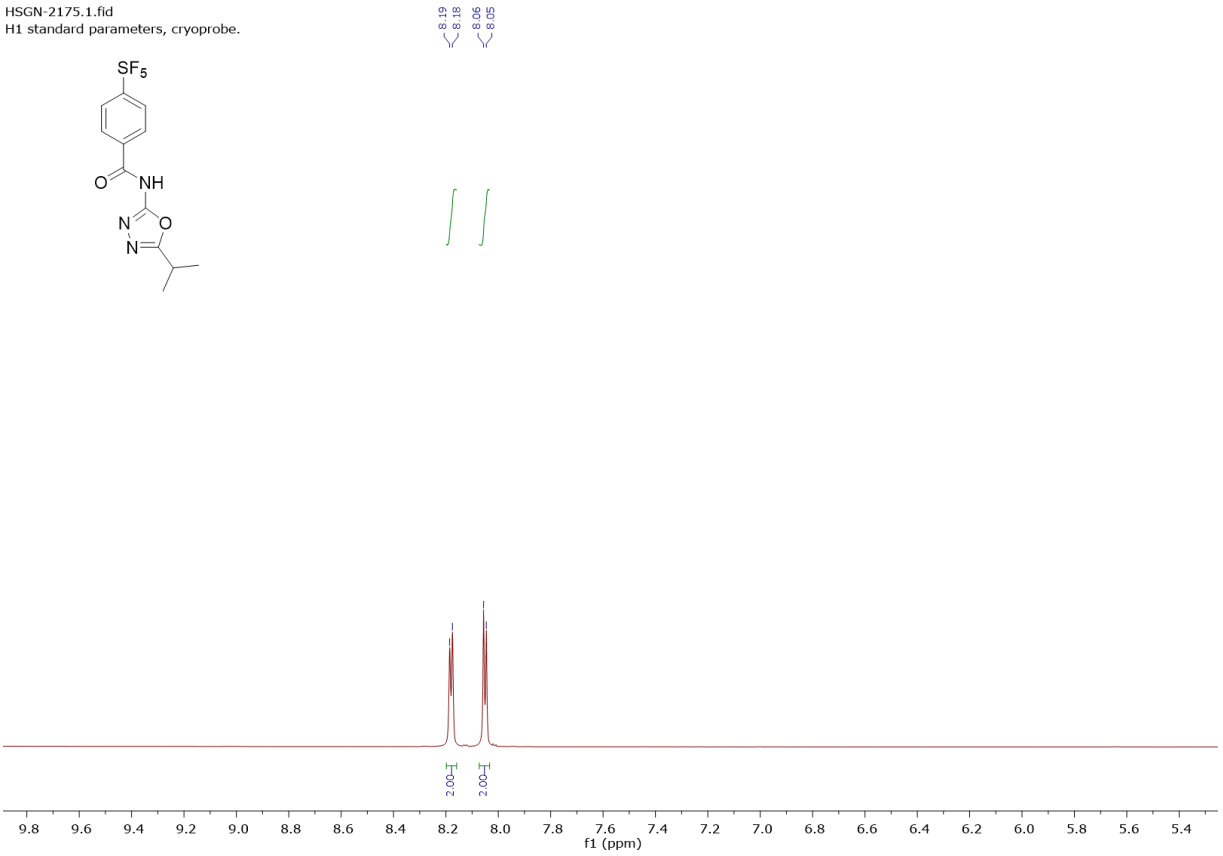
HSGN-2175.1.fid
H1 standard parameters, cryoprobe.
SF5
O
NH
N
O
N
8.19
8.18
8.06
8.05
2.00
2.00
9.8 9.6 9.4 9.2 9.0 8.8 8.6 8.4 8.2 8.0 7.8 7.6 7.4 7.2 7.0 6.8 6.6 6.4 6.2 6.0 5.8 5.6 5.4
f1 (ppm)

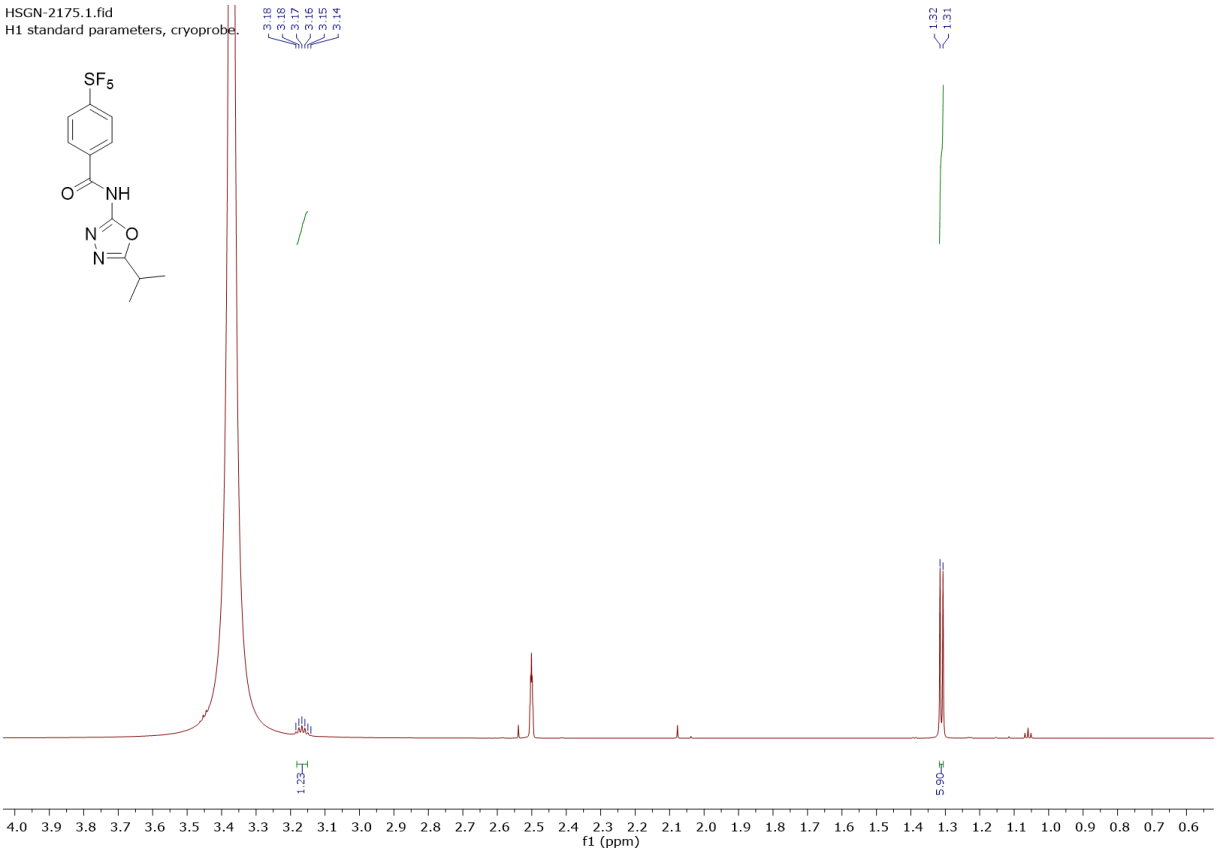
HSGN-2175.1.fid
H1 standard parameters, cryoprobe.
SF5
O
NH
N
O
N
3.18
3.18
3.17
3.16
3.15
3.14
1.32
1.31
1.23
5.90
4.0 3.9 3.8 3.7 3.6 3.5 3.4 3.3 3.2 3.1 3.0 2.9 2.8 2.7 2.6 2.5 2.4 2.3 2.2 2.1 2.0 1.9 1.8 1.7 1.6 1.5 1.4 1.3 1.2 1.1 1.0 0.9 0.8 0.7 0.6
f1 (ppm)

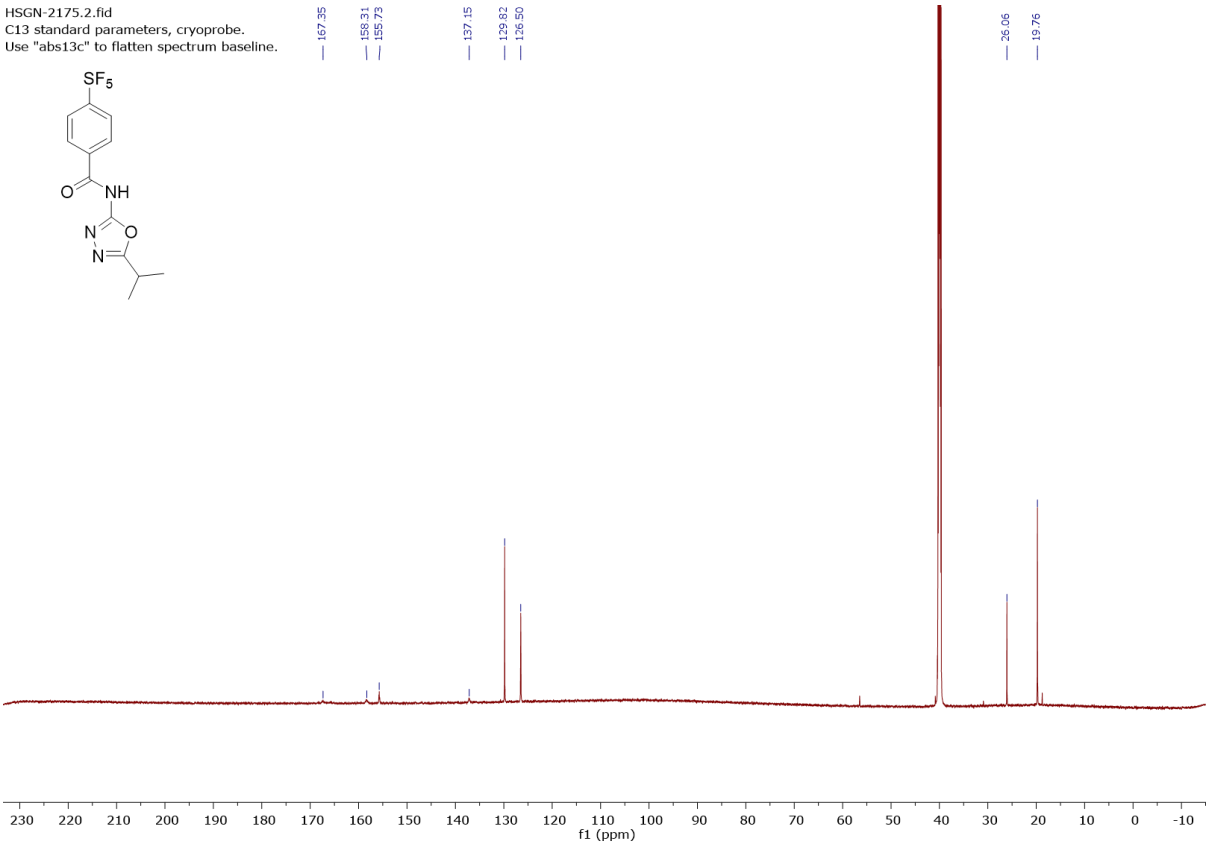
HSGN-2175.2.fid
C13 standard parameters, cryoprobe.
Use "abs13c" to flatten spectrum baseline.
167.35
158.31
155.73
137.15
129.82
126.50
26.06
19.76
SF5
O
NH
N
O
N
f1 (ppm)

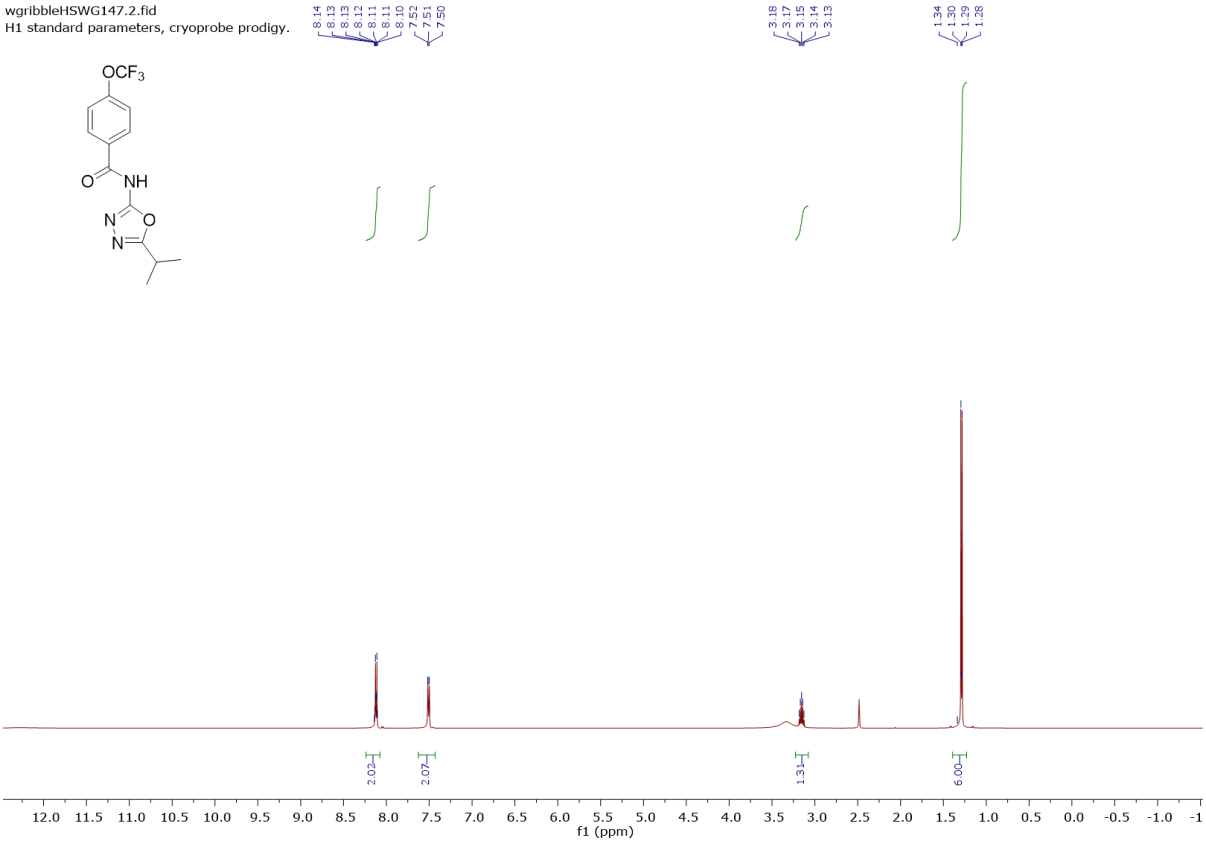
wgribbleHSWG147.2.fid
H1 standard parameters, cryoprobe prodigy.
8.14
8.13
8.13
8.12
8.11
8.11
8.10
7.52
7.51
7.50
3.18
3.17
3.15
3.14
3.13
1.34
1.30
1.29
1.28
OCF3
O
NH
N
O
N
2.02
2.07
1.31
6.00
f1 (ppm)

wgribbleHSWG147.2.fid
H1 standard parameters, cryoprobe prodigy.

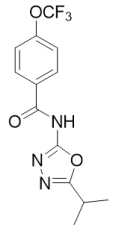

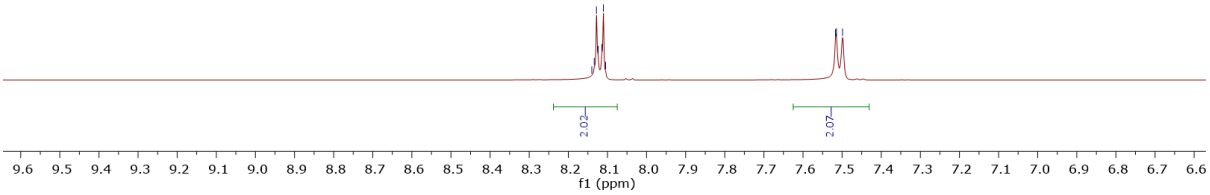

wgribbleHSWG147.2.fid
H1 standard parameters, cryoprobe prodigy.

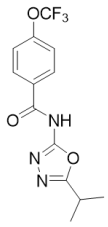

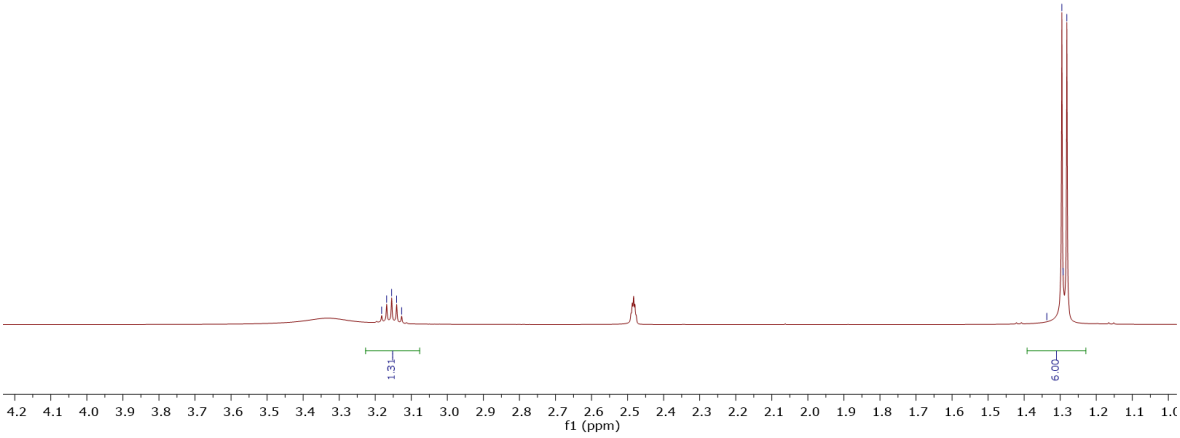

wgribbleHSWG147.1.fid
C13 standard parameters, cryoprobe prodigy. Pulprog = zgig30zr.jsh.

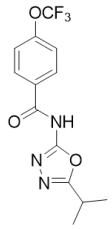

HSGN-2197.1.fid
H1 standard parameters, cryoprobe.

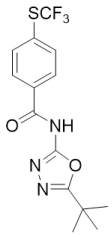

HSGN-2197.1.fid
H1 standard parameters, cryoprobe.

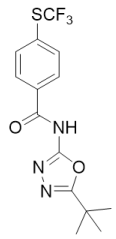

HSGN-2197.1.fid
H1 standard parameters, cryoprobe.

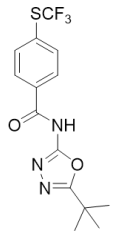

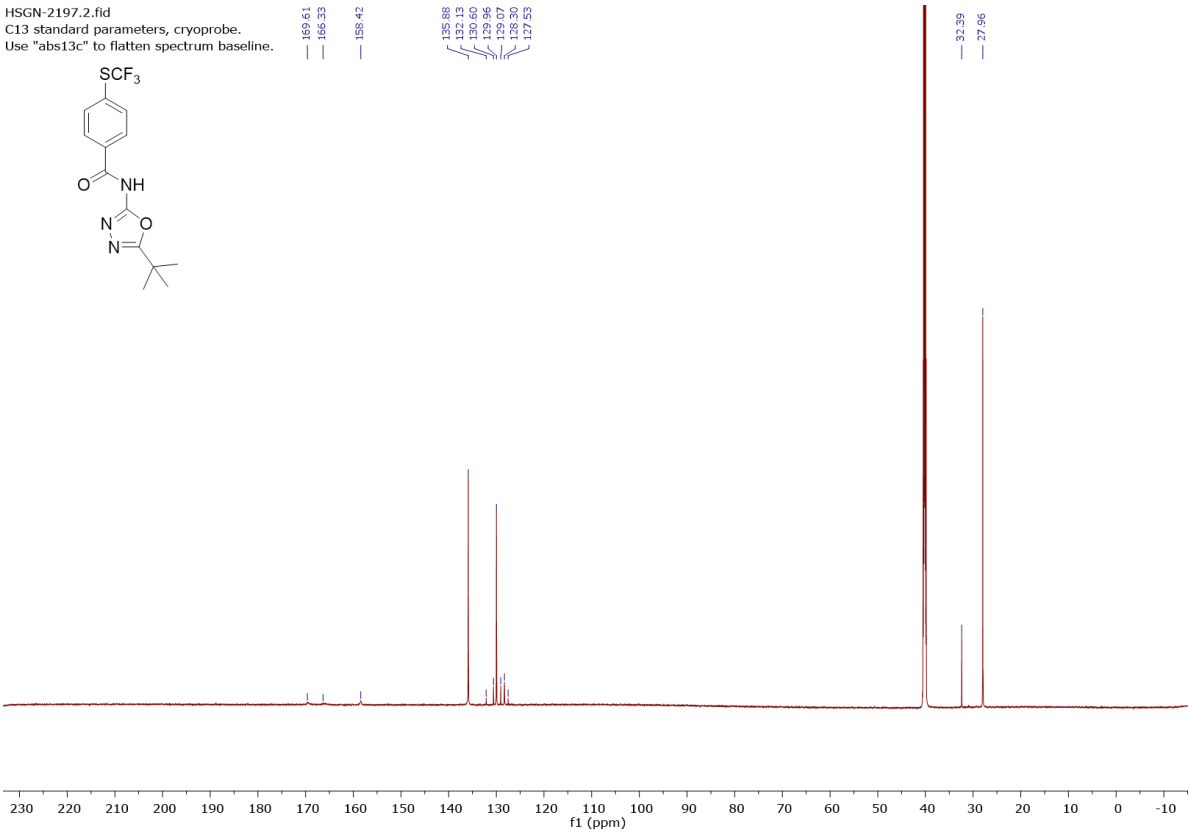
HSGN-2197.2.fid
C13 standard parameters, cryoprobe.
Use "abs13c" to flatten spectrum baseline.
169.61
166.33
158.42
135.88
132.13
130.60
129.96
129.07
128.30
127.53
32.39
27.96
SCF3
O
NH
N
O
N
230 220 210 200 190 180 170 160 150 140 130 120 110 100 90 80 70 60 50 40 30 20 10 0 -10
f1 (ppm)

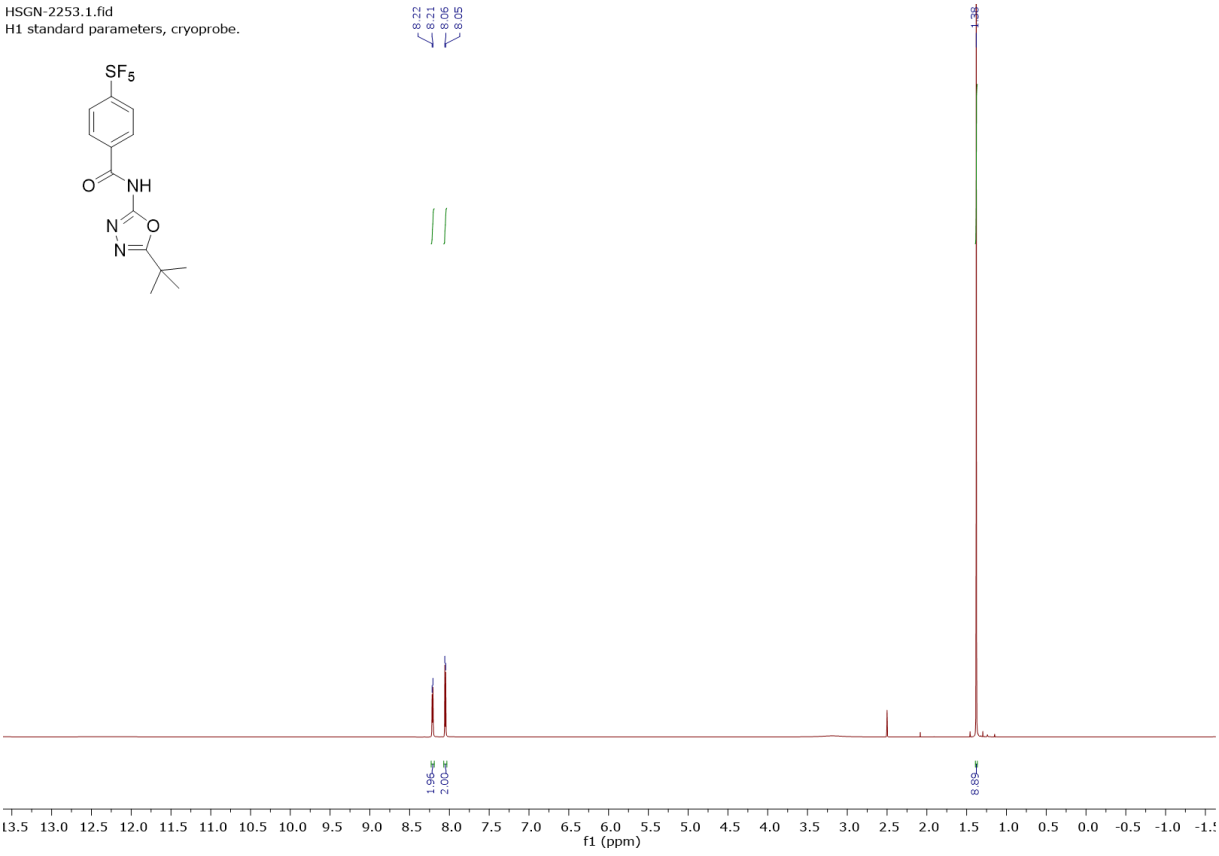
HSGN-2253.1.fid
H1 standard parameters, cryoprobe.
8.22
8.21
8.06
8.05
1.38
SF5
O
NH
N
O
N
1.96
2.00
8.89
13.5 13.0 12.5 12.0 11.5 11.0 10.5 10.0 9.5 9.0 8.5 8.0 7.5 7.0 6.5 6.0 5.5 5.0 4.5 4.0 3.5 3.0 2.5 2.0 1.5 1.0 0.5 0.0 -0.5 -1.0
f1 (ppm)

HSGN-2253.1.fid
H1 standard parameters, cryoprobe.

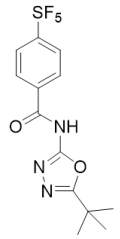

HSGN-2253.1.fid
H1 standard parameters, cryoprobe.

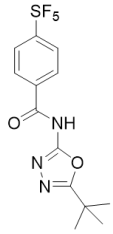

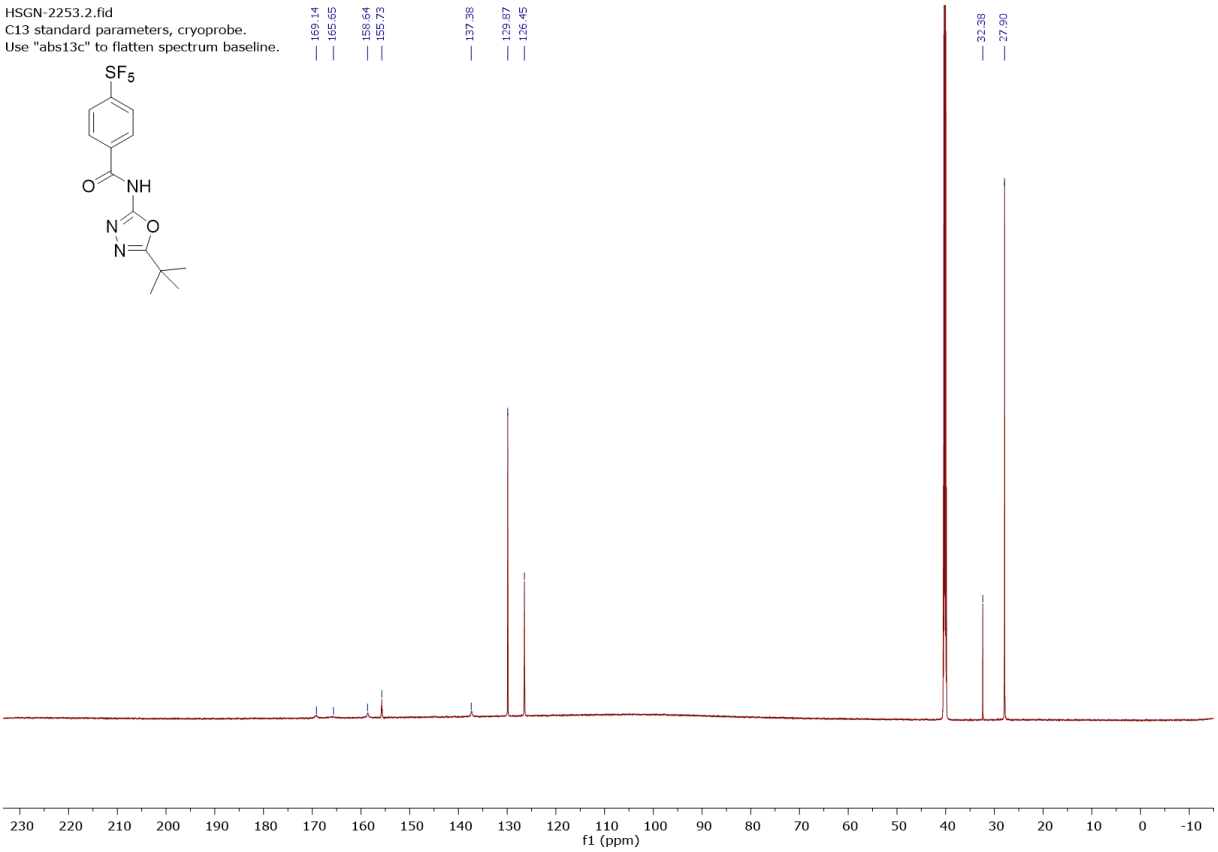
HSGN-2253.2.fid
C13 standard parameters, cryoprobe.
Use "abs13c" to flatten spectrum baseline.
169.14
165.65
158.64
155.73
137.38
129.87
126.45
32.38
27.90
SF5
O
NH
N
O
N
230 220 210 200 190 180 170 160 150 140 130 120 110 100 90 80 70 60 50 40 30 20 10 0 -10
f1 (ppm)

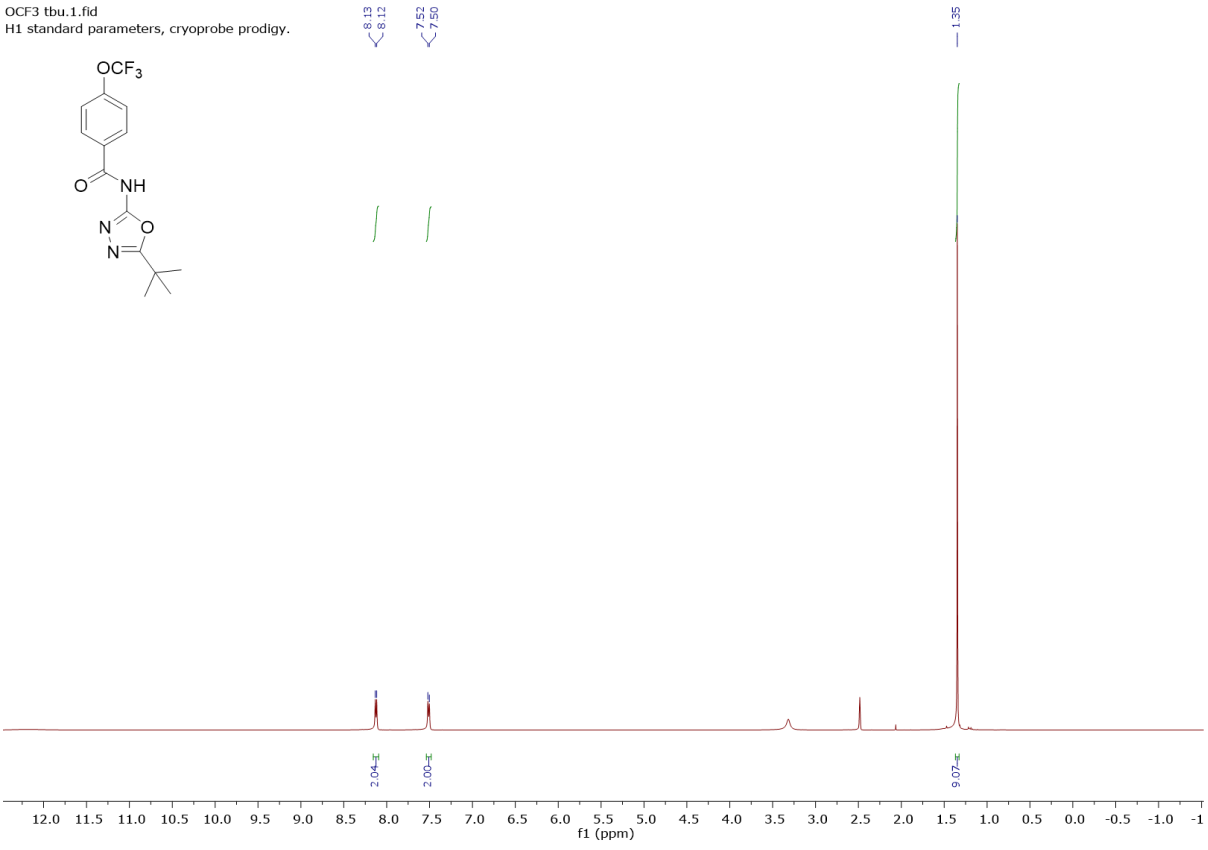
OCF3 tbu.1.fid
H1 standard parameters, cryoprobe prodigy.
8.13
8.12
7.52
7.50
1.35
OCF3
O
NH
N
O
N
2.04
2.00
9.07
12.0 11.5 11.0 10.5 10.0 9.5 9.0 8.5 8.0 7.5 7.0 6.5 6.0 5.5 5.0 4.5 4.0 3.5 3.0 2.5 2.0 1.5 1.0 0.5 0.0 -0.5 -1.0 -1
f1 (ppm)

OCF3 tbu.1.fid
H1 standard parameters, cryoprobe prodigy.

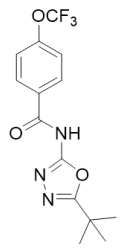

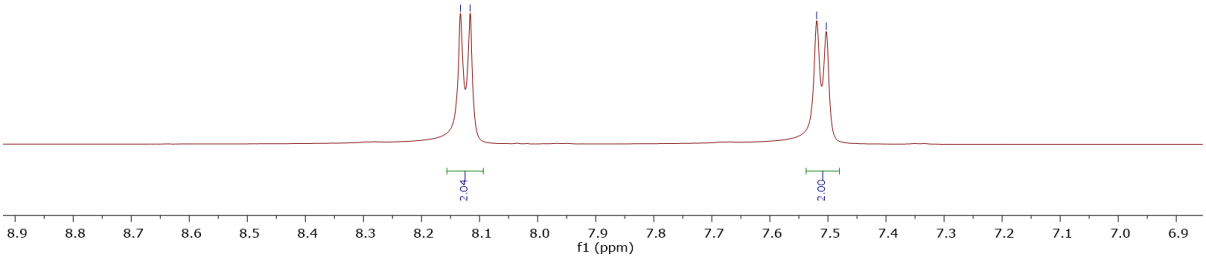

OCF3 tbu.1.fid
H1 standard parameters, cryoprobe prodigy.

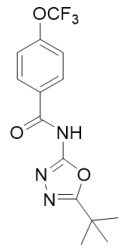

wgribble OCF3 tBu.2.fid
C13 standard parameters, cryoprobe.
Use "abs13c" to flatten spectrum baseline.

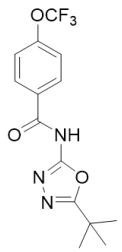

HSGN-2194.1.fid
H1 standard parameters, cryoprobe.

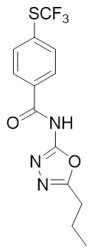

HSGN-2194.1.fid
H1 standard parameters, cryoprobe.

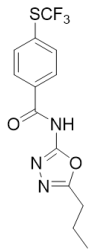

HSGN-2194.1.fid
H1 standard parameters, cryoprobe.

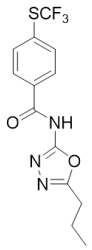

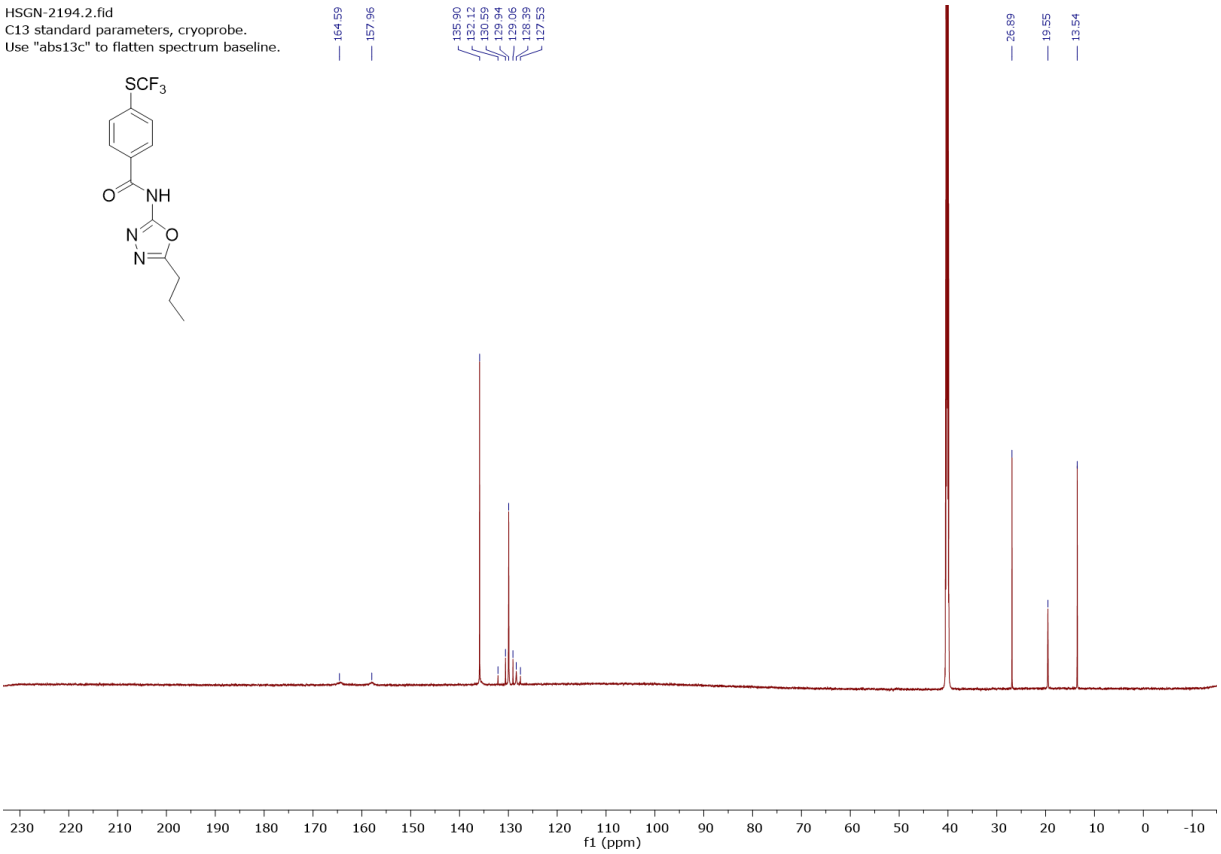
HSGN-2194.2.fid
C13 standard parameters, cryoprobe.
Use "abs13c" to flatten spectrum baseline.
164.59
157.96
135.90
132.12
130.59
129.94
129.06
128.39
127.53
26.89
19.55
13.54
SCF3
O
NH
N
O
N
f1 (ppm)

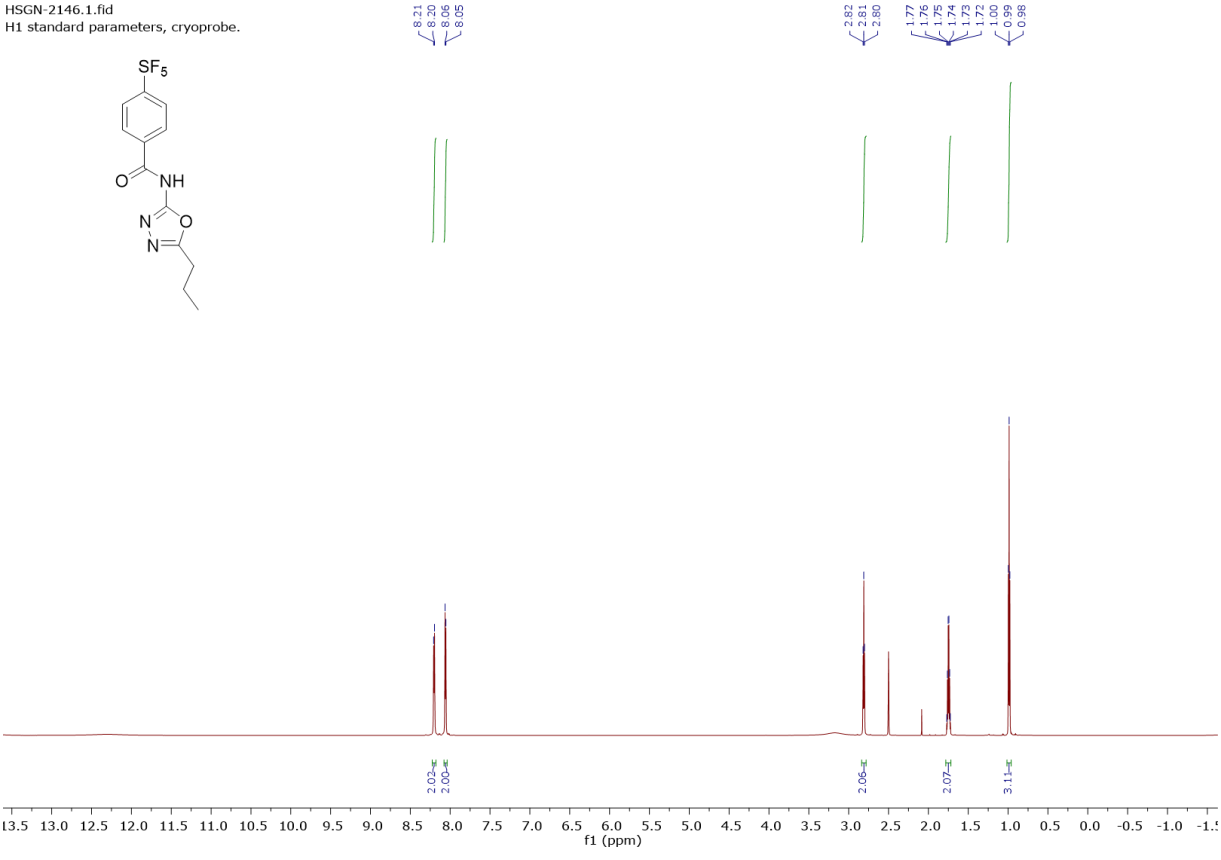
HSGN-2146.1.fid
H1 standard parameters, cryoprobe.
8.21
8.20
8.06
8.05
2.82
2.81
2.80
1.77
1.76
1.75
1.74
1.73
1.72
1.00
0.99
0.98
SF5
O
NH
N
O
N
2.02
2.00
2.06
2.07
3.11
f1 (ppm)

HSGN-2146.1.fid
H1 standard parameters, cryoprobe.

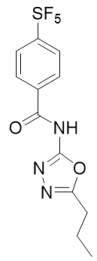

HSGN-2146.1.fid
H1 standard parameters, cryoprobe.

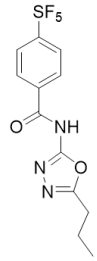

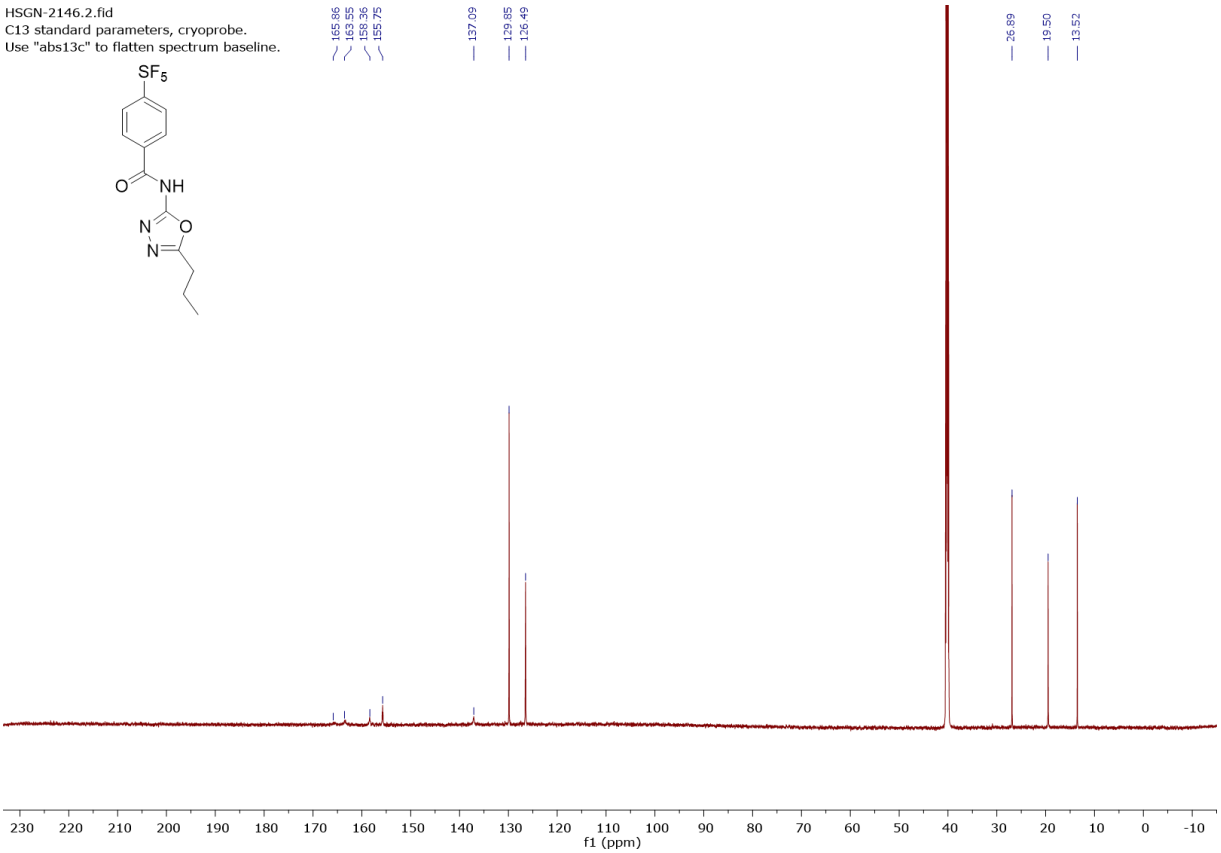
HSGN-2146.2.fid
C13 standard parameters, cryoprobe.
Use "abs13c" to flatten spectrum baseline.
165.86
163.55
158.36
155.75
137.09
129.85
126.49
26.89
19.50
13.52
SF5
O
NH
N
O
N
f1 (ppm)

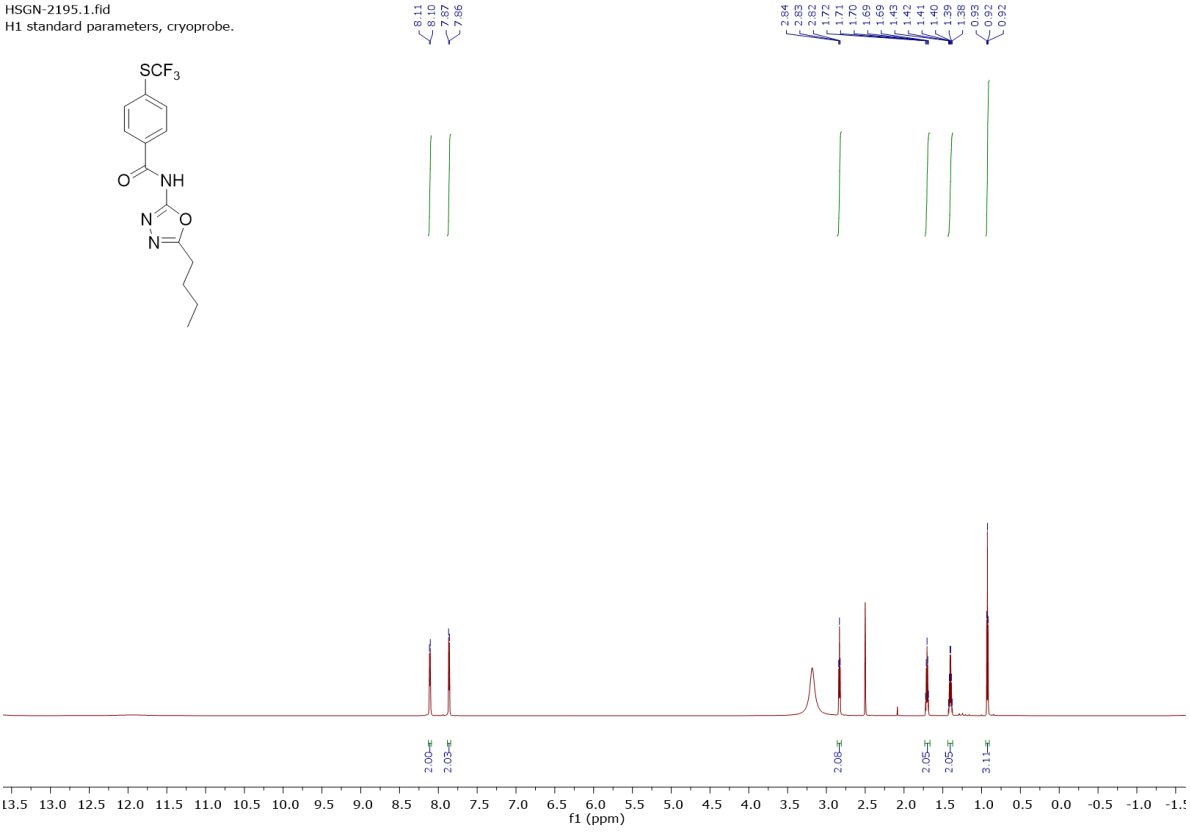
HSGN-2195.1.fid
H1 standard parameters, cryoprobe.
8.11
8.10
7.87
7.86
2.84
2.83
2.82
1.72
1.71
1.70
1.69
1.69
1.43
1.42
1.41
1.40
1.39
1.38
0.93
0.92
0.92
SCF3
O
NH
N
O
N
2.00
2.03
2.08
2.05
2.05
3.11
f1 (ppm)

HSGN-2195.1.fid
H1 standard parameters, cryoprobe.

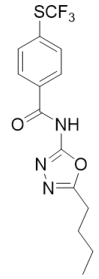

HSGN-2195.1.fid
H1 standard parameters, cryoprobe.

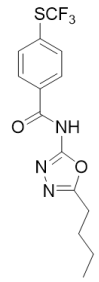

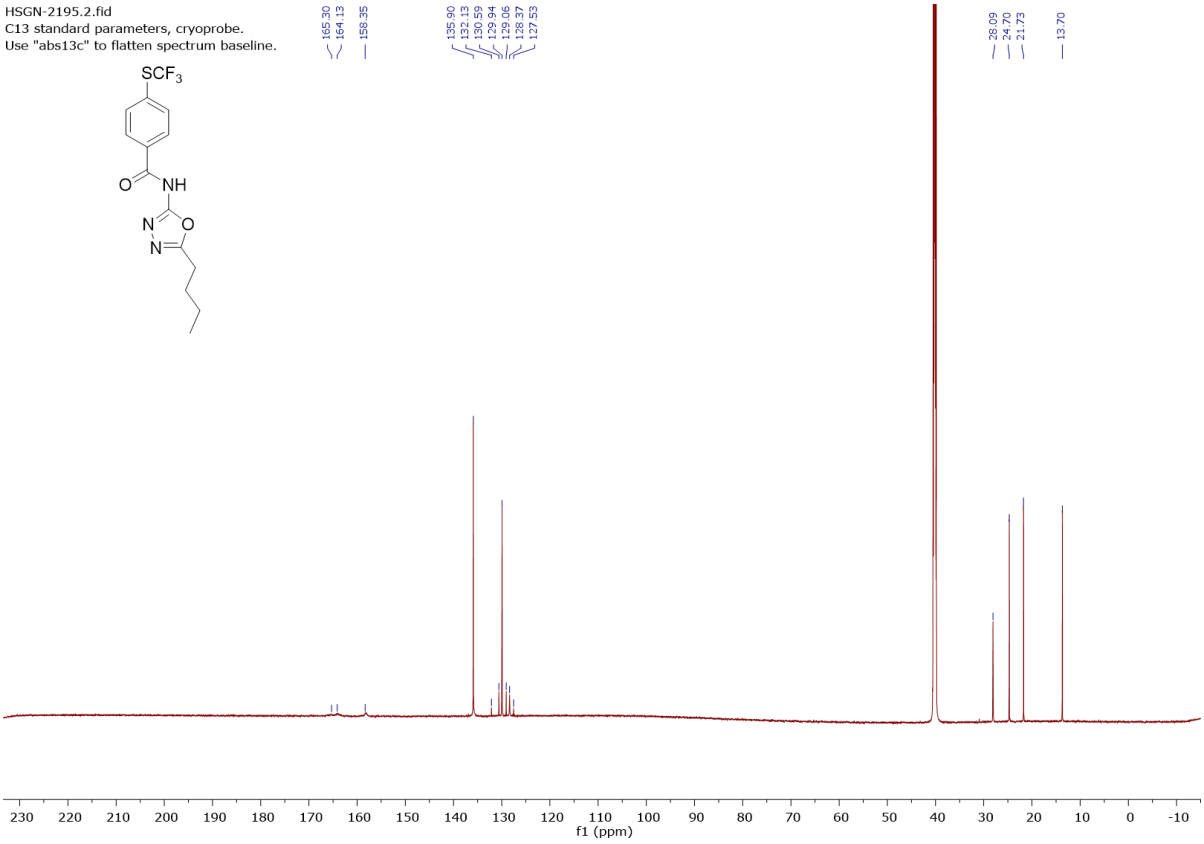
HSGN-2195.2.fid
C13 standard parameters, cryoprobe.
Use "abs13c" to flatten spectrum baseline.
SCF3
NH
O
N
O
N
165.30
164.13
158.35
135.90
132.13
130.59
129.94
129.06
128.37
127.53
28.09
24.70
21.73
13.70
f1 (ppm)

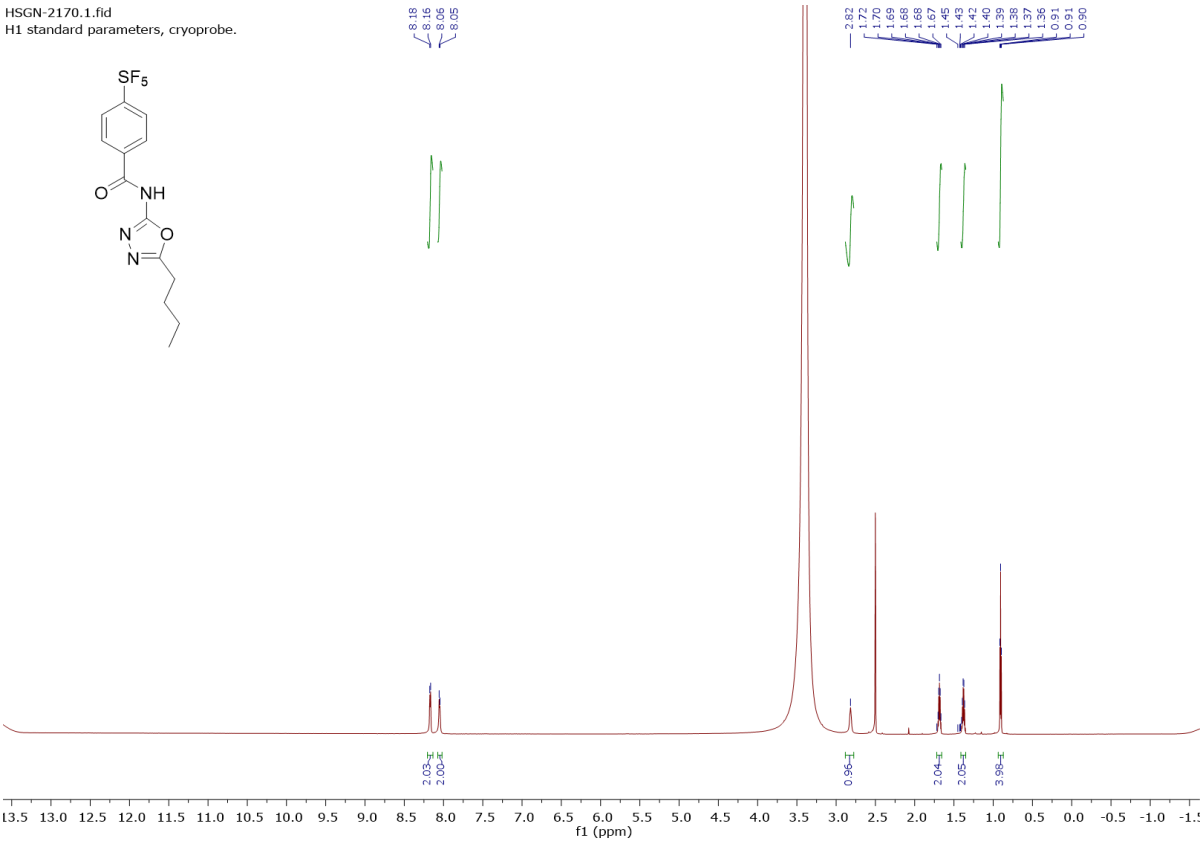
HSGN-2170.1.fid
H1 standard parameters, cryoprobe.
SF5
NH
O
N
O
N
8.18
8.16
8.06
8.05
2.82
1.72
1.70
1.69
1.68
1.68
1.67
1.45
1.43
1.42
1.40
1.39
1.38
1.37
1.36
0.91
0.91
0.90
2.03
2.00
0.96
2.04
2.05
3.98
f1 (ppm)

HSGN-2170.1.fid
H1 standard parameters, cryoprobe.

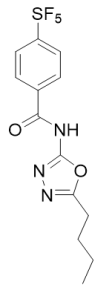

HSGN-2170.1.fid
H1 standard parameters, cryoprobe.

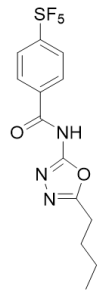

HSGN-2170.2.fid
C13 standard parameters, cryoprobe.
Use "abs13c" to flatten spectrum baseline.

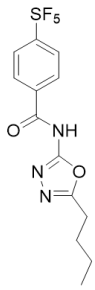

HSGN-2178.1.fid
H1 standard parameters, cryoprobe.

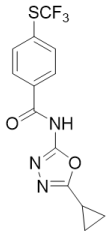

HSGN-2178.1.fid
H1 standard parameters, cryoprobe.

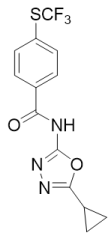

HSGN-2178.1.fid
H1 standard parameters, cryoprobe.

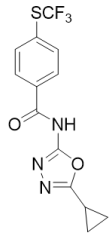

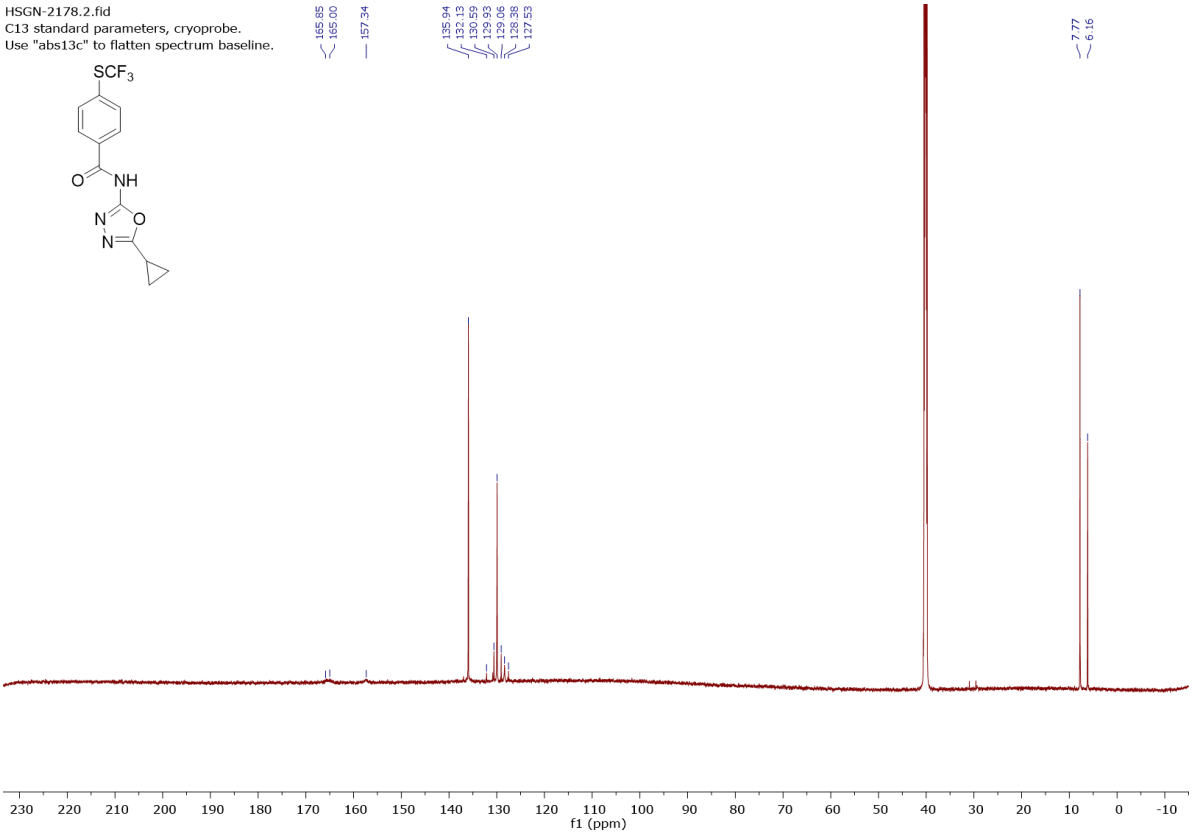
HSGN-2178.2.fid
C13 standard parameters, cryoprobe.
Use "abs13c" to flatten spectrum baseline.
SCF3
NH
f1 (ppm)

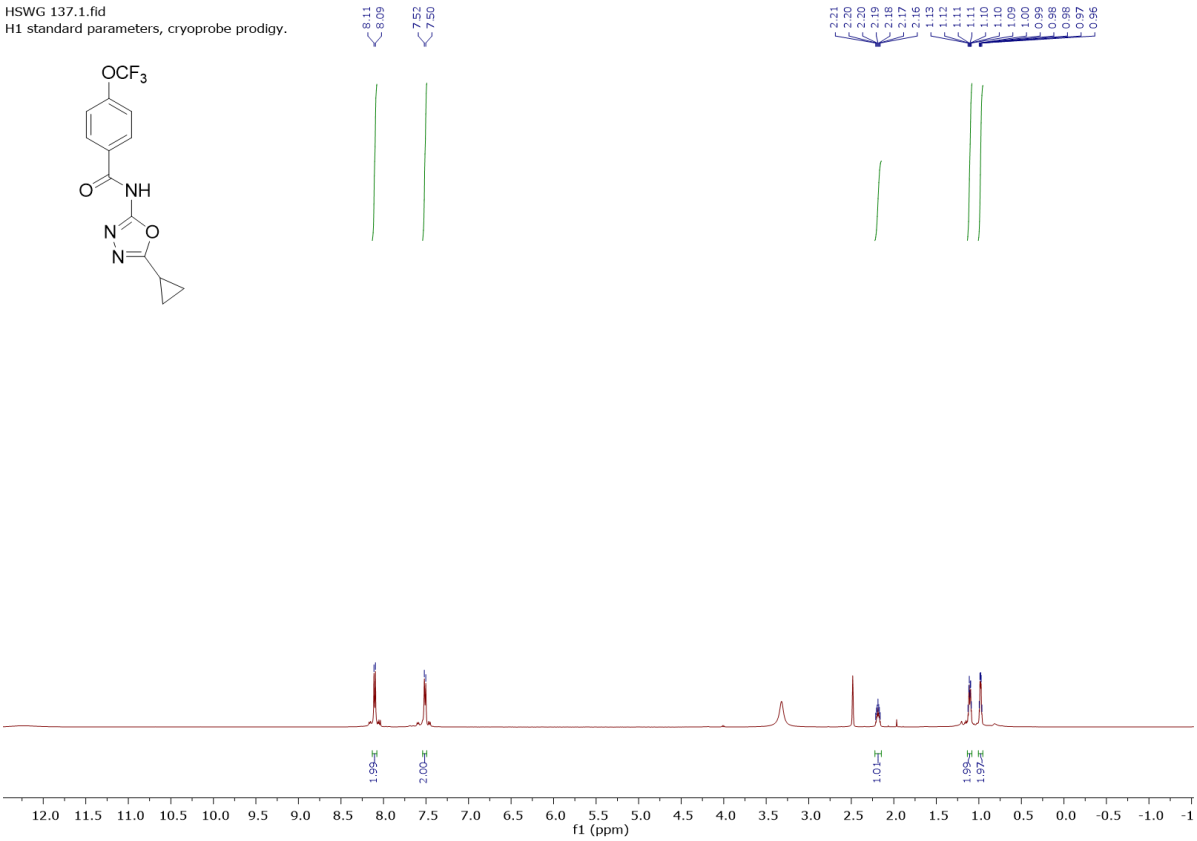
HSWG 137.1.fid
H1 standard parameters, cryoprobe prodigy.
OCF3
NH
f1 (ppm)

HSWG 137.1.fid
H1 standard parameters, cryoprobe prodigy.

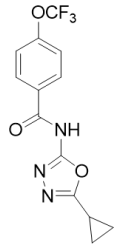

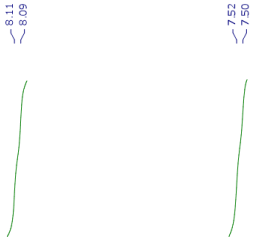

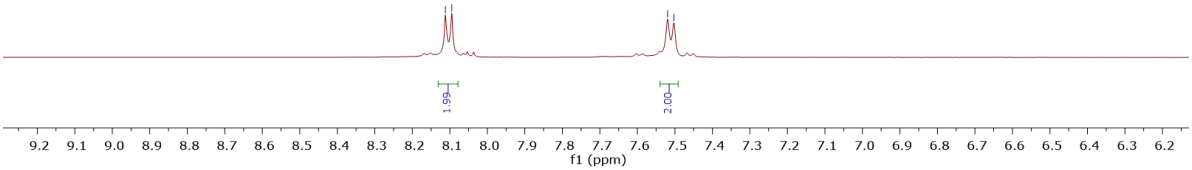

HSWG 137.1.fid
H1 standard parameters, cryoprobe prodigy.

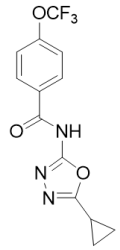

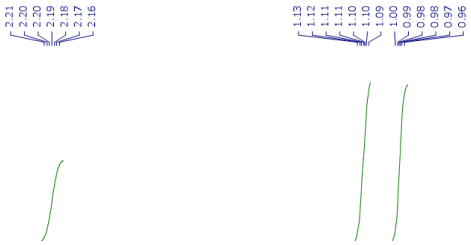

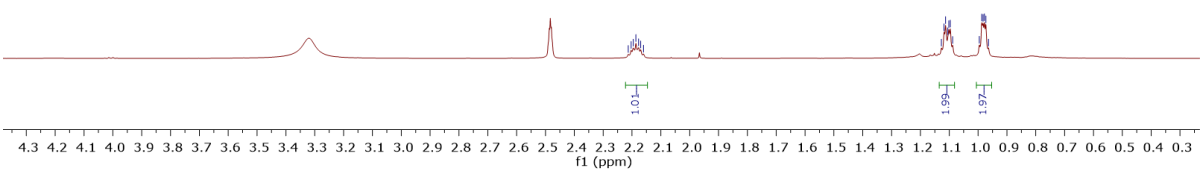

wgribble HSWG 137.2.fid
C13 standard parameters, cryoprobe.
Use "abs13c" to flatten spectrum baseline.

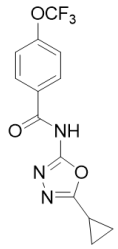

HSGN-2179.1.fid
H1 standard parameters, cryoprobe.

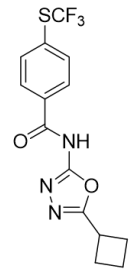

HSGN-2179.1.fid
H1 standard parameters, cryoprobe.

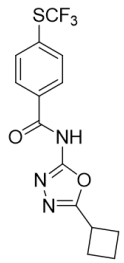

HSGN-2179.1.fid
H1 standard parameters, cryoprobe.

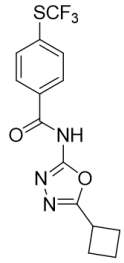

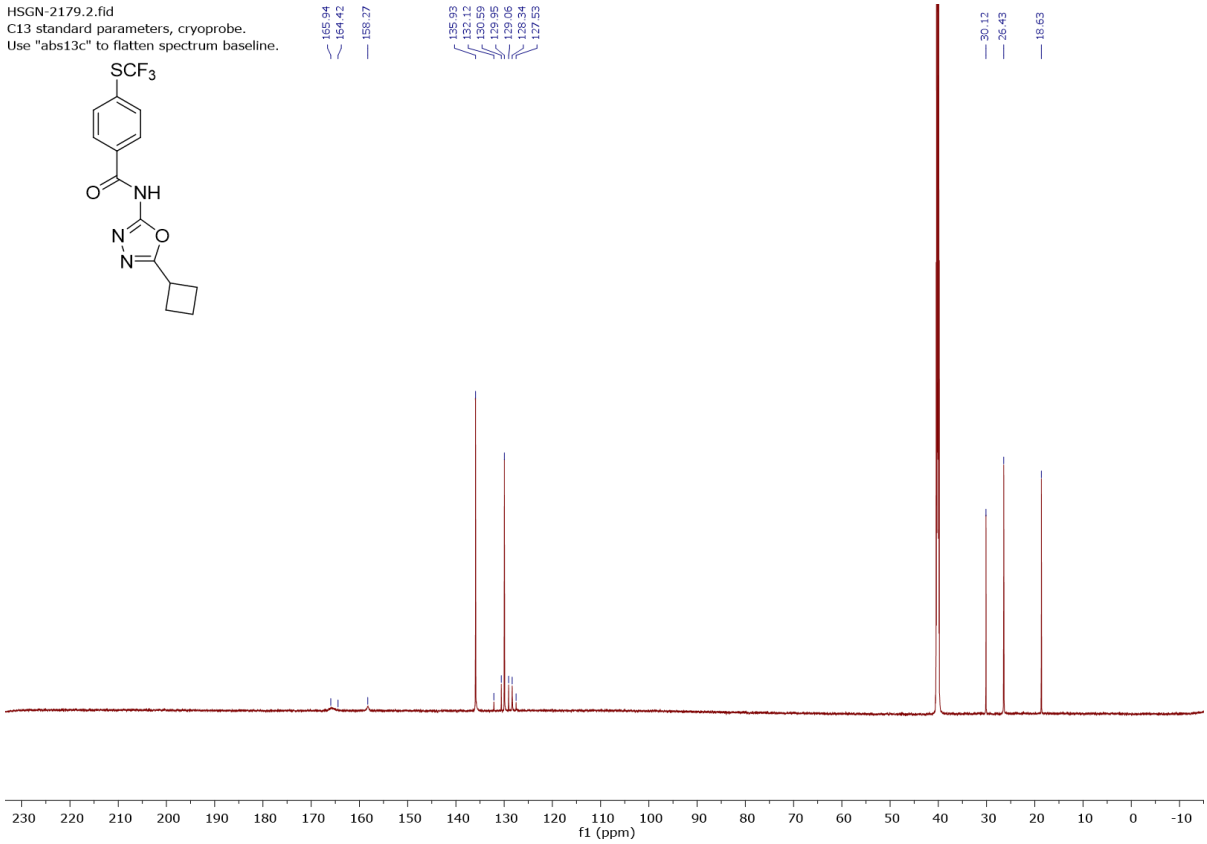
HSGN-2179.2.fid
C13 standard parameters, cryoprobe.
Use "abs13c" to flatten spectrum baseline.
SCF3
NH
O
N
O
N
165.94
164.42
158.27
135.93
132.12
130.59
129.95
129.06
128.34
127.53
30.12
26.43
18.63
f1 (ppm)

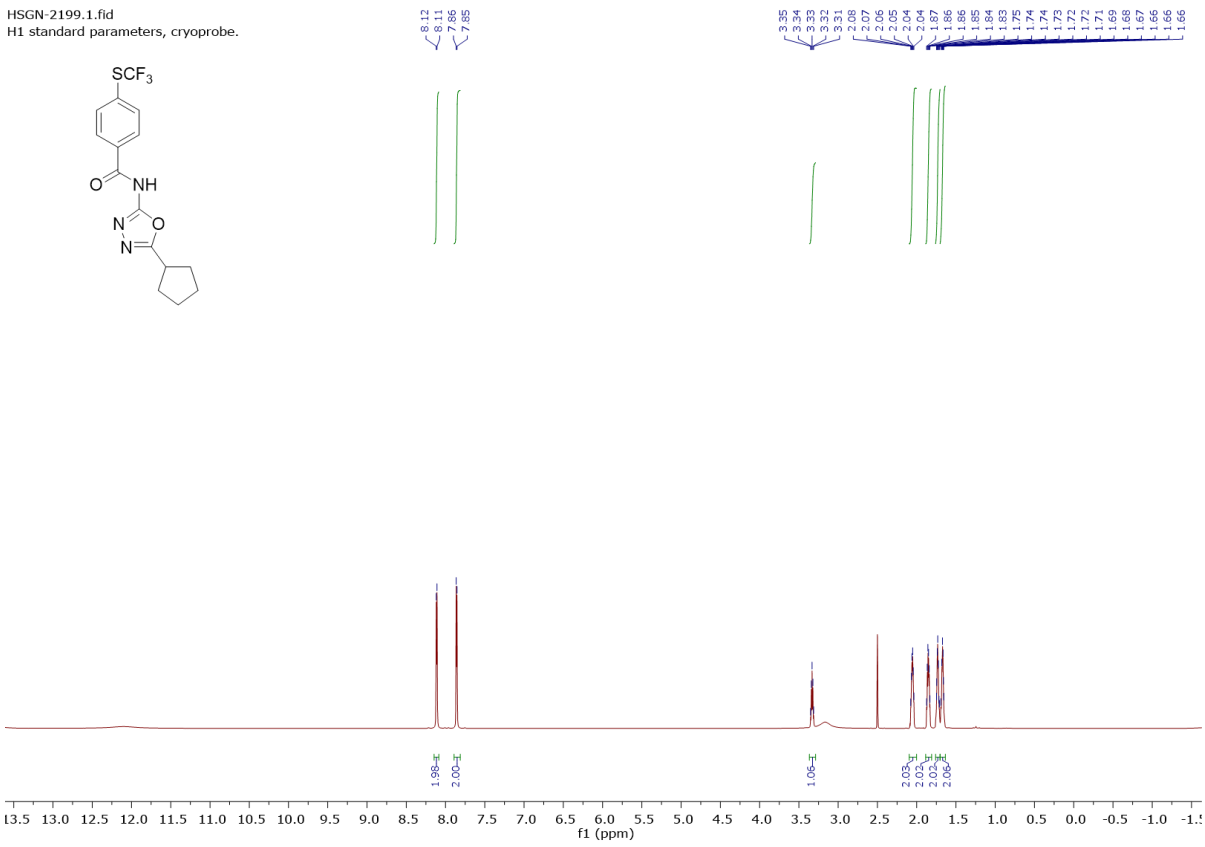
HSGN-2199.1.fid
H1 standard parameters, cryoprobe.
SCF3
NH
O
N
O
N
8.12
8.11
7.86
7.85
3.35
3.34
3.33
3.32
3.31
2.08
2.07
2.06
2.05
2.04
2.04
1.87
1.86
1.86
1.85
1.84
1.83
1.75
1.74
1.74
1.73
1.72
1.72
1.71
1.69
1.68
1.67
1.66
1.66
1.66
1.98
2.00
1.06
2.03
2.02
2.02
2.06
f1 (ppm)

HSGN-2199.1.fid
H1 standard parameters, cryoprobe.

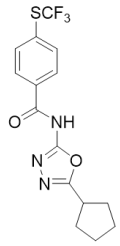

HSGN-2199.1.fid
H1 standard parameters, cryoprobe.

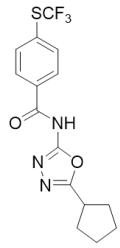

HSGN-2199.2.fid
C13 standard parameters, cryoprobe.
Use "abs13c" to flatten spectrum baseline.

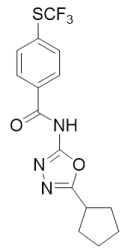

HSGN-2145.1.fid
H1 standard parameters, cryoprobe.

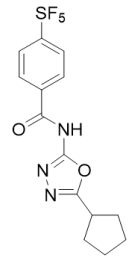

HSGN-2145.1.fid
H1 standard parameters, cryoprobe.

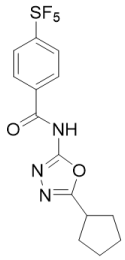

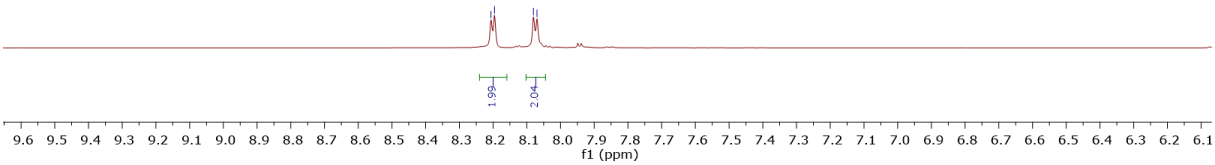

HSGN-2145.1.fid
H1 standard parameters, cryoprobe.

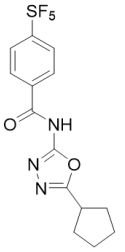

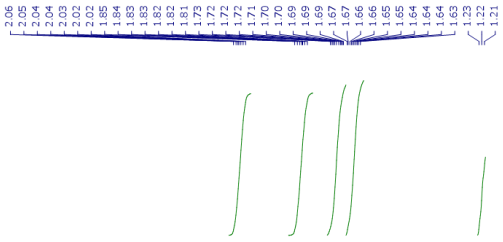

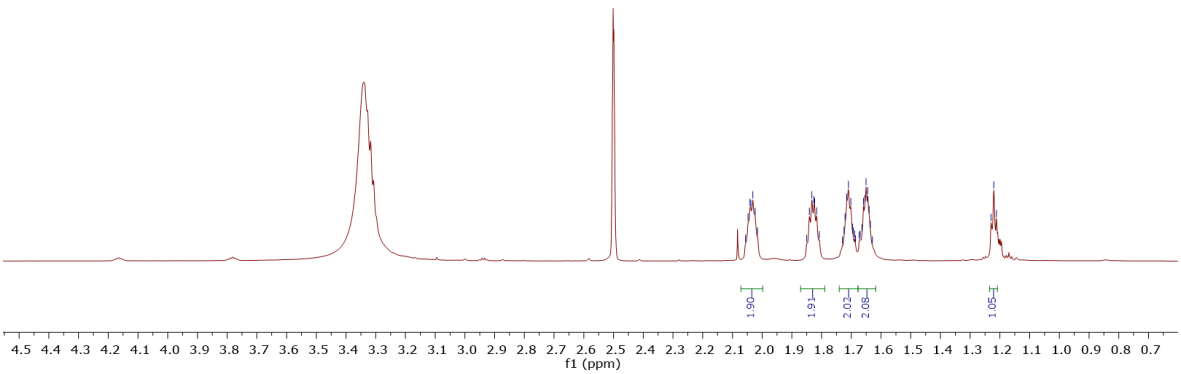

HSGN-2145.2.fid
C13 standard parameters, cryoprobe.
Use "abs13c" to flatten spectrum baseline.

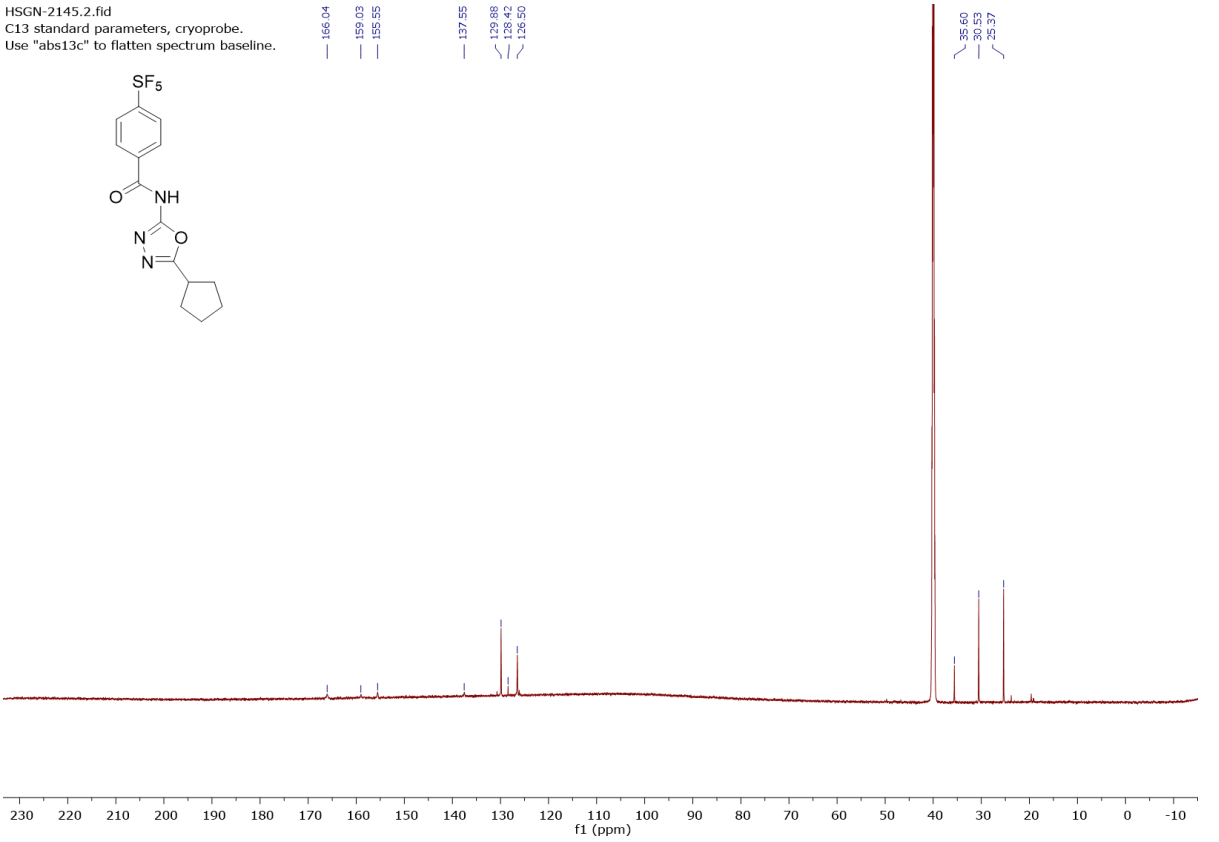

wgribble HSWG 148.1.fid
H1 standard parameters, cryoprobe.

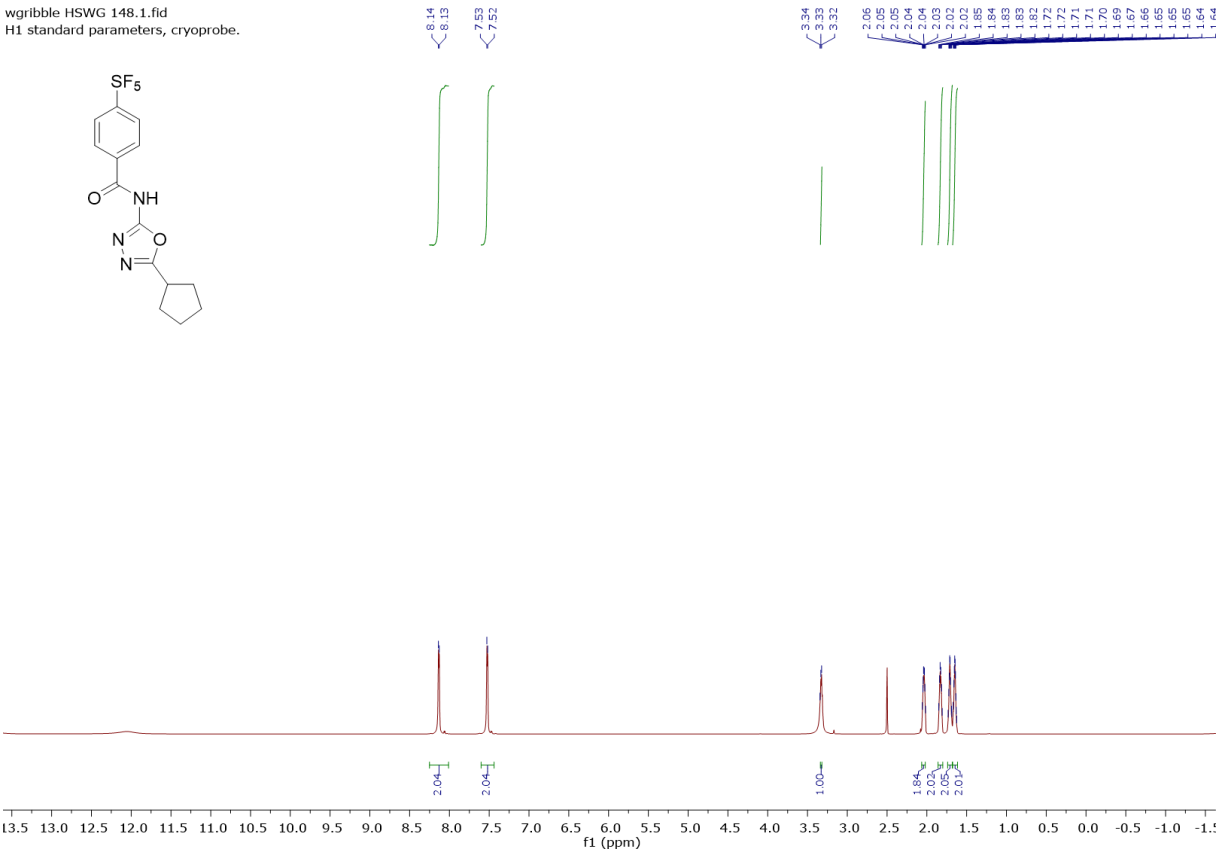

wgribble HSWG 148.1.fid
H1 standard parameters, cryoprobe.

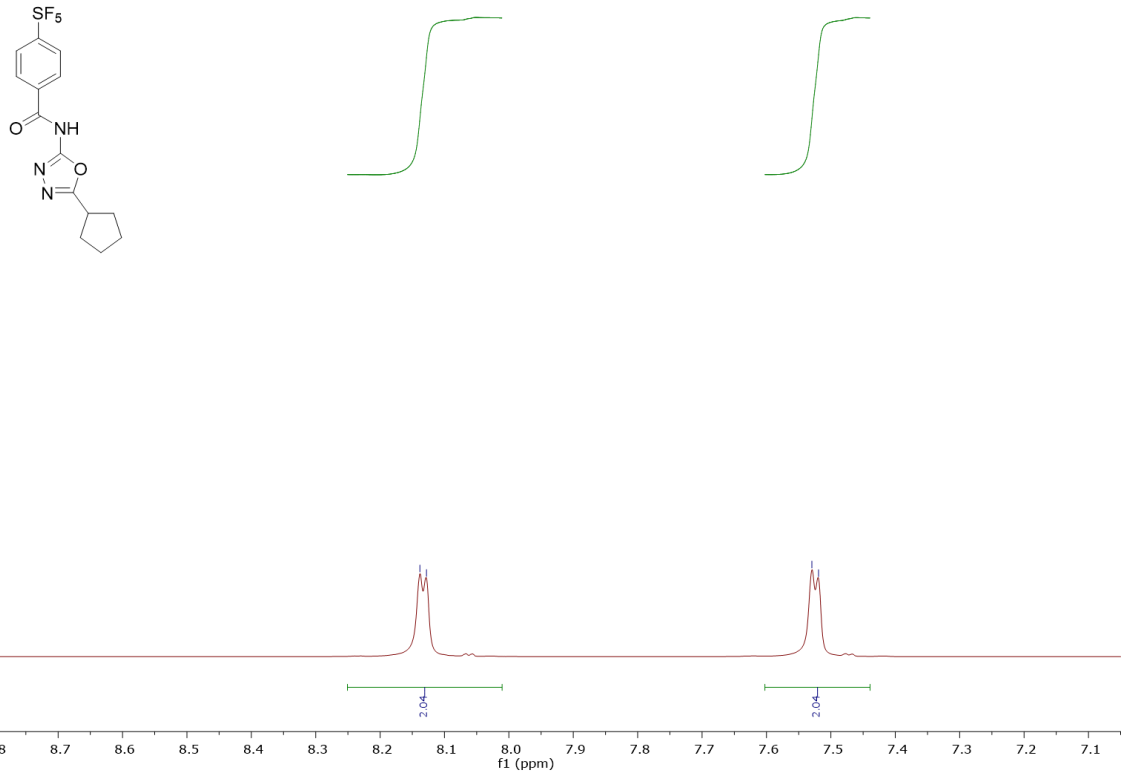

wgribble HSWG 148.1.fid
H1 standard parameters, cryoprobe.

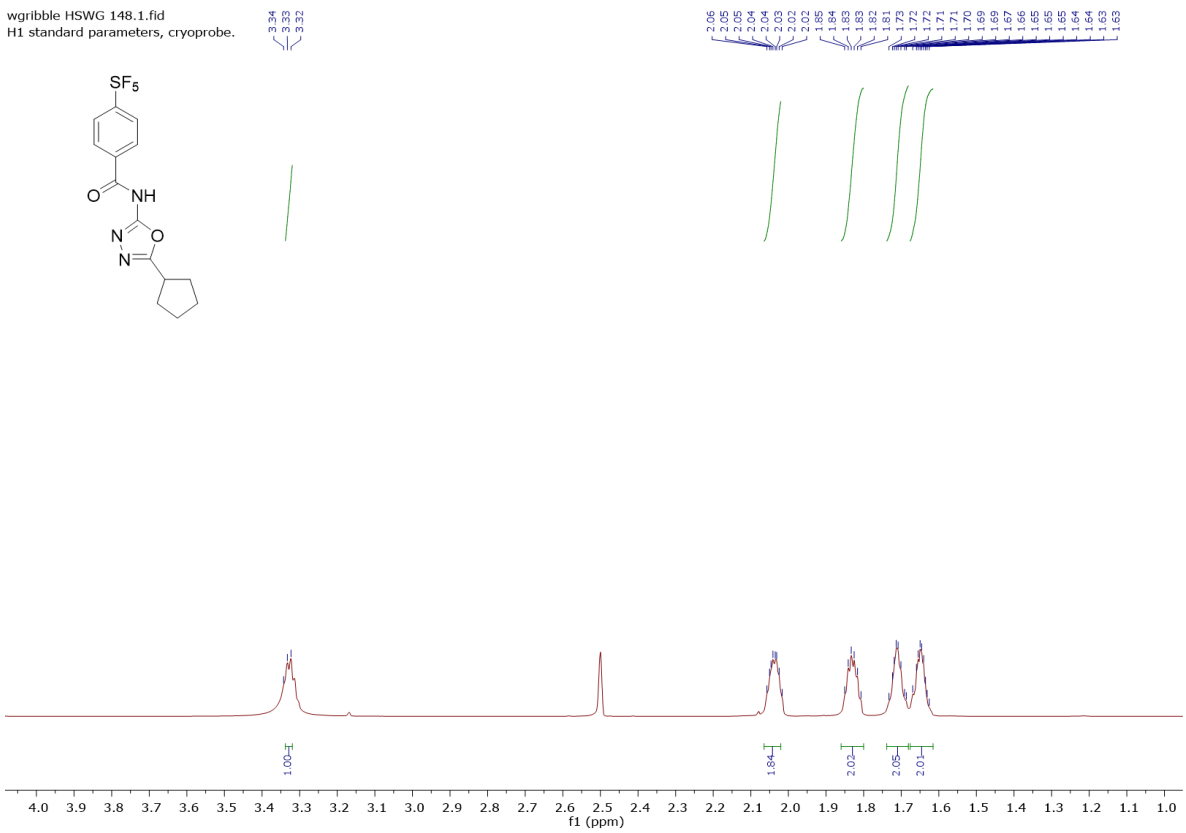

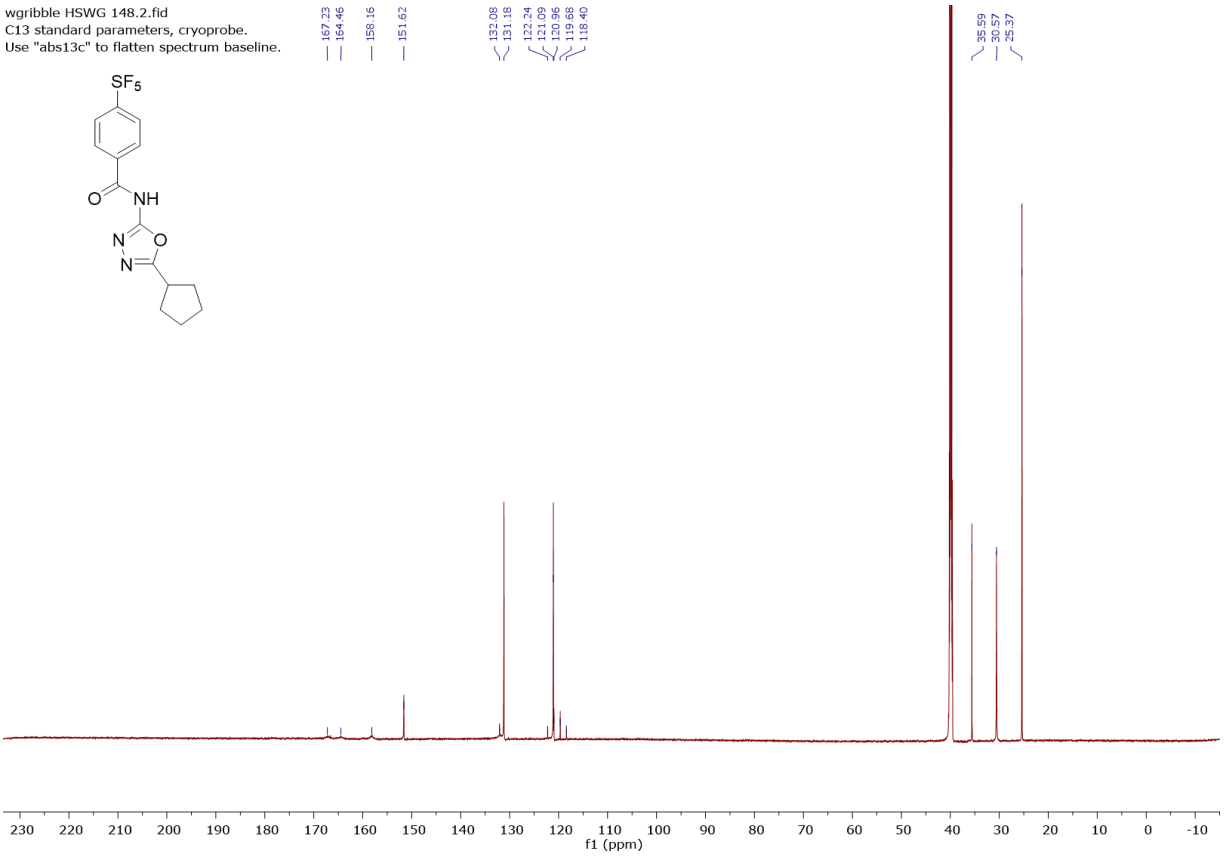
wgribble HSWG 148.2.fid
C13 standard parameters, cryoprobe.
Use "abs13c" to flatten spectrum baseline.
167.23
164.46
158.16
151.62
132.08
131.18
122.24
121.09
120.96
119.68
118.40
35.59
30.57
25.37
SF5
O
NH
N
O
N
f1 (ppm)

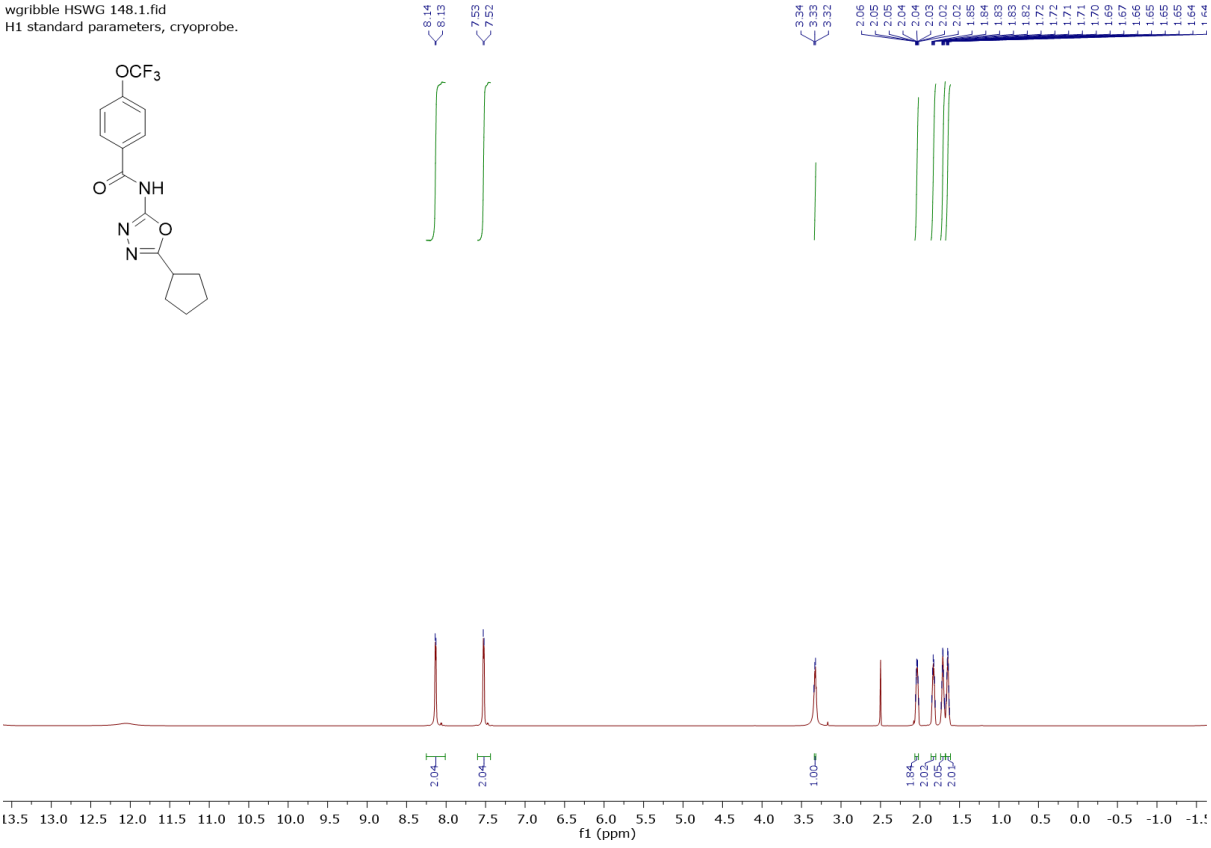
wgribble HSWG 148.1.fid
H1 standard parameters, cryoprobe.
8.14
8.13
7.53
7.52
3.34
3.33
3.32
OCF3
O
NH
N
O
N
2.04
2.04
1.00
1.84
2.02
2.05
2.01
f1 (ppm)

wgribble HSWG 148.1.fid
H1 standard parameters, cryoprobe.

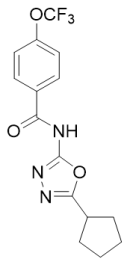

wgribble HSWG 148.1.fid
H1 standard parameters, cryoprobe.

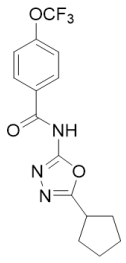

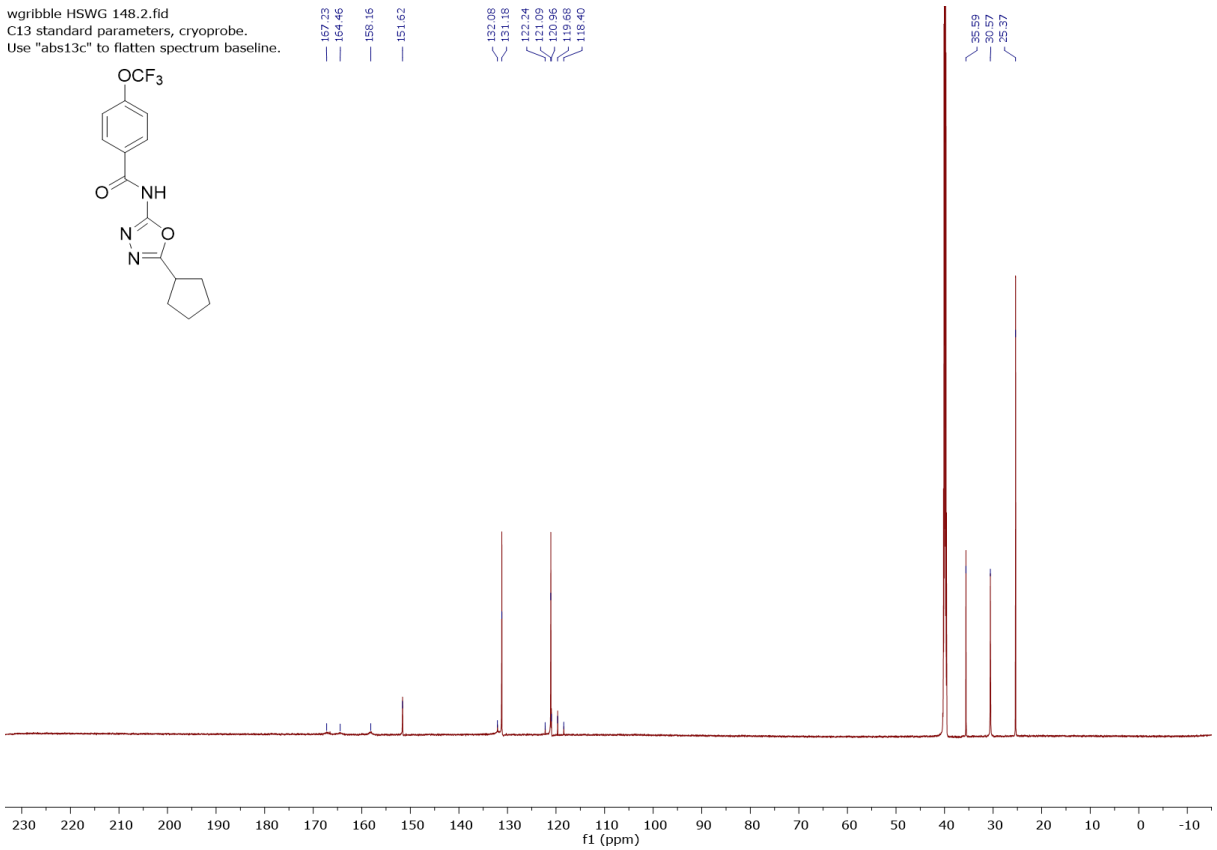
wgribble HSWG 148.2.fid
C13 standard parameters, cryoprobe.
Use "abs13c" to flatten spectrum baseline.
OCF3
O
NH
N
O
N
167.23
164.46
158.16
151.62
132.08
131.18
122.24
121.09
120.96
119.68
118.40
35.59
30.57
25.37
f1 (ppm)

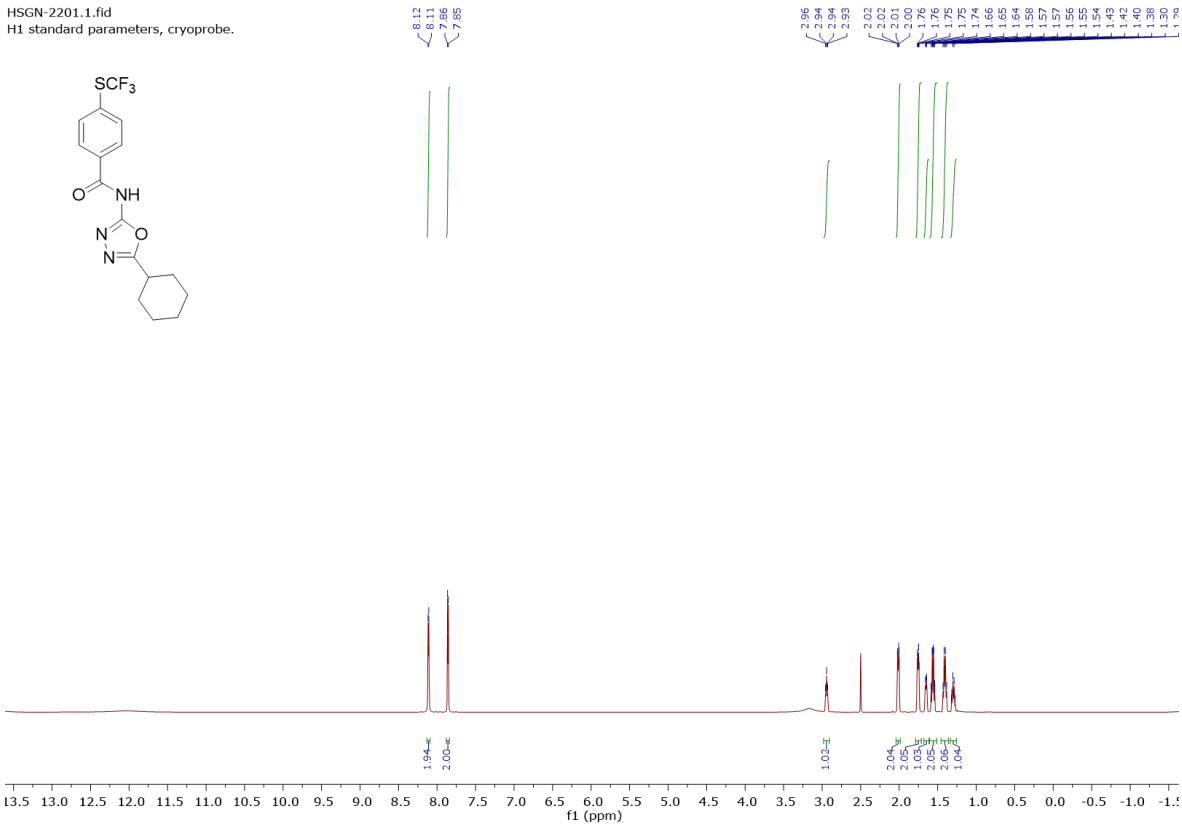
HSGN-2201.1.fid
H1 standard parameters, cryoprobe.
SCF3
O
NH
N
O
N
8.12
8.11
7.86
7.85
2.96
2.94
2.94
2.93
2.02
2.02
2.01
2.00
1.94
2.00
1.02
2.04
2.05
1.03
2.05
2.06
1.04
f1 (ppm)

HSGN-2201.1.fid
H1 standard parameters, cryoprobe.

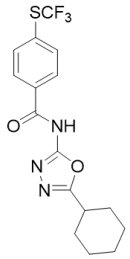

HSGN-2201.1.fid
H1 standard parameters, cryoprobe.

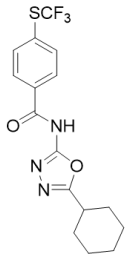

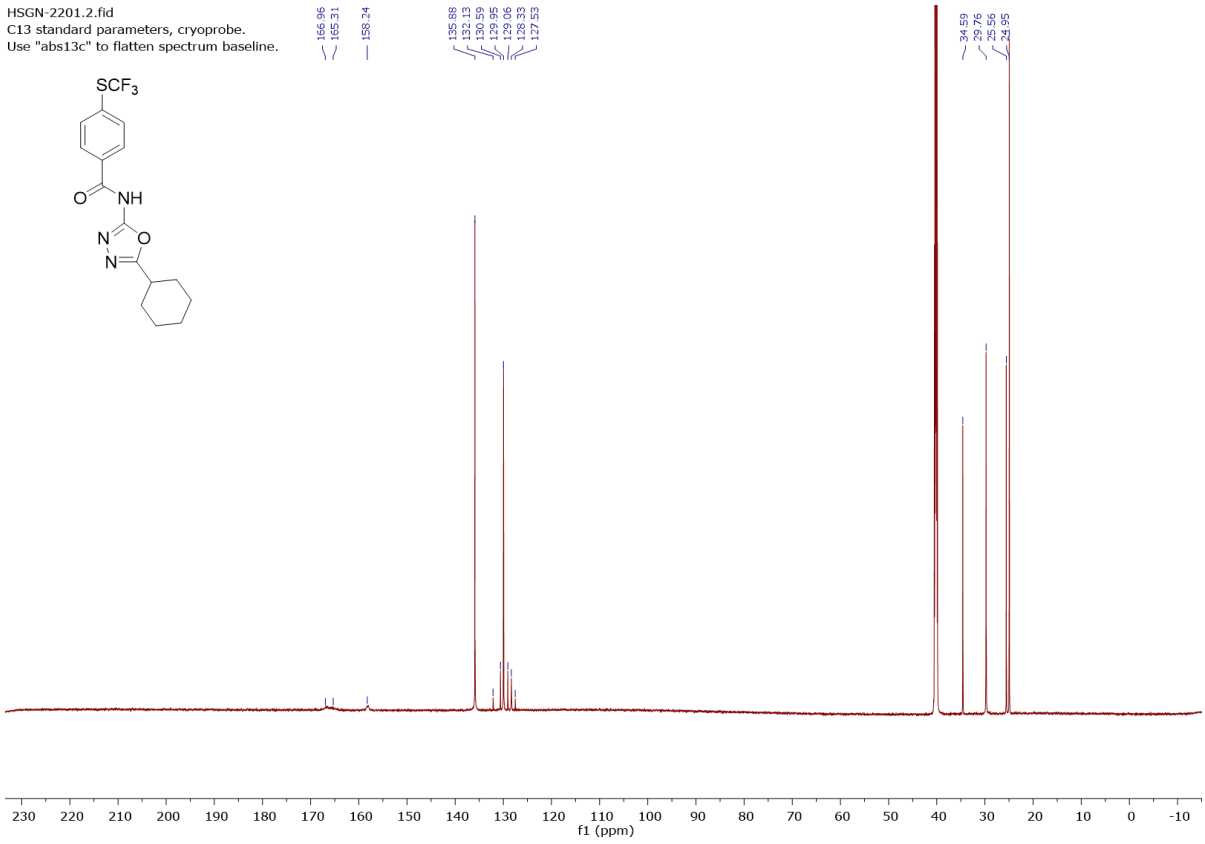
HSGN-2201.2.fid
C13 standard parameters, cryoprobe.
Use "abs13c" to flatten spectrum baseline.
166.96
165.31
158.24
135.88
132.13
130.59
129.95
129.06
128.33
127.53
34.59
29.76
25.56
24.95
SCF3
O
NH
N
O
N
f1 (ppm)

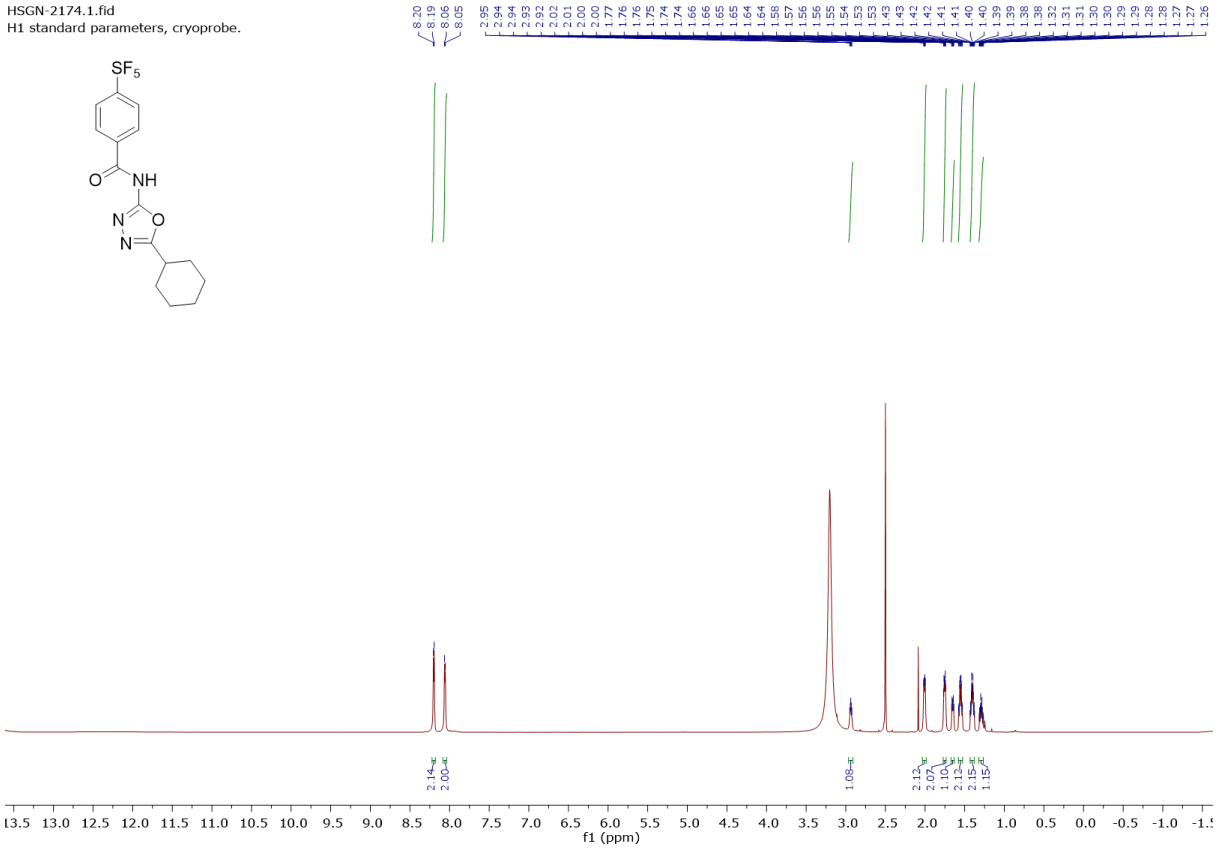
HSGN-2174.1.fid
H1 standard parameters, cryoprobe.
SF5
O
NH
N
O
N
2.14
2.00
1.08
2.12
2.07
1.10
2.13
2.15
1.15
f1 (ppm)

HSGN-2174.1.fid
H1 standard parameters, cryoprobe.

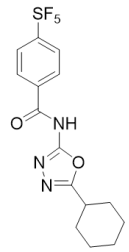

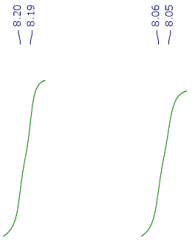

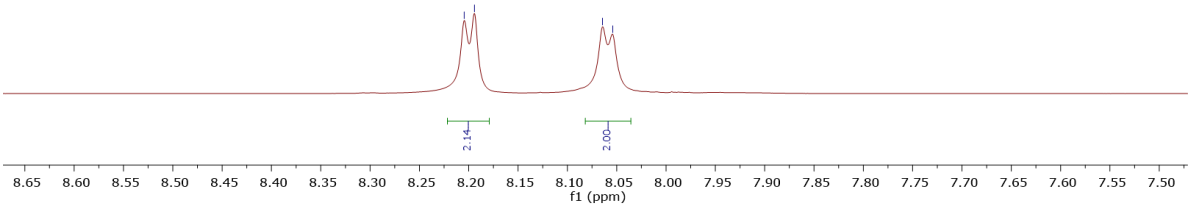

HSGN-2174.1.fid
H1 standard parameters, cryoprobe.

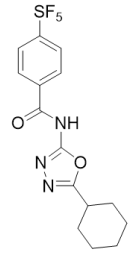

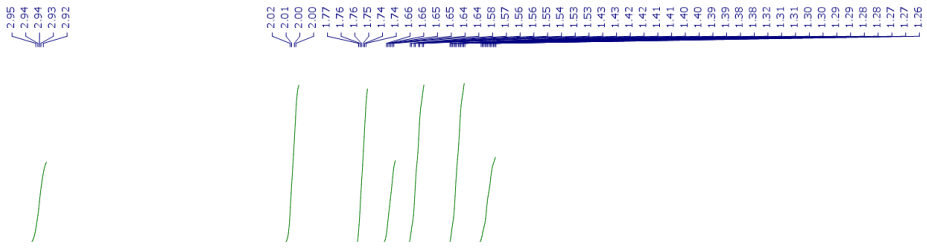

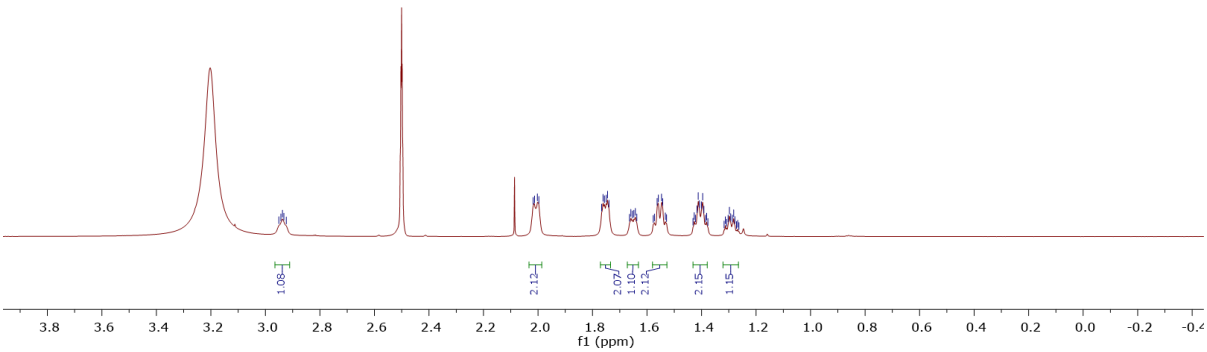

HSGN-2174.2.fid
C13 standard parameters, cryoprobe.
Use "abs13c" to flatten spectrum baseline.

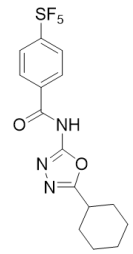

OCF3 Cyclohexane.1.fid
H1 standard parameters, cryoprobe prodigy.

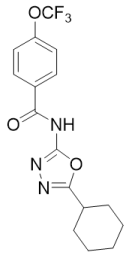

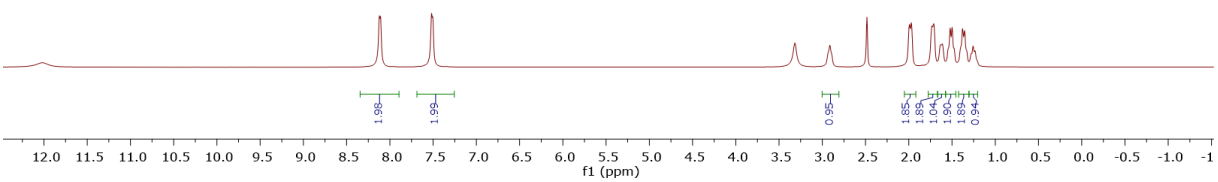

OCF3 Cyclohexane.1.fid
H1 standard parameters, cryoprobe prodigy.

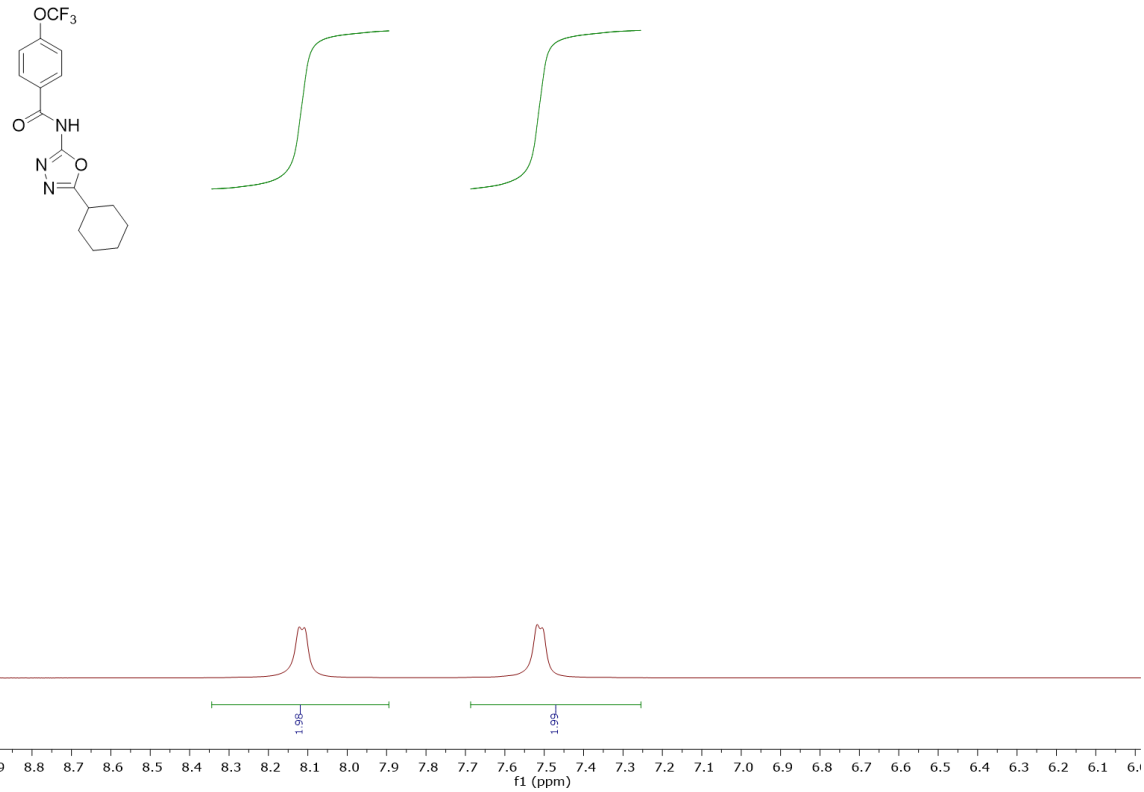

OCF3 Cyclohexane.1.fid
H1 standard parameters, cryoprobe prodigy.

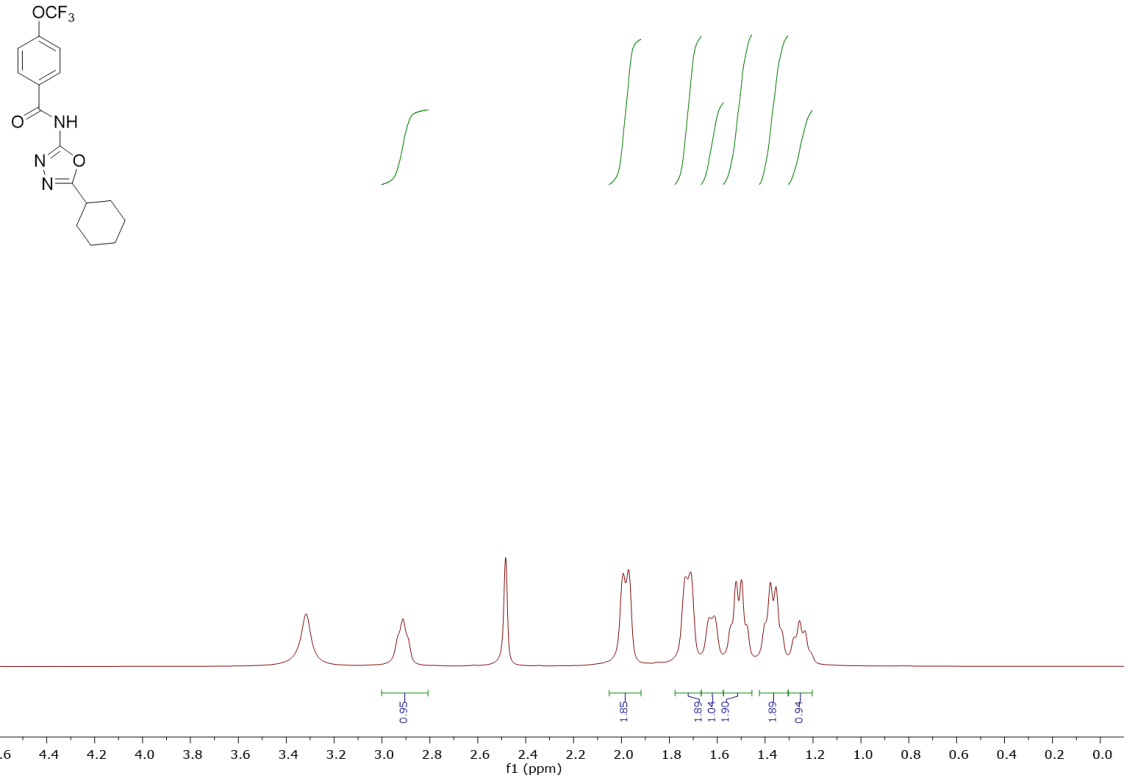

wgribble OCF3 cyclohexane.2.fid
C13 standard parameters, cryoprobe.
Use "abs13c" to flatten spectrum baseline.

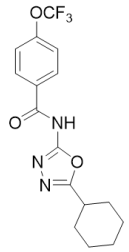

HSGN-2261.1.fid
H1 standard parameters, cryoprobe.

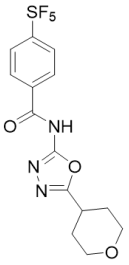

HSGN-2261.1.fid
H1 standard parameters, cryoprobe.

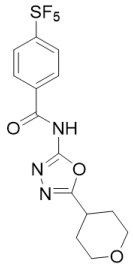

HSGN-2261.1.fid
H1 standard parameters, cryoprobe.

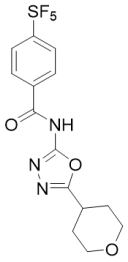

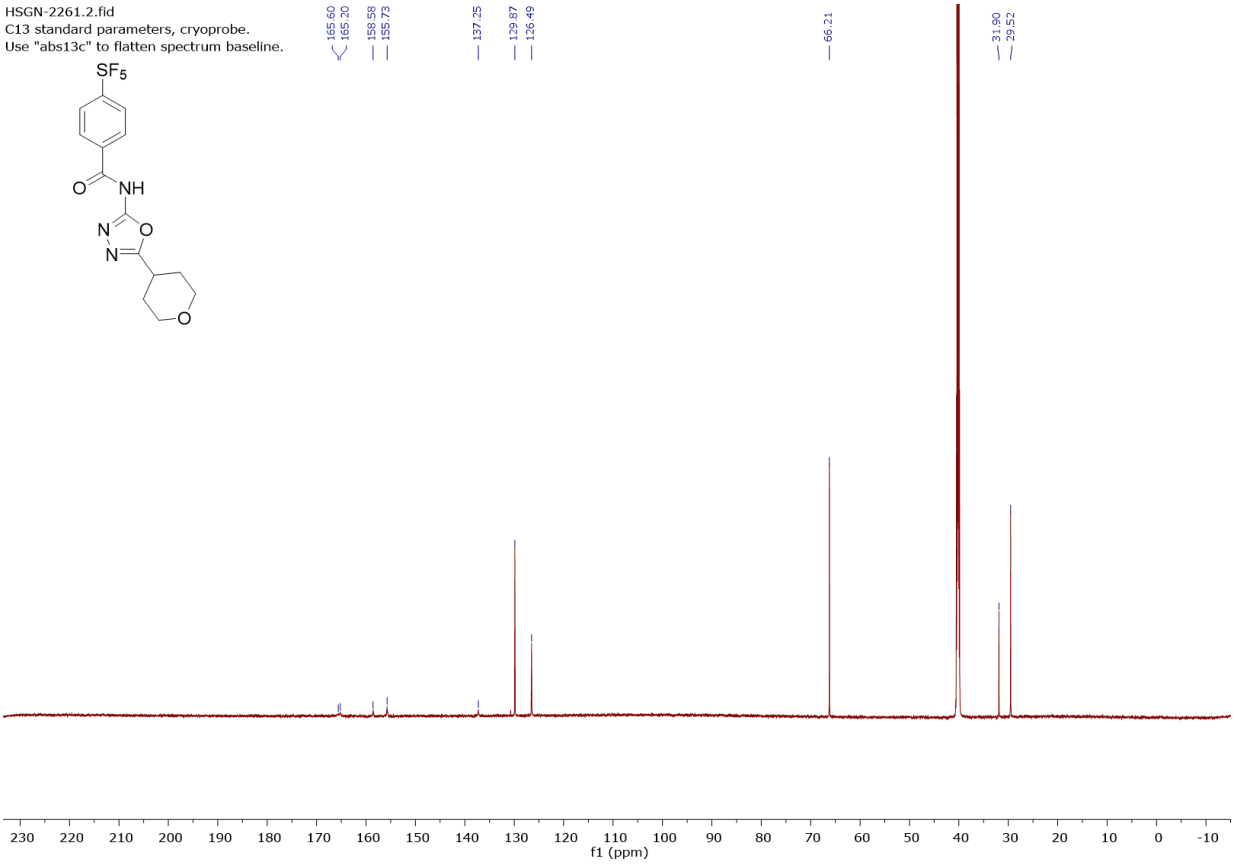
HSGN-2261.2.fid
C13 standard parameters, cryoprobe.
Use "abs13c" to flatten spectrum baseline.
165.60
165.20
158.58
155.73
137.25
129.87
126.49
66.21
31.90
29.52
SF5
O
NH
N
N
O
O
230 220 210 200 190 180 170 160 150 140 130 120 110 100 90 80 70 60 50 40 30 20 10 0 -10
f1 (ppm)

APPENDIX D. CHAPTER 10 SUPPORTING INFORMATION

II. Biological Analysis:

Table D.1. Bacterial strains, sources and characteristics

Staphylococcus aureus ATCC 25923	ATCC	Methicillin susceptible. Reference strain for antibiotic susceptibility testing
MRSA USA 300	ATCC/BEI resources	Methicillin resistant. Most prevalent MRSA clinical infection strain in the U.S
MRSA ATCC 33592	William Wuest, Emory University	Methicillin resistant, Gentamicin resistant. SCCmec: Type III
Enterococcus faecalis ATCC 29212	ATCC	Reference strain for antibiotic susceptibility testing. Susceptible to most GPC antibiotics
Enterococcus faecalis ATCC 51575 (VRE)	ATCC	Presence of *vanB*. Resistant to gentamicin, streptomycin, and vancomycin. Sensitive to teicoplanin.
Enterococcus faecium ATCC 700221 (VRE)	ATCC	Presence of *vanA*. Resistant to vancomycin and teicoplanin
Listeria monocytogenes ATCC 19115	ATCC	Reference strain for antibiotic susceptibility testing. Susceptible to most GPC antibiotics

ATCC = American Type Culture Collection, GPC = Gram positive cocci, ARLG = Antibacterial Resistance Leadership Group

Table D.2. MRSA clinical isolates used in study

Strain	PFGE Pattern / MLST Type	spa Type eGenomics (Ridom)	SCCmec	Other Genetic Characterization	Additional Non-MRSA resistance (dru Type)	Oxacillin MIC in μg/mL
ARLG 1561	USA 300	1	IVa	ACME+, pvl genes+	Ery	NT
ARLG 1567	USA 300	1	IVa	ACME+, pvl genes+	Ery, Cipro	NT
ARLG 1568	USA 300	1	IVa	ACME+, pvl genes+, MupA gene+	Mup, Ery, Cipro	NT
ARLG 1569	USA 300	1	IVa	ACME+, pvl genes+, MupA gene+	Mup, Ery, Cipro, Clinda	NT
ARLG 1570	USA 300	1	IVa	ACME+, pvl genes+, MupA gene+	Mup, Ery, Cipro, Clinda	NT
ARLG-1663	ST239	351 (t030)	3A.1.4	ccrC+, dcs+, Hg-J+, mecl+	(dt10a)	512
ARLG-1649	ST1312	351 (t030)	3A.1.4	ccrC+, dcs+, Hg-J+, mecl+	(dt10g)	256
ARLG-1664	ST239	351 (t030)	16691	ccrC+, Hg-J+, mecl+	(dt9x)	256

* ACME = arginine catabolic mobile element, PFGE = Pulsed field gel electrophoresis, MLST = Multilocus sequence typing, pvl = panton valentin leucocidin, Ery = Erythromycin, Mup = Mupirocin, Cipro = Ciprofloxacin, Clinda = Constitutive clindamycin resistance

Table D.3. Sequence of primers used in RT-PCR.

Primer Name	Sequence (5'- 3')	Source
eno Forward	AAACTGCCGTAGGTGACGAA	Kot et al.[426]
eno Reverse	TGTTTCAACAGCATCTTCAGTACCTT	Kot et al.[426]
ebps Forward	ACATTCAAATGACGCTCAAAACAAAAGT	Kot et al.[426]
ebps Reverse	CTTATCTTGAGACGCTTTATCCTCAGT	Kot et al.[426]
fib Forward	GAATATGGTGCACGTCCACAATT	Kot et al.[426]
fib Reverse	AAGATTTTGAGCTTGAATCAATTTTTGTTCTTTTT	Kot et al.[426]
cna Forward	GACTTACCGAAGTATGATGAAGGAAAGA	Kot et al.[426]
cna Reverse	ACCGTTGATGTCTGTTGTGTAGTC	Kot et al.[426]
icaA Forward	CAATACTATTTCGGGTGTCTTCACTCT	Kot et al.[426]
icaA Reverse	CAAGAAACTGCAATATCTTCGGTAATCAT	Kot et al.[426]
icaD Forward	TCAAGCCCAGACAGAGGGAATA	Kot et al.[426]
icaD Reverse	ACACGATATAGCGATAAGTGCTGTTT	Kot et al.[426]
rpoB Forward	CAGCTGACGAAGAAGATAGCTATGT	Kot et al.[426]
rpoB Reverse	ACTTCATCATCCATGAAACGACCAT	Kot et al.[426]

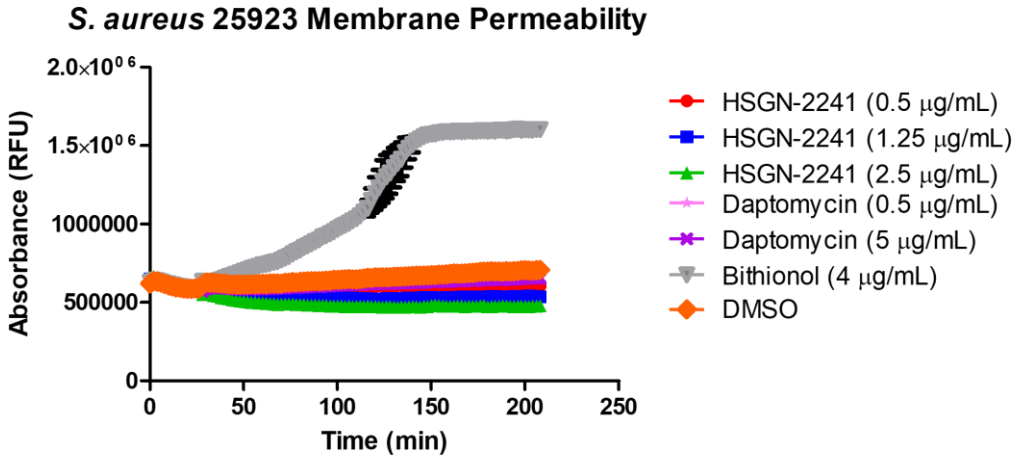

Figure D.1. Effects of HSGN-2241 on membrane permeability in *S. aureus* at 2X MIC, 5X MIC, and 10X MIC concentrations using sytox green dye. Increase in fluorescence indicates permeability. Bithionol (4 μg/mL) is used as positive control while 1% DMSO is used as negative control.

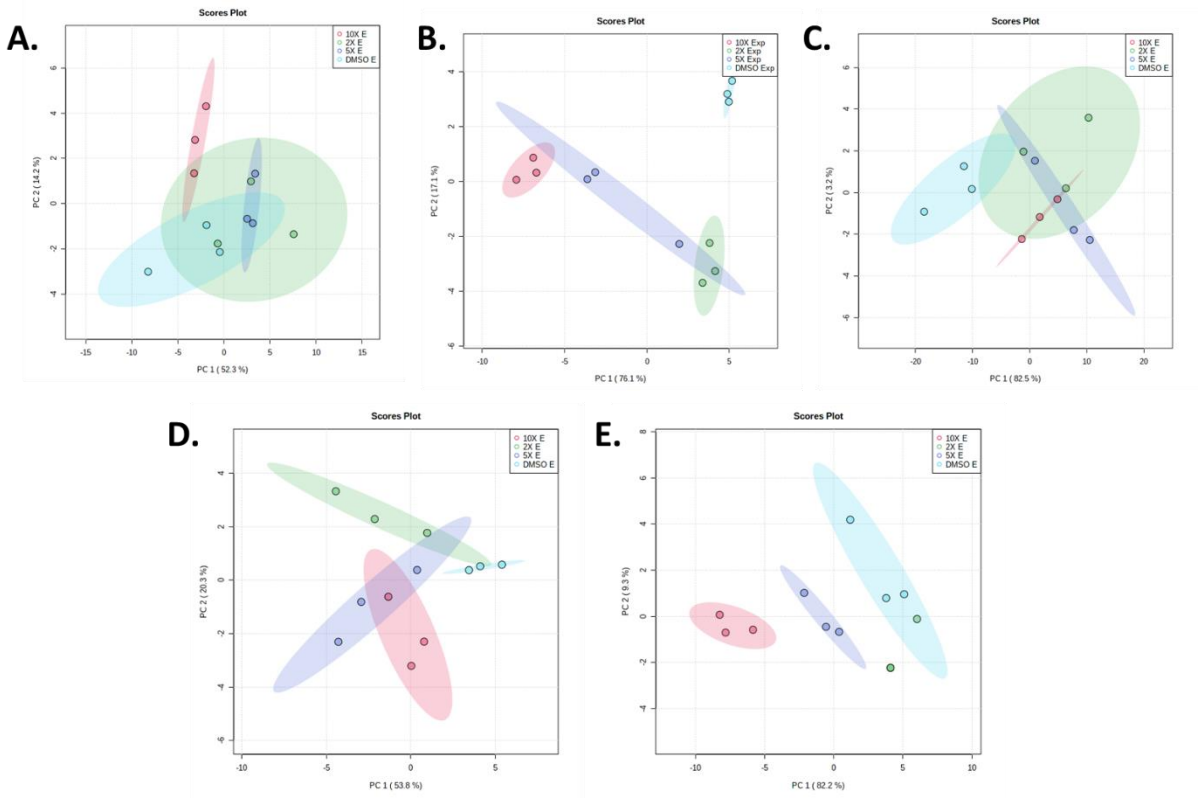

Figure D.2. PCA scores plots of exponential phase *S. aureus* treated with DMSO (control), 2X MIC HSGN-2241, 5X MIC HSGN-2241, and 10X HSGN-2241. (A) Effects on PC synthesis. (B) Effects on PG synthesis. (C) Effects on PE synthesis. (D) Effects on PEI synthesis. (E) Effects on free fatty acids.

II. ^{1}H, ^{13}C, and ^{19}F Spectra of Analogs:

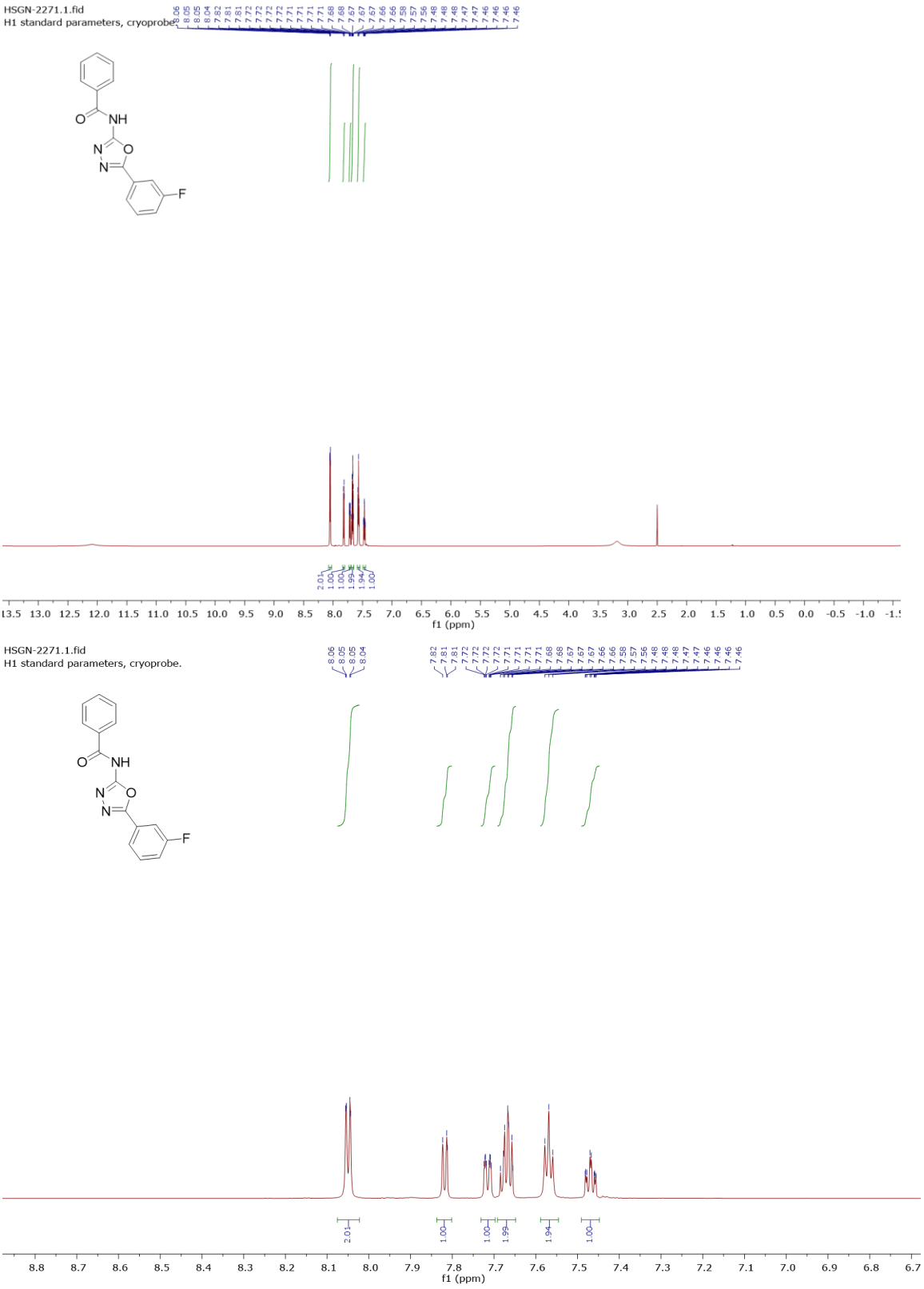

HSGN-2271.2.fid
C13 standard parameters, cryoprobe.
Use "abs13c" to flatten spectrum baseline.

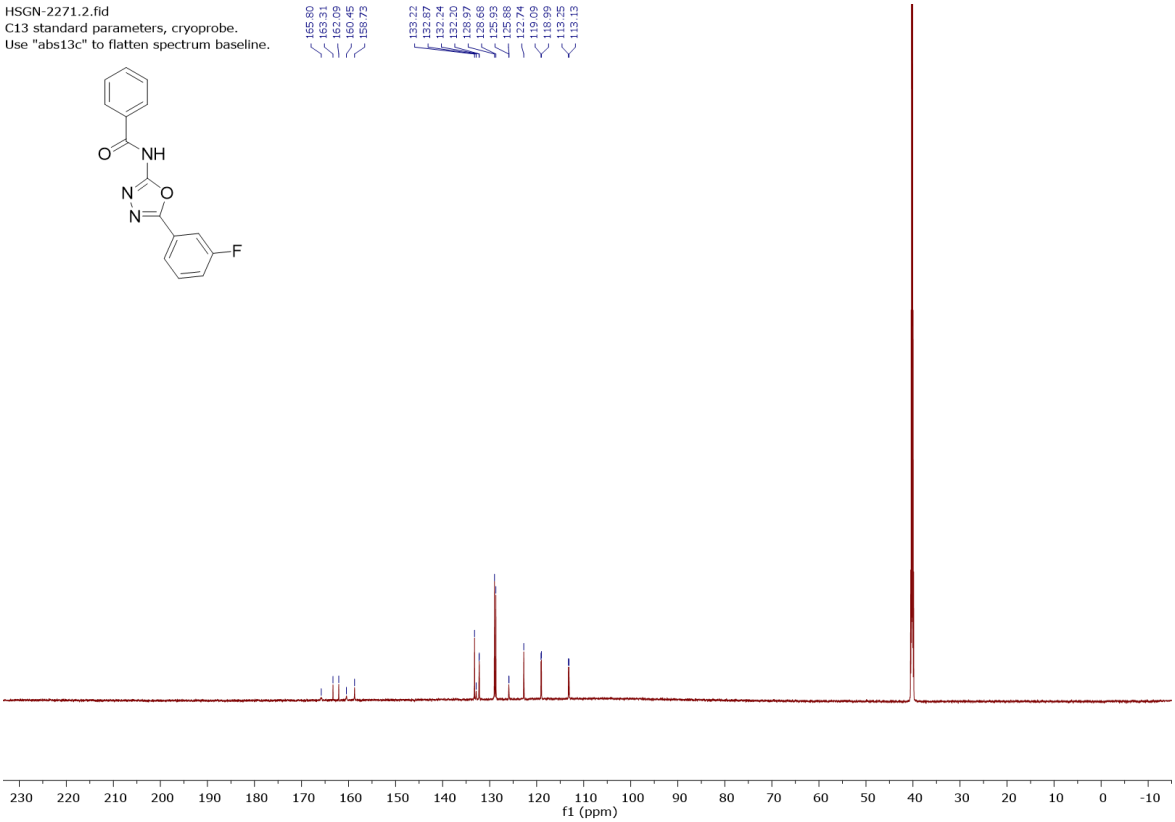

gnacleri_HSGN-2271.1.fid
F19 standard parameters, cryoprobe prodigy.
DE is lengthened compared to default.

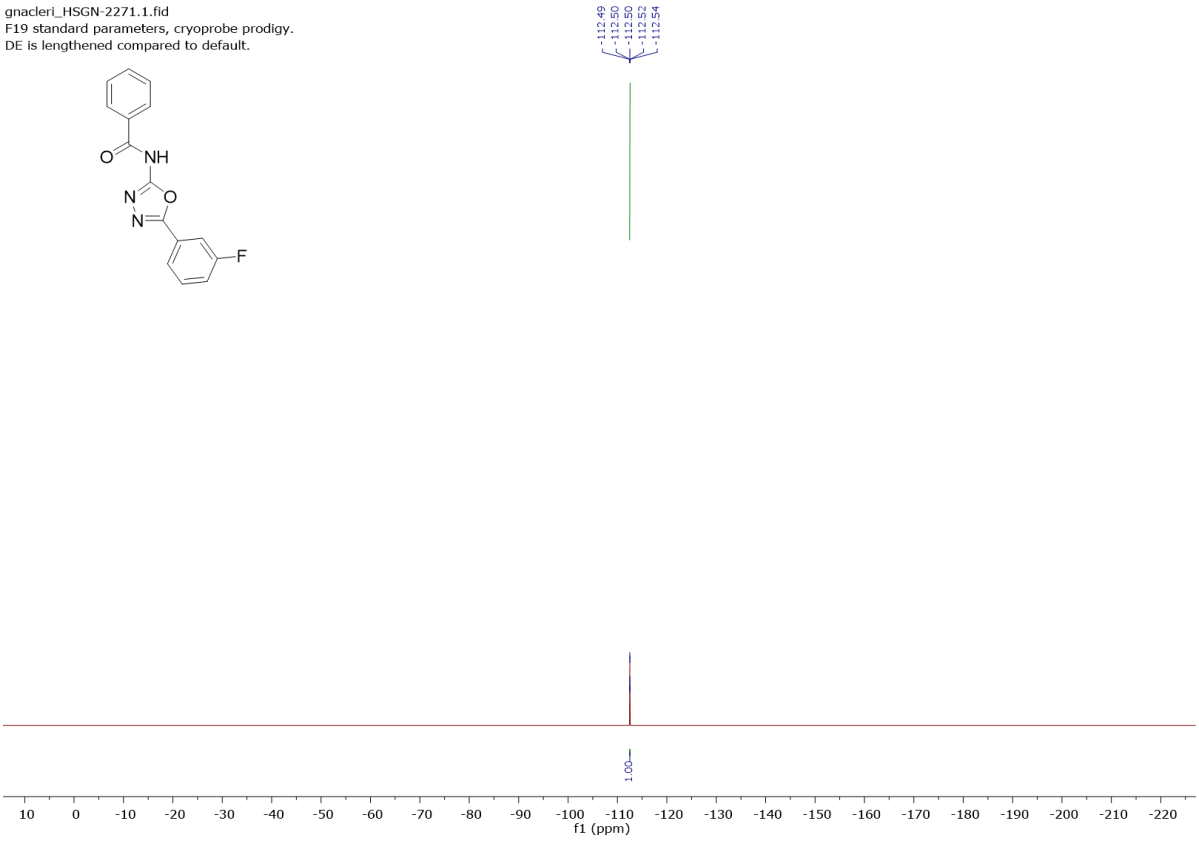

HSGN-2234.1.fid
H1 standard parameters, cryoprobe.

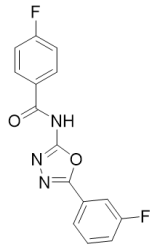

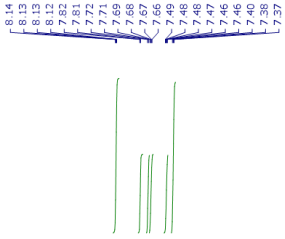

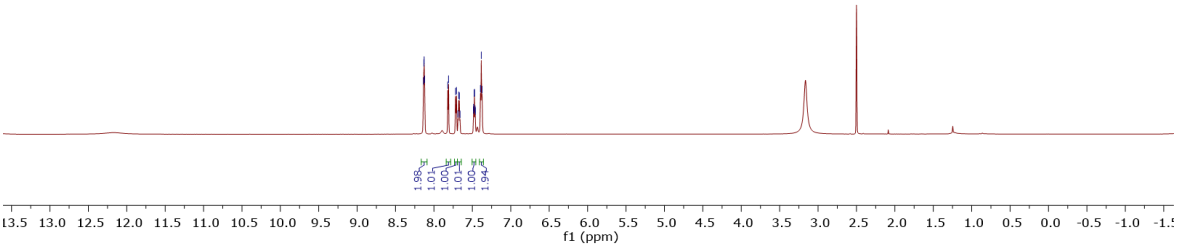

HSGN-2234.1.fid
H1 standard parameters, cryoprobe.

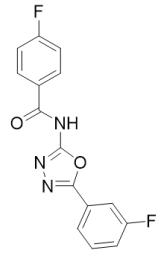

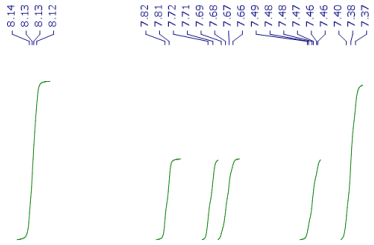

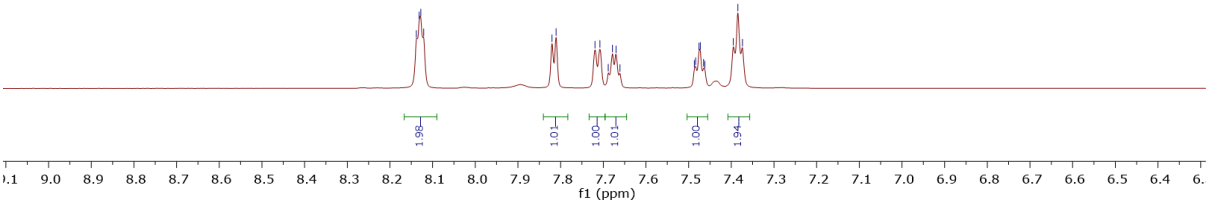

HSGN-2234.2.fid
C13 standard parameters, cryoprobe.
Use "abs13c" to flatten spectrum baseline.

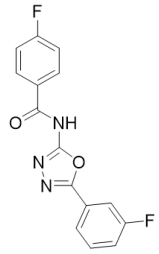

gnacleri_HSGN-2234.1.fid
F19 standard parameters, cryoprobe prodigy.
DE is lengthened compared to default.

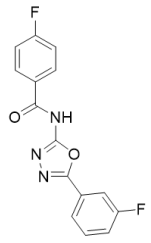

HSGN-2237.1.fid
H1 standard parameters, cryoprobe.

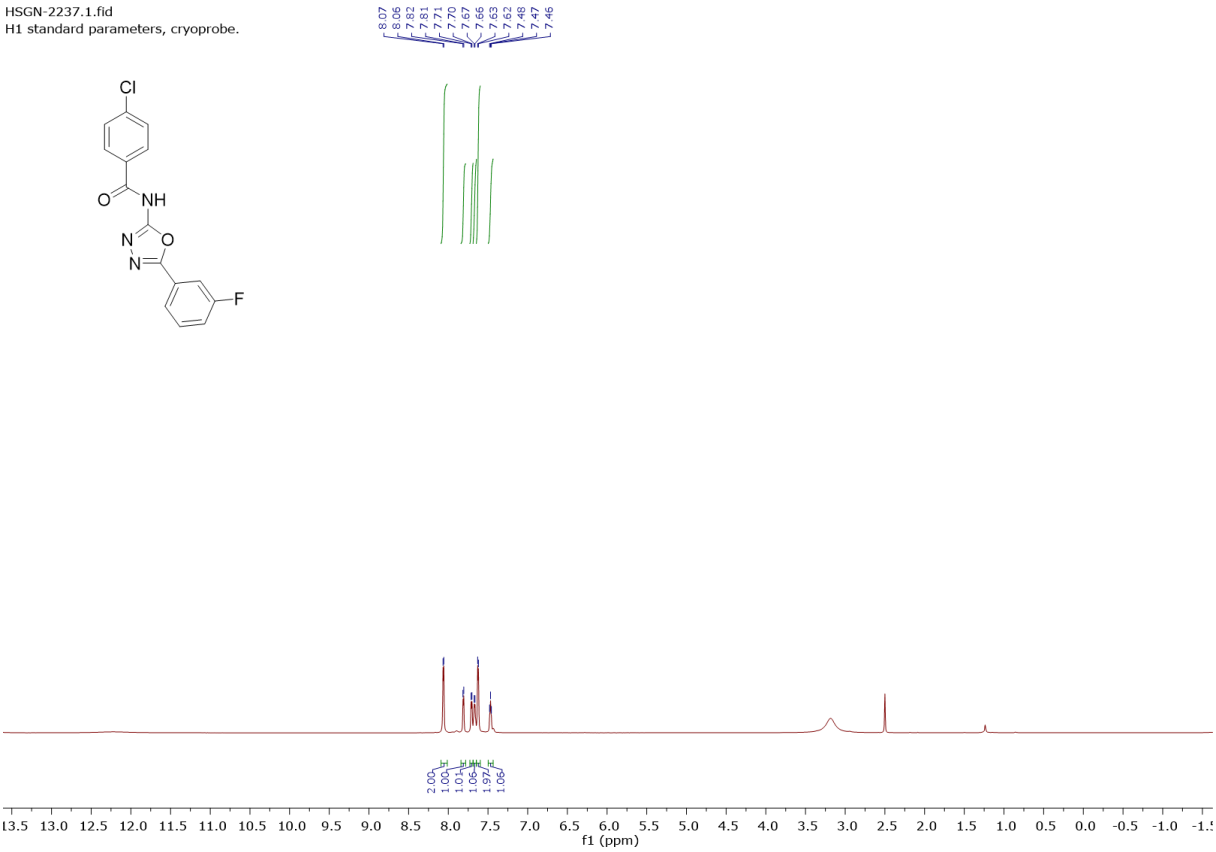

HSGN-2237.1.fid
H1 standard parameters, cryoprobe.

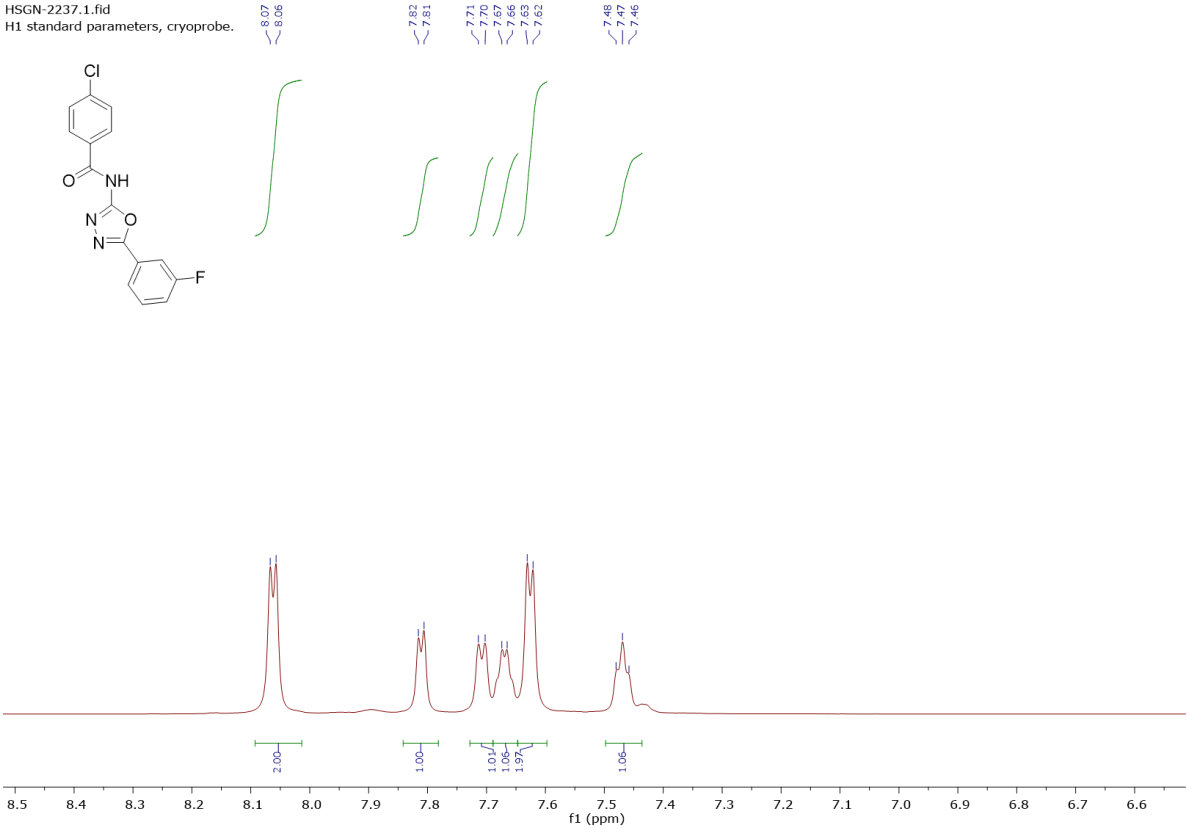

HSGN-2237.2.fid
C13 standard parameters, cryoprobe.
Use "abs13c" to flatten spectrum baseline.

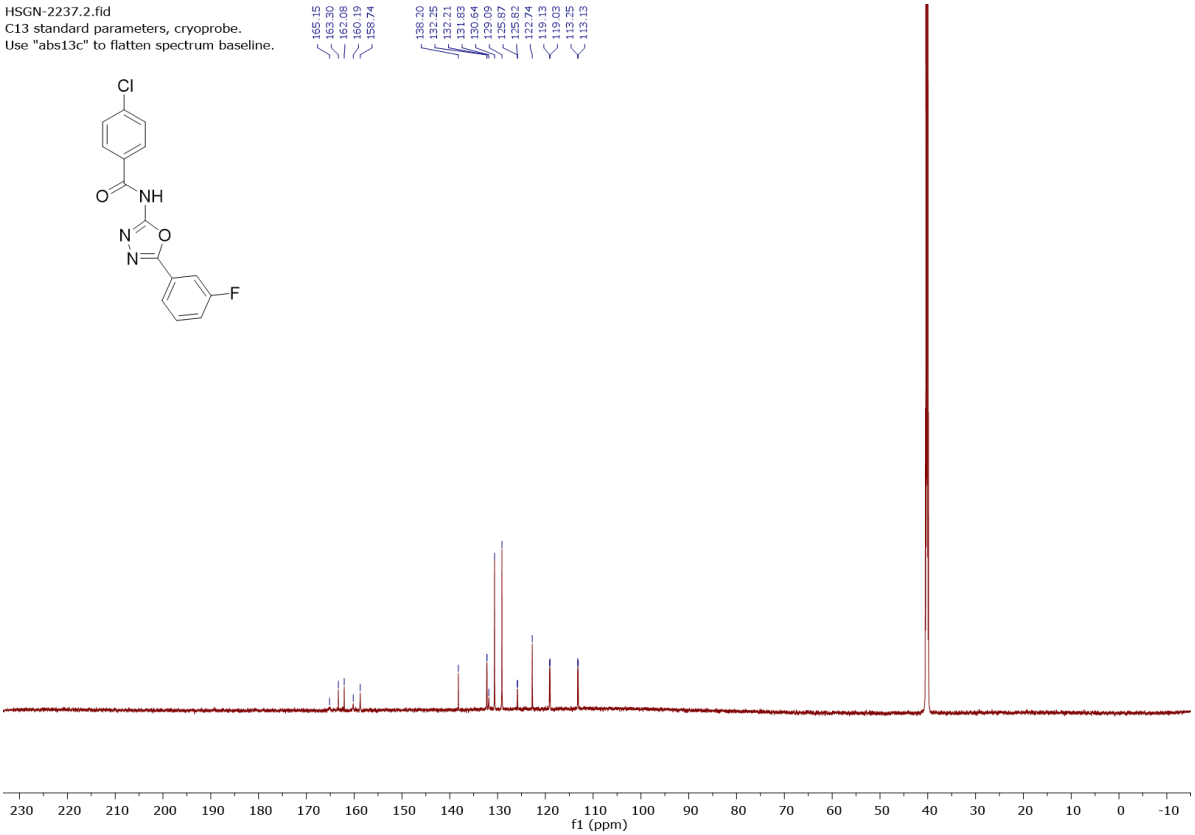

gnacleri_HSGN-2237.1.fid
F19 standard parameters, cryoprobe prodigy.
DE is lengthened compared to default.

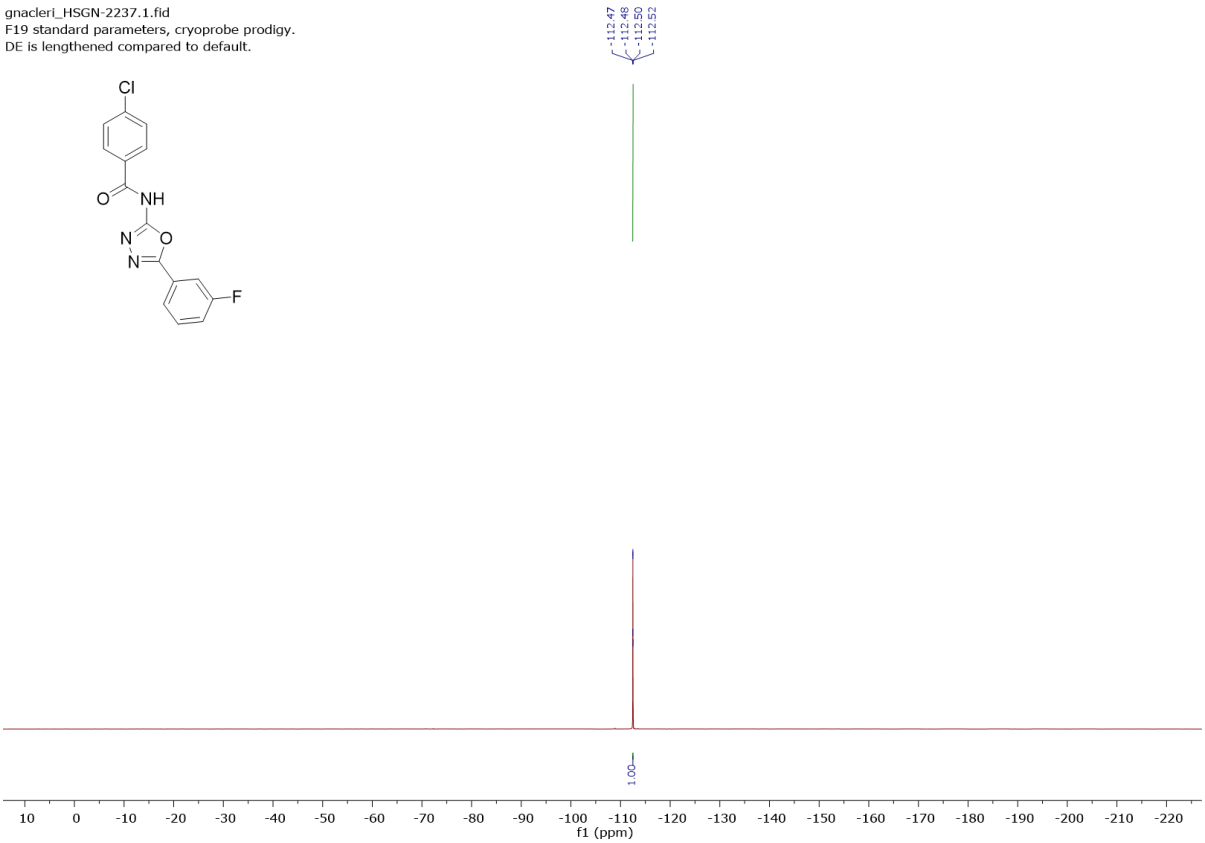

HSGN-2244.1.fid
H1 standard parameters, cryoprobe.

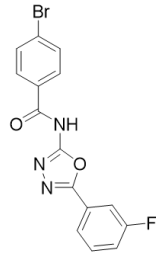

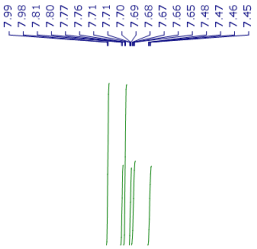

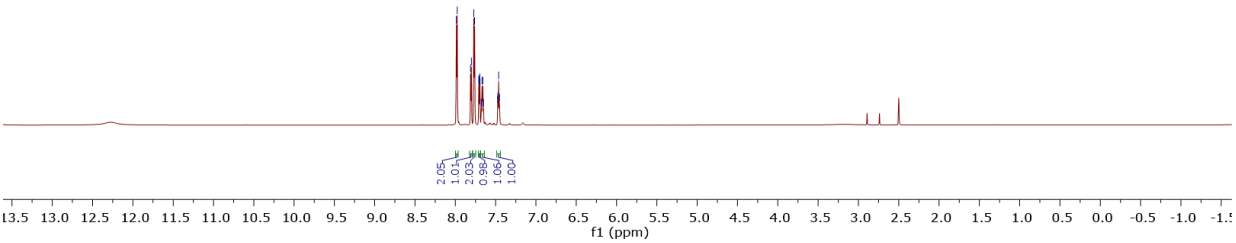

HSGN-2244.1.fid
H1 standard parameters, cryoprobe.

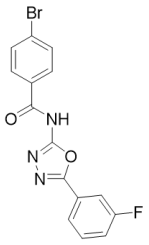

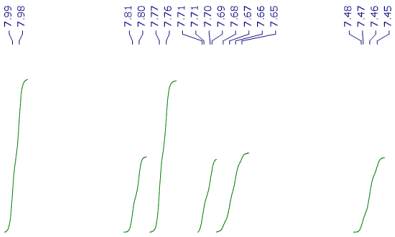

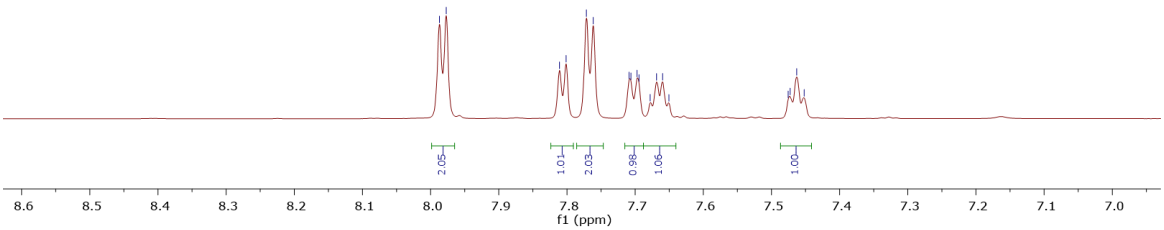

HSGN-2244.2.fid
C13 standard parameters, cryoprobe.
Use "abs13c" to flatten spectrum baseline.

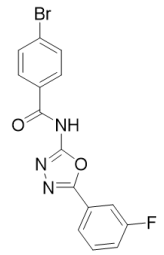

gnacleri_HSGN-2244.1.fid
F19 standard parameters, cryoprobe prodigy.
DE is lengthened compared to default.

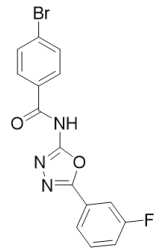

HSGN-2250.1.fid
H1 standard parameters, cryoprobe.

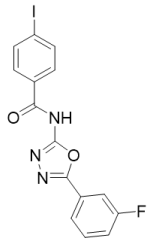

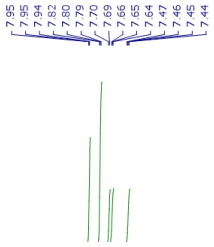

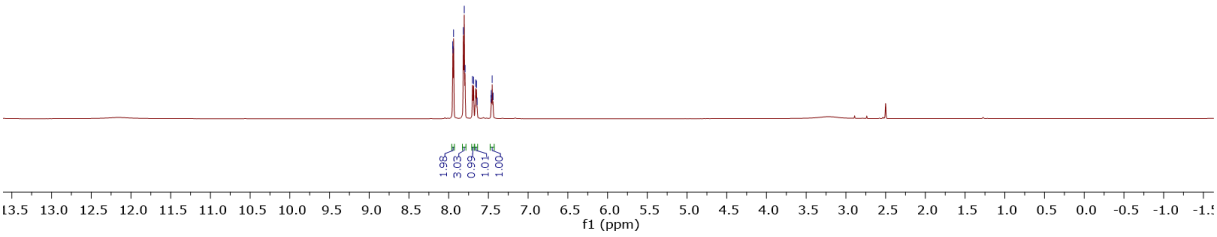

HSGN-2250.1.fid
H1 standard parameters, cryoprobe.

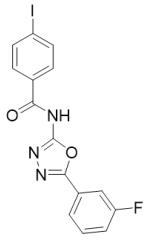

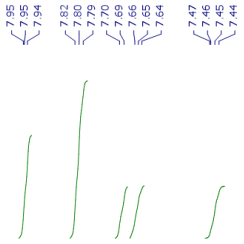

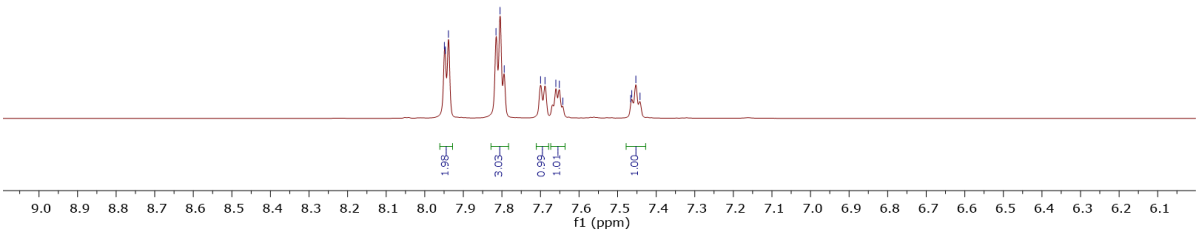

HSGN-2250.2.fid
C13 standard parameters, cryoprobe.
Use "abs13c" to flatten spectrum baseline.

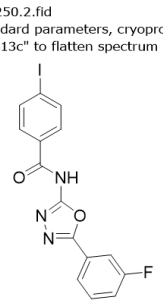

gnacleri_HSGN-2250.1.fid
F19 standard parameters, cryoprobe prodigy.
DE is lengthened compared to default.

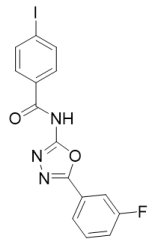

HSGN-2272.1.fid
H1 standard parameters, cryoprobe.

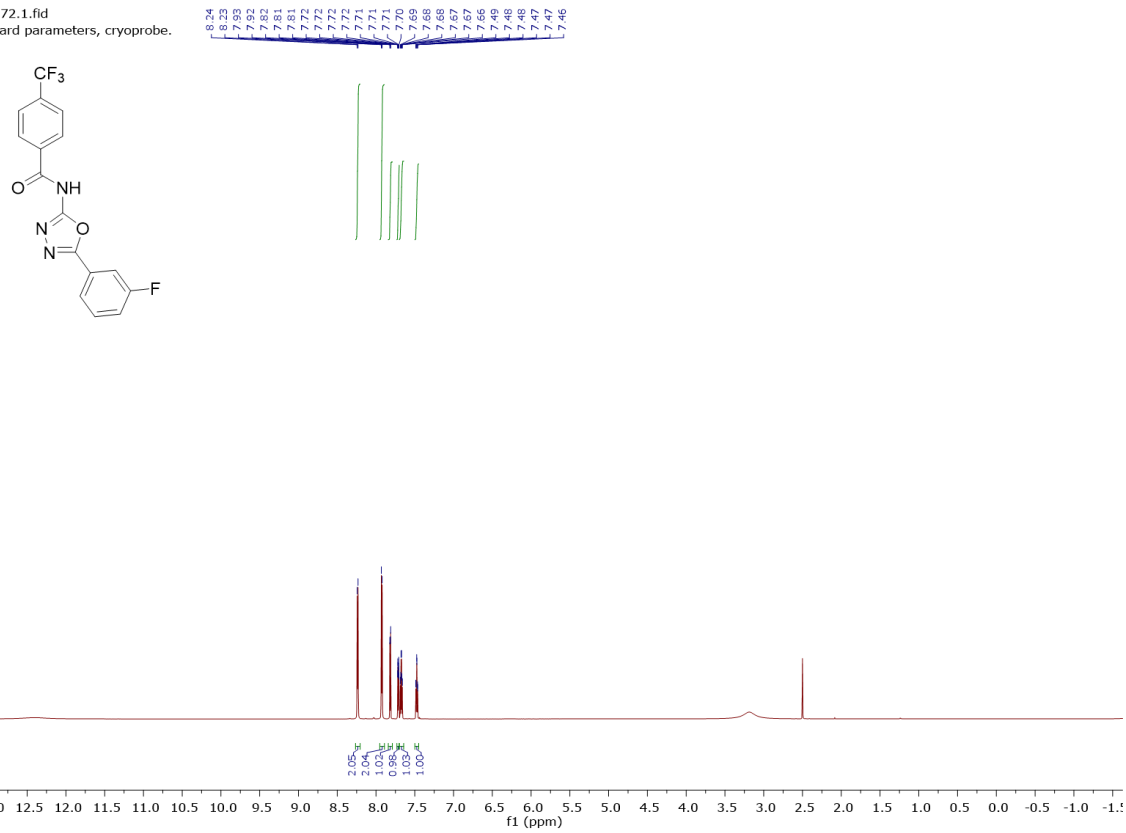

HSGN-2272.1.fid
H1 standard parameters, cryoprobe.

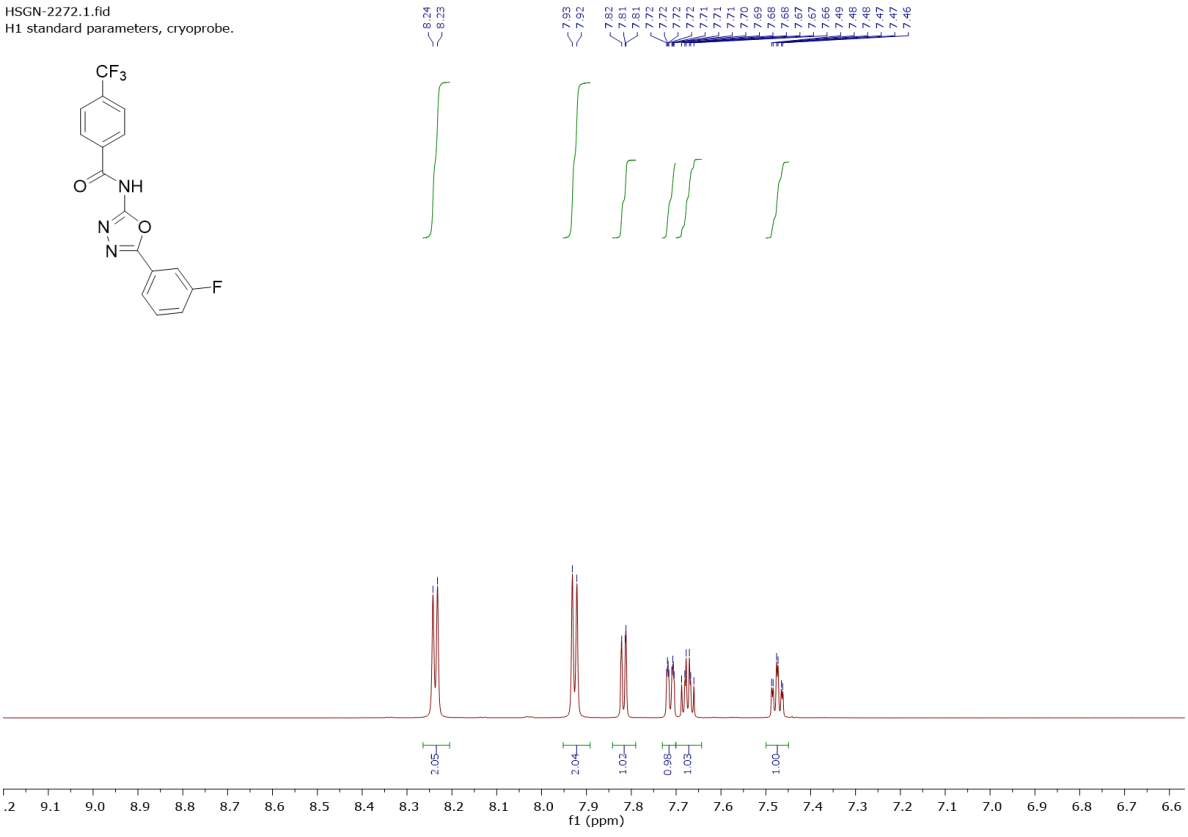

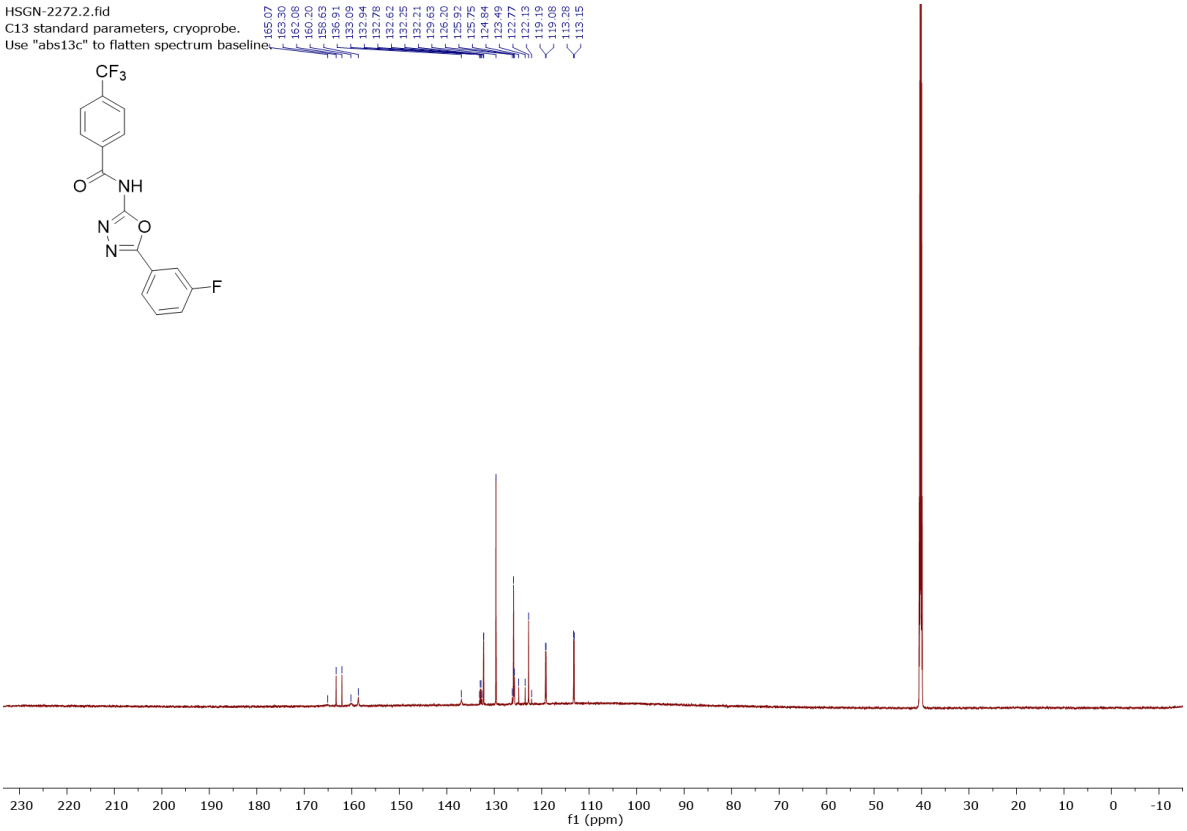
HSGN-2272.2.fid
C13 standard parameters, cryoprobe.
Use "abs13c" to flatten spectrum baseline.
165.07
163.30
162.08
160.20
158.63
136.91
133.09
132.94
132.78
132.62
132.25
132.21
129.63
126.20
125.92
125.75
124.84
123.49
122.77
122.13
119.19
119.08
113.38
113.15
CF3
O
NH
N
O
N
F
230 220 210 200 190 180 170 160 150 140 130 120 110 100 90 80 70 60 50 40 30 20 10 0 -10
f1 (ppm)

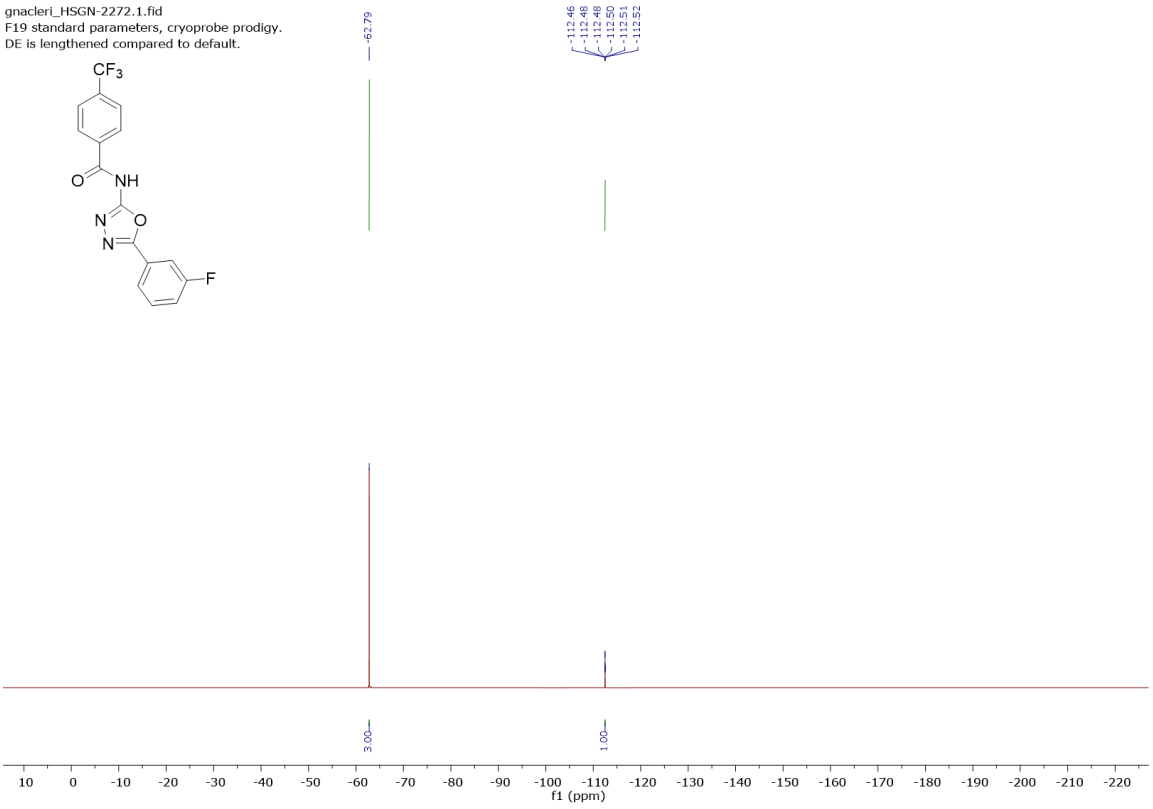
gnacleri_HSGN-2272.1.fid
F19 standard parameters, cryoprobe prodigy.
DE is lengthened compared to default.
-62.79
-112.46
-112.48
-112.48
-112.50
-112.51
-112.52
CF3
O
NH
N
O
N
F
3.00
1.00
10 0 -10 -20 -30 -40 -50 -60 -70 -80 -90 -100 -110 -120 -130 -140 -150 -160 -170 -180 -190 -200 -210 -220
f1 (ppm)

HSGN-2235.1.fid
H1 standard parameters, cryoprobe.

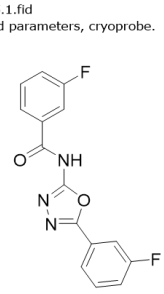

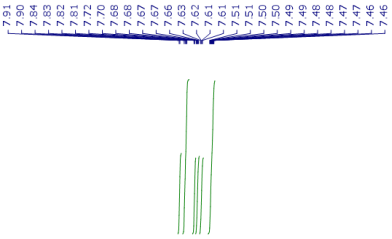

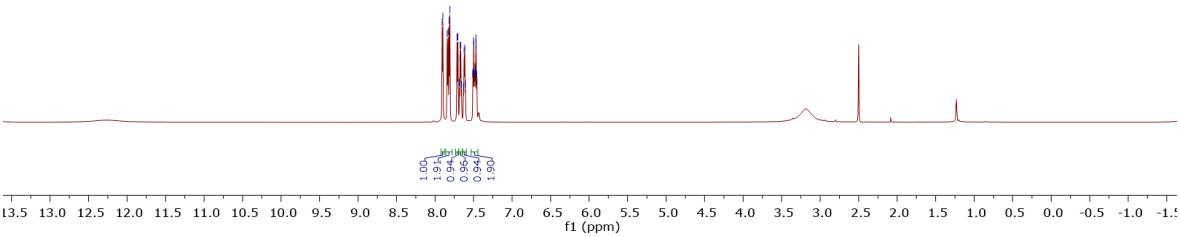

HSGN-2235.1.fid
H1 standard parameters, cryoprobe.

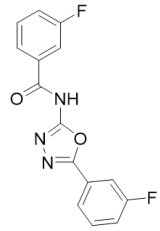

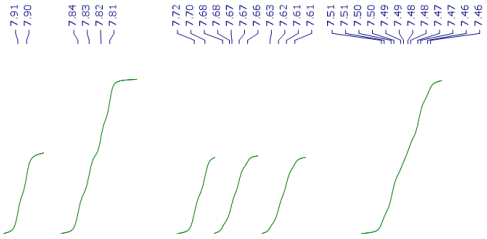

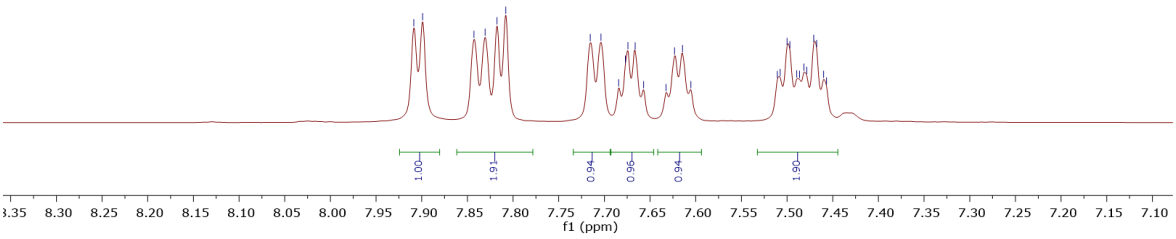

HSGN-2235.2.fid
C13 standard parameters, cryoprobe.
Use "abs13c" to flatten spectrum baseline.

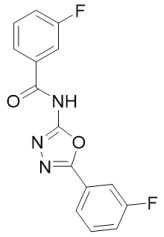

gnacleri_HSGN-2235.1.fid
F19 standard parameters, cryoprobe prodigy.
DE is lengthened compared to default.

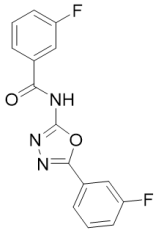

HSGN-2238.1.fid
H1 standard parameters, cryoprobe.

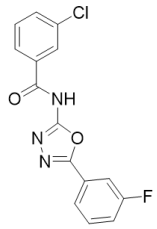

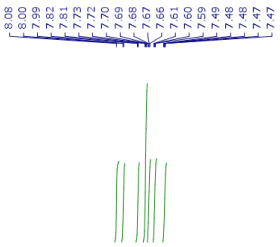

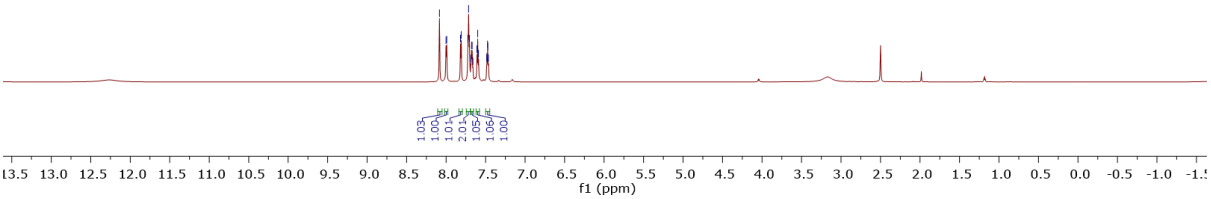

HSGN-2238.1.fid
H1 standard parameters, cryoprobe.

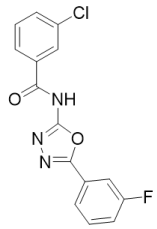

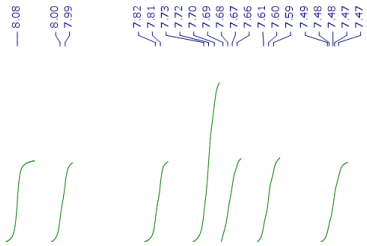

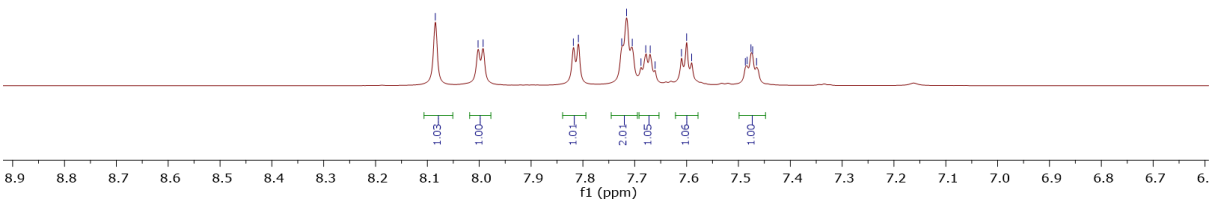

HSGN-2238.2.fid
C13 standard parameters, cryoprobe.
Use "abs13c" to flatten spectrum baseline.

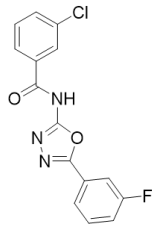

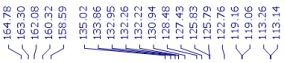

gnacleri_HSGN-2238.1.fid
F19 standard parameters, cryoprobe prodigy.
DE is lengthened compared to default.

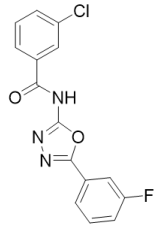

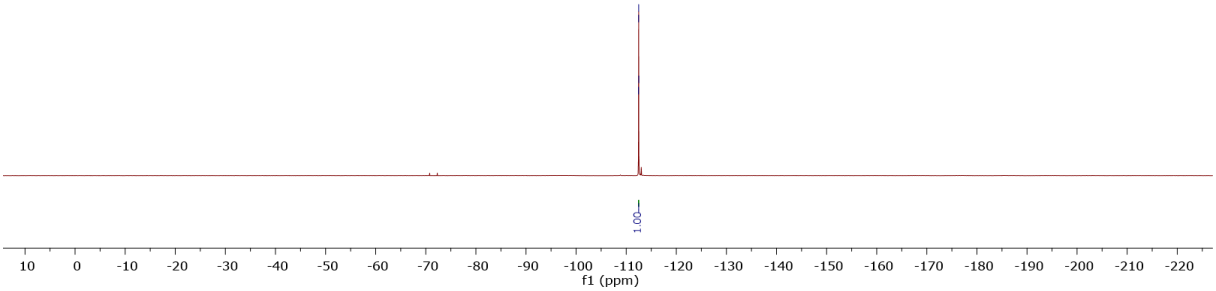

HSGN-2245.1.fid
H1 standard parameters, cryoprobe.

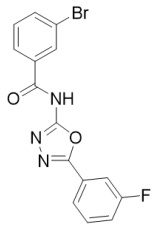

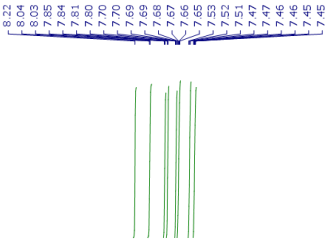

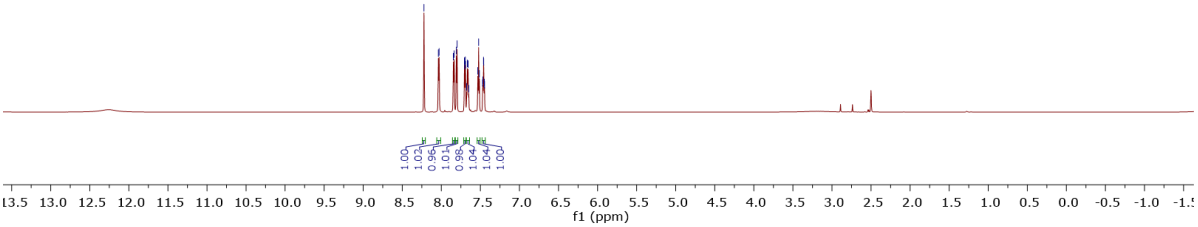

HSGN-2245.1.fid
H1 standard parameters, cryoprobe.

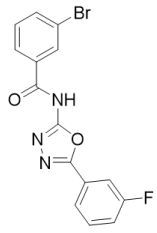

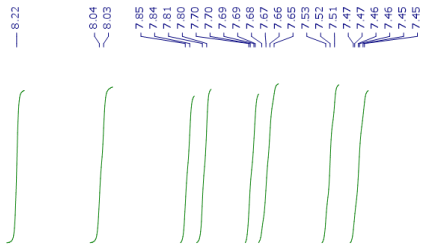

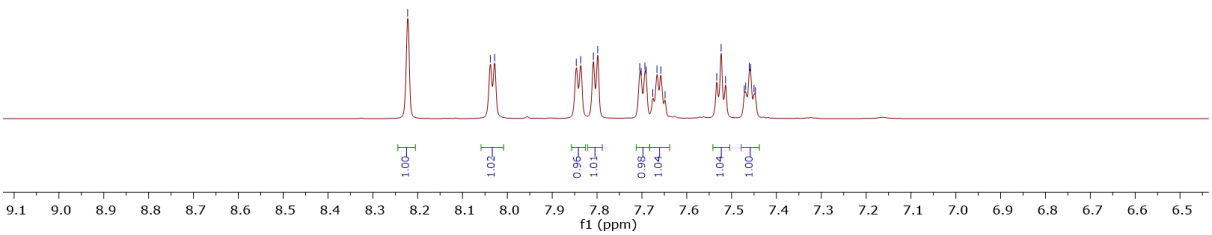

HSGN-2245.2.fid
C13 standard parameters, cryoprobe.
Use "abs13c" to flatten spectrum baseline.

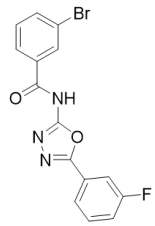

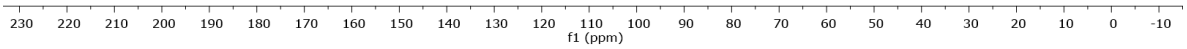

gnacleri_HSGN-2245.1.fid
F19 standard parameters, cryoprobe prodigy.
DE is lengthened compared to default.

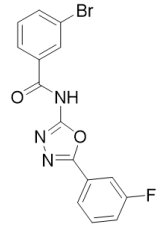

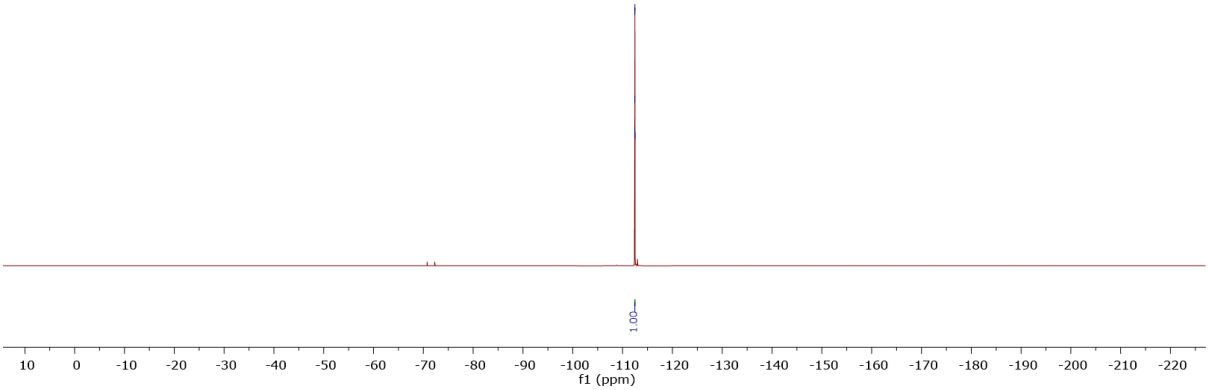

HSGN-2259.1.fid
H1 standard parameters, cryoprobe.

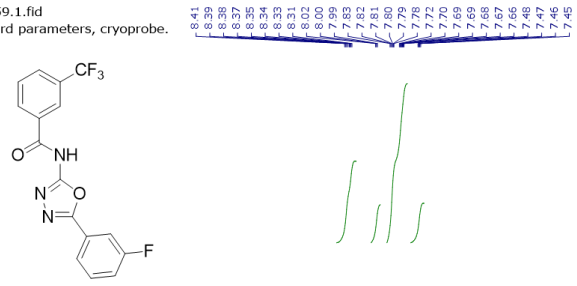

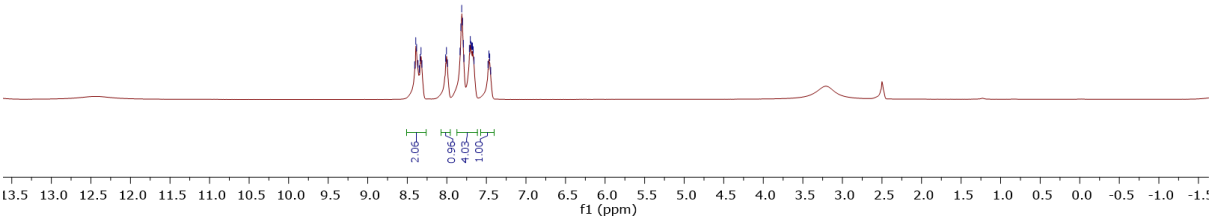

HSGN-2259.1.fid
H1 standard parameters, cryoprobe.

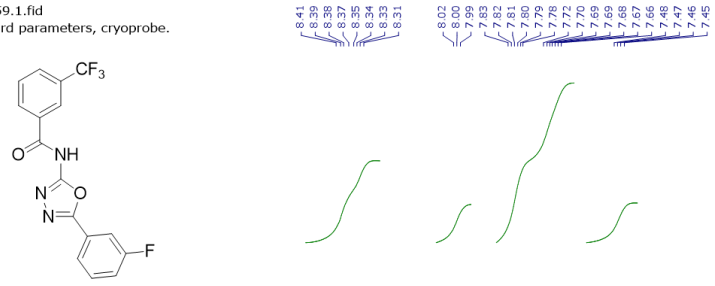

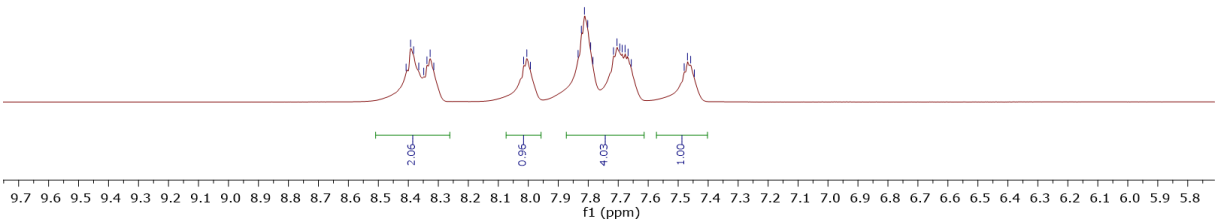

HSGN-2259.2.fid
C13 standard parameters, cryoprobe.
Use "abs13c" to flatten spectrum baseline.

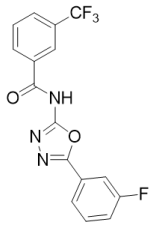

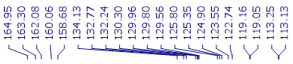

gnacleri_HSGN-2259.1.fid
F19 standard parameters, cryoprobe prodigy.
DE is lengthened compared to default.

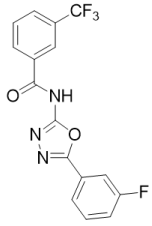

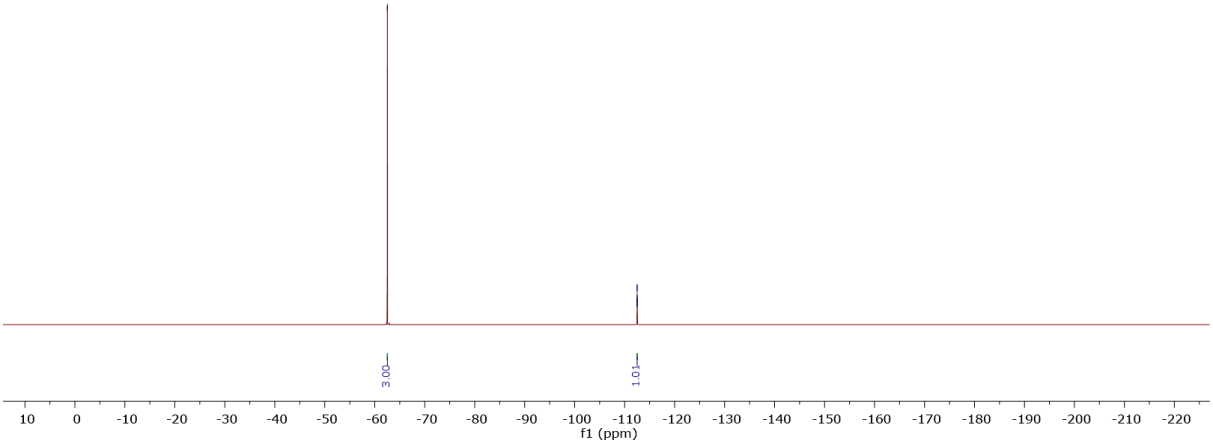

HSGN-2236.1.fid
H1 standard parameters, cryoprobe.

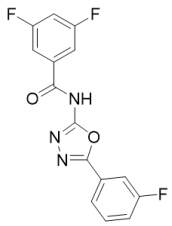

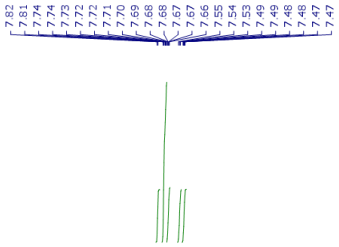

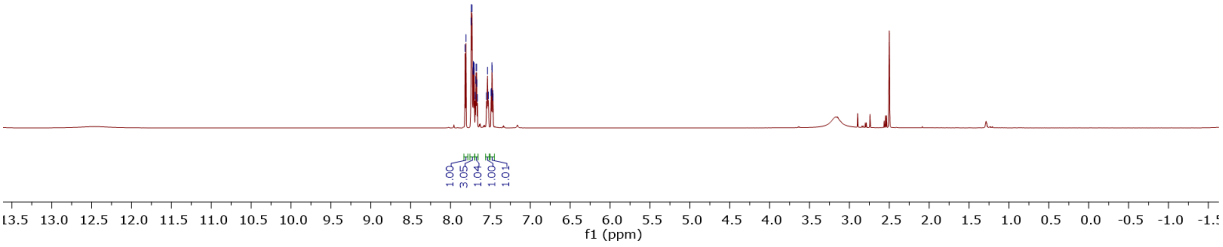

HSGN-2236.1.fid
H1 standard parameters, cryoprobe.

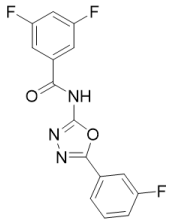

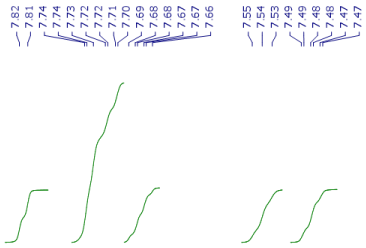

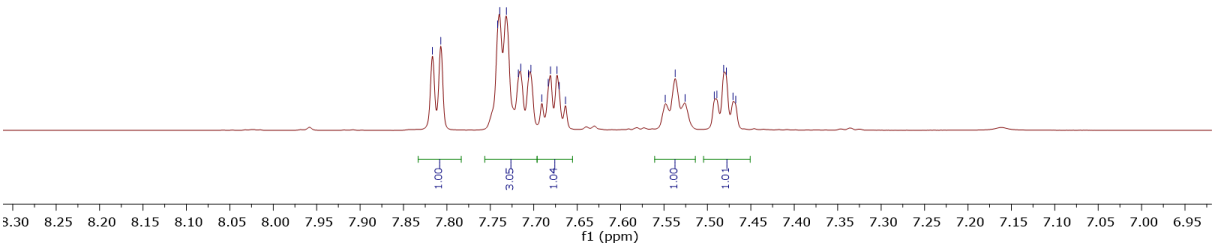

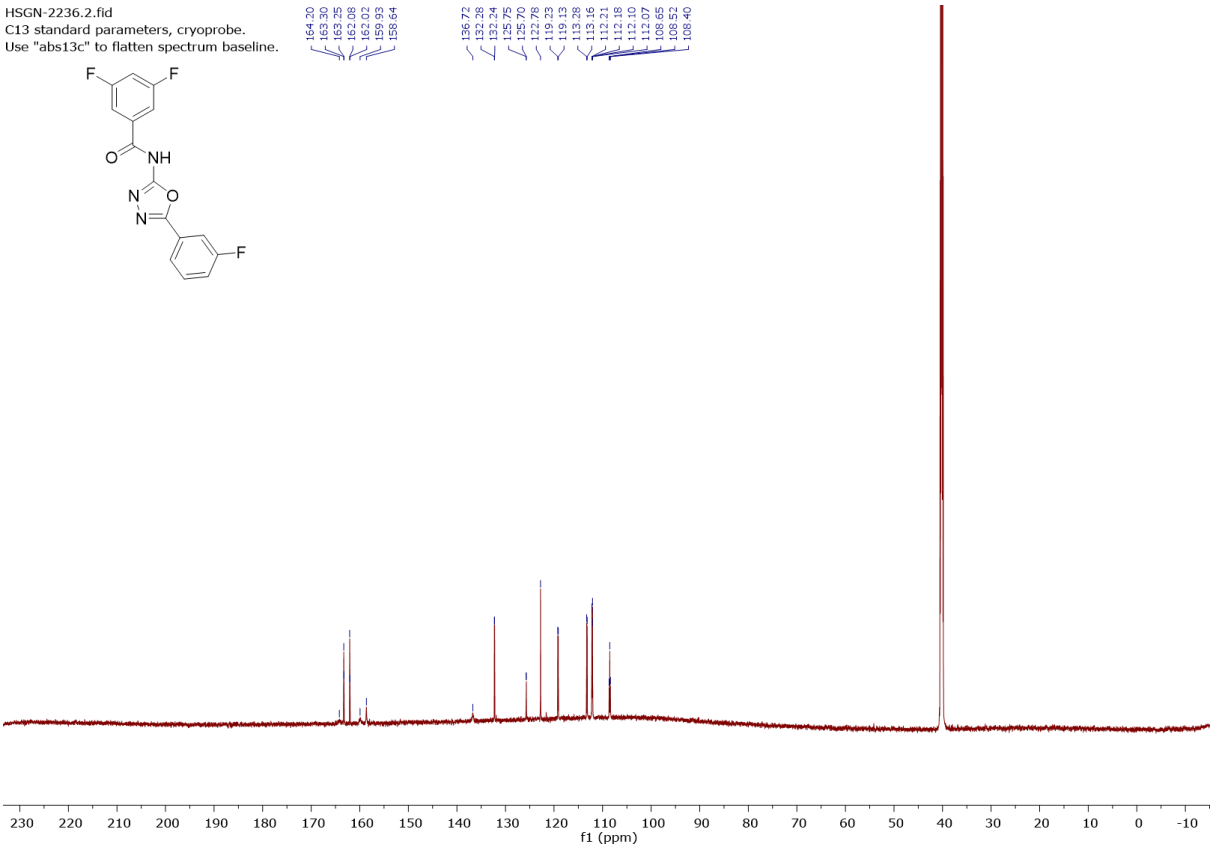
HSGN-2236.2.fid
C13 standard parameters, cryoprobe.
Use "abs13c" to flatten spectrum baseline.
164.20
163.30
163.25
162.08
162.02
159.93
158.64
136.72
132.28
132.24
125.75
125.70
122.78
119.23
119.13
113.28
113.16
112.21
112.18
112.10
112.07
108.65
108.52
108.40
F
F
O
NH
N
O
N
F
230 220 210 200 190 180 170 160 150 140 130 120 110 100 90 80 70 60 50 40 30 20 10 0 -10
f1 (ppm)

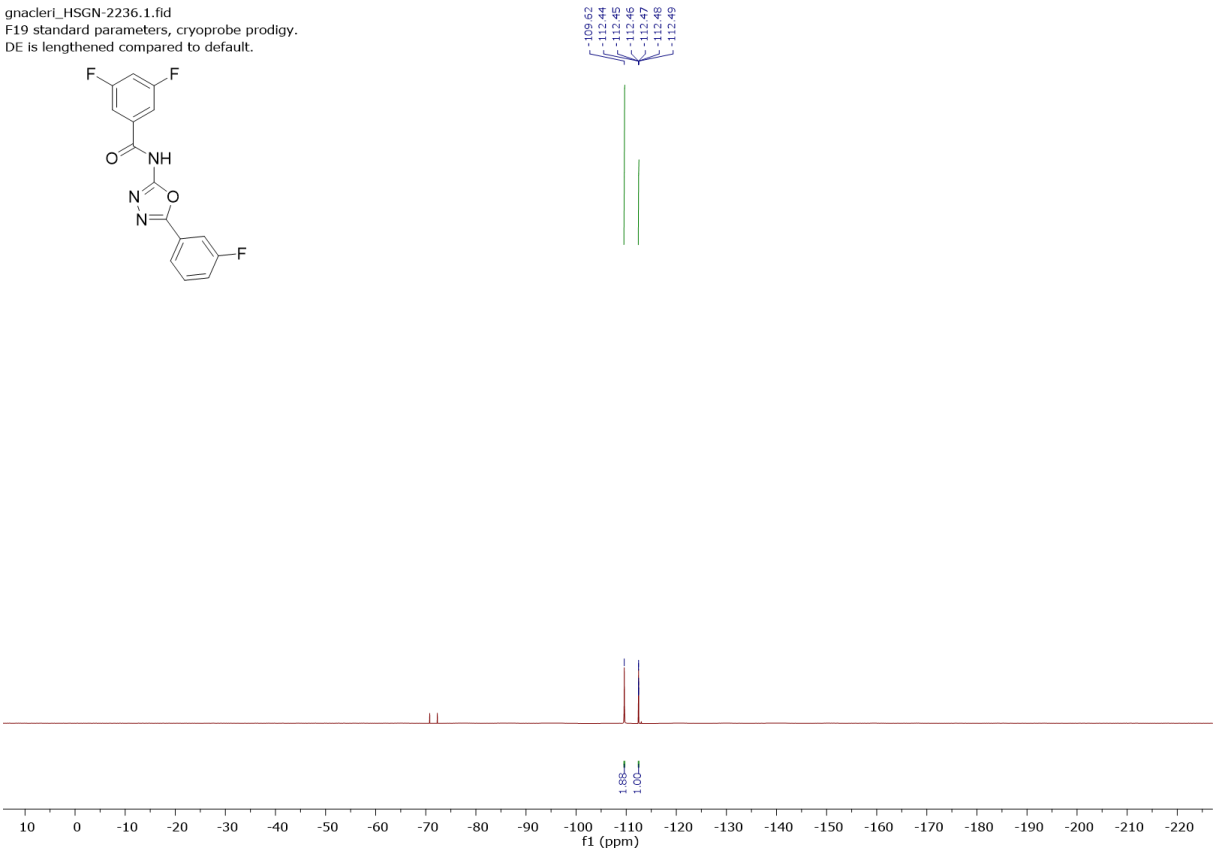
gnacleri_HSGN-2236.1.fid
F19 standard parameters, cryoprobe prodigy.
DE is lengthened compared to default.
-109.62
-112.44
-112.45
-112.46
-112.47
-112.48
-112.49
F
F
O
NH
N
O
N
F
1.88
1.00
10 0 -10 -20 -30 -40 -50 -60 -70 -80 -90 -100 -110 -120 -130 -140 -150 -160 -170 -180 -190 -200 -210 -220
f1 (ppm)

HSGN-2239.1.fid
H1 standard parameters, cryoprobe.

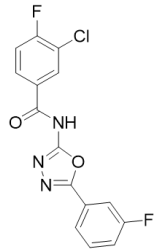

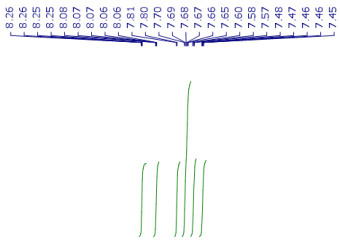

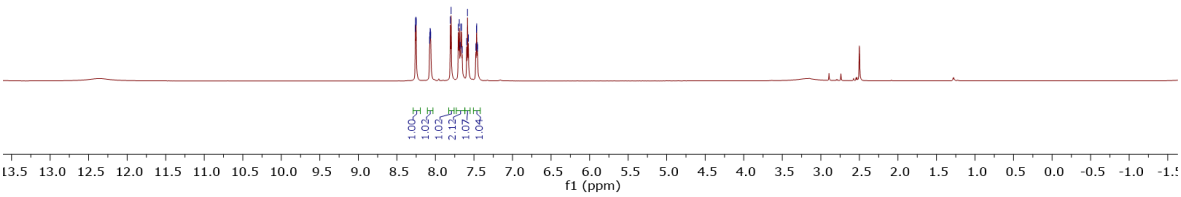

HSGN-2239.1.fid
H1 standard parameters, cryoprobe.

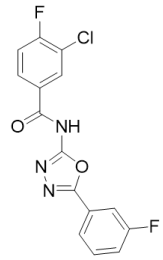

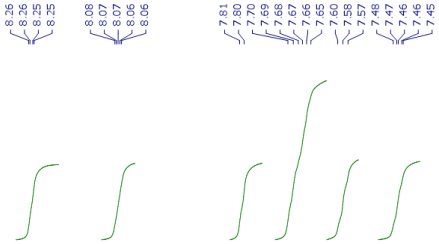

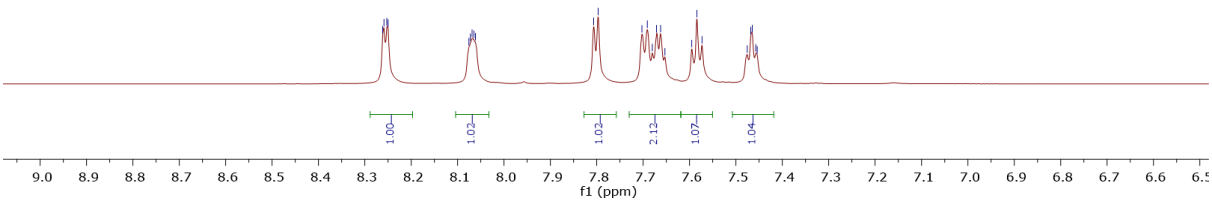

HSGN-2239.2.fid
C13 standard parameters, cryoprobe.
Use "abs13c" to flatten spectrum baseline.

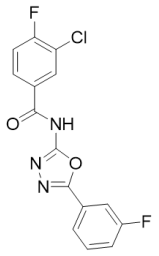

gnacleri_HSGN-2239.1.fid
F19 standard parameters, cryoprobe prodigy.
DE is lengthened compared to default.

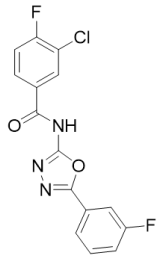

HSGN-2240.1.fid
H1 standard parameters, cryoprobe.

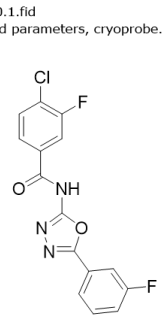

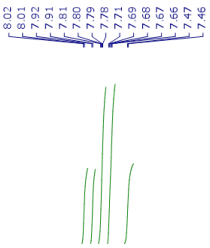

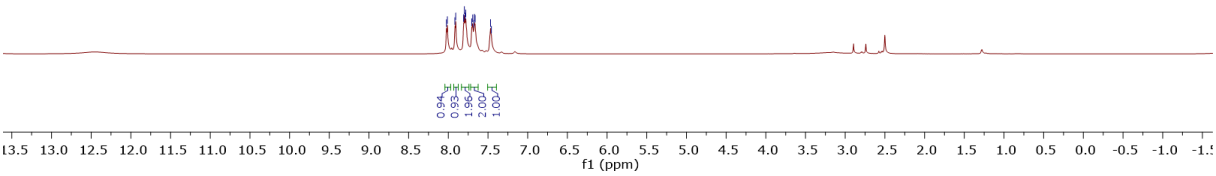

HSGN-2240.1.fid
H1 standard parameters, cryoprobe.

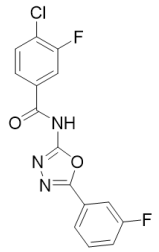

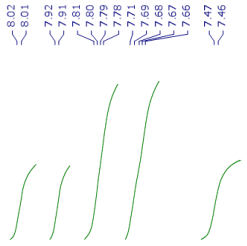

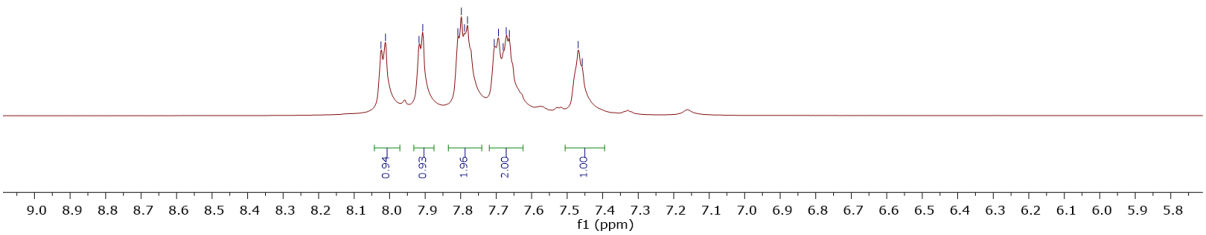

HSGN-2240.2.fid
C13 standard parameters, cryoprobe.
Use "abs13c" to flatten spectrum baseline.

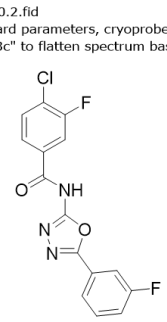

gnacleri_HSGN-2240.1.fid
F19 standard parameters, cryoprobe prodigy.
DE is lengthened compared to default.

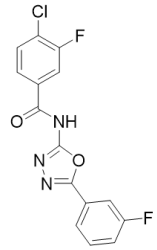

HSGN-2246.1.fid
H1 standard parameters, cryoprobe.

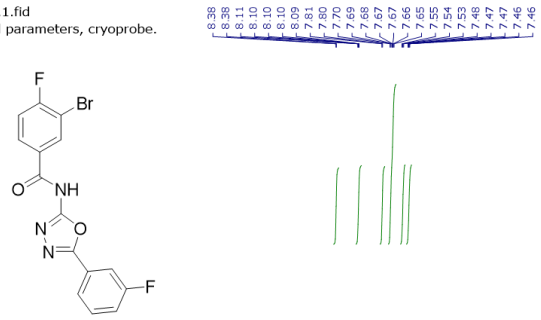

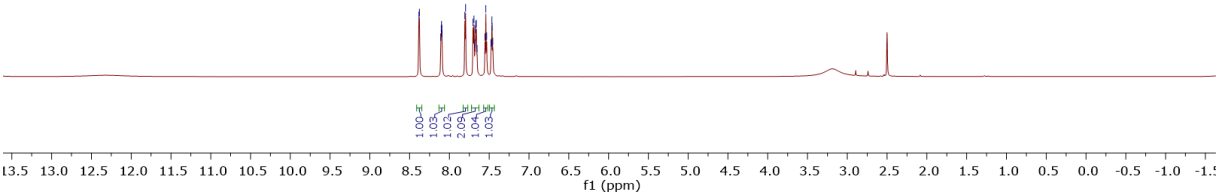

HSGN-2246.1.fid
H1 standard parameters, cryoprobe.

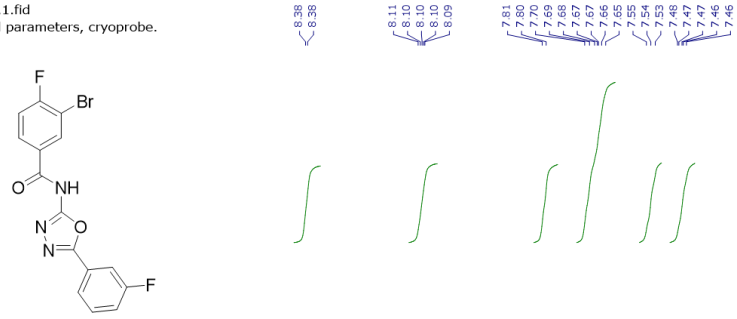

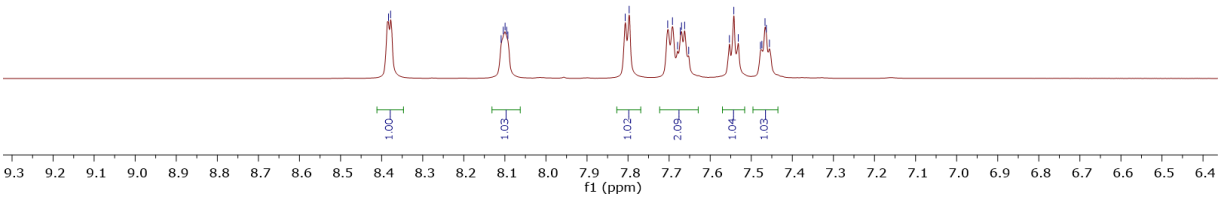

HSGN-2246.2.fid
C13 standard parameters, cryoprobe.
Use "abs13c" to flatten spectrum baseline.

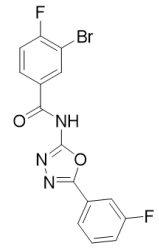

gnacleri_HSGN-2246.1.fid
F19 standard parameters, cryoprobe prodigy.
DE is lengthened compared to default.

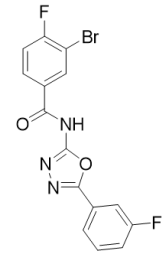

HSGN-2247.1.fid
H1 standard parameters, cryoprobe.

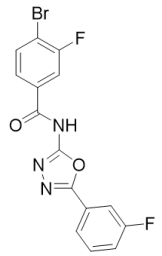

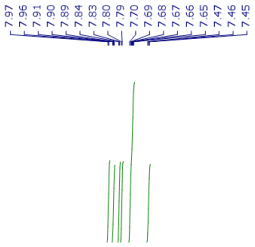

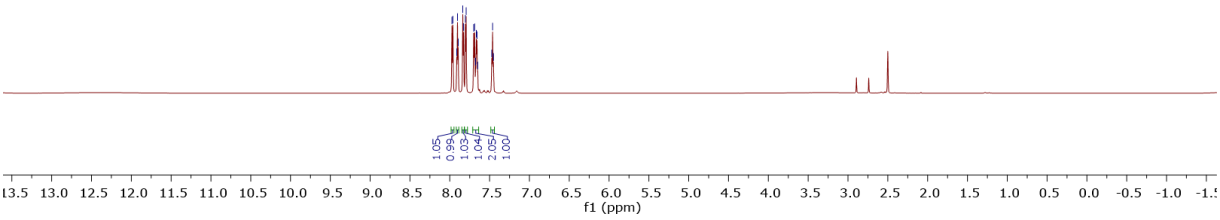

HSGN-2247.1.fid
H1 standard parameters, cryoprobe.

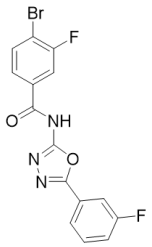

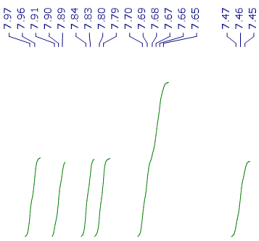

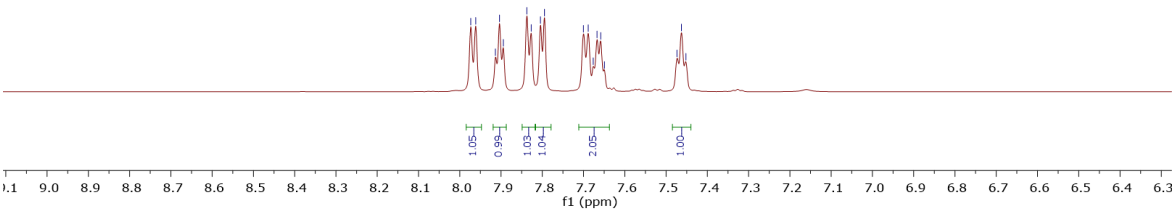

HSGN-2247.2.fid
C13 standard parameters, cryoprobe.
Use "abs13c" to flatten spectrum baseline.

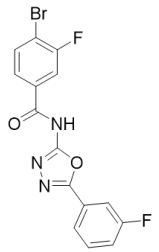

gnacleri_HSGN-2247.1.fid
F19 standard parameters, cryoprobe prodigy.
DE is lengthened compared to default.

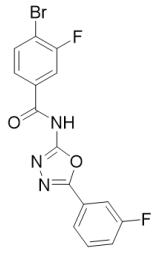

HSGN-2241.1.fid
H1 standard parameters, cryoprobe.

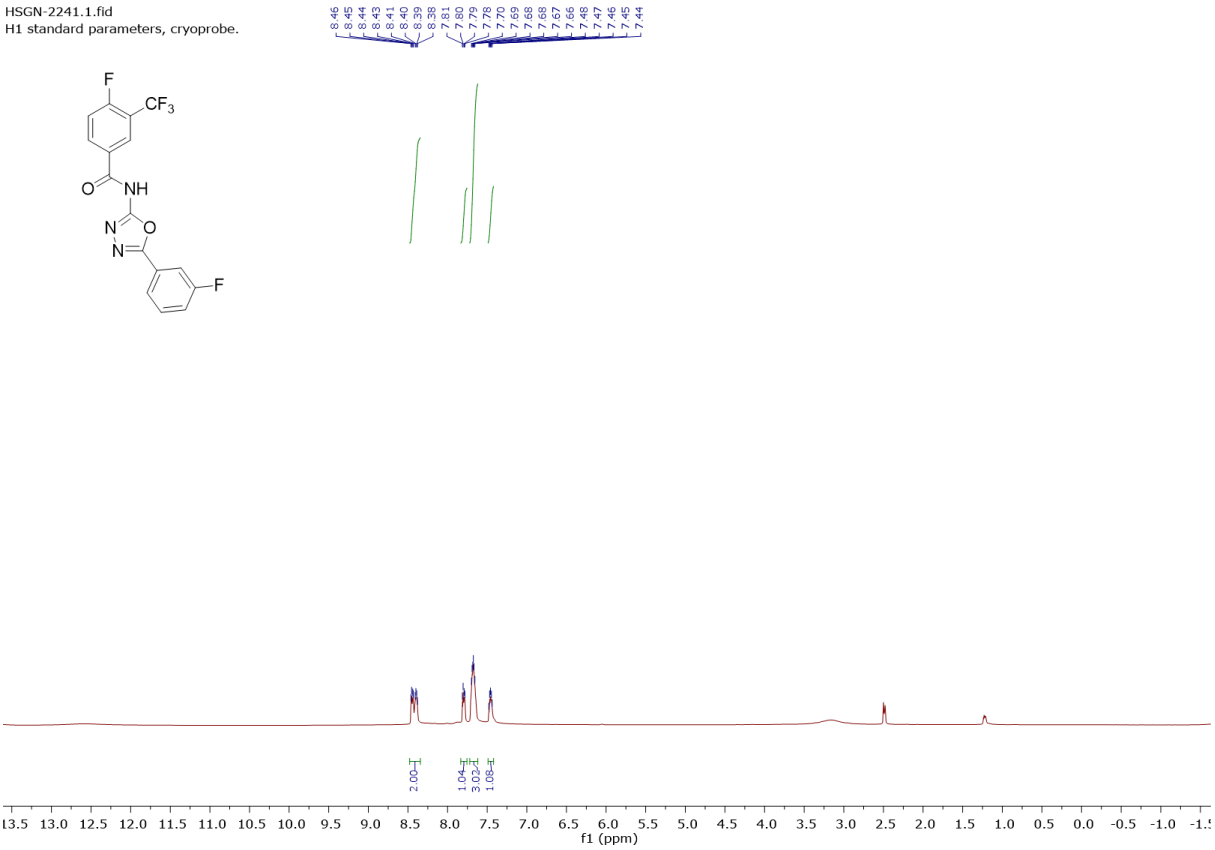

HSGN-2241.1.fid
H1 standard parameters, cryoprobe.

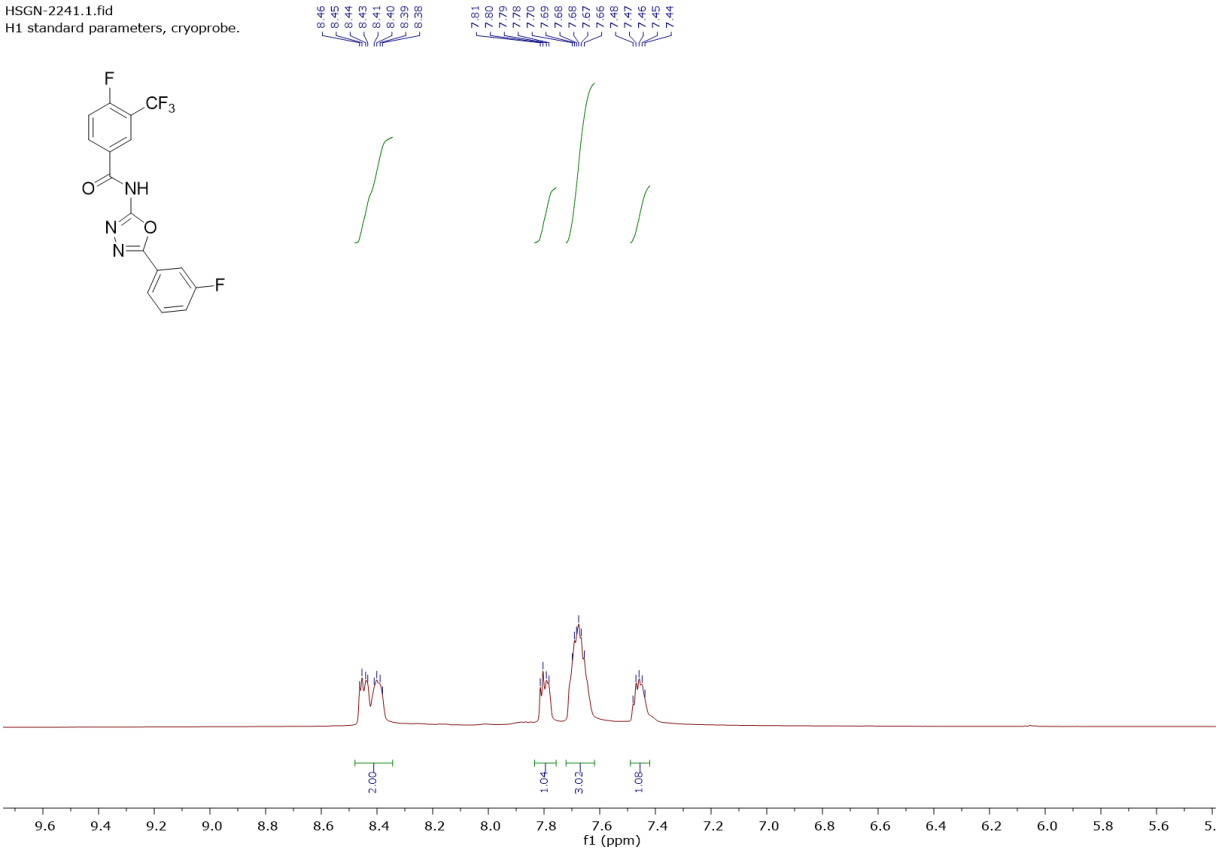

HSGN-2241.2.fid
C13 standard parameters, cryoprobe.
Use "abs13c" to flatten spectrum baseline.

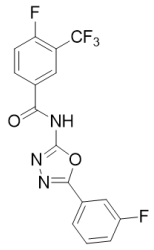

gnacleri_HSGN-2241.1.fid
F19 standard parameters, cryoprobe prodigy.
DE is lengthened compared to default.

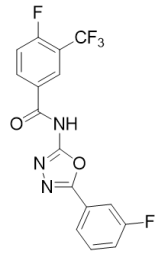

HSGN-2263_2.1.fid
H1 standard parameters, cryoprobe.

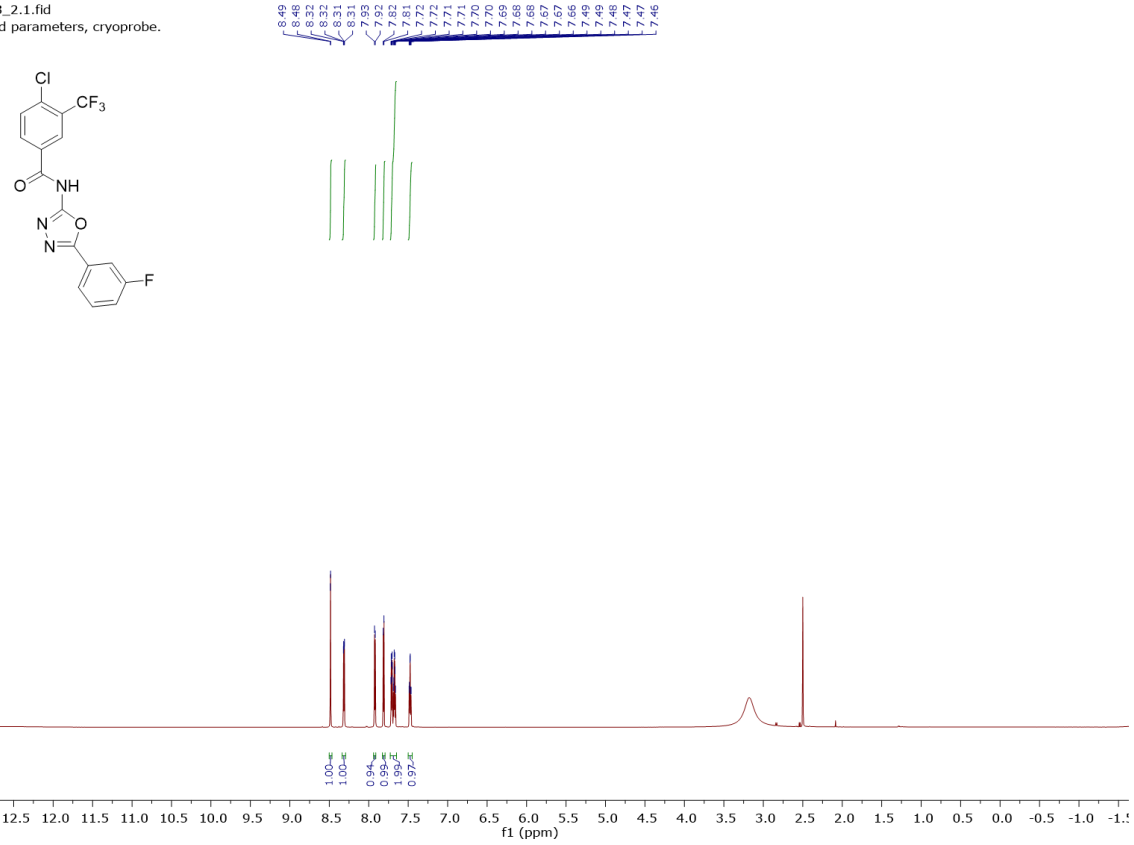

HSGN-2263_2.1.fid
H1 standard parameters, cryoprobe.

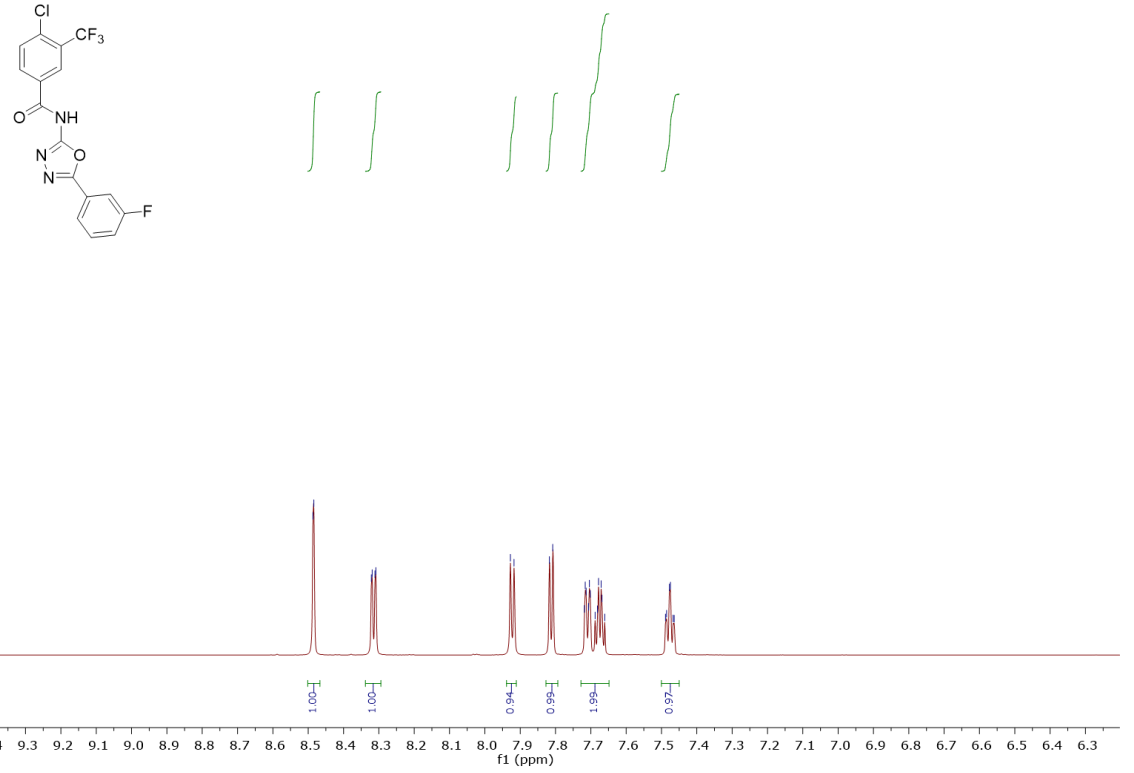

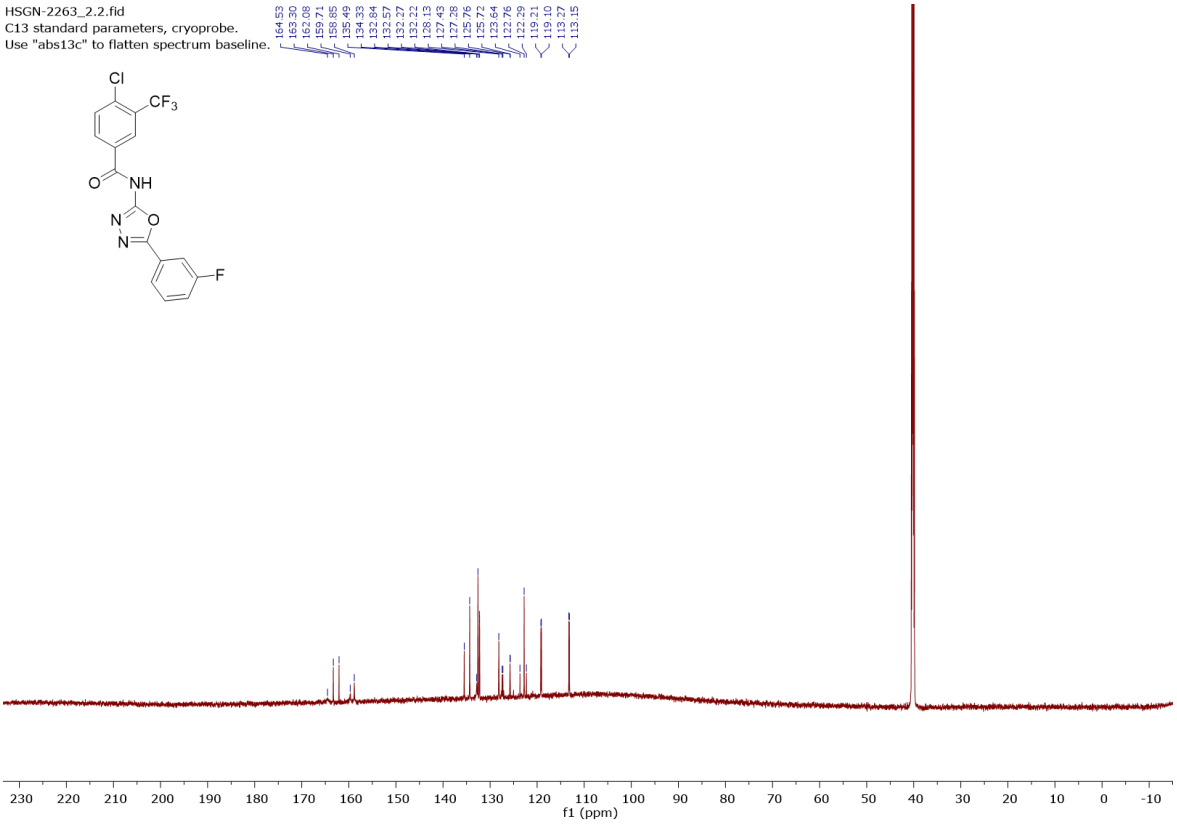
HSGN-2263_2.2.fid
C13 standard parameters, cryoprobe.
Use "abs13c" to flatten spectrum baseline.
164.53
163.30
162.08
159.71
158.85
135.49
134.33
132.84
132.57
132.27
132.22
130.13
127.43
127.28
125.76
125.72
123.64
122.76
122.29
119.21
119.10
113.27
113.15
Cl
CF3
O
NH
N
O
N
F
230 220 210 200 190 180 170 160 150 140 130 120 110 100 90 80 70 60 50 40 30 20 10 0 -10
f1 (ppm)

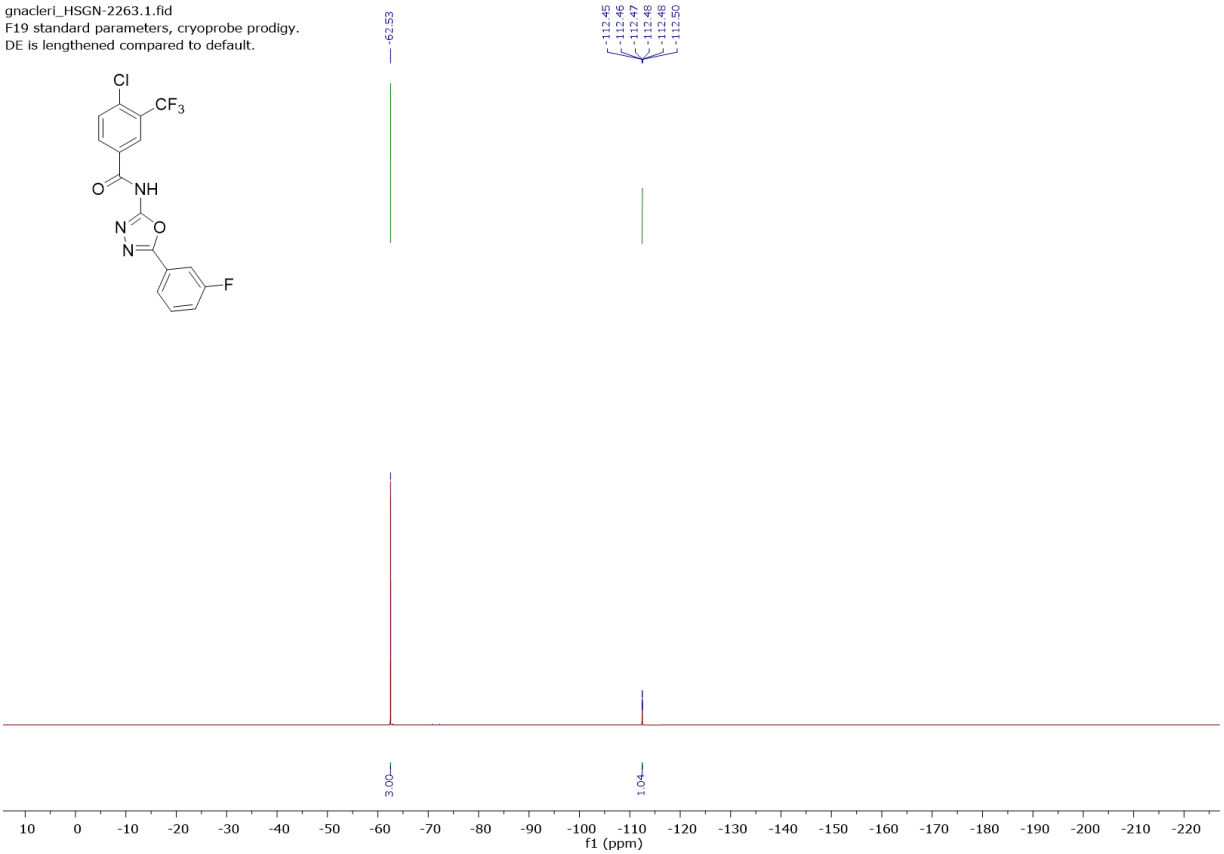
gnacleri_HSGN-2263.1.fid
F19 standard parameters, cryoprobe prodigy.
DE is lengthened compared to default.
-62.53
-112.45
-112.46
-112.47
-112.48
-112.48
-112.48
-112.50
Cl
CF3
O
NH
N
O
N
F
3.00
1.04
10 0 -10 -20 -30 -40 -50 -60 -70 -80 -90 -100 -110 -120 -130 -140 -150 -160 -170 -180 -190 -200 -210 -220
f1 (ppm)

HSGN-2262.1.fid
H1 standard parameters, cryoprobe.

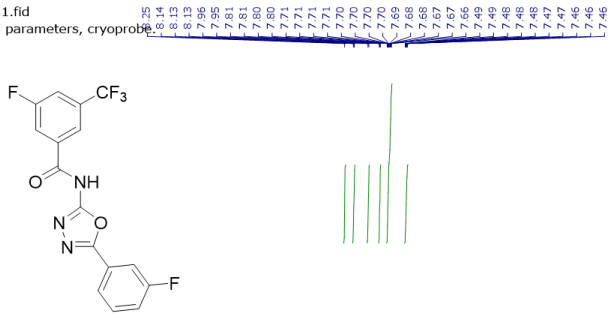

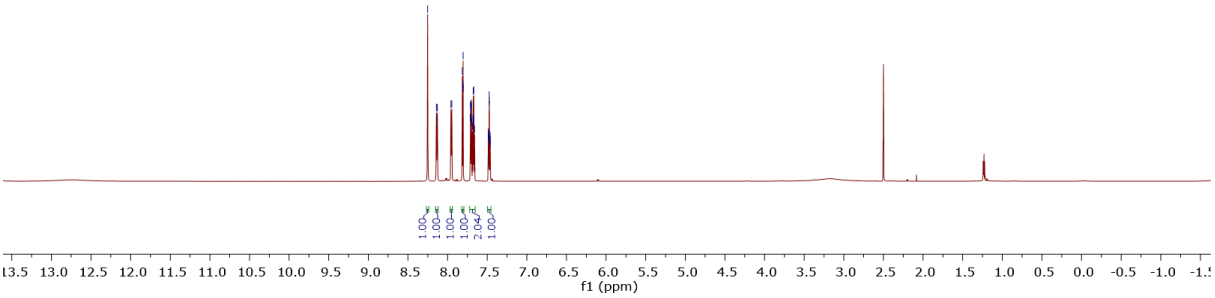

HSGN-2262.1.fid
H1 standard parameters, cryoprobe.

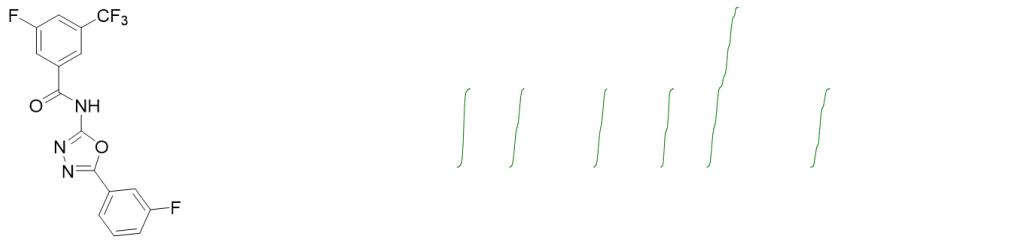

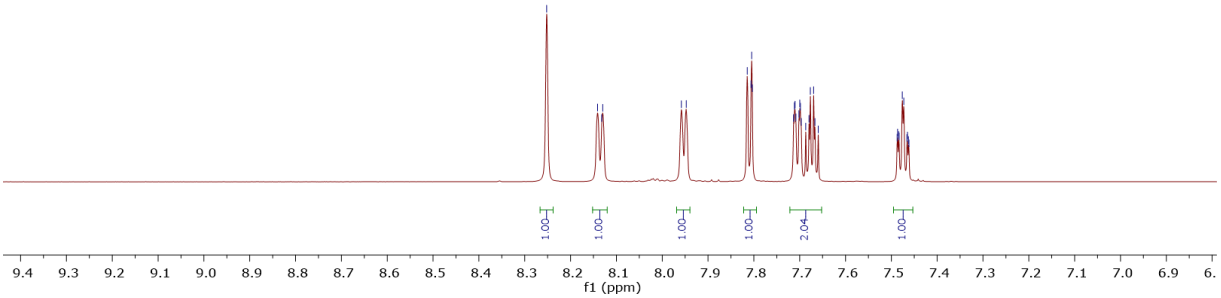

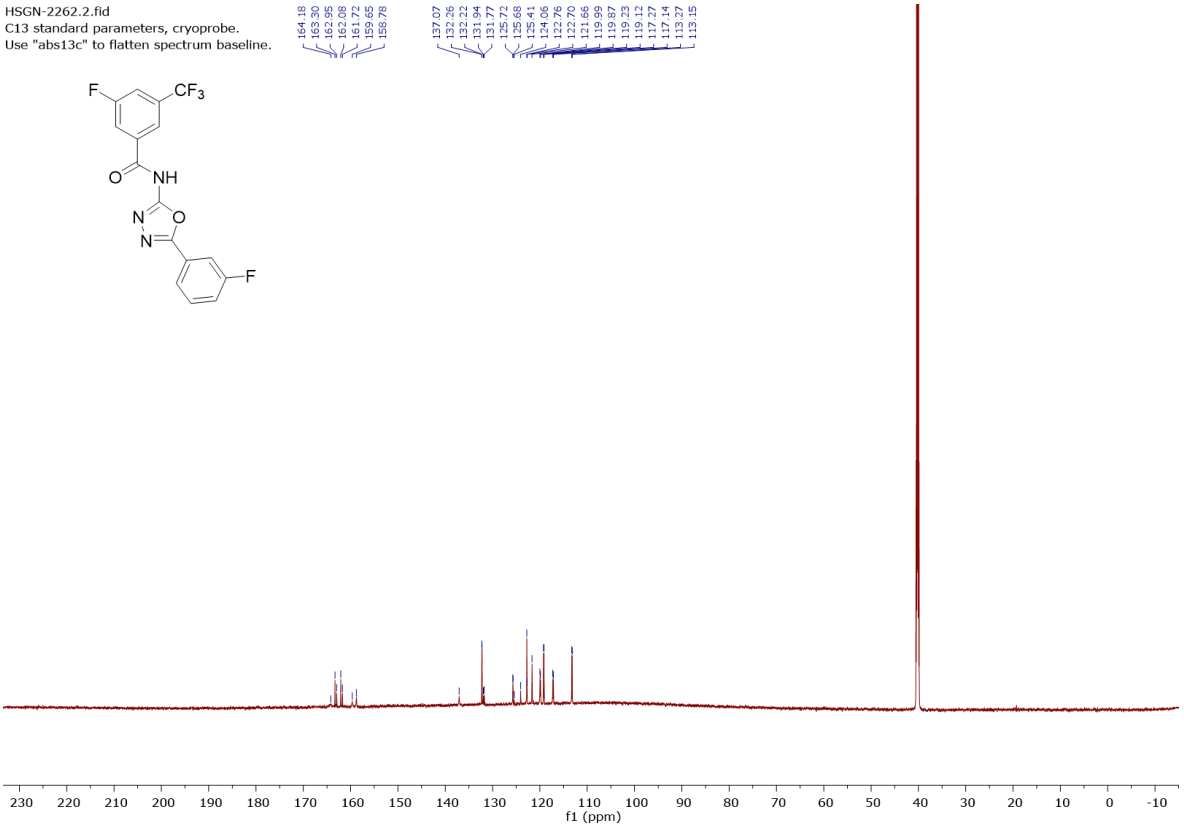
HSGN-2262.2.fid
C13 standard parameters, cryoprobe.
Use "abs13c" to flatten spectrum baseline.
164.18
163.30
162.85
162.08
161.72
159.65
158.78
137.07
132.26
132.22
131.94
131.77
125.72
125.68
125.41
124.06
122.76
122.70
121.66
119.99
119.87
119.23
119.12
117.27
117.14
113.27
113.15
F
CF3
O
NH
N
O
N
F
230 220 210 200 190 180 170 160 150 140 130 120 110 100 90 80 70 60 50 40 30 20 10 0 -10
f1 (ppm)

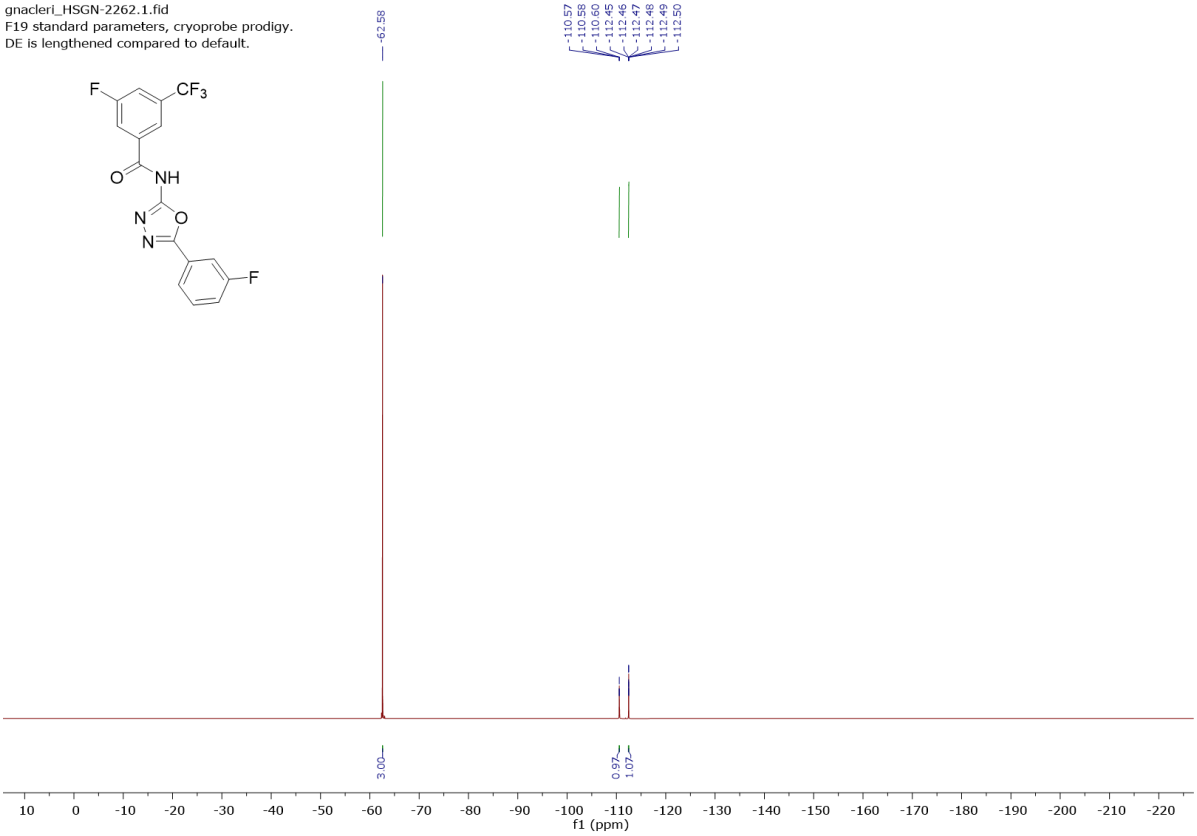
gnacleri_HSGN-2262.1.fid
F19 standard parameters, cryoprobe prodigy.
DE is lengthened compared to default.
-62.58
-110.57
-110.58
-110.60
-112.45
-112.46
-112.47
-112.48
-112.49
-112.50
F
CF3
O
NH
N
O
N
F
3.00
0.97
1.07
10 0 -10 -20 -30 -40 -50 -60 -70 -80 -90 -100 -110 -120 -130 -140 -150 -160 -170 -180 -190 -200 -210 -220
f1 (ppm)

HSGN-2242.1.fid
H1 standard parameters, cryoprobe.

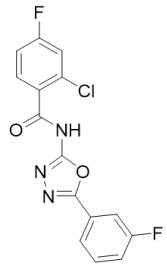

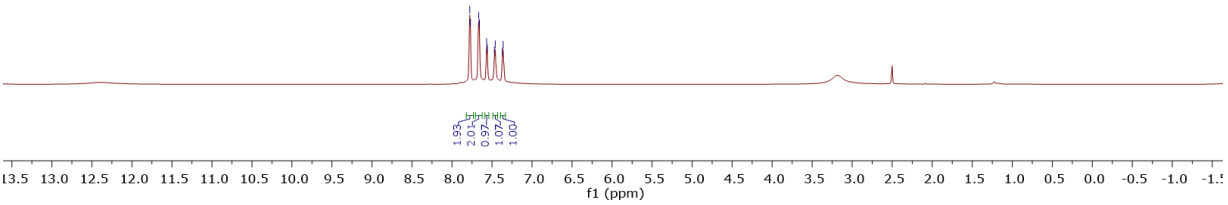

HSGN-2242.1.fid
H1 standard parameters, cryoprobe.

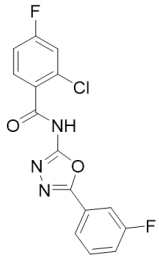

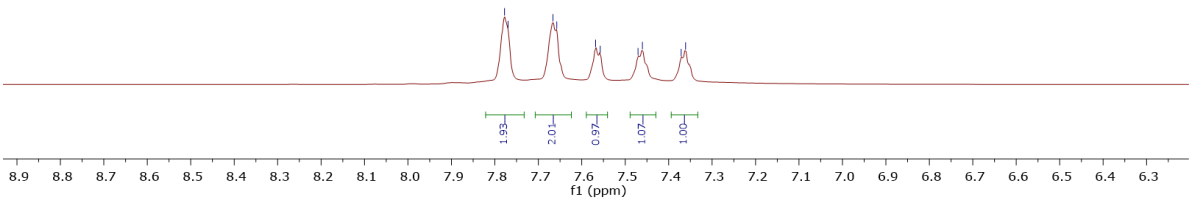

HSGN-2242.2.fid
C13 standard parameters, cryoprobe.
Use "abs13c" to flatten spectrum baseline.

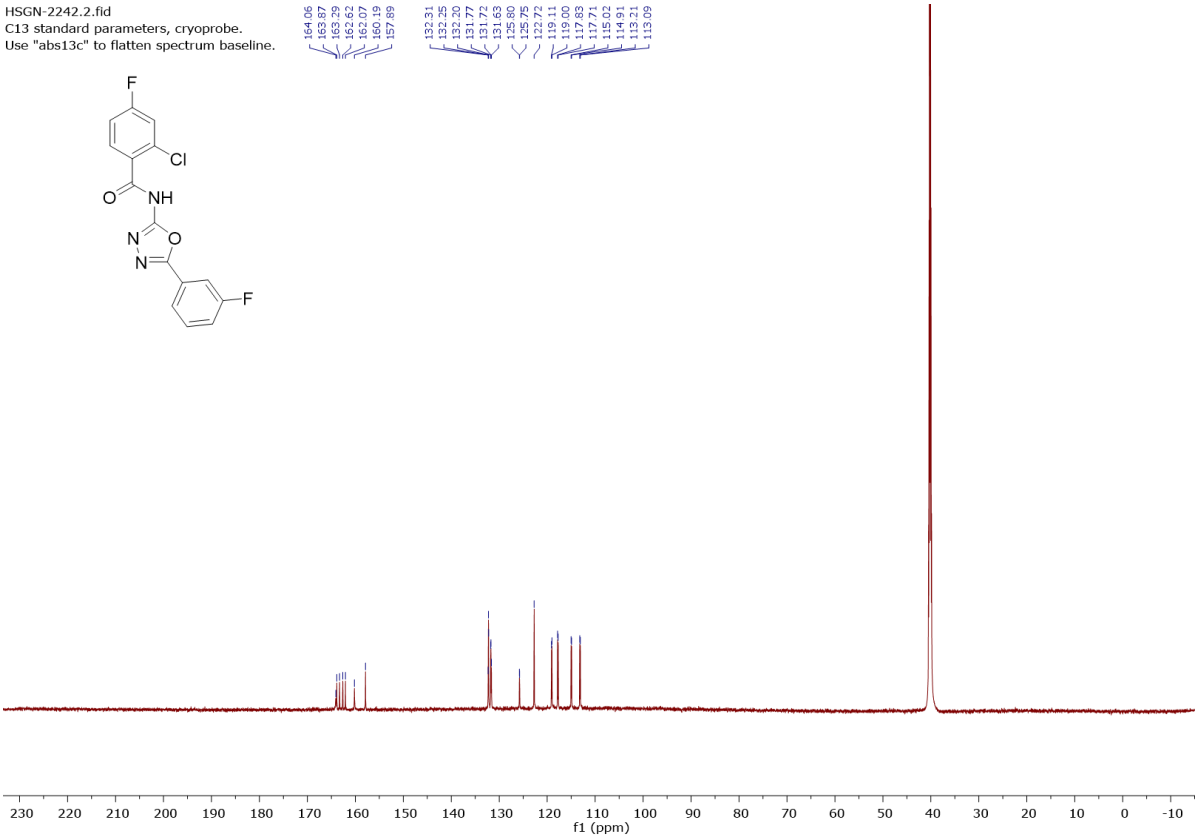

gnacleri_HSGN-2242.1.fid
F19 standard parameters, cryoprobe prodigy.
DE is lengthened compared to default.

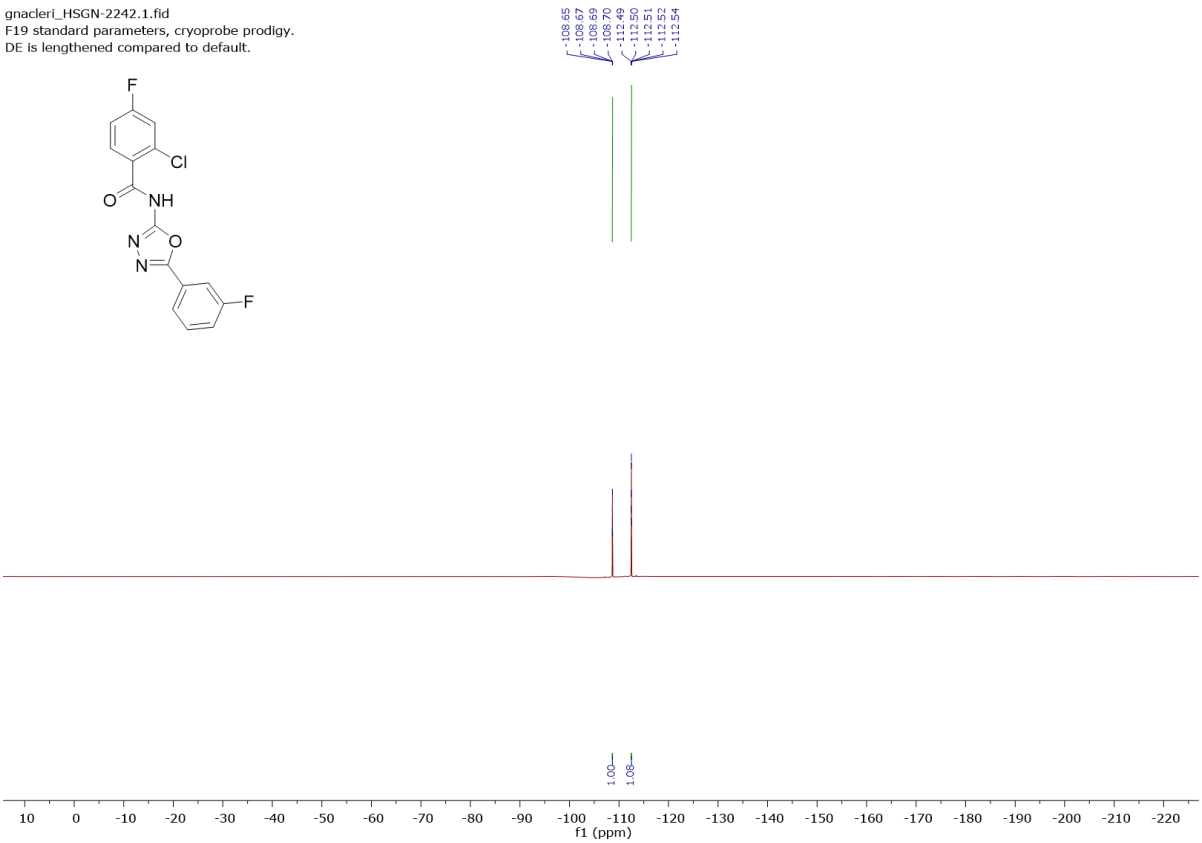

HSGN-2243.1.fid
H1 standard parameters, cryoprobe.

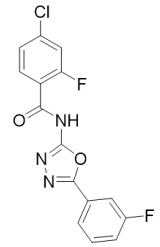

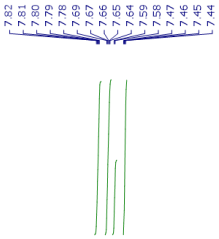

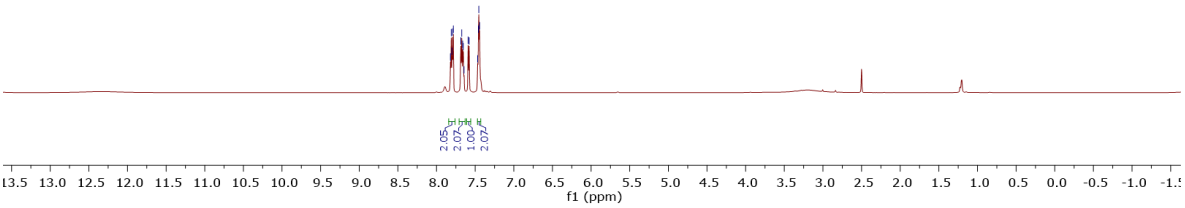

HSGN-2243.1.fid
H1 standard parameters, cryoprobe.

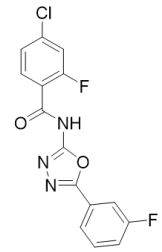

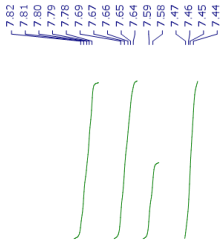

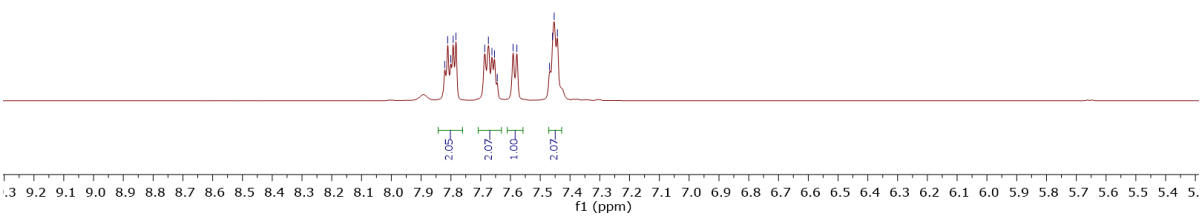

HSGN-2243.2.fid
C13 standard parameters, cryoprobe.
Use "abs13c" to flatten spectrum baseline.

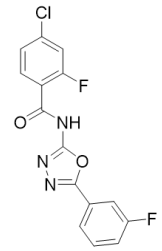

gnacleri_HSGN-2243.1.fid
F19 standard parameters, cryoprobe prodigy.
DE is lengthened compared to default.

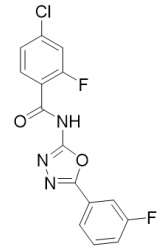

HSGN-2248.1.fid
H1 standard parameters, cryoprobe.

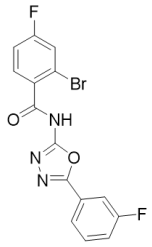

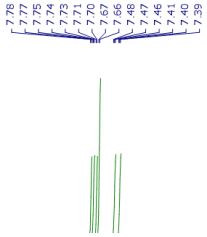

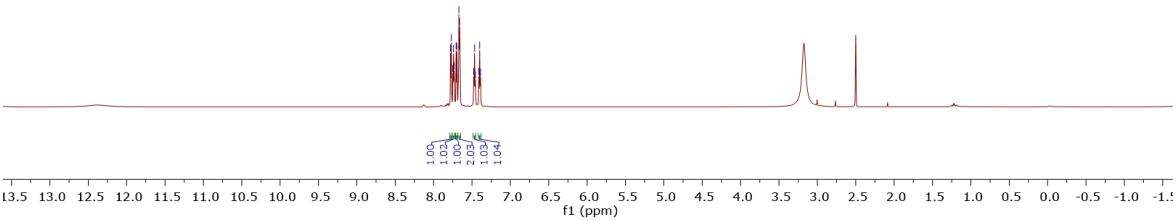

HSGN-2248.1.fid
H1 standard parameters, cryoprobe.

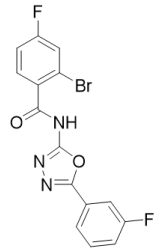

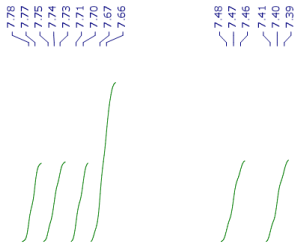

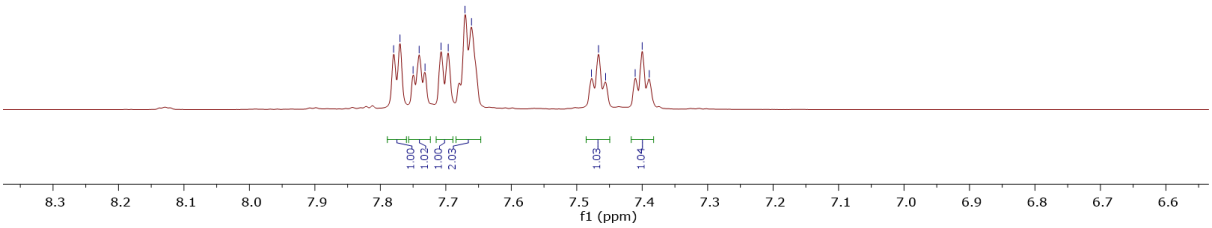

HSGN-2248.2.fid
C13 standard parameters, cryoprobe.
Use "abs13c" to flatten spectrum baseline.

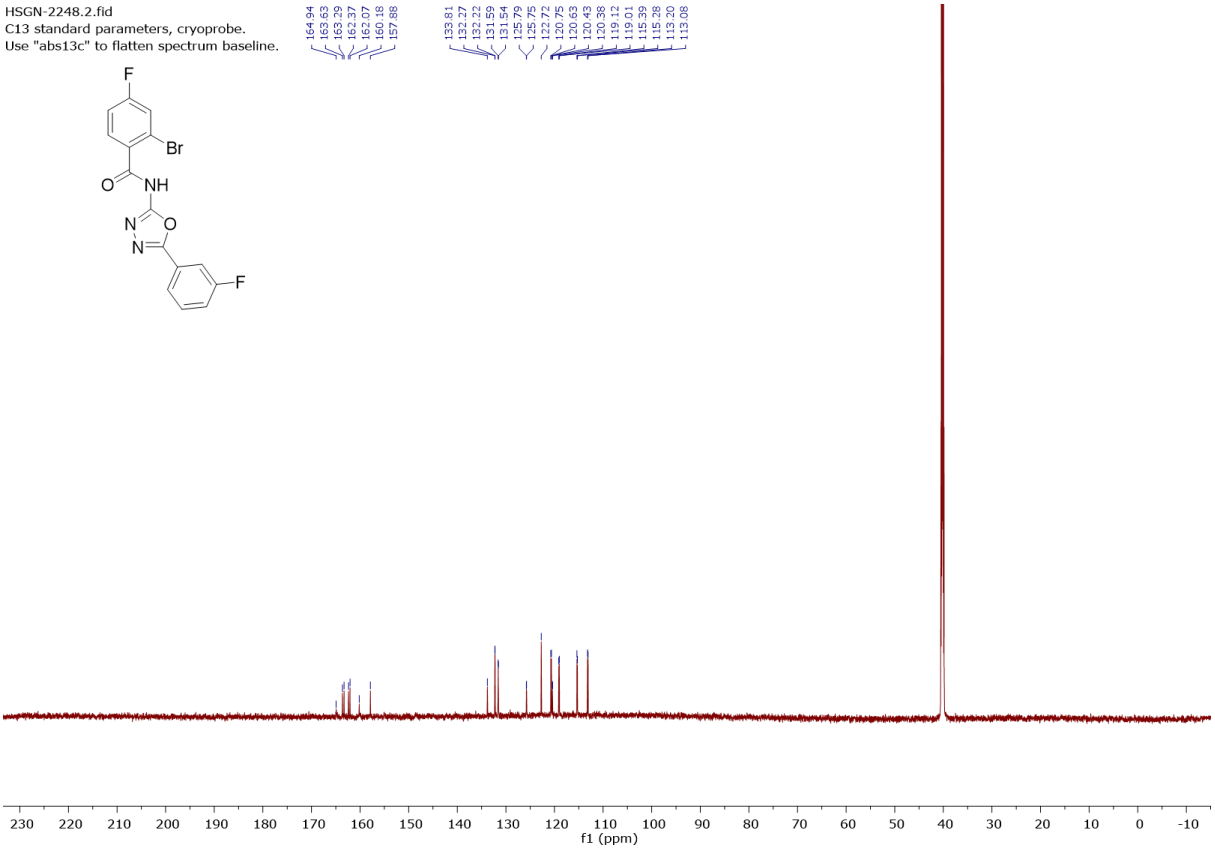

gnacleri_HSGN-2248.1.fid
F19 standard parameters, cryoprobe prodigy.
DE is lengthened compared to default.

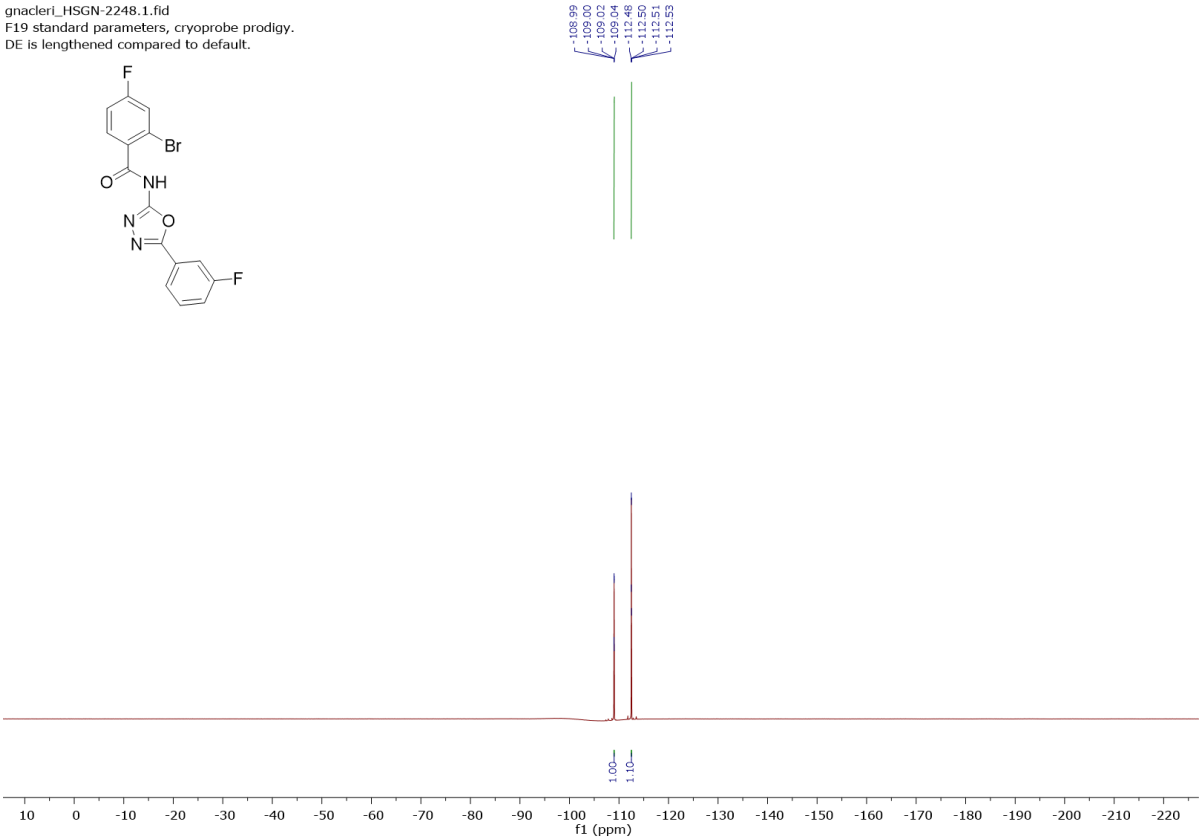

HSGN-2249.1.fid
H1 standard parameters, cryoprobe.

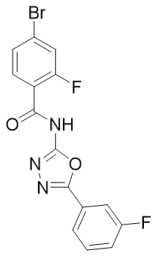

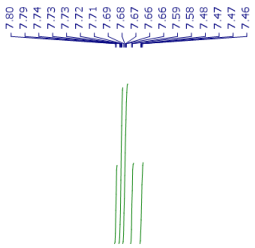

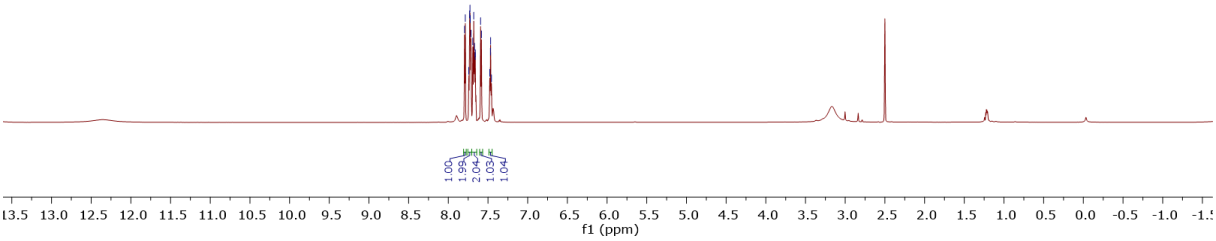

HSGN-2249.1.fid
H1 standard parameters, cryoprobe.

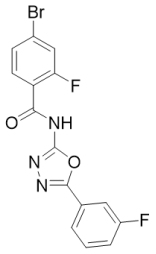

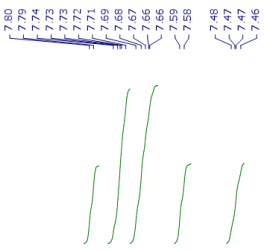

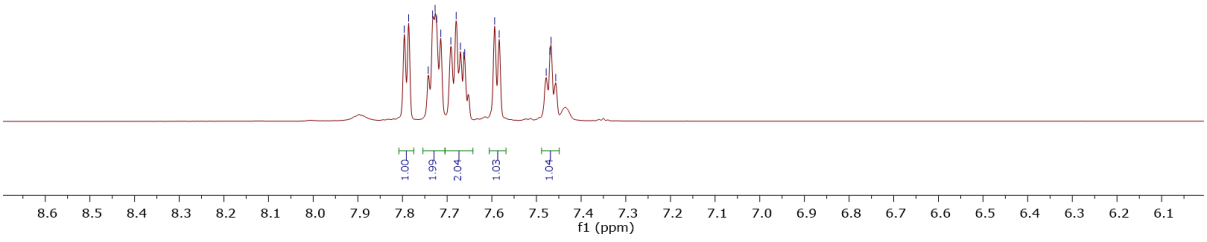

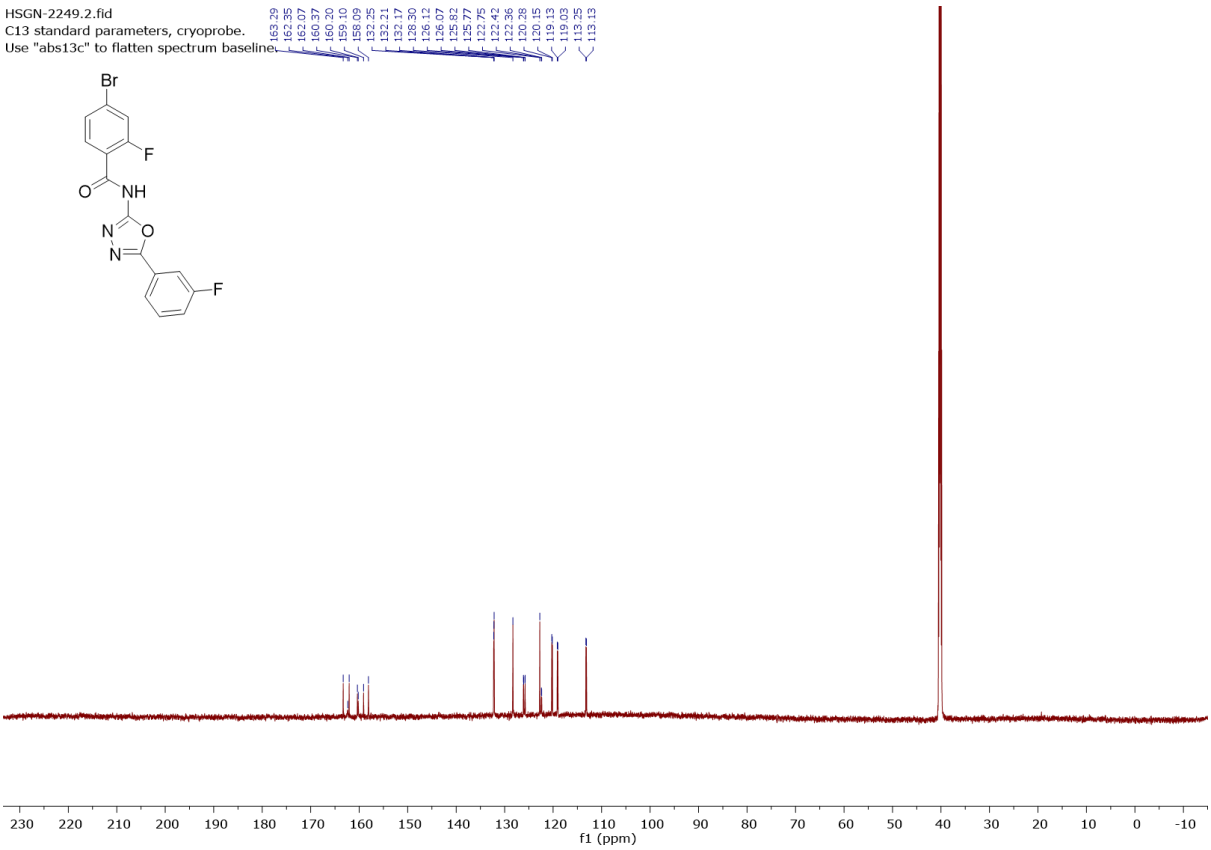
HSGN-2249.2.fid
C13 standard parameters, cryoprobe.
Use "abs13c" to flatten spectrum baseline.
163.29
162.35
162.07
160.37
160.20
159.10
158.09
132.25
132.21
132.17
128.30
126.12
126.07
125.82
125.77
122.75
122.42
122.36
120.28
120.15
119.13
119.03
113.25
113.13
Br
F
O
NH
N
O
N
F
230 220 210 200 190 180 170 160 150 140 130 120 110 100 90 80 70 60 50 40 30 20 10 0 -10
f1 (ppm)

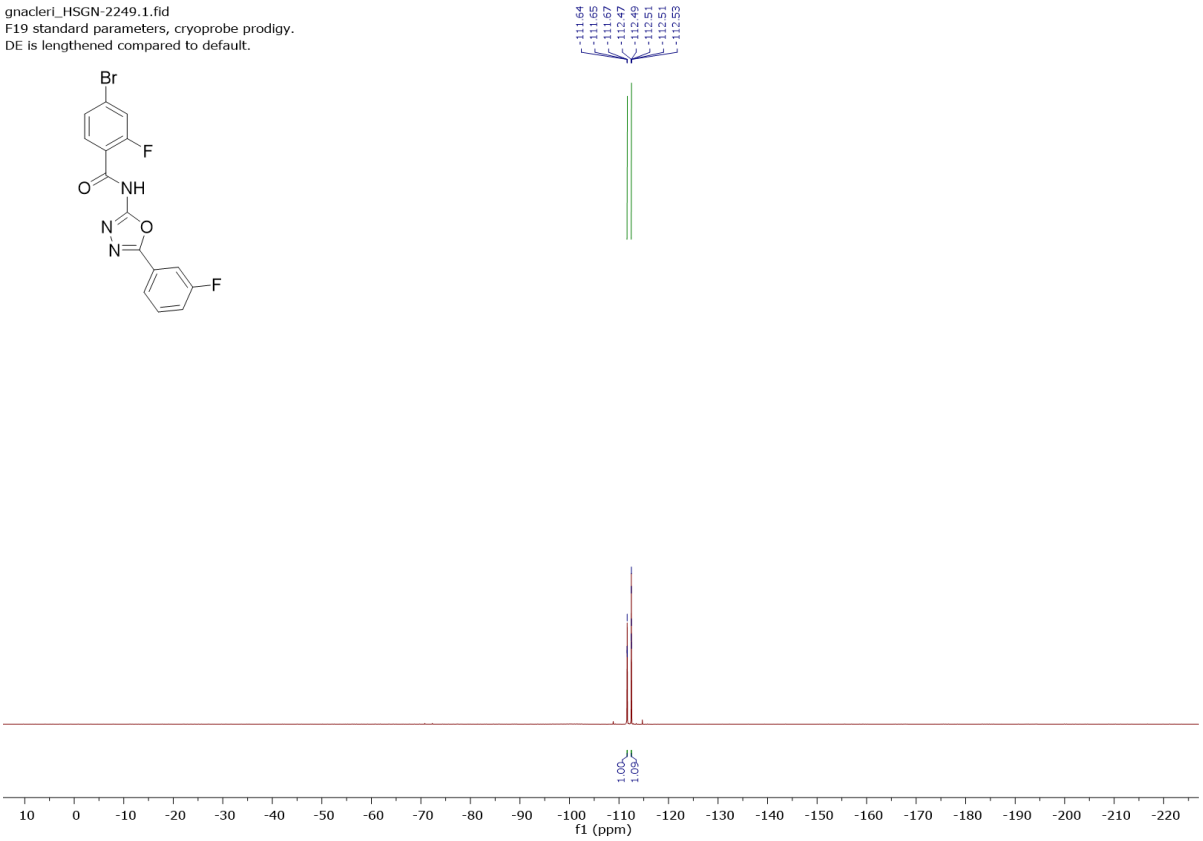
gnacleri_HSGN-2249.1.fid
F19 standard parameters, cryoprobe prodigy.
DE is lengthened compared to default.
-111.64
-111.65
-111.67
-112.47
-112.49
-112.51
-112.51
-112.51
-112.53
Br
F
O
NH
N
O
N
F
1.00
1.09
10 0 -10 -20 -30 -40 -50 -60 -70 -80 -90 -100 -110 -120 -130 -140 -150 -160 -170 -180 -190 -200 -210 -220
f1 (ppm)

HSGN-2252.1.fid
H1 standard parameters, cryoprobe.

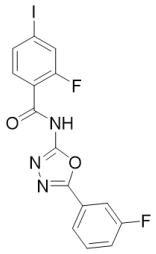

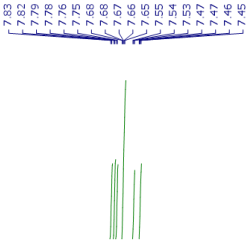

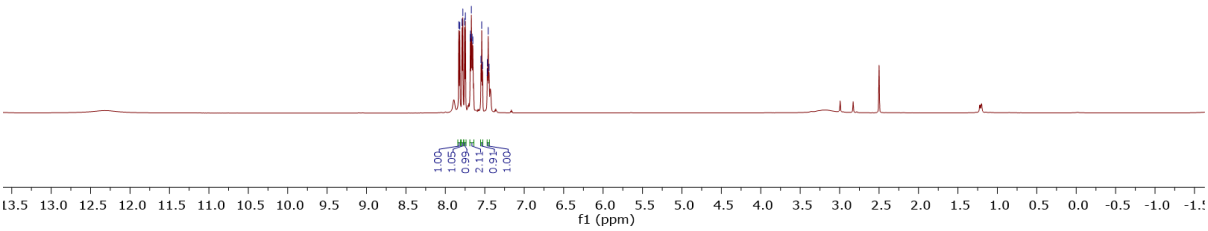

HSGN-2252.1.fid
H1 standard parameters, cryoprobe.

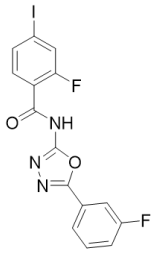

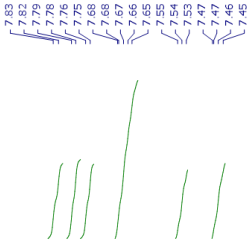

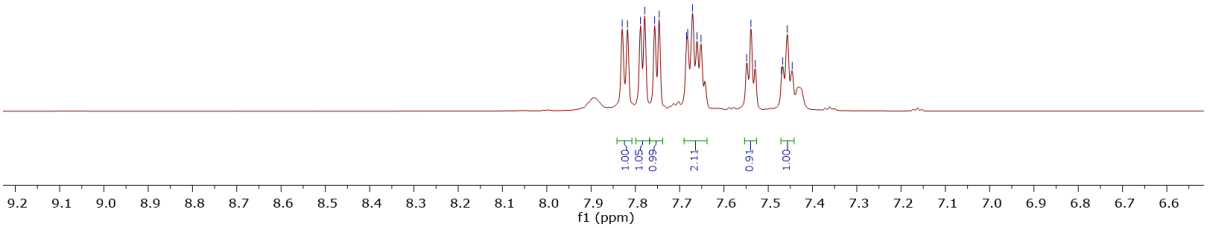

HSGN-2252.2.fid
C13 standard parameters, cryoprobe.
Use "abs13c" to flatten spectrum baseline.

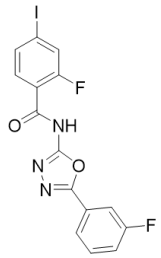

gnacleri_HSGN-2252.1.fid
F19 standard parameters, cryoprobe prodigy.
DE is lengthened compared to default.

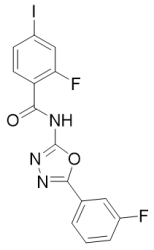

HSGN-2255.1.fid
H1 standard parameters, cryoprobe.

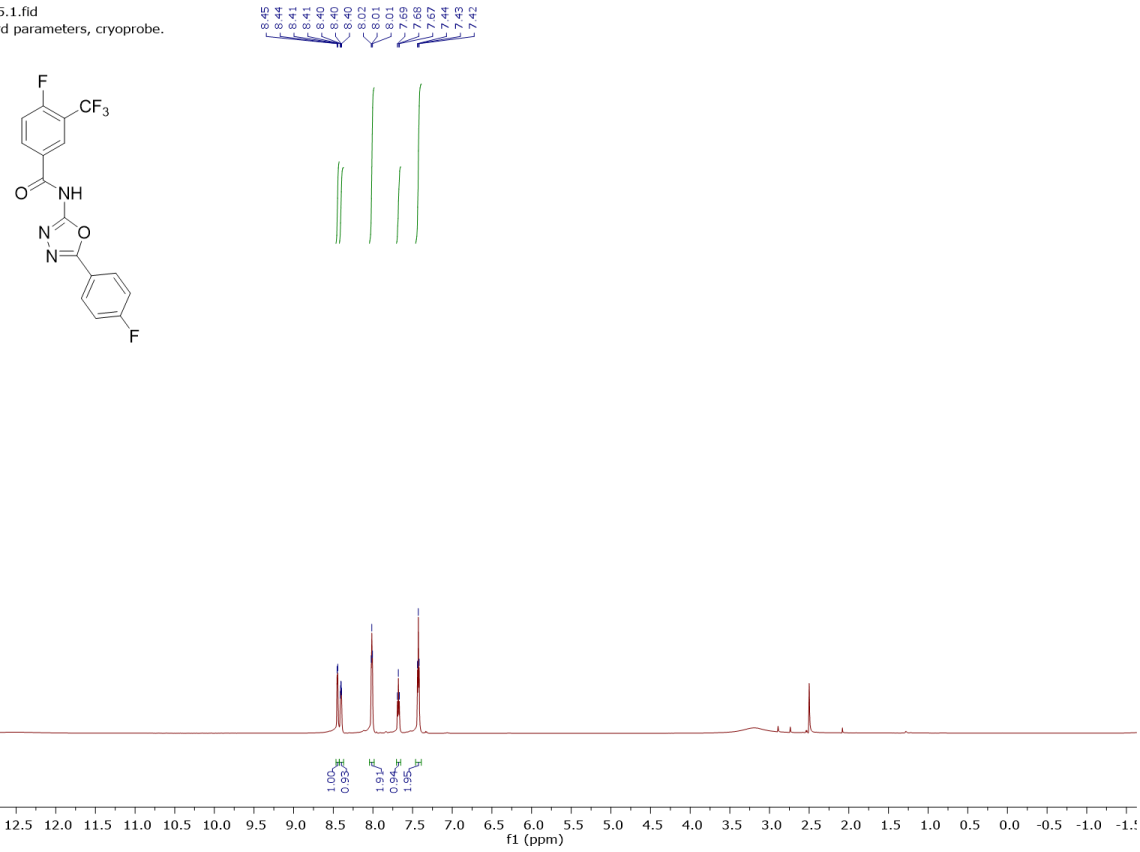

HSGN-2255.1.fid
H1 standard parameters, cryoprobe.

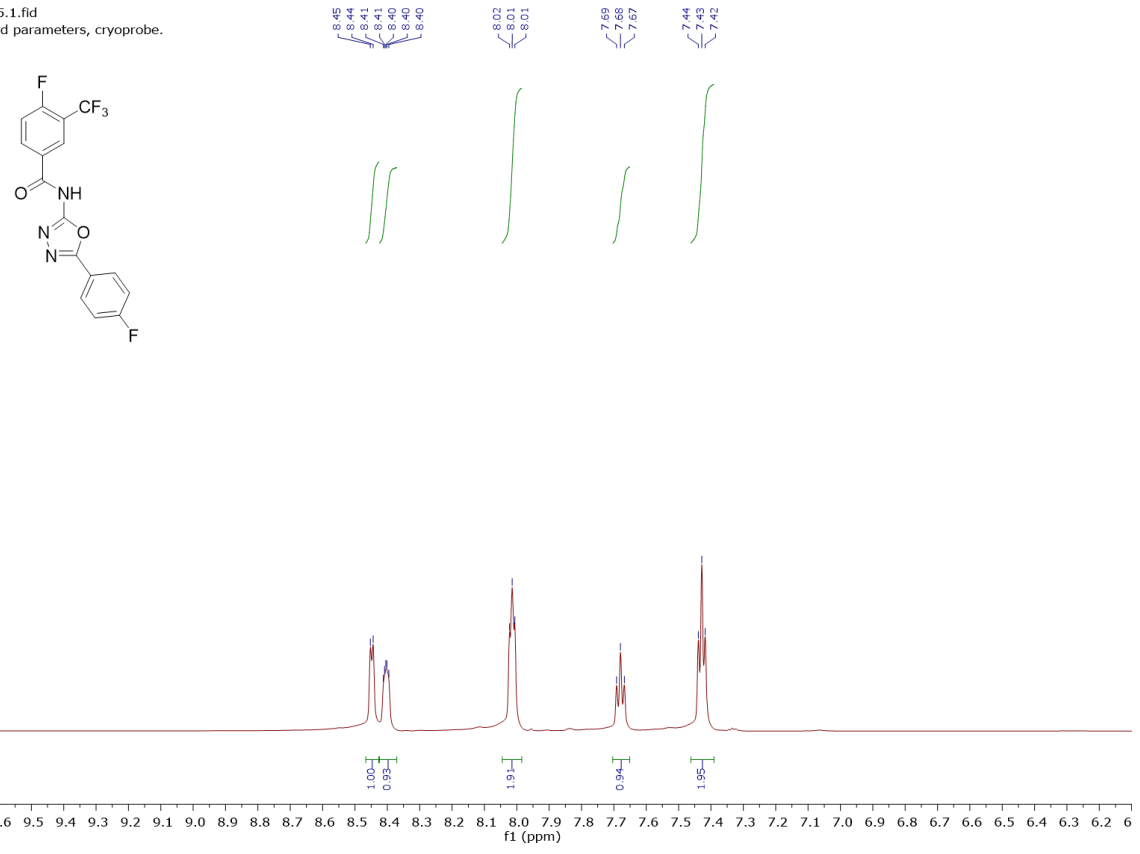

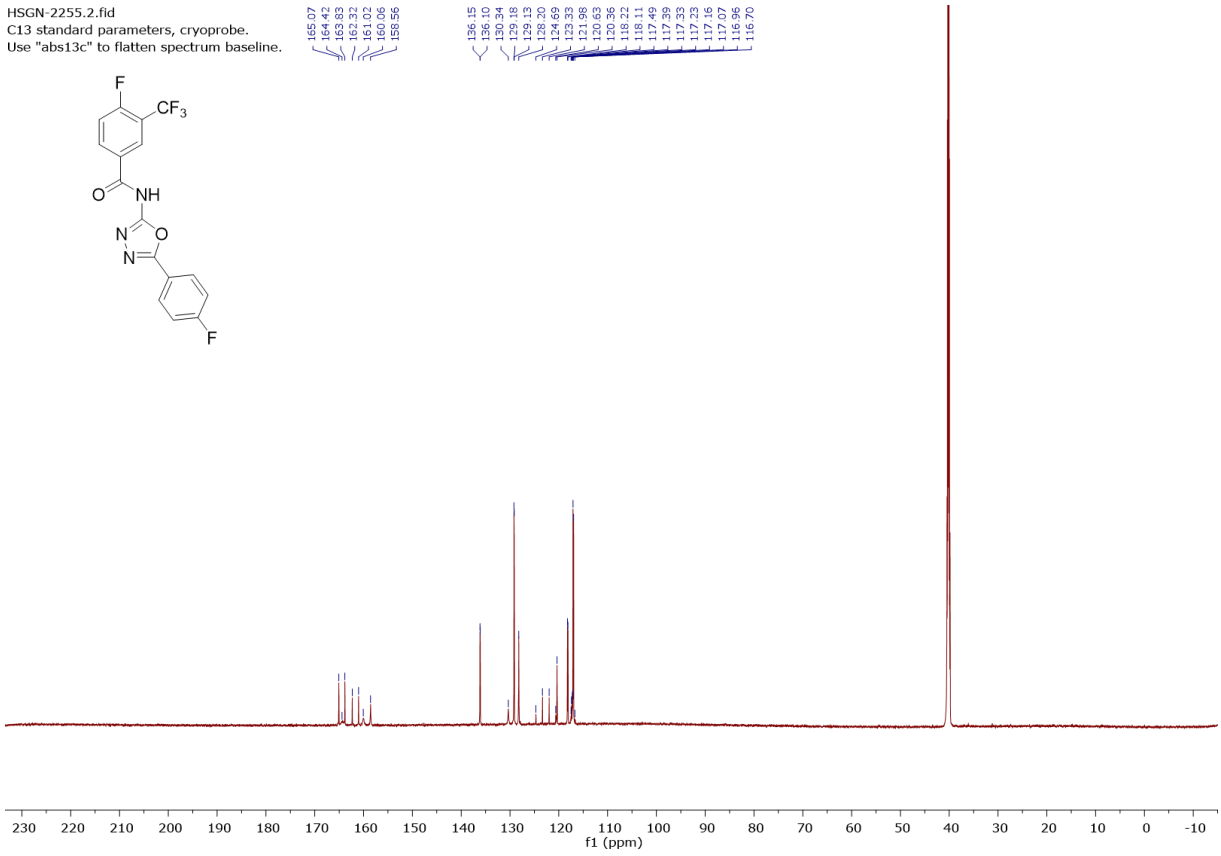
HSGN-2255.2.fid
C13 standard parameters, cryoprobe.
Use "abs13c" to flatten spectrum baseline.
165.07
164.42
163.83
162.32
161.02
160.06
158.56
136.15
136.10
130.34
129.18
129.13
128.20
124.69
123.33
121.98
120.65
120.35
118.22
118.11
117.49
117.39
117.33
117.23
117.16
117.07
116.96
116.70
F
CF3
O
NH
N
O
N
F
230 220 210 200 190 180 170 160 150 140 130 120 110 100 90 80 70 60 50 40 30 20 10 0 -10
f1 (ppm)

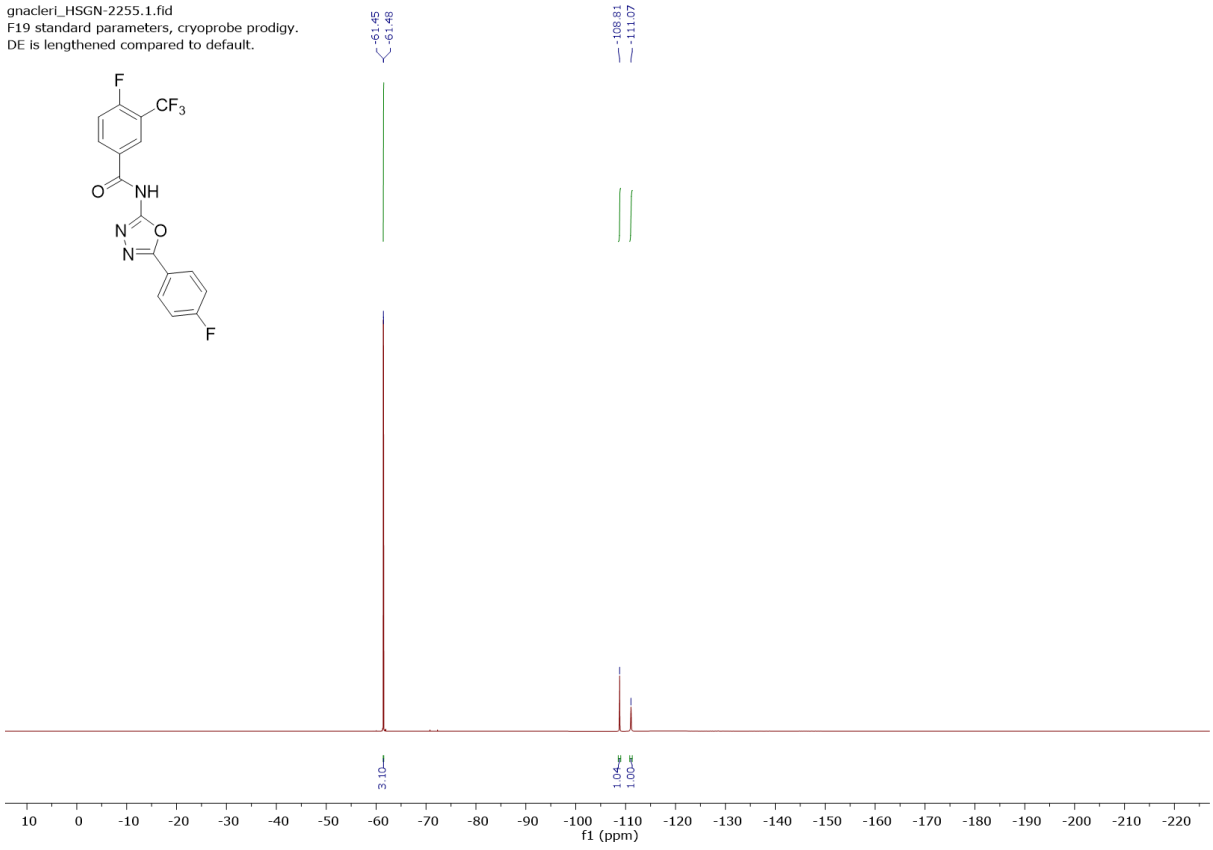
gnacleri_HSGN-2255.1.fid
F19 standard parameters, cryoprobe prodigy.
DE is lengthened compared to default.
-61.45
-61.48
-108.81
-111.07
F
CF3
O
NH
N
O
N
F
3.10
1.04
1.00
10 0 -10 -20 -30 -40 -50 -60 -70 -80 -90 -100 -110 -120 -130 -140 -150 -160 -170 -180 -190 -200 -210 -220
f1 (ppm)

HSGN-2256.1.fid
H1 standard parameters, cryoprobe.

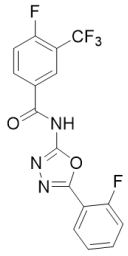

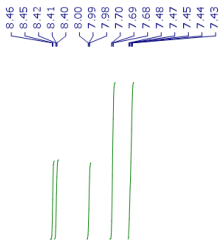

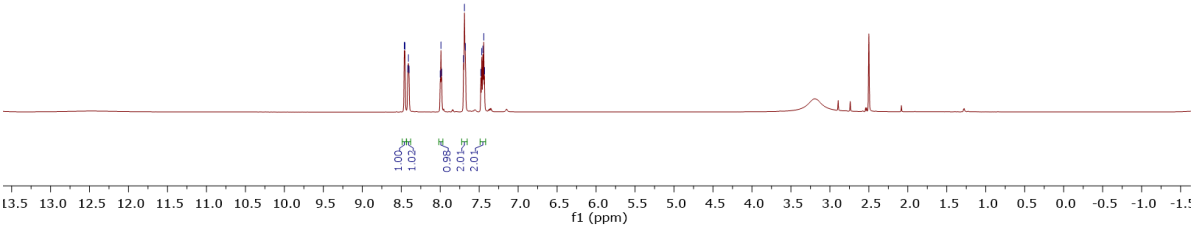

HSGN-2256.1.fid
H1 standard parameters, cryoprobe.

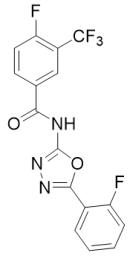

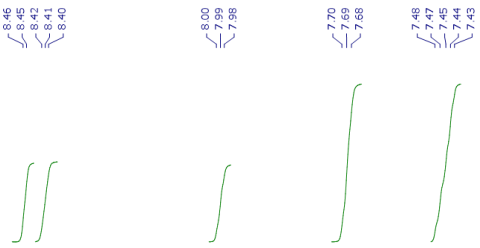

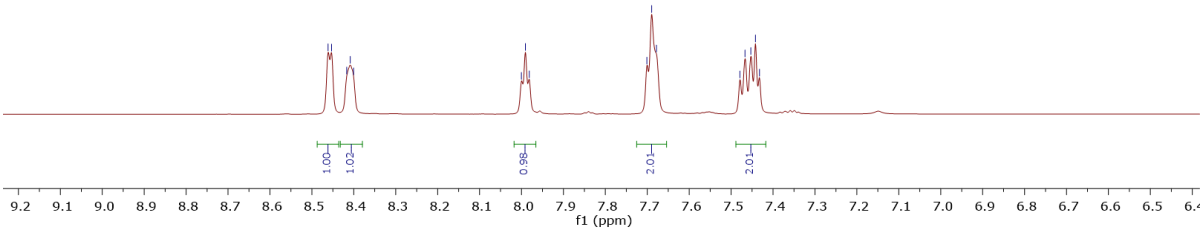

HSGN-2256.2.fid
C13 standard parameters, cryoprobe.
Use "abs13c" to flatten spectrum baseline.

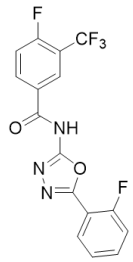

gnacleri_HSGN-2256.1.fid
F19 standard parameters, cryoprobe prodigy.
DE is lengthened compared to default.

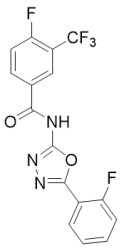

HSGN-2257.1.fid
H1 standard parameters, cryoprobe.

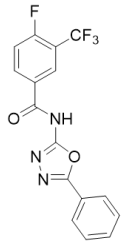

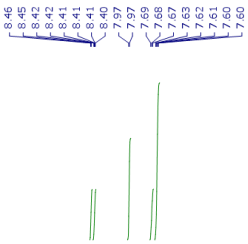

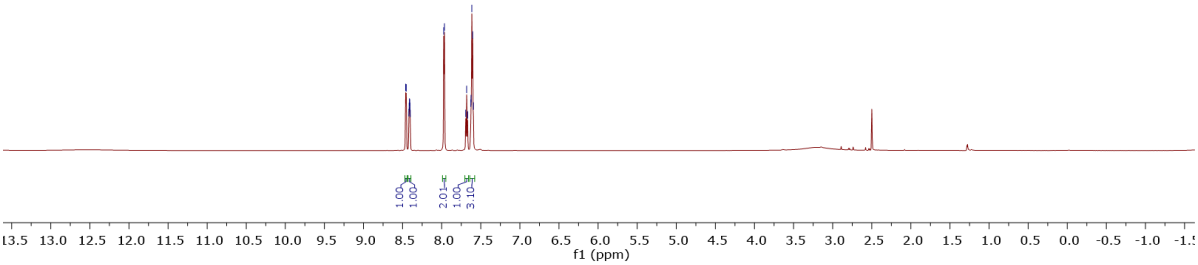

HSGN-2257.1.fid
H1 standard parameters, cryoprobe.

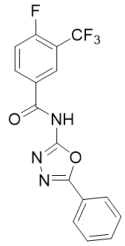

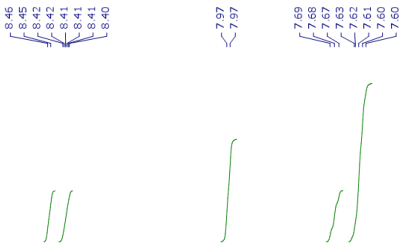

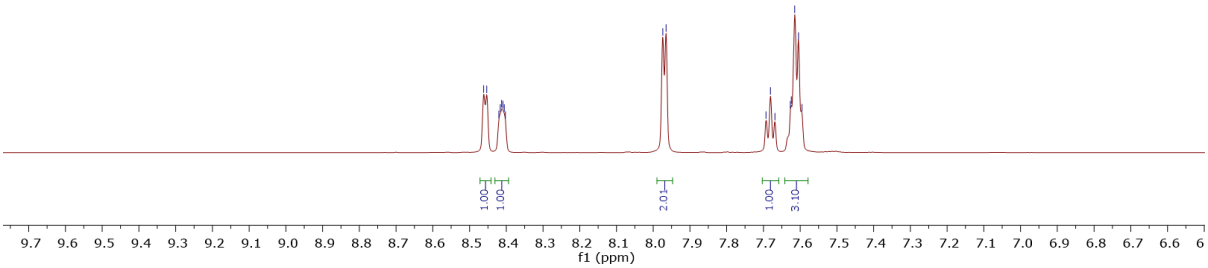

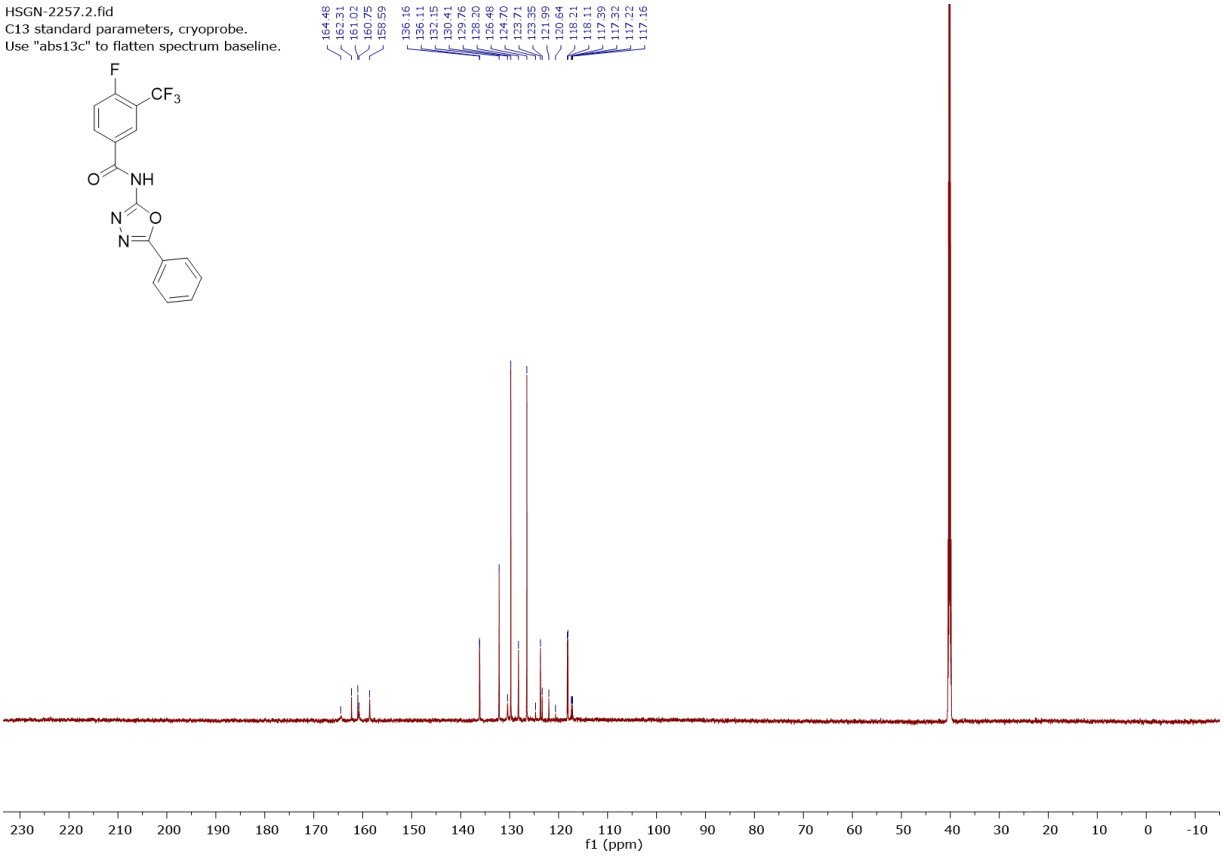
HSGN-2257.2.fid
C13 standard parameters, cryoprobe.
Use "abs13c" to flatten spectrum baseline.
164.48
162.31
161.02
160.75
158.59
136.16
136.11
132.15
130.41
129.76
128.20
126.48
124.70
123.71
123.35
121.99
120.64
118.21
118.11
117.39
117.32
117.22
117.16
F
CF3
O
NH
N
O
N
f1 (ppm)

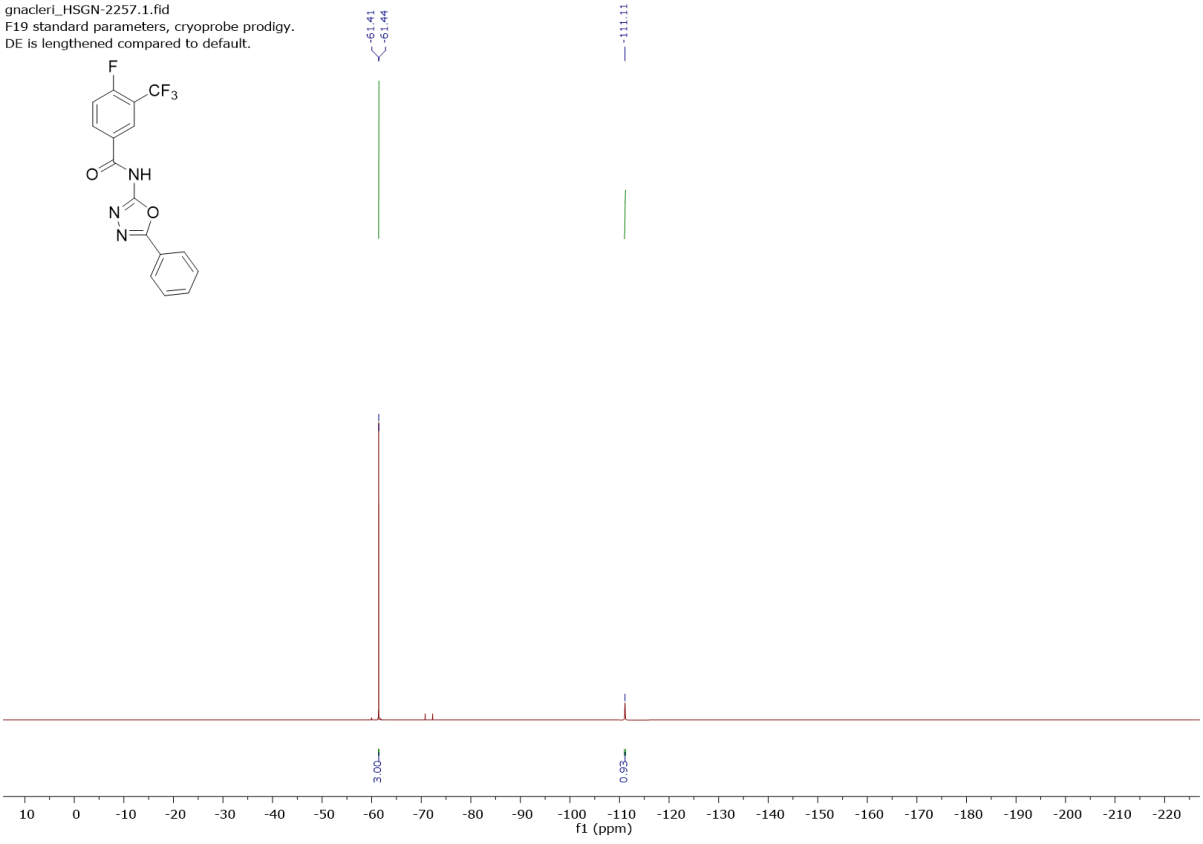
gnacleri_HSGN-2257.1.fid
F19 standard parameters, cryoprobe prodigy.
DE is lengthened compared to default.
-61.41
-61.44
-111.11
F
CF3
O
NH
N
O
N
3.00
0.93
f1 (ppm)

HSGN-2258.1.fid
H1 standard parameters, cryoprobe.

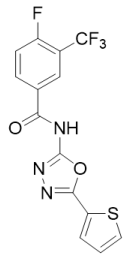

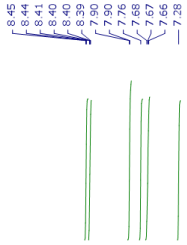

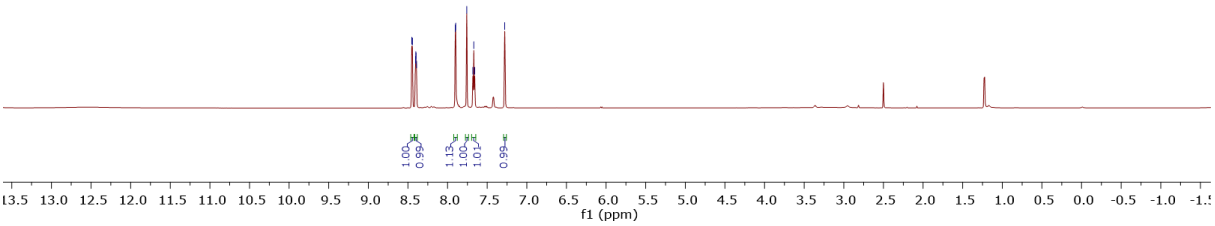

HSGN-2258.1.fid
H1 standard parameters, cryoprobe.

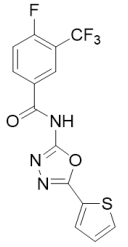

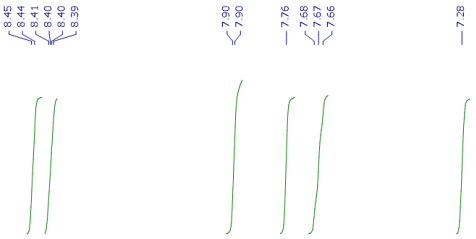

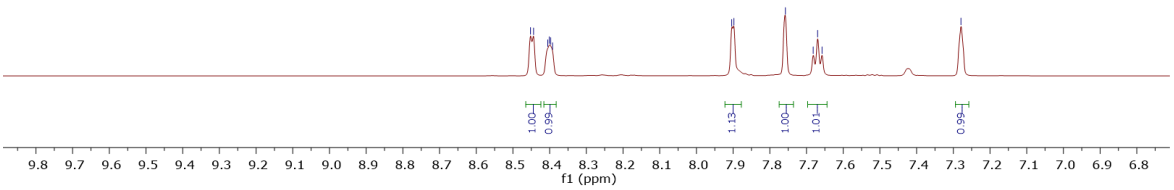

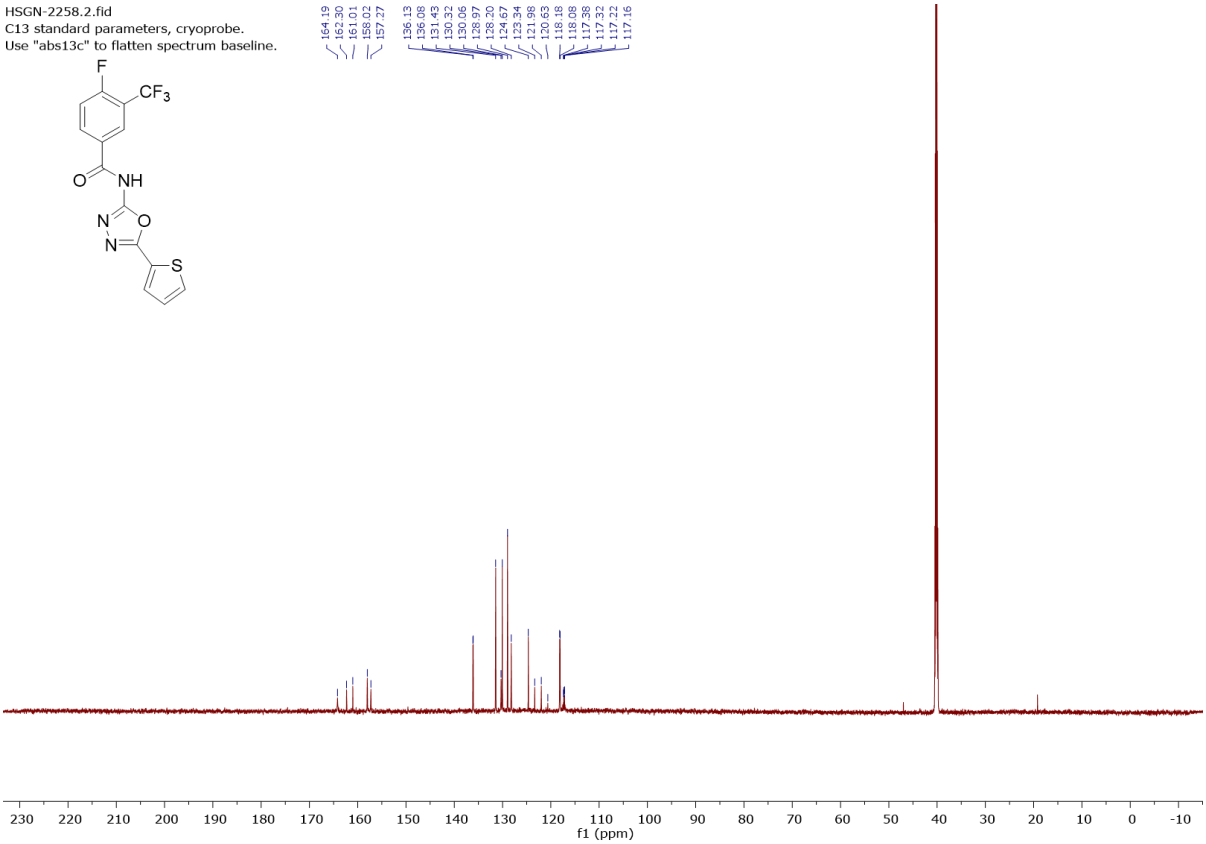
HSGN-2258.2.fid
C13 standard parameters, cryoprobe.
Use "abs13c" to flatten spectrum baseline.
164.19
162.30
161.01
158.02
157.27
136.13
136.08
131.43
130.32
130.06
128.97
128.20
124.67
123.34
121.98
120.63
118.18
118.08
117.38
117.32
117.22
117.16
F
CF3
O
NH
N
O
N
S
230 220 210 200 190 180 170 160 150 140 130 120 110 100 90 80 70 60 50 40 30 20 10 0 -10
f1 (ppm)

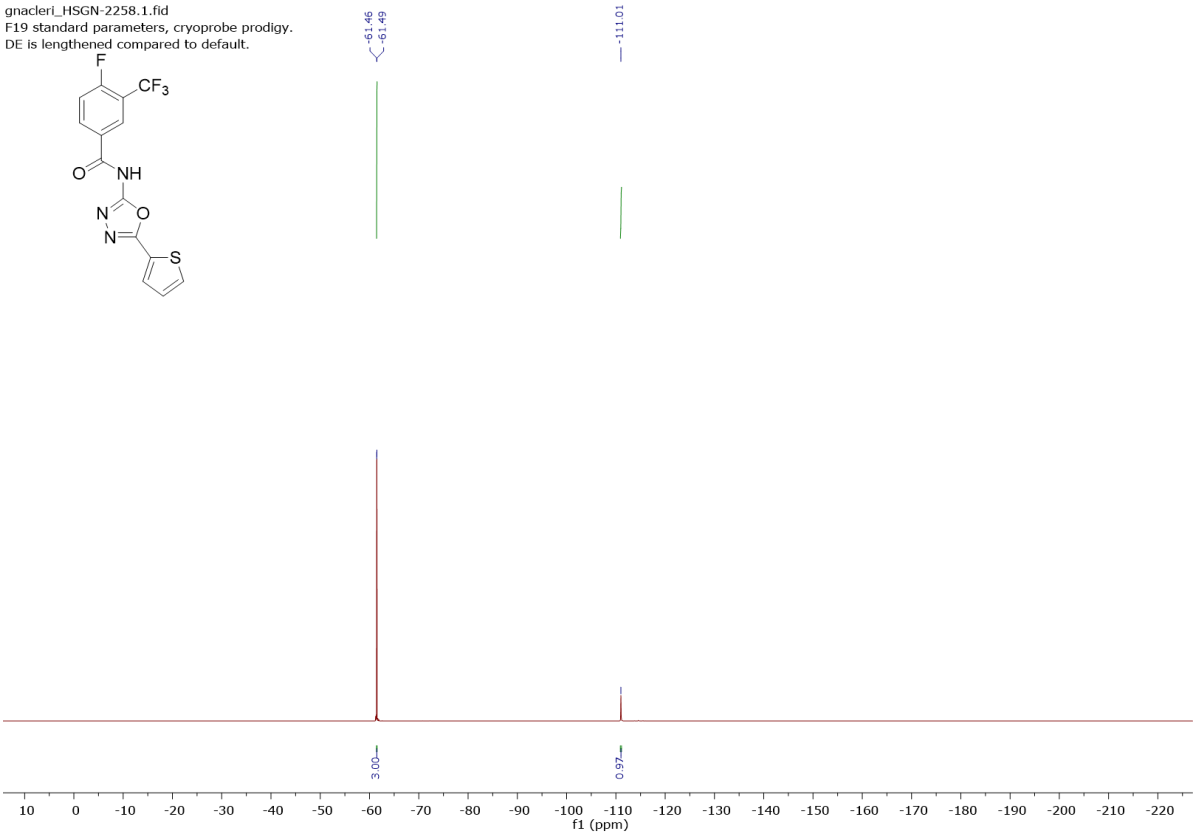
gnacleri_HSGN-2258.1.fid
F19 standard parameters, cryoprobe prodigy.
DE is lengthened compared to default.
-61.46
-61.49
-111.01
F
CF3
O
NH
N
O
N
S
3.00
0.97
10 0 -10 -20 -30 -40 -50 -60 -70 -80 -90 -100 -110 -120 -130 -140 -150 -160 -170 -180 -190 -200 -210 -220
f1 (ppm)

HSGN-2276.1.fid
H1 standard parameters, cryoprobe.

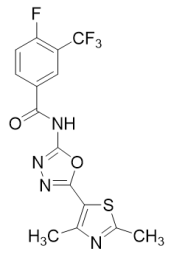

HSGN-2276.1.fid
H1 standard parameters, cryoprobe.

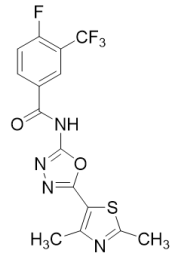

HSGN-2276.1.fid
H1 standard parameters, cryoprobe.

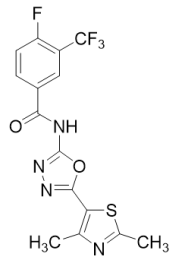

HSGN-2276.2.fid
C13 standard parameters, cryoprobe.
Use "abs13c" to flatten spectrum baseline.

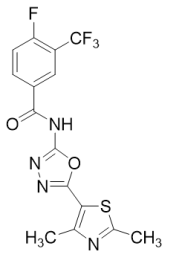

gnacleri_HSGN-2276.1.fid
F19 standard parameters, cryoprobe prodigy.
DE is lengthened compared to default.

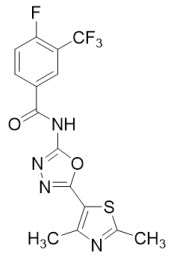

HSGN-2277.1.fid
H1 standard parameters, cryoprobe.

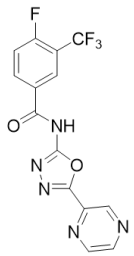

HSGN-2277.1.fid
H1 standard parameters, cryoprobe.

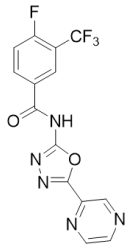

HSGN-2277.2.fid
C13 standard parameters, cryoprobe.
Use "abs13c" to flatten spectrum baseline.

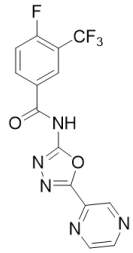

gnacleri_HSGN-2277.1.fid
F19 standard parameters, cryoprobe prodigy.
DE is lengthened compared to default.

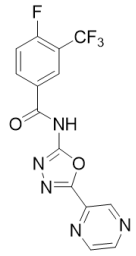

HSGN-2273.1.fid
H1 standard parameters, cryoprobe.

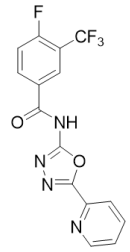

HSGN-2273.1.fid
H1 standard parameters, cryoprobe.

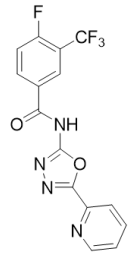

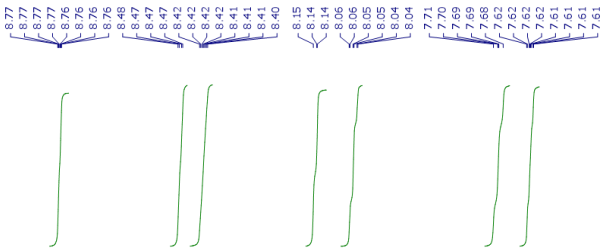

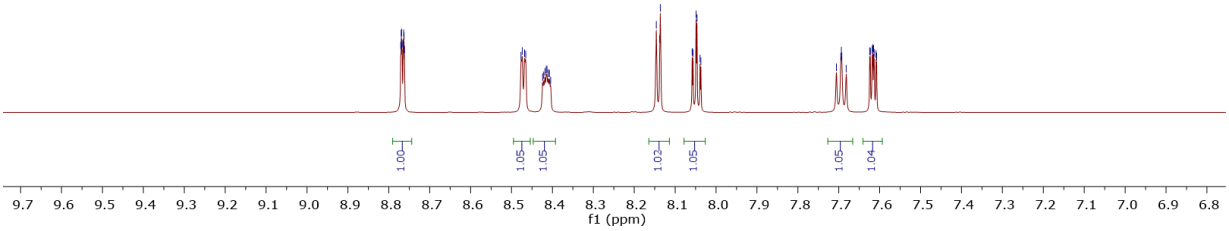

HSGN-2273.2.fid
C13 standard parameters, cryoprobe.
Use "abs13c" to flatten spectrum baseline.

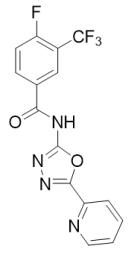

gnacleri_HSGN-2273.1.fid
F19 standard parameters, cryoprobe prodigy.
DE is lengthened compared to default.

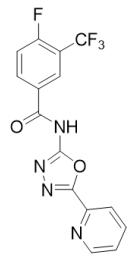

HSGN-2274.1.fid
H1 standard parameters, cryoprobe.

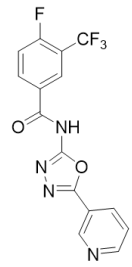

HSGN-2274.1.fid
H1 standard parameters, cryoprobe.

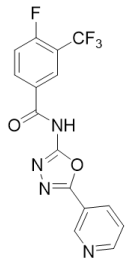

HSGN-2274.2.fid
C13 standard parameters, cryoprobe.
Use "abs13c" to flatten spectrum baseline.

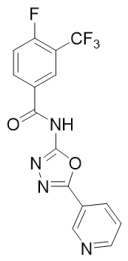

gnacleri_HSGN-2274.1.fid
F19 standard parameters, cryoprobe prodigy.
DE is lengthened compared to default.

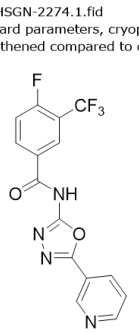

HSGN-2275.1.fid
H1 standard parameters, cryoprobe

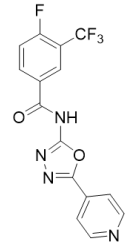

HSGN-2275.1.fid
H1 standard parameters, cryoprobe.

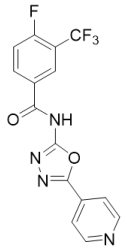

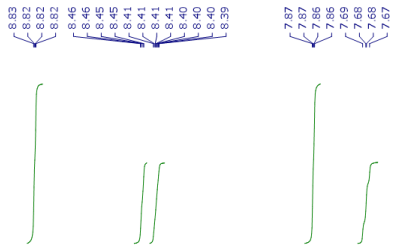

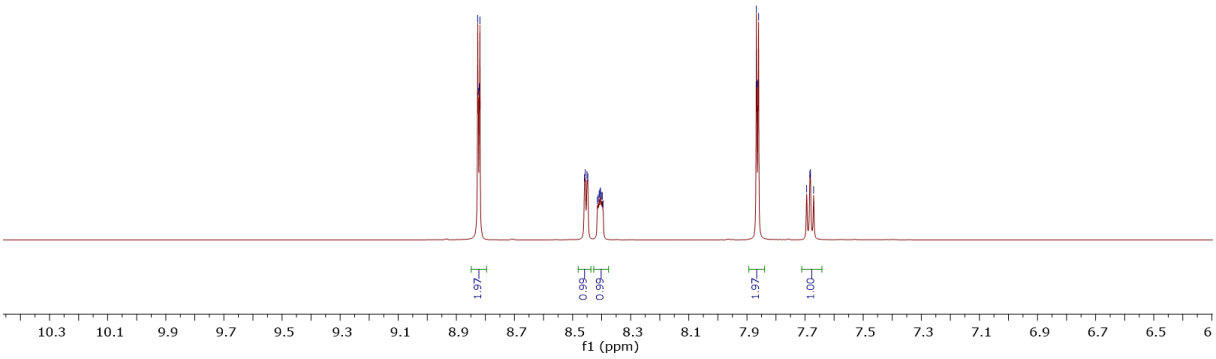

HSGN-2275.2.fid
C13 standard parameters, cryoprobe.
Use "abs13c" to flatten spectrum baseline.

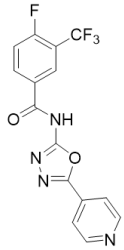

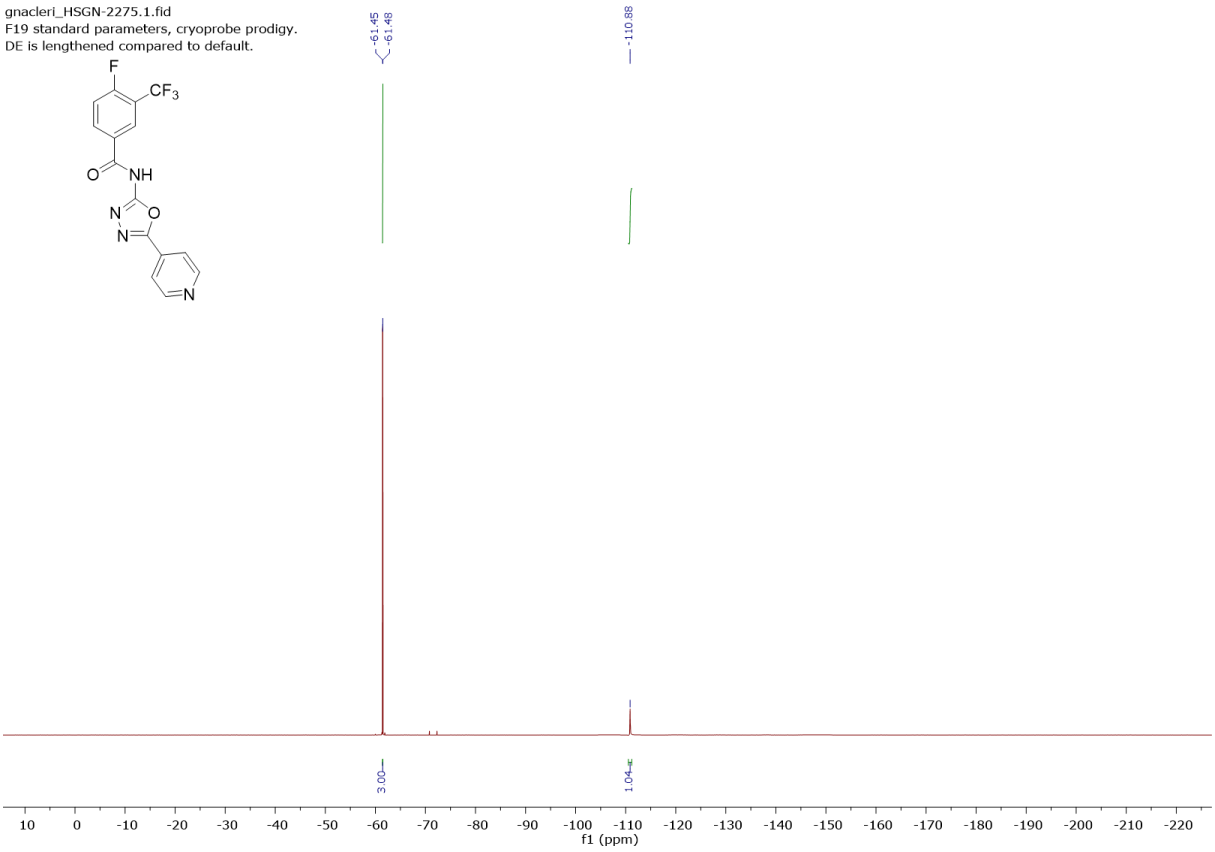
gnacleri_HSGN-2275.1.fid
F19 standard parameters, cryoprobe prodigy.
DE is lengthened compared to default.
-61.45
-61.48
-110.88
F
CF3
O
NH
N
O
N
N
3.00
1.04
10 0 -10 -20 -30 -40 -50 -60 -70 -80 -90 -100 -110 -120 -130 -140 -150 -160 -170 -180 -190 -200 -210 -220
f1 (ppm)

REFERENCES

1. Sizar, O.; Unakal, C. G., Gram-Positive Bacteria. In *StatPearls*, StatPearls Publishing: Treasure Island, FL, 2021.

2. Oliveira, J.; Reygaert, W. C., Gram-negative Bacteria. In *StatPearls*, StatPearls Publishing: Treasure Island, FL, 2021.

3. Tulchinsky, T. H.; Varavikova, E. A., Chapter 1 - A History of Public Health. In *The New Public Health (Third Edition)*, Tulchinsky, T. H.; Varavikova, E. A., Eds. Academic Press: San Diego, 2014; pp 1-42.

4. Smith, K. A., Louis pasteur, the father of immunology? *Front Immunol* **2012,** *3*, 68-68.

5. Berche, P., Louis Pasteur, from crystals of life to vaccination. *Clinical Microbiology and Infection* **2012,** *18*, 1-6.

6. Blevins, S. M.; Bronze, M. S., Robert Koch and the 'golden age' of bacteriology. *International Journal of Infectious Diseases* **2010,** *14* (9), e744-e751.

7. National Research Council (US) Committee to Update Science, M., and Animals. Science, Medicine, and Animals. Washington (DC), A Theory of Germs. *National Academies Press (US)* **2004**.

8. Perry, R. D.; Fetherston, J. D., Yersinia pestis--etiologic agent of plague. *Clinical Microbiology Reviews* **1997,** *10* (1), 35-66.

9. Acuna-Soto, R.; Stahle, D. W.; Cleaveland, M. K.; Therrell, M. D., Megadrought and megadeath in 16th century Mexico. *Emerg Infect Dis* **2002,** *8* (4), 360-362.

10. Martini, M.; Gazzaniga, V.; Bragazzi, N. L.; Barberis, I., The Spanish Influenza Pandemic: a lesson from history 100 years after 1918. *J Prev Med Hyg* **2019,** *60* (1), E64-E67.

11. Littman, R. J., The Plague of Athens: Epidemiology and Paleopathology. *Mount Sinai Journal of Medicine: A Journal of Translational and Personalized Medicine* **2009,** *76* (5), 456-467.

12. Bloom, D. E.; Cadarette, D., Infectious Disease Threats in the Twenty-First Century: Strengthening the Global Response. *Front Immunol* **2019,** *10*, 549-549.

13. Littman, R. J., The plague of Athens: epidemiology and paleopathology. *Mt Sinai J Med* **2009,** *76* (5), 456-67.

14. Stenseth, N. C.; Atshabar, B. B.; Begon, M.; Belmain, S. R.; Bertherat, E.; Carniel, E.; Gage, K. L.; Leirs, H.; Rahalison, L., Plague: past, present, and future. *PLoS Med* **2008,** *5* (1), e3.

15. Faruque, S. M.; Albert, M. J.; Mekalanos, J. J., Epidemiology, genetics, and ecology of toxigenic Vibrio cholerae. *Microbiol Mol Biol Rev* **1998,** *62* (4), 1301-14.

16. Mills, J. J.; Robinson, K. R.; Zehnder, T. E.; Pierce, J. G., Synthesis and Biological Evaluation of the Antimicrobial Natural Product Lipoxazolidinone A. *Angew Chem Int Ed Engl* **2018,** *57* (28), 8682-8686.

17. Hay, S. I.; Abajobir, A. A.; Abate, K. H.; Abbafati, C.; Abbas, K. M.; Abd-Allah, F.; Abdulkader, R. S.; Abdulle, A. M.; Abebo, T. A.; Abera, S. F.; Aboyans, V.; Abu-Raddad, L. J.; Ackerman, I. N.; Adedeji, I. A.; Adetokunboh, O.; Afshin, A.; Aggarwal, R.; Agrawal, S.; Agrawal, A.; Ahmed, M. B.; Aichour, M. T. E.; Aichour, A. N.; Aichour, I.; Aiyar, S.; Akinyemiju, T. F.; Akseer, N.; Al Lami, F. H.; Alahdab, F.; Al-Aly, Z.; Alam, K.; Alam, N.; Alam, T.; Alasfoor, D.; Alene, K. A.; Ali, R.; Alizadeh-Navaei, R.; Alkaabi, J. M.; Alkerwi, A. a.; Alla, F.; Allebeck, P.; Allen, C.; Al-Maskari, F.; AlMazroa, M. A.; Al-Raddadi, R.; Alsharif, U.; Alsowaidi, S.; Althouse, B. M.; Altirkawi, K. A.; Alvis-Guzman, N.; Amare, A. T.; Amini, E.; Ammar, W.; Amoako, Y. A.; Ansha, M. G.; Antonio, C. A. T.; Anwari, P.; Ärnlöv, J.; Arora, M.; Artaman, A.; Aryal, K. K.; Asgedom, S. W.; Atey, T. M.; Atnafu, N. T.; Avila-Burgos, L.; Avokpaho, E. F. G. A.; Awasthi, A.; Awasthi, S.; Azarpazhooh, M. R.; Azzopardi, P.; Babalola, T. K.; Bacha, U.; Badawi, A.; Balakrishnan, K.; Bannick, M. S.; Barac, A.; Barker-Collo, S. L.; Bärnighausen, T.; Barquera, S.; Barrero, L. H.; Basu, S.; Battista, R.; Battle, K. E.; Baune, B. T.; Bazargan-Hejazi, S.; Beardsley, J.; Bedi, N.; Béjot, Y.; Bekele, B. B.; Bell, M. L.; Bennett, D. A.; Bennett, J. R.; Bensenor, I. M.; Benson, J.; Berhane, A.; Berhe, D. F.; Bernabé, E.; Betsu, B. D.; Beuran, M.; Beyene, A. S.; Bhansali, A.; Bhatt, S.; Bhutta, Z. A.; Biadgilign, S.; Bicer, B. K.; Bienhoff, K.; Bikbov, B.; Birungi, C.; Biryukov, S.; Bisanzio, D.; Bizuayehu, H. M.; Blyth, F. M.; Boneya, D. J.; Bose, D.; Bou-Orm, I. R.; Bourne, R. R. A.; Brainin, M.; Brayne, C.; Brazinova, A.; Breitborde, N. J. K.; Briant, P. S.; Britton, G.; Brugha, T. S.; Buchbinder, R.; Bulto, L. N. B.; Bumgarner, B. R.; Butt, Z. A.; Cahuana-Hurtado, L.; Cameron, E.; Campos-Nonato, I. R.; Carabin, H.; Cárdenas, R.; Carpenter, D. O.; Carrero, J. J.; Carter, A.; Carvalho, F.; Casey, D.; Castañeda-Orjuela, C. A.; Castle, C. D.; Catalá-López, F.; Chang, J.-C.; Charlson, F. J.; Chaturvedi, P.; Chen, H.; Chibalabala, M.; Chibueze, C. E.; Chisumpa, V. H.; Chitheer, A. A.; Chowdhury, R.; Christopher, D. J.; Ciobanu, L. G.; Cirillo, M.; Colombara, D.; Cooper, L. T.; Cooper, C.; Cortesi, P. A.; Cortinovis, M.; Criqui, M. H.; Cromwell, E. A.; Cross, M.; Crump, J. A.; Dadi, A. F.; Dalal, K.; Damasceno, A.; Dandona, L.; Dandona, R.; das Neves, J.; Davitoiu, D. V.; Davletov, K.; de Courten, B.; De Leo, D.; De Steur, H.; Defo, B. K.; Degenhardt, L.; Deiparine, S.; Dellavalle, R. P.; Deribe, K.; Deribew, A.; Des Jarlais, D. C.; Dey, S.; Dharmaratne, S. D.; Dhillon, P. K.; Dicker, D.; Djalainia, S.; Do, H. P.; Dokova, K.; Doku, D. T.; Dorsey, E. R.; dos Santos, K. P. B.; Driscoll, T. R.; Dubey, M.; Duncan, B. B.; Ebel, B. E.; Echko, M.; El-Khatib, Z. Z.; Enayati, A.; Endries, A. Y.; Ermakov, S. P.; Erskine, H. E.; Eshetie, S.; Eshrati, B.; Esteghamati, A.; Estep, K.; Fanuel, F. B. B.; Farag, T.; Farinha, C. S. e. S.; Faro, A.; Farzadfar, F.; Fazeli, M. S.; Feigin, V. L.; Feigl, A. B.; Fereshtehnejad, S.-M.; Fernandes, J. C.; Ferrari, A. J.; Feyissa, T. R.; Filip, I.; Fischer, F.; Fitzmaurice, C.; Flaxman, A. D.; Foigt, N.; Foreman, K. J.; Franklin, R. C.; Frostad, J. J.; Fullman, N.; Fürst, T.; Furtado, J. M.; Futran, N. D.; Gakidou, E.; Garcia-Basteiro, A. L.; Gebre, T.; Gebregergs, G. B.; Gebrehiwot, T. T.; Geleijnse, J. M.; Geleto, A.; Gemechu, B. L.; Gesesew, H. A.; Gething, P. W.; Ghajar, A.; Gibney, K. B.; Gillum, R. F.; Ginawi, I. A. M.; Gishu, M. D.; Giussani,

G.; Godwin, W. W.; Goel, K.; Goenka, S.; Goldberg, E. M.; Gona, P. N.; Goodridge, A.; Gopalani, S. V.; Gosselin, R. A.; Gotay, C. C.; Goto, A.; Goulart, A. C.; Graetz, N.; Gugnani, H. C.; Gupta, P. C.; Gupta, R.; Gupta, T.; Gupta, V.; Gupta, R.; Gutiérrez, R. A.; Hachinski, V.; Hafezi-Nejad, N.; Hailu, A. D.; Hailu, G. B.; Hamadeh, R. R.; Hamidi, S.; Hammami, M.; Handal, A. J.; Hankey, G. J.; Hao, Y.; Harb, H. L.; Hareri, H. A.; Haro, J. M.; Harun, K. M.; Harvey, J.; Hassanvand, M. S.; Havmoeller, R.; Hay, R. J.; Hedayati, M. T.; Hendrie, D.; Henry, N. J.; Heredia-Pi, I. B.; Heydarpour, P.; Hoek, H. W.; Hoffman, H. J.; Horino, M.; Horita, N.; Hosgood, H. D.; Hostiuc, S.; Hotez, P. J.; Hoy, D. G.; Htet, A. S.; Hu, G.; Huang, J. J.; Huynh, C.; Iburg, K. M.; Igumbor, E. U.; Ikeda, C.; Irvine, C. M. S.; Islam, S. M. S.; Jacobsen, K. H.; Jahanmehr, N.; Jakovljevic, M. B.; James, P.; Jassal, S. K.; Javanbakht, M.; Jayaraman, S. P.; Jeemon, P.; Jensen, P. N.; Jha, V.; Jiang, G.; John, D.; Johnson, C. O.; Johnson, S. C.; Jonas, J. B.; Jürisson, M.; Kabir, Z.; Kadel, R.; Kahsay, A.; Kamal, R.; Kar, C.; Karam, N. E.; Karch, A.; Karema, C. K.; Karimi, S. M.; Karimkhani, C.; Kasaeian, A.; Kassa, G. M.; Kassaw, N. A.; Kassebaum, N. J.; Kastor, A.; Katikireddi, S. V.; Kaul, A.; Kawakami, N.; Keiyoro, P. N.; Kemmer, L.; Kengne, A. P.; Keren, A.; Kesavachandran, C. N.; Khader, Y. S.; Khalil, I. A.; Khan, E. A.; Khang, Y.-H.; Khoja, A. T.; Khosravi, A.; Khubchandani, J.; Kiadaliri, A. A.; Kieling, C.; Kim, Y. J.; Kim, D.; Kimokoti, R. W.; Kinfu, Y.; Kisa, A.; Kissimova-Skarbek, K. A.; Kissoon, N.; Kivimaki, M.; Knudsen, A. K.; Kokubo, Y.; Kolte, D.; Kopec, J. A.; Kosen, S.; Kotsakis, G. A.; Koul, P. A.; Koyanagi, A.; Kravchenko, M.; Krohn, K. J.; Kumar, G. A.; Kumar, P.; Kyu, H. H.; Lager, A. C. J.; Lal, D. K.; Lalloo, R.; Lallukka, T.; Lambert, N.; Lan, Q.; Lansingh, V. C.; Larsson, A.; Leasher, J. L.; Lee, P. H.; Leigh, J.; Leshargie, C. T.; Leung, J.; Leung, R.; Levi, M.; Li, Y.; Li, Y.; Liang, X.; Liben, M. L.; Lim, S. S.; Linn, S.; Liu, P. Y.; Liu, A.; Liu, S.; Liu, Y.; Lodha, R.; Logroscino, G.; Looker, K. J.; Lopez, A. D.; Lorkowski, S.; Lotufo, P. A.; Lozano, R.; Lucas, T. C. D.; Lunevicius, R.; Lyons, R. A.; Macarayan, E. R. K.; Maddison, E. R.; Magdy Abd El Razek, H. M. A.; Magdy Abd El Razek, M.; Magis-Rodriguez, C.; Mahdavi, M.; Majdan, M.; Majdzadeh, R.; Majeed, A.; Malekzadeh, R.; Malhotra, R.; Malta, D. C.; Mamun, A. A.; Manguerra, H.; Manhertz, T.; Mantovani, L. G.; Mapoma, C. C.; March, L. M.; Marczak, L. B.; Martinez-Raga, J.; Martins, P. H. V.; Martins-Melo, F. R.; Martopullo, I.; März, W.; Mathur, M. R.; Mazidi, M.; McAlinden, C.; McGaughey, M.; McGrath, J. J.; McKee, M.; Mehata, S.; Meier, T.; Meles, K. G.; Memiah, P.; Memish, Z. A.; Mendoza, W.; Mengesha, M. M.; Mengistie, M. A.; Mengistu, D. T.; Mensah, G. A.; Meretoja, T. J.; Meretoja, A.; Mezgebe, H. B.; Micha, R.; Millear, A.; Miller, T. R.; Minnig, S.; Mirarefin, M.; Mirrakhimov, E. M.; Misganaw, A.; Mishra, S. R.; Mitchell, P. B.; Mohammad, K. A.; Mohammadi, A.; Mohammed, M. S. K.; Mohammed, K. E.; Mohammed, S.; Mohan, M. B. V.; Mokdad, A. H.; Mollenkopf, S. K.; Monasta, L.; Montañez Hernandez, J. C.; Montico, M.; Moradi-Lakeh, M.; Moraga, P.; Morawska, L.; Mori, R.; Morrison, S. D.; Moses, M.; Mountjoy-Venning, C.; Mruts, K. B.; Mueller, U. O.; Muller, K.; Murdoch, M. E.; Murthy, G. V. S.; Murthy, S.; Musa, K. I.; Nachega, J. B.; Nagel, G.; Naghavi, M.; Naheed, A.; Naidoo, K. S.; Nangia, V.; Nasher, J. T.; Natarajan, G.; Negasa, D. E.; Negoi, R. I.; Negoi, I.; Newton, C. R.; Ngunjiri, J. W.; Nguyen, C. T.; Nguyen, Q. L.; Nguyen, T. H.; Nguyen, G.; Nguyen, M.; Nichols, E.; Ningrum, D. N. A.; Nong, V. M.; Norheim, O. F.; Norrving, B.; Noubiap, J. J. N.; Nyandwi, A.; Obermeyer, C. M.; O'Donnell, M. J.; Ogbo, F. A.; Oh, I.-H.; Okoro, A.; Oladimeji, O.; Olagunju, A. T.; Olagunju, T. O.; Olsen, H. E.; Olusanya, B. O.; Olusanya, J. O.; Ong, K.; Opio, J. N.; Oren, E.; Ortiz, A.; Osborne, R. H.; Osgood-Zimmerman, A.; Osman, M.; Ota,

E.; Owolabi, M. O.; Pa, M.; Pacella, R. E.; Panda, B. K.; Pandian, J. D.; Papachristou, C.; Park, E.-K.; Parry, C. D.; Parsaeian, M.; Patil, S. T.; Patten, S. B.; Patton, G. C.; Paudel, D.; Paulson, K.; Pearce, N.; Pereira, D. M.; Perez, K. M.; Perico, N.; Pesudovs, K.; Peterson, C. B.; Petri, W. A.; Petzold, M.; Phillips, M. R.; Phipps, G.; Pigott, D. M.; Pillay, J. D.; Pinho, C.; Piradov, M. A.; Plass, D.; Pletcher, M. A.; Popova, S.; Poulton, R. G.; Pourmalek, F.; Prabhakaran, D.; Prasad, N.; Purcell, C.; Purwar, M.; Qorbani, M.; Quintanilla, B. P. A.; Rabiee, R. H. S.; Radfar, A.; Rafay, A.; Rahimi, K.; Rahimi-Movaghar, A.; Rahimi-Movaghar, V.; Rahman, M. H. U.; Rahman, M. A.; Rahman, M.; Rai, R. K.; Rajsic, S.; Ram, U.; Ranabhat, C. L.; Rangaswamy, T.; Rankin, Z.; Rao, P. V.; Rao, P. C.; Rawaf, S.; Ray, S. E.; Reiner, R. C.; Reinig, N.; Reitsma, M.; Remuzzi, G.; Renzaho, A. M. N.; Resnikoff, S.; Rezaei, S.; Ribeiro, A. L.; Rivas, J. C.; Roba, H. S.; Robinson, S. R.; Rojas-Rueda, D.; Rokni, M. B.; Ronfani, L.; Roshandel, G.; Roth, G. A.; Rothenbacher, D.; Roy, A.; Rubagotti, E.; Ruhago, G. M.; Saadat, S.; Safdarian, M.; Safiri, S.; Sagar, R.; Sahathevan, R.; Sahraian, M. A.; Salama, J.; Saleh, M. M.; Salomon, J. A.; Salvi, S. S.; Samy, A. M.; Sanabria, J. R.; Sanchez-Niño, M. D.; Santomauro, D.; Santos, J. V.; Santos, I. S.; Santric Milicevic, M. M.; Sartorius, B.; Satpathy, M.; Sawhney, M.; Saxena, S.; Schelonka, K.; Schmidt, M. I.; Schneider, I. J. C.; Schöttker, B.; Schutte, A. E.; Schwebel, D. C.; Schwendicke, F.; Seedat, S.; Sepanlou, S. G.; Servan-Mori, E. E.; Shaheen, A.; Shaikh, M. A.; Shamsipour, M.; Sharma, R.; Sharma, J.; She, J.; Shi, P.; Shibuya, K.; Shields, C.; Shifa, G. T.; Shiferaw, M. S.; Shigematsu, M.; Shiri, R.; Shirkoohi, R.; Shirude, S.; Shishani, K.; Shoman, H.; Siabani, S.; Sibai, A. M.; Sigfusdottir, I. D.; Silberberg, D. H.; Silva, D. A. S.; Silva, J. P.; Silveira, D. G. A.; Singh, J. A.; Singh, O. P.; Singh, N. P.; Singh, V.; Sinha, D. N.; Skiadaresi, E.; Slepak, E. L.; Smith, D. L.; Smith, M.; Sobaih, B. H. A.; Sobngwi, E.; Soljak, M.; Sorensen, R. J. D.; Sousa, T. C. M.; Sposato, L. A.; Sreeramareddy, C. T.; Srinivasan, V.; Stanaway, J. D.; Stathopoulou, V.; Steel, N.; Stein, D. J.; Steiner, C.; Steinke, S.; Stokes, M. A.; Stovner, L. J.; Strub, B.; Subart, M.; Sufiyan, M. B.; Sunguya, B. F.; Sur, P. J.; Swaminathan, S.; Sykes, B. L.; Sylte, D.; Szoeke, C. E. I.; Tabarés-Seisdedos, R.; Tadakamadla, S. K.; Taffere, G. R.; Takala, J. S.; Tandon, N.; Tanne, D.; Tarekegn, Y. L.; Tavakkoli, M.; Taveira, N.; Taylor, H. R.; Tegegne, T. K.; Tehrani-Banihashemi, A.; Tekelab, T.; Terkawi, A. S.; Tesfaye, D. J.; Tesssema, B.; Thakur, J. S.; Thamsuwan, O.; Theadom, A. M.; Theis, A. M.; Thomas, K. E.; Thomas, N.; Thompson, R.; Thrift, A. G.; Tobe-Gai, R.; Tobollik, M.; Tonelli, M.; Topor-Madry, R.; Tortajada, M.; Touvier, M.; Traebert, J.; Tran, B. X.; Troeger, C.; Truelsen, T.; Tsoi, D.; Tuzcu, E. M.; Tymeson, H.; Tyrovolas, S.; Ukwaja, K. N.; Undurraga, E. A.; Uneke, C. J.; Updike, R.; Uthman, O. A.; Uzochukwu, B. S. C.; van Boven, J. F. M.; Varughese, S.; Vasankari, T.; Veerman, L. J.; Venkatesh, S.; Venketasubramanian, N.; Vidavalur, R.; Vijayakumar, L.; Violante, F. S.; Vishnu, A.; Vladimirov, S. K.; Vlassov, V. V.; Vollset, S. E.; Vos, T.; Wadilo, F.; Wakayo, T.; Wallin, M. T.; Wang, Y.-P.; Weichenthal, S.; Weiderpass, E.; Weintraub, R. G.; Weiss, D. J.; Werdecker, A.; Westerman, R.; Whiteford, H. A.; Wijeratne, T.; Williams, H. C.; Wiysonge, C. S.; Woldeyes, B. G.; Wolfe, C. D. A.; Woodbrook, R.; Woolf, A. D.; Workicho, A.; Xavier, D.; Xu, G.; Yadgir, S.; Yaghoubi, M.; Yakob, B.; Yan, L. L.; Yano, Y.; Ye, P.; Yihdego, M. G.; Yimam, H. H.; Yip, P.; Yonemoto, N.; Yoon, S.-J.; Yotebieng, M.; Younis, M. Z.; Yu, C.; Zaidi, Z.; Zaki, M. E. S.; Zegeye, E. A.; Zenebe, Z. M.; Zhang, X.; Zheng, Y.; Zhou, M.; Zipkin, B.; Zodpey, S.; Zoeckler, L.; Zuhlke, L. J.; Murray, C. J. L., Global, regional, and national disability-adjusted life-years (DALYs) for 333 diseases

and injuries and healthy life expectancy (HALE) for 195 countries and territories, 1990–2016: a systematic analysis for the Global Burden of Disease Study 2016. *The Lancet* **2017,** *390* (10100), 1260-1344.

18. Organization, W. H. *Global health risks*; 2009.

19. Bhutta, Z. A.; Salam, R. A.; Das, J. K.; Lassi, Z. S., Tackling the existing burden of infectious diseases in the developing world: existing gaps and the way forward. *Infectious Diseases of Poverty* **2014,** *3* (1), 28.

20. Miller, L. H.; Hoffman, S. L., Research toward vaccines against malaria. *Nat Med* **1998,** *4* (5 Suppl), 520-4.

21. Espinal, M. A., The global situation of MDR-TB. *Tuberculosis (Edinb)* **2003,** *83* (1-3), 44-51.

22. Williamson, D. A.; Chen, M. Y., Emerging and Reemerging Sexually Transmitted Infections. *N Engl J Med* **2020,** *382* (21), 2023-2032.

23. Warren, J. R.; Marshall, B., Unidentified curved bacilli on gastric epithelium in active chronic gastritis. *Lancet* **1983,** *1* (8336), 1273-5.

24. Bartlett, J. G.; Onderdonk, A. B.; Cisneros, R. L.; Kasper, D. L., Clindamycin-associated colitis due to a toxin-producing species of Clostridium in hamsters. *J Infect Dis* **1977,** *136* (5), 701-5.

25. Burgdorfer, W.; Barbour, A. G.; Hayes, S. F.; Benach, J. L.; Grunwaldt, E.; Davis, J. P., Lyme disease-a tick-borne spirochetosis? *Science* **1982,** *216* (4552), 1317-9.

26. Welinder-Olsson, C.; Kjellin, E.; Vaht, K.; Jacobsson, S.; Wenneras, C., First case of human "Candidatus Neoehrlichia mikurensis" infection in a febrile patient with chronic lymphocytic leukemia. *J Clin Microbiol* **2010,** *48* (5), 1956-9.

27. Clancy, C. J.; Nguyen, M. H., Buying Time: The AMR Action Fund and the State of Antibiotic Development in the United States 2020. *Open Forum Infect Dis* **2020,** *7* (11), ofaa464.

28. Bassett, E. J.; Keith, M. S.; Armelagos, G. J.; Martin, D. L.; Villanueva, A. R., Tetracycline-labeled human bone from ancient Sudanese Nubia (A.D. 350). *Science* **1980,** *209* (4464), 1532-4.

29. Nelson, M. L.; Dinardo, A.; Hochberg, J.; Armelagos, G. J., Brief communication: Mass spectroscopic characterization of tetracycline in the skeletal remains of an ancient population from Sudanese Nubia 350-550 CE. *Am J Phys Anthropol* **2010,** *143* (1), 151-4.

30. Cook, M.; Molto, E.; Anderson, C., Fluorochrome labelling in Roman period skeletons from Dakhleh Oasis, Egypt. *Am J Phys Anthropol* **1989,** *80* (2), 137-43.

31. Sobell, H. M., Actinomycin and DNA transcription. *Proc Natl Acad Sci U S A* **1985,** *82* (16), 5328-31.

32. Falkinham, J. O., 3rd; Wall, T. E.; Tanner, J. R.; Tawaha, K.; Alali, F. Q.; Li, C.; Oberlies, N. H., Proliferation of antibiotic-producing bacteria and concomitant antibiotic production as the basis for the antibiotic activity of Jordan's red soils. *Appl Environ Microbiol* **2009,** *75* (9), 2735-41.

33. Aminov, R. I., A brief history of the antibiotic era: lessons learned and challenges for the future. *Frontiers in microbiology* **2010,** *1*, 134-134.

34. Piddock, L. J. V., The crisis of no new antibiotics—what is the way forward? *The Lancet Infectious Diseases* **2012,** *12* (3), 249-253.

35. Lederberg, J., Infectious History. *Science* **2000,** *288* (5464), 287-293.

36. Adedeji, W. A., THE TREASURE CALLED ANTIBIOTICS. *Annals of Ibadan postgraduate medicine* **2016,** *14* (2), 56-57.

37. Rossolini, G. M.; Arena, F.; Pecile, P.; Pollini, S., Update on the antibiotic resistance crisis. *Current Opinion in Pharmacology* **2014,** *18*, 56-60.

38. Emmerich, R.; Low, O., Bakteriolytische Enzyme als Ursache der erworbenen Immunität und die Heilung von Infectionskrankheiten durch dieselben. *Zeitschr. f. Hygiene* **1899,** *31*, 1-65.

39. Buchwalow, I.; Boecker, W.; Tiemann, M., The contribution of Paul Ehrlich to histochemistry: a tribute on the occasion of the centenary of his death. *Virchows Archiv* **2015,** *466* (1), 111-116.

40. Schwartz, R. S., Paul Ehrlich's Magic Bullets. *New England Journal of Medicine* **2004,** *350* (11), 1079-1080.

41. Aminov, R. I., A brief history of the antibiotic era: lessons learned and challenges for the future. *Front Microbiol* **2010,** *1*, 134.

42. Fleming, A., On the Antibacterial Action of Cultures of a Penicillium, with Special Reference to their Use in the Isolation of B. influenzæ. *Br J Exp Pathol* **1929,** *10* (3), 226-236.

43. Chain, E.; Florey, H. W.; Gardner, A. D.; Heatley, N. G.; Jennings, M. A.; Orr-Ewing, J.; Sanders, A. G., THE CLASSIC: penicillin as a chemotherapeutic agent. 1940. *Clin Orthop Relat Res* **2005,** *439*, 23-6.

44. Gould, I. M.; Bal, A. M., New antibiotic agents in the pipeline and how they can help overcome microbial resistance. *Virulence* **2013,** *4* (2), 185-91.

45. Wright, G. D., Something old, something new: revisiting natural products in antibiotic drug discovery. *Can. J. Microbiol.* **2014,** *60* (3), 147-54.

46. Ventola, C. L., The antibiotic resistance crisis: part 1: causes and threats. *P T* **2015,** *40* (4), 277-83.

47. Centers for Disease Control and Prevention (CDC). Antibiotic / Antimicrobial Resistance (AR / AMR), Biggest Threats and Data. https://www.cdc.gov/drugresistance/biggest-threats.html

48. Bush, K.; Courvalin, P.; Dantas, G.; Davies, J.; Eisenstein, B.; Huovinen, P.; Jacoby, G. A.; Kishony, R.; Kreiswirth, B. N.; Kutter, E.; Lerner, S. A.; Levy, S.; Lewis, K.; Lomovskaya, O.; Miller, J. H.; Mobashery, S.; Piddock, L. J.; Projan, S.; Thomas, C. M.; Tomasz, A.; Tulkens, P. M.; Walsh, T. R.; Watson, J. D.; Witkowski, J.; Witte, W.; Wright, G.; Yeh, P.; Zgurskaya, H. I., Tackling antibiotic resistance. *Nat. Rev. Microbiol.* **2011,** *9* (12), 894-6.

49. Frieden, T., Antibiotic Resistance Threats in the United States, 2013. Centers for Disease Control and Prevention: Atlanta, GA, USA, 2013; p 114.

50. de Kraker, M. E.; Stewardson, A. J.; Harbarth, S., Will 10 million people die a year due to antimicrobial resistance by 2050? *PLoS Med.* **2016,** *13* (11), e1002184.

51. Wencewicz, T. A., Crossroads of Antibiotic Resistance and Biosynthesis. *J Mol Biol* **2019,** *431* (18), 3370-3399.

52. Epand, R. M.; Walker, C.; Epand, R. F.; Magarvey, N. A., Molecular mechanisms of membrane targeting antibiotics. *Biochim Biophys Acta* **2016,** *1858* (5), 980-7.

53. Bush, K., Antimicrobial agents targeting bacterial cell walls and cell membranes. *Rev Sci Tech* **2012,** *31* (1), 43-56.

54. Sarkar, P.; Yarlagadda, V.; Ghosh, C.; Haldar, J., A review on cell wall synthesis inhibitors with an emphasis on glycopeptide antibiotics. *Medchemcomm* **2017,** *8* (3), 516-533.

55. Norris, S. J., Antigenic variation with a twist--the Borrelia story. *Mol Microbiol* **2006,** *60* (6), 1319-22.

56. Redpath, S.; Ghazal, P.; Gascoigne, N. R., Hijacking and exploitation of IL-10 by intracellular pathogens. *Trends Microbiol* **2001,** *9* (2), 86-92.

57. Scott, C. C.; Botelho, R. J.; Grinstein, S., Phagosome maturation: a few bugs in the system. *J Membr Biol* **2003,** *193* (3), 137-52.

58. Brauner, A.; Fridman, O.; Gefen, O.; Balaban, N. Q., Distinguishing between resistance, tolerance and persistence to antibiotic treatment. *Nat Rev Microbiol* **2016,** *14*, 320-330.

59. Fisher, R. A.; Gollan, B.; Helaine, S., Persistent bacterial infections and persister cells. *Nat Rev Microbiol* **2017,** *15* (8), 453-464.

60. Michiels, J. E.; Van den Bergh, B.; Verstraeten, N.; Michiels, J., Molecular mechanisms and clinical implications of bacterial persistence. *Drug Resist Updat* **2016,** *29*, 76-89.

61. Helaine, S.; Kugelberg, E., Bacterial persisters: formation, eradication, and experimental systems. *Trends Microbiol* **2014,** *22* (7), 417-24.

62. Harms, A.; Maisonneuve, E.; Gerdes, K., Mechanisms of bacterial persistence during stress and antibiotic exposure. *Science* **2016,** *354* (6318).

63. Wood, T. K.; Knabel, S. J.; Kwan, B. W., Bacterial persister cell formation and dormancy. *Appl Environ Microbiol* **2013,** *79* (23), 7116-21.

64. Lewis, K., Persister cells. *Annu Rev Microbiol* **2010,** *64*, 357-72.

65. Costerton, J. W.; Stewart, P. S.; Greenberg, E. P., Bacterial biofilms: a common cause of persistent infections. *Science* **1999,** *284* (5418), 1318-22.

66. Lambe, D. W., Jr.; Ferguson, K. P.; Mayberry-Carson, K. J.; Tober-Meyer, B.; Costerton, J. W., Foreign-body-associated experimental osteomyelitis induced with Bacteroides fragilis and Staphylococcus epidermidis in rabbits. *Clin Orthop Relat Res* **1991,** (266), 285-94.

67. Mah, T. F.; O'Toole, G. A., Mechanisms of biofilm resistance to antimicrobial agents. *Trends Microbiol* **2001,** *9* (1), 34-9.

68. Conlon, B. P.; Rowe, S. E.; Lewis, K., Persister cells in biofilm associated infections. *Adv Exp Med Biol* **2015,** *831*, 1-9.

69. Kim, W.; Zou, G.; Hari, T. P. A.; Wilt, I. K.; Zhu, W.; Galle, N.; Faizi, H. A.; Hendricks, G. L.; Tori, K.; Pan, W.; Huang, X.; Steele, A. D.; Csatary, E. E.; Dekarske, M. M.; Rosen, J. L.; Ribeiro, N. Q.; Lee, K.; Port, J.; Fuchs, B. B.; Vlahovska, P. M.; Wuest, W. M.; Gao, H.; Ausubel, F. M.; Mylonakis, E., A selective membrane-targeting repurposed antibiotic with activity against persistent methicillin-resistant Staphylococcus aureus. *Proc Natl Acad Sci U S A* **2019,** *116* (33), 16529-16534.

70. Kim, W.; Steele, A. D.; Zhu, W.; Csatary, E. E.; Fricke, N.; Dekarske, M. M.; Jayamani, E.; Pan, W.; Kwon, B.; Sinitsa, I. F.; Rosen, J. L.; Conery, A. L.; Fuchs, B. B.; Vlahovska, P. M.; Ausubel, F. M.; Gao, H.; Wuest, W. M.; Mylonakis, E., Discovery and Optimization of nTZDpa as an Antibiotic Effective Against Bacterial Persisters. *ACS Infect Dis* **2018,** *4* (11), 1540-1545.

71. Kim, W.; Zhu, W.; Hendricks, G. L.; Van Tyne, D.; Steele, A. D.; Keohane, C. E.; Fricke, N.; Conery, A. L.; Shen, S.; Pan, W.; Lee, K.; Rajamuthiah, R.; Fuchs, B. B.; Vlahovska, P. M.; Wuest, W. M.; Gilmore, M. S.; Gao, H.; Ausubel, F. M.; Mylonakis, E., A new class of synthetic retinoid antibiotics effective against bacterial persisters. *Nature* **2018,** *556* (7699), 103-107.

72. Rajagopal, M.; Walker, S., Envelope Structures of Gram-Positive Bacteria. *Curr Top Microbiol Immunol* **2017,** *404*, 1-44.

73. Neuhaus, F. C.; Baddiley, J., A continuum of anionic charge: structures and functions of D-alanyl-teichoic acids in gram-positive bacteria. *Microbiol Mol Biol Rev* **2003,** *67* (4), 686-723.

74. Weidenmaier, C.; Kokai-Kun, J. F.; Kristian, S. A.; Chanturiya, T.; Kalbacher, H.; Gross, M.; Nicholson, G.; Neumeister, B.; Mond, J. J.; Peschel, A., Role of teichoic acids in Staphylococcus aureus nasal colonization, a major risk factor in nosocomial infections. *Nature Medicine* **2004,** *10*, 243.

75. Swoboda, J. G.; Campbell, J.; Meredith, T. C.; Walker, S., Wall teichoic acid function, biosynthesis, and inhibition. *Chembiochem* **2010,** *11* (1), 35-45.

76. Reichmann, N. T.; Grundling, A., Location, synthesis and function of glycolipids and polyglycerolphosphate lipoteichoic acid in Gram-positive bacteria of the phylum Firmicutes. *FEMS Microbiol Lett* **2011,** *319* (2), 97-105.

77. Xia, G.; Maier, L.; Sanchez-Carballo, P.; Li, M.; Otto, M.; Holst, O.; Peschel, A., Glycosylation of wall teichoic acid in Staphylococcus aureus by TarM. *J Biol Chem* **2010,** *285* (18), 13405-15.

78. Xia, G.; Kohler, T.; Peschel, A., The wall teichoic acid and lipoteichoic acid polymers of Staphylococcus aureus. *Int J Med Microbiol* **2010,** *300* (2-3), 148-54.

79. Brown, S.; Santa Maria, J. P., Jr.; Walker, S., Wall teichoic acids of gram-positive bacteria. *Annu Rev Microbiol* **2013,** *67*, 313-36.

80. Gründling, A.; Schneewind, O., Synthesis of glycerol phosphate lipoteichoic acid in Staphylococcus aureus. *Proceedings of the National Academy of Sciences of the United States of America* **2007,** *104* (20), 8478-8483.

81. Schirner, K.; Marles-Wright, J.; Lewis, R. J.; Errington, J., Distinct and essential morphogenic functions for wall- and lipo-teichoic acids in Bacillus subtilis. *EMBO J* **2009,** *28* (7), 830-42.

82. Schneewind, O.; Missiakas, D., Lipoteichoic acids, phosphate-containing polymers in the envelope of gram-positive bacteria. *J Bacteriol* **2014,** *196* (6), 1133-42.

83. Fischer, W., Physiology of lipoteichoic acids in bacteria. *Adv Microb Physiol* **1988,** *29*, 233-302.

84. Fischer, W., Lipoteichoic acids and lipoglycans. In *New comprehensive biochemistry*, Elsevier Science: Amsterdam, The Netherlands, 1994; Vol. 27, pp 199–215.

85. Schmidt, R. R.; Pedersen, C. M.; Qiao, Y.; Zahringer, U., Chemical synthesis of bacterial lipoteichoic acids: an insight on its biological significance. *Org Biomol Chem* **2011,** *9* (7), 2040-52.

86. Fischer, W., Pneumococcal lipoteichoic and teichoic acid. *Microb Drug Resist* **1997,** *3* (4), 309-25.

87. Seo, H. S.; Cartee, R. T.; Pritchard, D. G.; Nahm, M. H., A new model of pneumococcal lipoteichoic acid structure resolves biochemical, biosynthetic, and serologic inconsistencies of the current model. *J Bacteriol* **2008,** *190* (7), 2379-87.

88. Percy, M. G.; Gründling, A., Lipoteichoic Acid Synthesis and Function in Gram-Positive Bacteria. *Annual Review of Microbiology* **2014,** *68* (1), 81-100.

89. Campbell, J.; Singh, A. K.; Santa Maria, J. P., Jr.; Kim, Y.; Brown, S.; Swoboda, J. G.; Mylonakis, E.; Wilkinson, B. J.; Walker, S., Synthetic lethal compound combinations reveal a fundamental connection between wall teichoic acid and peptidoglycan biosyntheses in Staphylococcus aureus. *ACS Chem Biol* **2011,** *6* (1), 106-16.

90. Andre, G.; Deghorain, M.; Bron, P. A.; van, S., II; Kleerebezem, M.; Hols, P.; Dufrene, Y. F., Fluorescence and atomic force microscopy imaging of wall teichoic acids in Lactobacillus plantarum. *ACS Chem Biol* **2011,** *6* (4), 366-76.

91. Hess, N.; Waldow, F.; Kohler, T. P.; Rohde, M.; Kreikemeyer, B.; Gomez-Mejia, A.; Hain, T.; Schwudke, D.; Vollmer, W.; Hammerschmidt, S.; Gisch, N., Lipoteichoic acid deficiency permits normal growth but impairs virulence of Streptococcus pneumoniae. *Nat Commun* **2017,** *8* (1), 2093.

92. Novick, R. P., Autoinduction and signal transduction in the regulation of staphylococcal virulence. *Mol Microbiol* **2003,** *48* (6), 1429-49.

93. Vuong, C.; Gotz, F.; Otto, M., Construction and characterization of an agr deletion mutant of Staphylococcus epidermidis. *Infect Immun* **2000,** *68* (3), 1048-53.

94. Wanner, S.; Schade, J.; Keinhorster, D.; Weller, N.; George, S. E.; Kull, L.; Bauer, J.; Grau, T.; Winstel, V.; Stoy, H.; Kretschmer, D.; Kolata, J.; Wolz, C.; Broker, B. M.; Weidenmaier, C., Wall teichoic acids mediate increased virulence in Staphylococcus aureus. *Nat Microbiol* **2017,** *2*, 16257.

95. Poyart, C.; Pellegrini, E.; Marceau, M.; Baptista, M.; Jaubert, F.; Lamy, M. C.; Trieu-Cuot, P., Attenuated virulence of Streptococcus agalactiae deficient in D-alanyl-lipoteichoic acid is due to an increased susceptibility to defensins and phagocytic cells. *Mol Microbiol* **2003,** *49* (6), 1615-25.

96. Fedtke, I.; Mader, D.; Kohler, T.; Moll, H.; Nicholson, G.; Biswas, R.; Henseler, K.; Gotz, F.; Zahringer, U.; Peschel, A., A Staphylococcus aureus ypfP mutant with strongly reduced lipoteichoic acid (LTA) content: LTA governs bacterial surface properties and autolysin activity. *Mol Microbiol* **2007,** *65* (4), 1078-91.

97. Heilmann, C.; Schweitzer, O.; Gerke, C.; Vanittanakom, N.; Mack, D.; Gotz, F., Molecular basis of intercellular adhesion in the biofilm-forming Staphylococcus epidermidis. *Mol Microbiol* **1996,** *20* (5), 1083-91.

98. Gross, M.; Cramton, S. E.; Gotz, F.; Peschel, A., Key role of teichoic acid net charge in Staphylococcus aureus colonization of artificial surfaces. *Infect Immun* **2001,** *69* (5), 3423-6.

99. Fabretti, F.; Theilacker, C.; Baldassarri, L.; Kaczynski, Z.; Kropec, A.; Holst, O.; Huebner, J., Alanine esters of enterococcal lipoteichoic acid play a role in biofilm formation and resistance to antimicrobial peptides. *Infect Immun* **2006,** *74* (7), 4164-71.

100. Fedtke, I.; Mader, D.; Kohler, T.; Moll, H.; Nicholson, G.; Biswas, R.; Henseler, K.; Gotz, F.; Zahringer, U.; Peschel, A., A Staphylococcus aureus ypfP mutant with strongly reduced lipoteichoic acid (LTA) content: LTA governs bacterial surface properties and autolysin activity. *Mol Microbiol* **2007,** *65* (4), 1078-91.

101. May, J. J.; Finking, R.; Wiegeshoff, F.; Weber, T. T.; Bandur, N.; Koert, U.; Marahiel, M. A., Inhibition of the D-alanine:D-alanyl carrier protein ligase from Bacillus subtilis increases the bacterium's susceptibility to antibiotics that target the cell wall. *FEBS J* **2005,** *272* (12), 2993-3003.

102. Campbell, J.; Singh, A. K.; Swoboda, J. G.; Gilmore, M. S.; Wilkinson, B. J.; Walker, S., An antibiotic that inhibits a late step in wall teichoic acid biosynthesis induces the cell wall stress stimulon in Staphylococcus aureus. *Antimicrob Agents Chemother* **2012,** *56* (4), 1810-20.

103. Zhu, X.; Liu, D.; Singh, A. K.; Drolia, R.; Bai, X.; Tenguria, S.; Bhunia, A. K., Tunicamycin Mediated Inhibition of Wall Teichoic Acid Affects Staphylococcus aureus and Listeria monocytogenes Cell Morphology, Biofilm Formation and Virulence. *Front Microbiol* **2018,** *9*, 1352.

104. Wang, H.; Gill, C. J.; Lee, S. H.; Mann, P.; Zuck, P.; Meredith, T. C.; Murgolo, N.; She, X.; Kales, S.; Liang, L.; Liu, J.; Wu, J.; Santa Maria, J.; Su, J.; Pan, J.; Hailey, J.; McGuinness, D.; Tan, C. M.; Flattery, A.; Walker, S.; Black, T.; Roemer, T., Discovery of wall teichoic acid inhibitors as potential anti-MRSA beta-lactam combination agents. *Chem Biol* **2013,** *20* (2), 272-84.

105. Richter, S. G.; Elli, D.; Kim, H. K.; Hendrickx, A. P. A.; Sorg, J. A.; Schneewind, O.; Missiakas, D., Small molecule inhibitor of lipoteichoic acid synthesis is an antibiotic for Gram-positive bacteria. *Proc Natl Acad Sci U S A* **2013,** *110* (9), 3531-3536.

106. Vickery, C. R.; Wood, B. M.; Morris, H. G.; Losick, R.; Walker, S., Reconstitution of Staphylococcus aureus Lipoteichoic Acid Synthase Activity Identifies Congo Red as a Selective Inhibitor. *J Am Chem Soc* **2018,** *140* (3), 876-879.

107. Tong, S. Y. C.; Davis, J. S.; Eichenberger, E.; Holland, T. L.; Fowler, V. G., *Staphylococcus aureus* Infections: Epidemiology, Pathophysiology, Clinical Manifestations, and Management. *Clinical Microbiology Reviews* **2015,** *28* (3), 603.

108. Chambers, H. F.; Deleo, F. R., Waves of resistance: Staphylococcus aureus in the antibiotic era. *Nature reviews. Microbiology* **2009,** *7* (9), 629-641.

109. Cosgrove, S. E.; Sakoulas, G.; Perencevich, E. N.; Schwaber, M. J.; Karchmer, A. W.; Carmeli, Y., Comparison of Mortality Associated with Methicillin-Resistant and Methicillin-Susceptible Staphylococcus aureus Bacteremia: A Meta-analysis. *Clinical Infectious Diseases* **2003,** *36* (1), 53-59.

110. . Centers for disease control and prevention (CDC). Antibiotic resistance threats in the United State 2013. (accessed 02/20/2018).

111. Gross, M., Antibiotics in crisis. *Current Biology* **2013,** *23* (24), R1063-R1065.

112. Howden, B. P.; Davies, J. K.; Johnson, P. D. R.; Stinear, T. P.; Grayson, M. L., Reduced vancomycin susceptibility in Staphylococcus aureus, including vancomycin-intermediate and heterogeneous vancomycin-intermediate strains: resistance mechanisms, laboratory detection, and clinical implications. *Clinical Microbiology Reviews* **2010,** *23* (1), 99-139.

113. Malanovic, N.; Lohner, K., Gram-positive bacterial cell envelopes: The impact on the activity of antimicrobial peptides. *Biochimica et Biophysica Acta (BBA) - Biomembranes* **2016,** *1858* (5), 936-946.

114. Lu, D.; Wörmann, M. E.; Zhang, X.; Schneewind, O.; Gründling, A.; Freemont, P. S., Structure-based mechanism of lipoteichoic acid synthesis by Staphylococcus aureus LtaS. *Proceedings of the National Academy of Sciences* **2009,** *106* (5), 1584-1589.

115. Richter, S. G.; Elli, D.; Kim, H. K.; Hendrickx, A. P. A.; Sorg, J. A.; Schneewind, O.; Missiakas, D., Small molecule inhibitor of lipoteichoic acid synthesis is an antibiotic for Gram-positive bacteria. *Proceedings of the National Academy of Sciences* **2013,** *110* (9), 3531-3536.

116. Vickery, C. R.; Wood, B. M.; Morris, H. G.; Losick, R.; Walker, S., Reconstitution of Staphylococcus aureus Lipoteichoic Acid Synthase Activity Identifies Congo Red as a Selective Inhibitor. *Journal of the American Chemical Society* **2018,** *140* (3), 876-879.

117. Opoku-Temeng, C.; Naclerio, G. A.; Mohammad, H.; Dayal, N.; Abutaleb, N. S.; Seleem, M. N.; Sintim, H. O., N-(1,3,4-oxadiazol-2-yl)benzamide analogs, bacteriostatic agents against methicillin- and vancomycin-resistant bacteria. *Eur J Med Chem* **2018,** *155*, 797-805.

118. Sun, J.; Makawana, J. A.; Zhu, H. L., 1,3,4-oxadiazole derivatives as potential biological agents. *Mini Rev Med Chem* **2013,** *13* (12), 1725-43.

119. de Oliveira, C. S.; Lira, B. F.; Barbosa-Filho, J. M.; Lorenzo, J. G.; de Athayde-Filho, P. F., Synthetic approaches and pharmacological activity of 1,3,4-oxadiazoles: a review of the literature from 2000-2012. *Molecules* **2012,** *17* (9), 10192-231.

120. Steigbigel, R. T.; Cooper, D. A.; Kumar, P. N.; Eron, J. E.; Schechter, M.; Markowitz, M.; Loutfy, M. R.; Lennox, J. L.; Gatell, J. M.; Rockstroh, J. K.; Katlama, C.; Yeni, P.; Lazzarin, A.; Clotet, B.; Zhao, J.; Chen, J.; Ryan, D. M.; Rhodes, R. R.; Killar, J. A.; Gilde, L. R.; Strohmaier, K. M.; Meibohm, A. R.; Miller, M. D.; Hazuda, D. J.; Nessly, M. L.; DiNubile, M. J.; Isaacs, R. D.; Nguyen, B. Y.; Teppler, H.; Teams, B. S., Raltegravir with optimized background therapy for resistant HIV-1 infection. *N Engl J Med* **2008,** *359* (4), 339-54.

121. Trump, D. L.; Payne, H.; Miller, K.; de Bono, J. S.; Stephenson, J., 3rd; Burris, H. A., 3rd; Nathan, F.; Taboada, M.; Morris, T.; Hubner, A., Preliminary study of the specific endothelin a receptor antagonist zibotentan in combination with docetaxel in patients with metastatic castration-resistant prostate cancer. *Prostate* **2011,** *71* (12), 1264-75.

122. Barreiro, E. J.; Kummerle, A. E.; Fraga, C. A., The methylation effect in medicinal chemistry. *Chem Rev* **2011,** *111* (9), 5215-46.

123. Drewes, G.; Knapp, S., Chemoproteomics and Chemical Probes for Target Discovery. *Trends Biotechnol* **2018,** *36* (12), 1275-1286.

124. Mertes, F.; Elsharawy, A.; Sauer, S.; van Helvoort, J. M.; van der Zaag, P. J.; Franke, A.; Nilsson, M.; Lehrach, H.; Brookes, A. J., Targeted enrichment of genomic DNA regions for next-generation sequencing. *Brief Funct Genomics* **2011,** *10* (6), 374-86.

125. Lomenick, B.; Olsen, R. W.; Huang, J., Identification of direct protein targets of small molecules. *ACS Chem Biol* **2011,** *6* (1), 34-46.

126. Nguyen, H. M.; Graber, C. J., Limitations of antibiotic options for invasive infections caused by methicillin-resistant Staphylococcus aureus: is combination therapy the answer? *J Antimicrob Chemother* **2010,** *65* (1), 24-36.

127. Antonoplis, A.; Zang, X.; Huttner, M. A.; Chong, K. K. L.; Lee, Y. B.; Co, J. Y.; Amieva, M. R.; Kline, K. A.; Wender, P. A.; Cegelski, L., A Dual-Function Antibiotic-Transporter Conjugate Exhibits Superior Activity in Sterilizing MRSA Biofilms and Killing Persister Cells. *J Am Chem Soc* **2018,** *140* (47), 16140-16151.

128. Garrison, A. T.; Abouelhassan, Y.; Kallifidas, D.; Tan, H.; Kim, Y. S.; Jin, S.; Luesch, H.; Huigens, R. W., 3rd, An Efficient Buchwald-Hartwig/Reductive Cyclization for the Scaffold Diversification of Halogenated Phenazines: Potent Antibacterial Targeting, Biofilm Eradication, and Prodrug Exploration. *J Med Chem* **2018,** *61* (9), 3962-3983.

129. Huggins, W. M.; Barker, W. T.; Baker, J. T.; Hahn, N. A.; Melander, R. J.; Melander, C., Meridianin D Analogues Display Antibiofilm Activity against MRSA and Increase Colistin Efficacy in Gram-Negative Bacteria. *ACS Med Chem Lett* **2018,** *9* (7), 702-707.

130. Vermote, A.; Van Calenbergh, S., Small-Molecule Potentiators for Conventional Antibiotics against Staphylococcus aureus. *ACS Infect Dis* **2017,** *3* (11), 780-796.

131. de Kraker, M. E.; Stewardson, A. J.; Harbarth, S., Will 10 Million People Die a Year due to Antimicrobial Resistance by 2050? *PLoS Med* **2016,** *13* (11), e1002184.

132. Frieden, T. Centers for disease control and prevention (CDC). Antibiotic resistance threats in the United States 2013. (accessed 02/20/2018).

133. Ciofu, O.; Rojo-Molinero, E.; Macia, M. D.; Oliver, A., Antibiotic treatment of biofilm infections. *APMIS* **2017,** *125* (4), 304-319.

134. Naclerio, G. A.; Karanja, C. W.; Opoku-Temeng, C.; Sintim, H. O., Antibacterial Small Molecules That Potently Inhibit Staphylococcus aureus Lipoteichoic Acid Biosynthesis. *ChemMedChem* **2019,** *14* (10), 1000-1004.

135. Opoku-Temeng, C.; Zhou, J.; Zheng, Y.; Su, J.; Sintim, H. O., Cyclic dinucleotide (c-di-GMP, c-di-AMP, and cGAMP) signalings have come of age to be inhibited by small molecules. *Chem Commun (Camb)* **2016,** *52* (60), 9327-42.

136. Rabin, N.; Zheng, Y.; Opoku-Temeng, C.; Du, Y.; Bonsu, E.; Sintim, H. O., Biofilm formation mechanisms and targets for developing antibiofilm agents. *Future Med Chem* **2015,** *7* (4), 493-512.

137. Sugimoto, S.; Sato, F.; Miyakawa, R.; Chiba, A.; Onodera, S.; Hori, S.; Mizunoe, Y., Broad impact of extracellular DNA on biofilm formation by clinically isolated Methicillin-resistant and -sensitive strains of Staphylococcus aureus. *Sci Rep* **2018,** *8* (1), 2254.

138. Whitchurch, C. B.; Tolker-Nielsen, T.; Ragas, P. C.; Mattick, J. S., Extracellular DNA required for bacterial biofilm formation. *Science* **2002,** *295* (5559), 1487.

139. Kavanaugh, J. S.; Flack, C. E.; Lister, J.; Ricker, E. B.; Ibberson, C. B.; Jenul, C.; Moormeier, D. E.; Delmain, E. A.; Bayles, K. W.; Horswill, A. R., Identification of Extracellular DNA-Binding Proteins in the Biofilm Matrix. *MBio* **2019,** *10* (3).

140. Foulston, L.; Elsholz, A. K.; DeFrancesco, A. S.; Losick, R., The extracellular matrix of Staphylococcus aureus biofilms comprises cytoplasmic proteins that associate with the cell surface in response to decreasing pH. *MBio* **2014,** *5* (5), e01667-14.

141. Elchinger, P. H.; Delattre, C.; Faure, S.; Roy, O.; Badel, S.; Bernardi, T.; Taillefumier, C.; Michaud, P., Effect of proteases against biofilms of Staphylococcus aureus and Staphylococcus epidermidis. *Lett Appl Microbiol* **2014,** *59* (5), 507-13.

142. Kaplan, J. B.; LoVetri, K.; Cardona, S. T.; Madhyastha, S.; Sadovskaya, I.; Jabbouri, S.; Izano, E. A., Recombinant human DNase I decreases biofilm and increases antimicrobial susceptibility in staphylococci. *J Antibiot (Tokyo)* **2012,** *65* (2), 73-7.

143. Kiedrowski, M. R.; Kavanaugh, J. S.; Malone, C. L.; Mootz, J. M.; Voyich, J. M.; Smeltzer, M. S.; Bayles, K. W.; Horswill, A. R., Nuclease modulates biofilm formation in community-associated methicillin-resistant Staphylococcus aureus. *PLoS One* **2011,** *6* (11), e26714.

144. Darouiche, R. O.; Mansouri, M. D.; Gawande, P. V.; Madhyastha, S., Antimicrobial and antibiofilm efficacy of triclosan and DispersinB combination. *J Antimicrob Chemother* **2009,** *64* (1), 88-93.

145. Kaplan, J. B.; Ragunath, C.; Ramasubbu, N.; Fine, D. H., Detachment of Actinobacillus actinomycetemcomitans biofilm cells by an endogenous beta-hexosaminidase activity. *J Bacteriol* **2003,** *185* (16), 4693-8.

146. Suzuki, T.; Swoboda, J. G.; Campbell, J.; Walker, S.; Gilmore, M. S., In vitro antimicrobial activity of wall teichoic acid biosynthesis inhibitors against Staphylococcus aureus isolates. *Antimicrob Agents Chemother* **2011,** *55* (2), 767-74.

147. Nair, S.; Desai, S.; Poonacha, N.; Vipra, A.; Sharma, U., Antibiofilm Activity and Synergistic Inhibition of Staphylococcus aureus Biofilms by Bactericidal Protein P128 in Combination with Antibiotics. *Antimicrob Agents Chemother* **2016,** *60* (12), 7280-7289.

148. Eldesouky, H. E.; Li, X. Y.; Abutaleb, N. S.; Mohammad, H.; Seleem, M. N., Synergistic interactions of sulfamethoxazole and azole antifungal drugs against emerging multidrug-resistant Candida auris. *Int J Antimicrob Ag* **2018,** *52* (6), 754-761.

149. Mohammad, H.; Cushman, M.; Seleem, M. N., Antibacterial Evaluation of Synthetic Thiazole Compounds In Vitro and In Vivo in a Methicillin-Resistant Staphylococcus aureus (MRSA) Skin Infection Mouse Model. *PLoS One* **2015,** *10* (11).

150. Meletiadis, J.; Pournaras, S.; Roilides, E.; Walsh, T. J., Defining Fractional Inhibitory Concentration Index Cutoffs for Additive Interactions Based on Self-Drug Additive Combinations, Monte Carlo Simulation Analysis, and In Vitro-In Vivo Correlation Data for Antifungal Drug Combinations against Aspergillus fumigatus. *Antimicrob Agents Ch* **2010,** *54* (2), 602-609.

151. Moellering, R. C., Jr., Current treatment options for community-acquired methicillin-resistant Staphylococcus aureus infection. *Clin Infect Dis* **2008,** *46* (7), 1032-7.

152. Rasmussen, R. V.; Fowler, V. G., Jr.; Skov, R.; Bruun, N. E., Future challenges and treatment of Staphylococcus aureus bacteremia with emphasis on MRSA. *Future Microbiol* **2011,** *6* (1), 43-56.

153. Huovinen, P., Resistance to trimethoprim-sulfamethoxazole. *Clin Infect Dis* **2001,** *32* (11), 1608-14.

154. Azhar, A.; Rasool, S.; Haque, A.; Shan, S.; Saeed, M.; Ehsan, B.; Haque, A., Detection of high levels of resistance to linezolid and vancomycin in Staphylococcus aureus. *J Med Microbiol* **2017,** *66* (9), 1328-1331.

155. Roch, M.; Gagetti, P.; Davis, J.; Ceriana, P.; Errecalde, L.; Corso, A.; Rosato, A. E., Daptomycin Resistance in Clinical MRSA Strains Is Associated with a High Biological Fitness Cost. *Front Microbiol* **2017,** *8*, 2303.

156. Naclerio, G. A.; Sintim, H. O., Multiple ways to kill bacteria via inhibiting novel cell wall or membrane targets. *Future Med Chem* **2020,** *12* (13), 1253-1279.

157. Hesser, A. R.; Matano, L. M.; Vickery, C. R.; Wood, B. M.; Santiago, A. G.; Morris, H. G.; Do, T.; Losick, R.; Walker, S., The length of lipoteichoic acid polymers controls Staphylococcus aureus cell size and envelope integrity. *J Bacteriol* **2020**.

158. Collins, L. V.; Kristian, S. A.; Weidenmaier, C.; Faigle, M.; Van Kessel, K. P.; Van Strijp, J. A.; Gotz, F.; Neumeister, B.; Peschel, A., Staphylococcus aureus strains lacking D-alanine modifications of teichoic acids are highly susceptible to human neutrophil killing and are virulence attenuated in mice. *J Infect Dis* **2002,** *186* (2), 214-9.

159. Sheen, T. R.; Ebrahimi, C. M.; Hiemstra, I. H.; Barlow, S. B.; Peschel, A.; Doran, K. S., Penetration of the blood-brain barrier by Staphylococcus aureus: contribution of membrane-anchored lipoteichoic acid. *J Mol Med (Berl)* **2010,** *88* (6), 633-9.

160. Cabacungan, E.; Pieringer, R. A., Mode of elongation of the glycerol phosphate polymer of membrane lipoteichoic acid of Streptococcus faecium ATCC 9790. *J Bacteriol* **1981,** *147* (1), 75-9.

161. Taron, D. J.; Childs, W. C., 3rd; Neuhaus, F. C., Biosynthesis of D-alanyl-lipoteichoic acid: role of diglyceride kinase in the synthesis of phosphatidylglycerol for chain elongation. *J Bacteriol* **1983,** *154* (3), 1110-6.

162. Canepari, P.; Boaretti, M., Lipoteichoic acid as a target for antimicrobial action. *Microb Drug Resist* **1996,** *2* (1), 85-9.

163. Naclerio, G. A.; Abutaleb, N. S.; Li, D.; Seleem, M. N.; Sintim, H. O., Ultrapotent Inhibitor of Clostridioides difficile Growth, Which Suppresses Recurrence In Vivo. *J. Med. Chem.* **2020,** *63* (20), 11934-11944.

164. Naclerio, G. A.; Abutaleb, N. S.; Onyedibe, K. I.; Seleem, M. N.; Sintim, H. O., Potent trifluoromethoxy, trifluoromethylsulfonyl, trifluoromethylthio and pentafluorosulfanyl containing (1,3,4-oxadiazol-2-yl)benzamides against drug-resistant Gram-positive bacteria. *RSC Med Chem* **2020,** *11* (1), 102-110.

165. Naclerio, G. A.; Abutaleb, N. S.; Alhashimi, M.; Seleem, M. N.; Sintim, H. O., N-(1,3,4-Oxadiazol-2-yl)Benzamides as Antibacterial Agents against Neisseria gonorrhoeae. *Int J Mol Sci* **2021,** *22* (5), 2427.

166. Naclerio, G. A.; Onyedibe, K. I.; Sintim, H. O., Lipoteichoic Acid Biosynthesis Inhibitors as Potent Inhibitors of S. aureus and E. faecalis Growth and Biofilm Formation. *Molecules* **2020,** *25* (5), 2277.

167. Bridy-Pappas, A. E.; Margolis, M. B.; Center, K. J.; Isaacman, D. J., Streptococcus pneumoniae: description of the pathogen, disease epidemiology, treatment, and prevention. *Pharmacotherapy* **2005,** *25* (9), 1193-212.

168. Brooks, L. R. K.; Mias, G. I., Streptococcus pneumoniae's Virulence and Host Immunity: Aging, Diagnostics, and Prevention. *Front Immunol* **2018,** *9*, 1366.

169. Kourtis, A. P.; Hatfield, K.; Baggs, J.; Mu, Y.; See, I.; Epson, E.; Nadle, J.; Kainer, M. A.; Dumyati, G.; Petit, S.; Ray, S. M.; Ham, D.; Capers, C.; Ewing, H.; Coffin, N.; McDonald, L. C.; Jernigan, J.; Cardo, D., Vital Signs: Epidemiology and Recent Trends in Methicillin-Resistant and in Methicillin-Susceptible Staphylococcus Aureus Bloodstream Infections — United States. *MWR Morb Mortal Wkly Rep* **2019,** *68*, 214-219.

170. CDC. Antibiotic Resistance Threats in the United States. www.cdc.gov/DrugResistance/Biggest-Threats.html.

171. Abutaleb, N. S.; Elkashif, A.; Flaherty, D. P.; Seleem, M. N., In Vivo Antibacterial Activity of Acetazolamide. *Antimicrob Agents Chemother* **2021,** *65* (4).

172. Abutaleb, N. S.; Seleem, M. N., Antivirulence activity of auranofin against vancomycin-resistant enterococci: in vitro and in vivo studies. *Int J Antimicrob Agents* **2020,** *55* (3), 105828.

173. Abutaleb, N. S.; Elhassanny, A. E. M.; Flaherty, D. P.; Seleem, M. N., In vitro and in vivo activities of the carbonic anhydrase inhibitor, dorzolamide, against vancomycin-resistant enterococci. *PeerJ* **2021,** *9*, e11059.

174. Tyanova, S.; Temu, T.; Sinitcyn, P.; Carlson, A.; Hein, M. Y.; Geiger, T.; Mann, M.; Cox, J., The Perseus computational platform for comprehensive analysis of (prote)omics data. *Nat Methods* **2016,** *13* (9), 731-40.

175. Hu, Y.; Meng, J.; Shi, C.; Hervin, K.; Fratamico, P. M.; Shi, X., Characterization and comparative analysis of a second thermonuclease from Staphylococcus aureus. *Microbiol Res* **2013,** *168* (3), 174-82.

176. Parrish, J. Z.; Xue, D., Cuts can kill: the roles of apoptotic nucleases in cell death and animal development. *Chromosoma* **2006,** *115* (2), 89-97.

177. Kneuper, H.; Cao, Z. P.; Twomey, K. B.; Zoltner, M.; Jager, F.; Cargill, J. S.; Chalmers, J.; van der Kooi-Pol, M. M.; van Dijl, J. M.; Ryan, R. P.; Hunter, W. N.; Palmer, T., Heterogeneity in ess transcriptional organization and variable contribution of the Ess/Type VII protein secretion system to virulence across closely related Staphylocccus aureus strains. *Mol Microbiol* **2014,** *93* (5), 928-43.

178. Hsia, K. C.; Li, C. L.; Yuan, H. S., Structural and functional insight into sugar-nonspecific nucleases in host defense. *Curr Opin Struct Biol* **2005,** *15* (1), 126-34.

179. Lopez, M. S.; Tan, I. S.; Yan, D.; Kang, J.; McCreary, M.; Modrusan, Z.; Austin, C. D.; Xu, M.; Brown, E. J., Host-derived fatty acids activate type VII secretion in Staphylococcus aureus. *Proc Natl Acad Sci U S A* **2017,** *114* (42), 11223-11228.

180. Chaudhuri, R. R.; Allen, A. G.; Owen, P. J.; Shalom, G.; Stone, K.; Harrison, M.; Burgis, T. A.; Lockyer, M.; Garcia-Lara, J.; Foster, S. J.; Pleasance, S. J.; Peters, S. E.; Maskell, D. J.; Charles, I. G., Comprehensive identification of essential Staphylococcus aureus genes using Transposon-Mediated Differential Hybridisation (TMDH). *BMC Genomics* **2009,** *10*, 291.

181. Li, C.; Tan, B. K.; Zhao, J.; Guan, Z., In Vivo and in Vitro Synthesis of Phosphatidylglycerol by an Escherichia coli Cardiolipin Synthase. *J Biol Chem* **2016,** *291* (48), 25144-25153.

182. Zhang, Y. M.; Rock, C. O., Membrane lipid homeostasis in bacteria. *Nat Rev Microbiol* **2008,** *6* (3), 222-33.

183. Wright, M. H.; Sieber, S. A., Chemical proteomics approaches for identifying the cellular targets of natural products. *Nat Prod Rep* **2016,** *33* (5), 681-708.

184. Schenone, M.; Dancik, V.; Wagner, B. K.; Clemons, P. A., Target identification and mechanism of action in chemical biology and drug discovery. *Nat Chem Biol* **2013,** *9* (4), 232-40.

185. Ong, S.; Schenone, M.; Margolin, A. A.; Li, X. L.; Do, K.; Doud, M. K.; Mani, D. R.; Kuai, L.; Wang, X.; Wood, J. L.; Tolliday, N. J.; Koehler, A. N.; Marcaurelle, T. R.; Gould, R. J.; Schreiber, S.; Carr, S. A., Identifying the proteins to which small-molecule probes and drugs bind in cells. *Proc Natl Acad Sci U S A* **2009,** *106* (12), 4617-4622.

186. Chen, X.; Wang, Y.; Ma, N.; Tian, J.; Shao, Y.; Zhu, B.; Wong, Y. K.; Liang, Z.; Zou, C.; Wang, J., Target identification of natural medicine with chemical proteomics approach: probe synthesis, target fishing and protein identification. *Signal Transduct Target Ther* **2020,** *5* (1), 72.

187. Grundling, A.; Schneewind, O., Genes required for glycolipid synthesis and lipoteichoic acid anchoring in Staphylococcus aureus. *J Bacteriol* **2007,** *189* (6), 2521-30.

188. Kiriukhin, M. Y.; Debabov, D. V.; Shinabarger, D. L.; Neuhaus, F. C., Biosynthesis of the glycolipid anchor in lipoteichoic acid of Staphylococcus aureus RN4220: role of YpfP, the diglucosyldiacylglycerol synthase. *J Bacteriol* **2001,** *183* (11), 3506-14.

189. Xie, Z.; Gonzalez, L. E.; Ferreira, C. R.; Vorsilak, A.; Frabutt, D.; Sobreira, T. J. P.; Pugia, M.; Cooks, R. G., Multiple Reaction Monitoring Profiling (MRM-Profiling) of Lipids To Distinguish Strain-Level Differences in Microbial Resistance in Escherichia coli. *Anal Chem* **2019,** *91* (17), 11349-11354.

190. Wenzel, M., Do we really understand how antibiotics work? *Future Microbiol* **2020,** *15*, 1307-1311.

191. Grein, F.; Muller, A.; Scherer, K. M.; Liu, X.; Ludwig, K. C.; Klockner, A.; Strach, M.; Sahl, H. G.; Kubitscheck, U.; Schneider, T., Ca(2+)-Daptomycin targets cell wall biosynthesis by forming a tripartite complex with undecaprenyl-coupled intermediates and membrane lipids. *Nat Commun* **2020,** *11* (1), 1455.

192. Wenzel, M.; Dekker, M. P.; Wang, B.; Burggraaf, M. J.; Bitter, W.; van Weering, J. R.; Hamoen, L. W., A flat embedding method for transmission electron microscopy reveals an unknown mechanism of tetracycline. *Commun Biol* **2021,** *4*.

193. Montgomery, C. P.; Daniels, M. D.; Zhao, F.; Spellberg, B.; Chong, A. S.; Daum, R. S., Local inflammation exacerbates the severity of Staphylococcus aureus skin infection. *PLoS One* **2013,** *8* (7), e69508.

194. Kengatharan, K. M.; De Kimpe, S.; Robson, C.; Foster, S. J.; Thiemermann, C., Mechanism of gram-positive shock: identification of peptidoglycan and lipoteichoic acid moieties essential in the induction of nitric oxide synthase, shock, and multiple organ failure. *J Exp Med* **1998,** *188* (2), 305-15.

195. Kang, S. S.; Sim, J. R.; Yun, C. H.; Han, S. H., Lipoteichoic acids as a major virulence factor causing inflammatory responses via Toll-like receptor 2. *Arch Pharm Res* **2016,** *39* (11), 1519-1529.

196. Huang, B. R.; Tsai, C. F.; Lin, H. Y.; Tseng, W. P.; Huang, S. S.; Wu, C. R.; Lin, C.; Yeh, W. L.; Lu, D. Y., Interaction of inflammatory and anti-inflammatory responses in microglia by Staphylococcus aureus-derived lipoteichoic acid. *Toxicol Appl Pharmacol* **2013,** *269* (1), 43-50.

197. Brauweiler, A. M.; Goleva, E.; Leung, D. Y. M., Staphylococcus aureus Lipoteichoic Acid Damages the Skin Barrier through an IL-1-Mediated Pathway. *J Invest Dermatol* **2019,** *139* (8), 1753-1761 e4.

198. Fournier, B.; Philpott, D. J., Recognition of Staphylococcus aureus by the innate immune system. *Clin Microbiol Rev* **2005,** *18* (3), 521-40.

199. Yang, H.; Kundra, S.; Chojnacki, M.; Liu, K.; Fuse, M. A.; Abouelhassan, Y.; Kallifidas, D.; Zhang, P.; Huang, G.; Jin, S.; Ding, Y.; Luesch, H.; Rohde, K. H.; Dunman, P. M.; Lemos, J. A.; Huigens, R. W., 3rd, A Modular Synthetic Route Involving N-Aryl-2-nitrosoaniline Intermediates Leads to a New Series of 3-Substituted Halogenated Phenazine Antibacterial Agents. *J Med Chem* **2021,** *64* (11), 7275-7295.

200. Kaplan, A. R.; Musaev, D. G.; Wuest, W. M., Pyochelin Biosynthetic Metabolites Bind Iron and Promote Growth in Pseudomonads Demonstrating Siderophore-like Activity. *ACS Infect Dis* **2021,** *7* (3), 544-551.

201. Mattingly, A. E.; Cox, K. E.; Smith, R.; Melander, R. J.; Ernst, R. K.; Melander, C., Screening an Established Natural Product Library Identifies Secondary Metabolites That Potentiate Conventional Antibiotics. *ACS Infect Dis* **2020,** *6* (10), 2629-2640.

202. Weig, A. W.; Barlock, S. L.; O'Connor, P. M.; Marciano, O. M.; Smith, R.; Ernst, R. K.; Melander, R. J.; Melander, C., A scaffold hopping strategy to generate new aryl-2-amino pyrimidine MRSA biofilm inhibitors. *RSC Med Chem* **2021,** *12* (2), 293-296.

203. Milly, T. A.; Engler, E. R.; Chichura, K. S.; Buttner, A. R.; Koirala, B.; Tal-Gan, Y.; Bertucci, M. A., Harnessing Multiple, Nonproteogenic Substitutions to Optimize CSP:ComD Hydrophobic Interactions in Group 1 Streptococcus pneumoniae. *Chembiochem* **2021,** *22* (11), 1940-1947.

204. Garcia Chavez, M.; Garcia, A.; Lee, H. Y.; Lau, G. W.; Parker, E. N.; Komnick, K. E.; Hergenrother, P. J., Synthesis of Fusidic Acid Derivatives Yields a Potent Antibiotic with an Improved Resistance Profile. *ACS Infect Dis* **2021,** *7* (2), 493-505.

205. West, K. H. J.; Shen, W.; Eisenbraun, E. L.; Yang, T.; Vasquez, J. K.; Horswill, A. R.; Blackwell, H. E., Non-Native Peptides Capable of Pan-Activating the agr Quorum Sensing System across Multiple Specificity Groups of Staphylococcus epidermidis. *ACS Chem Biol* **2021,** *16* (6), 1070-1078.

206. Boudreau, M. A.; Ding, D.; Meisel, J. E.; Janardhanan, J.; Spink, E.; Peng, Z.; Qian, Y.; Yamaguchi, T.; Testero, S. A.; O'Daniel, P. I.; Leemans, E.; Lastochkin, E.; Song, W.; Schroeder, V. A.; Wolter, W. R.; Suckow, M. A.; Mobashery, S.; Chang, M., Structure-Activity Relationship for the Oxadiazole Class of Antibacterials. *ACS Med Chem Lett* **2020,** *11* (3), 322-326.

207. Peng, Z.; Nguyen, T. T.; Song, W.; Anderson, B.; Wolter, W. R.; Schroeder, V. A.; Hesek, D.; Lee, M.; Mobashery, S.; Chang, M., Selective MMP-9 Inhibitor (R)-ND-336 Alone or in Combination with Linezolid Accelerates Wound Healing in Infected Diabetic Mice. *ACS Pharmacol Transl Sci* **2021,** *4* (1), 107-117.

208. Lin, Y.; Ribaucourt, A.; Moazami, Y.; Pierce, J. G., Concise Synthesis and Antimicrobial Evaluation of the Guanidinium Alkaloid Batzelladine D: Development of a Stereodivergent Strategy. *J Am Chem Soc* **2020,** *142*, 9850-9857.

209. Yang, H.; Liu, K.; Jin, S.; Huigens, R. W., Design, synthesis and biological evaluation of a halogenated phenazine-erythromycin conjugate prodrug for antibacterial applications† *Org. Biomol. Chem.* **2021,** *19*, 1483-1487.

210. Kaur, J.; Soto-Velasquez, M.; Ding, Z.; Ghanbarpour, A.; Lill, M. A.; van Rijn, R. M.; Watts, V. J.; Flaherty, D. P., Optimization of a 1,3,4-oxadiazole series for inhibition of Ca(2+)/calmodulin-stimulated activity of adenylyl cyclases 1 and 8 for the treatment of chronic pain. *Eur J Med Chem* **2019,** *162*, 568-585.

211. Meo, P.; Khan, N. Antibiotic Compounds. 2017.

212. Clinical and Laboratory Standards Institute, C., Methods for dilution antimicrobial susceptibility tests for bacteria that grow aerobically. 9 ed.; 2012.

213. Hosny, Y.; Abutaleb, N. S.; Omara, M.; Alhashimi, M.; Elsebaei, M. M.; Elzahabi, H. S.; Seleem, M. N.; Mayhoub, A. S., Modifying the lipophilic part of phenylthiazole antibiotics to control their drug-likeness. *Eur J Med Chem* **2020,** *185*, 111830.

214. Elsebaei, M. M.; Abutaleb, N. S.; Mahgoub, A. A.; Li, D.; Hagras, M.; Mohammad, H.; Seleem, M. N.; Mayhoub, A. S., Phenylthiazoles with nitrogenous side chain: An approach to overcome molecular obesity. *Eur J Med Chem* **2019,** *182*, 111593.

215. Mohammad, H.; Abutaleb, N. S.; Seleem, M. N., Auranofin Rapidly Eradicates Methicillin-resistant Staphylococcus aureus (MRSA) in an Infected Pressure Ulcer Mouse Model. *Sci Rep* **2020,** *10*, 7251.

216. Mohammad, H.; Kyei-Baffour, K.; Abutaleb, N. S.; Dai, M.; Seleem, M. N., An aryl isonitrile compound with an improved physicochemical profile that is effective in two mouse models of multidrug-resistant Staphylococcus aureus infection. *J Glob Antimicrob Resist* **2019,** *19*, 1-7.

217. Opoku-Temeng, C.; Onyedibe, K. I.; Aryal, U. K.; Sintim, H. O., Proteomic analysis of bacterial response to a 4-hydroxybenzylidene indolinone compound, which re-sensitizes bacteria to traditional antibiotics. *J Proteomics* **2019,** *202*, 103368.

218. Cox, J.; Mann, M., MaxQuant enables high peptide identification rates, individualized p.p.b.-range mass accuracies and proteome-wide protein quantification. *Nat Biotechnol* **2008,** *26* (12), 1367-72.

219. Cox, J.; Hein, M. Y.; Luber, C. A.; Paron, I.; Nagaraj, N.; Mann, M., Accurate proteome-wide label-free quantification by delayed normalization and maximal peptide ratio extraction, termed MaxLFQ. *Mol Cell Proteomics* **2014,** *13* (9), 2513-26.

220. Cox, J.; Neuhauser, N.; Michalski, A.; Scheltema, R. A.; Olsen, J. V.; Mann, M., Andromeda: a peptide search engine integrated into the MaxQuant environment. *J Proteome Res* **2011,** *10* (4), 1794-805.

221. Bligh, E. G.; Dyer, W. J., A rapid method of total lipid extraction and purification. *Can J Biochem Physiol* **1959,** *37* (8), 911-7.

222. Dayal, N.; Opoku-Temeng, C.; Mohammad, H.; Abutaleb, N. S.; Hernandez, D.; Onyedibe, K. I.; Wang, M.; Zeller, M.; Seleem, M. N.; Sintim, H. O., Inhibitors of Intracellular Gram-Positive Bacterial Growth Synthesized via Povarov-Doebner Reactions. *ACS Infect Dis* **2019,** *5* (11), 1820-1830.

223. Brubaker, A. L.; Carter, S. R.; Kovacs, E. J., Experimental Approaches to Tissue Injury and Repair in Advanced Age. *Methods Mol Biol* **2015,** *1343*, 35-51.

224. Hoffmann, J. P.; Friedman, J. K.; Wang, Y.; McLachlan, J. B.; Sammarco, M. C.; Morici, L. A.; Roy, C. J., In situ Treatment With Novel Microbiocide Inhibits Methicillin Resistant Staphylococcus aureus in a Murine Wound Infection Model. *Front Microbiol* **2019,** *10*, 3106.

225. Vågesjö, E.; Öhnstedt, E.; Morier, A.; Lofton, H.; Huss, F.; Proost, P.; Roos, S.; Phillipson, M., Accelerated wound healing in mice by on-site production and delivery of CXCL12 by transformed lactic acid bacteria. *Proc Natl Acad Sci U S A* **2018,** *115* (8), 1895-1900.

226. Organization, W. H., WHO publishes list of bacteria for which new antibiotics are urgently needed. 2017.

227. Azhar, A.; Rasool, S.; Haque, A.; Shan, S.; Saeed, M.; Ehsan, B.; Haque, A., Detection of high levels of resistance to linezolid and vancomycin in Staphylococcus aureus. *J Med Microbiol* **2017,** *66* (9), 1328-1331.

228. Mangala, G. K.; Rao, P. N. S.; Vishwanath, G.; Suresh, K.; Vijayanath, V., Inducible Clindamycin Resistance, Glycopeptide Resistance and Mupirocin Resistance in Methicillin Resistant Staphylococcus aureus (MRSA) Isolated from Clinical Samples. *J Pure Appl Microbio* **2012,** *6* (1), 407-410.

229. Roch, M.; Gagetti, P.; Davis, J.; Ceriana, P.; Errecalde, L.; Corso, A.; Rosato, A. E., Daptomycin Resistance in Clinical MRSA Strains Is Associated with a High Biological Fitness Cost. *Front Microbiol* **2017,** *8*.

230. Fan, T.; Meng, W.; Xiao, Y.; Zhang, X., Synthesis of 5-pentafluorosulfanyl indazoles. *Tetrahedron Letters* **2017,** *58*, 4473-4475.

231. Zhang, Y. M.; Wang, Y. C.; He, C.; Liu, X. R.; Lu, Y. Z.; Chen, T. T.; Pan, Q.; Xiong, J. F.; She, M. Q.; Tu, Z. C.; Qin, X. C.; Li, M. K.; Tortorella, M. D.; Talley, J. J., Pentafluorosulfanyl-Substituted Benzopyran Analogues As New Cyclooxygenase-2 Inhibitors with Excellent Pharmacokinetics and Efficacy in Blocking Inflammation. *Journal of Medicinal Chemistry* **2017,** *60* (10), 4135-4146.

232. Curtis-Prior, P. B.; Prouteau, M., Qualitative and quantitative effects of fenfluramine and tiflorex on food consumption in trained rats offered dietary choices. *Int J Obes* **1983,** *7* (6), 575-81.

233. Bensimon, G.; Lacomblez, L.; Meininger, V., A controlled trial of riluzole in amyotrophic lateral sclerosis. ALS/Riluzole Study Group. *N Engl J Med* **1994,** *330* (9), 585-91.

234. Forhead, A. J.; Jellyman, J. K.; Gillham, K.; Ward, J. W.; Blache, D.; Fowden, A. L., Renal growth retardation following angiotensin II type 1 (AT(1)) receptor antagonism is associated with increased AT(2) receptor protein in fetal sheep. *J Endocrinol* **2011,** *208* (2), 137-45.

235. Harrold, M. W.; Zavod, R. M., *Basic Concepts in Medicinal Chemistry*. 1 ed.; American Society of Health-System Pharmacists, Inc.: Bethesda, MD, 2013.

236. Costerton, J. W.; Stewart, P. S.; Greenberg, E. P., Bacterial biofilms: a common cause of persistent infections. *science* **1999,** *284* (5418), 1318-1322.

237. Otto, M., Staphylococcus epidermidis—the'accidental'pathogen. *Nature reviews microbiology* **2009,** *7* (8), 555.

238. Khan, H. A.; Ahmad, A.; Mehboob, R., Nosocomial infections and their control strategies. *Asian pacific journal of tropical biomedicine* **2015,** *5* (7), 509-514.

239. Rajamuthiah, R.; Fuchs, B. B.; Conery, A. L.; Kim, W.; Jayamani, E.; Kwon, B.; Ausubel, F. M.; Mylonakis, E., Repurposing salicylanilide anthelmintic drugs to combat drug resistant Staphylococcus aureus. *Plos One* **2015,** *10* (4), e0124595.

240. Control, C. f. D.; Prevention, *Antibiotic resistance threats in the United States, 2013*. Centres for Disease Control and Prevention, US Department of Health and …: 2013.

241. Rapido, F., The potential adverse effects of haemolysis. *Blood Transfus* **2017,** *15* (3), 218-221.

242. Sowaileh, M. F.; Hazlitt, R. A.; Colby, D. A., Application of the Pentafluorosulfanyl Group as a Bioisosteric Replacement. *ChemMedChem* **2017,** *12* (18), 1481-1490.

243. Landelle, G.; Panossian, A.; Leroux, F. R., Trifluoromethyl ethers and -thioethers as tools for medicinal chemistry and drug discovery. *Curr Top Med Chem* **2014,** *14* (7), 941-51.

244. Meanwell, N. A., Synopsis of some recent tactical application of bioisosteres in drug design. *J Med Chem* **2011,** *54* (8), 2529-91.

245. Melehani, J. H.; James, D. B.; DuMont, A. L.; Torres, V. J.; Duncan, J. A., Staphylococcus aureus leukocidin A/B (LukAB) kills human monocytes via host NLRP3 and ASC when extracellular, but not intracellular. *PLoS pathogens* **2015,** *11* (6), e1004970.

246. Flannagan, R. S.; Heit, B.; Heinrichs, D. E., Intracellular replication of Staphylococcus aureus in mature phagolysosomes in macrophages precedes host cell death, and bacterial escape and dissemination. *Cell Microbiol* **2016,** *18* (4), 514-535.

247. Vanderauwera, P.; Prinz, G.; Petrikkos, G., Activity of Intracellular Antibiotics. *Infection* **1991,** *19*, S216-S223.

248. Bartash, R.; Nori, P., Beta-lactam combination therapy for the treatment of Staphylococcus aureus and Enterococcus species bacteremia: A summary and appraisal of the evidence. *Int J Infect Dis* **2017,** *63*, 7-12.

249. Abraham, G.; Finkelberg, D.; Spooner, L. M., Daptomycin-induced acute renal and hepatic toxicity without rhabdomyolysis. *Ann Pharmacother* **2008,** *42* (5), 719-721.

250. Li, B.; Ni, S.; Mao, F.; Chen, F.; Liu, Y.; Wei, H.; Chen, W.; Zhu, J.; Lan, L.; Li, J., Novel Terminal Bipheny-Based Diapophytoene Desaturases (CrtN) Inhibitors as Anti-MRSA/VISR/LRSA Agents with Reduced hERG Activity. *J Med Chem* **2018,** *61* (1), 224-250.

251. Lui, H. K.; Gao, W.; Cheung, K. C.; Jin, W. B.; Sun, N.; Kan, J. W. Y.; Wong, I. L. K.; Chiou, J.; Lin, D.; Chan, E. W. C.; Leung, Y. C.; Chan, T. H.; Chen, S.; Chan, K. F.; Wong, K. Y., Boosting the efficacy of anti-MRSA beta-lactam antibiotics via an easily accessible, non-cytotoxic and orally bioavailable FtsZ inhibitor. *Eur J Med Chem* **2019,** *163*, 95-115.

252. Opoku-Temeng, C.; Dayal, N.; Miller, J.; Sintim, H. O., Hydroxybenzylidene-indolinones, c-di-AMP synthase inhibitors, have antibacterial and anti-biofilm activities and also re-sensitize resistant bacteria to methicillin and vancomycin. *RSC Advances* **2017,** *7*, 8288-8294.

253. Richter, M. F.; Drown, B. S.; Riley, A. P.; Garcia, A.; Shirai, T.; Svec, R. L.; Hergenrother, P. J., Predictive compound accumulation rules yield a broad-spectrum antibiotic. *Nature* **2017,** *545* (7654), 299-304.

254. Rowe, I.; Guo, M.; Yasmann, A.; Cember, A.; Sintim, H. O.; Sukharev, S., Membrane Affinity of Platensimycin and Its Dialkylamine Analogs. *Int J Mol Sci* **2015,** *16* (8), 17909-32.

255. Smith, J. R.; Yim, J.; Rice, S.; Stamper, K.; Kebriaei, R.; Rybak, M. J., Combination of Tedizolid and Daptomycin against Methicillin-Resistant Staphylococcus aureus in an In Vitro Model of Simulated Endocardial Vegetations. *Antimicrob Agents Chemother* **2018,** *62* (5).

256. Wang, J.; Sintim, H. O., Dialkylamino-2,4-dihydroxybenzoic acids as easily synthesized analogues of platensimycin and platencin with comparable antibacterial properties. *Chemistry* **2011,** *17* (12), 3352-7.

257. Zhang, S.; Palazuelos-Munoz, S.; Balsells, E. M.; Nair, H.; Chit, A.; Kyaw, M. H., Cost of hospital management of Clostridium difficile infection in United States-a meta-analysis and modelling study. *BMC Infect Dis* **2016,** *16* (1), 447.

258. Kachrimanidou, M.; Malisiovas, N., Clostridium difficile Infection: A Comprehensive Review. *Crit Rev Microbiol* **2011,** *37* (3), 178-187.

259. Davies, A. H.; Roberts, A. K.; Shone, C. C.; Acharya, K. R., Super toxins from a super bug: structure and function of Clostridium difficile toxins. *The Biochemical journal* **2011,** *436* (3), 517-26.

260. Chumbler, N. M.; Farrow, M. A.; Lapierre, L. A.; Franklin, J. L.; Haslam, D.; Goldenring, J. R.; Lacy, D. B., Clostridium difficile Toxin B Causes Epithelial Cell Necrosis through an Autoprocessing-Independent Mechanism. *Plos Pathog* **2012,** *8* (12).

261. Awad, M. M.; Johanesen, P. A.; Carter, G. P.; Rose, E.; Lyras, D., *Clostridium difficile* virulence factors: Insights into an anaerobic spore-forming pathogen. *Gut Microbes* **2014,** *5* (5), 579-593.

262. Viswanathan, V. K.; Mallozzi, M. J.; Vedantam, G., Clostridium difficile infection: An overview of the disease and its pathogenesis, epidemiology and interventions. *Gut Microbes* **2010,** *1* (4), 234-242.

263. Dethlefsen, L.; Huse, S.; Sogin, M. L.; Relman, D. A., The pervasive effects of an antibiotic on the human gut microbiota, as revealed by deep 16S rRNA sequencing. *PLoS Biol* **2008,** *6* (11), e280.

264. McDonald, L. C.; Gerding, D. N.; Johnson, S.; Bakken, J. S.; Carroll, K. C.; Coffin, S. E.; Dubberke, E. R.; Garey, K. W.; Gould, C. V.; Kelly, C.; Loo, V.; Sammons, J. S.; Sandora, T. J.; Wilcox, M. H., Clinical Practice Guidelines for Clostridium difficile Infection in Adults and Children: 2017 Update by the Infectious Diseases Society of America (IDSA) and Society for Healthcare Epidemiology of America (SHEA). *Clin Infect Dis* **2018,** *66* (7), E1-E48.

265. Lamp, K. C.; Freeman, C. D.; Klutman, N. E.; Lacy, M. K., Pharmacokinetics and pharmacodynamics of the nitroimidazole antimicrobials. *Clin Pharmacokinet* **1999,** *36* (5), 353-73.

266. Bolton, R. P.; Culshaw, M. A., Faecal metronidazole concentrations during oral and intravenous therapy for antibiotic associated colitis due to Clostridium difficile. *Gut* **1986,** *27* (10), 1169-72.

267. Pepin, J.; Alary, M. E.; Valiquette, L.; Raiche, E.; Ruel, J.; Fulop, K.; Godin, D.; Bourassa, C., Increasing risk of relapse after treatment of Clostridium difficile colitis in Quebec, Canada. *Clin Infect Dis* **2005,** *40* (11), 1591-7.

268. Louie, T. J.; Cannon, K.; Byrne, B.; Emery, J.; Ward, L.; Eyben, M.; Krulicki, W., Fidaxomicin preserves the intestinal microbiome during and after treatment of Clostridium difficile infection (CDI) and reduces both toxin reexpression and recurrence of CDI. *Clin Infect Dis* **2012,** *55 Suppl 2*, S132-42.

269. Vardakas, K. Z.; Polyzos, K. A.; Patouni, K.; Rafailidis, P. I.; Samonis, G.; Falagas, M. E., Treatment failure and recurrence of *Clostridium difficile* infection following treatment with vancomycin or metronidazole: a systematic review of the evidence. *Int J Antimicrob Ag* **2012,** *40* (1), 1-8.

270. Smits, W. K.; Lyras, D.; Lacy, D. B.; Wilcox, M. H.; Kuijper, E. J., *Clostridium difficile* infection. *Nature reviews Disease primers* **2016,** *2*, 16020.

271. Orenstein, R., Fidaxomicin failures in recurrent Clostridium difficile infection: a problem of timing. *Clin Infect Dis* **2012,** *55* (4), 613-4.

272. Cornely, O. A.; Miller, M. A.; Louie, T. J.; Crook, D. W.; Gorbach, S. L., Treatment of first recurrence of *Clostridium difficile* infection: fidaxomicin versus vancomycin. *Clin Infect Dis* **2012,** *55 Suppl 2*, S154-61.

273. Zhanel, G. G.; Walkty, A. J.; Karlowsky, J. A., Fidaxomicin: A novel agent for the treatment of Clostridium difficile infection. *Can J Infect Dis Med* **2015,** *26* (6), 305-312.

274. Baines, S. D.; Wilcox, M. H., Antimicrobial Resistance and Reduced Susceptibility in Clostridium difficile: Potential Consequences for Induction, Treatment, and Recurrence of C. difficile Infection. *Antibiotics* **2015,** *4* (3), 267-98.

275. Bakken, J. S.; Borody, T.; Brandt, L. J.; Brill, J. V.; Demarco, D. C.; Franzos, M. A.; Kelly, C.; Khoruts, A.; Louie, T.; Martinelli, L. P.; Moore, T. A.; Russell, G.; Surawicz, C., Treating Clostridium difficile infection with fecal microbiota transplantation. *Clinical gastroenterology and hepatology : the official clinical practice journal of the American Gastroenterological Association* **2011,** *9* (12), 1044-9.

276. Woodworth, M. H.; Carpentieri, C.; Sitchenko, K. L.; Kraft, C. S., Challenges in fecal donor selection and screening for fecal microbiota transplantation: A review. *Gut Microbes* **2017,** *8* (3), 225-237.

277. Pamer, E. G., Fecal microbiota transplantation: effectiveness, complexities, and lingering concerns. *Mucosal immunology* **2014,** *7* (2), 210-4.

278. Mendez, L.; Henriquez, G.; Sirimulla, S.; Narayan, M., Looking Back, Looking Forward at Halogen Bonding in Drug Discovery. *Molecules* **2017,** *22* (9).

279. Hernandes, M. Z.; Cavalcanti, S. M.; Moreira, D. R.; de Azevedo Junior, W. F.; Leite, A. C., Halogen atoms in the modern medicinal chemistry: hints for the drug design. *Curr Drug Targets* **2010,** *11* (3), 303-14.

280. Wilcken, R.; Zimmermann, M. O.; Lange, A.; Joerger, A. C.; Boeckler, F. M., Principles and applications of halogen bonding in medicinal chemistry and chemical biology. *J Med Chem* **2013,** *56* (4), 1363-88.

281. Guo, M.; Zheng, Y.; Terell, J. L.; Ad, M.; Opoku-Temeng, C.; Bentley, W. E.; Sintim, H. O., Geminal dihalogen isosteric replacement in hydrated AI-2 affords potent quorum sensing modulators. *Chem Commun (Camb)* **2015,** *51* (13), 2617-20.

282. Suarez-Castro, A.; Valle-Sanchez, M.; Cortes-Garcia, C. J.; Chacon-Garcia, L., Molecular Docking in Halogen Bonding. In *Molecular Docking*, IntechOpen: 2018.

283. Gerebtzoff, G.; Li-Blatter, X.; Fischer, H.; Frentzel, A.; Seelig, A., Halogenation of drugs enhances membrane binding and permeation. *Chembiochem* **2004,** *5* (5), 676-84.

284. Gentry, C. L.; Egleton, R. D.; Gillespie, T.; Abbruscato, T. J.; Bechowski, H. B.; Hruby, V. J.; Davis, T. P., The effect of halogenation on blood-brain barrier permeability of a novel peptide drug. *Peptides* **1999,** *20* (10), 1229-38.

285. De Azevedo, W. F., Jr.; Mueller-Dieckmann, H. J.; Schulze-Gahmen, U.; Worland, P. J.; Sausville, E.; Kim, S. H., Structural basis for specificity and potency of a flavonoid inhibitor of human CDK2, a cell cycle kinase. *Proc Natl Acad Sci U S A* **1996,** *93* (7), 2735-40.

286. Valadon, P.; Dansette, P. M.; Girault, J. P.; Amar, C.; Mansuy, D., Thiophene sulfoxides as reactive metabolites: formation upon microsomal oxidation of a 3-aroylthiophene and fate in the presence of nucleophiles in vitro and in vivo. *Chem Res Toxicol* **1996,** *9* (8), 1403-13.

287. Dansette, P. M.; Bertho, G.; Mansuy, D., First evidence that cytochrome P450 may catalyze both S-oxidation and epoxidation of thiophene derivatives. *Biochem Biophys Res Commun* **2005,** *338* (1), 450-5.

288. Mansuy, D.; Dansette, P. M., Sulfenic acids as reactive intermediates in xenobiotic metabolism. *Arch Biochem Biophys* **2011,** *507* (1), 174-85.

289. Gramec, D.; Peterlin Masic, L.; Sollner Dolenc, M., Bioactivation potential of thiophene-containing drugs. *Chem Res Toxicol* **2014,** *27* (8), 1344-58.

290. Al-Nassir, W. N.; Sethi, A. K.; Li, Y.; Pultz, M. J.; Riggs, M. M.; Donskey, C. J., Both oral metronidazole and oral vancomycin promote persistent overgrowth of vancomycin-resistant enterococci during treatment of Clostridium difficile-associated disease. *Antimicrob Agents Chemother* **2008,** *52* (7), 2403-6.

291. Seiler, P.; Enderlin-Paput, M.; Pfaff, P.; Weiss, M.; Ritz, D.; Clozel, M.; Locher, H. H., Cadazolid Does Not Promote Intestinal Colonization of Vancomycin-Resistant Enterococci in Mice. *Antimicrob Agents Chemother* **2016,** *60* (1), 628-31.

292. Delmas, J.; Dalmasso, G.; Bonnet, R., Escherichia coli: The Good, the Bad and the Ugly. *Clin Microbiol* **2015,** *4* (2).

293. Hidalgo, I. J.; Raub, T. J.; Borchardt, R. T., Characterization of the human colon carcinoma cell line (Caco-2) as a model system for intestinal epithelial permeability. *Gastroenterology* **1989,** *96* (3), 736-49.

294. Kim, S.; Covington, A.; Pamer, E. G., The intestinal microbiota: Antibiotics, colonization resistance, and enteric pathogens. *Immunol Rev* **2017,** *279* (1), 90-105.

295. Yoon, S.; Yu, J.; McDowell, A.; Kim, S. H.; You, H. J.; Ko, G., Bile salt hydrolase-mediated inhibitory effect of Bacteroides ovatus on growth of Clostridium difficile. *J Microbiol* **2017,** *55* (11), 892-899.

296. Deng, H.; Yang, S.; Zhang, Y.; Qian, K.; Zhang, Z.; Liu, Y.; Wang, Y.; Bai, Y.; Fan, H.; Zhao, X.; Zhi, F., Bacteroides fragilis Prevents Clostridium difficile Infection in a Mouse Model by Restoring Gut Barrier and Microbiome Regulation. *Front Microbiol* **2018,** *9*, 2976.

297. Quigley, L.; Coakley, M.; Alemayehu, D.; Rea, M. C.; Casey, P. G.; O'Sullivan, O.; Murphy, E.; Kiely, B.; Cotter, P. D.; Hill, C.; Ross, R. P., Lactobacillus gasseri APC 678 Reduces Shedding of the Pathogen Clostridium difficile in a Murine Model. *Front Microbiol* **2019,** *10*, 273.

298. Naaber, P.; Smidt, I.; Stsepetova, J.; Brilene, T.; Annuk, H.; Mikelsaar, M., Inhibition of Clostridium difficile strains by intestinal Lactobacillus species. *J Med Microbiol* **2004,** *53* (Pt 6), 551-554.

299. Abutaleb, N. S.; Seleem, M. N., Repurposing the Antiamoebic Drug Diiodohydroxyquinoline for Treatment of Clostridioides difficile Infections. *Antimicrob Agents Chemother* **2020,** *64* (6).

300. Rafii, F.; Sutherland, J. B.; Cerniglia, C. E., Effects of treatment with antimicrobial agents on the human colonic microflora. *Ther Clin Risk Manag* **2008,** *4* (6), 1343-58.

301. Ajami, N. J.; Cope, J. L.; Wong, M. C.; Petrosino, J. F.; Chesnel, L., Impact of Oral Fidaxomicin Administration on the Intestinal Microbiota and Susceptibility to Clostridium difficile Colonization in Mice. *Antimicrob Agents Chemother* **2018,** *62* (5).

302. Mascio, C. T.; Chesnel, L.; Thorne, G.; Silverman, J. A., Surotomycin demonstrates low in vitro frequency of resistance and rapid bactericidal activity in Clostridium difficile, Enterococcus faecalis, and Enterococcus faecium. *Antimicrob Agents Chemother* **2014,** *58* (7), 3976-82.

303. Abutaleb, N. S.; Seleem, M. N., Auranofin, at clinically achievable dose, protects mice and prevents recurrence from Clostridioides difficile infection. *Sci Rep* **2020,** *10* (1), 7701.

304. Hutton, M. L.; Pehlivanoglu, H.; Vidor, C. J.; James, M. L.; Thomson, M. J.; Lyras, D., Repurposing auranofin as a Clostridioides difficile therapeutic. *J Antimicrob Chemother* **2020,** *75* (2), 409-417.

305. Chen, X.; Katchar, K.; Goldsmith, J. D.; Nanthakumar, N.; Cheknis, A.; Gerding, D. N.; Kelly, C. P., A mouse model of Clostridium difficile-associated disease. *Gastroenterology* **2008,** *135* (6), 1984-92.

306. AbdelKhalek, A.; Abutaleb, N. S.; Mohammad, H.; Seleem, M. N., Antibacterial and antivirulence activities of auranofin against Clostridium difficile. *Int J Antimicrob Agents* **2019,** *53* (1), 54-62.

307. Mody, D.; Athamneh, A. I. M.; Seleem, M. N., Curcumin: A natural derivative with antibacterial activity against Clostridium difficile. *J Glob Antimicrob Resist* **2019,** *21*, 154-161.

308. Pal, R.; Seleem, M. N., Screening of Natural Products and Approved Oncology Drug Libraries for Activity against Clostridioides difficile. *Sci Rep* **2020,** *10* (1), 5966.

309. Shao, X.; AbdelKhalek, A.; Abutaleb, N. S.; Velagapudi, U. K.; Yoganathan, S.; Seleem, M. N.; Talele, T. T., Chemical Space Exploration around Thieno[3,2-d]pyrimidin-4(3H)-one Scaffold Led to a Novel Class of Highly Active Clostridium difficile Inhibitors. *J Med Chem* **2019,** *62* (21), 9772-9791.

310. Kotb, A.; Abutaleb, N. S.; Seleem, M. A.; Hagras, M.; Mohammad, H.; Bayoumi, A.; Ghiaty, A.; Seleem, M. N.; Mayhoub, A. S., Phenylthiazoles with tert-Butyl side chain: Metabolically stable with anti-biofilm activity. *Eur J Med Chem* **2018,** *151*, 110-120.

311. ElAwamy, M.; Mohammad, H.; Hussien, A.; Abutaleb, N. S.; Hagras, M.; Serya, R. A. T.; Taher, A. T.; Abouzid, K. A.; Seleem, M. N.; Mayhoub, A. S., Alkoxyphenylthiazoles with broad-spectrum activity against multidrug-resistant gram-positive bacterial pathogens. *Eur J Med Chem* **2018,** *152*, 318-328.

312. Obach, R. S.; Baxter, J. G.; Liston, T. E.; Silber, B. M.; Jones, B. C.; MacIntyre, F.; Rance, D. J.; Wastall, P., The prediction of human pharmacokinetic parameters from preclinical and in vitro metabolism data. *J Pharmacol Exp Ther* **1997,** *283* (1), 46-58.

313. Hammad, A.; Abutaleb, N. S.; Elsebaei, M. M.; Norvil, A. B.; Alswah, M.; Ali, A. O.; Abdel-Aleem, J. A.; Alattar, A.; Bayoumi, S. A.; Gowher, H.; Seleem, M. N.; Mayhoub, A. S., From Phenylthiazoles to Phenylpyrazoles: Broadening the Antibacterial Spectrum toward Carbapenem-Resistant Bacteria. *J Med Chem* **2019,** *62* (17), 7998-8010.

314. AbdelKhalek A, M. H., Mayhoub AS, Seleem MN, Screening for potent and selective anticlostridial leads among FDA-approved drugs. *J Antibiot* **2020,** *73*, 392–409.

315. Thangamani, S.; Mohammad, H.; Abushahba, M. F.; Sobreira, T. J.; Hedrick, V. E.; Paul, L. N.; Seleem, M. N., Antibacterial activity and mechanism of action of auranofin against multi-drug resistant bacterial pathogens. *Sci Rep* **2016,** *6*, 22571.

316. Edwards, A. N.; McBride, S. M., Isolating and Purifying Clostridium difficile Spores. *Methods Mol Biol* **2016,** *1476*, 117-128.

317. Daina, A.; Michielin, O.; Zoete, V., SwissADME: a free web tool to evaluate pharmacokinetics, drug-likeness and medicinal chemistry friendliness of small molecules. *Sci Rep* **2017,** *7*, 42717.

318. Unemo, M.; Nicholas, R. A., Emergence of multidrug-resistant, extensively drug-resistant and untreatable gonorrhea. *Future Microbiol* **2012,** *7* (12), 1401-22.

319. Hill, S. A.; Masters, T. L.; Wachter, J., Gonorrhea - an evolving disease of the new millennium. *Microb Cell* **2016,** *3* (9), 371-389.

320. Burnett, A. M.; Anderson, C. P.; Zwank, M. D., Laboratory-confirmed gonorrhea and/or chlamydia rates in clinically diagnosed pelvic inflammatory disease and cervicitis. *Am J Emerg Med* **2012,** *30* (7), 1114-7.

321. Kirkcaldy, R. D.; Harvey, A.; Papp, J. R.; Del Rio, C.; Soge, O. O.; Holmes, K. K.; Hook, E. W., 3rd; Kubin, G.; Riedel, S.; Zenilman, J.; Pettus, K.; Sanders, T.; Sharpe, S.; Torrone, E., Neisseria gonorrhoeae Antimicrobial Susceptibility Surveillance - The Gonococcal Isolate Surveillance Project, 27 Sites, United States, 2014. *MMWR Surveill Summ* **2016,** *65* (7), 1-19.

322. Newman, L.; Rowley, J.; Vander Hoorn, S.; Wijesooriya, N. S.; Unemo, M.; Low, N.; Stevens, G.; Gottlieb, S.; Kiarie, J.; Temmerman, M., Global Estimates of the Prevalence and Incidence of Four Curable Sexually Transmitted Infections in 2012 Based on Systematic Review and Global Reporting. *PLoS One* **2015,** *10* (12), e0143304.

323. Kirkcaldy, R. D.; Weston, E.; Segurado, A. C.; Hughes, G., Epidemiology of gonorrhoea: a global perspective. *Sex Health* **2019,** *16* (5), 401-411.

324. WHO publishes list of bacteria for which new antibiotics are urgently needed. https://www.who.int/news-room/detail/27-02-2017-who-publishes-list-of-bacteria-for-which-new-antibiotics-are-urgently-needed.

325. Unemo, M.; Shafer, W. M., Antimicrobial resistance in Neisseria gonorrhoeae in the 21st century: past, evolution, and future. *Clin Microbiol Rev* **2014,** *27* (3), 587-613.

326. Workowski, K. A.; Bolan, G. A.; Centers for Disease, C.; Prevention, Sexually transmitted diseases treatment guidelines, 2015. *MMWR Recomm Rep* **2015,** *64* (RR-03), 1-137.

327. Wise, R.; Discovery, B. W. P. o. T. U. N. R. A. D.; Development, The urgent need for new antibacterial agents. *J Antimicrob Chemother* **2011,** *66* (9), 1939-40.

328. Blomquist, P. B.; Miari, V. F.; Biddulph, J. P.; Charalambous, B. M., Is gonorrhea becoming untreatable? *Future Microbiol* **2014,** *9* (2), 189-201.

329. Barbee, L. A., Preparing for an era of untreatable gonorrhea. *Curr Opin Infect Dis* **2014,** *27* (3), 282-7.

330. Feng, P.; Lee, K. N.; Lee, J. W.; Zhan, C.; Ngai, M. Y., Access to a new class of synthetic building blocks via trifluoromethoxylation of pyridines and pyrimidines. *Chem Sci* **2016,** *7* (1), 424-429.

331. Leroux, F. R.; Manteau, B.; Vors, J. P.; Pazenok, S., Trifluoromethyl ethers--synthesis and properties of an unusual substituent. *Beilstein J Org Chem* **2008,** *4*, 13.

332. van de Waterbeemd, H.; Testa, B.; Mannhold, R.; Kubinyi, H.; Folkers, G., *Drug Bioavailability: Estimation of Solubility, Permeability, Absorption and Bioavailability, 2nd Edition*. 2nd ed.; Wiley: 2008; p 649.

333. Unemo, M.; Golparian, D.; Sanchez-Buso, L.; Grad, Y.; Jacobsson, S.; Ohnishi, M.; Lahra, M. M.; Limnios, A.; Sikora, A. E.; Wi, T.; Harris, S. R., The novel 2016 WHO Neisseria gonorrhoeae reference strains for global quality assurance of laboratory investigations: phenotypic, genetic and reference genome characterization. *J Antimicrob Chemother* **2016,** *71* (11), 3096-3108.

334. Piddock, L. J., Multidrug-resistance efflux pumps - not just for resistance. *Nat. Rev. Microbiol.* **2006,** *4* (8), 629-36.

335. Opperman, T. J.; Nguyen, S. T., Recent advances toward a molecular mechanism of efflux pump inhibition. *Front. Microbiol.* **2015,** *6*, 421.

336. Li, J.; Xie, S.; Ahmed, S.; Wang, F.; Gu, Y.; Zhang, C.; Chai, X.; Wu, Y.; Cai, J.; Cheng, G., Antimicrobial Activity and Resistance: Influencing Factors. *Front Pharmacol* **2017,** *8*, 364.

337. Kaplan, N.; Awrey, D.; Bardouniotis, E.; Berman, J.; Yethon, J.; Pauls, H. W.; Hafkin, B., In vitro activity (MICs and rate of kill) of AFN-1252, a novel FabI inhibitor, in the presence of serum and in combination with other antibiotics. *J Chemother* **2013,** *25* (1), 18-25.

338. Zeitlinger, M. A.; Derendorf, H.; Mouton, J. W.; Cars, O.; Craig, W. A.; Andes, D.; Theuretzbacher, U., Protein binding: do we ever learn? *Antimicrob Agents Chemother* **2011,** *55* (7), 3067-74.

339. Tang, W.; Wang, C.; Liao, Y., Fetal bovine serum albumin inhibits antimicrobial peptide activity and binds drug only in complex with α1-antitrypsin. *Sci Rep* **2021,** *11*, 1267.

340. Schneider, E. K.; Huang, J. X.; Carbone, V.; Han, M.; Zhu, Y.; Nang, S.; Khoo, K. K.; Mak, J.; Cooper, M. A.; Li, J.; Velkov, T., Plasma Protein Binding Structure-Activity Relationships Related to the N-Terminus of Daptomycin. *ACS Infect Dis* **2017,** *3* (3), 249-258.

341. Hou, T. J.; Zhang, W.; Xia, K.; Qiao, X. B.; Xu, X. J., ADME evaluation in drug discovery. 5. Correlation of Caco-2 permeation with simple molecular properties. *J Chem Inf Comput Sci* **2004,** *44* (5), 1585-600.

342. Gres, M. C.; Julian, B.; Bourrie, M.; Meunier, V.; Roques, C.; Berger, M.; Boulenc, X.; Berger, Y.; Fabre, G., Correlation between oral drug absorption in humans, and apparent drug permeability in TC-7 cells, a human epithelial intestinal cell line: comparison with the parental Caco-2 cell line. *Pharm Res* **1998,** *15* (5), 726-33.

343. Artursson, P., Cell cultures as models for drug absorption across the intestinal mucosa. *Crit Rev Ther Drug Carrier Syst* **1991,** *8* (4), 305-30.

344. Alhashimi, M.; Mayhoub, A.; Seleem, M. N., Repurposing salicylamide for combating multidrug-resistant Neisseria gonorrhoeae. *Antimicrob Agents Chemother* **2019**.

345. Elkashif, A.; Seleem, M. N., Investigation of auranofin and gold-containing analogues antibacterial activity against multidrug-resistant Neisseria gonorrhoeae. *Sci Rep* **2020,** *10* (1), 5602.

346. Seong, Y. J.; Alhashimi, M.; Mayhoub, A.; Mohammad, H.; Seleem, M. N., Repurposing Fenamic Acid Drugs To Combat Multidrug-Resistant Neisseria gonorrhoeae. *Antimicrob Agents Chemother* **2020,** *64* (7).

347. Elsebaei, M. M.; Mohammad, H.; Samir, A.; Abutaleb, N. S.; Norvil, A. B.; Michie, A. R.; Moustafa, M. M.; Samy, H.; Gowher, H.; Seleem, M. N.; Mayhoub, A. S., Lipophilic efficient phenylthiazoles with potent undecaprenyl pyrophosphatase inhibitory activity. *Eur J Med Chem* **2019,** *175*, 49-62.

348. Kotb, A.; Abutaleb, N. S.; Hagras, M.; Bayoumi, A.; Moustafa, M. M.; Ghiaty, A.; Seleem, M. N.; Mayhoub, A. S., tert-Butylphenylthiazoles with an oxadiazole linker: a novel orally bioavailable class of antibiotics exhibiting antibiofilm activity. *RSC Adv* **2019,** *9*, 6770-6778.

349. Dokla, E. M. E.; Abutaleb, N. S.; Milik, S. N.; Li, D.; El-Baz, K.; Shalaby, M. W.; Al-Karaki, R.; Nasr, M.; Klein, C. D.; Abouzid, K. A. M.; Seleem, M. N., Development of benzimidazole-based derivatives as antimicrobial agents and their synergistic effect with colistin against gram-negative bacteria. *Eur J Med Chem* **2020,** *186*, 111850.

350. Hammad, S. G.; El-Gazzar, M. G.; Abutaleb, N. S.; Li, D.; Ramming, I.; Shekhar, A.; Abdel-Halim, M.; Elrazaz, E. Z.; Seleem, M. N.; Bilitewski, U.; Abouzid, K. A. M.; El-Hossary, E. M., Synthesis and antimicrobial evaluation of new halogenated 1,3-Thiazolidin-4-ones. *Bioorg Chem* **2020,** *95*, 103517.

351. OECD, *Stemming the Superbug Tide*. OECD Publishing: Paris, 2018.

352. Aron, Z. D.; Mehrani, A.; Hoffer, E. D.; Connolly, K. L.; Srinivas, P.; Torhan, M. C.; Alumasa, J. N.; Cabrera, M.; Hosangadi, D.; Barbor, J. S.; Cardinale, S. C.; Kwasny, S. M.; Morin, L. R.; Butler, M. M.; Opperman, T. J.; Bowlin, T. L.; Jerse, A.; Stagg, S. M.; Dunham, C. M.; Keiler, K. C., trans-Translation inhibitors bind to a novel site on the ribosome and clear Neisseria gonorrhoeae in vivo. *Nat Commun* **2021,** *12* (1), 1799.

353. Ramadoss, N. S.; Alumasa, J. N.; Cheng, L.; Wang, Y.; Li, S.; Chambers, B. S.; Chang, H.; Chatterjee, A. K.; Brinker, A.; Engels, I. H.; Keiler, K. C., Small molecule inhibitors of trans-translation have broad-spectrum antibiotic activity. *Proc. Natl. Acad. Sci. U.S.A.* **2013,** *110* (25), 10282-10287.

354. Tresse, C.; Radigue, R.; Gomes Von Borowski, R.; Thepaut, M.; Hanh Le, H.; Demay, F.; Georgeault, S.; Dhalluin, A.; Trautwetter, A.; Ermel, G.; Blanco, C.; van de Weghe, P.; Jean, M.; Giard, J. C.; Gillet, R., Synthesis and evaluation of 1,3,4-oxadiazole derivatives for development as broad-spectrum antibiotics. *Bioorg Med Chem* **2019,** *27* (21), 115097.

355. Mace, K.; Demay, F.; Guyomar, C.; Georgeault, S.; Giudice, E.; Goude, R.; Trautwetter, A.; Ermel, G.; Blanco, C.; Gillet, R., A Genetic Tool to Quantify trans-Translation Activity in Vivo. *J Mol Biol* **2017,** *429* (23), 3617-3625.

356. Farha, M. A.; Brown, E. D., Strategies for target identification of antimicrobial natural products. *Nat Prod Rep* **2016,** *33* (5), 668-80.

357. Gilbert, D. N.; Kohlhepp, S. J.; Slama, K. A.; Grunkemeier, G.; Lewis, G.; Dworkin, R. J.; Slaughter, S. E.; Leggett, J. E., Phenotypic resistance of Staphylococcus aureus, selected Enterobacteriaceae, and Pseudomonas aeruginosa after single and multiple in vitro exposures to ciprofloxacin, levofloxacin, and trovafloxacin. *Antimicrob Agents Chemother* **2001,** *45* (3), 883-92.

358. Mohammad, H.; Younis, W.; Ezzat, H. G.; Peters, C. E.; AbdelKhalek, A.; Cooper, B.; Pogliano, K.; Pogliano, J.; Mayhoub, A. S.; Seleem, M. N., Bacteriological profiling of diphenylureas as a novel class of antibiotics against methicillin-resistant Staphylococcus aureus. *PLoS One* **2017,** *12* (8), e0182821.

359. D'Lima, L.; Friedman, L.; Wang, L.; Xu, P.; Anderson, M.; Debabov, D., No decrease in susceptibility to NVC-422 in multiple-passage studies with methicillin-resistant Staphylococcus aureus, S. aureus, Pseudomonas aeruginosa, and Escherichia coli. *Antimicrob Agents Chemother* **2012,** *56* (5), 2753-5.

360. Timinskas, K.; Balvociute, M.; Timinskas, A.; Venclovas, C., Comprehensive analysis of DNA polymerase III alpha subunits and their homologs in bacterial genomes. *Nucleic Acids Res* **2014,** *42* (3), 1393-413.

361. Kaito, C.; Kurokawa, K.; Hossain, M. S.; Akimitsu, N.; Sekimizu, K., Isolation and characterization of temperature-sensitive mutants of the Staphylococcus aureus dnaC gene. *FEMS Microbiol Lett* **2002,** *210* (1), 157-64.

362. Henke, S. K.; Cronan, J. E., The Staphylococcus aureus group II biotin protein ligase BirA is an effective regulator of biotin operon transcription and requires the DNA binding domain for full enzymatic activity. *Mol Microbiol* **2016,** *102* (3), 417-429.

363. Cirz, R. T.; Jones, M. B.; Gingles, N. A.; Minogue, T. D.; Jarrahi, B.; Peterson, S. N.; Romesberg, F. E., Complete and SOS-mediated response of Staphylococcus aureus to the antibiotic ciprofloxacin. *J Bacteriol* **2007,** *189* (2), 531-9.

364. Xu, W.; Silverman, M. H.; Yu, X. Y.; Wright, G.; Brown, N., Discovery and development of DNA polymerase IIIC inhibitors to treat Gram-positive infections. *Bioorg Med Chem* **2019,** *27* (15), 3209-3217.

365. Kornberg, A.; Baker, T. A., *DNA Replication*. Second ed.; University Science Books: Sausalito, California, 2005.

366. Wright, G. E.; Brown, N. C., Inhibitors of Bacillus subtilis DNA polymerase III. 6-Anilinouracils and 6-(alkylamino)uracils. *J Med Chem* **1980,** *23* (1), 34-8.

367. Brown, N. C.; Gambino, J.; Wright, G. E., Inhibitors of Bacillus subtilis DNA polymerase III. 6-(arylalkylamino)uracils and 6-anilinouracils. *J Med Chem* **1977,** *20* (9), 1186-9.

368. Dvoskin, S.; Xu, W. C.; Brown, N. C.; Yanachkov, I. B.; Yanachkova, M.; Wright, G. E., A novel agent effective against Clostridium difficile infection. *Antimicrob Agents Chemother* **2012,** *56* (3), 1624-6.

369. Szklarczyk, D.; Morris, J. H.; Cook, H.; Kuhn, M.; Wyder, S.; Simonovic, M.; Santos, A.; Doncheva, N. T.; Roth, A.; Bork, P.; Jensen, L. J.; von Mering, C., The STRING database in 2017: quality-controlled protein-protein association networks, made broadly accessible. *Nucleic Acids Res* **2017,** *45* (D1), D362-D368.

370. Shineberg, B.; Young, I. G., Biosynthesis of bacterial menaquinones: the membrane-associated 1,4-dihydroxy-2-naphthoate octaprenyltransferase of Escherichia coli. *Biochemistry* **1976,** *15* (13), 2754-8.

371. Boersch, M.; Rudrawar, S.; Grant, G.; Zunk, M., Menaquinone biosynthesis inhibition: a review of advancements toward a new antibiotic mechanism. *RSC Adv* **2018,** *8*, 5099-5105.

372. Hiratsuka, T.; Furihata, K.; Ishikawa, J.; Yamashita, H.; Itoh, N.; Seto, H.; Dairi, T., An alternative menaquinone biosynthetic pathway operating in microorganisms. *Science* **2008,** *321* (5896), 1670-3.

373. Kurosu, M.; Begari, E., Vitamin K2 in electron transport system: are enzymes involved in vitamin K2 biosynthesis promising drug targets? *Molecules* **2010,** *15* (3), 1531-53.

374. Garcia-Villegas, M. R.; De La Vega, F. M.; Galindo, J. M.; Segura, M.; Buckingham, R. H.; Guarneros, G., Peptidyl-tRNA hydrolase is involved in lambda inhibition of host protein synthesis. *EMBO J* **1991,** *10* (11), 3549-55.

375. Atherly, A. G., Peptidyl-transfer RNA hydrolase prevents inhibition of protein synthesis initiation. *Nature* **1978,** *275* (5682), 769.

376. Menninger, J. R., Accumulation of peptidyl tRNA is lethal to Escherichia coli. *J Bacteriol* **1979,** *137* (1), 694-6.

377. Wakeman, C. A.; Hammer, N. D.; Stauff, D. L.; Attia, A. S.; Anzaldi, L. L.; Dikalov, S. I.; Calcutt, M. W.; Skaar, E. P., Menaquinone biosynthesis potentiates haem toxicity in Staphylococcus aureus. *Mol Microbiol* **2012,** *86* (6), 1376-92.

378. Matarlo, J. S.; Lu, Y.; Daryaee, F.; Daryaee, T.; Ruzsicska, B.; Walker, S. G.; Tonge, P. J., A Methyl 4-Oxo-4-phenylbut-2-enoate with in Vivo Activity against MRSA that Inhibits MenB in the Bacterial Menaquinone Biosynthesis Pathway. *ACS Infect Dis* **2016,** *2* (5), 329-340.

379. Meganathan, R.; Kwon, O., Biosynthesis of Menaquinone (Vitamin K2) and Ubiquinone (Coenzyme Q). *EcoSal Plus* **2009,** *3* (2).

380. Collins, M. D.; Jones, D., Distribution of isoprenoid quinone structural types in bacteria and their taxonomic implication. *Microbiol Rev* **1981,** *45* (2), 316-54.

381. Jeffries, L.; Cawthorne, M. A.; Harris, M.; Diplock, A. T.; Green, J.; Price, S. A., Distribution of menaquinones in aerobic Micrococcaceae. *Nature* **1967,** *215* (5098), 257-9.

382. Voynova, N. E.; Rios, S. E.; Miziorko, H. M., Staphylococcus aureus mevalonate kinase: isolation and characterization of an enzyme of the isoprenoid biosynthetic pathway. *J Bacteriol* **2004,** *186* (1), 61-7.

383. Gao, W.; Chua, K.; Davies, J. K.; Newton, H. J.; Seemann, T.; Harrison, P. F.; Holmes, N. E.; Rhee, H. W.; Hong, J. I.; Hartland, E. L.; Stinear, T. P.; Howden, B. P., Two novel point mutations in clinical Staphylococcus aureus reduce linezolid susceptibility and switch on the stringent response to promote persistent infection. *PLoS Pathog* **2010,** *6* (6), e1000944.

384. Godfrey, H. P.; Bugrysheva, J. V.; Cabello, F. C., The role of the stringent response in the pathogenesis of bacterial infections. *Trends Microbiol* **2002,** *10* (8), 349-51.

385. Peleg, A. Y.; Miyakis, S.; Ward, D. V.; Earl, A. M.; Rubio, A.; Cameron, D. R.; Pillai, S.; Moellering, R. C., Jr.; Eliopoulos, G. M., Whole genome characterization of the mechanisms of daptomycin resistance in clinical and laboratory derived isolates of Staphylococcus aureus. *PLoS One* **2012,** *7* (1), e28316.

386. Hammer, N. D.; Skaar, E. P., Molecular mechanisms of Staphylococcus aureus iron acquisition. *Annu Rev Microbiol* **2011,** *65*, 129-47.

387. Stauff, D. L.; Skaar, E. P., The heme sensor system of Staphylococcus aureus. *Contrib Microbiol* **2009,** *16*, 120-135.

388. Dale, S. E.; Sebulsky, M. T.; Heinrichs, D. E., Involvement of SirABC in iron-siderophore import in Staphylococcus aureus. *J Bacteriol* **2004,** *186* (24), 8356-62.

389. Beasley, F. C.; Marolda, C. L.; Cheung, J.; Buac, S.; Heinrichs, D. E., Staphylococcus aureus transporters Hts, Sir, and Sst capture iron liberated from human transferrin by Staphyloferrin A, Staphyloferrin B, and catecholamine stress hormones, respectively, and contribute to virulence. *Infect Immun* **2011,** *79* (6), 2345-55.

390. Naclerio, G. A.; Sintim, H. O., Starving Bacteria of Iron: A Potential Strategy to Disperse Bacterial Biofilms. *J Med Chem* **2021,** *64* (11), 7272-7274.

391. Speziali, C. D.; Dale, S. E.; Henderson, J. A.; Vines, E. D.; Heinrichs, D. E., Requirement of Staphylococcus aureus ATP-binding cassette-ATPase FhuC for iron-restricted growth and evidence that it functions with more than one iron transporter. *J Bacteriol* **2006,** *188* (6), 2048-55.

392. Sebulsky, M. T.; Hohnstein, D.; Hunter, M. D.; Heinrichs, D. E., Identification and characterization of a membrane permease involved in iron-hydroxamate transport in Staphylococcus aureus. *J Bacteriol* **2000,** *182* (16), 4394-400.

393. Onyedibe, K. I.; Dayal, N.; Sintim, H. O., SF5- and SCF3-substituted tetrahydroquinoline compounds as potent bactericidal agents against multidrug-resistant persister Gram-positive bacteria. *RSC Med Chem* **2021**.

394. Hurdle, J. G.; O'Neill, A. J.; Chopra, I.; Lee, R. E., Targeting bacterial membrane function: an underexploited mechanism for treating persistent infections. *Nat Rev Microbiol* **2011,** *9* (1), 62-75.

395. Zhang, Y. M.; Rock, C. O., Transcriptional regulation in bacterial membrane lipid synthesis. *J Lipid Res* **2009,** *50 Suppl*, S115-9.

396. Benarroch, J. M.; Asally, M., The Microbiologist's Guide to Membrane Potential Dynamics. *Trends Microbiol* **2020,** *28* (4), 304-314.

397. Padan, E.; Zilberstein, D.; Schuldiner, S., pH homeostasis in bacteria. *Biochim Biophys Acta* **1981,** *650* (2-3), 151-66.

398. Krulwich, T. A.; Sachs, G.; Padan, E., Molecular aspects of bacterial pH sensing and homeostasis. *Nat Rev Microbiol* **2011,** *9* (5), 330-43.

399. Poole, R. J., Energy Coupling for Membrane Transport. *Ann Rev Plant Physiol* **1978,** *29*, 437-460.

400. Miller, J. B.; Koshland, D. E., Jr., Sensory electrophysiology of bacteria: relationship of the membrane potential to motility and chemotaxis in Bacillus subtilis. *Proc Natl Acad Sci U S A* **1977,** *74* (11), 4752-6.

401. Damper, P. D.; Epstein, W., Role of the membrane potential in bacterial resistance to aminoglycoside antibiotics. *Antimicrob Agents Chemother* **1981,** *20* (6), 803-8.

402. Strahl, H.; Hamoen, L. W., Membrane potential is important for bacterial cell division. *Proc. Natl. Acad. Sci. U.S.A.* **2010,** *107* (27), 12281-12286.

403. Miller, J. B.; Koshland, D. E., Jr., Protonmotive force and bacterial sensing. *J Bacteriol* **1980,** *141* (1), 26-32.

404. Te Winkel, J. D.; Gray, D. A.; Seistrup, K. H.; Hamoen, L. W.; Strahl, H., Analysis of Antimicrobial-Triggered Membrane Depolarization Using Voltage Sensitive Dyes. *Front Cell Dev Biol* **2016,** *4*, 29.

405. Silverman, J. A.; Perlmutter, N. G.; Shapiro, H. M., Correlation of daptomycin bactericidal activity and membrane depolarization in Staphylococcus aureus. *Antimicrob Agents Chemother* **2003,** *47* (8), 2538-44.

406. Lebaron, P.; Catala, P.; Parthuisot, N., Effectiveness of SYTOX Green stain for bacterial viability assessment. *Appl Environ Microbiol* **1998,** *64* (7), 2697-700.

407. Sebulsky, M. T.; Speziali, C. D.; Shilton, B. H.; Edgell, D. R.; Heinrichs, D. E., FhuD1, a ferric hydroxamate-binding lipoprotein in Staphylococcus aureus: a case of gene duplication and lateral transfer. *J Biol Chem* **2004,** *279* (51), 53152-9.

408. Karl, J. P.; Fu, X.; Dolnikowski, G. G.; Saltzman, E.; Booth, S. L., Quantification of phylloquinone and menaquinones in feces, serum, and food by high-performance liquid chromatography-mass spectrometry. *J Chromatogr B Analyt Technol Biomed Life Sci* **2014,** *963*, 128-33.

409. Organization, W. H. New report calls for urgent action to avert antimicrobial resistance crisis 2019. https://www.who.int/news/item/29-04-2019-new-report-calls-for-urgent-action-to-avert-antimicrobial-resistance-crisis.

410. Endimiani, A.; Blackford, M.; Dasenbrook, E. C.; Reed, M. D.; Bajaksouszian, S.; Hujer, A. M.; Rudin, S. D.; Hujer, K. M.; Perreten, V.; Rice, L. B.; Jacobs, M. R.; Konstan, M. W.; Bonomo, R. A., Emergence of linezolid-resistant Staphylococcus aureus after prolonged treatment of cystic fibrosis patients in Cleveland, Ohio. *Antimicrob Agents Chemother* **2011,** *55* (4), 1684-92.

411. McGuinness, W. A.; Malachowa, N.; DeLeo, F. R., Vancomycin Resistance in Staphylococcus aureus. *Yale J Biol Med* **2017,** *90* (2), 269-281.

412. Rossolini, G. M.; Arena, F.; Pecile, P.; Pollini, S., Update on the antibiotic resistance crisis. *Curr Opin Pharmacol* **2014,** *18*, 56-60.

413. Britt, N. S.; Potter, E. M.; Patel, N.; Steed, M. E., Effect of Continuous and Sequential Therapy among Veterans Receiving Daptomycin or Linezolid for Vancomycin-Resistant Enterococcus faecium Bacteremia. *Antimicrob Agents Chemother* **2017,** *61* (5).

414. Watkins, R. R.; Lemonovich, T. L.; File, T. M., Jr., An evidence-based review of linezolid for the treatment of methicillin-resistant Staphylococcus aureus (MRSA): place in therapy. *Core Evid* **2012,** *7*, 131-43.

415. Dhanda, G.; Sarkar, P.; Samaddar, S.; Haldar, J., Battle against Vancomycin-Resistant Bacteria: Recent Developments in Chemical Strategies. *J Med Chem* **2019,** *62* (7), 3184-3205.

416. Costerton, J. W.; Montanaro, L.; Arciola, C. R., Biofilm in implant infections: its production and regulation. *Int J Artif Organs* **2005,** *28* (11), 1062-8.

417. Wingender, J.; Strathmann, M.; Rode, A.; Leis, A.; Flemming, H. C., Isolation and biochemical characterization of extracellular polymeric substances from Pseudomonas aeruginosa. *Methods Enzymol* **2001,** *336*, 302-14.

418. Mah, T. F., Biofilm-specific antibiotic resistance. *Future Microbiol* **2012,** *7* (9), 1061-72.

419. Wu, H.; Moser, C.; Wang, H. Z.; Hoiby, N.; Song, Z. J., Strategies for combating bacterial biofilm infections. *Int J Oral Sci* **2015,** *7* (1), 1-7.

420. Verderosa, A. D.; Totsika, M.; Fairfull-Smith, K. E., Bacterial Biofilm Eradication Agents: A Current Review. *Front Chem* **2019,** *7*, 824.

421. Mancy, A.; Abutaleb, N. S.; Elsebaei, M. M.; Saad, A. Y.; Kotb, A.; Ali, A. O.; Abdel-Aleem, J. A.; Mohammad, H.; Seleem, M. N.; Mayhoub, A. S., Balancing Physicochemical Properties of Phenylthiazole Compounds with Antibacterial Potency by Modifying the Lipophilic Side Chain. *ACS Infect Dis* **2020,** *6* (1), 80-90.

422. Ghasemian, A.; Najar Peerayeh, S.; Bakhshi, B.; Mirzaee, M., The Microbial Surface Components Recognizing Adhesive Matrix Molecules (MSCRAMMs) Genes among Clinical Isolates of Staphylococcus aureus from Hospitalized Children. *Iran J Pathol* **2015,** *10* (4), 258-64.

423. Agarwal, A.; Jain, A., Glucose & sodium chloride induced biofilm production & ica operon in clinical isolates of staphylococci. *Indian J Med Res* **2013,** *138*, 262-6.

424. Rayner, C.; Munckhof, W. J., Antibiotics currently used in the treatment of infections caused by Staphylococcus aureus. *Intern Med J* **2005,** *35 Suppl 2*, S3-16.

425. Thati, V.; Shivannavar, C. T.; Gaddad, S. M., Vancomycin resistance among methicillin resistant Staphylococcus aureus isolates from intensive care units of tertiary care hospitals in Hyderabad. *Indian J Med Res* **2011,** *134* (5), 704-8.

426. Kot, B.; Sytykiewicz, H.; Sprawka, I.; Witeska, M., Effect of manuka honey on biofilm-associated genes expression during methicillin-resistant Staphylococcus aureus biofilm formation. *Sci Rep* **2020,** *10* (1), 13552.

PUBLICATIONS

1. **G.A. Naclerio** & H.O. Sintim, Starving Bacteria of Iron: A Potential Strategy to Disperse Bacterial Biofilms, *J Med Chem*, **2021**, *64*(11), 7272-7274.

2. **G.A. Naclerio,** N.S. Abutaleb, M. Alhashimi, M.N. Seleem, H.O. Sintim, *N*-(1,3,4-Oxadiazol-2-yl)Benzamides as Antibacterial Agents against *Neisseria gonorrhoeae*, *Int J Mol Sci* **2021,** *22* (5), 2427.

3. **G.A. Naclerio,** N.S. Abutaleb, D. Li, M.N. Seleem, H.O. Sintim, Ultrapotent inhibitor of *Clostridioides difficile* growth, which suppresses recurrence *in vivo*, *J Med Chem*, **2020**, *63*, 11934–11944.

4. **G.A. Naclerio** & H. O. Sintim, Many ways to kill bacteria via inhibiting novel cell wall or membrane targets, *Future Med Chem,* **2020**, *12*, doi: 10.4155/fmc-2020-0046.

5. **G.A. Naclerio** K.I. Onyedibe, H.O. Sintim, Lipoteichoic Acid Biosynthesis Inhibitors as Potent Inhibitors of *S. aureus* and *E. faecalis* Growth and Biofilm Formation, *Molecules*, **2020**, *25*, E2277.

6. **G.A. Naclerio**, N.S. Abutaleb, K.I. Onyedibe, M.N. Seleem, H.O. Sintim, Potent trifluoromethoxy, trifluoromethyl sulfonyl, trifluoromethylthio and pentafluorosulfanyl containing (1,3,4-oxadiazol-2-yl)benzamides against drug-resistant Gram-positive bacteria, *RSC Med Chem*, **2020,** *11*, 102-110.

7. N. Dayal, C.G. Mikek, D. Hernandez; **G.A. Naclerio**, E. Chu, R. Lapidus, B. Carter-Cooper, H.O. Sintim, Potently Inhibiting Cancer Cell Migration with Novel 3H-pyrazolo[4,3-f]quinoline boronic acid ROCK Kinase Inhibitors, *Eur J Med Chem,* **2019**, *180*, 449-456.

8. **G.A. Naclerio**, C.W. Karanja, C. Opoku-Temeng, H.O. Sintim, Antibacterial small molecules that potently inhibit Staphylococcus aureus lipoteichoic acid synthesis, *ChemMedChem*, **2019**, *14, 10*. 1000-1004.

9. C. Opoku-Temeng[1], **G.A. Naclerio[1]**, H. Mohammad, N. Dayal, N.S. Abutaleb, M.N. Seleem, H.O. Sintim, N-(1,3,4-oxadiazol-2-yl)benzamide analogs, bacteriostatic agents against methicillin- and vancomycin-resistant bacteria, *Eur J Med Chem,* **2018**, *155*. 797-805 ([1]Equal Contribution).

10. Van Dyke, A. R.; Etemad, L. S.; Vessicchio, M. J.; **Naclerio, G. A.**; Jedson, T. E. Capture-Tag-Release: A strategy for small molecule labeling of native enzymes. *ChemBioChem,* **2016**, *17*, 1602–1605